

Characterization of transcriptionally active chicken erythrocyte chromatin

by

Sanzida Jahan

A Thesis submitted to the Faculty of Graduate Studies
of The University of Manitoba
in partial fulfilment of the requirements of the degree of

DOCTOR OF PHILOSOPHY

Department of Biochemistry and Medical Genetics
Max Rady College of Medicine, Rady Faculty of Health Sciences
University of Manitoba
Winnipeg

Copyright © 2017 by Sanzida Jahan

Abstract

Transcriptionally active chicken polychromatic erythrocytes are nucleated, terminally differentiated cells that are no longer replicating. Thus, provide a suitable system to study the mechanisms of transcription and transcription-related events in the absence of replication. In higher eukaryotes, genomes are organized into chromosomal domains. The combination of dynamic histone acetylation, histone modifications and histone modifying enzymes along with DNase sensitive regions ensure the conformation of the transcriptionally active chromosomal loci. Histone deacetylases (HDACs) and lysine acetyltransferases (KATs) work in combination with bromodomain-containing enzymes and chromatin remodeling factors to produce open chromatin structures. Further, protein arginine methyltransferase 1 (PRMT1), a major type I PRMT, plays a critical role in establishing and maintaining active histone marks as demonstrated for the chicken erythroid β globin domain. Type II PRMT, PRMT5 generates a modified histone, which is recognized by lysine methyltransferases complexes that contain WD repeat-containing protein 5 to establish active chromatin signature to the site. However, PRMT5-mediated arginine methylation and HDAC2 can lead to repressed chromatin state as well. Therefore, I hypothesize that the recruitment of HDAC2, PRMT1 and 5 to the active chromosomal regions is a critical event in sustaining open chromatin structure in chicken polychromatic erythrocyte cells.

Several biochemical techniques along with Next-generation DNA, RNA and ChIP-sequencing, were employed in this thesis to map the salt-soluble transcriptionally active chromatin regions in chicken polychromatic erythrocyte cells (Chapter III). Our investigation revealed that chromatin structures vary with respect salt solubility and are correlated with the transcriptional status of the gene. Subsequently, we demonstrated that both total HDAC2 and HDAC2-S394ph are associated with active chromatin fractions and recruitment of HDAC2 to transcribed genes is transcription-dependent (Chapter IV). Further, we explored the distribution of arginine modifications H3R2me2s and H4R3me2a in the active chromosomal locus (Chapter V). Genome-wide distribution of H3K4me3, H3K27ac, H3R2me2s, and H4R3me2a showed the unique distribution of these modifications with immune genes in active chromatin fractions (Chapter VI).

The findings from this study will provide novel insights into the mechanisms of how HDAC2, PRMT1 and 5 regulate a complex network of gene expression. Thus, our studies supply useful

information on the structural and functional organization of the chicken polychromatic erythrocyte epigenome and may also provide insights into the human erythrocyte genome organization.

Acknowledgements

This work is in its present form due to the contribution of many individuals. Foremost, I would like to express my sincere gratitude to my supervisor and mentor **Dr. Jim Davie** for his wisdom, guidance, motivation, patience, support and encouragement throughout my Ph.D. program. He has taught me valuable life lessons of work ethic, integrity, perseverance, and teamwork. He has truly been an inspiration for me to become an independent researcher. He has been and will continue to be a role model for me.

I also sincerely thank the members of my advisory committee- **Drs. Jeffrey Wigle, Sam Kung, Wayne Xu** for their generous support, insightful feedback and mentorship throughout my graduate program. I am grateful to **Dr. Wayne Xu**, who performed the bioinformatics analysis which is an integral part of this study.

This work would not have been possible without the tremendous support and technical assistance of **past and present members of the Davie lab: Cheryl Peltier, Dr. Shihua he, Carolina Gonzaleg, Dr. Deborah Tsuyuki, Dr. Shannon Healy, Dr. Dilshad Khan and Dr. Soma Mandal**. I am greatly thankful to **Ms. Cheryl Peltier** who not only helps me in learning techniques and to start up my project but always been there as a support. I greatly appreciate the tremendous support and technical assistance of **Ms. Cheryl Peltier**. I extend my gratitude to **Ms. Carolina Gonzaleg** who was involved in the library preparation for the first part of the study. She was my bench mate and a very supportive friend. It was a pleasure to work with such a friendly and supportive person. I am grateful to **Aleksandar Ilic** who performed the library preparation for most part of the study. He was a wonderful person to work with. We started the lab at the same time, shared struggle and frustration about experiments during the learning process. Also, thank you for taking the pain of proofreading part of my thesis. I would like to acknowledge Mr. Mario from Dr. Vernon Dolinsky lab for lending me their apparatus whenever I needed to set my gigantic experiments. I thank my **present and fellow lab members** for their pleasant company in the lab.

I am grateful to: Cathy Webber and Philip Dufresne of Biochemistry and Medical Genetics; Debbie Korpesho of Child health research institute of Manitoba; Wendy Benchrasky, Research Institute of oncology and hematology, for their administrative support; staff at the animal facility

for animal maintenance. I acknowledge Nichola Wigle, Chief Operating Officer of Child health research institute of Manitoba for her tremendous effort to maintain the institute as an excellent place to work.

Pursuing a Ph.D. program is like a marathon - scholarship support from Research Manitoba, Child health research institute of Manitoba and Cancer care Manitoba, made the run gratifying. I would like to acknowledge Faculty of Graduate Studies for providing me travel awards during my tenure as a Ph.D. student. This research was supported by several grants; CIHR, Canada Research Chair and NSERC (to **J.R.D.**)

Lastly, but not the least, I thank my parents for their unconditional love and support throughout my life. Moreover, I thank my loving husband **Rony**, for his love, patience, understanding and encouragement. Finally, this thesis would be incomplete without thanking my very smart daughter Suri Jahan Kabir, who always been a source of peace after the exhausting day in the lab and unsuccessful experiments. I thank the Almighty for all the wonderful things in my life.

Dedication

I dedicate this thesis

To my family

My parents Md.Shah Jahan and Mrs.Sabera Khatun,

my husband Rony and my daughter Suri

-For their love and support

TABLE OF CONTENTS

Abstract	i
Acknowledgements	iii
Dedication	v
List of Abbreviations	xiii
List of Tables	xix
List of Copyrighted Material for which Permission was obtained	xxiii
CHAPTER I: INTRODUCTION	1
1.1 Chromatin structure, histone modifications	2
1.1.1 Chromatin domain	4
1.1.1.1 Defining the barrier element	5
1.1.1.2 Examples of some insulators and chromatin domains in vertebrates	7
1.1.1.3 Disease associated with altered chromatin structure	10
1.1.2 Histone modifications and their distribution in the genome	12
1.1.3 Histone acetylation	15
1.1.4 Histone lysine methylation	15
1.1.5 Histone arginine methylation	16
1.1.6 Citrullination of histones	17
1.1.7 Phosphorylation of histone	18
1.1.8 Other histone modifications	18
1.2 Chromatin modifying enzymes: Histone deacetylases	18
1.2.1 Classifications of class I HDAC	19
1.2.2 Complexes of unmodified and phosphorylated HDAC2	19
1.2.3 Distribution of HDAC2 and pHDAC2	20
1.3 Chromatin modifying enzymes: Protein arginine methyltransferases	22
1.3.1 Overview of mammalian PRMTs	22
1.3.2 Mammalian PRMTs and their substrates	23
1.3.3 Arginine modifications by PRMTs	26
1.3.4 Biological functions of PRMTs	29
1.3.4.1 PRMTs and transcriptional co-activator activity	29
1.3.4.2 PRMTs and transcriptional co-repressor activity	29

1.3.4.3	PRMTs and chromatin barrier function	30
1.3.5	Association of PRMTs with human disease	30
1.3.6	Regulating the regulator	31
1.4	Chromatin fractionation	32
1.4.1	Description of chromatin fractionation for different cell sources	32
1.5	Innate immunity in avian system.....	35
1.5.1	Chicken TLRs.....	37
1.5.2	Chicken TLR 1, 2, 4, 5	39
1.5.3	TLR3, TLR7, TLR8, and TLR9	39
1.5.4	TLR15.....	39
1.5.5	TLR21.....	40
1.5.6	RIG-1 like receptors	40
1.5.7	NLR	41
1.5.8	Cytokines	41
1.5.9	Immune regulatory pathways in avian erythrocytes	42
1.5.10	Immune stimulants to induce immune pathways	47
1.6	Rationale, hypothesis and study objectives	48
1.6.1	General hypothesis	50
1.7	References	51
CHAPTER II: MATERIALS & METHODS		83
2.1	Cell processing and related techniques	83
2.1.1	Animal Ethics and source of cells	83
2.1.2	Types of cells used in the study	83
2.1.3	Treatment of chickens	83
2.1.4	Harvesting chicken erythrocytes and storage.....	83
2.1.5	Preparation of media for erythrocyte cell treatment.....	84
2.1.6	Chromatin fractionation	84
2.3	Protein-based techniques.....	86
2.3.1	Preparation of cellular extract	86
2.3.2	Electrophoresis and Immunoblotting	87
2.3.3	Peptide Dot Blot assay	87
2.3.4	Immunoprecipitation	88

2.3.5 Histone co-IP	88
2.3.6 Chromatin immunoprecipitation (ChIP) assay and ChIP-seq assay	89
2.4 RNA-based technique	90
2.4.1 RNA extraction and cDNA preparation	90
2.4.2 Isolation of nuclear RNA	91
2.5 Polymerase chain reaction (PCR).....	91
2.5.1 RT-qPCR.....	91
2.6 Library preparation for F1 DNA, total RNA, and ChIP-seq DNA.....	91
2.6.1 Genomic DNA and ChIP DNA libraries, Sequencing and data analyses	91
2.6.2 ChIP-Seq with the MiSeq.....	92
2.6.3 RNAseq library preparation for SOLiD	92
2.7 Bioinformatics analysis.....	92
2.7.1 SOLiD next-generation sequencing data analyses	92
2.7.2 Detection of transcriptionally active chromatin domains	92
2.7.3 RNA-seq data analyses.....	93
2.7.4 ChIP-seq data analyses.....	93
2.8 References	94
CHAPTER III: CHICKEN ERYTHROCYTE EPIGENOME	95
3.1 Abstract.....	95
3.2 Introduction.....	97
3.3 Results:.....	98
3.3.1 Genome-wide mapping of polychromatic erythrocyte transcribed chromosomal domains 98	
3.3.2 Features of salt-soluble chromatin.....	104
3.4 Discussion.....	108
3.5 Conclusions.....	110
3.6 Methods.....	110
3.6.1 Isolation of chicken erythrocytes.....	110
3.6.2 Salt fractionation.....	110
3.6.3 ChIP-seq assays	110
3.6.4 Sequencing and mapping of data.....	111
3.6.5 RNA Isolation and Real-time RT-qPCR Analysis	111
3.6.6 Active chromatin detection and genomic distribution.....	112

3.6.7 Chromatin profiling of transcriptionally active genes	112
3.7 Data availability	112
3.8 Acknowledgements	112
3.9 References	113
3.10 Supporting informations	117
4.1 Abstract	122
4.2 Introduction	124
4.3 Results	125
4.3.1 HDAC2 and phosphorylated HDAC2 association with active chromatin	125
4.3.2 HDAC2 co-maps with interchromatin channels of the nuclei	126
4.3.3 Phosphorylated HDAC2 binds to regulatory regions of transcribed genes.....	127
4.3.4 Recruitment of HDAC2 to promoter and coding region is dependent on transcription	129
4.3.5 Chicken erythrocyte HDAC2 associates with RNA splicing factors	130
4.3.6 Association of HDAC2, but not HDAC2S394ph, with RNAPII	131
4.4 Discussion	132
4.5.1 Ethics	134
4.5.2 Chicken erythrocyte chromatin fractionation and HDAC2 isolation.....	134
4.5.3 Mass Spectrometry.....	134
4.5.4 Immunoblotting.....	134
4.5.5 Immunofluorescence assay.....	134
4.5.6 Immunoprecipitation (IP) and co-immunoprecipitation (co-IP) assays.....	135
4.5.7 Cell Culture and Treatments.....	135
4.5.8 Chromatin Immunoprecipitation (ChIP) assay	135
4.5.9 Statistical analysis	135
4.6 References	136
4.7 Supplementary informations	138
CHAPTER V: PRMT1 AND 5 MEDIATED H4R3ME2A AND H3R2ME2S MODIFICATIONS IN TRANSCRIPTIONALLY ACTIVE CHROMATIN	140
5.1 Abstract	140
5.2 Introduction	142
5.3 Results	143

5.3.1 Association of PRMT1, PRMT5 and their products (H4R3me2a and H3R2me2s) with active chromatin fractions	143
5.3.2 Correlation of H4R3me2a and H3R2me2s arginine methylation with highly transcribed genes	146
5.3.3 Profile of H4R3me2a and H3R2me2s arginine methylation in highly transcribed genes	148
5.3.4 Profile of arginine methylation in lowly expressed genes of polychromatic erythrocyte cells	154
5.3.5 Analysis of correlation between H4R3me2a with H3K27ac ChIP-seq peaks	157
5.3.6 H3 arginine dimethylation relationship with H3K4me3 and H3K27ac	158
5.3.7 RNAPIIS2ph dependent recruitment of PRMT1 and 5 to transcribed gene regions .	160
5.3.8 Association of PRMT1 and 5 with the nuclear matrix	161
5.4 Discussion	162
5.4.1 PRMT1 and 5 associate with active chromatin	162
5.4.2 H4R3me2a associate with promoters of transcriptionally active genes	163
5.4.3 H4R3me2a co-localize with H3R2me2s at the hypersensitive sites HS1-HS4 and other distal regulatory region of transcriptionally active genes	164
5.4.4 H3R2me2s co-localize with H3K4me3 at the 5' end of the gene body of highly expressed genes	165
5.4.5 H3 modified at R2me2s has K4me1 and H3K27ac	165
5.4.6 PRMT1 and 5 recruited through RNAPIIS2ph	165
5.4.7 PRMT1 and 5 binds to the nuclear matrix	166
5.5 Methods	167
5.5.1 Chromatin fractionation	167
5.5.2 Immunoblotting	167
5.5.3 Dot-blot assay.....	168
5.5.4 Co-association of modification on H3 tail	168
5.5.5 Chromatin immunoprecipitation (ChIP) assay and ChIP-seq assay	169
5.5.6 Immunoprecipitation and co-IP	169
5.5.7 Isolation of nuclear matrix	170
5.5.8 Bioinformatics analysis	170
5.5.8.1 RNA-seq and ChIP-seq analysis	170
5.5.8.2 ChIP-seq peak distribution	170
5.5.8.3 ChIP-seq peak Correlation	171

5.6 References	172
5.7 Supporting informations	176
5.7.1 Supporting figures	176
5.7.1.1 Determining antibody specificity and cross reactivity	176
5.7.1.2 Association of PRMT1, PRMT5 and H3 and H4 arginine methylation with transcriptionally active chromatin	177
5.7.1.3 ChIP assay for H3R2me2s and H4R3me2a for highly transcribing genes of polychromatic erythrocyte cells.	179
5.7.2 Supporting table	181
CHAPTER VI: EPIGENOMIC LANDSCAPE OF IMMUNE GENES IN CHICKEN ERYTHROCYTES	183
6.1 Abstract	183
6.2 Introduction	185
6.3 Results	187
6.3.1 Circos plot for immune genes enrichment in F1	187
6.3.2 Transcriptome profile of immune genes in polychromatic erythrocytes and 6C2 cells	189
6.3.3 Chromatin profile of highly expressed immune genes.....	195
6.3.4 Chromatin profile of low expressed immune genes	197
6.3.5 Induction of immune genes in polychromatic cells	202
6.4 Discussion	204
6.5 Methods	208
6.5.1 Cell culture and Treatment	208
6.5.2 RNA extraction and RT-PCR.....	209
6.5.3 Statistical analysis	209
6.6 References	210
6.7 Supporting informations	214
6.7 Supporting informations	214
6.7.1 Supporting figures	214
6.7.1.1 Transcriptome profile of several immune genes	214
6.7.1.2 Chromatin profile of several immune genes in polychromatic erythrocytes	218
6.7.1.3 Microscopy for polychromatic erythrocytes	226
6.7.2 Supporting tables.....	227

CHAPTER VII: DISCUSSION AND FUTURE PERSPECTIVE	228
7.1 Summary	228
7.2 Insight and perspectives from the studies	228
7.2.1 Insights and perspectives from the study-1 “Chicken erythrocyte epigenome”..	228
7.2.2 Insights and perspectives from the study-2 “Transcription-Dependent Association of HDAC2 with Active Chromatin.”	229
7.2.3 Insights and perspectives from the study-3 “PRMT1 and 5 mediated H4R3me2a and H3R2me2s modifications in transcriptionally active chromatin”	230
7.2.4 Insights and perspectives from the study-4	231
7.3 Conclusion, significance and study limitations	232
7.4 References	238

List of Abbreviations

A260	Absorbance at 260 nm
A280	Absorbance at 280 nm
ASF/SF2	Alternative-splicing factor 1/Splicing factor-2
ATF	Activating transcription factor
ATP	Adenosine triphosphate
BAD	Bcl-2-associated death promoter
BAK	Bcl-2 homologous antagonist killer
BAX	Bcl-2-associated X protein
BME	β -mercaptoethanol
bp	Base pair
BRG1	Brahma-related gene-1
BSA	Bovine serum albumin
cDNA	Complementary deoxyribonucleic acid
C/EBP	CCAAT/Enhancer-binding protein
CHD1	Chromodomain helicase DNA binding protein-1
ChIP	Chromatin immunoprecipitation
ChIP-seq	ChIP followed by high-throughput sequencing
CLIP	UV cross-linking and immunoprecipitation
CLIP-seq	CLIP followed by high-throughput sequencing
DAPI	4',6-diamidino-2-phenylindole
DMEM	Dulbecco's modified eagle medium

DMSO	Dimethyl sulfoxide
DNA	Deoxyribonucleic acid
DRB	5,6-dichloro-1- β -D-ribofuranosylbenzimidazole
DSP	Dithiobis[succinimidylpropionate]
EDTA	(Ethylenedinitrilo) tetraacetic acid
EGTA	Ethylene glycol-bis(2-aminoethylether)- <i>N,N,N',N'</i> -tetraacetic acid
eRNA	Enhancer RNA
FACS	Fluorescence-activated cell sorting
FBS	Fetal bovine serumH Hours
H3K9ac	Histone H3 acetylation on lysine 9
H3K14ac	Histone H3 acetylation on lysine 14
H3 K9me3	Histone H3 trimethylation on lysine 9
H3S10ph	Histone H3 phosphorylation on serine 10
H3S28ph	Histone H3 phosphorylation on serine 28
H3R2me2s	Histone H3 dimethyl symmetric
H3R2me2a	Histone H3 dimethyl asymmetric
H4R3me2a	Histone H4 dimethyl asymmetric
H4R3me2s	Histone H3 dimethyl symmetric
HAT	Histone acetyltransferases
H3K4me3	Histone H3 trimethylation on lysine 4
H3K36me3	Histone H3 trimethylation on lysine 36
HCT116	Human colorectal cancer cell line
HDAC	Histone deacetylase

HDAC1	Histone deacetylase 1
HDAC2	Histone deacetylase 2
HeLa	Henrietta Lacks (Human cervical cancer cell line)
HEK293	Human embryonic kidney 293 cell line
HP1	Heterochromatin protein-1
IB	Immunoblot
ID	Immunodepleted fraction
IEG	Immediate-early gene
ING	Inhibitor of growth
IP	Immunoprecipitated fraction
JNK	c-Jun N-terminal kinase
K562	Chronic myeloid leukemia cell line
KAT	Lysine acetyltransferases
KDa	Kilodalton
KMT	Lysine methyltransferase
LSD1	Lysine-specific histone demethylase-1
MAPK	Mitogen-activated protein kinase
MBD	Methyl-CpG-binding domain-containing protein
MCF7	Michigan Cancer Foundation-7
Min	Minutes
miRNA	MicroRNA
MLL	Mixed-lineage leukemia gene
MNase	Micrococcal nuclease

NAD	Nicotinamide adenine dinucleotide
NCoR	Nuclear receptor corepressor
ncRNA	Non-coding RNA
NF- κ B	Nuclear factor-kappa B
NuRD	Nucleosome-remodeling and deacetylase repressor
p53	protein 53
PAGE	Polyacrylamide gel electrophoresis
PBS	Phosphate buffered saline
PCR	Polymerase chain reaction
P _E	EDTA insoluble chromatin fraction
P ₁₅₀	150 mM NaCl insoluble chromatin fraction
ph	Phosphorylation
PIC	Pre-initiation complex
PKA	c-AMP dependent protein kinase A
PKC	Protein kinase C
PCE	Polychromatic erythrocyte cells
pHDAC2	Phosphorylated HDAC2
PolyI:C	Polyinosinic:polycytidylic acid
PRMTs	Protein arginine methyltransferases
PTM	Post-translational modification
qPCR	Real time PCR
RbAp	Retinoblastoma-associated protein
RNA	Ribonucleic acid

RNA-seq	Next-generation RNA-sequencing
RNAPII	RNA polymerase II
RNAPIIS2ph	RNA polymerase II phosphorylated at serine 2
RNAPIIS5ph	RNA polymerase II phosphorylated at serine 5
RNase	Ribonuclease
RNP	Ribonucleoprotein
RRM	RNA recognition motif
RT	Reverse transcriptase
RT-PCR	Reverse transcription-polymerase chain reaction
SDC	Sodium deoxycholate
SDS	Sodium dodecyl sulfate
SDS-PAGE	SDS-Polyacrylamide gel electrophoresis
Sec	Seconds
S _E	EDTA insoluble chromatin fraction
S ₁₅₀	150 mM NaCl insoluble chromatin fraction
SETD1A	SET Domain Containing 1A
SETD1B	SET Domain Containing 1B
SF2/ASF	Splicing factor 2/Alternative splicing factor 1
siRNA	Small interfering RNA
SMRT	Silencing mediator of retinoid and thyroid hormone receptor
Sp1/Sp3	Specificity protein 1/3
snRNPs	Small ribonucleoprotein particles
SR	proteins Serine/arginine-rich proteins

SRSF1	Serine/arginine-rich splicing factor 1
SUMO	Small ubiquitin-like modifier
SWI/SNF	Switch/sucrose non-fermentable
TBB	4,5,6,7-tetrabromobenzotriazole
TBP	TATA-box binding protein
TBS	Tris buffered saline
TBP	TATA-binding protein
TE	Tris-EDTA
TFF1	Trefoil factor 1
TIP60	Tat-interactive protein 60
TLR	Toll-like receptor
TPA	12-O-tetradecanoate 13-acetate
Tris	Tris (hydroxymethyl)aminomethane
TSA	Trichostatin A
TTBS	Tris buffered saline with Tween-20
U2AF	U2snRNP auxiliary factor
UPR	Upstream promoter region
UsnRNPs	Uridine-rich small ribonucleoprotein particles
USF1	Upstream stimulatory factor 1
UTR	Untranslated region
UV	Ultraviolet
YY1	Yin Yang 1

List of Tables

Table 1: PRMT-catalyzed methylation marks on mammalian histones.....	24
Table 2: Properties of 150 mM salt soluble and salt-insoluble chromatin isolated from chicken erythrocytes.....	33
Table 3: Pattern recognition receptors between human and chicken.....	34
Table 4: List of cytokine repertoire between human and chicken.....	39
Table 5: Table reports functions associated to erythrocytes in mammals, fish, amphibian, reptiles and birds. References are numbered according to appearance.....	41
Table 6: Analysis of cytokine and other immunological genes in chicken erythrocytes after 3h post stimulation.....	42
Table S3.1: Table with information regarding all sequencing tracks.....	81
Table S3.1: Description of polychromatic erythrocyte sample sources.....	84
Table S3.2: Primers for RT-qPCR assays.....	85
Table 4.1: Protein composition of HAP-unbound HDAC2 complexes in the polynucleosome fraction (F1) of chicken erythrocytes.....	95
Table S4.1: List of antibodies used in immunoblotting (IB) and immunoprecipitation (IP).....	104
Table S4.2: Primers used in ChIP-qPCR experiments.....	105
Table S5.1: Primers used for ChIP qPCR.....	145
Table 6.1: Expression of immune components in chicken polychromatic erythrocytes and Chicken erythroleukemia cell (6C2) cells.....	167
Table S6.1: Primers used for ChIP qPCR.....	191

List of Figures

Figure 1.1: Higher order chromatin structure.....	1
Figure 1.2: Chromosome territories within the nucleus.....	2
Figure 1.3: Chromosome domain, barrier.....	6
Figure 1.4: Histone modifications in the N-terminal tail of core histone.....	13
Figure 1.5: Distribution of histone modifications across the genome.....	15
Figure 1.6: Citrullination of arginine by PADs.....	16
Figure 1.7a: Binding of phosphorylated and unmodified HDAC2 to chromatin.....	19
Figure 1.7b: Recruitment of HDAC1/2ph complexes to the regulatory region and non-ph HDAC1/2 to the coding region of expressed genes	21
Figure 1.8: Methylation of arginine residue by PRMTs. Amino acid Arginine contains five potential hydrogen bond donor site.....	23
Figure 1.9: Overview of chromatin fractionation process in chicken erythrocyte cells.....	34
Figure 1.10: PAMP recognition by intracellularTLRs.....	38
Figure 1.11: Innate immunity in birds.....	46
Figure 3.1: Representative browser snapshots of F1 and S _E chromatin DNA-seq.....	63
Figure 3.2: Active chromatin distribution and transcriptional activity.....	64
Figure 3.3: Chromatin profile and transcriptional activity of β -globin domain.....	69
Figure 3.4: Chromatin profile and transcriptional activity of region of interest on chromosome Z.....	71
Figure 3.5: Chromatin profile and transcriptional activity of moderately and poorly expressed genes.	72
Figure 4.1. HDAC2, HDAC2-S394ph, SRSF1 and H3K36me3 are associated with the transcriptionally active chromatin fraction of polychromatic erythrocytes.....	91
Figure 4.2. Association of HDAC2 with the interchromatin channel of the polychromatic erythrocytes.....	92

Figure 4.3. Distribution of HDAC2, phosphorylated HDAC2 (HDAC2-S394ph) and acetylated H3 (H3Ac) within the <i>CA2</i> and <i>GAS41</i> gene regions.....	93
Figure 4.4. Transcription-dependent recruitment of unmodified HDAC2 to <i>CA2</i> and <i>GAS41</i> gene regions.....	95
Figure 4.5. Interaction of HDAC2 but not HDAC2-S394ph with RNAPIIS2ph and RNAPIIS5ph in polychromatic erythrocytes is RNA-dependent.....	97
Figure 5.1: Association of PRMT1 and PRMT5 with the active chromatin fractions of polychromatic erythrocytes.....	111
Figure 5.2: Association of H3 and H4 arginine modifications with active chromatin fractions.....	112
Figure 5.3: Association of H3, H4 arginine modifications with the active chromatin fractions.....	113
Figure 5.4: Profile of H4R3me2a as function of gene expression.....	114
Figure 5.5: Profile of H3R2me2s as function of gene expression.....	115
Figure 5.6: Distribution of H3R2me2s and H4R3me2a along the β -globin domain of polychromatic erythrocytes.....	116
Figure 5.7: Distribution of H3R2me2s and H4R3me2a along expressed genes of polychromatic erythrocytes.....	117
Figure 5.8: Distribution of H3R2me2s and H4R3me2a along <i>FTH1</i> gene of polychromatic erythrocytes.....	118
Figure 5.9: Distribution of H3R2me2s and H4R3me2a along <i>CA2</i> gene of polychromatic erythrocytes.....	120
Figure 5.10: Distribution of H3R2me2s and H4R3me2a along <i>HDAC2</i> gene of polychromatic erythrocytes.....	122
Figure 5.11: Distribution of H3R2me2s and H4R3me2a along the <i>PRMT7</i> gene of polychromatic erythrocytes.....	123
Figure 5.12: Correlation between H4R3me2a and H3K27ac ChIP-seq peaks.....	124
Figure 5.13: Correlation between H4R3me2a and H3R2me2s ChIP-seq peaks.....	125
Figure 5.14: H3R2me2s arginine methylation with lysine methylation and acetylation.....	126
Figure 5.15: PRMT1 and 5 associate with the RNAPIIS2ph complex.....	128
Figure 5.16: Interaction of PRMT1 and PRMT5 with the nuclear matrix.....	129

Figure 6.1: Distribution of salt soluble immune genes in chicken erythrocyte genome.....	153
Figure 6.2. Transcriptional activity of a. <i>TLR3</i> and b. <i>TLR21</i> gene in chicken erythrocytes.....	154
Figure 6.3. Transcriptional activity of <i>TLR6</i> in chicken erythrocytes.....	155
Figure 6.4 shows <i>IFNA3</i> and <i>IFNW1</i> had low level of expression in polychromatic erythrocytes and 6C2 cells.....	156
Figure 6.5: Transcriptional activity of a. <i>IL1B</i> and b. <i>IL15</i> gene in chicken polychromatic erythrocytes.....	158
Figure 6.6. Chromatin profile and transcriptional activity of <i>IRF1</i> gene.....	162
Figure 6.7: Chromatin profile and transcriptional activity of <i>TLR3</i> gene.....	164
Figure 6.8: Chromatin profile and transcriptional activity of <i>IL1B</i> gene.....	165
Figure 6.9: Chromatin profile and transcriptional activity of <i>IFNA3</i> gene.....	167
Figure 6.10: Poly I:C mediated induction of immune genes in chicken polychromatic erythrocytes.....	168
Figure 7.1: Interplay between arginine methylation and lysine methylation and acetylation in transcriptionally chromosomal location.....	199
Figure 7.2: Chromatin organization in chicken erythrocyte nuclei.....	200

List of Copyrighted Material for which Permission was obtained

1. Jahan S, Davie JR (2014) Protein arginine methyltransferases (PRMTs): Role in chromatin organization. *Advances in biological regulation*. 57:173-84. © 2014 Elsevier Ltd.
2. Jahan S, Wayne Xu, Shihua He, Carolina Gonzalez, Geneviève P. Delcuve and James R. Davie. The chicken erythrocyte epigenome. *Epigenetics & Chromatin* (2016) 9:19. © The Author(s). 2016.
3. Jahan S, Jian-Min Sun, Shihua He, Davie JR. Transcription-dependent association of HDAC2 with active chromatin. *J Cell Physiol*. 2017;1–8. © 2017 Wiley Periodicals, Inc.
4. Figure 1.1: Higher order chromatin structure (Reprinted with permission from *Science*, volume 297: 1824-7 © 2002, The American Association for the Advancement of Science).
5. Figure 1.2: Chromosome territories within the nucleus (Reprinted with permission from *Nat Struct Mol Biol*, volume 20(3): p. 290-9. © 2002, Annual reviews).
6. Figure 1.3: Good Fences Make Good Neighbors (Reprinted with permission from *Molecular cell*, volume 16: 500-502 © 2004, Elsevier Ltd.).
7. Figure 1.4: Histone modifications in the N-terminal tail of core histone (Reprinted with permission from *Reproduction*, volume 136(2): p. 131-46 © 2008, Bioscientifica Ltd.).
8. Figure 1.5: Distribution of histone modifications across the genome (Reprinted with permission from *Curr Drug Targets*, 16(7): p. 700-10. © 2007, Elsevier).
9. Figure 1.6: Binding of phosphorylated and unmodified HDAC2 to chromatin (Reprinted with permission from *Clin Epigenetics*, 4(1): p. 5. © ©2012 Delcuve et al; licensee BioMed Central Ltd.).
10. Figure 1.10: PAMP recognition by intracellular TLRs (Adapted with permission from *Nat Immunol*, 11(5): p. 373-84. ©2010 nature publishing group).
11. Figure 11: Innate immunity in birds (Adapted with permission from *Vet Res*, 44: p. 82. © 2013 Chen et al.; licensee BioMed Central Ltd.).
12. Table 3: Comparison of pattern recognition repertoire between human and chicken (Reprinted with permission from *Avian Pathol*, 39(5): p. 309-24. © 2010 Taylor and Francis).
13. Table 4: Comparison of the cytokine repertoire between human and chicken (Reprinted with permission from *Avian Pathol*, 39(5): p. 309-24. © 2010 Taylor and Francis).

14. Table 5: Table reports functions associated to erythrocytes in mammals, fish, amphibian, reptiles and birds (Reprinted with permission from *Vet Res*, 42: p. 89©2011 Morera and MacKenzie; licensee BioMed Central Ltd.).

15. Table 6: Expression levels of cytokine and other immunological genes in chicken erythrocytes at 3 h post-poly I:C-stimulation (Reprinted with permission from *Res Vet Sci*, 95(1): p. 87-91© 2013 Elsevier Ltd.).

CHAPTER I: INTRODUCTION

This chapter contains materials from the following publication:

Jahan S, Davie JR (2014) Protein arginine methyltransferases (PRMTs): Role in chromatin organization. Advances in biological regulation. doi:10.1016/j.jbior.2014.09.003

1.1 Chromatin structure, histone modifications

During the interphase stage of the cell cycle, when cells are not undergoing cell division, chromatin exists in various structures. Chromatin is a nucleoprotein complex composed of histones and DNA molecules. Nucleosomes, the unit of chromatin, consists of four core histones (H2A, H2B, H3 and H4) along with 146 base pairs of DNA [1]. Histones are evolutionarily conserved, basic proteins. The histone octamer contains an $(H3)_2(H4)_2$ tetramer flanked by two dimers of H2A-H2B [1]. Core histones have three domains; globular central domain organized by three α helices (histone fold), a N- and a C-terminal domain. The globular central domain binds to DNA as depicted in the crystal structure. The N-terminal and C-terminal tails of the histones undergo several post-translational modifications [1]. In a recent study, it was demonstrated that the globular domain of histones is also subjected to posttranslational modifications [2, 3]. Histone H1 (linker histone) binds to the linker DNA, which joins the nucleosomes together. H1 histone contributes to condensation of the chromatin fiber resulting in higher order chromatin structures. Unlike the core histones, which are highly conserved among species, histone H1s are less conserved [4]. Histone H5 is one of the isoforms of H1 and is found in nucleated erythrocytes of birds and fish [5].

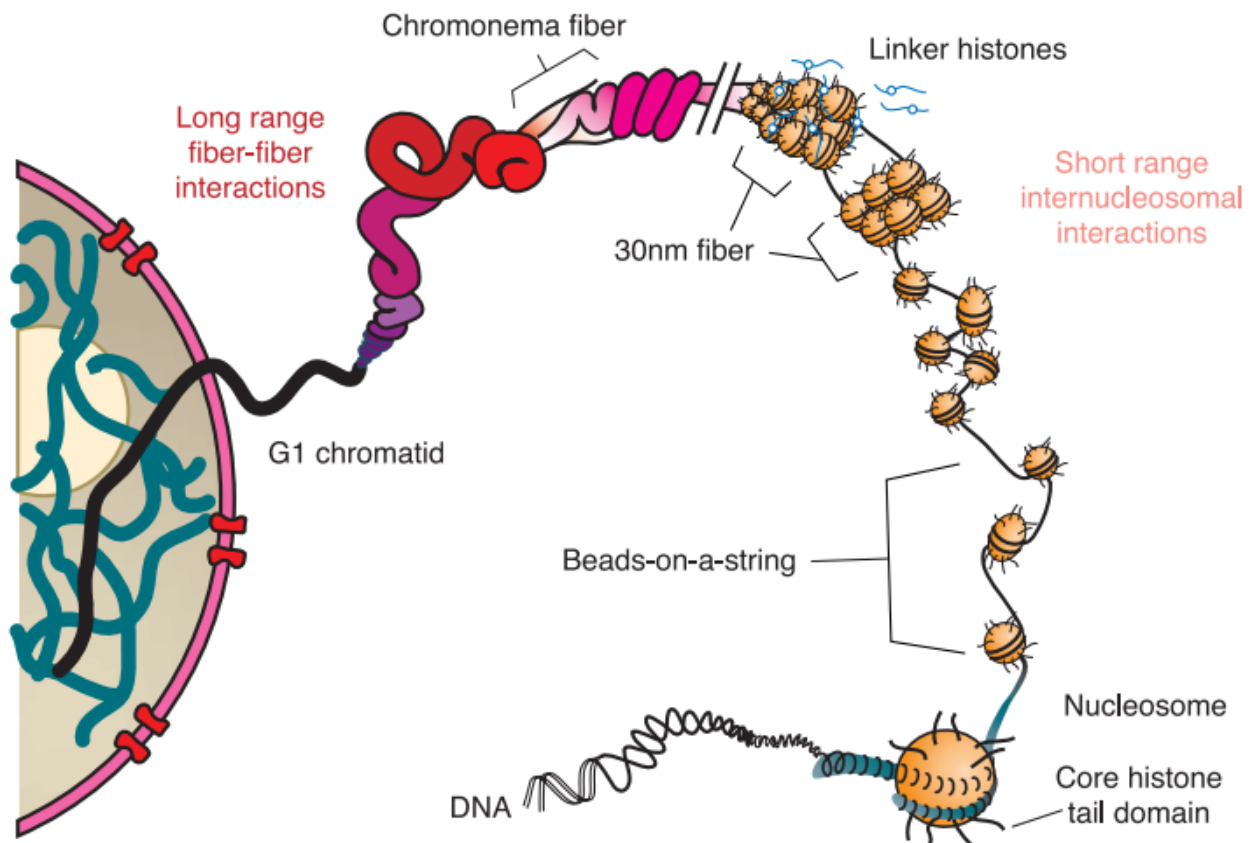


Figure 1.1: Higher order chromatin structure. In the interphase stage of the nuclei, chromatin has higher order structures. Interaction of nucleosome with neighboring nucleosomes gives rise to 30 nm structure, and fiber-fiber interactions lead to the tertiary structure of the chromatin [6]. The figure and the text were reproduced with permission from Figure 1 [6].

Chromatin states can be changed between euchromatin and heterochromatin based on the type of modifications at the N-terminal core histone tail. Euchromatic regions are organized as a decondensed chromatin, which allows access of transcription factors, transcription initiation complex, histone remodellers and histone modifying enzymes to bind to sites to turn on the active transcription. On the contrary, the heterochromatic region is in a condensed chromatin configuration built up due to fiber-fibre interactions, which are inaccessible to RNA polymerase and other transcription-related machinery [7].

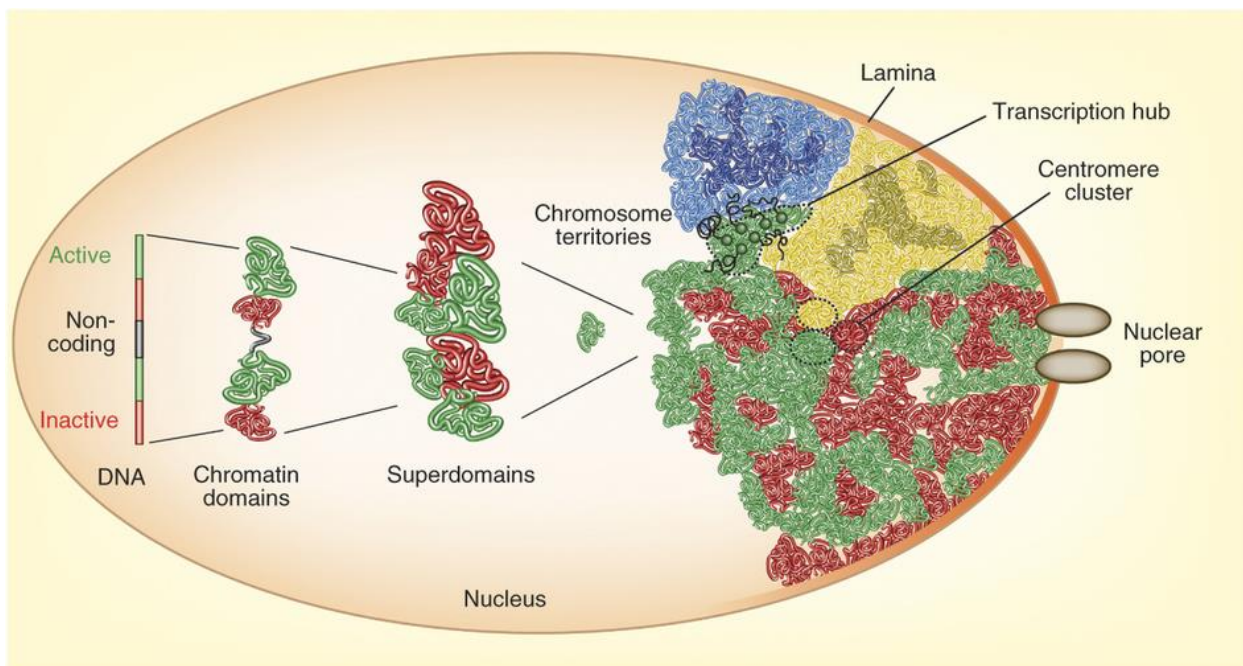


Figure 1.2: Chromosome territories within the nucleus. Chromatin domain folding is determined by the transcriptional activity of genome regions. Boundaries form at the interface of active and inactive parts of the genome. Higher-order domains of similar activity status cluster to form chromatin domains, which assemble into chromosome territories. Repressive regions of chromosomes tend to contact other repressive regions on the same chromosome arm, whereas active domains are more exposed to the outside of chromosome territories. Active chromosomes have a higher chance of contacting active domains on the

other chromosome arm and other chromosomes, giving rise to topological 'superdomains' composed of multiple, functionally similar genome domains. The location of territories is constrained by their association with the nuclear periphery, transcription hubs, nuclear bodies and centromere clusters. *The figure and the text were reproduced with permission from Figure 1 [8].*

In higher eukaryotes, genomes are organized spatially in a non-random way within the nucleus. Individual chromosomes are located in specific nuclear locations, defining a chromosome territory [9]. The interchromatin compartment that creates a channel around the chromosome territory is believed to facilitate the transportation/diffusion of nuclear-molecules to the chromosomal regions [10]. A gene-rich transcriptionally active chromosome tends to reside in the nuclear interior, while gene-poor chromosomes tend to reside at the periphery [9]. The location of active chromosomal regions in the nuclear interior may facilitate access of the active genomic region to the “transcription factories” where transcription occurs within the nucleus [11].

1.1.1 Chromatin domain

Chromatin domains have individual genes or gene clusters, with the genes in the cluster exhibiting distinct expression patterns during developmental stages and in differentiated cells [12-14]. Expression of the genes within a domain is controlled by several regulatory elements, namely enhancers, silencers, promoters and locus control regions. Enhancers are regulatory elements that can activate target genes in *cis* over a significant distance, while silencers repress transcription [15]. In vertebrates, euchromatin or transcribed gene regions are separated from the adjacent heterochromatin regions by chromatin boundaries [16]. A chromatin boundary separates active and inactive chromatin states which differ in histone and/or DNA modifications or chromatin accessibility. In fact, boundaries are transition regions between heterochromatin and euchromatin that comprise boundary element-specific or non-specific DNA sequences or specific proteins (**Figure 1.3**). Therefore, boundary elements regulate the expression of genes within individual domains independent of their surroundings [16].

The barrier chromatin boundaries mostly act as insulators to shield genes from nonspecific signals that exude from its surroundings [17, 18]. Insulators can inhibit the action of a distal enhancer on a promoter when they are located between an enhancer and promoter. Moreover, acting as barriers, they can prevent the encroachment of nearby condensed chromatin and prevent silencing of gene expression [19]. Some insulators can at the same time block enhancers and act as a barrier in a particular gene region while others limit their function to either one. The mechanisms underlying an insulator's specific role in a particular

system are still elusive [15, 20, 21]. It was suggested that insulators employ protein–protein interactions to interfere with enhancer–promoter communication [22]. However, insulators may also protect the propagation of heterochromatin into active chromatin regions through histone modifications which set up protein complexes. It was demonstrated that deletion of the histone modifying enzyme, protein arginine methyltransferase 1 (PRMT1), at the chicken β -globin barrier site resulted in the loss of active histone PTMs and spread of repressed histone PTMs along the globin domain [23]. Therefore, the protein complex that binds to the insulator region can recruit histone-modifying enzymes and thereby constitutes a barrier to prevent the spread of condensed chromatin region by creating localized region of open chromatin [24, 25]. Histone modifying enzymes maintain the open chromatin region by sustaining specific modifications of histone tail. These histone modifications are acetylation and H3K4 methylation in the active chromatin domain [26]. However, the mechanisms that segregates the open chromatin domain from heterochromatin region remain poorly characterized.

1.1.1.1 Defining the barrier element

Boundary elements are present in almost all eukaryotes from yeast to human, but they do not possess any consensus motif across species [27]. The lack of a fixed boundary is the basis of position-effect variegation (PEV), where the stochastic spread of heterochromatin formation results in the heritable silencing of a neighboring gene [16]. Insulators bind specific transcription factors, and their location is confined to DNase I hypersensitive sites. Insulators recruit histone modifying and chromatin remodeling enzymes, which aid in the formation of the hypersensitive site. Moreover, insulators form ‘insulator bodies’ by clustering together to separate gene and regulatory elements in distinct loops. As a result, genes are sequestered into specific compartments in the nucleus [28-30]. Proteins in vertebrates that have barrier activity include CTCF, USF1/2, VEZF1, and TFIIC (GTF3C5) [31-33].

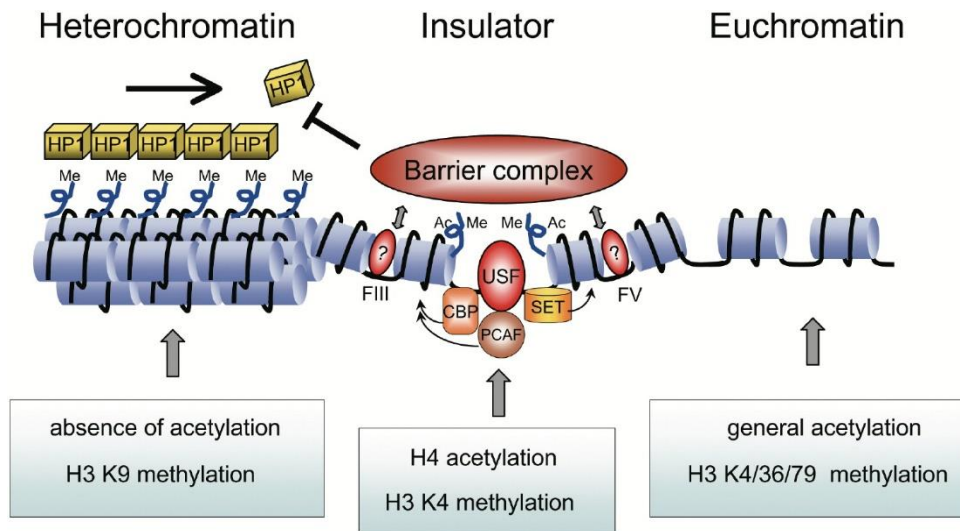


Figure 1.3: A Model for Chromatin Barrier. The chromatin barrier function of the HS4 insulator from the chicken β -globin LCR requires the USF1/USF2 proteins, which interact with footprint IV (FIV) sites of HS4 and recruit PCAF and CBP/P300 to acetylate K9/14 of H3, and SET7/9 to methylate K4 of H3. These and possibly other modifications work together to prevent the assembly of heterochromatin typified by the lack of histone acetylation, H3 K9 methylation, and HP1 recruitment. *The figure and the text were reproduced with permission from Figure 1 [34].*

1.1.1.1.1 CTCF

CTCF is a transcription factor which is also known as insulator binding protein or 11 zinc finger protein [35, 36]. CTCF is considered to be the primary insulator protein in mammals and is the first factor shown to act as an insulator in vertebrates [25]. This protein binds to the three regularly spaced direct repeats of the core sequence CCCTC, and therefore it named as CCCTC binding factor or CTCF [37]. CTCF is a highly conserved protein sharing 100% amino acid sequence homology among mouse, chicken and human within its eleven zinc finger central DNA-binding domains [38]. This protein forms a CTCF-DNA complex that is DNA methylation sensitive and is involved in gene activation, repression, silencing and chromatin insulation [38]. The CTCF-DNA complexes customize their structure with the involvement of zinc fingers to make base contacts and target specific surfaces to enable interaction with other nuclear proteins [38]. This property of CTCF confers its versatile functions because different zinc fingers have different consensus sequences which result in various binding partners, different posttranslational modifications, and ultimately multiple functional roles [39].

1.1.1.1.2 USF1/2

Upstream stimulatory factor 1 or 2 (USF1/2) is a basic helix-loop-helix leucine zipper transcription factor that binds to DNA at the pyrimidine-rich initiator (Inr) elements and E-box motifs to allow transcription activation [40, 41]. These transcription factors bind to a typical symmetrical DNA sequence (E-boxes) (5'-CACGTG-3') in a dimer conformation. They recognize and bind to the degenerate E-box sequence CACGGG found in the insulator at the 5' hypersensitive site HS4 of the chicken β -globin domain as a USF1/USF2 heterodimer [42]. USF proteins also bind to the human β -globin HS2 enhancer site [43, 44]. It is suggested that both at insulator and enhancer sites, USF is involved in recruiting histone modifying enzymes resulting in nucleosome modifications that make the region more accessible for other factors to bind [45].

1.1.1.1.3 VEZF1

Vascular endothelial zinc finger 1 or VEZF1 is a transcriptional regulator. This novel chromatin barrier protein plays a role in the protection of the gene promoters from DNA methylation. VEZF1 binds to the (dG-dC) string of the 5'-HS4 region of the chicken β -globin domain but does not interact with the 3' HS enhancer-blocking element, which lacks the dG-dC string like motifs and barrier activity [46]. Binding of VEZF1 to the globin cHS4 site and *APRT* gene promoter region was sufficient to protect these regions from DNA methylation [46]. Therefore, this barrier element protects a gene promoter from DNA methylation-mediated silencing possibly by preventing the binding of DNA methyltransferase to the site.

1.1.1.1.4 TFIIC (GTFC5)

General transcription factor IIC (TFIIC) is involved in RNA polymerase III-mediated transcription. TFIIC has a boundary function with both barrier and enhancer-blocker activities [47]. It binds to two internal control regions (ICR) named as box A and box B of *tRNA* gene [48].

1.1.1.2 Examples of some insulators and chromatin domains in vertebrates

1.1.1.2.1 The H19 ICR insulator

The insulin-like growth factor (*Igf2*) and *H19* genes in the mouse are reciprocally imprinted. Imprinting refers to the sex-specific gene marking process that starts at the germ line where expression of a subset of genes depends on their parental origin [49]. *Igf2* and *H19* genes lie within a large imprinted region on mouse chromosome 7 separated by a 70 kb region. Only the paternal allele of *Igf2* is expressed in males whereas only the maternal allele of *H19* is expressed in females [50]. It is suggested that the imprinting of this region is controlled by the imprinting control region (ICR) which is located far upstream of the

mouse/human *H19* gene [51]. *H19* ICR contains two DNaseI hypersensitive sites, each of which has two CTCF binding sites in mouse and seven CTCF binding sites in humans [52-55]. Insulator activity of the ICR is responsible for the imprinting of the *Igf2/ H19* gene. Several groups have reported that CTCF dependent chromatin insulator that is residing within ICR is crucial for *Igf2* repression in somatic cells [53, 54, 56, 57]. However, there are two differentially methylated regions (DMRs), with DMR1 being a methylation-sensitive silencer and DMR2 being a methylation sensitive activator lying upstream of *Igf2* gene [58-60]. Unmethylated ICR acts as an insulator in the maternal chromosome setting, facilitating *H19* transcription and *Igf2* gene repression in *cis*. Moreover, the enhancer, which is located downstream of the mouse *H19* gene, forms a small chromosome loop by interacting with the ICR. This loop blocks the access of RNA polymerase to *Igf2* [50]. Upstream DMRs and downstream enhancers are two regulatory regions that control the parental allele-specific expression of *H19* gene. Nevertheless, CTCF binding sites within the *H19* ICR confer the protection against *de novo* methylation as methylation of this site abolishes CTCF binding [61-64]. CTCF binding to the *H19* ICR is a key component of the higher order chromatin structure of this region. CTCF binding to this ICR is prevented by DNA methylation [65].

1.1.1.2.2 Chicken β -globin gene domain

One of the best-characterized and first identified insulators in vertebrates is the HS4 insulator of the chicken β globin gene domain located at the 5' end of the locus control region (LCR) in this gene domain. This insulator contains both enhancer blocking and barrier activities [66-69]. Chicken β globin domain is demarcated by two DNaseI hypersensitive sites, 5'-HS4 and 3'-HS where 5'-HS4 separates the β -globin domain from condensed chromatin region and the upstream folate receptor gene [70]. On the other hand, 3'HS separates β -globin domain from chicken olfactory receptor (*OR*) genes which are inactive in the chicken erythroid cell but active in olfactory epithelium and brain cells [71]. In chicken erythrocytes 5'-HS4 acts as an insulator having both enhancer blocking and barrier activities whereas 3'-HS acts only as an enhancer blocker [71]. CTCF binds to both enhancers and is involved in the enhancer blocking activity by creating a loop and independent transcription unit with the insulator site [25, 68]. The barrier function of 5'-HS4 is mediated through upstream stimulatory factors USF1 and USF2. The USF1/2 recruits chromatin-modifying enzymes (e.g., acetyltransferases) to this site. Proteins responsible for heterochromatin formation, e.g., HP1 (heterochromatin protein 1) and Suv39H1 (lysine methyltransferase) are also recruited upstream of 5'-HS4 site. The 5'-HS4 is always active independent of the type of tissue and stage of development. This element separates the pattern of active or inactive histone modifications (acetylation and methylation) on both sides of the element depending on the expression of

either β -globin domain or folate gene [42]. Studies showed that chicken HS4 can exert insulation property both in human and *Drosophila* cells when expressed exogenously [66]. Barrier activity of 5'-HS4 is depend upon the binding of USF1 and USF2 to the site which recruit histone modifying enzymes. This was demonstrated in chicken and mouse erythroid cell [45, 72]. Therefore, it indicates that chicken HS4 maintain its insulator property irrespective of cell type and prevent the propagation of condensed chromatin [73].

1.1.1.2.3 The human β -globin locus

Human β -globin locus is approximately 50 kb in breadth and contains five functional β -like globin genes ϵ , γ^G , γ^A , δ and β positioned in 5' to 3' order. The expression of these genes is controlled developmentally through a LCR located 6 kb upstream of ϵ globin gene. The LCR in the human β globin locus is composed of five developmentally stable DNaseI hypersensitive sites among which four are erythroid-specific (5' HS1–4) and one ubiquitous (5' HS5) [74]. In human β -globin locus, olfactory receptor (*OR*) genes replace the folate receptor locus of the avian β -globin locus [74]. Similar to the chicken β -globin locus, human 5'-HS5 and 3'-HS1 act as enhancer blockers as they contain CTCF binding site [74]. Moreover, similar to chicken, the human 5'-HS5 also possesses barrier activity as demonstrated using the position-effect assay [75]. Deletion of the LCR and 5'-HS5 results in heterochromatinization and inactivation of globin gene expression that pathologically gives rise to thalassemia [76].

1.1.1.2.4 The murine β -globin locus

Genomic organization of murine β -globin locus is more similar to human β -globin locus than it is to the chicken β -globin locus [77]. It contains six DNaseI hypersensitive sites 5'-HS1–5'-HS6 in the 5' region and one 3'-HS at 3' end of the locus. Within the 5'-HS6 and 3'HS, the murine β -globin locus has four genes ϵ^y , β^{h1} , β^{maj} and β^{min} [74, 78]. The hypersensitive sites in murine β -globin locus contain enhancer blocker properties and have CTCF binding sites [74, 78, 79]. The 3'-HS also contain a USF binding site in the CTCF binding region. Deletion of the hypersensitive site in this locus does not lead to heterochromatinization of this region which indicates they lack barrier activity [80].

1.1.1.2.5 The human apolipoprotein locus

Human apolipoprotein locus is approximately 47 kb long, and is composed of four genes *APOA1*, *APOC3*, *APOA4*, and *APOA5* genes [81]. *APOA1*, *APOA4*, and *APOA5* genes are transcribed in the same direction, whereas *APOC3* gene is transcribed in the opposite direction [81]. These genes are involved in metabolism and redistribution of lipoproteins and lipids [82]. The expression of *APOA1*, *APOA4*, and *APOA5* gene

products contribute to the formation of high-density lipoprotein (HDL). The plasma level of HDL is negatively correlated with atherosclerosis. In contrast, the *APOC3* gene product is involved in the production of very low-density lipoprotein (VLDL). Therefore, expression of these genes needs to be controlled properly [82]. The insulators AC1, AC2, AC3, and AR1 in this locus harbor CTCF and cohesin protein RAD21 binding sites. These insulators have enhancer blocking properties and maintain higher order chromatin architecture by making two long-range interactive chromatin loops *in vivo* [81]. Insulators AC2, AR1 and AC3 often co-localize together and undergo loop formation in *APO* gene locus. However, insulator AC1 does not co-localize with AC2 and AC3 and undergo loop formation. It is hypothesized that the binding of cohesion at AR1 leads to the connection AC2 to AC3 and thus gives rise to two chromatin loops in the region [81].

1.1.1.2.6 Human *tRNA* locus

Human *tRNA* genes are transcribed by RNAPIII and their expression is cell-cycle dependent and regulated developmentally [83]. The *tDNA* is composed of internal promoter A and B box, which are involved in the recruitment of TFIIC. TFIIC participates in the recruitment of TFIIB, followed by RNAPIII recruitment to initiate transcription at this site [84, 85]. Barrier insulator and enhancer blocking activity of *tRNA* was shown to be dependent partly on the binding of TFIIC to the B-box promoter of *tDNA*. Moreover, *tRNA* genes are often organized in clusters. Analysis of two *tRNA* clusters revealed that they contain binding sites for CTCF. This observation further added that in addition to CTCF and TFIIC other factors may also involve in long-range chromatin interaction for *tRNA* gene [86-90]. Moreover, *tRNA* genes are often found near boundaries of repressed chromatin domains and function as repressed chromatin blockers in preventing heterochromatinization [31]. *tDNA* flanking regions contain active histone marks, possibly due to the interaction of TFIIC with acetyltransferase p300 at this site. Thus, p300 acetylates histones in this region which helps to provide an open chromatin structure for other factors to bind [91]. Further, transcription factors such as OCT, FOS/JUN, MYC, and CTCF bind to the *tDNA* flanking region and can thus help to regulate transcription of the *tDNA* gene [92-95].

1.1.1.3 Disease associated with altered chromatin structure

Disruption of barrier binding and mutation of barrier elements leads to disease pathogenesis. Some of the diseases are listed below.

1.1.1.3.1 Hispanic $\gamma\delta\beta$ -thalassemia

Mutations in the human β globin locus affect thousands of people worldwide [96]. Though the β globin locus has been extensively studied, the mechanisms regulating genes in the locus remain poorly understood. Deletion of β -globin LCR and 27 kb upstream causes Hispanic $\gamma\delta\beta$ -thalassemia, leading to heterochromatinization and silencing of the β globin locus [76, 97-99]. This observation indicates that the DNA region upstream of the LCR known as an upstream Hispanic region (UHR) contains a *cis*-acting sequence that contributes to maintaining “open” chromatin structure in β -globin locus. In Hispanic $\gamma\delta\beta$ -thalassemia, the entire Hispanic locus transforms into a DNaseI-resistant chromatin structure, which is transcriptionally inactive. In healthy individuals, the downstream LCR is DNaseI-sensitive and the chromatin is in a transcriptionally active state. The Hispanic deletion prevents the transcriptional activation of the *cis*-linked β -globin genes at any developmental stage. Moreover, either all or a subset of the developmentally stable hypersensitive sites upstream of the ϵ -globin gene are deleted in every $\gamma\delta\beta$ -thalassemia. In Hispanic thalassaemia, replication of the globin locus occurs late at S phase compared to early S phase replication of the normal β globin locus. In the diseased state, the globin locus was devoid of DNaseI hypersensitive sites [76, 98, 99].

1.1.1.3.2 Hereditary spherocytosis syndromes

“Hereditary spherocytosis syndromes” involve disorders such as anemia, recurrent jaundice, splenomegaly, and the existence of sphere-shaped erythrocytes on peripheral blood smears [100]. In people of northern European ancestry, it is the common cause of inherited anemia. However, it can also affect people from all over the world. The primary cause of spherocytosis is a frameshift or nonsense mutations in the erythrocyte membrane protein *ankyrin-1* gene [101, 102]. A recent study reported that a region of the erythroid *ankyrin* promoter shows barrier insulator activity and that a mutation in this site leads to defects in barrier function and therefore a reduction in ankyrin expression. Mutation at –108/–153 upstream of the *ankyrin-1* promoter, harboring spherocytosis-associated mutations, results in the perturbation of barrier function and failure to bind barrier proteins in this region. Restoration of erythroid *ankyrin* gene expression was possible when the cHS4 barrier insulator was inserted into transgenic mice flanking the mutant –108/–153 *ankyrin* gene’s erythroid promoter, showing the crucial role of the barrier elements in spherocytosis disease [103].

1.1.1.3.3 CTCF in cancer

CTCF binds to a crucial gene regulatory element that plays a diverse role for regulating gene expression. CTCF can act as transcriptional repressor when binding to the promoter and upstream silencer region of the chicken lysozyme, and to the promoter region of chicken and human *MYC* gene. On the other hand, a CTCF acts as a transcriptional activator when it binds to the amyloid beta-protein precursor (*APP*) gene promoter and *ARF* gene promoter (also known as p14ARF in human and p19ARF in mouse) [104, 105]. Altered expression of these genes was shown to be linked with tumour progression. Given its diverse function in gene regulation and genome organization, it was predicted that CTCF might have been involved in cancer development. Tumor-specific missense mutations in ZF domain of CTCF were reported for breast, prostate, and Wilms' tumors [106, 107]. CTCF ZF domain mutations modify CTCF's binding to promoters/insulators of genes that are involved in cell proliferation (*MYC*, *ARF*, *PIMI*, *PLK*, and *Igf2*), and reduces the expression of these genes. In contrast, CTCF binding to other loci (e.g., the β -globin insulator, *lysozyme* silencer, *APP* promoter) remains unaffected by CTCF ZF domain mutations. Thus, mutations in CTCF can change the function of some genes and thereby is considered as a novel tumor suppressor [107]. In another study, the role of CTCF was described in tumor initiation or proliferation in individual cases of invasive ductal breast carcinoma [106].

In addition, CTCF was reported to have the ability to inhibit apoptosis of breast cancer cells [107]. Thus CTCF has a direct effect at transcriptional level or indirect effect on the post-translational level of proteins involved in apoptosis (e.g., anti-apoptotic proteins BCL-2, BCL-XL, MCL-1 and pro-apoptotic proteins BAX, BAK, BAD, BIK, BID, and BOK) [107]. However, the molecular mechanism by which CTCF renders breast cancer cells resistant to apoptosis is still elusive.

1.1.2 Histone modifications and their distribution in the genome

Histones are subjected to various posttranslational modifications, which are mostly reversible. Histone posttranslational modifications can affect almost all genomic events such as transcription, replication, recombination, DNA repair, and kinetochore and centromere formation [108]. In respect to transcription, appropriate histone modifications can alter the active chromatin into an inactive state and *vice versa*. Together with histone modifying enzymes, which are categorized as "Reader," "Writer," "Eraser," "Effector" and "Presenter", histone modifications can regulate the transcriptional state [109, 110]. Histone cross talk is defined as a combination of histone posttranslational modifications that can code for transcriptional activation or repression in a context-dependent manner [111]. Histone crosstalk can occur

either *cis* or *trans*, involving events on the same histone tail or nearby histone tail within the same or neighboring nucleosome [112]. It was demonstrated that serine 10 phosphorylation on H3 enhances the GCN5 mediated acetylation of H3 at lysine 14 [113]. Histone crosstalk can be initiated by preventing the nearby histone modifications. Histone H3 asymmetric di-methylation (H3R2me2a) was shown to prevent the MLL mediated formation of di- and tri- methylation of H3 lysine 4 (H3K4me3/H3K4me2). Interestingly, the presence of H3K4me3 prevents PRMT6-mediated H3R2me2a [114]. The advancement in the technology with tools such as chromatin immunoprecipitation (ChIP) and ChIP-sequencing (ChIP-seq) enables one to determine the crosstalk between different writers and readers or effector molecules.

Lysine acetylation (H3, H4, H2A, and H2B), lysine and arginine methylation (H3, H4, and H2B), serine and threonine phosphorylation (all), and lysine ubiquitination (H2A, H2B), ADP-ribosylation at glutamine (H1) and sumoylation are some of the well-known histone modifications. Several of the histone marks are exclusively associated with active chromatin state, while others are with the inactive chromatin state [112].

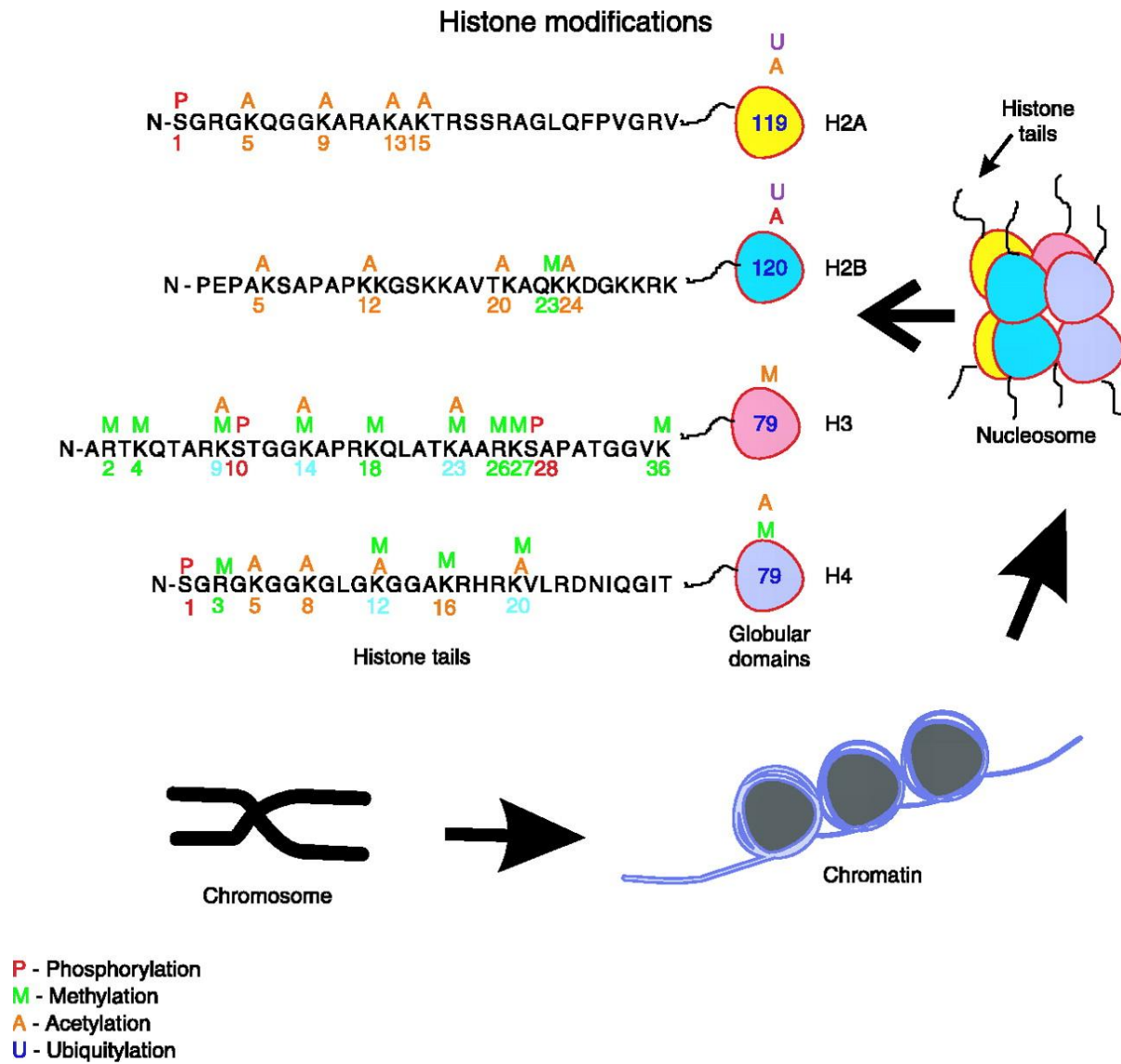


Figure 1.4: Histone modifications in the N-terminal tail of core histone. Histone tail modifications. Specific arginine residues (R) can be methylated. Specific lysine residues (K) can be either acetylated, methylated or ubiquitylated. Specific serine residues (S) can be phosphorylated. Acetylation, orange; methylation, green; phosphorylation, red; ubiquitination, purple. *The figure and the text were reproduced with permission from Figure 2 [115].*

1.1.3 Histone acetylation

Histone acetylation was first reported by Vincent Allfrey and his group in 1964. Allfrey's group described the dynamic and rapid histone acetylation using nuclei isolated from calf thymus [116]. Following on this study, they later reported that histone acetylation occurs on ϵ -amino lysine residue, and they also identified histone deacetylase activity in the nuclei. In 1978, both Dr. Davie and Dr. Allfrey reported for the first time that n-butyrate acts as an HDAC inhibitor [117, 118]. Hyperacetylation of histone H3 and H4 and to a lesser extent H2A and H2B was observed upon sodium butyrate treatment in the cell line investigated [117]. DNA sequences associated with the hyperacetylated histones showed increased DNaseI sensitivity in HeLa and chicken erythrocyte cells [118]. The first report of a direct link between histone acetylation and transcriptionally active chromatin came from the study by Dr. Crane Robinson's group using chicken erythrocytes [119]. In this study, chromatin immunoprecipitation (ChIP) assay was used for the first time to demonstrate that acetylated histones are associated with transcriptionally active DNA sequences [119]. The relationship between histone acetylation and transcription became established after the discovery of lysine acetyltransferases (KATs) were co-activators [120]. Acetylation of histone and non-histone proteins is catalyzed by KATs [121]. Dynamic and reversible histone acetylation is catalyzed by KATs and histone deacetylases (HDACs). The rate of histone acetylation can vary across the genomic regions with some regions having a faster rate of dynamic acetylation while some have slower or none [122]. Histone acetylation can modulate the chromatin-condensing feature of linker histone H1, facilitate solubility of the region at physiological salt concentration and maintain the unfolded chromatin structure [123, 124]. KATs are categorized into four different groups; GCN5, MYST (SAS/MOZ), P300/CBP and SRC/p160 nuclear receptor coactivator family [122].

1.1.4 Histone lysine methylation

The N-terminal tail of histone lysine and arginine is methylated by lysine methyltransferases (KMTs) or protein arginine methyltransferases (PRMTs). Mono, di or trimethylation of lysine and mono or di methylation of arginine can be distinguished as active or repressive chromatin marks [125, 126]. Lysine and arginine methylation of histones can serve either as a binding site or occlude the binding of other modifiers to the site and thereby play a crucial role in histone posttranslational mediated signaling event. Due to the existing signaling event, aberrant binding of the modifying enzymes can lead to diseased state as observed for several cancers [127-129]. EZ, SET1, SET2, SMYD, SUV39, SUV4-20, RIZ are among the major family of lysine methyltransferases [130]. S-Adenosyl methionine (SAM) serves as methyl

donor and co-factor for both KMTs and PRMTs [131]. Genomic distribution of lysine methylation varies depending on the type of marks or degree of methylation as illustrated in **Figure 1.5**.

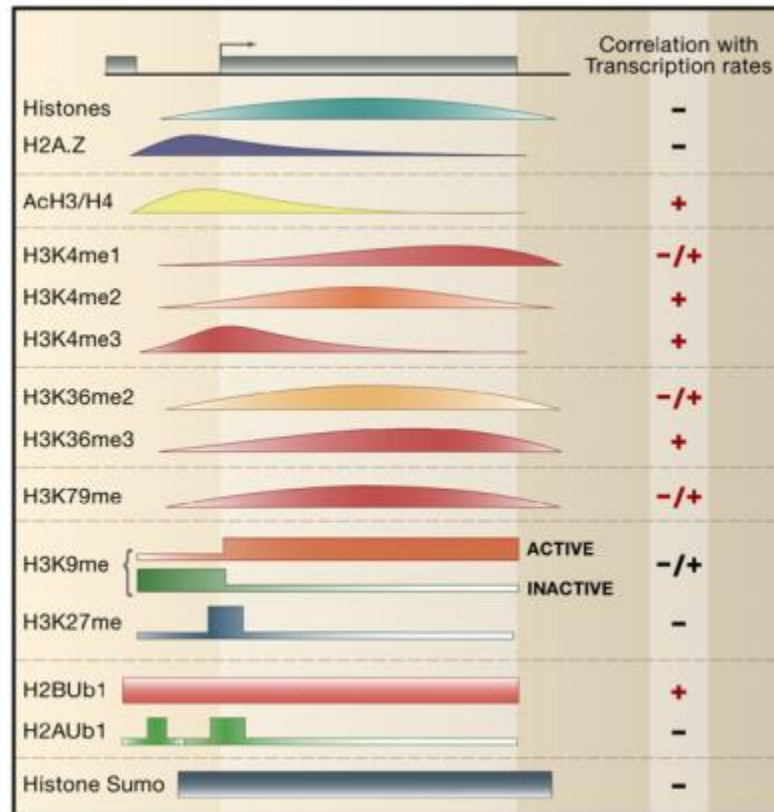


Figure 1.5: Distribution of histone modifications across the genome. The distribution of histones and their modifications are mapped on an arbitrary gene relative to its promoter (5' IGR), ORF, and 3' IGR. The curves represent the patterns that are determined via genome-wide approaches. The squares indicate that the data are based on only a few case studies. Except for the data on K9 and K27 methylation, most of the data are based on yeast genes. *The figure and the text were reproduced with permission from Figure 1 [108].*

1.1.5 Histone arginine methylation

Arginine methylation of histones by PRMTs can be either symmetrical or asymmetrical, and they are categorized based on this chemical feature. Similar to lysine methylation, arginine methylation can

contribute to the active or repress the chromatin state in a context-dependent manner [132]. More details of these modifications will be discussed in the later section of the chapter.

1.1.6 Citrullination of histones

Protein arginine deiminase (PAD) family of enzymes catalyze citrullination from the amino acid arginine. To date, PADs have been identified PAD1-4 and PAD6 [133]. As shown in **Figure 1.6**, PADs replace the ketamine (=NH) group of arginine to keto group (=O), thereby resulting in no net charge from the positively charged arginine. This change in charge due to citrullination alters the structure and function of the protein as well affect the binding of protein interacting partners [134].

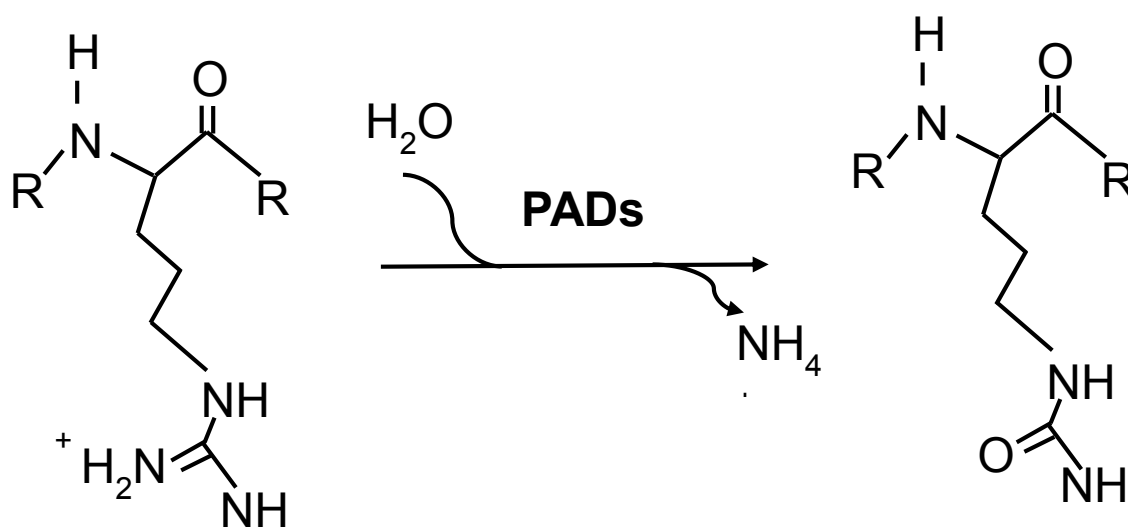


Figure 1.6: Citrullination of arginine by PADs. Protein arginine deiminase enzyme hydrolyzed arginine molecule and converted it to peptidyl-citrulline. The primary amine group of arginine is converted to keto group upon reaction with cysteine of PADs.

It was reported that both PAD2 and PAD4 could catalyze citrullination on a histone tail, albeit it is PAD4 which is involved in citrullination of monomethyl arginine [135, 136]. Symmetric and asymmetric mono and dimethylation of arginine H3/H4 were reported to be catalyzed by Jumonji domain-containing 6 protein (JMJD6) [137]. However, later it was shown that JMJD6 is involved only in the demethylation of mono and di-methyl H4 arginine residue [138]. Although JMJD6 has been reported as a candidate for demethylation of arginine, there is still a lack of sufficient biochemical evidence for that. Moreover, demethylation of H3R2 was not been detected yet.

1.1.7 Phosphorylation of histone

Histone phosphorylation on serine, threonine or tyrosine residue is catalyzed by kinases and dephosphorylated by phosphatases [139]. Histone phosphorylation regulates the DNA damage response pathway, transcription, chromatin compaction and apoptosis [140-143]. Although most of the phosphorylated modifications are associated with chromatin condensation, phosphorylation of serine at 10 and 28 in histone H3 is correlated with gene activation of inducible genes and after exposure to different stimuli during interphase state [139, 144, 145]. Phosphorylation of H3S10 prevents the binding of heterochromatin protein 1 (HP1) to the H3K9 dimethylated site [146]. Moreover, phosphorylation of H3S10 enhances the ability of GCN5 to bind and generate H3K14ac [147].

1.1.8 Other histone modifications

Histone ubiquitination or ubiquitylation refers to the addition of ubiquitin molecule to the lysine residue. Lysine can be mono or poly-ubiquitinated. Ubiquitination of lysine in the histone molecule is associated with active and repressed chromatin regions. Monoubiquitination of H2A leads to gene silencing, whereas mono-ubiquitination of H2B is linked to gene activation [148]. RING1A/RING1B/BMI1 is the enzyme involved in the monoubiquitination of H2A and mediating polycomb-mediated gene silencing [149, 150]. RAD6A/B, RNF20/40 are the enzymes that catalyze monoubiquitination of H2B [151].

SUMOylation is a less studied histone modification which is the addition of small ubiquitin-related modifier (SUMO) to the histone [152]. Unlike ubiquitination, SUMOylation does not lead to protein degradation; rather it is involved in inhibition of ubiquitin-mediated degradation, protein-protein interaction, protein localization and transcription regulation. Binding of H4 to SUMO conjugating enzymes leads to sumoylation of H4 both *in vivo* and *in vitro* resulting in the silent chromatin state [152].

1.2 Chromatin modifying enzymes: Histone deacetylases

HDACs are enzymes involved in removing an acetyl group from ϵ -amino lysine of histone. It has the opposing action of KATs which catalyze lysine acetylation. HDACs and KATs together maintain the dynamic histone acetylation state in transcriptionally active chromatin region *via* the opposing action of these two enzymes [153]. In vertebrates, four classes of HDACs have been identified. Class I HDACs are HDAC1, 2, 3 and 8; class II are HDAC 4, 5, 6, 7, 9 and 10; class III include the sirtuin family of NAD⁺ dependent HDACs. HDAC11 is in class IV HDAC. All classes of HDACs except for class III HDACs uses Zn²⁺ as a cofactor [154].

1.2.1 Classifications of class I HDAC

Class I HDAC, which includes HDAC1, 2, 3 and 8, are mainly located in the nucleus except for HDAC8. HDAC8 is found equally distributed in the nucleus and cytoplasm. Class I HDACs show ubiquitous expression among tissues [154]. Among the class I HDACs, HDAC1 and HDAC2 share sequence similarity of 85% as they evolved from a recent gene duplication [153]. HDAC1 and HDAC2 form homodimers and heterodimers. Formation of dimer complex is a required for catalytic activity. The enhanced enzymatic activity of HDAC1/2 dimer has been observed when these dimers are present in multiprotein complexes such as Sin3, nucleosome remodeling histone deacetylase (NuRD) and CoREST. Formation of these complexes depends on HDAC1 and HDAC2 phosphorylation. The Sin3 complex consists of HDAC1 and HDAC2, Sin3A or Sin3B, SAP18, SAP30 and retinoblastoma-associated proteins (RbAps) RbAp46 and RbAp48. Corepressor complex NuRD contain HDAC1 and/or HDAC2, Mi-2 α and/or Mi-2 β , RbAp46/RbAp48, p66 α or p66 β , metastasis-associated protein family (MTA1, MTA2 or MTA3) and lysine-specific demethylase 1 (KDM1/LSD1) [155-157]. A different NuRD complex has been reported which consists of HDAC1 and HDAC2, MTA1 or MTA2, p66 α or p66 β , Nanog, Oct4 and helicase-like ATPase Mi-2. This complex is also known as Nanog- and Oct4-associated deacetylase (NODE) complex [158]. The CoREST complex contains HDAC1, HDAC2, RCOR1/CoREST, HMG20B/BRAF35, PHF21A/BHC80 KDM1/LSD1 and sometimes zinc finger protein ZNF217 and chromatin remodeling complex SWI/SNF or the C-terminal binding protein (CtBP) [159]. These complexes may also contain several other proteins or protein complexes [160].

1.2.2 Complexes of unmodified and phosphorylated HDAC2

In vitro studies have shown that HDAC2 is phosphorylated at S394, S422, and S424 by casein kinase 2 (CK2), and that phosphorylation increases its enzymatic [161, 162]. Phosphorylation of HDAC2 at these sites is a prerequisite for the formation of Sin3, NuRD, and CoREST corepressor complexes. Highly phosphorylated HDAC2 is recruited to regulatory regions, and the status of phosphorylation is crucial for this event [162-164]. However, studies have demonstrated that unphosphorylated HDAC2 is recruited to the coding region of transcribed genes [163, 165]. Recruitment of phosphorylated HDAC2 to the regulatory region was reported to be mediated by transcription factors, for example, Sp1, Sp3, p53, NF- κ B and YY1 [154, 163]. Non-phosphorylated HDAC2 is targeted to the coding region in a complex with splicing factors in a RNA-dependent manner [165]. Loss of RNA showed the reduced recruitment of HDAC2 to the transcribed gene as well as resulted in the loss of its interaction with splicing factor SRSF1

[165]. However, the interaction of HDAC2 to pre-mRNA was indirect as the binding of HDAC2 was considerable lower in UV crosslinked cells compared to that in DSP and UV crosslinked cells [165].

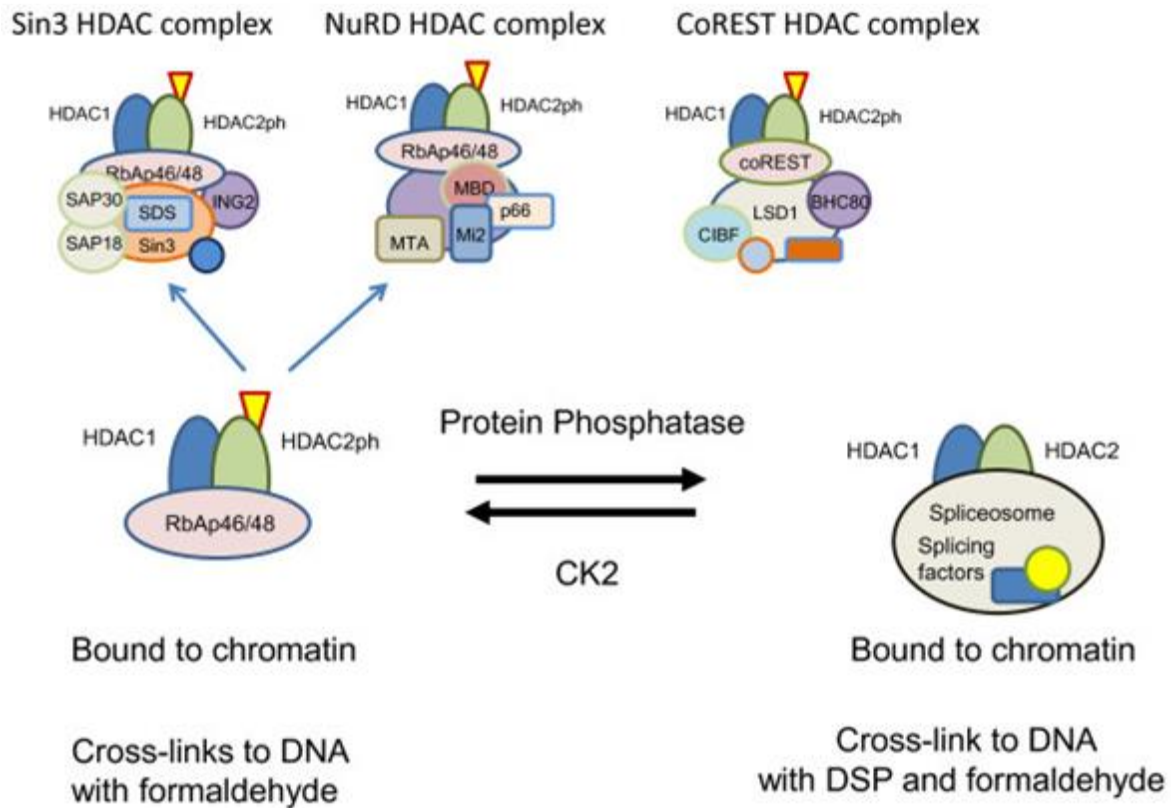


Figure 1.7a: Binding of phosphorylated and unmodified HDAC2 to chromatin. Multiprotein complexes containing HDAC1-HDAC2 homo- or heterodimers are shown. HDAC2 is shown as phosphorylated, which is a requirement for multiprotein complex formation. Phosphorylation is indicated by a red-outlined yellow triangle. *The figure and the text were reproduced with permission from Figure 1 [166].*

1.2.3 Distribution of HDAC2 and pHDAC2

It has been demonstrated that there is more unmodified HDAC2 than phosphorylated-HDAC2. In both human breast cancer T5 cells and MCF7 cells, more unmodified HDAC2 was observed compared to phosphorylated-HDAC2 [163, 167]. When HDAC2 is phosphorylated it shows reduced mobility on electrophoretic gel. When lysates from cisplatin (protein-protein cross linker) cross-linked T5 and MCF7 cells were treated with alkaline phosphatase, it resulted in the disappearance of the slow migrating phosphorylated form of HDAC2 leaving the unmodified form. Crosslinking using formaldehyde can

efficiently map phosphorylated HDAC2 to the chromatin but only poorly maps unmodified HDAC2 to chromatin (**Figure 1.7b**) [163]. Standard ChIP conditions with formaldehyde thus can map phosphorylated HDAC2 but are not sufficient to map unmodified HDAC2. Therefore, an additional crosslinking process (protein-protein crosslinking) was used to map all forms of HDAC2 (phosphorylated and unmodified) across the genomic region (**Figure 1.7b**) [163, 165]. Dual crosslinking ChIP assays which combine the crosslinking of cells with 2 mM disuccinimidyl glutarate followed by 1% formaldehyde were applied for genome-wide profiling of HDACs (HDAC1, HDAC2, HDAC3, HDAC6) and KATs (CBP, p300, PCAF, Tip60, MO) in human CD4⁺ T cells. This study revealed that HDACs and KATs were mainly located in active chromatin regions [168].

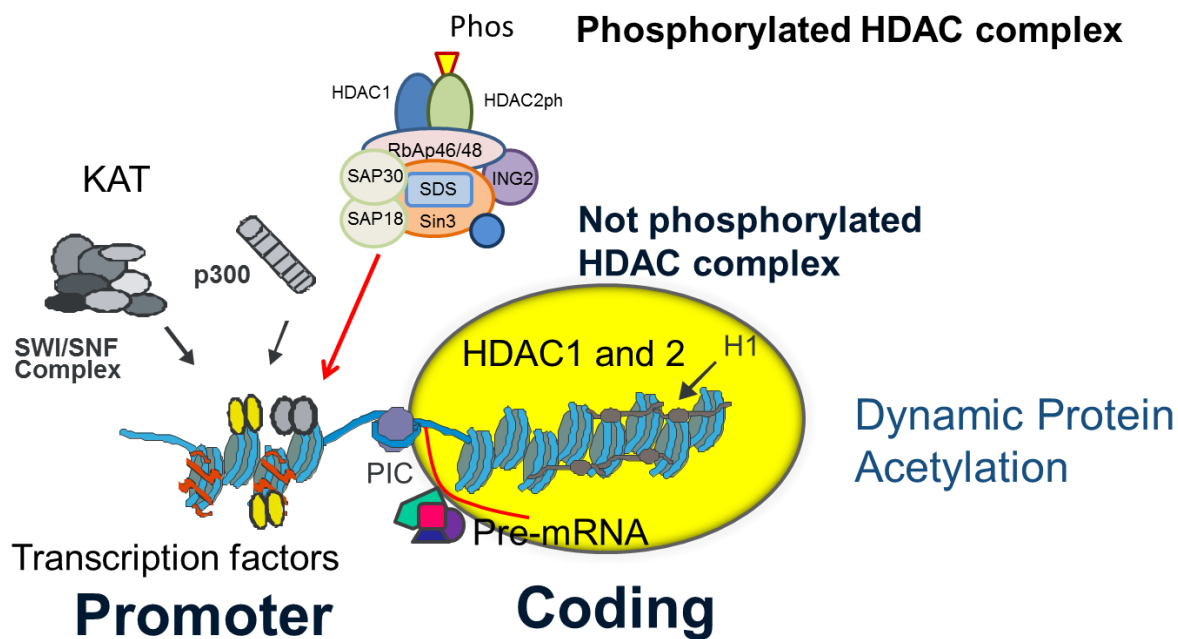


Figure 1.7b: Recruitment of HDAC1/2ph complexes to the regulatory region and non-ph HDAC1/2 to the coding region of expressed genes. *The figure was reproduced with permission from Dr. Jim Davie.* Phosphorylated HDAC2 is in a large multiprotein complex (Sin3, NuRD, CoREST) which is recruited to the promoter region through its interaction with transcription factors. KATs are also recruited by transcription factors to these regulatory regions. Together the KAT and HDAC1/2ph complexes mediate dynamic acetylation of nucleosomal histones in this region. The non-phosphorylated HDAC2 is associated with RNA binding proteins and is recruited to the newly formed transcripts. It is from the transcript that non-phosphorylated HDAC1/2 deacetylate nucleosomal acetylated histones present at the 5' end of the coding region of expressed genes. PIC, transcription pre-initiation complex.

Interestingly, the association of HDACs is positively correlated with the level of RNAPII bound to transcribed genes [168]. The function of HDACs in transcribed gene region has been attributed to reset acetylation and chromatin modifications after transcription [168]. Primed genes (genes poised for transcription) that contain H3K4me3 undergo dynamic histone acetylation and deacetylation; however repressed genes lacking H3K4me3 do not contain KAT/HDACs [168]. Nucleosomes containing H3K4me3 undergo dynamic histone acetylation by KATs and HDACs [165, 169]. There is evidence that non-phosphorylated HDAC2 act from the transcript to deacetylate acetylated nucleosomal histones associated with the coding of region of transcribed genes. Non-phosphorylated HDAC2 binds to RNA binding proteins that are involved in pre-mRNA splicing [165].

1.3 Chromatin modifying enzymes: Protein arginine methyltransferases

1.3.1 Overview of mammalian PRMTs

The amino acid arginine contains five potential hydrogen bond donors in its guanidino group (**Figure 1.7**). These can interact with a wide range of hydrogen bond acceptors in DNA, RNA and proteins, imparting a unique feature to this amino acid [169]. For each methyl group added, one hydrogen donor is released from arginine. This methylation event changes the amino acid conformation, making it slightly more hydrophobic. As a consequence, methylation of an arginine may impact the structure of the protein and/or the protein's interaction surface [169]. In the context of nucleosomal histones, methylation of specific arginine residues will influence interactions with chromatin readers and effectors, either providing docking sites or preventing binding [170, 171]. Mono and dimethylation of arginine are catalyzed by three types of protein arginine methyltransferases (PRMTs): PRMT1, 3, 4, 6 and 8 belonging to type I, PRMT5 and 9 belonging to type II, and PRMT7 being a type III methyltransferase [172]. PRMTs catalyze arginine methylation by using S-adenosyl-L-methionine (SAM) to form monomethyl arginine (MMA), and asymmetric (ω -NG, ω -NG-dimethyl-arginine or ADMA) (type I) or symmetric (ω -NG, ω -N'G-dimethylarginine or SDMA) (type II) (**Figure 1.8**) [169, 173]. Arginine methylation is evolutionarily conserved and is ubiquitous across species, such as fungi, plants, *Caenorhabditis elegans*, *Drosophila* and vertebrate animals [174]. Other than histones, a wide range of proteins, including RNA binding proteins, proteins involved in signal transduction processes such as interferons, cytokines, and T-cell signaling proteins are also substrates for PRMTs [175-177]. Therefore, aberrant expression of many of these enzymes is involved in several pathological conditions such as pulmonary diseases, cardiovascular diseases, cancer and diabetes [129, 178-180].

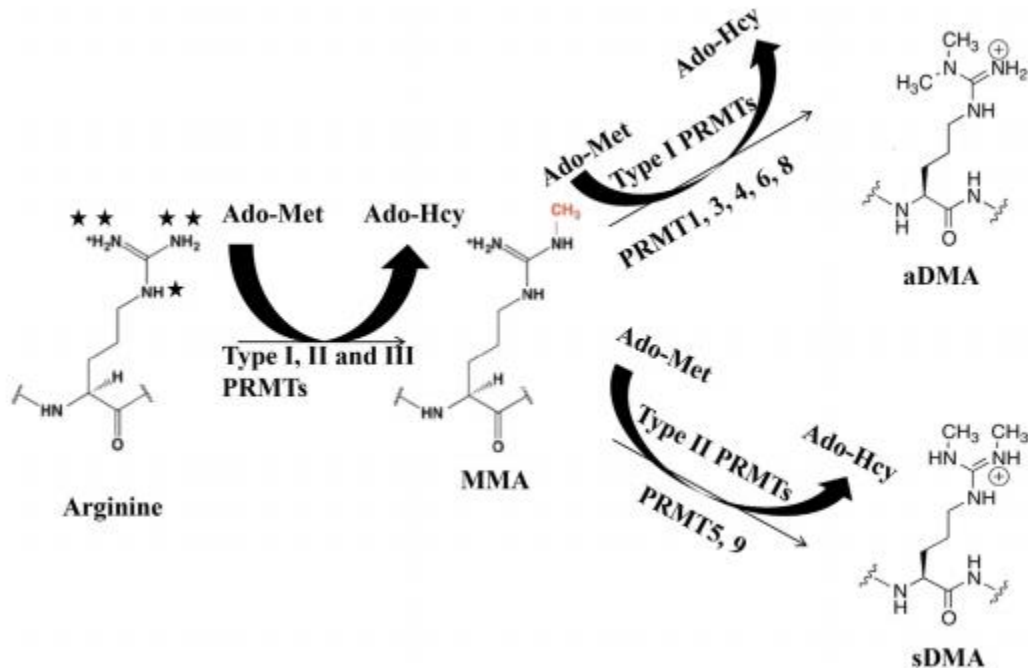


Figure 1.8: Methylation of arginine residue by PRMTs. Amino acid Arginine contains five potential hydrogen bond donor site. PRMTs transfer methyl group to these sites from S-adenosylmethionine (SAM) resulting in S-adenosylhomocysteine (AdoHcy) and methylarginine. This reaction gives rise to monomethyl arginine (MMA); asymmetric dimethylarginines (aDMA) and symmetric dimethylarginines (sDMA). *The figure and the text were reproduced with permission from Figure 1 [181].*

1.3.2 Mammalian PRMTs and their substrates

Eleven PRMTs have been reported and categorized into three groups; type I, II and III. PRMT1, categorized under the type I, was the first identified mammalian PRMT [182]. It is primarily localized in the nucleus [183]. The majority of the arginine methylation is catalyzed by PRMT1, which has a preference for an arginine residue flanked by one or more glycine residues [184]. PRMT1 is active as a homodimer; the evidence of which is supported by its three-dimensional structure [185]. PRMT1 catalyzes the formation of H4R3me2a and H2AR11me1 [23, 186].

PRMT2 contains the SH3 domain along with the methyltransferase domain. This SH3 domain can interact with N-terminal region of PRMT8 to present it to its substrate [187]. PRMT2 harbors a very weak *in vitro* type I methyltransferase activity towards H4. PRMT2 was reported to bind to and act as co-activator of both androgen receptor and estrogen receptor alpha. PRMT2 can inhibit NF- κ B-dependent transcription in a similar way as PRMT4 by decreasing the binding of NF- κ B to DNA. It causes the nuclear

accumulation of I κ B- α and thereby increases the cell's susceptibility to apoptosis [188]. *In vitro*, PRMT2 will produce H3R8me2a [189, 190].

PRMT3 is localized in the cytoplasm. The N-terminus zinc finger domain of PRMT3 binds to its substrate. One such substrate is the 40s ribosomal protein S2 [191].

PRMT4 (CARM1): Correlation between arginine methylation and transcription event was first made evident with PRMT4 which is also designated as an activator of steroid receptors. It acts as a co-activator of p160 family of transcriptional activators. This is the reason that this enzyme is also known as the co-activator of the associated arginine methyltransferase or CARM1 [132]. PRMT4 null mice showed prenatal death and exhibited smaller size compared to their littermates [192]. Moreover, PRMT4-deficient mice showed aberrant estrogen-responsive gene expression in their fibroblasts and the embryos [192]. PRMT4 is responsible for thymocyte differentiation because *Carm1*(-/-) cells do not show methylation of thymocyte cyclic AMP-regulated phosphoprotein [193]. The *Carm1*(-/-) mice had delayed endochondral ossification and decreased chondrocyte proliferation [194]. Moreover, the loss of PRMT4 in mice increases pulmonary cell proliferation and alveolar cell differentiation [195]. PRMT4 catalyzes the formation of H3R17me2a, H3R26me2a and H3R42me2a [196, 197].

PRMT5 is expressed at a higher level in heart, muscle, and testis than in other tissues [198]. The subcellular localization of PRMT5 is predominantly within the nucleus, but this enzyme is also localized in the cytoplasm and Golgi apparatus. The enzyme is important in maintaining the Golgi architecture [199]. PRMT5 recognizes GAR motifs, and its targets include spliceosome proteins along with histones. PRMT5 methylates several Sm proteins and is involved in snRNP biogenesis in the cytoplasm [200]. Similar to PRMT4, PRMT5 acts as a transcriptional co-activator by associating with hSWI/SNF ATP-dependent chromatin remodeling proteins [201]. However, when PRMT5 interacts with COPR5 (cooperator of PRMT5), it acts as transcriptional co-repressor [202]. It was indicated that COPR5 could regulate the substrate specificity for the PRMT5 complex in nuclei. COPR5 acts as an adaptor for the nuclear PRMT5 complex to drive it towards target genomic site in chromatin [202]. So far, it was reported that H3R2me2s, H3R8me2s, H4R3me2s, and H2AR3me2s are produced by PRMT5 [186, 203].

PRMT6 is localized primarily in the nucleus [204]. PRMT6 catalyzes asymmetric dimethylation of arginine residues. This enzyme is involved in transcriptional repression of tumor suppressor genes; therefore promoting cell proliferation and preventing senescence [205]. PRMT6 methylates H3R2, preventing the methylation of Lys 4 by the MLL complex. The enzyme has a higher affinity for

monomethylated substrates compared to unmodified one [206]. H3R42me2a, H3R2me2a (*in vitro*), H2AR3 (*in vitro*) and H2AR29me2a are also produced by this enzyme [171, 186, 197].

PRMT7 is categorized as a type III PRMT and is dependent on other polypeptides for its functionality [207]. This enzyme is present mainly in thymus, dendritic cells, and testis. PRMT7 is localized in the nucleus and cytoplasm. This enzyme catalyzes monomethylation of arginine residues though some studies have also documented their involvement in dimethylation of arginine [172]. In conjunction with PRMT5, this enzyme is involved in the snRNP biogenesis in human cells [208]. PRMT7 showed both sensitivity and resistance towards DNA damaging agents, and thus it serves as a marker for kidney damage due to antibiotic treatment [209-211]. In pluripotent stem cells, PRMT7 acts as a marker similar to OCT4; loss of expression of PRMT7 was observed in differentiated embryonic stem cells [212]. PRMT7 catalyzes monomethylation of several R sites in histones, including H3R2, H3R17, and H3R19 [186].

PRMT8 is a type I PRMT and shares 80% homology to PRMT1 [213]. PRMT8 is found primarily in the neuronal region of the brain [187, 214]. The subcellular localization of this enzyme is within the plasma membrane as it interacts with membrane lipid by its N-terminal myristoylation motif [187]. The N-terminal region also harbors two proline-rich motifs that enable it to interact with several SH3 domains and also with PRMT2 [187]. The enzymatic activity of this enzyme resides in the conformation of its N-terminal end which increases with the loss of this domain.

PRMT9 (FBXO11) contains two Ado-met binding domains similar to PRMT7. Its N-terminus contains two tetratricopeptide repeats which facilitate protein-protein interaction [215]. PRMT9 is a type II PRMT, which is widely expressed in mammalian tissues. This enzyme is localized in the cytoplasm and nucleus [173]. Loss of PRMT9 activity was associated with middle ear inflammation [216].

PRMT 10 and 11 are homologous to PRMT7 and PRMT9, respectively. These two enzymes and their substrates have not been characterized.

Active marks

H3	R2me2s	PRMT5	[217]
	R8me2a	PRMT2*	[190]
	R17me2a	PRMT4	[196, 218, 219]
	R26me2a	PRMT4	[218, 219]
	R42me2a	PRMT4/6	[197]**
H4	R3me2a	PRMT1/6*	[23, 220, 221]

Repressive marks

H3	R2me2a	PRMT6	[114, 221, 222]
	R8me2s	PRMT5	[203, 223]
H4	R3me2s	PRMT5	[203, 224]
H2A	R29me2a	PRMT6	[225]

* Only observed *in vitro*, ** Transcriptional stimulation only observed *in vitro*

Table 1. PRMT-catalyzed methylation marks on mammalian histones. The first column represents the histone molecule, the second column represents the type of arginine modification on the histone tail and the third column represents PRMT enzyme responsible for the particular modification. *The Table and the text were reproduced with permission from Figure 1 [181].*

1.3.3 Arginine modifications by PRMTs

Arginine modifications of histones have important roles in chromatin modeling and transcriptional state [226, 227]. Studies using chromatin immunoprecipitation assays have determined the location of the modified histones, and in some studies, knockdown of specific PRMTs have given us an idea of the enzyme substrates and their function (**Table 1**).

H3R17me2a: PRMT4/CARM1 catalyzes the production of H3R17me2a. This H3 PTM is found within the upstream promoter region of several genes such as *TFF1*, *E2F1*, *CCNE1*, *AP2*, *Oct 4* and *Sox2*, *CITED2*, and *Scn3*, suggesting a role for this PTM in transcriptional activation [129, 228, 229]. Increased H3R17me2a parallels the increased occupancy of the KAT CBP/p300, suggesting that acetylation of H3K18 by CBP/300 is important for the recruitment of PRMT4/CARM1 [230]. Upon cellular stimulation (such as by estradiol) histone cross-talk can be initiated at specific gene promoters as described for the estrogen-responsive gene *TFF1*. In this case, acetylation at H3K18 and K23 promotes H3R17 methylation by PRMT4 upon estrogen stimulation resulting in the activation of the *TFF1* promoter [230, 231]. This phenomenon was also reported for *GADD45* gene [232]. Acetylation at specific sites of H3 increases the rate of the CARM1 reaction or the binding affinity [233]. Acetylation of H3K18 can neutralize the positive charge, which increases the nucleophilic attack on the sulfur methyl bond of S-adenosyl methionine. Thus this modification on H3 makes PRMT4 more amenable to bind to the H3K18ac peptide. Moreover, loading of PRMT4 at the estrogen responsive *TFF1* gene promoter was found to occur in a cyclic manner at 40-minute intervals [234]. Additional analysis revealed the enrichment of H3R17 methylation in M-phase cells which is correlated with the appearance of H3S10 phosphorylation [235]. Using ChIP-chip analysis for H3R17me2a in the estrogen receptor alpha (ER α) positive MCF7 breast cancer cell line, it was found that this PTM mark is enriched at the enhancer-rich clusters Ec1 and Ec3, which bind to ER α . CARM1 was recruited to these distant enhancer regions following the addition of estradiol [236]. In addition to marking the ER α associated enhancer regions, H3R17me2 locates with the upstream promoter region of the *TFF1* gene [234, 237].

H3R26me2a: H3R26me2a is a less studied H3 PTM than H3R17me2a, and it is also produced by PRMT4/CARM1. This H3 PTM is associated with the upstream promoter region of *cyclin E1* gene (*CCNE1*) which is transiently expressed before the cells enter into the S phase [219]. H3R26me2a may have a crucial role in regulating gene expression as it is adjacent to the repressive mark H3K27me3. Further experiments are needed to determine whether H3R26me2 has a role in blocking the binding of the H3K27 modifier EZH2 or making the binding sites unavailable for the carboxy terminal domain of polycomb protein EED [238].

H3R2me2a: PRMT6 is the major methyltransferase responsible for the genesis of H3R2me2a *in vivo*. This H3 PTM antagonizes the MLL1 (mixed lineage leukemia1)-mediated trimethylation of H3K4, by preventing the recruitment of WDR5, a subunit of the MLL complex [221]. Thus, H3R2me2a by blocking

the docking site for MLL1 and the subsequent methylation of H3K4 functions as a transcription repressor [221, 222]. This phenomenon was supported by the ChIP-sequencing data of human upstream promoter regions [114, 239]. H3R2me2a was present at pericentromeric regions, while H3R2me1 was found at subtelomeric regions [240]. H3R2me2a was not enriched in the promoters of active genes [241].

H3R2me2s: Symmetric dimethylation of H3R2 is catalyzed by both PRMT5 and PRMT7 WDR-77 complex. This modification usually localizes at the -1 nucleosome relative to the TSS where its role is to keep the region free of nucleosomes. Moreover, it prevents the binding of CAF1 by blocking RBBP7 (retinoblastoma binding protein 7) interaction with H3 to prevent the heterochromatinization [217]. The underlying mechanism to prevent heterochromatinization is to prevent H3K27 methylation by PRC2 and deacetylation by NURD and Sin3a. H3R2me2s recruits WDR5 which is a subunit of several co-activator complexes (MLL, SET1A, SET1B, NLS1, and ATAC) that produce H3K4me3. WDR5 is the reader of the H3R2me2s mark, and this interaction is mediated through the WD40 domain of WDR5 [217]. H3R2me2s at distal promoter sites binds to the WDR5 binding pocket, and these regions are also enriched with H3K4me1 and H3, H4 acetylation.

H4R3me2a and H2AR3me2a: Histone H4 and H2A contain identical residues at the first five amino acids and therefore possess functional similarity. Together these two sites are known as the 'R3' motif [171]. PRMT1 and PRMT6 are involved in the asymmetric dimethylation of H4R3 located on the active promoter region. The upstream promoter regions of *TFF1*, *CYP3A4*, *CITED2* and β globin gene locus were enriched with H4R3me2a [23, 242-244]. Top-down mass spectrometry analysis showed the association H4R3me with acetylation of lysine residues and often in combination with the H4K20me2 mark [245, 246].

H4R3me2s and H2AR3me2s: PRMT5 is responsible for the catalysis of H4R3me2s and H2AR3me2s marks [223, 247]. H4R3me2s is associated with promoters and CpG islands independent of transcriptional activity or DNA methylation [247]. H4R3me2s is associated with the imprinting control regions (ICRs) where it resides with other repressive marks (H3K9me3, H4K20me3 and DNA methylation) [247]. H4R3me2s is localized within silenced upstream promoter region (e.g. that of the silenced fetal globin gene and H19 imprinting control region) [203, 248, 249]. H4R3me2s was not present at enhancers with H3K4me1 or repressed regions with H3K9me3. It is possible that PRMT5-mediated H4R3me2s marks poised promoter regions, while PRMT1-mediated H4R3me2a marks transcriptionally active promoters.

Further sequential ChIP assays will be required to determine whether H3K4me3 is associated with a nucleosome with H4R3me2a but not with H4R3me2s.

H3R8me2s: This symmetric methylation is also catalyzed by PRMT5 which marks transcriptionally repressed gene regions [223]. This mark is associated with H4R3me2s as PRMT5 catalyzes both. ChIP analysis indicated its presence along the repressed promoter region where PRMT5 is recruited through several factors such as Snail, ZNF224, Ski and BRD7 [203, 250-253]. H3R8 methylation was shown to be prevented by the acetylation of H3K9 and H3K14, but the reverse effect of these modifications has not been tested yet [254]. However, H3R8 methylation can block the methylation event by the protein methyltransferase G9a [254]. More research is needed to decipher the mechanism of how PRMT5 mediated H3R8me2s is associated with the transcriptionally repressed status.

1.3.4 Biological functions of PRMTs

PRMTs regulate chromatin structure and function through transcriptional activation, repression and their interaction with chromatin barrier elements [226, 227]. PRMTs are also involved in pre-mRNA splicing, nuclear/cytoplasmic shuttling, cell cycle and DNA repair [255-257]. The focus of next sections will be on the role of PRMTs in transcription and chromatin organization.

1.3.4.1 PRMTs and transcriptional co-activator activity

PRMTs methylate several transcriptional coactivators such as p300, CBP, and SRC3, which indicates their role in regulating the activity of these coactivators. Moreover, as described in the earlier section of this review, PRMT4/CARM1 acts as a nuclear receptor coactivator whereas PRMT4 and PRMT1 have a synergistic effect on the steroid hormone-induced gene activation [258]. This observation was supported by single and double knockout studies and transcriptome analysis where the loss of both PRMT1 and PRMT4 leads to the downregulation of transcription factor STAT5 [243]. A wide range of transcription factors such as USF1, p53, YY1, NF- κ B, PPAR γ , RUNX1, and E2F1 are regulated by PRMTs [23, 243, 259]. So far the only reported mechanism of action of PRMT1 as a transcriptional coactivator was described for RUNX1. Methylation of RUNX1 by PRMT1 leads to the dissociation of the transcriptional repressor SIN3A, thus promoting the transcriptional activation of RUNX1 [259].

1.3.4.2 PRMTs and transcriptional co-repressor activity

PRMT5 mediated symmetrical methylation was reported to be associated with transcriptional repression. PRMT5 can interact with MBD2 (methyl-DNA-binding protein 2)/NuRD histone deacetylase complex. Methylation of DNA at the CpG island causes the recruitment of PRMT5 to the promoter where it confers

symmetric H4R3 methylation at the promoter site to repress the target gene [260]. A role of PRMT5 similar to the suppressor of tumorigenicity 7 (ST7) and nonmetastatic 23 (NM23) tumor-suppressor genes was observed upon its interaction with SWI/SNF chromatin remodeling complexes. In this instance, PRMT5 overexpression in these cells was accompanied by H3R8 methylation and H3K9 deacetylation [223].

1.3.4.3 PRMTs and chromatin barrier function

The proteins binding to barrier elements recruit chromatin modifying enzymes which elevate the steady state level of active histone PTMs at the barrier element and across the active chromosomal domain [23, 261]. The USF1/2 heterodimer recruits PRMT1 to HS4 of the chicken β -globin domain. PRMT1-mediated H4R3me2a plays a critical role in establishing and maintaining active histone marks, such as H3K4me2 and acetylated histones, at the avian β -globin domain by recruiting lysine methyltransferases (SET1) and KATs [23, 261]. H3R2me2s is also an active histone mark, which is catalyzed by PRMT5 [217, 262]. It is currently not known whether USF recruits PRMT5 to the HS4 barrier element.

1.3.5 Association of PRMTs with human disease

PRMTs, as with other chromatin modifiers, are aberrantly expressed in cancer cells. Also, a common theme in cancer cells is alterations in splicing, with different cancer cell types expressing alternative PRMT isoforms, which may have different properties [263, 264]. In the case of acute myeloid leukemia (AML), PRMT1 was found to be a component of MLL-EEN oncoprotein complex where PRMT1-catalyzed H4R3 dimethylation was involved in leukemic transformation [178]. This is further explained by the knockdown study of PRMT1 which resulted in the suppression of MLL-mediated transformation. The MLL-PRMT1 fusion protein will transform primary myeloid progenitors [178]. The catalytic activity of PRMT1 was required for transformation. Moreover, the methylation of RUNX1/AML1 by PRMT1 promote myeloid cell differentiation. Methylated RUNX1 lost its interaction with SIN3A co-repressor driving to leukemic stage [259]. Thus, a PRMT1 specific inhibitor could be considered a candidate for a therapeutic approach for AML [265]. TDRD3, which is a methylarginine effector molecule and transcriptional coactivator, interacts with H4R3me2a and H3R17me2a. Interestingly, increased levels of TDRD3 was associated with poor prognosis of breast cancer patients [266]. The association of PRMT1 and PRMT4/CARM1 with several nuclear receptors have made these proteins of interest in cancer research [267, 268]. Elevated PRMT4 levels were observed in several castration-resistant prostate cancers. For example, the growth and differentiation of prostate cancer cell line LNCaP required PRMT4 [269].

PRMT4 expression was analyzed in clinical samples where more than the 75% patients showed aberrant PRMT4 expression relating to clonal survival and anchorage-independent growth [269, 270].

PRMT5 is overexpressed in various types of cancers, and it has a role in the inhibition of tumor suppressor genes [271]. The symmetric methylation of H3R8 or H4R3 by PRMT5 promotes cancer cell survival. It also induces anchorage-independent cell growth because the loss of PRMT5 results in increased E-cadherin expression [203, 223]. Reducing the expression of PRMT1 and 6 in bladder and lung cancer cells resulted in the suppression of cell growth [272]. Based on these observations, PRMT5 is considered as an oncoprotein [273].

1.3.6 Regulating the regulator

PADI4 (peptidyl arginine deaminase 4) and JMJD6 (jumonji domain-containing protein 6) catalyze arginine demethylation [274]. Human PADI4 catalyzes the deamination of arginine and monomethyl arginine to citrulline, but it is unable to act on symmetrical or asymmetrical dimethylarginine. However, PADI4 is not considered to be a true demethylase as it is unable to directly convert methylarginine to arginine through the removal of the methyl group [136, 275]. JMJD6, a family of the Jumonji domain-containing proteins, is capable of removing the mono methyl H3R2 and H4R3 groups *in vitro* and *in vivo* but is not capable of doing so for H3R8, H3R17, H3R26 or H2A sites [138]. It will be of interest to further characterize the existence of additional arginine demethylases [275].

PRMT activity is also regulated by PRMT interacting protein partners that regulate arginine methyltransferase activity. hCAF1 [CCR4 (CC chemokine receptor 4)-associated factor-1] is one such protein that inhibits the PRMT1 catalyzed H4R3 methylation in a substrate and dose-dependent manner although it does not show any effect on the target of PRMT1, which is hnRNPA1 [276]. Differentially expressed in adenocarcinoma of the lung (DAL-1) is a tumor suppressor protein which was shown to interfere with the activities of PRMT3 and PRMT5 [277]. Nuclear protein COPR5 (co-operator of PRMT5) can regulate the recruitment of PRMT5 at its target gene which also sustains a specific enzymatic function for PRMT5. It causes PRMT5 to catalyze H4R3 but not H3R8 at the target site [202].

There is considerable evidence for the involvement of PRMTs in cancer cell proliferation and differentiation, making these proteins promising candidates for therapeutic targets in various types of cancer [278]. Our appreciation of the role of the PRMT catalyzing histone modifications is increasing but is limited by not having high-quality antibodies to each arginine (R) methylated histone site. We are also gaining an appreciation of the mechanisms by which the various histone modifications influence each

other and the readers these histone modifications attract or repel [186, 231]. This knowledge will be required to understand the role the PRMTs and their histone substrates have in regulating epigenetic events and in the organization of the genome.

1.4 Chromatin fractionation

Chromatin fractionation is a popular method to characterize the features of chromatin. Chromatin fractionation to profile chromatin accessibility was first described by Sanders in 1978 using rat liver [279]. Varying salt concentrations were used to separate chromatin subfractions from micrococcal nuclease digested nuclei. Characterization of these chromatin subfractions revealed that they differ in molecular composition, DNA fragment size, contents of linker histones, histone, non-histone protein composition. Based on these varying features three different types of chromatin structure was identified. In that study, it was shown that low salt extraction of nuclei (0.2 M NaCl) released chromatin regions that were MNase sensitive and structurally open [279]. In contrast, the salt concentration of 0.6 M NaCl released mostly bulk chromatin. The step wise increase in NaCl concentrations of micrococcal nuclease digested nuclei released nucleosomes with different compositions. This study showed that chromatin fractionation using a salt extraction procedure can separate functionally different parts of the genome. Such chromatin fractionation protocols were used to isolate and characterize structurally different chromatin populations in various cell types. Fractionation in *Drosophila* and chicken erythrocytes are described next.

1.4.1 Description of chromatin fractionation for different cell sources

Chromatin fractionation in Drosophila

The chromatin fraction isolated with low salt concentrations (80 mM or 150 mM NaCl) from micrococcal digested nuclei from *Drosophila melanogaster* S2 cells contain mostly mononucleosomes and represent the ‘active’ chromatin properties [280]. Chromatin isolated with low salt was enriched at the 5’end upstream gene promoter, 3’end of gene and regulatory region. High salt (600 mM NaCl) extracted chromatin was mostly oligomers enriched with a different “active” population, presumably transcribed chromatin associated with the nuclear matrix. Transcriptionally active chromatin is both low salt soluble and insoluble (nuclear matrix associated) [280-282]. Due to the presence of larger complexes such as RNAPII and splicing factors, transcriptionally active regions attached to these complexes are insoluble and nuclear matrix associated [281-283]. Separation of two different ‘active’ chromatin regions with low

and high salt concentration indicates that two fractions exhibit different active chromatin properties, albeit sequence derived from same or overlapping genomic region.

Chromatin fractionation process to isolate transcriptionally active chromatin from chicken erythrocytes

Chicken erythrocytes express linker histone variant H5 in addition to H1. Chicken polychromatic erythrocyte chromatin has about 1.3 molecules of histone H1/H5 per nucleosome [282, 284, 285]. Most vertebrate cells have an average coverage of only 0.8-1.0 molecules of H1/nucleosome [284]. Chicken polychromatic erythrocytes, isolated from anemic birds, are cells at the stage before maturation and are transcriptionally active [286]. A very small population (~1-2%) of chromatin of chicken polychromatic erythrocytes undergoes dynamic histone acetylation. With the aid of low salt solubilization process, it was possible to isolate and characterize these active chromatin populations from chicken polychromatic erythrocytes (**Figure 1.9**) [285, 287]. In our experience, chicken erythrocytes are the only eukaryotic cell source in which a biochemical fractionation protocol is capable of isolating polynucleosomes (fraction F1) that are soluble at physiological ionic strength (0.15 M NaCl) and are highly enriched in transcribed DNA (**Figure 1.9**) [282, 285]. Similar salt fractionation protocols applied to other chromatin sources yielded mononucleosomes associated with the 5' end of the transcribed gene body [280]. Our publications showed that the combination of localized highly acetylated histones and the higher than usual levels of H1/H5 explains why the chromatin fractionation protocol with polychromatic erythrocytes yields salt soluble polynucleosomes enriched in transcribed DNA [124, 288]. Furthermore, the DNaseI sensitivity of a polychromatic erythrocyte chromatin region is directly proportional to the region's solubility at physiological ionic strength [289]. The majority of the polychromatic erythrocyte chromatin does not have highly acetylated histones and is insoluble at physiological ionic strength. Thus, histone acetylation and solubility at physiological ionic strength are features of DNaseI sensitive active chromosomal domains in erythroid cells. Salt-soluble (150 mM NaCl) chromatin fractions isolated from chicken erythrocytes were mostly enriched with mononucleosomes. However, polynucleosome and oligonucleosome fragments (F1, F2) were also enriched in the 150 mM NaCl soluble chromatin fragment with distinct features [287]. The F1 fraction polynucleosomes are dynamic atypical structures exchanging with newly synthesized H2A and H2B and to a lesser extent with newly synthesized H3 and H4 [285, 291-293]. It should be noted that G0 phase cells synthesize the four core histone in the absence of DNA replication [294, 295]. Properties of the transcriptionally active polynucleosome chromatin isolated from chicken erythrocytes are listed in **Table 2**.

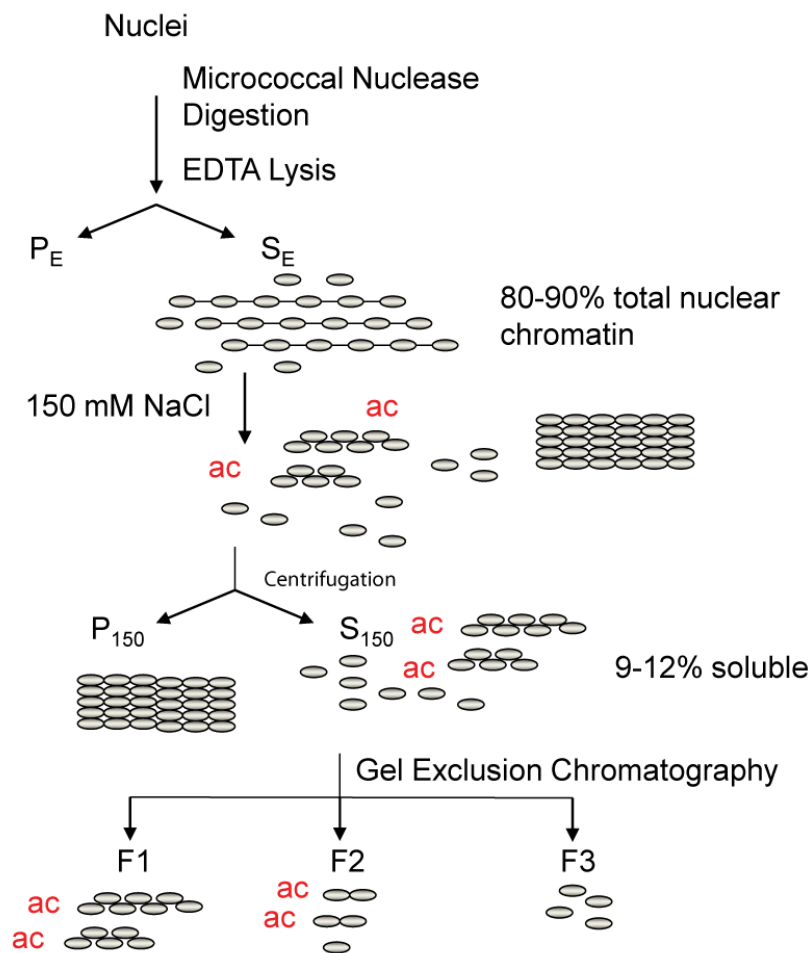


Figure 1.9: Overview of chromatin fractionation process in chicken erythrocyte cells [285]. Fractionation of chicken erythrocyte chromatin. Chicken polychromatic erythrocyte nuclei were incubated with micrococcal nuclease, and chromatin fragments soluble in a low ionic strength solution containing 10 mM EDTA were recovered in fraction S_E . Chromatin fraction S_E was made 150 mM in NaCl, and chromatin fragments from the salt-soluble fraction (S_{150}) were size-resolved on a Bio-Gel A-1.5 m column to isolate the F1 fraction containing polynucleosomes. *The figure and the text were reproduced with permission from Additional Figure 1a* [285].

1.4.1.1.1 Features of low salt soluble transcriptionally active chromatin F1

Features of salt soluble chromatin S150, F1, F2	Features of salt insoluble chromatin P150
Active/poised DNA	Repressed DNA
Acetylated histones	Unacetylated histones
HDAC1 and 2	HDAC1/2 low or absent
uH2B	lacks uH2B
H3K4me2, me3	H3K9me3
H3.3 S28p	H3.2
Newly synthesized H2A, H2B, H3.3	No histone exchange
On-going H3 and H4 methylation	No on-going histone methylation
Atypical nucleosomes (U-shaped)	Canonical nucleosomes

Table 2: Properties of 150 mM salt soluble and salt-insoluble chromatin isolated from chicken erythrocytes [124, 163, 287, 290, 291].

Finally, the longer (poly/oligonucleosome) fragment size of transcriptionally active chromatin resembles more the state of native transcriptionally active chromatin. Under the physiological conditions, the regulatory region may locate further away from the target gene region. Therefore, characterizing polynucleosome chromatin fragments is valuable regarding analyzing the interrelationship between transcription and higher order chromatin structure.

1.5 Innate immunity in avian system

Innate immunity is the first line of defense against infectious pathogen. Adaptive immunity or acquired immune response rely on the signal generated by pattern recognition receptors (PRR) for proper recognition and effective clearance of the pathogen from the system [292]. Different types of PRRs exist in vertebrate cells to detect pathogen-associated molecular patterns (PAMPs). Upon exposure to infection, PAMP triggers the activation of the PRR mediated downstream pathway that involves different adaptor proteins, transcription factors, expression of interleukins and release of cytokines [293]. Innate immunity in the avian system is different from its mammalian counterpart despite sharing an evolutionary conserved

genomic region [294]. The site of B-cell development and hematopoiesis in birds is the bursa of Fabricius as they lack lymph nodes present in mammals. Birds lack functional eosinophils and have heterophils to replace the function of the neutrophil. In birds, Harderian glands located behind the eyeballs play a crucial role in the adaptive immune response. Chickens have a somewhat similar and distinct Toll-like receptors (TLRs), chemokines, defensins, antibodies, cytokines and several other immunological particles when compared to humans as demonstrated in **Table 3** [294-299].

Pattern recognition receptor	Human	Chicken
Membrane-bound		
TLRs (signalling) recognizing cell surface PAMPs	TLR1/6/10 TLR2 TLR4 TLR5 TLR11 ^a	TLR1LA and TLR1LB TLR2A and TLR2B Present Present Absent TLR15 (predicted ^b)
TLRs (signalling) recognizing pathogen nucleic acid	TLR3 TLR7 TLR8 TLR9	Present Present Pseudogene TLR9 absent; CpG recognized by TLR21
Endocytic	Mannose receptor Glucan receptors Scavenger receptors	Present Present Present
Cytoplasmic		
NLRs		
NODs	NOD1 NOD2	Present Absent
NALPs	14 genes	All absent
RNA helicases	RIG-I MDA5 LPG2	Absent, but present in duck Present Absent

Table 3: Comparison of pattern recognition repertoire between human and chicken. *The table and the text were reproduced with permission from table 1 [294].*

PRRs are present in various immune and non-immune cells such as macrophages, dendritic cells, lymphocytes, mucosal epithelial, endothelial and fibroblasts cells. Cytosolic PRRs include Toll-like receptors (TLR), retinoic acid-inducible gene I (RIG-I)-like receptors (RLR), and nucleotide-binding oligomerization domain (NOD)-like receptors (NLR). These PRRs play a crucial role in recognizing double-strand RNA (dsRNA), single-strand RNA (ssRNA) and foreign DNA molecules [300, 301]. In mammalian system, 12 TLRs have been discovered whereas human contain 10 and mouse possess 12; among them, chickens share orthologues for some of the TLRs. However, some of the TLRs are specific to chicken, and chicken lack some of mammalian TLRs [302-306].

1.5.1 Chicken TLRs

TLRs are type I transmembrane proteins, which consist of three separate domains. The N-terminal extracellular domain, which contains leucine-rich repeats, is involved in the detection of PAMP. Both the transmembrane domain and intracellular Toll-interleukin 1 (IL-1) receptor (TIR) domain mediate downstream signaling events due to exposure to PAMP [306, 307]. TLRs are unique to their ligand or PAMP such as lipids, nucleic acid, lipoprotein and proteins derived from microorganisms [308]. TLRs are distributed in the plasma membrane, endosome-lysosome, and endolysosomes to defend against a ligand of bacterial, viral, parasitic or fungal origin. TLRs recruit specific adaptor molecules in response to signal, and their mechanism of action varies with cell type [307, 309, 310].

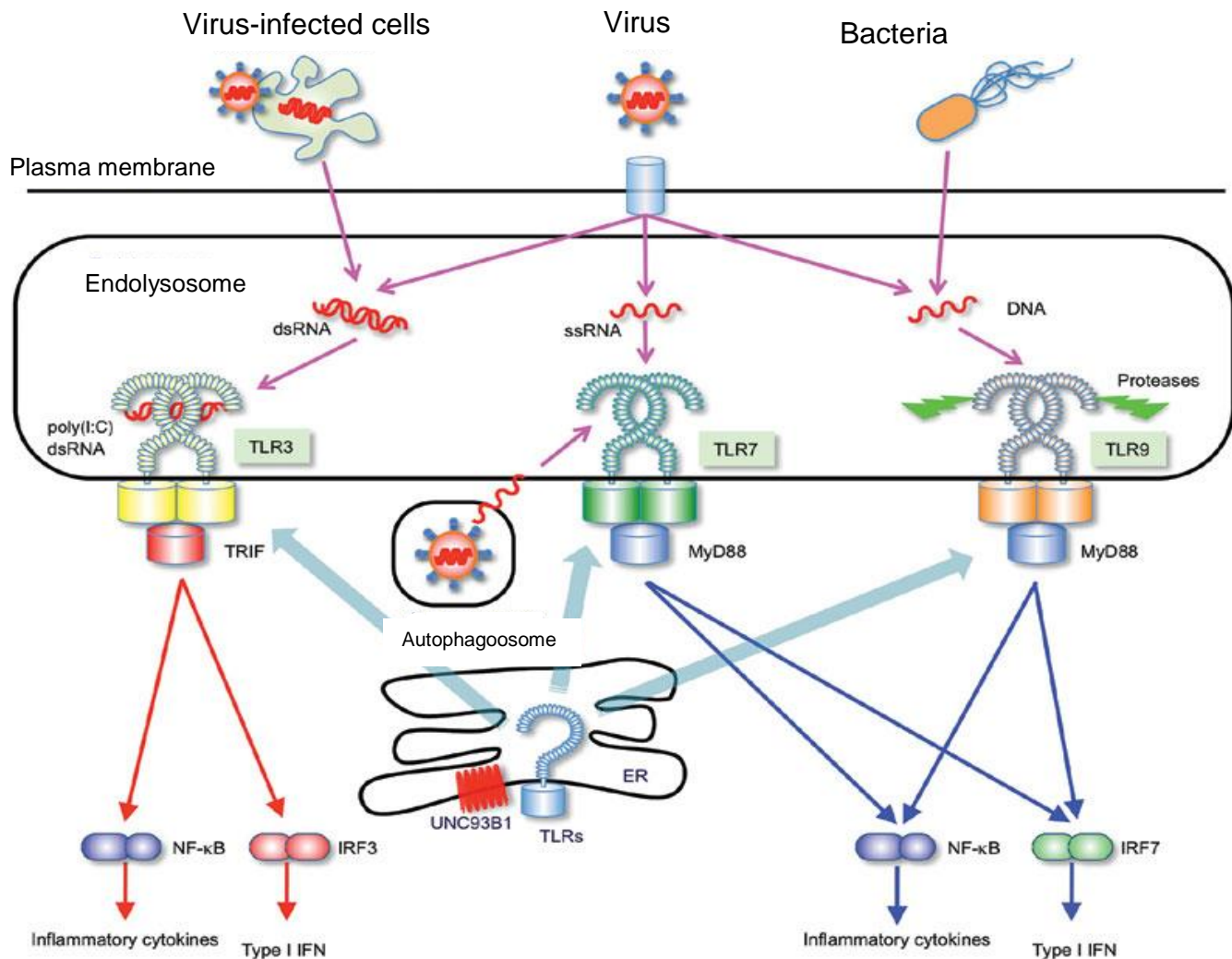


Figure 1.10: PAMP recognition by intracellular TLRs. TLR3 recognizes dsRNA derived from viruses or virus-infected cells; dsRNA binds to N- and C-terminal sites on the lateral side of the convex surface of the TLR3 ectodomain, which facilitates the formation of a homodimer via the C-terminal region. TLR3 activates the TRIF-dependent pathway to induce type I interferon and inflammatory cytokines. In pDCs, TLR7 recognizes ssRNA derived from ssRNA viruses in endolysosomes and activates NF- κ B and IRF7 via MyD88 to induce inflammatory cytokines and type I interferon, respectively. Also, autophagy is involved in delivering ssRNA to TLR7-expressing vesicles. TLR9 recognizes DNA derived from both DNA viruses and bacteria. Proteolytic cleavage of TLR9 by cellular proteases is required for downstream signal transduction. TLR9 recruits MyD88 to activate NF- κ B and IRF7 in pDCs. TLR3, TLR7, and TLR9 localize mainly to the ER in the steady state and traffic to the endolysosomes, where they engage with their ligands. UNC93B1 interacts with these TLRs in the ER and is essential for this trafficking. *The figure and the text were reproduced with permission from Figure 2 [306].*

1.5.2 Chicken TLR 1, 2, 4, 5

Chicken TLR 2, 4, 5 and 7 are orthologous to mammalian TLRs where chicken contains duplicated TLR2 gene chTLR2a and chTLR2b. In the chicken genome, human TLR1/6/10 locus substituted by TLR1LA and TLR1LB and hence inferred they recognize a narrow range of antimicrobial agents [311]. TLR1LA and TLR1LB are unique to birds and form a heterodimer with chicken TLR2a and b [312, 313]. Chicken TLR5 gene shows polymorphism, which leads to inferring the distinct ability of this receptor than a mammalian counterpart for recognizing PAMPs. However, the antiviral immune response for chTLR1 and chTLR5 has not been demonstrated [314]. On the other hand, mammalian TLR2 binds to hemagglutinin from measles virus [315] and envelop protein of human cytomegalovirus (HCMV) [316], varicella virus [317], herpes simplex virus-1 [318]. Similarly, TLR4 was also involved in recognition of viral components such as viral protein from Respiratory Syncytial virus (RSV) [319], Mouse mammary tumor virus (MMTV) [320], Coxsackievirus B3 [320].

1.5.3 TLR3, TLR7, TLR8, and TLR9

TLR3 recognizes the viral antigen and triggers the pathway for type I IFNs mediated antiviral defense. Endosomal TLR3 detects viral dsRNA which is produced during replication cycle of the virus within endoplasmic reticulum [306]. Chicken *TLR3* is homologous to its human orthologues and shares 48% amino acid sequence similarity. Similar to human, ch*TLR3* is distributed in a wide range of tissues; with moderate expression observed in bone marrow, skin, muscle cells and as well as chicken CD4⁺ T cells [321]. chTLR7 recognize viral nucleic acid similar to chTLR3 and shares 63% of amino acid sequence similarity with that of human [295]. In contrast to its human orthologues, the distribution of chTLR7 is restricted to immune cells only. Chicken erythrocytes that showed expression of ch*TLR2*, *3*, *4*, *5* and *21* lack the expression for ch*TLR7* [322]. Chicken lack the *TLR9* gene, *TLR8* exists as a pseudogene [323, 324].

1.5.4 TLR15

One of the avian specific TLRs is TLR15, which has been identified in chicken, turkey, goose and Japanese quail [311, 325, 326]. Experiments in chicken embryonic fibroblasts (CEF) cells treated with heat killed *S. enteric serovar Typhimurium* showed that this TLR presumably plays a defensive role against bacterial antigens [325]. In chicken, the expression of *TLR15* gene has been observed in bone marrow, bursa, and spleen [325]. TLR15 upregulates the production of IL1 β in myeloid differentiation primary response gene (Myd88) dependent pathway in response to unmethylated CpG

oligodeoxynucleotides (CpG ODN) as demonstrated in the chicken macrophage cell line HD11. Moreover, crosstalk between TLR2 and 15 signaling events can lead to a IL1b reduction in these cells [327]. *TLR15* can be highly expressed in response to Marek's disease virus (MDV) infection in chicken. This demonstrates the potential role of TLR15 against antiviral infection similar to mammalian TLR4 and 9 [328]. However, this research area needs more investigation.

1.5.5 TLR21

TLR21 has been identified in chicken and turkey and is homologous to fish and amphibian *TLR21* with amino acid sequence similarity >60% [329]. It shares 47% sequence similarity with murine *tlr13* [329]. ChTLR15 and chTLR21 recognize mammalian TLR9 ligand CpG ODN and can generate an antiviral immune response. Similar to human TLR9, chTLR21 is localized in the endoplasmic reticulum [330]. Expression of ch*TLR21* was found highest in spleen and bursa of Fabricius with a low level detected in chicken intestinal CD4+ and CD8+ T cells, skin, lung, kidney, brain and liver [331, 332].

1.5.6 RIG-1 like receptors

RIG-1 like receptors (RLRs) are cytosolic and detect RNA viruses. This family includes RIG-I, melanoma differentiation-associated gene 5 (MDA5) and laboratory of genetics and physiology 2 (LGP2) [333]. Both RIG-1 and MDA5 receptors contain four domains. These domains include two N-terminal caspase activation and recruitment domains (CARD). RIG-1 and MDA5 contain one of each DEX (D/H) box RNA helicase domain, C-terminal RNA-binding domain and a repressor domain. LGP2 contain all of these domains except for the CARD domain. Among vertebrates, the gene synteny of the region containing *MDA5* and *LGP2* receptor gene is well conserved compared to the conservation of synteny for *RIG-1* gene [334]. However, *RIG-1* homologues are absent in chicken and most fish species [334, 335].

RIG-1: *RIG-1* is categorized as a IFN-stimulated gene (ISG) family. It is involved in the generation of IFN type I and III-mediated immune stimulation in response to RNA viruses [336]. The *RIG-1* gene was identified in duck and goose, but not in chicken. It can recognize dsDNA from Epstein-Barr virus, dsRNA and 5'-triphosphate (5'ppp) dsRNA derivative of viral RNA polymerase [335, 337, 338].

MDA5: Similar as RIG-1, this is a key cytosolic receptor and both are conserved in their mechanism for recognizing viral pathogens in vertebrate [334]. Human and chicken *MDA5* share 60% of sequence similarity with the C-terminal end of the gene being most conserved (70%) [339]. MDA5 detects the invading virus and activates the type I interferon response pathway. MDA5 can be activated by dsRNA and analog of dsRNA, poly (I:C). It was demonstrated that the length of poly I:C could activate either

RIG-1 or MDA5; long poly I:C sequences (>1 kbp) potentially activate the MDA5 mediated immune response pathway while small poly(I:C) sequences (<1 kbp) activate the RIG-1 dependent pathway [340]. Chicken *MDA5* shows the highest expression in the intestine; however, *MDA5* is also expressed in other tissues [341]. Due to the strong IFN β immune response with MDA5 N-terminal 483 amino acid residue, it is considered for use as a vaccine adjuvant against highly pathogenic avian influenza virus H5N1 [342].

LGP2: LGP2 is a negative regulator of RLR-mediated signaling. *LGP2* shares 53% of amino acid sequence similarity with human and 52% with mouse [343]. In DF-1 chicken fibroblasts and HD-11 chicken macrophage-like cells, siRNA mediated knockdown assay was performed for LGP2 followed by viral co-transfection to stimulate the RLR mediated signaling pathway [344]. The result demonstrated that reduction of LGP2 correlates with the reduced level of type I IFN secretion in these cells. Consistent with mammalian system overexpression of *LGP2*, there was a down regulation of *IFN β* expression in these chicken cells [344]. Therefore, chicken LGP2 is functional, and a part of the RLR-mediated signaling event. More investigations are required to decipher the connection between the MDA5 and LGP2 signaling events in response to influenza virus infection in chicken.

1.5.7 NLR

NLR is another cytosolic receptor that contains more than 20 members in the group. These receptors can detect both PAMP and non-PAMP molecules and act in response to cellular stress to secrete inflammatory cytokines [345]. These receptors mainly recognize bacterial agents and provide an immune response. However, in mammal NLR has been demonstrated to recognize viral pathogens including DNA and RNA virus and regulate the antiviral immune response [346]. There are three domains in NLR receptor; N-terminal domain which confers protein-protein interaction, C-terminal leucine-rich repeats (LRR) that recognize PAMP, and a central domain which provides nucleotide binding and self-oligomerization [347]. NLRC5 is one of the members of NLR family group receptors. Based on the experiments with the chicken HD11 cell, NLRC5 expression increased with LPS but not with poly I:C treatment [348]. This demonstrates that NLRC5 is activated mainly by a bacterial infection. Subsequently, loss of NLRC5 was found associated with downregulation of type I IFN (IFN- α and IFN- β), but not IL-6 and MHC class I [349].

1.5.8 Cytokines

The chicken genome contains fewer cytokine genes than human [350]. However, there are several human orthologues of chicken cytokines that have identified so far (**Table 4**). A total of 23 interleukins and 24

chemokines (*XCL*, *14 CCL*, *8 CXCL* and *CX3CL*) have been identified in the chicken genome. All type I interferons and type II interferon IFN γ were also detected in chicken. The chicken genome contains all of the colony stimulating factors (*GM-CSF*) present in human as well as the tumor necrosis factor superfamily (*TNFSF*) members.

Cytokine	Human	Chicken
Interferons		
Type I	IFN- α , IFN- β , IFN- κ , IFN- ω , IFN- τ	All present except IFN- τ
Type II	IFN- γ	Present
Type III	IFN- λ 1 to IFN- λ 3	Single IFN- λ gene only
Interleukins		
IL-1 family	11 members (IL-1 α , IL-1 β , IL-1RN, IL-18, IL-1F5 to IL1-F10, IL-33)	4 members (IL-1 β , IL-1RN, IL-18, IL-1F5)
IL-10 family	6 members (IL-10, IL-19, IL-20, IL-22, IL-24, IL-26)	4 members (IL-10, IL-19, IL-22, IL-26)
IL-12 family	4 members (IL-12, IL-23, IL-27, IL-35)	Two members (IL-12, IL-23)
IL-17 family	6 members (IL-17A to IL-17F)	5 members (IL-17E (aka IL-25) absent)
T-cell proliferative	IL-2, IL-15, IL-21	All present
Th2 family	4 members (IL-4, IL-5, IL-13, IL-31)	3 members (IL-31 absent)
Others	IL-3, IL-6, IL-7, IL-9, IL-11, IL-32, IL-34	All present except IL-32
Transforming growth factors	3 members	All present
Tumour necrosis factors ^a	17 members	11 members
Colony-stimulating factors	3 members	All present
Chemokines^a		
XCL	2 members	1 member
CCL	28 members	14 members
CXCL	16 members	8 members
CX3CL	1 member	Present

^aFor TNFSF members and the chemokines, there are some direct orthologous relationships between human and chicken, but also distinct family members between the two species.

Table 4: Comparison of the cytokine repertoire between human and chicken. *The table and the text were reproduced with permission from table 2 [294].*

1.5.9 Immune regulatory pathways in avian erythrocytes

The major function of vertebrate erythrocytes is oxygen transport and gas exchange in lungs and tissues (**Table 5**). Non-mammalian vertebrates with a few exceptions have a nucleus and other organelles in their erythrocytes. These includes birds, reptiles, amphibians and fish [351]. The presence of the nucleus; however, does not affect the oxygen-carrying capacity of birds as results this erythrocyte function is well conserved between human and birds [352]. The half-life of erythrocytes vary among vertebrates with a range of 120 days for human, 40 days for avian, 600-800 for reptiles, 300-1400 for amphibians and 80-500 days in fish [351, 353-355]. As nucleated cells, chicken polychromatic erythrocytes are transcriptionally active but do not replicate. For this reason, chicken erythrocytes have been a popular system to investigate the relationship between transcription and transcription related mechanisms in the

absence of replication [285, 356]. Therefore, due to the presence of a nucleus, the physiological function of nucleated erythrocytes could extend to more than oxygen transport. Mammalian nucleated erythrocytes can produce cytokines such as interleukins, interferons, transforming growth factors and tumor necrosis factors as demonstrated for the first time in a study conducted on human erythroblast antigen+ and glycophorin A+ cells isolated from human bone marrow [357]. Several studies reported that nucleated erythrocytes in vertebrates, such as in fish, chicken or trout; possess an immune response capability [322, 358, 359]. IFN α is produced by salmon erythrocytes upon exposure to salmon anemia virus [360]. In a different study, macrophage effector function was stimulated in trout in response to *Candida albicans* [361]. Further, the phagocytic capacity of macrophages was increased in response to soluble molecules from chicken erythrocytes when treated with *Candida albicans* [362].

Proposed functions	Mammals	Fish	Amphibia n	Reptiles	Birds
Gas exchange function	[363]	[363]	[363]	[363]	[363]
Sugar transport	[364]	[372]	[379]	[381]	[385]
Calcium homeostasis	[365]	[373]	[380]	[382]	[386]
Redox homeostasis	[366]	[374]	-	[383]	[387]
Cell proliferation	[367]	-	-	-	[388]
Antiviral response		[360]	-	-	-
Antimicrobial activity			-	-	-
Immune complex	[368]	[375]	-	-	-
ROS production	[369]	[376]	-	-	-
Hemoglobin	[370]	[377]	-		-
Other related function	[371]	[378]	-	[384]	[362]

Table 5: Table reports functions associated to erythrocytes in mammals, fish, amphibian, reptiles and birds. References are numbered according to their appearance in this introductory chapter. The table and the text were reproduced with permission from Table 1 [359].

In a study to demonstrate the immune response in nucleated mature chicken erythrocytes, it was found that the erythrocytes respond against several tested PAMPs [358]. Production of chemokine CCL4, interferon IFN α , myxovirus resistance 1 (Mx 1), TLR3 and TLR21 showed different responses against three different tested PAMPs LPS, poly I:C, PGN, and a recombinant cytokine, rainbow trout tumor necrosis factor-alpha (rTNF) [358]. IFN α was stimulated in response to LPS, poly I:C, PGN, and rTNF,

while MX showed a low level of induction for all these PAMPs. Expression of CCL4 was low or none for all the PAMPs except for LPS and PGN. TLR3 showed the highest induction with LPS and rTNF and a lower induction for poly I:C and PGN. In contrast, TLR21 was induced highly in response to LPS and PGN [358]. Therefore, the stimulation of the genes was dependent on both the type of PAMP and the time of incubation [358]. This emphasizes that functional activity of nucleated erythrocytes in producing an immune response in a PAMP-PRR driven way and extends the possibility that this could be a possible function for non-mammalian nucleated erythrocyte in addition to O₂ transport.

Expression levels of cytokine and other immunological genes in chicken erythrocytes at 3 h post-poly I:C-stimulation.	
Gene	Expression
IFN- α	+++
IFN- β	+++
iNOS	+++
2'-5' OAS	++
MHC II	+
CD80	+
CD40	-
IL-1 β	-
IL-8	++

A "+++" indicates a high degree of expression, while a "++" indicates a moderate degree of expression, while a "+" indicates a low level of expression, while a "-" indicates no expression, as determined by real-time PCR.

Table 6: Expression levels of cytokine and other immunological genes in chicken erythrocytes at 3 h post-poly I:C-stimulation. *The table and the text were reproduced with permission from Table 2 [322].*

To understand the immune response in chicken erythrocytes, a second study addressed the expression profile of several TLRs in response to different PAMPs [322]. The study demonstrated the differential expression of TLRs including TLRs 2, 3, 4, 5 and 21, type I IFNs, and interleukins such as IL8 in response to different PAMPs. IFN α , IFN β , and IL8 were upregulated at 3-hour post poly I:C stimulation of chicken erythrocytes (**Table 6**) [322]. A low dose of poly I:C upregulated both IFN α and IFN β at 1-hour and 3-hour post-treatment. On the contrary, high dose of poly I:C downregulated the IFN response and upregulated IL8. However, both low and high dose of CpG ODN upregulated the expression of both interferons [322]. Interestingly, poly I:C of varying length has been shown to stimulate varying repertoires of TLRs in murine myeloid and fibroblasts cells [389]. These findings indicate a PRR response can be driven in a dose and time-dependent as well as cell type specific manner.

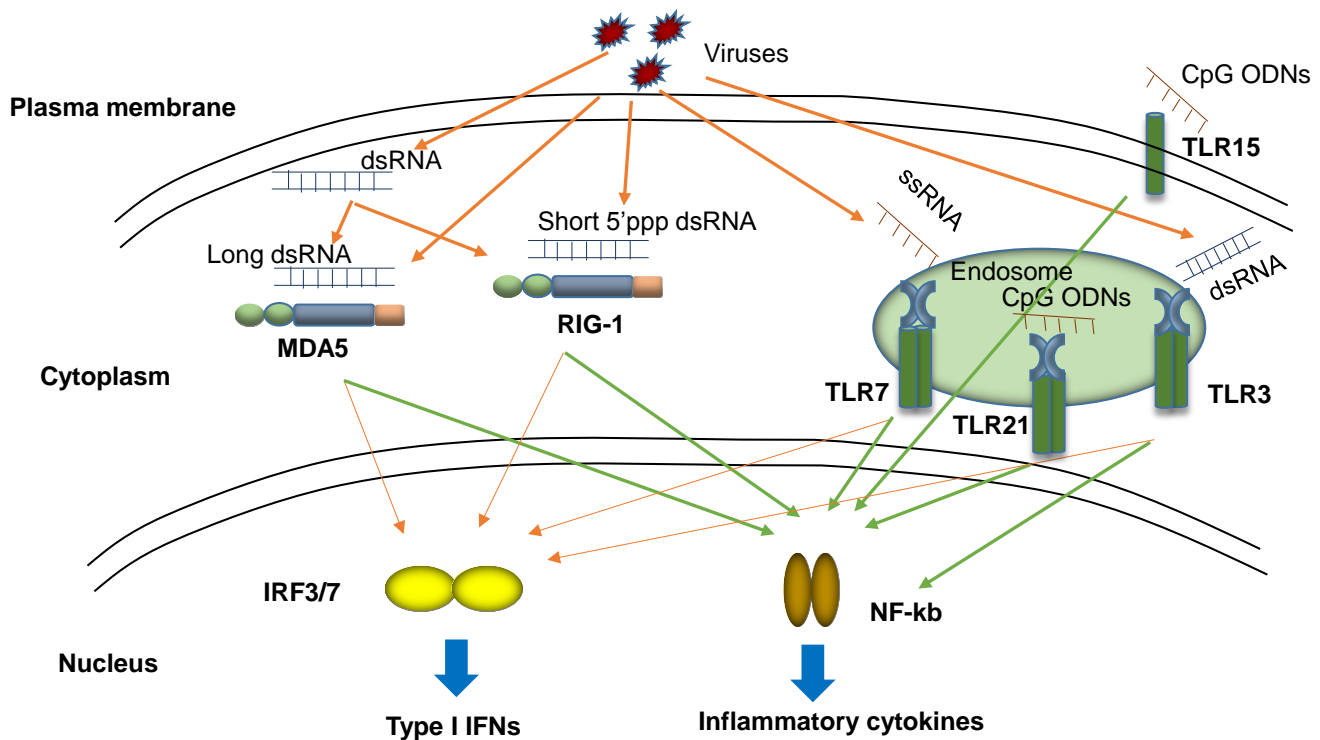


Figure 1.11: Innate immunity in birds. The plasma membrane receptor of TLR15 recognizes CpG-ODN derived from viruses and bacteria. Viral recognition relies on intracellular vesicles of PRR, whose ligands are dsRNA derived from viruses or virus-infected cells (TLR3), ssRNA derived from RNA viruses (TLR7), CpG-ODN (TLR21), short 5'ppp dsRNA (RIG-I), and long dsRNA (MDA5). TLR3, TLR7 and TLR21 localize mainly in the ER in the steady state and traffic to the endosome, where they engage with their ligands. The recognition triggers the downstream signal transduction to activate NF- κ B or IRF3/7, finally induces interferon and inflammatory cytokine production. *The figure and the text were adapted with permission from Figure 1 [293].*

Dose-dependent response of TLR3 against poly I:C was explained by the possibility that poly I:C may interact with other dsRNA binding receptors, which antagonize TLR3 mediated antiviral IFN response [322]. Chicken erythrocytes showed higher induction of pro-inflammatory cytokine IL8 compared to thrombocytes, monocytes or heterophils against poly I:C treatment. IL8 is a chemokine and usually released from macrophages or endothelial cells to attract heterophils and other cells causing them to migrate to the site of infection [390]. This indicates that nucleated erythrocytes may play a significant role in the innate immune defense against pathogens invading the bloodstream or blood borne pathogens

(Figure 1.11). Chicken erythrocytes' function is somewhat similar to leukocytes in birds, albeit there is a lack of evidence that they exhibit phagocytic functions.

1.5.10 Immune stimulants to induce immune pathways

The immune stimulants that are commercially available and used for research purposes are discussed next.

Polyinosinic-polycytidylic acid (poly I:C): poly I:C is an immune stimulant and a synthetic analog for dsRNA virus. It binds to Toll-like receptor TLR3 that is usually expressed at the surfaces of B-cells, macrophages and dendritic cells [391]. Poly I:C from different suppliers and sources varying in length can elicit different immune modulatory pathways. A study reported that the length of poly I:C has a different effect and it is cell type specific [389]. Poly I:C with a smaller molecular weight have greater immune induction potential in myeloid cells as compared to larger molecular weight poly I:C. In contrast, the result was *vice versa* for fibroblast cells [389]. In another report, it was shown that long poly I:C induces antiviral immune response mediated through the MDA-5 pathway [392].

Lipopolysaccharide (LPS): Commercially used immune stimulant LPS is derived from the outer membrane of Gram-negative bacteria *Escherichia coli*. It induces the TLR4-mediated innate immune response and known agonist for TLR4. However, LPS from *P. gingivitis* has been shown to activate the TLR2-mediated immune pathway [393-395]. LPS stimulate rapid NF- κ B activation and production of pro-inflammatory cytokines via MyD88 dependent pathway. However, LPS activated MyD88 independent pathway results in rapid induction of interferon regulatory factor genes and thereby production of IFN β . But NF- κ B activation was delayed in the later pathway [396].

Peptidoglycan (PGN): PGN is derived from a surface component of gram-positive bacteria *Staphylococcus aureus*. It binds to TLR2 to activate NF- κ B and TNF- α mediated immune response. NOD1 and NOD2 pattern recognition receptor can sense PGN through D- γ -glutamyl-meso-DAP dipeptide and muramyl dipeptide respectively [397-402].

CpG oligodeoxynucleotides (CpG ODN): CpG motif from bacterial DNA has potential pathogen-associated molecular patterns (PAMPs) that are lacking in the vertebrate genome. It mediates signal through binding to TLR9 and stimulates pro-inflammatory cytokines. Synthetic ssDNA molecule that mimics bacterial unmethylated CpG dinucleotides (CpG motifs) are commercially available to investigate the immune stimulant property of CpG ODN. Several classes of synthetic CpG ODN has been generated

based on number and location of CpG dimers. They vary in the mechanism in stimulating IFN and TLR9-dependent NF- κ B signaling [403-405].

These immune stimulants are often used as a vaccine adjuvant and therefore the mechanism of action in different cell type needs to be characterized.

1.6 Rationale, hypothesis and study objectives

In chicken polychromatic erythrocytes active/competent genes that are associated with dynamically acetylated histones are soluble at low ionic strength (50–150 mM NaCl). Acetylation is the key feature that prevent histone H1/H5-induced chromatin insolubility for these regions at physiological ionic strength [124, 406]. We applied a powerful chromatin fractionation procedure to isolate the active/competent chromatin from chicken polychromatic erythrocytes. Our findings revealed that salt-soluble polynucleosome chromatin fraction (F1) is enriched in active DNA-sequences, active histone marks, and dynamically acetylated four core histones [282, 291]. Transcriptionally active/poised genes such as β -globin, ϵ globin, histone H5 were enriched in salt soluble polynucleosome chromatin fractions [282]. However, repressed genes such as vitellogenin was depleted in 150 mM NaCl soluble chromatin fractions [282, 407]. **Further, it is important to characterize the chromatin features of genes that are soluble at physiological ionic (F1 chromatin) strength.**

Transcriptionally active chromatin undergo dynamic histone modifications by the opposing activities of two enzymes; HDACs and KATs [408]. HDAC2 is a major histone-modifying enzyme involved in dynamic histone acetylation-deacetylation process along with KATs. Phosphorylated HDAC2 in association with HDAC1 forms Sin3 and NuRD multiprotein complexes that are recruited to the promoter of the target gene and involved in transcriptional regulation [154]. Alternatively, unphosphorylated or monophosphorylated HDAC2 binds to serine/arginine (SR)-rich proteins and the RNA-binding protein Hu antigen R (HuR/ELAVL1) which then assembles into the spliceosome complex within the coding region and hence involved in splicing [163, 166]. **Nevertheless, the chromatin components that retain HDAC2 onto the coding region and the distribution of HDAC2/phosphorylated HDAC2 along active chromatin region are not fully characterized.**

PRMTs are involved in the transfer of a methyl group from SAM to the guanidine nitrogen of arginine. PRMTs catalyze arginine methylation by using a molecule of SAM to form asymmetric (ω -NG, NG-dimethyl- arginine) (Type I) or symmetric (ω -NG, N'G-dimethylarginine) (Type II) or monomethyl arginine [181]. PRMT1 which is a major type I PRMT appears to be critical in maintaining H4R3me2a,

acetylated histones and H3K4me2 as the loss of PRMT1 causes loss of these histone PTMs and disruption of the chicken active β globin domain conformation [23]. PRMT5 is the major type II PRMT, responsible for the symmetric methylation of H4R3me2s (inactive mark) and H3R2me2s (active mark) *in vivo*. H3R2me2s recruits WDR5, which is a subunit of several co-activator complexes that produce H3K4me3 (an active mark) while H3R2me2a (inactive mark by PRMT6) prevents the binding of WDR5 to the site [114, 217]. Thus, methylation of histones by PRMTs can block the docking site for other effector molecules and can interfere with the orchestration of histone PTMs (active marks). Although genome-wide distribution of H3R2me2s has been demonstrated in human and mouse B-cell line [217, 409], **there is no current report on the genome-wide distribution of H4R3me2a. Moreover, the distribution and recruitment of PRMT1 and 5 enzymes yet to be characterized.**

Arginine methylation of H4 by PRMT1 at HS4 barrier site and transcribed gene body of chicken β -globin showed a difference in the distribution of this modification at different developmental stages of erythrocyte cell [23]. Distribution of H4R3 methylation was found to be enriched in HSA regulatory elements near the promoter of the Folate receptor (FR) gene, at the 5'HS4 insulator site and over the HS2 globin locus control region (LCR) in 6C2 cells. In contrast, this mark had a peak at β H promoter in 10-d embryonic erythrocyte cells. This indicates a transcription dependent role of PRMT1 in the regulation of globin domain structure during erythroid differentiation [23, 125]. **Therefore, it is necessary to characterize the distribution of PRMTs and arginine modifications in chromatin fractions.** Previous studies done by Gary Felsenfeld's group showed that PRMT1 was recruited to regulatory regions of the β -globin gene by the transcription factor USF1 [45]. **However, it is currently unknown how PRMT1 and 5 are recruited to the body of transcribed genes.**

Interaction of PRMTs with a wide range of RNA associated proteins indicates the involvement of these enzymes in a splicing-associated event possibly through interaction with RNA [175]. Using 'interactome capture' analysis to define the mRNA interactome in proliferating HeLa cells, the Hentze group reported PRMT1 as one of the candidate RNA binding protein [410]. Recent findings from our lab provided evidence that the chromatin modifiers HDAC1/2 are associated with hnRNP, suggesting via interaction with RNA, HDACs catalyze dynamic histone acetylation along the transcribed gene body [165]. We have previously demonstrated that histone deacetylase is a component of nuclear matrix [281]. **It is possible that similar as HDAC2, PRMT1 and 5 could be targeted to the transcription machineries that are associated with nuclear matrix.**

1.6.1 General hypothesis

The histone-modifying enzymes, HDAC2, PRMT1 and PRMT5, associate with active chromatin regions and are recruited to transcriptionally active chromosomal domains in a RNA-dependent manner. PRMTs establish and maintain active histone PTMs, which are responsible for the open chromatin structure of transcriptionally active chromatin.

Thesis objectives:

Specific objectives of experiments in this thesis are:

- A) To map salt soluble transcriptionally active chromatin domains in the chicken polychromatic erythrocytes.
- B) Genome wide characterization of active histone PTMs in chicken polychromatic erythrocyte.
- C) To characterize the distribution of HDAC2 and HDAC2-S394ph in the transcribed regions of chromatin and to determine the association of HDAC2 to the transcribed region.
- D) To characterize the distribution of PRMTs and their substrates in chicken erythroid cells, and to elucidate the mechanism of PRMTs recruitment to the active chromosomal domains.
- E) To characterize the epigenomic features of immune genes in erythrocyte cells.

1.7 References

1. Luger K, Mader AW, Richmond RK, Sargent DF, Richmond TJ. Crystal structure of the nucleosome core particle at 2.8 Å resolution. *Nature*. 1997;389(6648):251-60. doi: 10.1038/38444. PubMed PMID: 9305837.
2. Tropberger P, Schneider R. Going global: novel histone modifications in the globular domain of H3. *Epigenetics*. 2010;5(2):112-7. PubMed PMID: 20160509.
3. Cosgrove MS, Boeke JD, Wolberger C. Regulated nucleosome mobility and the histone code. *Nat Struct Mol Biol*. 2004;11(11):1037-43. doi: 10.1038/nsmb851. PubMed PMID: 15523479.
4. Allan J, Mitchell T, Harborne N, Bohm L, Crane-Robinson C. Roles of H1 domains in determining higher order chromatin structure and H1 location. *J Mol Biol*. 1986;187(4):591-601. PubMed PMID: 3458926.
5. Izzo A, Kamieniarz K, Schneider R. The histone H1 family: specific members, specific functions? *Biol Chem*. 2008;389(4):333-43. doi: 10.1515/BC.2008.037. PubMed PMID: 18208346.
6. Horn PJ, Peterson CL. Molecular biology. Chromatin higher order folding--wrapping up transcription. *Science*. 2002;297(5588):1824-7. doi: 10.1126/science.1074200. PubMed PMID: 12228709.
7. International Human Genome Sequencing C. Finishing the euchromatic sequence of the human genome. *Nature*. 2004;431(7011):931-45. doi: 10.1038/nature03001. PubMed PMID: 15496913.
8. Cavalli G, Misteli T. Functional implications of genome topology. *Nat Struct Mol Biol*. 2013;20(3):290-9. doi: 10.1038/nsmb.2474. PubMed PMID: 23463314.
9. Lanctot C, Cheutin T, Cremer M, Cavalli G, Cremer T. Dynamic genome architecture in the nuclear space: regulation of gene expression in three dimensions. *Nat Rev Genet*. 2007;8(2):104-15. doi: 10.1038/nrg2041. PubMed PMID: 17230197.
10. Albiez H, Cremer M, Tiberi C, Vecchio L, Schermelleh L, Dittrich S, et al. Chromatin domains and the interchromatin compartment form structurally defined and functionally interacting nuclear networks. *Chromosome Res*. 2006;14(7):707-33. doi: 10.1007/s10577-006-1086-x. PubMed PMID: 17115328.
11. Osborne CS, Chakalova L, Brown KE, Carter D, Horton A, Debrand E, et al. Active genes dynamically colocalize to shared sites of ongoing transcription. *Nat Genet*. 2004;36(10):1065-71. doi: 10.1038/ng1423. PubMed PMID: 15361872.
12. Wei GH, Liu DP, Liang CC. Chromatin domain boundaries: insulators and beyond. *Cell Res*. 2005;15(4):292-300. doi: 10.1038/sj.cr.7290298. PubMed PMID: 15857584.
13. de Wit E, Braunschweig U, Greil F, Bussemaker HJ, van Steensel B. Global chromatin domain organization of the *Drosophila* genome. *PLoS Genet*. 2008;4(3):e1000045. doi: 10.1371/journal.pgen.1000045. PubMed PMID: 18369463; PubMed Central PMCID: PMC2274884.
14. Goldman MA. The chromatin domain as a unit of gene regulation. *Bioessays*. 1988;9(2-3):50-5. doi: 10.1002/bies.950090204. PubMed PMID: 3066357.

15. Oki M, Kamakaka RT. Blockers and barriers to transcription: competing activities? *Curr Opin Cell Biol.* 2002;14(3):299-304. PubMed PMID: 12067651.
16. Barkess G, West AG. Chromatin insulator elements: establishing barriers to set heterochromatin boundaries. *Epigenomics.* 2012;4(1):67-80. doi: 10.2217/epi.11.112. PubMed PMID: 22332659.
17. Geyer PK, Corces VG. DNA position-specific repression of transcription by a *Drosophila* zinc finger protein. *Genes Dev.* 1992;6(10):1865-73. PubMed PMID: 1327958.
18. Kellum R, Schedl P. A position-effect assay for boundaries of higher order chromosomal domains. *Cell.* 1991;64(5):941-50. PubMed PMID: 1848159.
19. Sun FL, Elgin SC. Putting boundaries on silence. *Cell.* 1999;99(5):459-62. PubMed PMID: 10589674.
20. West AG, Gaszner M, Felsenfeld G. Insulators: many functions, many mechanisms. *Genes Dev.* 2002;16(3):271-88. doi: 10.1101/gad.954702. PubMed PMID: 11825869.
21. Yang J, Corces VG. Chromatin insulators: a role in nuclear organization and gene expression. *Adv Cancer Res.* 2011;110:43-76. doi: 10.1016/B978-0-12-386469-7.00003-7. PubMed PMID: 21704228; PubMed Central PMCID: PMC3175007.
22. Ghirlando R, Giles K, Gowher H, Xiao T, Xu Z, Yao H, et al. Chromatin domains, insulators, and the regulation of gene expression. *Biochim Biophys Acta.* 2012;1819(7):644-51. doi: 10.1016/j.bbagr.2012.01.016. PubMed PMID: 22326678; PubMed Central PMCID: PMC3484685.
23. Huang S, Litt M, Felsenfeld G. Methylation of histone H4 by arginine methyltransferase PRMT1 is essential in vivo for many subsequent histone modifications. *Genes Dev.* 2005;19(16):1885-93. doi: 10.1101/gad.1333905. PubMed PMID: 16103216; PubMed Central PMCID: PMC1186188.
24. Bell AC, West AG, Felsenfeld G. Insulators and boundaries: versatile regulatory elements in the eukaryotic genome. *Science.* 2001;291(5503):447-50. PubMed PMID: 11228144.
25. Bell AC, West AG, Felsenfeld G. The protein CTCF is required for the enhancer blocking activity of vertebrate insulators. *Cell.* 1999;98(3):387-96. PubMed PMID: 10458613.
26. Litt MD, Simpson M, Gaszner M, Allis CD, Felsenfeld G. Correlation between histone lysine methylation and developmental changes at the chicken beta-globin locus. *Science.* 2001;293(5539):2453-5. doi: 10.1126/science.1064413. PubMed PMID: 11498546.
27. Lunyak VV. Boundaries. Boundaries...Boundaries??? *Curr Opin Cell Biol.* 2008;20(3):281-7. doi: 10.1016/j.ceb.2008.03.018. PubMed PMID: 18524562.
28. Bushey AM, Dorman ER, Corces VG. Chromatin insulators: regulatory mechanisms and epigenetic inheritance. *Mol Cell.* 2008;32(1):1-9. doi: 10.1016/j.molcel.2008.08.017. PubMed PMID: 18851828; PubMed Central PMCID: PMC2576288.
29. Maeda RK, Karch F. Making connections: boundaries and insulators in *Drosophila*. *Curr Opin Genet Dev.* 2007;17(5):394-9. doi: 10.1016/j.gde.2007.08.002. PubMed PMID: 17904351.
30. Raab JR, Kamakaka RT. Insulators and promoters: closer than we think. *Nat Rev Genet.* 2010;11(6):439-46. doi: 10.1038/nrg2765. PubMed PMID: 20442713; PubMed Central PMCID: PMC3477808.

31. Raab JR, Chiu J, Zhu J, Katzman S, Kurukuti S, Wade PA, et al. Human tRNA genes function as chromatin insulators. *EMBO J.* 2012;31(2):330-50. doi: 10.1038/emboj.2011.406. PubMed PMID: 22085927; PubMed Central PMCID: PMC3261562.
32. Wang J, Lunyak VV, Jordan IK. Genome-wide prediction and analysis of human chromatin boundary elements. *Nucleic Acids Res.* 2012;40(2):511-29. doi: 10.1093/nar/gkr750. PubMed PMID: 21930510; PubMed Central PMCID: PMC3258141.
33. Yocum AO, Steiner LA, Seidel NE, Cline AP, Rout ED, Lin JY, et al. A tissue-specific chromatin loop activates the erythroid ankyrin-1 promoter. *Blood.* 2012;120(17):3586-93. doi: 10.1182/blood-2012-08-450262. PubMed PMID: 22968456; PubMed Central PMCID: PMC3482866.
34. Zhou J, Berger SL. Good fences make good neighbors: barrier elements and genomic regulation. *Mol Cell.* 2004;16(4):500-2. doi: 10.1016/j.molcel.2004.11.005. PubMed PMID: 15546609.
35. Filippova GN, Fagerlie S, Klenova EM, Myers C, Dehner Y, Goodwin G, et al. An exceptionally conserved transcriptional repressor, CTCF, employs different combinations of zinc fingers to bind diverged promoter sequences of avian and mammalian c-myc oncogenes. *Mol Cell Biol.* 1996;16(6):2802-13. PubMed PMID: 8649389; PubMed Central PMCID: PMC3231272.
36. Rubio ED, Reiss DJ, Welch PL, Distèche CM, Filippova GN, Baliga NS, et al. CTCF physically links cohesin to chromatin. *Proc Natl Acad Sci U S A.* 2008;105(24):8309-14. doi: 10.1073/pnas.0801273105. PubMed PMID: 18550811; PubMed Central PMCID: PMC2448833.
37. Lobanekov VV, Nicolas RH, Adler VV, Paterson H, Klenova EM, Polotskaja AV, et al. A novel sequence-specific DNA binding protein which interacts with three regularly spaced direct repeats of the CCCTC-motif in the 5'-flanking sequence of the chicken c-myc gene. *Oncogene.* 1990;5(12):1743-53. PubMed PMID: 2284094.
38. Ohlsson R, Renkawitz R, Lobanekov V. CTCF is a uniquely versatile transcription regulator linked to epigenetics and disease. *Trends Genet.* 2001;17(9):520-7. PubMed PMID: 11525835.
39. Phillips JE, Corces VG. CTCF: master weaver of the genome. *Cell.* 2009;137(7):1194-211. doi: 10.1016/j.cell.2009.06.001. PubMed PMID: 19563753; PubMed Central PMCID: PMC3040116.
40. Groenen PM, Garcia E, Debeer P, Devriendt K, Fryns JP, Van de Ven WJ. Structure, sequence, and chromosome 19 localization of human USF2 and its rearrangement in a patient with multicystic renal dysplasia. *Genomics.* 1996;38(2):141-8. PubMed PMID: 8954795.
41. Shieh BH, Sparkes RS, Gaynor RB, Lusk AJ. Localization of the gene-encoding upstream stimulatory factor (USF) to human chromosome 1q22-q23. *Genomics.* 1993;16(1):266-8. doi: 10.1006/geno.1993.1174. PubMed PMID: 8486371.
42. West AG, Huang S, Gaszner M, Litt MD, Felsenfeld G. Recruitment of histone modifications by USF proteins at a vertebrate barrier element. *Mol Cell.* 2004;16(3):453-63. doi: 10.1016/j.molcel.2004.10.005. PubMed PMID: 15525517.
43. Bresnick EH, Felsenfeld G. Evidence that the transcription factor USF is a component of the human beta-globin locus control region heteromeric protein complex. *J Biol Chem.* 1993;268(25):18824-34. PubMed PMID: 8360172.

44. Leach KM, Vieira KF, Kang SH, Aslanian A, Teichmann M, Roeder RG, et al. Characterization of the human beta-globin downstream promoter region. *Nucleic Acids Res.* 2003;31(4):1292-301. PubMed PMID: 12582249; PubMed Central PMCID: PMCPMC150227.
45. Huang S, Li X, Yusufzai TM, Qiu Y, Felsenfeld G. USF1 recruits histone modification complexes and is critical for maintenance of a chromatin barrier. *Mol Cell Biol.* 2007;27(22):7991-8002. doi: 10.1128/MCB.01326-07. PubMed PMID: 17846119; PubMed Central PMCID: PMCPMC2169148.
46. Dickson J, Gowher H, Strogantsev R, Gaszner M, Hair A, Felsenfeld G, et al. VEZF1 elements mediate protection from DNA methylation. *PLoS Genet.* 2010;6(1):e1000804. doi: 10.1371/journal.pgen.1000804. PubMed PMID: 20062523; PubMed Central PMCID: PMCPMC2795164.
47. Simms TA, Dugas SL, Gremillion JC, Ibos ME, Dandurand MN, Toliver TT, et al. TFIIC binding sites function as both heterochromatin barriers and chromatin insulators in *Saccharomyces cerevisiae*. *Eukaryot Cell.* 2008;7(12):2078-86. doi: 10.1128/EC.00128-08. PubMed PMID: 18849469; PubMed Central PMCID: PMCPMC2593192.
48. Oettel S, Kober I, Seifart KH. The activity binding to the termination region of several pol III genes represents a separate entity and is distinct from a novel component enhancing U6 snRNA transcription. *Nucleic Acids Res.* 1998;26(19):4324-31. PubMed PMID: 9742231; PubMed Central PMCID: PMCPMC147850.
49. Nakao M, Sasaki H. Genomic imprinting: significance in development and diseases and the molecular mechanisms. *J Biochem.* 1996;120(3):467-73. PubMed PMID: 8902605.
50. Banerjee S, Smallwood A. A chromatin model of IGF2/H19 imprinting. *Nat Genet.* 1995;11(3):237-8. doi: 10.1038/ng1195-237. PubMed PMID: 7581444.
51. Brenton JD, Drewell RA, Viville S, Hilton KJ, Barton SC, Ainscough JF, et al. A silencer element identified in *Drosophila* is required for imprinting of H19 reporter transgenes in mice. *Proc Natl Acad Sci U S A.* 1999;96(16):9242-7. PubMed PMID: 10430927; PubMed Central PMCID: PMCPMC17764.
52. Kanduri C, Holmgren C, Pilartz M, Franklin G, Kanduri M, Liu L, et al. The 5' flank of mouse H19 in an unusual chromatin conformation unidirectionally blocks enhancer-promoter communication. *Curr Biol.* 2000;10(8):449-57. PubMed PMID: 10801414.
53. Bell AC, Felsenfeld G. Methylation of a CTCF-dependent boundary controls imprinted expression of the *Igf2* gene. *Nature.* 2000;405(6785):482-5. doi: 10.1038/35013100. PubMed PMID: 10839546.
54. Hark AT, Schoenherr CJ, Katz DJ, Ingram RS, Levorse JM, Tilghman SM. CTCF mediates methylation-sensitive enhancer-blocking activity at the H19/*Igf2* locus. *Nature.* 2000;405(6785):486-9. doi: 10.1038/35013106. PubMed PMID: 10839547.
55. Szabo P, Tang SH, Rentsendorj A, Pfeifer GP, Mann JR. Maternal-specific footprints at putative CTCF sites in the H19 imprinting control region give evidence for insulator function. *Curr Biol.* 2000;10(10):607-10. PubMed PMID: 10837224.
56. Kanduri C, Pant V, Loukinov D, Pugacheva E, Qi CF, Wolffe A, et al. Functional association of CTCF with the insulator upstream of the H19 gene is parent of origin-specific and methylation-sensitive. *Curr Biol.* 2000;10(14):853-6. PubMed PMID: 10899010.

57. Holmgren C, Kanduri C, Dell G, Ward A, Mukhopadhyaya R, Kanduri M, et al. CpG methylation regulates the Igf2/H19 insulator. *Curr Biol.* 2001;11(14):1128-30. PubMed PMID: 11509237.
58. Eden S, Constancia M, Hashimshony T, Dean W, Goldstein B, Johnson AC, et al. An upstream repressor element plays a role in Igf2 imprinting. *EMBO J.* 2001;20(13):3518-25. doi: 10.1093/emboj/20.13.3518. PubMed PMID: 11432838; PubMed Central PMCID: PMC125515.
59. Constancia M, Dean W, Lopes S, Moore T, Kelsey G, Reik W. Deletion of a silencer element in Igf2 results in loss of imprinting independent of H19. *Nat Genet.* 2000;26(2):203-6. doi: 10.1038/79930. PubMed PMID: 11017078.
60. Murrell A, Heeson S, Bowden L, Constancia M, Dean W, Kelsey G, et al. An intragenic methylated region in the imprinted Igf2 gene augments transcription. *EMBO Rep.* 2001;2(12):1101-6. doi: 10.1093/embo-reports/kve248. PubMed PMID: 11743023; PubMed Central PMCID: PMC1084166.
61. Pant V, Kurukuti S, Pugacheva E, Shamsuddin S, Mariano P, Renkawitz R, et al. Mutation of a single CTCF target site within the H19 imprinting control region leads to loss of Igf2 imprinting and complex patterns of de novo methylation upon maternal inheritance. *Mol Cell Biol.* 2004;24(8):3497-504. PubMed PMID: 15060168; PubMed Central PMCID: PMC1381662.
62. Pant V, Mariano P, Kanduri C, Mattsson A, Lobanenko V, Heuchel R, et al. The nucleotides responsible for the direct physical contact between the chromatin insulator protein CTCF and the H19 imprinting control region manifest parent of origin-specific long-distance insulation and methylation-free domains. *Genes Dev.* 2003;17(5):586-90. doi: 10.1101/gad.254903. PubMed PMID: 12629040; PubMed Central PMCID: PMC196004.
63. Schoenherr CJ, Levorse JM, Tilghman SM. CTCF maintains differential methylation at the Igf2/H19 locus. *Nat Genet.* 2003;33(1):66-9. doi: 10.1038/ng1057. PubMed PMID: 12461525.
64. Rand E, Ben-Porath I, Keshet I, Cedar H. CTCF elements direct allele-specific undermethylation at the imprinted H19 locus. *Curr Biol.* 2004;14(11):1007-12. doi: 10.1016/j.cub.2004.05.041. PubMed PMID: 15182675.
65. Chao W, Huynh KD, Spencer RJ, Davidow LS, Lee JT. CTCF, a candidate trans-acting factor for X-inactivation choice. *Science.* 2002;295(5553):345-7. doi: 10.1126/science.1065982. PubMed PMID: 11743158.
66. Chung JH, Whiteley M, Felsenfeld G. A 5' element of the chicken beta-globin domain serves as an insulator in human erythroid cells and protects against position effect in *Drosophila*. *Cell.* 1993;74(3):505-14. PubMed PMID: 8348617.
67. Pikaart MJ, Recillas-Targa F, Felsenfeld G. Loss of transcriptional activity of a transgene is accompanied by DNA methylation and histone deacetylation and is prevented by insulators. *Genes Dev.* 1998;12(18):2852-62. PubMed PMID: 9744862; PubMed Central PMCID: PMC1317165.
68. Recillas-Targa F, Pikaart MJ, Burgess-Beusse B, Bell AC, Litt MD, West AG, et al. Position-effect protection and enhancer blocking by the chicken beta-globin insulator are separable activities. *Proc Natl Acad Sci U S A.* 2002;99(10):6883-8. doi: 10.1073/pnas.102179399. PubMed PMID: 12011446; PubMed Central PMCID: PMC124498.

69. Rincon-Arano H, Furlan-Magaril M, Recillas-Targa F. Protection against telomeric position effects by the chicken *CHS4* beta-globin insulator. *Proc Natl Acad Sci U S A*. 2007;104(35):14044-9. doi: 10.1073/pnas.0704999104. PubMed PMID: 17715059; PubMed Central PMCID: PMC1955792.
70. Prioleau MN, Nony P, Simpson M, Felsenfeld G. An insulator element and condensed chromatin region separate the chicken beta-globin locus from an independently regulated erythroid-specific folate receptor gene. *EMBO J*. 1999;18(14):4035-48. doi: 10.1093/emboj/18.14.4035. PubMed PMID: 10406808; PubMed Central PMCID: PMC1171479.
71. Saitoh N, Bell AC, Recillas-Targa F, West AG, Simpson M, Pikaart M, et al. Structural and functional conservation at the boundaries of the chicken beta-globin domain. *EMBO J*. 2000;19(10):2315-22. doi: 10.1093/emboj/19.10.2315. PubMed PMID: 10811622; PubMed Central PMCID: PMC1384375.
72. Li X, Wang S, Li Y, Deng C, Steiner LA, Xiao H, et al. Chromatin boundaries require functional collaboration between the hSET1 and NURF complexes. *Blood*. 2011;118(5):1386-94. doi: 10.1182/blood-2010-11-319111. PubMed PMID: 21653943; PubMed Central PMCID: PMC3152501.
73. Amouyal M. Gene insulation. Part II: natural strategies in vertebrates. *Biochem Cell Biol*. 2010;88(6):885-98. doi: 10.1139/O10-111. PubMed PMID: 21102651.
74. Farrell CM, Grinberg A, Huang SP, Chen D, Pichel JG, Westphal H, et al. A large upstream region is not necessary for gene expression or hypersensitive site formation at the mouse beta-globin locus. *Proc Natl Acad Sci U S A*. 2000;97(26):14554-9. doi: 10.1073/pnas.97.26.14554. PubMed PMID: 11121056; PubMed Central PMCID: PMC118957.
75. Li Q, Zhang M, Han H, Rohde A, Stamatoyannopoulos G. Evidence that DNase I hypersensitive site 5 of the human beta-globin locus control region functions as a chromosomal insulator in transgenic mice. *Nucleic Acids Res*. 2002;30(11):2484-91. PubMed PMID: 12034837; PubMed Central PMCID: PMC117184.
76. Driscoll MC, Dobkin CS, Alter BP. Gamma delta beta-thalassemia due to a de novo mutation deleting the 5' beta-globin gene activation-region hypersensitive sites. *Proc Natl Acad Sci U S A*. 1989;86(19):7470-4. PubMed PMID: 2798417; PubMed Central PMCID: PMC298086.
77. Bulger M, Schubeler D, Bender MA, Hamilton J, Farrell CM, Hardison RC, et al. A complex chromatin landscape revealed by patterns of nuclease sensitivity and histone modification within the mouse beta-globin locus. *Mol Cell Biol*. 2003;23(15):5234-44. PubMed PMID: 12861010; PubMed Central PMCID: PMC165715.
78. Bender MA, Byron R, Ragozy T, Telling A, Bulger M, Groudine M. Flanking HS-62.5 and 3' HS1, and regions upstream of the LCR, are not required for beta-globin transcription. *Blood*. 2006;108(4):1395-401. doi: 10.1182/blood-2006-04-014431. PubMed PMID: 16645164; PubMed Central PMCID: PMC1895883.
79. Bulger M, van Doorninck JH, Saitoh N, Telling A, Farrell C, Bender MA, et al. Conservation of sequence and structure flanking the mouse and human beta-globin loci: the beta-globin genes are embedded within an array of odorant receptor genes. *Proc Natl Acad Sci U S A*. 1999;96(9):5129-34. PubMed PMID: 10220430; PubMed Central PMCID: PMC121828.

80. Farrell CM, West AG, Felsenfeld G. Conserved CTCF insulator elements flank the mouse and human beta-globin loci. *Mol Cell Biol.* 2002;22(11):3820-31. PubMed PMID: 11997516; PubMed Central PMCID: PMCPMC133827.
81. Mishiro T, Ishihara K, Hino S, Tsutsumi S, Aburatani H, Shirahige K, et al. Architectural roles of multiple chromatin insulators at the human apolipoprotein gene cluster. *EMBO J.* 2009;28(9):1234-45. doi: 10.1038/emboj.2009.81. PubMed PMID: 19322193; PubMed Central PMCID: PMCPMC2683055.
82. Lai CQ, Parnell LD, Ordovas JM. The APOA1/C3/A4/A5 gene cluster, lipid metabolism and cardiovascular disease risk. *Curr Opin Lipidol.* 2005;16(2):153-66. PubMed PMID: 15767855.
83. Dieci G, Fiorino G, Castelnuovo M, Teichmann M, Pagano A. The expanding RNA polymerase III transcriptome. *Trends Genet.* 2007;23(12):614-22. doi: 10.1016/j.tig.2007.09.001. PubMed PMID: 17977614.
84. Geiduschek EP, Kassavetis GA. The RNA polymerase III transcription apparatus. *J Mol Biol.* 2001;310(1):1-26. doi: 10.1006/jmbi.2001.4732. PubMed PMID: 11419933.
85. Schramm L, Hernandez N. Recruitment of RNA polymerase III to its target promoters. *Genes Dev.* 2002;16(20):2593-620. doi: 10.1101/gad.1018902. PubMed PMID: 12381659.
86. Donze D, Kamakaka RT. RNA polymerase III and RNA polymerase II promoter complexes are heterochromatin barriers in *Saccharomyces cerevisiae*. *EMBO J.* 2001;20(3):520-31. doi: 10.1093/emboj/20.3.520. PubMed PMID: 11157758; PubMed Central PMCID: PMCPMC133458.
87. Noma K, Cam HP, Maraia RJ, Grewal SI. A role for TFIIC transcription factor complex in genome organization. *Cell.* 2006;125(5):859-72. doi: 10.1016/j.cell.2006.04.028. PubMed PMID: 16751097.
88. Biswas M, Maqani N, Rai R, Kumaran SP, Iyer KR, Sendinc E, et al. Limiting the extent of the RDN1 heterochromatin domain by a silencing barrier and Sir2 protein levels in *Saccharomyces cerevisiae*. *Mol Cell Biol.* 2009;29(10):2889-98. doi: 10.1128/MCB.00728-08. PubMed PMID: 19289503; PubMed Central PMCID: PMCPMC2682026.
89. Lunnyak VV, Prefontaine GG, Nunez E, Cramer T, Ju BG, Ohgi KA, et al. Developmentally regulated activation of a SINE B2 repeat as a domain boundary in organogenesis. *Science.* 2007;317(5835):248-51. doi: 10.1126/science.1140871. PubMed PMID: 17626886.
90. Scott KC, Merrett SL, Willard HF. A heterochromatin barrier partitions the fission yeast centromere into discrete chromatin domains. *Curr Biol.* 2006;16(2):119-29. doi: 10.1016/j.cub.2005.11.065. PubMed PMID: 16431364.
91. McNairn AJ, Gerton JL. The chromosome glue gets a little stickier. *Trends Genet.* 2008;24(8):382-9. doi: 10.1016/j.tig.2008.06.002. PubMed PMID: 18602182.
92. Hoeffler WK, Roeder RG. Enhancement of RNA polymerase III transcription by the E1A gene product of adenovirus. *Cell.* 1985;41(3):955-63. PubMed PMID: 4005953.
93. Felton-Edkins ZA, Kenneth NS, Brown TR, Daly NL, Gomez-Roman N, Grandori C, et al. Direct regulation of RNA polymerase III transcription by RB, p53 and c-Myc. *Cell Cycle.* 2003;2(3):181-4. PubMed PMID: 12734418.
94. Oler AJ, Alla RK, Roberts DN, Wong A, Hollenhorst PC, Chandler KJ, et al. Human RNA polymerase III transcriptomes and relationships to Pol II promoter chromatin and enhancer-binding

factors. *Nat Struct Mol Biol.* 2010;17(5):620-8. doi: 10.1038/nsmb.1801. PubMed PMID: 20418882; PubMed Central PMCID: PMCPMC2945309.

95. Woiwode A, Johnson SA, Zhong S, Zhang C, Roeder RG, Teichmann M, et al. PTEN represses RNA polymerase III-dependent transcription by targeting the TFIIB complex. *Mol Cell Biol.* 2008;28(12):4204-14. doi: 10.1128/MCB.01912-07. PubMed PMID: 18391023; PubMed Central PMCID: PMCPMC2423115.

96. Blau CA, Stamatoyannopoulos G. Hemoglobin switching and its clinical implications. *Curr Opin Hematol.* 1994;1(2):136-42. PubMed PMID: 9371272.

97. Curtin P, Pirastu M, Kan YW, Gobert-Jones JA, Stephens AD, Lehmann H. A distant gene deletion affects beta-globin gene function in an atypical gamma delta beta-thalassemia. *J Clin Invest.* 1985;76(4):1554-8. doi: 10.1172/JCI112136. PubMed PMID: 2997283; PubMed Central PMCID: PMCPMC424127.

98. Forrester WC, Epner E, Driscoll MC, Enver T, Brice M, Papayannopoulou T, et al. A deletion of the human beta-globin locus activation region causes a major alteration in chromatin structure and replication across the entire beta-globin locus. *Genes Dev.* 1990;4(10):1637-49. PubMed PMID: 2249769.

99. Taramelli R, Kioussis D, Vanin E, Bartram K, Groffen J, Hurst J, et al. Gamma delta beta-thalassaemias 1 and 2 are the result of a 100 kbp deletion in the human beta-globin cluster. *Nucleic Acids Res.* 1986;14(17):7017-29. PubMed PMID: 3763397; PubMed Central PMCID: PMCPMC311714.

100. Eber S, Lux SE. Hereditary spherocytosis--defects in proteins that connect the membrane skeleton to the lipid bilayer. *Semin Hematol.* 2004;41(2):118-41. PubMed PMID: 15071790.

101. Perrotta S, Gallagher PG, Mohandas N. Hereditary spherocytosis. *Lancet.* 2008;372(9647):1411-26. doi: 10.1016/S0140-6736(08)61588-3. PubMed PMID: 18940465.

102. Gallagher PG. Hematologically important mutations: ankyrin variants in hereditary spherocytosis. *Blood Cells Mol Dis.* 2005;35(3):345-7. doi: 10.1016/j.bcmd.2005.08.008. PubMed PMID: 16223590.

103. Gallagher PG, Steiner LA, Liem RI, Owen AN, Cline AP, Seidel NE, et al. Mutation of a barrier insulator in the human ankyrin-1 gene is associated with hereditary spherocytosis. *J Clin Invest.* 2010;120(12):4453-65. doi: 10.1172/JCI42240. PubMed PMID: 21099109; PubMed Central PMCID: PMCPMC2993586.

104. Vostrov AA, Quitschke WW. The zinc finger protein CTCF binds to the APBbeta domain of the amyloid beta-protein precursor promoter. Evidence for a role in transcriptional activation. *J Biol Chem.* 1997;272(52):33353-9. PubMed PMID: 9407128.

105. Qi CF, Martensson A, Mattioli M, Dalla-Favera R, Lobanenko VV, Morse HC, 3rd. CTCF functions as a critical regulator of cell-cycle arrest and death after ligation of the B cell receptor on immature B cells. *Proc Natl Acad Sci U S A.* 2003;100(2):633-8. doi: 10.1073/pnas.0237127100. PubMed PMID: 12524457; PubMed Central PMCID: PMCPMC141048.

106. Aulmann S, Blaker H, Penzel R, Rieker RJ, Otto HF, Sinn HP. CTCF gene mutations in invasive ductal breast cancer. *Breast Cancer Res Treat.* 2003;80(3):347-52. doi: 10.1023/A:1024930404629. PubMed PMID: 14503807.

107. Docquier F, Farrar D, D'Arcy V, Chernukhin I, Robinson AF, Loukinov D, et al. Heightened expression of CTCF in breast cancer cells is associated with resistance to apoptosis. *Cancer Res.* 2005;65(12):5112-22. doi: 10.1158/0008-5472.CAN-03-3498. PubMed PMID: 15958555.
108. Li B, Carey M, Workman JL. The role of chromatin during transcription. *Cell.* 2007;128(4):707-19. doi: 10.1016/j.cell.2007.01.015. PubMed PMID: 17320508.
109. Musselman CA, Lalonde ME, Cote J, Kutateladze TG. Perceiving the epigenetic landscape through histone readers. *Nat Struct Mol Biol.* 2012;19(12):1218-27. doi: 10.1038/nsmb.2436. PubMed PMID: 23211769; PubMed Central PMCID: PMC3645987.
110. Tarakhovskiy A. Tools and landscapes of epigenetics. *Nat Immunol.* 2010;11(7):565-8. doi: 10.1038/ni0710-565. PubMed PMID: 20562839.
111. Lee JS, Smith E, Shilatifard A. The language of histone crosstalk. *Cell.* 2010;142(5):682-5. doi: 10.1016/j.cell.2010.08.011. PubMed PMID: 20813257; PubMed Central PMCID: PMC3711869.
112. Zhang T, Cooper S, Brockdorff N. The interplay of histone modifications - writers that read. *EMBO Rep.* 2015;16(11):1467-81. doi: 10.15252/embr.201540945. PubMed PMID: 26474904; PubMed Central PMCID: PMC4641500.
113. Cheung P, Tanner KG, Cheung WL, Sassone-Corsi P, Denu JM, Allis CD. Synergistic coupling of histone H3 phosphorylation and acetylation in response to epidermal growth factor stimulation. *Mol Cell.* 2000;5(6):905-15. PubMed PMID: 10911985.
114. Guccione E, Bassi C, Casadio F, Martinato F, Cesaroni M, Schuchlantz H, et al. Methylation of histone H3R2 by PRMT6 and H3K4 by an MLL complex are mutually exclusive. *Nature.* 2007;449(7164):933-7. doi: 10.1038/nature06166. PubMed PMID: 17898714.
115. Zamudio NM, Chong S, O'Bryan MK. Epigenetic regulation in male germ cells. *Reproduction.* 2008;136(2):131-46. doi: 10.1530/REP-07-0576. PubMed PMID: 18515312.
116. Allfrey V, Faulkner R, Mirsky A. Acetylation and methylation of histones and their possible role in the regulation of RNA synthesis. *Proceedings of the National Academy of Sciences.* 1964;51(5):786-94.
117. Candido EP, Reeves R, Davie JR. Sodium butyrate inhibits histone deacetylation in cultured cells. *Cell.* 1978;14(1):105-13. PubMed PMID: 667927.
118. Vidali G, Boffa LC, Bradbury EM, Allfrey VG. Butyrate suppression of histone deacetylation leads to accumulation of multiacetylated forms of histones H3 and H4 and increased DNase I sensitivity of the associated DNA sequences. *Proc Natl Acad Sci U S A.* 1978;75(5):2239-43. PubMed PMID: 276864; PubMed Central PMCID: PMC392527.
119. Hebbes TR, Thorne AW, Crane-Robinson C. A direct link between core histone acetylation and transcriptionally active chromatin. *EMBO J.* 1988;7(5):1395-402. PubMed PMID: 3409869; PubMed Central PMCID: PMC458389.
120. Brownell JE, Allis CD. An activity gel assay detects a single, catalytically active histone acetyltransferase subunit in *Tetrahymena* macronuclei. *Proc Natl Acad Sci U S A.* 1995;92(14):6364-8. PubMed PMID: 7603997; PubMed Central PMCID: PMC41518.
121. Davie JR, Chadee DN. Regulation and regulatory parameters of histone modifications. *J Cell Biochem Suppl.* 1998;30-31:203-13. PubMed PMID: 9893272.

122. Davie JR, Spencer VA. Control of histone modifications. *J Cell Biochem.* 1999;Suppl 32-33:141-8. PubMed PMID: 10629113.
123. Spencer VA, Davie JR. Role of covalent modifications of histones in regulating gene expression. *Gene.* 1999;240(1):1-12. PubMed PMID: 10564807.
124. Ridsdale JA, Hendzel MJ, Delcuve GP, Davie JR. Histone acetylation alters the capacity of the H1 histones to condense transcriptionally active/competent chromatin. *J Biol Chem.* 1990;265(9):5150-6. PubMed PMID: 2318888.
125. Schneider R, Bannister AJ, Myers FA, Thorne AW, Crane-Robinson C, Kouzarides T. Histone H3 lysine 4 methylation patterns in higher eukaryotic genes. *Nat Cell Biol.* 2004;6(1):73-7. doi: 10.1038/ncb1076. PubMed PMID: 14661024.
126. Jackson JP, Johnson L, Jasencakova Z, Zhang X, PerezBurgos L, Singh PB, et al. Dimethylation of histone H3 lysine 9 is a critical mark for DNA methylation and gene silencing in *Arabidopsis thaliana*. *Chromosoma.* 2004;112(6):308-15. doi: 10.1007/s00412-004-0275-7. PubMed PMID: 15014946.
127. Zhang K, Dent SY. Histone modifying enzymes and cancer: going beyond histones. *J Cell Biochem.* 2005;96(6):1137-48. doi: 10.1002/jcb.20615. PubMed PMID: 16173079.
128. Wu SC, Zhang Y. Minireview: role of protein methylation and demethylation in nuclear hormone signaling. *Mol Endocrinol.* 2009;23(9):1323-34. doi: 10.1210/me.2009-0131. PubMed PMID: 19407220; PubMed Central PMCID: PMCPMC2737564.
129. Yang Y, Bedford MT. Protein arginine methyltransferases and cancer. *Nat Rev Cancer.* 2013;13(1):37-50. doi: 10.1038/nrc3409. PubMed PMID: 23235912.
130. Feng Q, Wang H, Ng HH, Erdjument-Bromage H, Tempst P, Struhl K, et al. Methylation of H3-lysine 79 is mediated by a new family of HMTases without a SET domain. *Curr Biol.* 2002;12(12):1052-8. PubMed PMID: 12123582.
131. Helin K, Dhanak D. Chromatin proteins and modifications as drug targets. *Nature.* 2013;502(7472):480-8. doi: 10.1038/nature12751. PubMed PMID: 24153301.
132. Chen D, Ma H, Hong H, Koh SS, Huang SM, Schurter BT, et al. Regulation of transcription by a protein methyltransferase. *Science.* 1999;284(5423):2174-7. PubMed PMID: 10381882.
133. Vossenaar ER, Zendman AJ, van Venrooij WJ, Pruijn GJ. PAD, a growing family of citrullinating enzymes: genes, features and involvement in disease. *Bioessays.* 2003;25(11):1106-18. doi: 10.1002/bies.10357. PubMed PMID: 14579251.
134. Witalison EE, Thompson PR, Hofseth LJ. Protein Arginine Deiminases and Associated Citrullination: Physiological Functions and Diseases Associated with Dysregulation. *Curr Drug Targets.* 2015;16(7):700-10. PubMed PMID: 25642720; PubMed Central PMCID: PMCPMC4520219.
135. Zhang X, Bolt M, Guertin MJ, Chen W, Zhang S, Cherrington BD, et al. Peptidylarginine deiminase 2-catalyzed histone H3 arginine 26 citrullination facilitates estrogen receptor alpha target gene activation. *Proc Natl Acad Sci U S A.* 2012;109(33):13331-6. doi: 10.1073/pnas.1203280109. PubMed PMID: 22853951; PubMed Central PMCID: PMCPMC3421185.
136. Wang Y, Wysocka J, Sayegh J, Lee YH, Perlin JR, Leonelli L, et al. Human PAD4 regulates histone arginine methylation levels via demethyliminium. *Science.* 2004;306(5694):279-83. doi: 10.1126/science.1101400. PubMed PMID: 15345777.

137. Chang B, Chen Y, Zhao Y, Bruick RK. JMJD6 is a histone arginine demethylase. *Science*. 2007;318(5849):444-7. doi: 10.1126/science.1145801. PubMed PMID: 17947579.
138. Liu W, Ma Q, Wong K, Li W, Ohgi K, Zhang J, et al. Brd4 and JMJD6-associated anti-pause enhancers in regulation of transcriptional pause release. *Cell*. 2013;155(7):1581-95. doi: 10.1016/j.cell.2013.10.056. PubMed PMID: 24360279; PubMed Central PMCID: PMC3886918.
139. Rossetto D, Avvakumov N, Cote J. Histone phosphorylation: a chromatin modification involved in diverse nuclear events. *Epigenetics*. 2012;7(10):1098-108. doi: 10.4161/epi.21975. PubMed PMID: 22948226; PubMed Central PMCID: PMC3469451.
140. van Attikum H, Gasser SM. The histone code at DNA breaks: a guide to repair? *Nat Rev Mol Cell Biol*. 2005;6(10):757-65. doi: 10.1038/nrm1737. PubMed PMID: 16167054.
141. Choi HS, Choi BY, Cho YY, Mizuno H, Kang BS, Bode AM, et al. Phosphorylation of histone H3 at serine 10 is indispensable for neoplastic cell transformation. *Cancer Res*. 2005;65(13):5818-27. doi: 10.1158/0008-5472.CAN-05-0197. PubMed PMID: 15994958; PubMed Central PMCID: PMC2227263.
142. Wei Y, Mizzen CA, Cook RG, Gorovsky MA, Allis CD. Phosphorylation of histone H3 at serine 10 is correlated with chromosome condensation during mitosis and meiosis in *Tetrahymena*. *Proc Natl Acad Sci U S A*. 1998;95(13):7480-4. PubMed PMID: 9636175; PubMed Central PMCID: PMC22657.
143. Ajiro K. Histone H2B phosphorylation in mammalian apoptotic cells. An association with DNA fragmentation. *J Biol Chem*. 2000;275(1):439-43. PubMed PMID: 10617636.
144. Clayton AL, Mahadevan LC. MAP kinase-mediated phosphoacetylation of histone H3 and inducible gene regulation. *FEBS Lett*. 2003;546(1):51-8. PubMed PMID: 12829236.
145. Cerutti H, Casas-Mollano JA. Histone H3 phosphorylation: universal code or lineage specific dialects? *Epigenetics*. 2009;4(2):71-5. PubMed PMID: 19242092.
146. Fischle W, Wang Y, Allis CD. Histone and chromatin cross-talk. *Curr Opin Cell Biol*. 2003;15(2):172-83. PubMed PMID: 12648673.
147. Lo WS, Trievel RC, Rojas JR, Duggan L, Hsu JY, Allis CD, et al. Phosphorylation of serine 10 in histone H3 is functionally linked in vitro and in vivo to Gcn5-mediated acetylation at lysine 14. *Mol Cell*. 2000;5(6):917-26. PubMed PMID: 10911986.
148. Cao J, Yan Q. Histone ubiquitination and deubiquitination in transcription, DNA damage response, and cancer. *Front Oncol*. 2012;2:26. doi: 10.3389/fonc.2012.00026. PubMed PMID: 22649782; PubMed Central PMCID: PMC3355875.
149. Cao R, Tsukada Y, Zhang Y. Role of Bmi-1 and Ring1A in H2A ubiquitylation and Hox gene silencing. *Mol Cell*. 2005;20(6):845-54. doi: 10.1016/j.molcel.2005.12.002. PubMed PMID: 16359901.
150. Gearhart MD, Corcoran CM, Wamstad JA, Bardwell VJ. Polycomb group and SCF ubiquitin ligases are found in a novel BCOR complex that is recruited to BCL6 targets. *Mol Cell Biol*. 2006;26(18):6880-9. doi: 10.1128/MCB.00630-06. PubMed PMID: 16943429; PubMed Central PMCID: PMC1592854.

151. Kim J, Hake SB, Roeder RG. The human homolog of yeast BRE1 functions as a transcriptional coactivator through direct activator interactions. *Mol Cell*. 2005;20(5):759-70. doi: 10.1016/j.molcel.2005.11.012. PubMed PMID: 16337599.
152. Shio Y, Eisenman RN. Histone sumoylation is associated with transcriptional repression. *Proc Natl Acad Sci U S A*. 2003;100(23):13225-30. doi: 10.1073/pnas.1735528100. PubMed PMID: 14578449; PubMed Central PMCID: PMCPMC263760.
153. Gregoret IV, Lee YM, Goodson HV. Molecular evolution of the histone deacetylase family: functional implications of phylogenetic analysis. *J Mol Biol*. 2004;338(1):17-31. doi: 10.1016/j.jmb.2004.02.006. PubMed PMID: 15050820.
154. de Ruijter AJ, van Gennip AH, Caron HN, Kemp S, van Kuilenburg AB. Histone deacetylases (HDACs): characterization of the classical HDAC family. *Biochem J*. 2003;370(Pt 3):737-49. doi: 10.1042/BJ20021321. PubMed PMID: 12429021; PubMed Central PMCID: PMCPMC1223209.
155. Hayakawa T, Nakayama J. Physiological roles of class I HDAC complex and histone demethylase. *J Biomed Biotechnol*. 2011;2011:129383. doi: 10.1155/2011/129383. PubMed PMID: 21049000; PubMed Central PMCID: PMCPMC2964911.
156. Denslow SA, Wade PA. The human Mi-2/NuRD complex and gene regulation. *Oncogene*. 2007;26(37):5433-8. doi: 10.1038/sj.onc.1210611. PubMed PMID: 17694084.
157. Wang Y, Zhang H, Chen Y, Sun Y, Yang F, Yu W, et al. LSD1 is a subunit of the NuRD complex and targets the metastasis programs in breast cancer. *Cell*. 2009;138(4):660-72. doi: 10.1016/j.cell.2009.05.050. PubMed PMID: 19703393.
158. Liang J, Wan M, Zhang Y, Gu P, Xin H, Jung SY, et al. Nanog and Oct4 associate with unique transcriptional repression complexes in embryonic stem cells. *Nat Cell Biol*. 2008;10(6):731-9. doi: 10.1038/ncb1736. PubMed PMID: 18454139.
159. Lee MG, Wynder C, Cooch N, Shiekhattar R. An essential role for CoREST in nucleosomal histone 3 lysine 4 demethylation. *Nature*. 2005;437(7057):432-5. doi: 10.1038/nature04021. PubMed PMID: 16079794.
160. Delcuve GP, Khan DH, Davie JR. Targeting class I histone deacetylases in cancer therapy. *Expert Opin Ther Targets*. 2013;17(1):29-41. doi: 10.1517/14728222.2013.729042. PubMed PMID: 23062071.
161. Segre CV, Chiocca S. Regulating the regulators: the post-translational code of class I HDAC1 and HDAC2. *J Biomed Biotechnol*. 2011;2011:690848. doi: 10.1155/2011/690848. PubMed PMID: 21197454; PubMed Central PMCID: PMCPMC3004424.
162. Tsai SC, Seto E. Regulation of histone deacetylase 2 by protein kinase CK2. *J Biol Chem*. 2002;277(35):31826-33. doi: 10.1074/jbc.M204149200. PubMed PMID: 12082111.
163. Sun JM, Chen HY, Davie JR. Differential distribution of unmodified and phosphorylated histone deacetylase 2 in chromatin. *J Biol Chem*. 2007;282(45):33227-36. doi: 10.1074/jbc.M703549200. PubMed PMID: 17827154.
164. Pflum MK, Tong JK, Lane WS, Schreiber SL. Histone deacetylase 1 phosphorylation promotes enzymatic activity and complex formation. *J Biol Chem*. 2001;276(50):47733-41. doi: 10.1074/jbc.M105590200. PubMed PMID: 11602581.

165. Khan DH, Gonzalez C, Cooper C, Sun JM, Chen HY, Healy S, et al. RNA-dependent dynamic histone acetylation regulates MCL1 alternative splicing. *Nucleic Acids Res.* 2014;42(3):1656-70. doi: 10.1093/nar/gkt1134. PubMed PMID: 24234443; PubMed Central PMCID: PMC3919583.
166. Delcuve GP, Khan DH, Davie JR. Roles of histone deacetylases in epigenetic regulation: emerging paradigms from studies with inhibitors. *Clin Epigenetics.* 2012;4(1):5. doi: 10.1186/1868-7083-4-5. PubMed PMID: 22414492; PubMed Central PMCID: PMC3320549.
167. Sun JM, Chen HY, Moniwa M, Litchfield DW, Seto E, Davie JR. The transcriptional repressor Sp3 is associated with CK2-phosphorylated histone deacetylase 2. *J Biol Chem.* 2002;277(39):35783-6. doi: 10.1074/jbc.C200378200. PubMed PMID: 12176973.
168. Wang Z, Zang C, Cui K, Schones DE, Barski A, Peng W, et al. Genome-wide mapping of HATs and HDACs reveals distinct functions in active and inactive genes. *Cell.* 2009;138(5):1019-31. doi: 10.1016/j.cell.2009.06.049. PubMed PMID: 19698979; PubMed Central PMCID: PMC2750862.
169. Bedford MT, Clarke SG. Protein arginine methylation in mammals: who, what, and why. *Molecular cell.* 2009;33(1):1-13. doi: 10.1016/j.molcel.2008.12.013. PubMed PMID: 19150423; PubMed Central PMCID: PMC3372459.
170. Migliori V, Phalke S, Bezzi M, Guccione E. Arginine/lysine-methyl/methyl switches: biochemical role of histone arginine methylation in transcriptional regulation. *Epigenomics.* 2010;2(1):119-37. doi: 10.2217/epi.09.39. PubMed PMID: 22122749.
171. Di Lorenzo A, Bedford MT. Histone arginine methylation. *FEBS Lett.* 2011;585(13):2024-31. doi: 10.1016/j.febslet.2010.11.010. PubMed PMID: 21074527; PubMed Central PMCID: PMC3409563.
172. Zurita-Lopez CI, Sandberg T, Kelly R, Clarke SG. Human protein arginine methyltransferase 7 (PRMT7) is a type III enzyme forming omega-NG-monomethylated arginine residues. *The Journal of biological chemistry.* 2012;287(11):7859-70. doi: 10.1074/jbc.M111.336271. PubMed PMID: 22241471; PubMed Central PMCID: PMC3318701.
173. Wolf SS. The protein arginine methyltransferase family: an update about function, new perspectives and the physiological role in humans. *Cell Mol Life Sci.* 2009;66(13):2109-21. doi: 10.1007/s00018-009-0010-x. PubMed PMID: 19300908.
174. Krause CD, Yang ZH, Kim YS, Lee JH, Cook JR, Pestka S. Protein arginine methyltransferases: evolution and assessment of their pharmacological and therapeutic potential. *Pharmacol Ther.* 2007;113(1):50-87. doi: 10.1016/j.pharmthera.2006.06.007. PubMed PMID: 17005254.
175. Pahlich S, Zakaryan RP, Gehring H. Protein arginine methylation: Cellular functions and methods of analysis. *Biochim Biophys Acta.* 2006;1764(12):1890-903. doi: 10.1016/j.bbapap.2006.08.008. PubMed PMID: 17010682.
176. Wei H, Mundade R, Lange KC, Lu T. Protein arginine methylation of non-histone proteins and its role in diseases. *Cell Cycle.* 2014;13(1):32-41. doi: 10.4161/cc.27353. PubMed PMID: 24296620; PubMed Central PMCID: PMC3925732.
177. Boisvert FM, Chenard CA, Richard S. Protein interfaces in signaling regulated by arginine methylation. *Sci STKE.* 2005;2005(271):re2. doi: 10.1126/stke.2712005re2. PubMed PMID: 15713950.

178. Cheung N, Chan LC, Thompson A, Cleary ML, So CW. Protein arginine-methyltransferase-dependent oncogenesis. *Nat Cell Biol.* 2007;9(10):1208-15. doi: 10.1038/ncb1642. PubMed PMID: 17891136.
179. Sugai M, Ohta A, Ogata Y, Nakanishi M, Ueno S, Kawata T, et al. Asymmetric dimethylarginine (ADMA) in the aqueous humor of diabetic patients. *Endocr J.* 2007;54(2):303-9. PubMed PMID: 17379959.
180. Valkonen VP, Tuomainen TP, Laaksonen R. DDAH gene and cardiovascular risk. *Vasc Med.* 2005;10 Suppl 1:S45-8. PubMed PMID: 16444868.
181. Jahan S, Davie JR. Protein arginine methyltransferases (PRMTs): role in chromatin organization. *Adv Biol Regul.* 2015;57:173-84. doi: 10.1016/j.jbior.2014.09.003. PubMed PMID: 25263650.
182. Lin WJ, Gary JD, Yang MC, Clarke S, Herschman HR. The mammalian immediate-early TIS21 protein and the leukemia-associated BTG1 protein interact with a protein-arginine N-methyltransferase. *The Journal of biological chemistry.* 1996;271(25):15034-44. PubMed PMID: 8663146.
183. Tang J, Gary JD, Clarke S, Herschman HR. PRMT 3, a type I protein arginine N-methyltransferase that differs from PRMT1 in its oligomerization, subcellular localization, substrate specificity, and regulation. *The Journal of biological chemistry.* 1998;273(27):16935-45. Epub 1998/06/27. PubMed PMID: 9642256.
184. Lee J, Bedford MT. PABP1 identified as an arginine methyltransferase substrate using high-density protein arrays. *EMBO Rep.* 2002;3(3):268-73. doi: 10.1093/embo-reports/kvf052. PubMed PMID: 11850402; PubMed Central PMCID: PMC1084016.
185. Zhang X, Cheng X. Structure of the predominant protein arginine methyltransferase PRMT1 and analysis of its binding to substrate peptides. *Structure.* 2003;11(5):509-20. PubMed PMID: 12737817.
186. Gayatri S, Bedford MT. Readers of histone methylarginine marks. *Biochimica et biophysica acta.* 2014;1839(8):702-10. Epub 2014/03/04. doi: 10.1016/j.bbagr.2014.02.015. PubMed PMID: 24583552; PubMed Central PMCID: PMC4099268.
187. Sayegh J, Webb K, Cheng D, Bedford MT, Clarke SG. Regulation of protein arginine methyltransferase 8 (PRMT8) activity by its N-terminal domain. *The Journal of biological chemistry.* 2007;282(50):36444-53. doi: 10.1074/jbc.M704650200. PubMed PMID: 17925405.
188. Ganesh L, Yoshimoto T, Moorthy NC, Akahata W, Boehm M, Nabel EG, et al. Protein methyltransferase 2 inhibits NF-kappaB function and promotes apoptosis. *Molecular and cellular biology.* 2006;26(10):3864-74. doi: 10.1128/MCB.26.10.3864-3874.2006. PubMed PMID: 16648481; PubMed Central PMCID: PMC1488990.
189. Blythe SA, Cha SW, Tadjuidje E, Heasman J, Klein PS. beta-Catenin primes organizer gene expression by recruiting a histone H3 arginine 8 methyltransferase, Prmt2. *Developmental cell.* 2010;19(2):220-31. Epub 2010/08/17. doi: 10.1016/j.devcel.2010.07.007. PubMed PMID: 20708585; PubMed Central PMCID: PMC2923644.
190. Su X, Zhu G, Ding X, Lee SY, Dou Y, Zhu B, et al. Molecular basis underlying histone H3 lysine-arginine methylation pattern readout by Spin/Ssty repeats of Spindlin1. *Genes & development.* 2014;28(6):622-36. Epub 2014/03/05. doi: 10.1101/gad.233239.113. PubMed PMID: 24589551; PubMed Central PMCID: PMC3967050.

191. Swiercz R, Cheng D, Kim D, Bedford MT. Ribosomal protein rpS2 is hypomethylated in PRMT3-deficient mice. *The Journal of biological chemistry*. 2007;282(23):16917-23. doi: 10.1074/jbc.M609778200. PubMed PMID: 17439947.
192. Yadav N, Lee J, Kim J, Shen J, Hu MC, Aldaz CM, et al. Specific protein methylation defects and gene expression perturbations in coactivator-associated arginine methyltransferase 1-deficient mice. *Proceedings of the National Academy of Sciences of the United States of America*. 2003;100(11):6464-8. doi: 10.1073/pnas.1232272100. PubMed PMID: 12756295; PubMed Central PMCID: PMC164469.
193. Kim J, Lee J, Yadav N, Wu Q, Carter C, Richard S, et al. Loss of CARM1 results in hypomethylation of thymocyte cyclic AMP-regulated phosphoprotein and deregulated early T cell development. *The Journal of biological chemistry*. 2004;279(24):25339-44. doi: 10.1074/jbc.M402544200. PubMed PMID: 15096520.
194. Ito T, Yadav N, Lee J, Furumatsu T, Yamashita S, Yoshida K, et al. Arginine methyltransferase CARM1/PRMT4 regulates endochondral ossification. *BMC Dev Biol*. 2009;9:47. doi: 10.1186/1471-213X-9-47. PubMed PMID: 19725955; PubMed Central PMCID: PMC2754437.
195. O'Brien KB, Alberich-Jorda M, Yadav N, Kocher O, Diruscio A, Ebraliidze A, et al. CARM1 is required for proper control of proliferation and differentiation of pulmonary epithelial cells. *Development*. 2010;137(13):2147-56. doi: 10.1242/dev.037150. PubMed PMID: 20530543; PubMed Central PMCID: PMC2882134.
196. Wu J, Cui N, Wang R, Li J, Wong J. A role for CARM1-mediated histone H3 arginine methylation in protecting histone acetylation by releasing corepressors from chromatin. *PloS one*. 2012;7(6):e34692. Epub 2012/06/23. doi: 10.1371/journal.pone.0034692. PubMed PMID: 22723830; PubMed Central PMCID: PMC3377634.
197. Casadio F, Lu X, Pollock SB, LeRoy G, Garcia BA, Muir TW, et al. H3R42me2a is a histone modification with positive transcriptional effects. *Proceedings of the National Academy of Sciences of the United States of America*. 2013;110(37):14894-9. Epub 2013/08/28. doi: 10.1073/pnas.1312925110. PubMed PMID: 23980157; PubMed Central PMCID: PMC3773778.
198. Pollack BP, Kotenko SV, He W, Izotova LS, Barnoski BL, Pestka S. The human homologue of the yeast proteins Skb1 and Hsl7p interacts with Jak kinases and contains protein methyltransferase activity. *The Journal of biological chemistry*. 1999;274(44):31531-42. PubMed PMID: 10531356.
199. Zhou Z, Sun X, Zou Z, Sun L, Zhang T, Guo S, et al. PRMT5 regulates Golgi apparatus structure through methylation of the golgin GM130. *Cell Res*. 2010;20(9):1023-33. doi: 10.1038/cr.2010.56. PubMed PMID: 20421892.
200. Neuenkirchen N, Chari A, Fischer U. Deciphering the assembly pathway of Sm-class U snRNPs. *FEBS Lett*. 2008;582(14):1997-2003. doi: 10.1016/j.febslet.2008.03.009. PubMed PMID: 18348870.
201. Dacwag CS, Ohkawa Y, Pal S, Sif S, Imbalzano AN. The protein arginine methyltransferase Prmt5 is required for myogenesis because it facilitates ATP-dependent chromatin remodeling. *Molecular and cellular biology*. 2007;27(1):384-94. doi: 10.1128/MCB.01528-06. PubMed PMID: 17043109; PubMed Central PMCID: PMC1800640.
202. Lacroix M, El Messaoudi S, Rodier G, Le Cam A, Sardet C, Fabrizio E. The histone-binding protein COPR5 is required for nuclear functions of the protein arginine methyltransferase PRMT5. *EMBO*

Rep. 2008;9(5):452-8. doi: 10.1038/embor.2008.45. PubMed PMID: 18404153; PubMed Central PMCID: PMC2373370.

203. Wang L, Pal S, Sif S. Protein arginine methyltransferase 5 suppresses the transcription of the RB family of tumor suppressors in leukemia and lymphoma cells. *Molecular and cellular biology*. 2008;28(20):6262-77. doi: 10.1128/MCB.00923-08. PubMed PMID: 18694959; PubMed Central PMCID: PMC2577430.

204. Di Lorenzo A, Yang Y, Macaluso M, Bedford MT. A gain-of-function mouse model identifies PRMT6 as a NF-kappaB coactivator. *Nucleic Acids Res*. 2014;42(13):8297-309. Epub 2014/06/19. doi: 10.1093/nar/gku530. PubMed PMID: 24939901; PubMed Central PMCID: PMC4117762.

205. Stein C, Riedl S, Ruthnick D, Notzold RR, Bauer UM. The arginine methyltransferase PRMT6 regulates cell proliferation and senescence through transcriptional repression of tumor suppressor genes. *Nucleic Acids Res*. 2012;40(19):9522-33. doi: 10.1093/nar/gks767. PubMed PMID: 22904088; PubMed Central PMCID: PMC3479209.

206. Lakowski TM, Frankel A. A kinetic study of human protein arginine N-methyltransferase 6 reveals a distributive mechanism. *The Journal of biological chemistry*. 2008;283(15):10015-25. doi: 10.1074/jbc.M710176200. PubMed PMID: 18263580.

207. Lee JH, Cook JR, Yang ZH, Mirochnitchenko O, Gunderson SI, Felix AM, et al. PRMT7, a new protein arginine methyltransferase that synthesizes symmetric dimethylarginine. *The Journal of biological chemistry*. 2005;280(5):3656-64. doi: 10.1074/jbc.M405295200. PubMed PMID: 15494416.

208. Gonsalvez GB, Tian L, Ospina JK, Boisvert FM, Lamond AI, Matera AG. Two distinct arginine methyltransferases are required for biogenesis of Sm-class ribonucleoproteins. *J Cell Biol*. 2007;178(5):733-40. doi: 10.1083/jcb.200702147. PubMed PMID: 17709427; PubMed Central PMCID: PMC2064538.

209. Zheng Z, Schmidt-Ott KM, Chua S, Foster KA, Frankel RZ, Pavlidis P, et al. A Mendelian locus on chromosome 16 determines susceptibility to doxorubicin nephropathy in the mouse. *Proceedings of the National Academy of Sciences of the United States of America*. 2005;102(7):2502-7. doi: 10.1073/pnas.0409786102. PubMed PMID: 15699352; PubMed Central PMCID: PMC549022.

210. Gros L, Delaporte C, Frey S, Decesse J, de Saint-Vincent BR, Cavarec L, et al. Identification of new drug sensitivity genes using genetic suppressor elements: protein arginine N-methyltransferase mediates cell sensitivity to DNA-damaging agents. *Cancer Res*. 2003;63(1):164-71. PubMed PMID: 12517794.

211. Bleibel WK, Duan S, Huang RS, Kistner EO, Shukla SJ, Wu X, et al. Identification of genomic regions contributing to etoposide-induced cytotoxicity. *Hum Genet*. 2009;125(2):173-80. doi: 10.1007/s00439-008-0607-4. PubMed PMID: 19089452; PubMed Central PMCID: PMC2714550.

212. Buhr N, Carapito C, Schaeffer C, Kieffer E, Van Dorsselaer A, Viville S. Nuclear proteome analysis of undifferentiated mouse embryonic stem and germ cells. *Electrophoresis*. 2008;29(11):2381-90. doi: 10.1002/elps.200700738. PubMed PMID: 18449859.

213. Lee J, Sayegh J, Daniel J, Clarke S, Bedford MT. PRMT8, a new membrane-bound tissue-specific member of the protein arginine methyltransferase family. *The Journal of biological chemistry*. 2005;280(38):32890-6. doi: 10.1074/jbc.M506944200. PubMed PMID: 16051612.

214. Scaramuzzino C, Monaghan J, Milioto C, Lanson NA, Jr., Maltare A, Aggarwal T, et al. Protein arginine methyltransferase 1 and 8 interact with FUS to modify its sub-cellular distribution and toxicity in vitro and in vivo. *PloS one*. 2013;8(4):e61576. Epub 2013/04/27. doi: 10.1371/journal.pone.0061576. PubMed PMID: 23620769; PubMed Central PMCID: PMC3631215.
215. Andrade MA, Perez-Iratxeta C, Ponting CP. Protein repeats: structures, functions, and evolution. *J Struct Biol*. 2001;134(2-3):117-31. doi: 10.1006/jsbi.2001.4392. PubMed PMID: 11551174.
216. Hardisty-Hughes RE, Tateossian H, Morse SA, Romero MR, Middleton A, Tymowska-Lalanne Z, et al. A mutation in the F-box gene, *Fbxo11*, causes otitis media in the Jeff mouse. *Hum Mol Genet*. 2006;15(22):3273-9. doi: 10.1093/hmg/ddl403. PubMed PMID: 17035249.
217. Migliori V, Muller J, Phalke S, Low D, Bezzi M, Mok WC, et al. Symmetric dimethylation of H3R2 is a newly identified histone mark that supports euchromatin maintenance. *Nat Struct Mol Biol*. 2012;19(2):136-44. doi: 10.1038/nsmb.2209. PubMed PMID: 22231400.
218. Schurter BT, Koh SS, Chen D, Bunick GJ, Harp JM, Hanson BL, et al. Methylation of histone H3 by coactivator-associated arginine methyltransferase 1. *Biochemistry*. 2001;40(19):5747-56. Epub 2001/05/09. PubMed PMID: 11341840.
219. El Messaoudi S, Fabrizio E, Rodriguez C, Chuchana P, Fauquier L, Cheng D, et al. Coactivator-associated arginine methyltransferase 1 (CARM1) is a positive regulator of the Cyclin E1 gene. *Proceedings of the National Academy of Sciences of the United States of America*. 2006;103(36):13351-6. doi: 10.1073/pnas.0605692103. PubMed PMID: 16938873; PubMed Central PMCID: PMC1569167.
220. Wang H, Huang ZQ, Xia L, Feng Q, Erdjument-Bromage H, Strahl BD, et al. Methylation of histone H4 at arginine 3 facilitating transcriptional activation by nuclear hormone receptor. *Science*. 2001;293(5531):853-7. Epub 2001/06/02. doi: 10.1126/science.1060781. PubMed PMID: 11387442.
221. Hyllus D, Stein C, Schnabel K, Schiltz E, Imhof A, Dou Y, et al. PRMT6-mediated methylation of R2 in histone H3 antagonizes H3 K4 trimethylation. *Genes & development*. 2007;21(24):3369-80. doi: 10.1101/gad.447007. PubMed PMID: 18079182; PubMed Central PMCID: PMC2113036.
222. Iberg AN, Espejo A, Cheng D, Kim D, Michaud-Levesque J, Richard S, et al. Arginine methylation of the histone H3 tail impedes effector binding. *The Journal of biological chemistry*. 2008;283(6):3006-10. doi: 10.1074/jbc.C700192200. PubMed PMID: 18077460.
223. Pal S, Vishwanath SN, Erdjument-Bromage H, Tempst P, Sif S. Human SWI/SNF-associated PRMT5 methylates histone H3 arginine 8 and negatively regulates expression of ST7 and NM23 tumor suppressor genes. *Molecular and cellular biology*. 2004;24(21):9630-45. doi: 10.1128/MCB.24.21.9630-9645.2004. PubMed PMID: 15485929; PubMed Central PMCID: PMC522266.
224. Zhao Q, Rank G, Tan YT, Li H, Moritz RL, Simpson RJ, et al. PRMT5-mediated methylation of histone H4R3 recruits DNMT3A, coupling histone and DNA methylation in gene silencing. *Nature structural & molecular biology*. 2009;16(3):304-11. Epub 2009/02/24. doi: 10.1038/nsmb.1568. PubMed PMID: 19234465.
225. Waldmann T, Izzo A, Kamieniarz K, Richter F, Vogler C, Sarg B, et al. Methylation of H2AR29 is a novel repressive PRMT6 target. *Epigenetics & chromatin*. 2011;4:11. Epub 2011/07/22. doi: 10.1186/1756-8935-4-11. PubMed PMID: 21774791; PubMed Central PMCID: PMC3164600.

226. Aravind L, Abhiman S, Iyer LM. Natural history of the eukaryotic chromatin protein methylation system. *Progress in molecular biology and translational science*. 2011;101:105-76. Epub 2011/04/22. doi: 10.1016/B978-0-12-387685-0.00004-4. PubMed PMID: 21507350.
227. Pal S, Sif S. Interplay between chromatin remodelers and protein arginine methyltransferases. *Journal of cellular physiology*. 2007;213(2):306-15. Epub 2007/08/22. doi: 10.1002/jcp.21180. PubMed PMID: 17708529.
228. Cheng X, Collins RE, Zhang X. Structural and sequence motifs of protein (histone) methylation enzymes. *Annu Rev Biophys Biomol Struct*. 2005;34:267-94. doi: 10.1146/annurev.biophys.34.040204.144452. PubMed PMID: 15869391; PubMed Central PMCID: PMC2733851.
229. Selvi BR, Batta K, Kishore AH, Mantelingu K, Varier RA, Balasubramanyam K, et al. Identification of a novel inhibitor of coactivator-associated arginine methyltransferase 1 (CARM1)-mediated methylation of histone H3 Arg-17. *The Journal of biological chemistry*. 2010;285(10):7143-52. Epub 2009/12/22. doi: 10.1074/jbc.M109.063933. PubMed PMID: 20022955; PubMed Central PMCID: PMC2844164.
230. Daujat S, Bauer UM, Shah V, Turner B, Berger S, Kouzarides T. Crosstalk between CARM1 methylation and CBP acetylation on histone H3. *Curr Biol*. 2002;12(24):2090-7. PubMed PMID: 12498683.
231. Molina-Serrano D, Schiza V, Kirmizis A. Cross-talk among epigenetic modifications: lessons from histone arginine methylation. *Biochemical Society transactions*. 2013;41(3):751-9. Epub 2013/05/24. doi: 10.1042/BST20130003. PubMed PMID: 23697934.
232. An W, Kim J, Roeder RG. Ordered cooperative functions of PRMT1, p300, and CARM1 in transcriptional activation by p53. *Cell*. 2004;117(6):735-48. Epub 2004/06/10. doi: 10.1016/j.cell.2004.05.009. PubMed PMID: 15186775.
233. Yue WW, Hassler M, Roe SM, Thompson-Vale V, Pearl LH. Insights into histone code syntax from structural and biochemical studies of CARM1 methyltransferase. *The EMBO journal*. 2007;26(20):4402-12. doi: 10.1038/sj.emboj.7601856. PubMed PMID: 17882261; PubMed Central PMCID: PMC2034666.
234. Metivier R, Penot G, Hubner MR, Reid G, Brand H, Kos M, et al. Estrogen receptor-alpha directs ordered, cyclical, and combinatorial recruitment of cofactors on a natural target promoter. *Cell*. 2003;115(6):751-63. PubMed PMID: 14675539.
235. Sakabe K, Hart GW. O-GlcNAc transferase regulates mitotic chromatin dynamics. *The Journal of biological chemistry*. 2010;285(45):34460-8. doi: 10.1074/jbc.M110.158170. PubMed PMID: 20805223; PubMed Central PMCID: PMC2966060.
236. Lupien M, Eeckhoute J, Meyer CA, Krum SA, Rhodes DR, Liu XS, et al. Coactivator function defines the active estrogen receptor alpha cisrome. *Molecular and cellular biology*. 2009;29(12):3413-23. doi: 10.1128/MCB.00020-09. PubMed PMID: 19364822; PubMed Central PMCID: PMC2698732.
237. Bauer UM, Daujat S, Nielsen SJ, Nightingale K, Kouzarides T. Methylation at arginine 17 of histone H3 is linked to gene activation. *EMBO Rep*. 2002;3(1):39-44. doi: 10.1093/embo-reports/kvf013. PubMed PMID: 11751582; PubMed Central PMCID: PMC1083932.

238. Margueron R, Justin N, Ohno K, Sharpe ML, Son J, Drury WJ, 3rd, et al. Role of the polycomb protein EED in the propagation of repressive histone marks. *Nature*. 2009;461(7265):762-7. doi: 10.1038/nature08398. PubMed PMID: 19767730; PubMed Central PMCID: PMC3772642.
239. Guccione E, Martinato F, Finocchiaro G, Luzi L, Tizzoni L, Dall' Olio V, et al. Myc-binding-site recognition in the human genome is determined by chromatin context. *Nature cell biology*. 2006;8(7):764-70. Epub 2006/06/13. doi: 10.1038/ncb1434. PubMed PMID: 16767079.
240. Rosenfeld JA, Wang Z, Schones DE, Zhao K, DeSalle R, Zhang MQ. Determination of enriched histone modifications in non-genic portions of the human genome. *BMC Genomics*. 2009;10:143. doi: 10.1186/1471-2164-10-143. PubMed PMID: 19335899; PubMed Central PMCID: PMC2667539.
241. Barski A, Cuddapah S, Cui K, Roh TY, Schones DE, Wang Z, et al. High-resolution profiling of histone methylations in the human genome. *Cell*. 2007;129(4):823-37. doi: 10.1016/j.cell.2007.05.009. PubMed PMID: 17512414.
242. Denis H, Deplus R, Putmans P, Yamada M, Metivier R, Fuks F. Functional connection between deimination and deacetylation of histones. *Molecular and cellular biology*. 2009;29(18):4982-93. doi: 10.1128/MCB.00285-09. PubMed PMID: 19581286; PubMed Central PMCID: PMC2738279.
243. Kleinschmidt MA, Streubel G, Samans B, Krause M, Bauer UM. The protein arginine methyltransferases CARM1 and PRMT1 cooperate in gene regulation. *Nucleic Acids Res*. 2008;36(10):3202-13. doi: 10.1093/nar/gkn166. PubMed PMID: 18413343; PubMed Central PMCID: PMC2425501.
244. Xie Y, Ke S, Ouyang N, He J, Xie W, Bedford MT, et al. Epigenetic regulation of transcriptional activity of pregnane X receptor by protein arginine methyltransferase 1. *The Journal of biological chemistry*. 2009;284(14):9199-205. doi: 10.1074/jbc.M806193200. PubMed PMID: 19144646; PubMed Central PMCID: PMC2666572.
245. Pesavento JJ, Bullock CR, LeDuc RD, Mizzen CA, Kelleher NL. Combinatorial modification of human histone H4 quantitated by two-dimensional liquid chromatography coupled with top down mass spectrometry. *The Journal of biological chemistry*. 2008;283(22):14927-37. doi: 10.1074/jbc.M709796200. PubMed PMID: 18381279; PubMed Central PMCID: PMC2397456.
246. Phanstiel D, Brumbaugh J, Berggren WT, Conard K, Feng X, Levenstein ME, et al. Mass spectrometry identifies and quantifies 74 unique histone H4 isoforms in differentiating human embryonic stem cells. *Proceedings of the National Academy of Sciences of the United States of America*. 2008;105(11):4093-8. doi: 10.1073/pnas.0710515105. PubMed PMID: 18326628; PubMed Central PMCID: PMC2393763.
247. Girardot M, Hirasawa R, Kacem S, Fritsch L, Pontis J, Kota SK, et al. PRMT5-mediated histone H4 arginine-3 symmetrical dimethylation marks chromatin at G + C-rich regions of the mouse genome. *Nucleic Acids Res*. 2014;42(1):235-48. doi: 10.1093/nar/gkt884. PubMed PMID: 24097435; PubMed Central PMCID: PMC3874197.
248. Jelinic P, Stehle JC, Shaw P. The testis-specific factor CTCFL cooperates with the protein methyltransferase PRMT7 in H19 imprinting control region methylation. *PLoS Biol*. 2006;4(11):e355. doi: 10.1371/journal.pbio.0040355. PubMed PMID: 17048991; PubMed Central PMCID: PMC1609128.

249. Rank G, Cerruti L, Simpson RJ, Moritz RL, Jane SM, Zhao Q. Identification of a PRMT5-dependent repressor complex linked to silencing of human fetal globin gene expression. *Blood*. 2010;116(9):1585-92. doi: 10.1182/blood-2009-10-251116. PubMed PMID: 20495075; PubMed Central PMCID: PMC2938845.
250. Hou Z, Peng H, Ayyanathan K, Yan KP, Langer EM, Longmore GD, et al. The LIM protein AJUBA recruits protein arginine methyltransferase 5 to mediate SNAIL-dependent transcriptional repression. *Molecular and cellular biology*. 2008;28(10):3198-207. doi: 10.1128/MCB.01435-07. PubMed PMID: 18347060; PubMed Central PMCID: PMC2423142.
251. Cesaro E, De Cegli R, Medugno L, Florio F, Grosso M, Lupo A, et al. The Kruppel-like zinc finger protein ZNF224 recruits the arginine methyltransferase PRMT5 on the transcriptional repressor complex of the aldolase A gene. *The Journal of biological chemistry*. 2009;284(47):32321-30. doi: 10.1074/jbc.M109.043349. PubMed PMID: 19741270; PubMed Central PMCID: PMC2781646.
252. Tabata T, Kokura K, Ten Dijke P, Ishii S. Ski co-repressor complexes maintain the basal repressed state of the TGF-beta target gene, SMAD7, via HDAC3 and PRMT5. *Genes Cells*. 2009;14(1):17-28. doi: 10.1111/j.1365-2443.2008.01246.x. PubMed PMID: 19032343.
253. Tae S, Karkhanis V, Velasco K, Yaneva M, Erdjument-Bromage H, Tempst P, et al. Bromodomain protein 7 interacts with PRMT5 and PRC2, and is involved in transcriptional repression of their target genes. *Nucleic Acids Res*. 2011;39(13):5424-38. Epub 2011/03/31. doi: 10.1093/nar/gkr170. PubMed PMID: 21447565; PubMed Central PMCID: PMC3141267.
254. Rathert P, Dhayalan A, Murakami M, Zhang X, Tamas R, Jurkowska R, et al. Protein lysine methyltransferase G9a acts on non-histone targets. *Nature chemical biology*. 2008;4(6):344-6. doi: 10.1038/nchembio.88. PubMed PMID: 18438403; PubMed Central PMCID: PMC2696268.
255. Kuhn P, Xu W. Protein arginine methyltransferases: nuclear receptor coregulators and beyond. *Progress in molecular biology and translational science*. 2009;87:299-342. Epub 2009/01/01. doi: 10.1016/S1877-1173(09)87009-9. PubMed PMID: 20374708.
256. Bezzi M, Teo SX, Muller J, Mok WC, Sahu SK, Vardy LA, et al. Regulation of constitutive and alternative splicing by PRMT5 reveals a role for Mdm4 pre-mRNA in sensing defects in the spliceosomal machinery. *Genes & development*. 2013;27(17):1903-16. Epub 2013/09/10. doi: 10.1101/gad.219899.113. PubMed PMID: 24013503; PubMed Central PMCID: PMC3778243.
257. Karkhanis V, Hu YJ, Baiocchi RA, Imbalzano AN, Sif S. Versatility of PRMT5-induced methylation in growth control and development. *Trends in biochemical sciences*. 2011;36(12):633-41. Epub 2011/10/07. doi: 10.1016/j.tibs.2011.09.001. PubMed PMID: 21975038; PubMed Central PMCID: PMC3225484.
258. Bedford MT, Richard S. Arginine methylation an emerging regulator of protein function. *Molecular cell*. 2005;18(3):263-72. doi: 10.1016/j.molcel.2005.04.003. PubMed PMID: 15866169.
259. Zhao X, Jankovic V, Gural A, Huang G, Pardanani A, Menendez S, et al. Methylation of RUNX1 by PRMT1 abrogates SIN3A binding and potentiates its transcriptional activity. *Genes Dev*. 2008;22(5):640-53. doi: 10.1101/gad.1632608. PubMed PMID: 18316480; PubMed Central PMCID: PMC2259033.

260. Le Guezennec X, Vermeulen M, Brinkman AB, Hoeijmakers WA, Cohen A, Lasonder E, et al. MBD2/NuRD and MBD3/NuRD, two distinct complexes with different biochemical and functional properties. *Molecular and cellular biology*. 2006;26(3):843-51. doi: 10.1128/MCB.26.3.843-851.2006. PubMed PMID: 16428440; PubMed Central PMCID: PMC1347035.
261. Ma MK, Heath C, Hair A, West AG. Histone crosstalk directed by H2B ubiquitination is required for chromatin boundary integrity. *PLoSGenet*. 2011;7(7):e1002175.
262. Yuan CC, Matthews AG, Jin Y, Chen CF, Chapman BA, Ohsumi TK, et al. Histone H3R2 symmetric dimethylation and histone H3K4 trimethylation are tightly correlated in eukaryotic genomes. *Cell Rep*. 2012;1(2):83-90.
263. Baldwin RM, Morettin A, Cote J. Role of PRMTs in cancer: Could minor isoforms be leaving a mark? *World J Biol Chem*. 2014;5(2):115-29. doi: 10.4331/wjbc.v5.i2.115. PubMed PMID: 24921003; PubMed Central PMCID: PMC4050107.
264. Van Rechem C, Whetstine JR. Examining the impact of gene variants on histone lysine methylation. *Biochim Biophys Acta*. 2014;1839(12):1463-76. doi: 10.1016/j.bbagr.2014.05.014. PubMed PMID: 24859469; PubMed Central PMCID: PMC4752941.
265. Wang J, Chen L, Sinha SH, Liang Z, Chai H, Muniyan S, et al. Pharmacophore-based virtual screening and biological evaluation of small molecule inhibitors for protein arginine methylation. *J Med Chem*. 2012;55(18):7978-87. doi: 10.1021/jm300521m. PubMed PMID: 22928876; PubMed Central PMCID: PMC4150255.
266. Yang Y, Lu Y, Espejo A, Wu J, Xu W, Liang S, et al. TDRD3 is an effector molecule for arginine-methylated histone marks. *Mol Cell*. 2010;40(6):1016-23. doi: 10.1016/j.molcel.2010.11.024. PubMed PMID: 21172665; PubMed Central PMCID: PMC3090733.
267. Majumder S, Liu Y, Ford OH, 3rd, Mohler JL, Whang YE. Involvement of arginine methyltransferase CARM1 in androgen receptor function and prostate cancer cell viability. *Prostate*. 2006;66(12):1292-301. doi: 10.1002/pros.20438. PubMed PMID: 16705743.
268. Yager JD, Davidson NE. Estrogen carcinogenesis in breast cancer. *N Engl J Med*. 2006;354(3):270-82. doi: 10.1056/NEJMra050776. PubMed PMID: 16421368.
269. Ou CY, LaBonte MJ, Manegold PC, So AY, Ianculescu I, Gerke DS, et al. A coactivator role of CARM1 in the dysregulation of beta-catenin activity in colorectal cancer cell growth and gene expression. *Mol Cancer Res*. 2011;9(5):660-70. doi: 10.1158/1541-7786.MCR-10-0223. PubMed PMID: 21478268; PubMed Central PMCID: PMC3096696.
270. Kim YR, Lee BK, Park RY, Nguyen NT, Bae JA, Kwon DD, et al. Differential CARM1 expression in prostate and colorectal cancers. *BMC Cancer*. 2010;10:197. doi: 10.1186/1471-2407-10-197. PubMed PMID: 20462455; PubMed Central PMCID: PMC2881889.
271. Chung J, Karkhanis V, Tae S, Yan F, Smith P, Ayers LW, et al. Protein arginine methyltransferase 5 (PRMT5) inhibition induces lymphoma cell death through reactivation of the retinoblastoma tumor suppressor pathway and polycomb repressor complex 2 (PRC2) silencing. *J Biol Chem*. 2013;288(49):35534-47. doi: 10.1074/jbc.M113.510669. PubMed PMID: 24189068; PubMed Central PMCID: PMC3853299.

272. Yoshimatsu M, Toyokawa G, Hayami S, Unoki M, Tsunoda T, Field HI, et al. Dysregulation of PRMT1 and PRMT6, Type I arginine methyltransferases, is involved in various types of human cancers. *Int J Cancer*. 2011;128(3):562-73. doi: 10.1002/ijc.25366. PubMed PMID: 20473859.
273. Wei TY, Juan CC, Hisa JY, Su LJ, Lee YC, Chou HY, et al. Protein arginine methyltransferase 5 is a potential oncoprotein that upregulates G1 cyclins/cyclin-dependent kinases and the phosphoinositide 3-kinase/AKT signaling cascade. *Cancer Sci*. 2012;103(9):1640-50. doi: 10.1111/j.1349-7006.2012.02367.x. PubMed PMID: 22726390.
274. Kooistra SM, Helin K. Molecular mechanisms and potential functions of histone demethylases. *Nat Rev Mol Cell Biol*. 2012;13(5):297-311. doi: 10.1038/nrm3327. PubMed PMID: 22473470.
275. Cuthbert GL, Daujat S, Snowden AW, Erdjument-Bromage H, Hagiwara T, Yamada M, et al. Histone deimination antagonizes arginine methylation. *Cell*. 2004;118(5):545-53. doi: 10.1016/j.cell.2004.08.020. PubMed PMID: 15339660.
276. Robin-Lespinasse Y, Sentis S, Kolytcheff C, Rostan MC, Corbo L, Le Romancer M. hCAF1, a new regulator of PRMT1-dependent arginine methylation. *J Cell Sci*. 2007;120(Pt 4):638-47. doi: 10.1242/jcs.03357. PubMed PMID: 17264152.
277. Singh V, Miranda TB, Jiang W, Frankel A, Roemer ME, Robb VA, et al. DAL-1/4.1B tumor suppressor interacts with protein arginine N-methyltransferase 3 (PRMT3) and inhibits its ability to methylate substrates in vitro and in vivo. *Oncogene*. 2004;23(47):7761-71. doi: 10.1038/sj.onc.1208057. PubMed PMID: 15334060.
278. Cha B, Jho EH. Protein arginine methyltransferases (PRMTs) as therapeutic targets. *Expert Opin Ther Targets*. 2012;16(7):651-64. doi: 10.1517/14728222.2012.688030. PubMed PMID: 22621686.
279. Sanders MM. Fractionation of nucleosomes by salt elution from micrococcal nuclease-digested nuclei. *J Cell Biol*. 1978;79(1):97-109. PubMed PMID: 701381; PubMed Central PMCID: PMC2110209.
280. Henikoff S, Henikoff JG, Sakai A, Loeb GB, Ahmad K. Genome-wide profiling of salt fractions maps physical properties of chromatin. *Genome Res*. 2009;19(3):460-9. doi: 10.1101/gr.087619.108. PubMed PMID: 19088306; PubMed Central PMCID: PMC2661814.
281. Hendzel MJ, Sun JM, Chen HY, Rattner JB, Davie JR. Histone acetyltransferase is associated with the nuclear matrix. *J Biol Chem*. 1994;269(36):22894-901. PubMed PMID: 8077241.
282. Delcuve GP, Davie JR. Chromatin structure of erythroid-specific genes of immature and mature chicken erythrocytes. *Biochem J*. 1989;263(1):179-86. PubMed PMID: 2604693; PubMed Central PMCID: PMC21133406.
283. Hebbes TR, Allen SC. Multiple histone acetyltransferases are associated with a chicken erythrocyte chromatin fraction enriched in active genes. *J Biol Chem*. 2000;275(40):31347-52. doi: 10.1074/jbc.M004830200. PubMed PMID: 10896666.
284. Bates DL, Thomas JO. Histones H1 and H5: one or two molecules per nucleosome? *Nucleic Acids Res*. 1981;9(22):5883-94. PubMed PMID: 7312631; PubMed Central PMCID: PMC21133406.
285. Jahan S, Xu W, He S, Gonzalez C, Delcuve GP, Davie JR. The chicken erythrocyte epigenome. *Epigenetics Chromatin*. 2016;9:19. doi: 10.1186/s13072-016-0068-2. PubMed PMID: 27226810; PubMed Central PMCID: PMC4879735.

286. Williams AF. DNA synthesis in purified populations of avian erythroid cells. *J Cell Sci.* 1972;10(1):27-46. PubMed PMID: 5017428.
287. Ridsdale JA, Davie JR. Chicken erythrocyte polynucleosomes which are soluble at physiological ionic strength and contain linker histones are highly enriched in beta-globin gene sequences. *Nucleic Acids Res.* 1987;15(3):1081-96. PubMed PMID: 3822820; PubMed Central PMCID: PMCPMC340509.
288. Shogren-Knaak M, Ishii H, Sun JM, Pazin MJ, Davie JR, Peterson CL. Histone H4-K16 acetylation controls chromatin structure and protein interactions. *Science.* 2006;311(5762):844-7. doi: 10.1126/science.1124000. PubMed PMID: 16469925.
289. Ridsdale JA, Rattner JB, Davie JR. Erythroid-specific gene chromatin has an altered association with linker histones. *Nucleic Acids Res.* 1988;16(13):5915-26. PubMed PMID: 3399383; PubMed Central PMCID: PMCPMC336837.
290. Locklear L, Jr., Ridsdale JA, Bazett-Jones DP, Davie JR. Ultrastructure of transcriptionally competent chromatin. *Nucleic Acids Res.* 1990;18(23):7015-24. PubMed PMID: 2263461; PubMed Central PMCID: PMCPMC332764.
291. Sun JM, Chen HY, Espino PS, Davie JR. Phosphorylated serine 28 of histone H3 is associated with destabilized nucleosomes in transcribed chromatin. *Nucleic Acids Res.* 2007;35(19):6640-7. doi: 10.1093/nar/gkm737. PubMed PMID: 17913747; PubMed Central PMCID: PMCPMC2095820.
292. Clark R, Kupper T. Old meets new: the interaction between innate and adaptive immunity. *J Invest Dermatol.* 2005;125(4):629-37. doi: 10.1111/j.0022-202X.2005.23856.x. PubMed PMID: 16185260.
293. Chen S, Cheng A, Wang M. Innate sensing of viruses by pattern recognition receptors in birds. *Vet Res.* 2013;44:82. doi: 10.1186/1297-9716-44-82. PubMed PMID: 24016341; PubMed Central PMCID: PMCPMC3848724.
294. Kaiser P. Advances in avian immunology--prospects for disease control: a review. *Avian Pathol.* 2010;39(5):309-24. doi: 10.1080/03079457.2010.508777. PubMed PMID: 20954007.
295. Temperley ND, Berlin S, Paton IR, Griffin DK, Burt DW. Evolution of the chicken Toll-like receptor gene family: a story of gene gain and gene loss. *BMC Genomics.* 2008;9:62. doi: 10.1186/1471-2164-9-62. PubMed PMID: 18241342; PubMed Central PMCID: PMCPMC2275738.
296. Boyd A, Philbin VJ, Smith AL. Conserved and distinct aspects of the avian Toll-like receptor (TLR) system: implications for transmission and control of bird-borne zoonoses. *Biochem Soc Trans.* 2007;35(Pt 6):1504-7. doi: 10.1042/BST0351504. PubMed PMID: 18031254.
297. Lynn DJ, Higgs R, Lloyd AT, O'Farrelly C, Herve-Grepinet V, Nys Y, et al. Avian beta-defensin nomenclature: a community proposed update. *Immunol Lett.* 2007;110(1):86-9. doi: 10.1016/j.imlet.2007.03.007. PubMed PMID: 17467809.
298. Kaiser P, Poh TY, Rothwell L, Avery S, Balu S, Pathania US, et al. A genomic analysis of chicken cytokines and chemokines. *J Interferon Cytokine Res.* 2005;25(8):467-84. doi: 10.1089/jir.2005.25.467. PubMed PMID: 16108730.
299. Kaiser P. The avian immune genome--a glass half-full or half-empty? *Cytogenet Genome Res.* 2007;117(1-4):221-30. doi: 10.1159/000103183. PubMed PMID: 17675863.

300. Petrilli V, Dostert C, Muruve DA, Tschopp J. The inflammasome: a danger sensing complex triggering innate immunity. *Curr Opin Immunol.* 2007;19(6):615-22. doi: 10.1016/j.coi.2007.09.002. PubMed PMID: 17977705.
301. Takeuchi O, Akira S. Innate immunity to virus infection. *Immunol Rev.* 2009;227(1):75-86. doi: 10.1111/j.1600-065X.2008.00737.x. PubMed PMID: 19120477.
302. Fukui A, Inoue N, Matsumoto M, Nomura M, Yamada K, Matsuda Y, et al. Molecular cloning and functional characterization of chicken toll-like receptors. A single chicken toll covers multiple molecular patterns. *J Biol Chem.* 2001;276(50):47143-9. doi: 10.1074/jbc.M103902200. PubMed PMID: 11590137.
303. Kogut MH, Iqbal M, He H, Philbin V, Kaiser P, Smith A. Expression and function of Toll-like receptors in chicken heterophils. *Dev Comp Immunol.* 2005;29(9):791-807. doi: 10.1016/j.dci.2005.02.002. PubMed PMID: 15936435.
304. Schwarz H, Schneider K, Ohnemus A, Lavric M, Kothlow S, Bauer S, et al. Chicken toll-like receptor 3 recognizes its cognate ligand when ectopically expressed in human cells. *J Interferon Cytokine Res.* 2007;27(2):97-101. doi: 10.1089/jir.2006.0098. PubMed PMID: 17316136.
305. He H, Genovese KJ, Nisbet DJ, Kogut MH. Profile of Toll-like receptor expressions and induction of nitric oxide synthesis by Toll-like receptor agonists in chicken monocytes. *Mol Immunol.* 2006;43(7):783-9. doi: 10.1016/j.molimm.2005.07.002. PubMed PMID: 16098593.
306. Kawai T, Akira S. The role of pattern-recognition receptors in innate immunity: update on Toll-like receptors. *Nat Immunol.* 2010;11(5):373-84. doi: 10.1038/ni.1863. PubMed PMID: 20404851.
307. Akira S, Takeda K, Kaisho T. Toll-like receptors: critical proteins linking innate and acquired immunity. *Nat Immunol.* 2001;2(8):675-80. doi: 10.1038/90609. PubMed PMID: 11477402.
308. Akira S, Uematsu S, Takeuchi O. Pathogen recognition and innate immunity. *Cell.* 2006;124(4):783-801. doi: 10.1016/j.cell.2006.02.015. PubMed PMID: 16497588.
309. Kawai T, Akira S. Innate immune recognition of viral infection. *Nat Immunol.* 2006;7(2):131-7. doi: 10.1038/ni1303. PubMed PMID: 16424890.
310. Barbalat R, Lau L, Locksley RM, Barton GM. Toll-like receptor 2 on inflammatory monocytes induces type I interferon in response to viral but not bacterial ligands. *Nat Immunol.* 2009;10(11):1200-7. doi: 10.1038/ni.1792. PubMed PMID: 19801985; PubMed Central PMCID: PMCPMC2821672.
311. Brownlie R, Allan B. Avian toll-like receptors. *Cell Tissue Res.* 2011;343(1):121-30. doi: 10.1007/s00441-010-1026-0. PubMed PMID: 20809414.
312. Keestra AM, de Zoete MR, van Aabel RA, van Putten JP. The central leucine-rich repeat region of chicken TLR16 dictates unique ligand specificity and species-specific interaction with TLR2. *J Immunol.* 2007;178(11):7110-9. PubMed PMID: 17513760.
313. Higuchi M, Matsuo A, Shingai M, Shida K, Ishii A, Funami K, et al. Combinational recognition of bacterial lipoproteins and peptidoglycan by chicken Toll-like receptor 2 subfamily. *Dev Comp Immunol.* 2008;32(2):147-55. doi: 10.1016/j.dci.2007.05.003. PubMed PMID: 17614130.
314. Ruan W, Wu Y, Zheng SJ. Different genetic patterns in avian Toll-like receptor (TLR)5 genes. *Mol Biol Rep.* 2012;39(4):3419-26. doi: 10.1007/s11033-011-1113-7. PubMed PMID: 21717059.

315. Bieback K, Lien E, Klagge IM, Avota E, Schneider-Schaulies J, Duprex WP, et al. Hemagglutinin protein of wild-type measles virus activates toll-like receptor 2 signaling. *J Virol.* 2002;76(17):8729-36. PubMed PMID: 12163593; PubMed Central PMCID: PMCPMC136986.
316. Compton T, Kurt-Jones EA, Boehme KW, Belko J, Latz E, Golenbock DT, et al. Human cytomegalovirus activates inflammatory cytokine responses via CD14 and Toll-like receptor 2. *J Virol.* 2003;77(8):4588-96. PubMed PMID: 12663765; PubMed Central PMCID: PMCPMC152130.
317. Wang JP, Kurt-Jones EA, Shin OS, Manchak MD, Levin MJ, Finberg RW. Varicella-zoster virus activates inflammatory cytokines in human monocytes and macrophages via Toll-like receptor 2. *J Virol.* 2005;79(20):12658-66. doi: 10.1128/JVI.79.20.12658-12666.2005. PubMed PMID: 16188968; PubMed Central PMCID: PMCPMC1235827.
318. Kurt-Jones EA, Chan M, Zhou S, Wang J, Reed G, Bronson R, et al. Herpes simplex virus 1 interaction with Toll-like receptor 2 contributes to lethal encephalitis. *Proc Natl Acad Sci U S A.* 2004;101(5):1315-20. doi: 10.1073/pnas.0308057100. PubMed PMID: 14739339; PubMed Central PMCID: PMCPMC337050.
319. Kurt-Jones EA, Popova L, Kwinn L, Haynes LM, Jones LP, Tripp RA, et al. Pattern recognition receptors TLR4 and CD14 mediate response to respiratory syncytial virus. *Nat Immunol.* 2000;1(5):398-401. doi: 10.1038/80833. PubMed PMID: 11062499.
320. Courreges MC, Burzyn D, Nepomnaschy I, Piazzon I, Ross SR. Critical role of dendritic cells in mouse mammary tumor virus in vivo infection. *J Virol.* 2007;81(8):3769-77. doi: 10.1128/JVI.02728-06. PubMed PMID: 17267484; PubMed Central PMCID: PMCPMC1866091.
321. St Paul M, Barjesteh N, Paolucci S, Pei Y, Sharif S. Toll-like receptor ligands induce the expression of interferon-gamma and interleukin-17 in chicken CD4+ T cells. *BMC Res Notes.* 2012;5:616. doi: 10.1186/1756-0500-5-616. PubMed PMID: 23116495; PubMed Central PMCID: PMCPMC3508843.
322. St Paul M, Paolucci S, Barjesteh N, Wood RD, Sharif S. Chicken erythrocytes respond to Toll-like receptor ligands by up-regulating cytokine transcripts. *Res Vet Sci.* 2013;95(1):87-91. doi: 10.1016/j.rvsc.2013.01.024. PubMed PMID: 23433682.
323. Philbin VJ, Iqbal M, Boyd Y, Goodchild MJ, Beal RK, Bumstead N, et al. Identification and characterization of a functional, alternatively spliced Toll-like receptor 7 (TLR7) and genomic disruption of TLR8 in chickens. *Immunology.* 2005;114(4):507-21. doi: 10.1111/j.1365-2567.2005.02125.x. PubMed PMID: 15804288; PubMed Central PMCID: PMCPMC1782111.
324. Vleugels B, Ververken C, Goddeeris BM. Stimulatory effect of CpG sequences on humoral response in chickens. *Poult Sci.* 2002;81(9):1317-21. PubMed PMID: 12269610.
325. Higgs R, Cormican P, Cahalane S, Allan B, Lloyd AT, Meade K, et al. Induction of a novel chicken Toll-like receptor following *Salmonella enterica* serovar Typhimurium infection. *Infect Immun.* 2006;74(3):1692-8. doi: 10.1128/IAI.74.3.1692-1698.2006. PubMed PMID: 16495540; PubMed Central PMCID: PMCPMC1418683.
326. Ramasamy KT, Reddy MR, Verma PC, Murugesan S. Expression analysis of turkey (*Meleagris gallopavo*) toll-like receptors and molecular characterization of avian specific TLR15. *Mol Biol Rep.* 2012;39(8):8539-49. doi: 10.1007/s11033-012-1709-6. PubMed PMID: 22699880.

327. Ciraci C, Lamont SJ. Avian-specific TLRs and downstream effector responses to CpG-induction in chicken macrophages. *Dev Comp Immunol.* 2011;35(3):392-8. doi: 10.1016/j.dci.2010.11.012. PubMed PMID: 21095203.
328. Heidari M, Sarson AJ, Huebner M, Sharif S, Kireev D, Zhou H. Marek's disease virus-induced immunosuppression: array analysis of chicken immune response gene expression profiling. *Viral Immunol.* 2010;23(3):309-19. doi: 10.1089/vim.2009.0079. PubMed PMID: 20565294.
329. Roach JC, Glusman G, Rowen L, Kaur A, Purcell MK, Smith KD, et al. The evolution of vertebrate Toll-like receptors. *Proc Natl Acad Sci U S A.* 2005;102(27):9577-82. doi: 10.1073/pnas.0502272102. PubMed PMID: 15976025; PubMed Central PMCID: PMCPMC1172252.
330. Brownlie R, Zhu J, Allan B, Mutwiri GK, Babiuk LA, Potter A, et al. Chicken TLR21 acts as a functional homologue to mammalian TLR9 in the recognition of CpG oligodeoxynucleotides. *Mol Immunol.* 2009;46(15):3163-70. doi: 10.1016/j.molimm.2009.06.002. PubMed PMID: 19573927.
331. Keestra AM, de Zoete MR, Bouwman LI, van Putten JP. Chicken TLR21 is an innate CpG DNA receptor distinct from mammalian TLR9. *J Immunol.* 2010;185(1):460-7. doi: 10.4049/jimmunol.0901921. PubMed PMID: 20498358.
332. Brisbin JT, Parvizi P, Sharif S. Differential cytokine expression in T-cell subsets of chicken caecal tonsils co-cultured with three species of *Lactobacillus*. *Benef Microbes.* 2012;3(3):205-10. doi: 10.3920/BM2012.0014. PubMed PMID: 22968409.
333. Yoneyama M, Fujita T. RNA recognition and signal transduction by RIG-I-like receptors. *Immunol Rev.* 2009;227(1):54-65. doi: 10.1111/j.1600-065X.2008.00727.x. PubMed PMID: 19120475.
334. Zou J, Chang M, Nie P, Secombes CJ. Origin and evolution of the RIG-I like RNA helicase gene family. *BMC Evol Biol.* 2009;9:85. doi: 10.1186/1471-2148-9-85. PubMed PMID: 19400936; PubMed Central PMCID: PMCPMC2686710.
335. Pichlmair A, Schulz O, Tan CP, Naslund TI, Liljestrom P, Weber F, et al. RIG-I-mediated antiviral responses to single-stranded RNA bearing 5'-phosphates. *Science.* 2006;314(5801):997-1001. doi: 10.1126/science.1132998. PubMed PMID: 17038589.
336. Matsumiya T, Stafforini DM. Function and regulation of retinoic acid-inducible gene-I. *Crit Rev Immunol.* 2010;30(6):489-513. PubMed PMID: 21175414; PubMed Central PMCID: PMCPMC3099591.
337. Samanta M, Iwakiri D, Kanda T, Imaizumi T, Takada K. EB virus-encoded RNAs are recognized by RIG-I and activate signaling to induce type I IFN. *EMBO J.* 2006;25(18):4207-14. doi: 10.1038/sj.emboj.7601314. PubMed PMID: 16946700; PubMed Central PMCID: PMCPMC1570431.
338. Hornung V, Ellegast J, Kim S, Brzozka K, Jung A, Kato H, et al. 5'-Triphosphate RNA is the ligand for RIG-I. *Science.* 2006;314(5801):994-7. doi: 10.1126/science.1132505. PubMed PMID: 17038590.
339. Karpala AJ, Stewart C, McKay J, Lowenthal JW, Bean AG. Characterization of chicken Mda5 activity: regulation of IFN-beta in the absence of RIG-I functionality. *J Immunol.* 2011;186(9):5397-405. doi: 10.4049/jimmunol.1003712. PubMed PMID: 21444763.
340. Kato H, Takeuchi O, Mikamo-Satoh E, Hirai R, Kawai T, Matsushita K, et al. Length-dependent recognition of double-stranded ribonucleic acids by retinoic acid-inducible gene-I and melanoma

differentiation-associated gene 5. *J Exp Med*. 2008;205(7):1601-10. doi: 10.1084/jem.20080091. PubMed PMID: 18591409; PubMed Central PMCID: PMCPMC2442638.

341. Lee CC, Wu CC, Lin TL. Characterization of chicken melanoma differentiation-associated gene 5 (MDA5) from alternative translation initiation. *Comp Immunol Microbiol Infect Dis*. 2012;35(4):335-43. doi: 10.1016/j.cimid.2012.02.004. PubMed PMID: 22459580.

342. Liniger M, Summerfield A, Ruggli N. MDA5 can be exploited as efficacious genetic adjuvant for DNA vaccination against lethal H5N1 influenza virus infection in chickens. *PLoS One*. 2012;7(12):e49952. doi: 10.1371/journal.pone.0049952. PubMed PMID: 23227156; PubMed Central PMCID: PMCPMC3515599.

343. Childs K, Stock N, Ross C, Andrejeva J, Hilton L, Skinner M, et al. mda-5, but not RIG-I, is a common target for paramyxovirus V proteins. *Virology*. 2007;359(1):190-200. doi: 10.1016/j.virol.2006.09.023. PubMed PMID: 17049367.

344. Liniger M, Summerfield A, Zimmer G, McCullough KC, Ruggli N. Chicken cells sense influenza A virus infection through MDA5 and CARDIF signaling involving LGP2. *J Virol*. 2012;86(2):705-17. doi: 10.1128/JVI.00742-11. PubMed PMID: 22072756; PubMed Central PMCID: PMCPMC3255855.

345. Franchi L, Eigenbrod T, Munoz-Planillo R, Nunez G. The inflammasome: a caspase-1-activation platform that regulates immune responses and disease pathogenesis. *Nat Immunol*. 2009;10(3):241-7. doi: 10.1038/ni.1703. PubMed PMID: 19221555; PubMed Central PMCID: PMCPMC2820724.

346. Muruve DA, Petrilli V, Zaiss AK, White LR, Clark SA, Ross PJ, et al. The inflammasome recognizes cytosolic microbial and host DNA and triggers an innate immune response. *Nature*. 2008;452(7183):103-7. doi: 10.1038/nature06664. PubMed PMID: 18288107.

347. Inohara, Chamaillard, McDonald C, Nunez G. NOD-LRR proteins: role in host-microbial interactions and inflammatory disease. *Annu Rev Biochem*. 2005;74:355-83. doi: 10.1146/annurev.biochem.74.082803.133347. PubMed PMID: 15952891.

348. Lian L, Ciraci C, Chang G, Hu J, Lamont SJ. NLRC5 knockdown in chicken macrophages alters response to LPS and poly (I:C) stimulation. *BMC Vet Res*. 2012;8:23. doi: 10.1186/1746-6148-8-23. PubMed PMID: 22401171; PubMed Central PMCID: PMCPMC3349563.

349. Ciraci C, Tuggle CK, Wannemuehler MJ, Nettleton D, Lamont SJ. Unique genome-wide transcriptome profiles of chicken macrophages exposed to Salmonella-derived endotoxin. *BMC Genomics*. 2010;11:545. doi: 10.1186/1471-2164-11-545. PubMed PMID: 20929591; PubMed Central PMCID: PMCPMC3091694.

350. Kaufman J, Milne S, Gobel TW, Walker BA, Jacob JP, Auffray C, et al. The chicken B locus is a minimal essential major histocompatibility complex. *Nature*. 1999;401(6756):923-5. doi: 10.1038/44856. PubMed PMID: 10553909.

351. Claver JA, Quaglia AI. Comparative Morphology, Development, and Function of Blood Cells in Nonmammalian Vertebrates. *Journal of Exotic Pet Medicine*. 2009;18(2):87-97.

352. Hawkey CM, Bennett PM, Gascoyne SC, Hart MG, Kirkwood JK. Erythrocyte size, number and haemoglobin content in vertebrates. *Br J Haematol*. 1991;77(3):392-7. PubMed PMID: 2012765.

353. Avery EH, Lee BL, Freedland RA, Cornelius CE. Bile pigments in gallbladder and freshly-secreted hepatic duct bile from fed and fasted rainbow trout, *Oncorhynchus mykiss*. *Comp Biochem Physiol Comp Physiol*. 1992;101(4):857-61. PubMed PMID: 1351461.
354. O'Malley B. *Clinical anatomy and physiology of exotic species*: WB Saunders Company; 2005.
355. Davies AJ, Johnston MR. The biology of some intraerythrocytic parasites of fishes, amphibia and reptiles. *Adv Parasitol*. 2000;45:1-107. PubMed PMID: 10751939.
356. Zhang DE, Nelson DA. Histone acetylation in chicken erythrocytes. Rates of deacetylation in immature and mature red blood cells. *Biochem J*. 1988;250(1):241-5. PubMed PMID: 3355515; PubMed Central PMCID: PMC1148839.
357. Sennikov SV, Injelevskaya TV, Krysov SV, Silkov AN, Kovinev IB, Dyachkova NJ, et al. Production of hemo- and immunoregulatory cytokines by erythroblast antigen+ and glycophorin A+ cells from human bone marrow. *BMC Cell Biol*. 2004;5(1):39. doi: 10.1186/1471-2121-5-39. PubMed PMID: 15488155; PubMed Central PMCID: PMC1524510.
358. Morera D, Roher N, Ribas L, Balasch JC, Donate C, Callol A, et al. RNA-Seq reveals an integrated immune response in nucleated erythrocytes. *PLoS One*. 2011;6(10):e26998. doi: 10.1371/journal.pone.0026998. PubMed PMID: 22046430; PubMed Central PMCID: PMC3203173.
359. Morera D, MacKenzie SA. Is there a direct role for erythrocytes in the immune response? *Vet Res*. 2011;42:89. doi: 10.1186/1297-9716-42-89. PubMed PMID: 21801407; PubMed Central PMCID: PMC3199785.
360. Workenhe ST, Kibenge MJ, Wright GM, Wadowska DW, Groman DB, Kibenge FS. Infectious salmon anaemia virus replication and induction of alpha interferon in Atlantic salmon erythrocytes. *Virology*. 2008;5:36. doi: 10.1186/1743-422X-5-36. PubMed PMID: 18307775; PubMed Central PMCID: PMC2292172.
361. Passantino L, Altamura M, Cianciotta A, Jirillo F, Ribaud MR, Jirillo E, et al. Maturation of fish erythrocytes coincides with changes in their morphology, enhanced ability to interact with *Candida albicans* and release of cytokine-like factors active upon autologous macrophages. *Immunopharmacol Immunotoxicol*. 2004;26(4):573-85. doi: 10.1081/IPH-200042323. PubMed PMID: 15658606.
362. Passantino L, Massaro MA, Jirillo F, Di Modugno D, Ribaud MR, Modugno GD, et al. Antigenically activated avian erythrocytes release cytokine-like factors: a conserved phylogenetic function discovered in fish. *Immunopharmacol Immunotoxicol*. 2007;29(1):141-52. doi: 10.1080/08923970701284664. PubMed PMID: 17464774.
363. Nikinmaa M. Oxygen and carbon dioxide transport in vertebrate erythrocytes: an evolutionary change in the role of membrane transport. *J Exp Biol*. 1997;200(Pt 2):369-80. PubMed PMID: 9050246.
364. Montel-Hagen A, Sitbon M, Taylor N. Erythroid glucose transporters. *Curr Opin Hematol*. 2009;16(3):165-72. doi: 10.1097/MOH.0b013e328329905c. PubMed PMID: 19346941.
365. Perez-Gordones MC, Lugo MR, Winkler M, Cervino V, Benaim G. Diacylglycerol regulates the plasma membrane calcium pump from human erythrocytes by direct interaction. *Arch Biochem Biophys*. 2009;489(1-2):55-61. doi: 10.1016/j.abb.2009.07.010. PubMed PMID: 19631607.

366. Tsantes AE, Bonovas S, Travlou A, Sitaras NM. Redox imbalance, macrocytosis, and RBC homeostasis. *Antioxid Redox Signal*. 2006;8(7-8):1205-16. doi: 10.1089/ars.2006.8.1205. PubMed PMID: 16910768.
367. Fonseca AM, Pereira CF, Porto G, Arosa FA. Red blood cells promote survival and cell cycle progression of human peripheral blood T cells independently of CD58/LFA-3 and heme compounds. *Cell Immunol*. 2003;224(1):17-28. PubMed PMID: 14572797.
368. Gershon H. The anti-inflammatory role of the erythrocyte: impairment in the elderly. *Arch Gerontol Geriatr*. 1997;24(2):157-65. PubMed PMID: 15374122.
369. Jiang N, Tan NS, Ho B, Ding JL. Respiratory protein-generated reactive oxygen species as an antimicrobial strategy. *Nat Immunol*. 2007;8(10):1114-22. doi: 10.1038/ni1501. PubMed PMID: 17721536.
370. Liepke C, Baxmann S, Heine C, Breithaupt N, Standker L, Forssmann WG. Human hemoglobin-derived peptides exhibit antimicrobial activity: a class of host defense peptides. *J Chromatogr B Analyt Technol Biomed Life Sci*. 2003;791(1-2):345-56. PubMed PMID: 12798194.
371. Morariu AM, Maathuis MH, Asgeirsdottir SA, Leuvenink HG, Boonstra PW, van Oeveren W, et al. Acute isovolemic hemodilution triggers proinflammatory and procoagulatory endothelial activation in vital organs: role of erythrocyte aggregation. *Microcirculation*. 2006;13(5):397-409. doi: 10.1080/10739680600745992. PubMed PMID: 16815825.
372. Pesquero J, Albi JL, Gallardo MA, Planas J, Sanchez J. Glucose metabolism by trout (*Salmo trutta*) red blood cells. *J Comp Physiol B*. 1992;162(5):448-54. PubMed PMID: 1401338.
373. Orlov SN, Aksentsev SL, Kotelevtsev SV. Extracellular calcium is required for the maintenance of plasma membrane integrity in nucleated cells. *Cell Calcium*. 2005;38(1):53-7. doi: 10.1016/j.ceca.2005.03.006. PubMed PMID: 15936814.
374. Jensen FB. The role of nitrite in nitric oxide homeostasis: a comparative perspective. *Biochim Biophys Acta*. 2009;1787(7):841-8. doi: 10.1016/j.bbabbio.2009.02.010. PubMed PMID: 19248757.
375. Schraml B, Baker MA, Reilly BD. A complement receptor for opsonized immune complexes on erythrocytes from *Oncorhynchus mykiss* but not *Ictalurus punctatus*. *Mol Immunol*. 2006;43(10):1595-603. doi: 10.1016/j.molimm.2005.09.014. PubMed PMID: 16271392.
376. Fedeli D, Carloni M, Falcioni G. Oxidative damage in trout erythrocyte in response to "in vitro" copper exposure. *Mar Environ Res*. 2010;69(3):172-7. doi: 10.1016/j.marenvres.2009.10.001. PubMed PMID: 19880173.
377. Ullal AJ, Litaker RW, Noga EJ. Antimicrobial peptides derived from hemoglobin are expressed in epithelium of channel catfish (*Ictalurus punctatus*, Rafinesque). *Dev Comp Immunol*. 2008;32(11):1301-12. doi: 10.1016/j.dci.2008.04.005. PubMed PMID: 18538841.
378. Fernandes JM, Smith VJ. Partial purification of antibacterial proteinaceous factors from erythrocytes of *Oncorhynchus mykiss*. *Fish Shellfish Immunol*. 2004;16(1):1-9. PubMed PMID: 14675829.
379. Kaloyianni M, Doukakis I. Effect of adrenaline on glucose transport in red cells of *Rana balcanica*. *Gen Physiol Biophys*. 2003;22(1):69-80. PubMed PMID: 12870702.

380. Light DB, Attwood AJ, Siegel C, Baumann NL. Cell swelling increases intracellular calcium in *Necturus erythrocytes*. *J Cell Sci*. 2003;116(Pt 1):101-9. PubMed PMID: 12456720.
381. Mauro NA, Isaacks RE. Examination of reptilian erythrocytes as models of the progenitor of mammalian red blood cells. *Comp Biochem Physiol A Physiol*. 1997;116(4):323-7. PubMed PMID: 9125684.
382. Bagnaresi P, Rodrigues MT, Garcia CR. Calcium signaling in lizard red blood cells. *Comp Biochem Physiol A Mol Integr Physiol*. 2007;147(3):779-87. doi: 10.1016/j.cbpa.2006.09.015. PubMed PMID: 17095273.
383. Torsoni MA, Ogo SH. Hemoglobin-sulfhydryls from tortoise (*Geochelone carbonaria*) can reduce oxidative damage induced by organic hydroperoxide in erythrocyte membrane. *Comp Biochem Physiol B Biochem Mol Biol*. 2000;126(4):571-7. PubMed PMID: 11026669.
384. Parish CA, Jiang H, Tokiwa Y, Berova N, Nakanishi K, McCabe D, et al. Broad-spectrum antimicrobial activity of hemoglobin. *Bioorg Med Chem*. 2001;9(2):377-82. PubMed PMID: 11249130.
385. Braun EJ, Sweazea KL. Glucose regulation in birds. *Comp Biochem Physiol B Biochem Mol Biol*. 2008;151(1):1-9. doi: 10.1016/j.cbpb.2008.05.007. PubMed PMID: 18571448.
386. Alves-Ferreira M, Scofano HM, Ferreira-Pereira A. Ca(2+)-ATPase from chicken (*Gallus domesticus*) erythrocyte plasma membrane: effects of calmodulin and taurine on the Ca(2+)-dependent ATPase activity and Ca²⁺ uptake. *Comp Biochem Physiol B Biochem Mol Biol*. 1999;122(3):269-76. PubMed PMID: 10374256.
387. Di Simplicio P, Cacace MG, Lusini L, Giannerini F, Giustarini D, Rossi R. Role of protein -SH groups in redox homeostasis--the erythrocyte as a model system. *Arch Biochem Biophys*. 1998;355(2):145-52. doi: 10.1006/abbi.1998.0694. PubMed PMID: 9675020.
388. Bertram EM, Jilbert AR, Kotlarski I. Optimization of an in vitro assay which measures the proliferation of duck T lymphocytes from peripheral blood in response to stimulation with PHA and ConA. *Dev Comp Immunol*. 1997;21(3):299-310. PubMed PMID: 9258611.
389. Mian MF, Ahmed AN, Rad M, Babaian A, Bowdish D, Ashkar AA. Length of dsRNA (poly I:C) drives distinct innate immune responses, depending on the cell type. *J Leukoc Biol*. 2013;94(5):1025-36. doi: 10.1189/jlb.0312125. PubMed PMID: 23911868.
390. Brat DJ, Bellail AC, Van Meir EG. The role of interleukin-8 and its receptors in gliomagenesis and tumoral angiogenesis. *Neuro-oncology*. 2005;7(2):122-33.
391. Fortier ME, Kent S, Ashdown H, Poole S, Boksa P, Luheshi GN. The viral mimic, polyinosinic:polycytidylic acid, induces fever in rats via an interleukin-1-dependent mechanism. *Am J Physiol Regul Integr Comp Physiol*. 2004;287(4):R759-66. doi: 10.1152/ajpregu.00293.2004. PubMed PMID: 15205185.
392. DeWitte-Orr SJ, Mehta DR, Collins SE, Suthar MS, Gale M, Jr., Mossman KL. Long double-stranded RNA induces an antiviral response independent of IFN regulatory factor 3, IFN-beta promoter stimulator 1, and IFN. *J Immunol*. 2009;183(10):6545-53. doi: 10.4049/jimmunol.0900867. PubMed PMID: 19864603; PubMed Central PMCID: PMC2885285.

393. Poltorak A, He X, Smirnova I, Liu MY, Van Huffel C, Du X, et al. Defective LPS signaling in C3H/HeJ and C57BL/10ScCr mice: mutations in Tlr4 gene. *Science*. 1998;282(5396):2085-8. PubMed PMID: 9851930.
394. Shimazu R, Akashi S, Ogata H, Nagai Y, Fukudome K, Miyake K, et al. MD-2, a molecule that confers lipopolysaccharide responsiveness on Toll-like receptor 4. *J Exp Med*. 1999;189(11):1777-82. PubMed PMID: 10359581; PubMed Central PMCID: PMCPMC2193086.
395. Netea MG, van Deuren M, Kullberg BJ, Cavaillon JM, Van der Meer JW. Does the shape of lipid A determine the interaction of LPS with Toll-like receptors? *Trends Immunol*. 2002;23(3):135-9. PubMed PMID: 11864841.
396. Kawai T, Takeuchi O, Fujita T, Inoue J, Muhlradt PF, Sato S, et al. Lipopolysaccharide stimulates the MyD88-independent pathway and results in activation of IFN-regulatory factor 3 and the expression of a subset of lipopolysaccharide-inducible genes. *J Immunol*. 2001;167(10):5887-94. PubMed PMID: 11698465.
397. Shah SM, Ravi Kumar GV, Brah GS, Santra L, Pawar H. Differential Expression of Th1- and Th2-Type Cytokines in Peripheral Blood Mononuclear Cells of Murrah Buffalo (*Bubalus Bubalis*) on TLR2 Induction by *B. Subtilis* Peptidoglycan. *Asian-Australas J Anim Sci*. 2012;25(7):1021-8. doi: 10.5713/ajas.2012.12033. PubMed PMID: 25049659; PubMed Central PMCID: PMCPMC4092975.
398. Schwandner R, Dziarski R, Wesche H, Rothe M, Kirschning CJ. Peptidoglycan- and lipoteichoic acid-induced cell activation is mediated by toll-like receptor 2. *J Biol Chem*. 1999;274(25):17406-9. PubMed PMID: 10364168.
399. Takeuchi O, Hoshino K, Kawai T, Sanjo H, Takada H, Ogawa T, et al. Differential roles of TLR2 and TLR4 in recognition of gram-negative and gram-positive bacterial cell wall components. *Immunity*. 1999;11(4):443-51. PubMed PMID: 10549626.
400. Chamaillard M, Hashimoto M, Horie Y, Masumoto J, Qiu S, Saab L, et al. An essential role for NOD1 in host recognition of bacterial peptidoglycan containing diaminopimelic acid. *Nat Immunol*. 2003;4(7):702-7. doi: 10.1038/ni945. PubMed PMID: 12796777.
401. Girardin SE, Boneca IG, Carneiro LA, Antignac A, Jehanno M, Viala J, et al. Nod1 detects a unique muropeptide from gram-negative bacterial peptidoglycan. *Science*. 2003;300(5625):1584-7. doi: 10.1126/science.1084677. PubMed PMID: 12791997.
402. Girardin SE, Boneca IG, Viala J, Chamaillard M, Labigne A, Thomas G, et al. Nod2 is a general sensor of peptidoglycan through muramyl dipeptide (MDP) detection. *J Biol Chem*. 2003;278(11):8869-72. doi: 10.1074/jbc.C200651200. PubMed PMID: 12527755.
403. Bauer S, Wagner H. Bacterial CpG-DNA licenses TLR9. *Curr Top Microbiol Immunol*. 2002;270:145-54. PubMed PMID: 12467249.
404. Rothenfusser S, Tuma E, Endres S, Hartmann G. Plasmacytoid dendritic cells: the key to CpG. *Hum Immunol*. 2002;63(12):1111-9. PubMed PMID: 12480254.
405. Vollmer J, Krieg AM. Immunotherapeutic applications of CpG oligodeoxynucleotide TLR9 agonists. *Adv Drug Deliv Rev*. 2009;61(3):195-204. doi: 10.1016/j.addr.2008.12.008. PubMed PMID: 19211030.

406. Zhang DE, Nelson DA. Histone acetylation in chicken erythrocytes. Rates of acetylation and evidence that histones in both active and potentially active chromatin are rapidly modified. *Biochem J.* 1988;250(1):233-40. PubMed PMID: 2451508; PubMed Central PMCID: PMCPMC1148838.
407. Rocha E, Davie JR, van Holde KE, Weintraub H. Differential salt fractionation of active and inactive genomic domains in chicken erythrocyte. *J Biol Chem.* 1984;259(13):8558-63. PubMed PMID: 6736042.
408. Spencer VA, Davie JR. Dynamically acetylated histone association with transcriptionally active and competent genes in the avian adult beta-globin gene domain. *J Biol Chem.* 2001;276(37):34810-5. doi: 10.1074/jbc.M104886200. PubMed PMID: 11435438.
409. Yuan CC, Matthews AG, Jin Y, Chen CF, Chapman BA, Ohsumi TK, et al. Histone H3R2 symmetric dimethylation and histone H3K4 trimethylation are tightly correlated in eukaryotic genomes. *Cell Rep.* 2012;1(2):83-90. doi: 10.1016/j.celrep.2011.12.008. PubMed PMID: 22720264; PubMed Central PMCID: PMCPMC3377377.
410. Castello A, Fischer B, Eichelbaum K, Horos R, Beckmann BM, Strein C, et al. Insights into RNA biology from an atlas of mammalian mRNA-binding proteins. *Cell.* 2012;149(6):1393-406. doi: 10.1016/j.cell.2012.04.031. PubMed PMID: 22658674.

CHAPTER II: MATERIALS & METHODS

2.1 Cell processing and related techniques

2.1.1 Animal Ethics and source of cells

Animal ethics approval was obtained from University of Manitoba Animal Protocol Management and Review Committee before starting all chicken work. Authorization to use controlled drug was obtained from Health Canada. All methods involving the use of chickens were approved by the committee and carried out in accordance with its guidelines and regulations. All egg-laying hens were purchased from Clarks Poultry and then raised in a pullet to grow for 18 weeks before moving into the animal care facility, University of Manitoba. Chickens were purchased through Central Animal Care Services, University of Manitoba. They were housed under standard conditions in Central Animal Care Services, Basic Medical Science Building. All methods involving the use of chickens were approved by and carried out in accordance with the University of Manitoba Animal Care Committee guidelines and regulations. A biological sample consisted of a pool of red blood cells from 11-12 anemic chickens.

2.1.2 Types of cells used in the study

In this study, chicken polychromatic erythrocytes were used for most experiments. For some parts of the study, chicken mature erythrocytes and 6C2 cells were used. Chicken polychromatic erythrocytes represent the stage of erythrocytes before final maturation stage [286]. Mature erythrocytes were collected from non-anemic chicken. 6C2 cells are transformed cells with erythroblastosis virus and represent the early colony forming unit (CFU) stage of erythropoiesis [411]. The 6C2 cells were a generous gift from Dr. Suming Huang from University of Florida.

2.1.3 Treatment of chickens

Chickens were made anemic with the administration of phenylhydrazine solution (3.5 mL 95% ethanol, 2.5 mL double distilled water and 0.15 g acetyl-phenylhydrazine) in a dose-dependent manner for 6 consecutive days. They were injected intramuscularly with 0.7 mL on the first two days, 0.4 mL on the 3rd day, 0.6 mL on the 4th day, 0.7 mL on the 5th day and 0.8 mL on the 6th day.

2.1.4 Harvesting chicken erythrocytes and storage

Chickens were anesthetized with the following anesthetic solution: 3 parts of Ketamine, 1 part of Rompun, 2 parts of saline (collection buffer pH 7.4: 75 mM NaCl, 25 mM EDTA, pH 8.0, 25 mM Tris-HCl, pH 7.5). Birds were injected with anesthetic in the breast (0.2 mL or 0.5 mL for larger size chickens). When

the chicken was fully anesthetized, the jugular vein was severed with a blade, and blood was collected quickly in a large 2 litre plastic jug containing an amount of collection buffer equal to the final volume of collected blood. The blood was filtered through at least 4 layers of cheese cloth lining a buchner funnel into a 500 mL or 2L flask placed on ice. Approximately 30 mL of blood was aliquoted into ice-cold, polycarbonate tubes (clear, open-topped and non-flexible tubes). It was then centrifuged at 3.5K rotations per minute (rpm) for 5-10 minute at 4°C in a SS-34 rotor. Supernatant and the white cell layer were removed immediately above the red blood cell pellet with a vacuum aspirator. The pellet was resuspended in approximately 30 mL collection buffer, and centrifugation was performed at 3.5K rpm for 5-10 minute at 4°C in a SS-34 Rotor. The pellet was washed with collection buffer for at least 3 more times. Packed cells were stored at -20°C overnight and then transferred to -80°C for long term storage.

2.1.5 Preparation of media for erythrocyte cell treatment

MEM Alpha (1X) minimum essential medium (Life Technologies, cat#12571-063) containing L-glutamine, ribonucleosides, deoxyribonucleosides. Media was supplemented with 10% FBS (Life Technologies), 2% chicken serum (Sigma), 1 mM HEPES (Life Technologies), 0.5 mM β -mercaptoethanol (Sigma) and 0.1M penicillin-streptomycin (Life Technologies).

2.1.6 Chromatin fractionation

1. Packed chicken erythrocytes were washed for four times with RSB buffer (10 mM Tris-Cl pH 7.5, 10 mM NaCl, 3 mM MgCl₂, 5 mM Na-butyrate). 300 uL NP-40 (stock of 25% v/v) and 300 uL PMSF of 100 mM stock solution were added to 30 mL RSB buffer (stored at 4°C) to the cell pellet.
2. Resuspended cells were homogenized for five times in slow motion using a glass homogenizer. Cells were pelleted by centrifuging at 3.5K rpm for 10 minute at 4°C (SS34 rotor).
3. Supernatant was decanted carefully using capillary pipette. Pellet was then resuspended with chilled 30 mL RSB buffer containing Na-butyrate, 300 uL NP-40 (stock of 25% v/v) and 300 uL PMSF (stock 100 mM) followed by centrifugation at 3.5K rpm for 10 minute at 4°C.
4. The pellet was washed with RSB buffer after the removal of supernatant and centrifugation at the above-mentioned speed. Pellet was resuspended with 8-10 mL of cold W&S buffer (1 M hexylene glycol, 10 mM PIPES pH 7.0, 2 mM MgCl₂, 1% thiodiglycol, 30 mM Na-butyrate), and A260 was determined.
5. Resuspended nuclei were diluted to 50 A260nm U/mL, and absorbance was re-measured. Nuclei were incubated in a 37°C water bath with shaking for 10 minute in order to ensure the sample mixes well.

6. CaCl_2 was added to a final concentration of 1 mM and incubated for 10 minute.
7. Micrococcal nuclease (MNase) (Worthington) was added to a final concentration of 15 units/mL and incubation was continued in the shaking water bath for 12 minute. The concentration and time of MNase digestion should be optimized prior to the experiment to get polynucleosome-sized fragment sizes (average size 1.5-2 kb). When using a new enzyme or if activity was lower over time of MNase storage, a series of digestions need to be performed by keeping the digestion time constant and increasing the amount of enzyme (ie. 1x, 1.5x, 2x, 2.5x, 3x, 3.5x, 4x 15 units/ml). To resuspend the enzyme, 2 mL of 50% glycerol was added to a vial of 45k units of MNase (Worthington). This makes a stock of 22.5k U/mL of MNase enzyme. After the digestion, a quick DNA extraction can be performed by adding an equal volume of phenol/chloroform followed by mixing and centrifugation at 13K rpm for 15 minute. Subsequently RNase A (5 ug/mL final) was added and incubated at 37°C for 30 minute. To view the DNA sizes samples were run on a 1% agarose gel.
8. MNase reaction was stopped by adding EGTA to a final concentration of 10 mM.
9. Nuclei was centrifuged in two pre-cooled tubes, at 10K rpm and 4°C for 10 minute.
10. Supernatant was discarded, and the pellet was resuspended in 10 mM EDTA/5 mM sodium butyrate pH 7.4 with a glass pipette and was left on ice for 30 minutes. To enhance the release of chromatin, the suspension may be homogenized for three times.
11. Chromatin was centrifuged at 10K rpm and 4°C in a SS34 rotor for 10 minutes. EDTA-soluble (S_E fraction) chromatin fraction was collected as supernatant while EDTA insoluble pellet (P_E fraction) as pellet fraction.
12. A260 units/mL of the S_E fraction was measured and multiplied by the total volume for total A260 of S_E . The total recovered A260 nm units of the S_E fraction should amount to 60-70% of the total A260 nm units of nuclei (i.e., total S_E /total nuclei = 60-70%). The pellet (P_E fraction) was saved and stored at 4°C.
13. In order to make S_{150} or P_{150} fraction, the S_E fraction was diluted to 30 A260 nm units/mL with 10 mM EDTA/5 mM sodium butyrate pH 7.4. Absorbance was measured in quadruplicate to confirm S_E has been diluted to 30 A260 nm units/mL.
14. NaCl was added dropwise from a 4 M stock to a final concentration of 150 mM to the S_E solution followed by centrifugation at 10K rpm and 4°C for 10 min (SS34 rotor). Caution should be followed to

gently mix the solution while adding NaCl in order to ensure proper mixing of the chromatin with salt. The pellet (P₁₅₀ fraction) was saved and stored while the supernatant (S₁₅₀ fraction) was measured for total volume.

15. An A260 nm measurement was taken for S₁₅₀ to determine the concentration. The total recovered A260 nm units of the S₁₅₀ fraction should be approximately 10% of the total S_E A260 nm units used in preparing the S₁₅₀ fraction.

16. S₁₅₀ must be concentrated using polyethylene glycol (PEG) 8000 (Fisher), and absorbance was measured. S₁₅₀ was placed in a pre-wetted dialysis membrane, and the sample was placed onto a bed of PEG. The top of the S₁₅₀ containing dialysis bag was covered with PEG and placed at 4°C. Samples should be checked every hour or two to ensure concentrating process is running smoothly.

17. S₁₅₀ should be concentrated down to 8-10 ml. In the meantime, the Biogel A1.5 column (BioRad) should be washed with Column Running buffer (100 mM Tris-pH 8.0, 10 mM EDTA, 150 mM NaCl).

18. Chromatin fractions F1 (polynucleosomes), F2 (oligonucleosomes), F3 (oligonucleosomes/mononucleosomes) and F4 (mononucleosomes) were separated from S₁₅₀ chromatin by gel exclusion chromatography with a Biogel A1.5 column at a flow rate of 0.11 mL/minute.

19. Fraction collector (BioRad, model #2110) was set at 13 minute to collect 5 mL fraction in each tube. The run should take 16-18 hours to complete.

20. Absorbance was measured from each tube, and the DNA isolated from the fractions were run on 1% agarose gel to determine the size of collected fragments.

2.3 Protein-based techniques

2.3.1 Preparation of cellular extract

Erythrocytes were washed with RSB buffer twice and resuspended in an appropriate volume of cold lysis buffer (50 mM Tris-HCl, pH 8.0, 150 mM NaCl, 1.0 mM EDTA, 0.5% NP-40) containing phosphatase and protease inhibitors (Roche). The cell suspension was sonicated using probe sonicator (Fisher scientific, sonic dismembrator, model #100) 2-3 times 3X 10 sec each with 1 minute interval on ice. Supernatant was collected after centrifugation at 7,000 g for 10 minutes at 4°C. The protein concentration of the supernatant was measured using BCA protein assay kit (Thermo Fisher Scientific) as per

manufacturer's instructions using BSA (bovine serum albumin) as a standard. The cell extracts were stored at -20°C or -80°C.

2.3.2 Electrophoresis and Immunoblotting

Equal A260 (2.0 A260) of each chromatin fraction (P_E , S_E , S_{150} , P_{150} , F1-F4) was denatured by boiling for 5-6 minute in SDS-loading buffer [65 mM Tris-HCl, pH 6.8, 2% SDS, 10% glycerol, 2-5% v/v β -mercaptoethanol (BME), and 0.01 mg bromophenol blue]. Proteins were resolved by SDS-polyacrylamide gel electrophoresis (SDS-PAGE) to separate proteins based on their molecular weight under denaturing conditions, according to Laemmli's protocol [412]. Proteins was separated depending on size on 8%, 10% or 15% polyacrylamide gels using Mini-Protean® 3 Cell apparatus (BioRad). In order to get the desired resolution, gels were run at a constant voltage of 120V for approximately 1.5-2.0 hour. Proteins were transferred from SDS gel to 0.45 μ m nitrocellulose membranes (BioRad) using the wet transfer apparatus (BioRad) at a constant voltage of 100V for 1 hour at 4°C. Membranes were stained after transfer with Ponceau S [0.5% (w/v) Ponceau S, 1% acetic acid] to determine the efficiency of the transfer. Membranes were blocked with 5% (w/v) non-fat dry milk in 0.05% TTBS (0.05% Tween-20, 50 mM Tris-HCl, pH 7.5, 150 mM NaCl) for 1.0-1.5 hour at room temperature on a rocking platform (VWR, Model 200). Membrane was incubated with primary antibody for 2 hour at room temperature or overnight at 4°C on an orbitron (Boekel Scientific, Model 260200) depending on the antibody. Next day, membranes were washed three times with 0.05% TTBS (10 minute/wash). After the washing step, membranes were incubated with secondary antibody (isotype-specific to primary antibody) by placing on rocking platform (VWR, model# 200) for 1 hour at room temperature. Secondary antibodies conjugated with horseradish peroxidase (HRP). Using the Hyper film ECL (Amersham) with Western 221 Lightning™ Plus-ECL reagent (Perkin Elmer) according to the supplier's instructions, the antibodies to proteins of interest were visualized.

2.3.3 Peptide Dot Blot assay

Nitrocellulose membrane was labelled to specify the location of the peptides. Peptides were directly added onto the membrane and allowed to dry at 65°C for 15 minute. Membrane was incubated with blocking solution (5.0 % skim milk-0.05% TTBS) for 1 hour at room temperature. Membrane was then incubated with primary antibody solution for overnight. After three washes with 0.05%, TTBS incubation with the secondary antibody solution (diluted in blocking solution) was performed for 1 hour at room temperature

with rotation. After incubation with the chemiluminescent ECL, the film was developed for the signal of the antibody.

2.3.4 Immunoprecipitation

Cells were washed with RSB buffer (10 mM Tris-HCl pH7.5, 10 mM NaCl, 3 mM MgCl) twice. Cell pellet was dissolved with low stringency IP buffer (50 mM Tris-HCl, pH 8.0; 150 mM NaCl, 0.5% NP-40, 1 mM EDTA). Cellular extract was then sonicated using probe sonicator (Fisher scientific, sonic dismembrator, model#100) at setting 2 for 10 seconds twice. Supernatant was collected after 10 minute centrifugation at high speed using benchtop centrifuge (Sorvall Legend Micro 17).

2.3.5 Histone co-IP

Packed erythrocytes were washed with RSB buffer (10 mM Tris-HCl pH 7.5, 10 mM NaCl, 3 mM MgCl). Nuclei were isolated using cell lysis buffer (5 mM PIPES [pHed with KOH to 8.0], 85 mM KCl, 0.5% NP-40) buffer with the incubation at 4°C. Supernatant was discarded after centrifugation for 10 minute at 10,000 rpm using microcentrifuge (Hettich Mikro 20 Centrifuge). The nuclear pellet was resuspended in MNase Digestion Buffer (10 mM Tris-HCl pH 7.5, 0.25 M sucrose, 75 mM NaCl) plus phosphatase/protease inhibitors. A260 of the suspension was measured. CaCl₂ was added to the samples to a final concentration of 3 mM and incubated at 37°C for 10 minute. MNase was added to a concentration of 4.5 U/mL and incubated for 20 minute. MNase condition was optimized to get mononucleosome size fragments. Reaction was stopped by adding EDTA pH 8.0 to a final concentration of 5 mM. Nuclei was lysed with SDS (0.5% final concentration) by rotating at room temperature for 1 hour. Insoluble material was separated by centrifugation (10k rpm, 5 minute) (Sorvall Legend Micro 17) and discarded. Nuclear lysate was diluted with RIPA buffer (10 mM Tris-HCl pH 8.0, 1% Triton-X-100, 0.1% SDS, 0.1% sodium deoxycholate-SDC) plus phosphatase/protease inhibitors added freshly. Lysate was pre-cleared with protein A/G agarose (Santa Cruz) beads (40 µl per mL of lysate) for 1 hour at 4°C. Beads were pelleted by centrifugation by using microcentrifuge (Hettich Mikro 20 Centrifuge) for 2-3 minute at 1200 rpm. Supernatant was transferred to new tubes. After measuring the A260, 1 ug of antibody was used per A260 of lysate. It was allowed to incubate overnight at 4°C with rotation. Next day Dynabeads Protein G (Invitrogen) were added and incubated for 2 hours with rotation at 4°C. Beads were washed with RIPA buffer 4 times at room temperature for 5 minutes with rotation. One A260 of supernatant was collected for immunodepleted (ID) fraction. Immunoprecipitant (IP) was eluted by adding appropriate volume

(usually 40 μ L) of SDS loading buffer to the beads. Equal amounts of input and ID (usually 0.2 A260) and 1 A260 IP were loaded onto gel for Western blot analysis.

2.3.6 Chromatin immunoprecipitation (ChIP) assay and ChIP-seq assay

1. Packed blood cells were washed twice with 1X PBS.
2. Cells were incubated with 0.5% (v/v) formaldehyde at room temperature for 10 minutes.
3. Subsequently, 125 mM glycine (final concentration) was added to stop cross-linking (made up in 1xPBS).
4. After 5 minute, incubation at room temperature supernatant was removed by aspiration after centrifuging cells at 4k rpm for 10 minute.
5. Cells were washed twice with RSB buffer and pelleted by centrifuging at 1200 rpm (300 xg) for 3 minutes. RSB was removed and cells were stored at -80°C if needed or continue with next step.
6. Cell pellet was suspended in 5 mL of cell lysis buffer (RSB plus 0.5% NP-40) plus phosphatase/protease inhibitors and incubated for 5-10 minutes at 4°C with gentle shaking on a rotor.
7. To obtain the nuclei, the resuspended pellet was centrifuged for 5 minutes (2000g). This wash step was repeated at least one more time. Nuclei were observed under a microscope after second wash step to ensure the proper isolation of nuclei.
8. The nuclear pellet was resuspended with an appropriate volume (approximately 2 mL) of MNase digestion buffer (10 mM Tris-HCl pH 7.5, 0.25M sucrose, 75 mM NaCl) with phosphatase/protease inhibitors depending on the pellet size.
9. Nuclei were lysed using 0.5% SDS and rotating at room temperature for 30 minutes.
10. Chromatin was sheared using probe sonicator (Fisher scientific, sonic dismembrator, model#100) at setting 3. Sonication was performed for 10 sec then leave tube on ice for 30 sec. Sonication time has to be optimized until the average fragment size is 200-300 bp of the fragment.
11. Nuclear lysate was diluted (5 fold) with RIPA buffer (10 mM Tris-HCl pH 8.0, 1% Triton-X-100, 0.1% SDS, 0.1% SDC) plus phosphatase/protease inhibitors (4 mL of RIPA to 1 mL of sonicated lysate).
12. The lysate was pre-cleared with protein A/G agarose beads (300 μ L) for 1 hour at 4°C (60 μ L of A/G beads per mL of lysate). Beads were pelleted by centrifugation at 1200rpm for 2-3 minute using microcentrifuge (Hettich Mikro 20 Centrifuge).

13. Approximately 5 A260 of the lysate was incubated with rotation overnight at 4°C with 5 ug of specific antibody. Isotype-specific IgG was included as a control to the ChIP experiment.
14. Next day, magnetic Dynabeads protein G beads (Invitrogen, cat# 100.04D) were added and incubated for 2 hours with rotation at 4°C (7 µl of Beads per A260). Magnetic beads were pelleted using MagneSphere® Technology Stands (from Promega), and supernatants were removed.
15. Beads were washed with Low Salt Wash Buffer (0.1% SDS, 1% Triton-X-100, 2 mM EDTA, 20 mM Tris-HCl pH 8.1, 150 mM NaCl), High Salt Wash Buffer (0.1% SDS, 1% Triton-X-100, 2 mM EDTA, 20 mM Tris- HCl pH 8.1, 500 mM NaCl), LiCl Wash Buffer (250 mM LiCl, 1% NP-40, 1% deoxycholate, 1 mM EDTA, 10 mM Tris-HCl pH 8.1) and 1xTE Buffer (10 mM Tris-HCl pH 7.5, 1 mM EDTA) at least twice.
16. Antibody/chromatin complexes were eluted by adding 200 uL of Elution Buffer (1% SDS, 100 mM NaHCO₃) to the beads.
17. After reverse crosslinking at 65°C overnight, samples were treated with proteinase K (Sigma) (0.5 µg/mL final concentration) for 1 hour at 55°C and RNase A (Sigma) (0.02 µg/mL final concentration) for 30 minutes at 37°C. DNA was purified using the Qiagen PCR purification kit.

2.4 RNA-based technique

2.4.1 RNA extraction and cDNA preparation

RNA from polychromatic erythrocytes were isolated using RNeasy Plus mini kit (Qiagen) following manufacturer's instruction. DNase digestion was performed (Promega) to remove any genomic DNA in the purified RNA. RNA stock was diluted to 100 ng and cDNA preparation reaction mixture was set up as follows using GeneAmp® PCR system 2700 from applied biosystem.

4 ul RT mix (iScript™ Reverse Transcription Supermix from BioRad)

8 ul ddH₂O

8ul of you diluted RNA (100 ng RNA)

Total 20 uL

cDNA was synthesized using the following program,

Priming	5 minutes at 25°C
Reverse transcription	30 minute at 42°C
RT Inactivation	5 minute at 85°C

2.4.2 Isolation of nuclear RNA

Nuclei were isolated from polychromatic erythrocytes using the previously described protocol [287]. RNA was isolated from the nuclei using commercially available RNeasy plus mini kit from Qiagen.

2.5 Polymerase chain reaction (PCR)

2.5.1 RT-qPCR

RT-qPCR was performed using 3 ng of prepared cDNA (stock 100ng), 0.2 uM of forward and reverse primer. 10 uL of Universal sybergreen Supermix from BioRad and 6.6 uL of ddH2O. Program used for PCR reaction was as follows,

98°C for 3minute

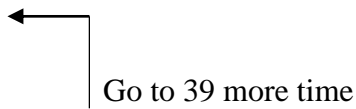
98°C for 0:15minute

60°C for 0:30 minute

72°C for 0:15 minute+ Plate read

95°C for 0:10 minute

Melting curve 60°C / or the temperature specific for specific primer to 95 for 0:05 minute + plate read



2.6 Library preparation for F1 DNA, total RNA, and ChIP-seq DNA

2.6.1 Genomic DNA and ChIP DNA libraries, Sequencing and data analyses

Genomic DNA libraries and ChIP-Seq libraries for H3K4me3, H3K27ac, H3R2me2s, and H4R3me2a were prepared according to the 5500 SOLiD fragment library protocol (Life Technologies). Five µg of sheared genomic DNA and 30 ng of ChIP DNA were end-repaired and size selected (100-250bp), followed

by dA tailing, ligation of SOLiD barcodes and library PCR amplification. Libraries were subjected to emulsion PCR (ePCR) and loaded on the flowchip for sequencing.

2.6.2 ChIP-Seq with the MiSeq

ChIP-Seq library preparation was performed according to the NEBNext ChIP-Seq library preparation protocol. Twenty ng of ChIP DNA was end-repaired and dA-tailed. Ligation products were size selected, and PCR enriched. Libraries were quantified by qPCR and normalized. ChIP DNA and Input libraries were sequenced using the MiSeq platform and v3 sequencing reagents.

2.6.3 RNAseq library preparation for SOLiD

SOLiD total RNA-seq kit was used to prepare whole transcriptome libraries. RNA quality and integrity were assessed using the RNA pico Kit and 2000 Bioanalyzer (Agilent Technologies). Four to six μg of total RNA was subjected to ribosomal depletion (RiboMinus Eukaryote system v2, Life Technologies) followed by RNaseIII fragmentation, adaptor hybridization and reverse transcription. Reversed transcribed DNA was size-selected and PCR amplified. Libraries were sequenced in a multiplex manner, pooling two libraries per lane.

2.7 Bioinformatics analysis

2.7.1 SOLiD next-generation sequencing data analyses

The DNA-seq, RNA-seq, and ChIP-seq were mapped on the chicken reference genome (Galgal3) Lifescope v2.5.1 software (Life Technologies) with 2-mismatch settings after quality check and filtering. The mapped bam or wiggle files were visualized by IGV or Partek Genomics Suite v6.6 (Partek Incorporated, St. Louis, Missouri, USA). Genes were annotated using Ensembl Transcripts database release-70 or UCSC refGenes.

2.7.2 Detection of transcriptionally active chromatin domains

Since the domain could span a region as large as tens of kilobases, we applied a clustering approach (SICER) for identification of islands of DNA-seq enrichment using F1 DNA-seq-mapped BAM files as inputs [413]. These islands separated by gaps of size less than or equal to a predetermined parameter formed a contingent domain. For identical reads, only one read was used to remove the repeats from genome structure or PCR amplification. SICER parameters of window size 1000 bp and gap size of 1000 bp was used. The island scores represent the negative logarithm of the probability of finding l reads in the window if the reads can land anywhere on the genome with equal probability, i.e. a background model

of random reads. The higher the score is the more reads the domain has. We used the island scores to plot the domains using CIRCOS [414].

Total number of islands: 9467, score ≥ 100 , 4409, size $>10k$ size,

We rank the genes by a z-score. We first calculate the gene enrichment values (including exon and introns of each gene) as per 300 bp coverage subtracted by the normalized enriched value of relevant gene of S_E control. We then calculate the background mean and standard deviation (SD) by simulating every 300 bases on the whole genome of each sample for 20,000 regions. The z-score is the gene normalized value subtracted by the mean and further divided by SD.

2.7.3 RNA-seq data analyses

The SOLiD sequence reads were counted against gal3 ensembl release-70 genes by the Lifescope whole Transcriptome WT counts module. The reads per kilobase per million reads (rpkm) of greater than 5 of each gene were further z-normalized to zRPKM [415].

2.7.4 ChIP-seq data analyses

We used the model-based analysis of ChIP-seq (MACS) to process ChIP-Seq mapped bam files for histone modifications by removing redundant reads, estimating fragment length, building signal profile, calculating peak enrichment, and refining and reporting peak calls. The genes within the peaks were annotated by using software CEAS [416]. We use IGV and Partek to visualize ChIP-seq data.

2.8 References

1. Williams AF. DNA synthesis in purified populations of avian erythroid cells. *J Cell Sci.* 1972;10(1):27-46. PubMed PMID: 5017428.
2. Beug H, von Kirchbach A, Doderlein G, Conscience JF, Graf T. Chicken hematopoietic cells transformed by seven strains of defective avian leukemia viruses display three distinct phenotypes of differentiation. *Cell.* 1979;18(2):375-90. PubMed PMID: 227607.
3. Laemmli UK. Cleavage of structural proteins during the assembly of the head of bacteriophage T4. *Nature.* 1970;227(5259):680-5. PubMed PMID: 5432063.
4. Ridsdale JA, Davie JR. Chicken erythrocyte polynucleosomes which are soluble at physiological ionic strength and contain linker histones are highly enriched in beta-globin gene sequences. *Nucleic acids research.* 1987;15(3):1081-96. PubMed PMID: 3822820; PubMed Central PMCID: PMC340509.
5. Zang C, Schones DE, Zeng C, Cui K, Zhao K, Peng W. A clustering approach for identification of enriched domains from histone modification ChIP-Seq data. *Bioinformatics.* 2009;25(15):1952-8. doi: 10.1093/bioinformatics/btp340. PubMed PMID: 19505939; PubMed Central PMCID: PMC2732366.
6. Krzywinski M, Schein J, Birol I, Connors J, Gascoyne R, Horsman D, et al. Circos: an information aesthetic for comparative genomics. *Genome Res.* 2009;19(9):1639-45. doi: 10.1101/gr.092759.109. PubMed PMID: 19541911; PubMed Central PMCID: PMC2752132.
7. Li H, Handsaker B, Wysoker A, Fennell T, Ruan J, Homer N, et al. The Sequence Alignment/Map format and SAMtools. *Bioinformatics.* 2009;25(16):2078-9. doi: 10.1093/bioinformatics/btp352. PubMed PMID: 19505943; PubMed Central PMCID: PMC2723002.
8. Shin H, Liu T, Manrai AK, Liu XS. CEAS: cis-regulatory element annotation system. *Bioinformatics.* 2009;25(19):2605-6. doi: 10.1093/bioinformatics/btp479. PubMed PMID: 19689956.

CHAPTER III: CHICKEN ERYTHROCYTE EPIGENOME

3.1 Abstract

Background: Transcriptional regulation is impacted by multiple layers of genomic organization. A general feature of transcriptionally active chromatin is its sensitivity to DNase I and its association with acetylated histones. However, very few of these active DNase I-sensitive domains, such as the chicken erythrocyte β -globin domain, have been identified and characterized. In chicken polychromatic erythrocytes, dynamically acetylated histones associated with DNase I-sensitive, transcriptionally active chromatin prevent histone H1/H5-induced insolubility at physiological ionic strength.

Results: Here, we globally identified and mapped all of the transcriptionally active chromosomal domains in the chicken polychromatic erythrocyte genome by combining a powerful chromatin fractionation method with next-generation DNA and RNA sequencing. Two classes of transcribed chromatin organizations were identified on the basis of the extent of solubility at physiological ionic strength. Highly transcribed genes were present in multigenic salt-soluble chromatin domains ranging in length from 30 to over 150 kb. We identified over 100 highly expressed genes that were organized in broad dynamically highly acetylated, salt-soluble chromatin domains. Highly expressed genes were associated with H3K4me3 and H3K27ac and produced discernible antisense transcripts. The moderately- and low-expressing genes had highly acetylated, salt-soluble chromatin regions that were confined to the 5' end of the gene.

Conclusions: Our data provide a genome-wide profile of chromatin signatures in relation to expression levels in chicken polychromatic erythrocytes.

Keywords: Chromatin fractionation, Chromosomal domains, Histone acetylation, H3K27ac, Histone methylation, H3K4me3, Chicken erythrocyte transcriptome

This collaborative work was published as:

Sanzida Jahan, Wayne Xu, Shihua He, Carolina Gonzalez, Geneviève P. Delcuve and
James R. Davie.

The chicken erythrocyte epigenome.

Epigenetics & Chromatin (2016) 9:19

Sanzida Jahan carried out the chromatin fractionation procedures, the ChIP-seq assays and RT-PCR validation experiments, participated in data interpretation and prepared figures. WX performed the bioinformatics analyses. SH participated in ChIP-seq assays. CG prepared the DNA and RNA libraries. GPD participated in data interpretation, drafted and wrote the manuscript. JRD conceived of the study, participated in its design and coordination and reviewed manuscript.

3.2 Introduction

Histone acetylation plays a critical role in the structure of transcriptionally active chromatin. The seminal studies of Weintraub and Groudine demonstrated that transcribed chromatin has an increased sensitivity to DNase I (approximately twofold to threefold greater than the bulk of chromatin) [1]. The dynamically acetylated histones bound to transcribed chromatin are largely responsible for this DNase I sensitivity. Genomic mapping of acetylated histones (H3K9/14ac, H4K16ac) demonstrated that the acetylated histones are located around the transcription start site of expressed genes [2–4]. However, for α - and β -globin genes in mammalian and chicken erythroid cells, the dynamically highly acetylated histones are broadly distributed to encompass transcriptionally competent and active globin genes. These extensive acetylation patterns display sharp edges where acetylation drops abruptly, defining acetylation domains [5–7]. The boundaries of the acetylated β -globin domain co-map with those of the DNase I-sensitive β -globin chromatin domain [8]. The dynamically acetylated histones also render the active/competent chromatin soluble at low ionic strength (50–150 mM NaCl), by preventing histone H1/H5-mediated chromatin insolubility at physiological ionic strength [9, 10]. In parallel with the decline in acetylated histones and DNase I sensitivity, the chromatin salt solubility at physiological ionic strength falls sharply at the 5' boundary of the β -globin domain [11]. The DNase I sensitive and dynamically highly acetylated chromatin of the 33-kb chicken erythroid β -globin domain is one of the better characterized domains [12]. Other DNase I-sensitive domains containing one or more expressed genes have been mapped in chicken and mammalian cells. In the chicken hen oviduct, the *SERPINB14* (ovalbumin) gene and two pseudogenes of the *GAPDH* gene lies in a 15-kb DNase I-sensitive domain [14]. In human hepatocytes, the *APOB* gene resides in a 50-kb DNase I-sensitive domain [15]. Within the DNase I-sensitive domains are regions of hypersensitivity (about 100-fold more sensitive than bulk chromatin), which are nucleosome-depleted regions associated with regulatory elements such as enhancers, locus control regions and promoters. The study of the chromatin structure of chicken mature erythrocytes and polychromatic erythrocytes from anemic birds has advanced the field. Polychromatic erythrocytes are transcriptionally active, while mature erythrocytes are transcriptionally inert [16]. Polychromatic and mature erythrocytes are nucleated, non-replicating G₀-phase cells. Thus, histone posttranslational modifications related to cell cycle do not confound the analyses of transcribed chromatin. Polychromatic erythrocytes express the adult β^A -globin gene as do 15-day chicken embryo erythrocytes, but do not express the β^H -globin gene as do cells of late embryos and newly hatched chickens [17–19]. Approximately 1–2 % of polychromatic and mature erythrocyte chromatin has dynamically acetylated histones [10, 20, 21]. Due to a particularly high density

of H1/H5 linker histones [22], the bulk of chicken polychromatic erythrocyte chromatin is extremely condensed and insoluble at physiological ionic strength. However, the dynamically highly acetylated histones associated with transcriptionally active/poised chromatin prevent H1/H5 from rendering active/poised gene polynucleosomes insoluble at physiological ionic strength [9]. Exploiting these properties of chicken polychromatic erythrocyte chromatin, we designed a chromatin fractionation protocol to isolate transcriptionally active/competent chromatin. The polynucleosomes (fraction F1) are enriched in active histone marks including the dynamically highly acetylated four core histones, H3K4me3 and uH2B [23, 24]. Furthermore, F1 chromatin is enriched in u-shaped atypical nucleosomes, which were first discovered by Allfrey's laboratory [25–27]. The nucleosomes in the F1 fraction rapidly exchange with newly synthesized histones (replication-independent class of histones) and are readily dissociated by DNA intercalators [28–30], demonstrating the lability of the F1 nucleosomes.

Our previous studies have mapped the 5' boundary of the β -globin chromatin domain that was soluble at physiological ionic strength [11, 23]. We exploited this powerful chromatin fractionation procedure to further map the salt-soluble organization of the β -globin chromatin domain and determine whether other regions of the chicken polychromatic erythrocyte genome had domains of salt solubility akin to the β -globin chromatin domain. In conjunction with next-generation DNA and RNA sequencing (DNA-seq and RNA-seq) as well as chromatin immunoprecipitation-DNA sequencing (ChIP-seq), we could identify all the active chromosomal domains that were soluble at physiological ionic strength. Furthermore, we determined their structural signatures in relation to expression levels of genes contained within the domain. Herein, we present the functional organization of the chicken polychromatic erythrocyte genome.

3.3 Results:

3.3.1 Genome-wide mapping of polychromatic erythrocyte transcribed chromosomal domains

To isolate fraction F1 chromatin, chicken polychromatic erythrocyte nuclei were incubated with micrococcal nuclease, bulk chromatin (S_E) was released, and chromatin fragments soluble at 150 mM NaCl were isolated and size-resolved [22]. The F1 chromatin consisted of chromatin fragments ranging in size from 0.4 to 3.4 kb, with the average DNA length being 1.5 kb (**Figure S3.1**). Next-generation DNA sequencing of F1 chromatin generated an uneven profile with clusters of read enrichment varying in intensity and breadth, interspersed with regions depleted of reads. In contrast, the track of bulk chromatin (S_E) was flat. These data are exemplified in Fig. 1 showing the sequence reads for a 1,000 kb region on chromosome 1 and a 2,300 kb region on chromosome 9. Both regions displayed long stretches (500-1,000 kb) of salt-soluble chromatin interrupted with equally long stretches of salt-insoluble chromatin. Within a

F1-enriched region, chromatin salt-solubility fluctuated, and when we looked closely, we could distinguish several distinct domains within this region, for example see the β -globin (HBB) domain (**Figure 3.1a, S3.1b**). The profiles generated from two biological repeats of F1 chromatin (F1-1 and F1-2) were similar. Thus, we only show tracks from F1-2 in the following figures.

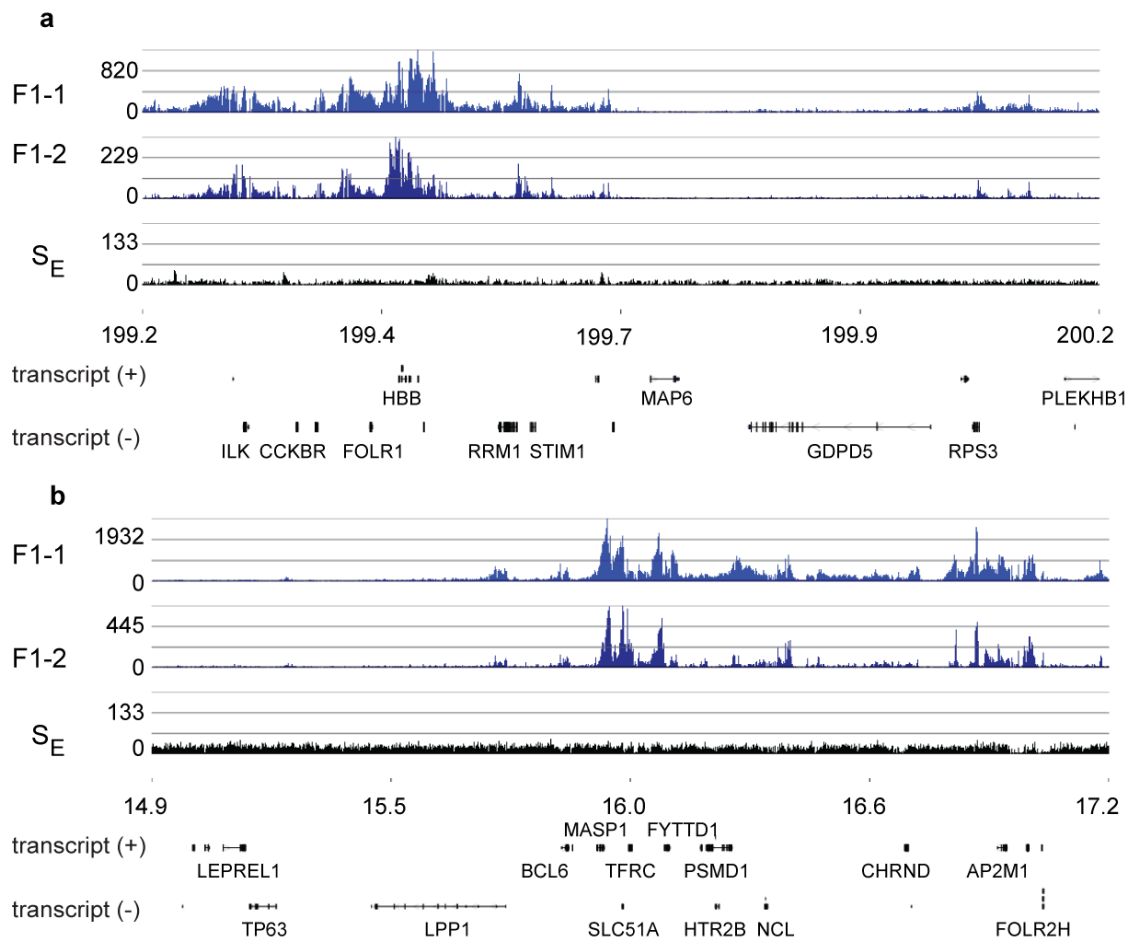
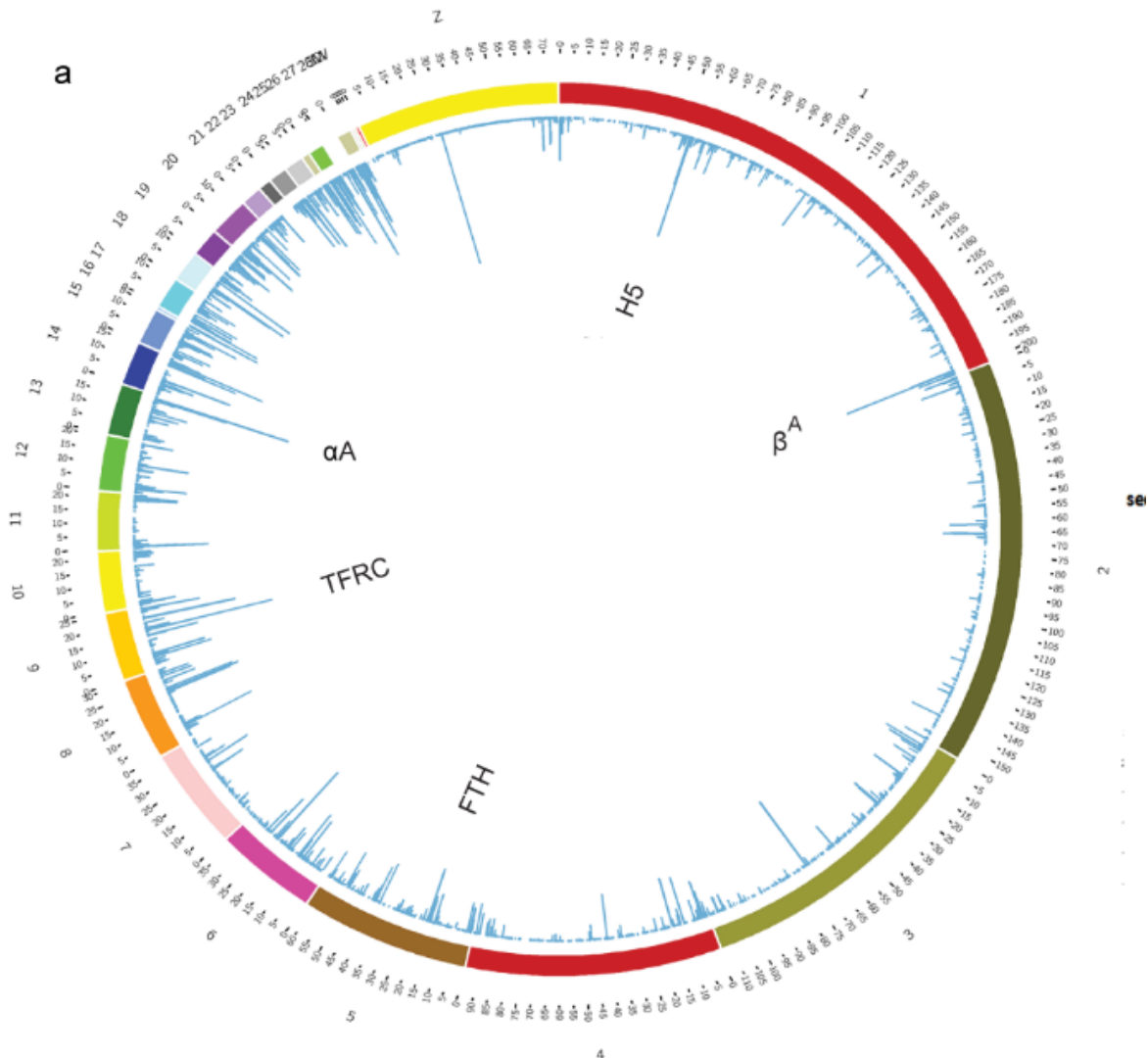


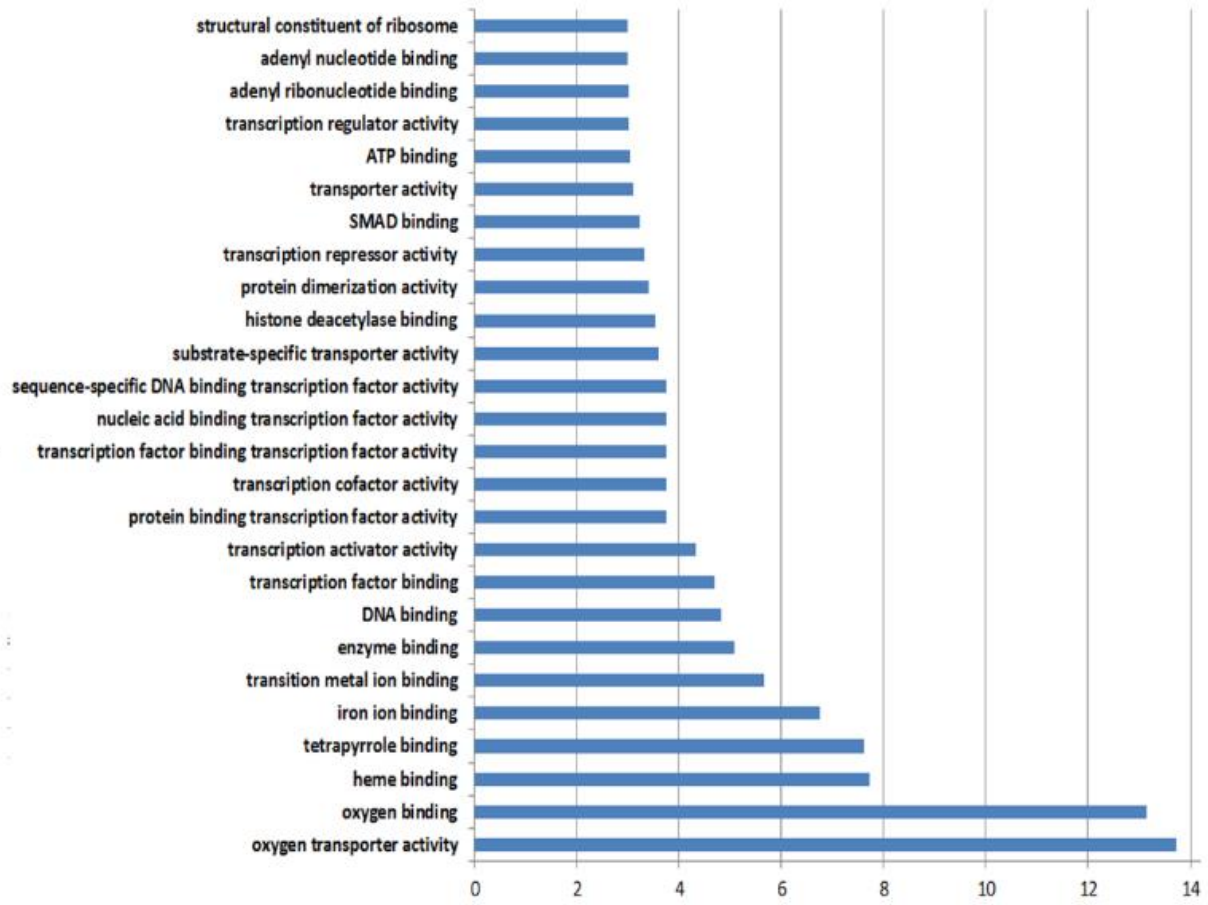
Figure 3.1: Representative browser snapshots of F1 and S_E chromatin DNA-seq. The DNA from two biological repeats of F1 (F1-1 and F1-2) and S_E chromatin fractions isolated from chicken polychromatic erythrocytes was sequenced. The positions are indicated in Mbs. a Region of chromosome 1. b Region of chromosome 9.

To visualize the genome-wide profiling of salt-soluble chromatin, we show a Circos plot of F1-enriched sequences (**Figure 3.2a**). The chicken karyotype consists of 38 autosomes and a pair of sex chromosomes (ZW female, ZZ male), and is made up of macro- and microchromosomes. Several arbitrary chromosome classifications exist [30-33]. Here, we use the initial categorization, defining chromosomes 9-38 and W as cytologically indistinguishable microchromosomes [34]. Early studies estimated that

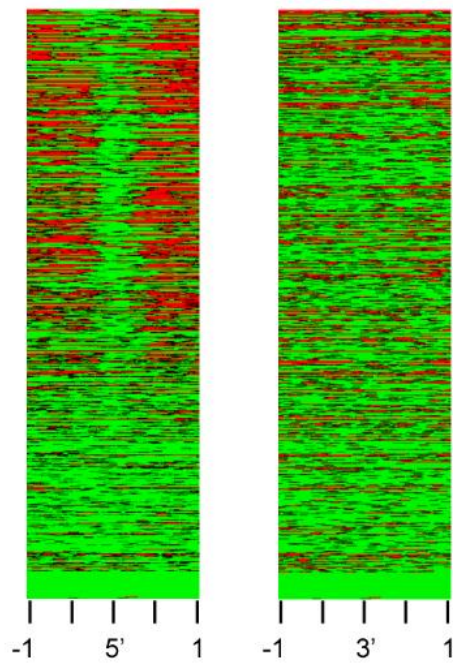
microchromosomes constitute 23% of the chicken genome and contain 48% of all genes [31]. In agreement, sequencing of the genome showed that gene density is inversely correlated to chromosome length [32]. As seen in the Circos plot of F1-enriched sequences (**Figure 3.2a**), there was a higher density of salt-soluble chromatin in polychromatic erythrocytes on microchromosomes than on macrochromosomes. The F1 reads were used to rank genes contained within salt-soluble chromatin domain. The rank order of these genes was used for GO term analysis. In terms of molecular functions, genes involved in the hemoglobin synthesis pathway were the predominant sets of active genes in F1 chromatin, followed by genes encoding proteins involved in transcription regulation (**Figure 3.2b**). In summary, the chicken polychromatic erythrocyte genome is organized in clusters of discrete salt-soluble chromatin domains, and these expanses of chromatin exhibiting an open structure alternating with long stretches of salt-insoluble chromatin.



b



c



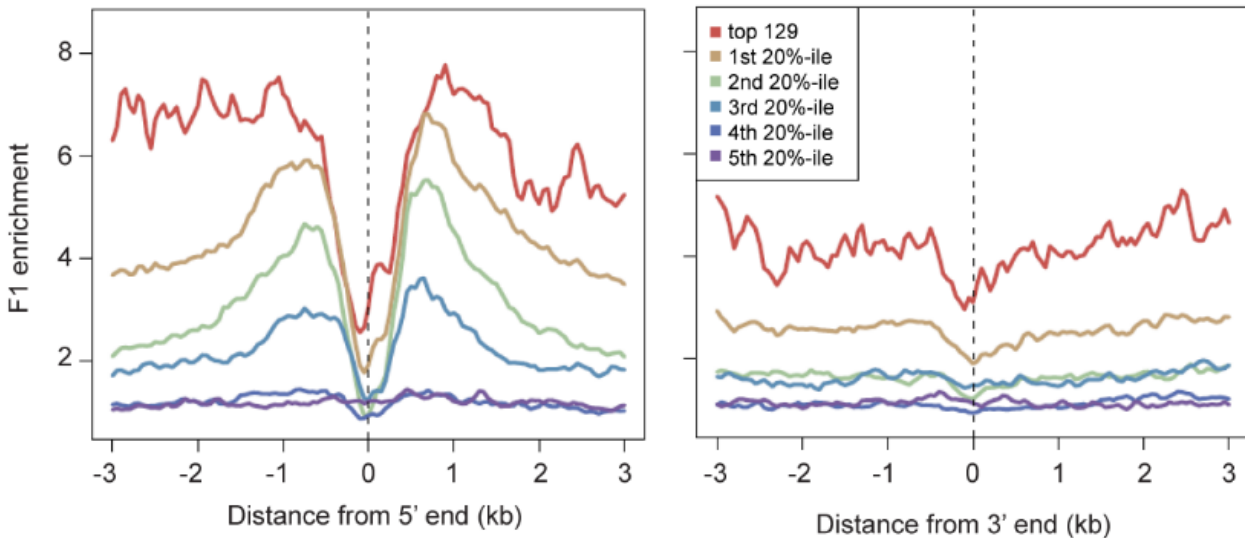
d

Figure 3.2: Active chromatin distribution and transcriptional activity. **a** Circos plot of DNA sequence enrichment in fraction F1 polynucleosomes. The *outer ring* represents the chicken chromosomes, and the inner ring details the peak of F1 DNA-seq reads. Some of the most enriched genes are identified. **b** Gene ontology function analysis of fraction F1. The most significantly enriched GO groups ($P < 0.001$ in one-tailed Fisher's exact test) are displayed. The *X-axis* represents the $-\log_{10}(P \text{ value})$. **c** TSS- and TTS-centered profiles of F1 chromatin enrichment for the 129 most expressed genes and for quintile classes based on gene expression levels (Additional file 2). **d** Heatmap of F1 chromatin DNA-seq signals spanning 1 kb on each side of TSS and TTS of genes from the galGal3 RefSeq database. All 5479 genes were ranked from top to bottom, according to their level of expression (**Appendix 2**).

Chromatin domain organization correlates with gene expression levels. Snapshots of F1 and SE chromatin DNA-seq confirmed that the active β A-globin resided in a salt-soluble domain (HBB) while sequences from the inactive ovalbumin locus were depleted in F1 (**Figure 3.1 and S3.1b**). To determine the correlation between transcriptional activity and chromatin salt-solubility at the genome-wide level, the chicken polychromatic erythrocyte transcriptome was characterized by cellular RNA-seq analyses. The 5479 genes annotated in the galGal3 RefSeq database were placed in order of their level of expression (**Appendix 2**). RNA-seq assessment of cellular transcript levels by RPKM was validated by RT-qPCR analyses. We show that genes with high (*HBG2*), intermediate (*CA2* and *FTH1*) or low (*HDAC2* and

PRMT7) RPKM values had relatively similar transcript levels in our validation studies (Additional file 3). We also isolated and sequenced nuclear RNA and found a very high correlation ($r=0.82$) between cellular and nuclear RNA-seq data sets, as seen in the scatterplot and snapshots of β -globin and *HIF0* (coding for *H5*) transcripts (**Figure S3.4**). Moreover, RNA-seq data analysis revealed that for the most highly expressed genes, that is about the first 20th-percentile class, there was a low level (about 1%) of antisense transcription of the coding region (**Appendix 3**). This antisense transcription was observed for coding regions of cellular and nuclear transcripts (**Appendix 3**).

There are two types of histone genes; those that are replication-dependent and those that are replication-independent. The polychromatic erythrocyte, which has ceased replication, had low expression of replication dependent histone H1 (*HIST1H1C*), H2A (*HIST2H2AC_dup2*), H2B (*HIST1H2BO*, *H2B-V*) and H4 (*H4*, *H4-VII*). However, expression of the replication-independent histone genes (*H3F3C*, *H2AFZ*, *HIF0*) was high.

Chicken erythroid progenitor cells undergo a restructuring of the cytoskeleton during the terminal differentiation program [35]. We observed that the polychromatic erythrocytes expressed several cytoskeleton associated genes such as *SPTAN1* (spectrin, alpha, non-erythrocytic 1) gene, *EPB41* (protein 4.1), genes (*ANKHD1*, *ANKRD27*) coding for ankyrin repeat domain proteins, and spectrin genes (*SPTAN1*, spectrin, alpha, non-erythrocytic 1 and *SPTBNI*, spectrin, beta, non-erythrocytic 1). However, the polychromatic erythrocytes did not express ankyrin genes (*ANK1*, *ANK2*, *ANK3*), erythrocytic specific spectrin genes *SPTAI* (spectrin, alpha, erythrocytic 1), *SPTB* (spectrin, beta, erythrocytic), or band 3 gene/anion exchange gene 1 (*SLC4A1/AE1*).

To determine if enrichment in F1 chromatin paralleled gene expression levels, the 5479 genes placed in order of their level of expression (**Appendix 2**), were divided into five 20th-percentile classes in relation to expression level. For each class, as well as for the top 129 expressors (number chosen to include *HIF0* gene known to be expressed in polychromatic erythrocytes [17]), sequence enrichment in F1 chromatin was analyzed at the transcription start site (TSS) and termination site (TTS) of each gene (**Figure 3.2c**). The first 20th-percentile group with highest gene expression levels, and even more so the top 129 expressors, showed the highest sequence enrichment in the F1 chromatin fraction, while the last two 20th-percentile groups were not enriched, further validating the ability of this salt fractionation method to isolate transcriptionally active chromatin. For all classes, enrichment in F1 chromatin was higher at the TSS than at the TTS, although the difference between F1 enrichment at TSS and TTS was not as marked for the top 129 expressors. The sequence enrichment profile extending over 3 kb on both sides of

nucleosome-free TSS demonstrated that solubility of chromatin at physiological ionic strength was not limited to the first nucleosome of the gene as in the case of other chromatin sources (**Figure 3.2b**) [36, 37]. Heatmaps of F1 chromatin DNA-seq reads around the TSS and TTS of the 5479 genes ranked from top to bottom were consistent with the enrichment plots for the quintile classes, showing a marked enrichment for about the top 60% of expressors around the TSS, but for only about 10% around the TTS (**Figure 3.2d**).

Regarding the chromosomal location, microchromosomes held 43% of the genes from the first 20th percentile group. Slightly more of the actively expressed genes (56%) in the first 20th percentile group were located on the macrochromosomes. Thus, the genomic distribution of the most active genes in polychromatic erythrocytes was slightly in favor of the macrochromosomes. To conclude, there was an overall correlation between levels of gene expression and the extent of salt-solubility of their associated chromatin.

3.3.2 Features of salt-soluble chromatin

To compliment the F1 chromatin sequence and transcriptome analyses, we mapped the positions of two active chromatin marks (H3K4me3 and H3K27ac) (**Figure S3.3**). H3K27ac is the signature of active enhancers and promoters [417], while H3K4me3 maps to the 5' end of the body of active genes in mammals [125, 418, 419]. H3K27ac or H3K4me3 average coverage around the TSS was determined for each of the 20th-percentile classes described above. Both H3K27ac and H3K4me3 were only significantly enriched in the 5' region of the most highly expressed genes (first 20th-percentile). The average profile was sharper for H3K4me3 than H3K27ac, with H3K4me3 peaking between 0.5 and 1.5 kb downstream of the TSS. Consistent with these data, H3K4me3 and H3K27ac heatmaps spanning 1 kb on each side of the TSS showed enrichment for the top 40% expressors.

Genes from the first 20th percentile group had distinct salt-soluble chromatin organizations. The genes with the highest expression were present in broad salt-soluble chromatin regions, while moderately or poorly expressed genes had the salt-soluble chromatin confined to their 5' regions. To illustrate the broad salt-soluble domains, we show the chromatin profile of the β -globin locus. Figure 3a shows that salt-solubility co-mapped with the well known 33 kb β -globin domain, as defined by DNase I sensitivity, histone acetylation and CTCF binding sites marking the boundaries. Moreover, within the domain, F1-enrichment reads paralleled the high acetylation profile [71, 420, 421]. Similar data were obtained for the α -globin locus [422] (data not shown). Beside the abundant β^A -globin mRNA and low level of antisense transcription (about 1% of sense transcript), we detected LCR-associated RNAs or enhancer-derived

RNAs (eRNAs), which originated from the HS1, HS2 and HS3 sites (**Figure 3.3a, b**). Attribution of transcriptional activity from $\beta^{A/\epsilon}$ enhancer was precluded by the massive β^A gene transcription. The H3K27ac mark was positioned at HS1, HS2, HS3 and $\beta^{A/\epsilon}$ enhancer, as well at the promoter and along the body of the β^A gene, while H3K4me3 was enriched in the body of the β^A -globin gene (Fig. 3a). These results demonstrate that the β -globin genes are present in a salt-soluble chromatin domain, with the boundaries of the 33 kb domain defined by a loss of a salt-soluble chromatin structure. The LCR chromatin region is organized into salt-soluble chromatin regions enriched in H3K27ac, with MNase hypersensitive sites demarcating the boundaries of each region of the LCR.

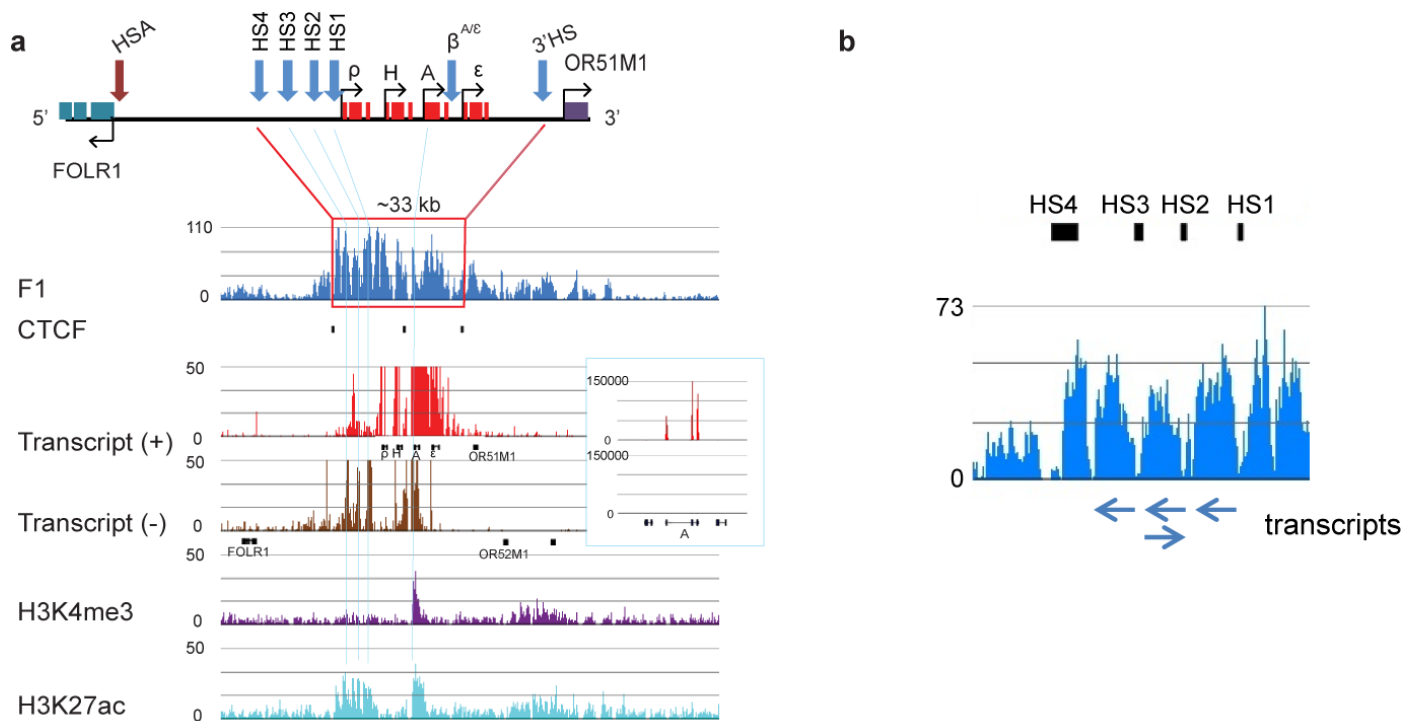


Figure 3.3: Chromatin profile and transcriptional activity of β -globin domain. a. Schematic of the β -globin domain, detailing the developmentally regulated β -globin genes and DNase I-hypersensitive sites (HS4 and 3'HS delimiting the locus). HS1, HS2, HS3 and β^A/ϵ enhancer are collectively known as locus control region (LCR) and regulate the expression of the four β -globin genes. Below the maps, are signal tracks showing DNA enrichment in F1 fraction, CTCF-binding sites (as vertical bars), transcripts on (+) and (-) strands and H3 modifications. mRNAs (with exons as black boxes) are shown below their template strand. The inset to the right shows the level of transcripts on an expanded scale. Vertical blue lines illustrate the position within the domain of prominent features (H3K27ac and/or H3K4me3 peaks and

eRNAs). b Amplification of signal tracks showing F1-enriched DNA and transcribed RNAs in the β -globin LCR region.

We looked in detail at the chromatin features of nine other genes among the 129 top expressors and found out that those genes resided in broad salt-soluble chromatin domains: the α -globin (*HBA*) gene (expressor # 1, in a 60-kb domain), *CA2* (expressor # 13, in a 86-kb domain), *FTH1* (expressor # 14, in a 46-kb domain), *IFRDI* (expressor # 21, in a 33-kb domain), *NCOA4* (expressor # 23, in a 22-kb domain), *TFRC* (expressor # 51, in a 35-kb domain), *ARIH1* (expressor # 125, in a 154-kb domain), *AK2* (not annotated in the galGal3 RefSeq gene database, in a 44-kb domain) and *HIF0* (expressor # 129, in a 48-kb domain).

As to genes associated with a salt-soluble chromatin limited to their 5' regions, the Circos plot (**Figure 3.2a**) displayed a very high F1 enrichment of chromatin (at approximately 28,000,000) on the sex chromosome Z. This peak was mapped to a region containing two MHM (male hypermethylated) locus genes believed to play a role in localized dosage compensation (**Figure 3.4**). The two genes ENSGALG00000023324 (transcript: ENSGALT00000038395) and ENSGALG00000018479 (transcript: ENSGALT00000035390) showed a large increase of expression in gonads of female (ZW) chickens compared to male (ZZ) chickens [43, 44]. They code for uncharacterized proteins of 103 and 60 amino acids, respectively. The ENSGALG00000018479 gene was found overexpressed in the brain (hypothalamus and thalamus) of 21 days old females compared to males [43]. Our results show that the salt-soluble F1 chromatin on the chromosome Z identified the presence of the MHM locus genes (**Figure 3.4**).

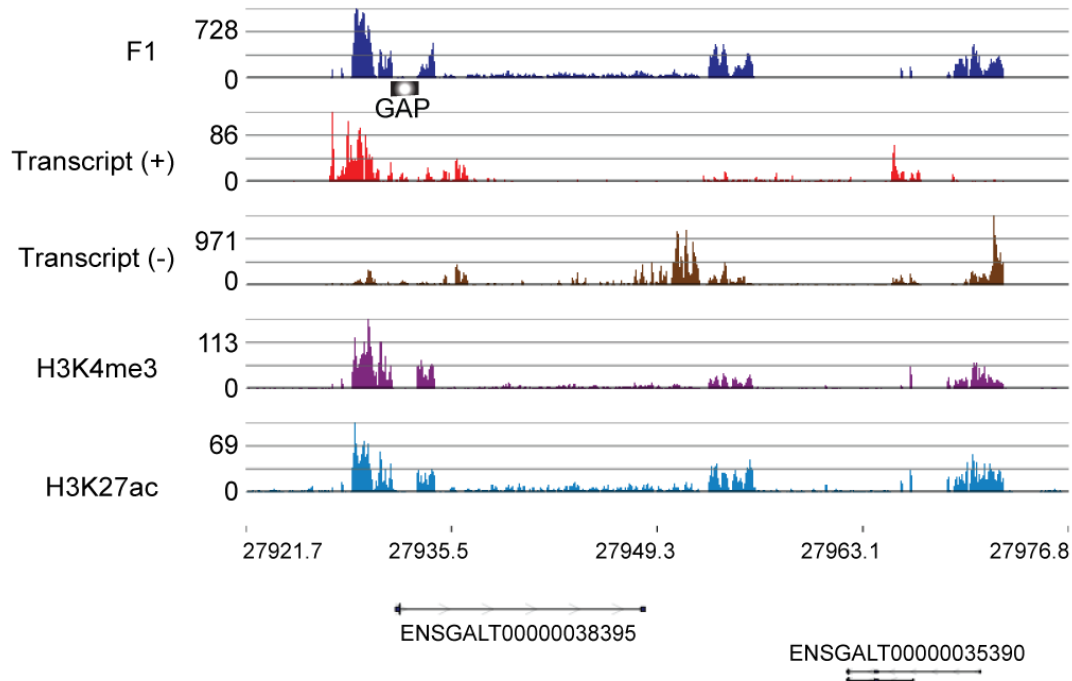


Figure 3.4: Chromatin profile and transcriptional activity of region of interest on chromosome Z. The positions are indicated in kbs. It should be noted that the dips in the F1-enrichment, H3K4me3 and H3K27ac profiles are due to a gap in the genome sequence.

Other genes with very small region of salt-soluble chromatin at their 5' end or body were moderately or poorly expressed in chicken polychromatic erythrocytes, e.g., *HDAC2* (histone deacetylase 2) and *PRMT7* (protein arginine methyltransferase 7) (**Figure 5**). No particular feature (H3K27ac or H3K4me3) or enhancer-associated chromatin feature could be identified for either gene.

Our results have identified several domains that have extended salt-soluble chromatin domains similar to the α - and β -globin gene domains. The genes with this chromatin organization tend to be highly expressed. A larger number of genes, which are expressed at lower levels, have a salt-soluble chromatin organization confined to the 5' end of the gene.

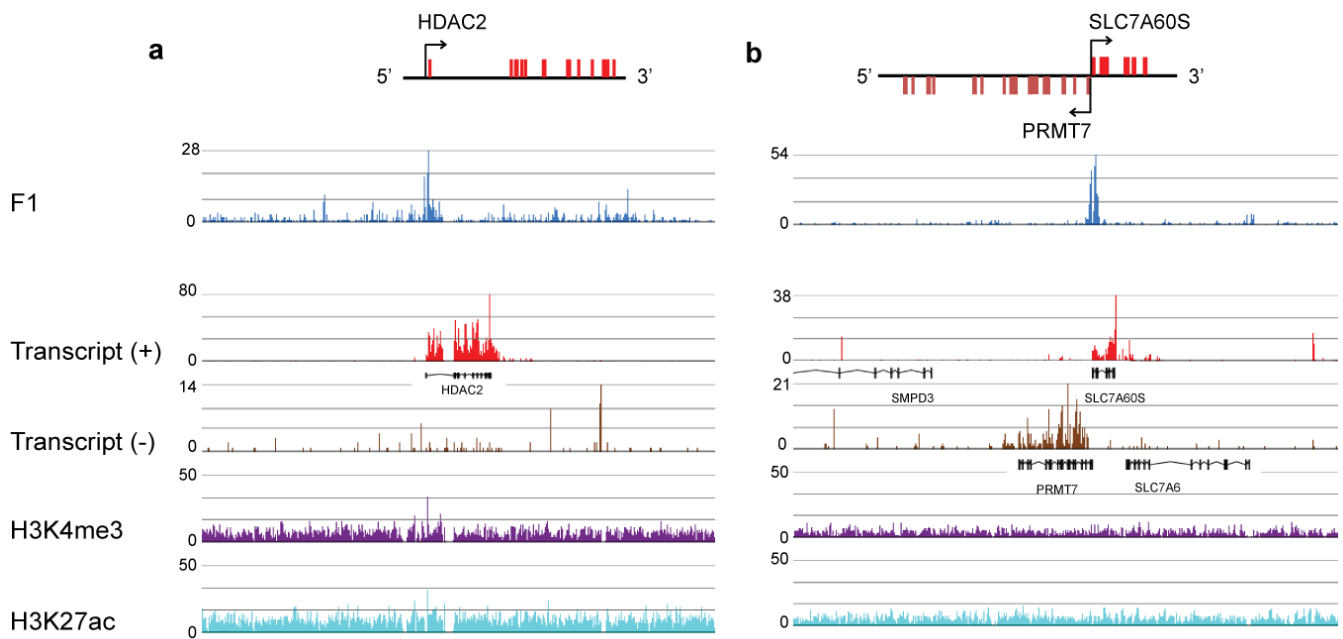


Figure 3.5: Chromatin profile and transcriptional activity of moderately and poorly expressed genes. a *HDAC2*. b *PRMT7*.

3.4 Discussion

Our results demonstrate that the broad highly acetylated, salt-soluble chromatin domain organization of the α - and β -globin genes is a characteristic of many highly expressed genes in the chicken polychromatic erythrocytes. The boundaries of the salt-soluble chromatin containing the α - and β -globin genes mapped precisely with the boundaries defined by highly acetylated histones (H3K9/14ac; acetylated H4). For highly expressed genes the broad salt-soluble, highly acetylated regions were present 5' and 3' to the TSS and sustained to lesser extent around the TTS. It is possible that the antisense transcripts are a feature of the highly acetylated chromatin state of these genes. It is of note that antisense transcripts for the α - and β^A -globin genes have been reported previously [7, 45]. Less actively expressed genes have highly acetylated F1 chromatin regions restricted to their 5' ends. This restricted highly acetylated domain is typical of mammalian genes [3].

The majority of the polychromatic erythroid chromatin is highly condensed due to the excessive amount of histone H5 present and the low acetylated state of the bulk of chromatin. Nevertheless, we find that the

genomic distribution of the H3K4me3 at the 5' of the coding region of expressed genes and the presence of H3K27ac at enhancers and LCR is typical of mammalian cells. It is also noteworthy that the repressive environment in chicken polychromatic erythrocytes also facilitated its transcriptome characterization. Typically, high-throughput sequencing of steady state cellular RNA is not a suitable method to detect the rarer and/or less stable transcripts resulting from antisense transcription or originating from enhancers [46, 47]. However, cellular RNA-seq analyses allowed us to identify such transcripts. For the β A-globin LCR, we observed transcripts originating from HS1, HS2 and HS3 sites. This is in contrast to human erythroid cells in which RNA polymerase II-mediated transcription from one of the LCR elements goes in the globin mRNA sense direction [48, 49], transcription in chicken polychromatic erythrocytes occurred on the (–) strand from HS2 and HS1 and in both directions from HS3. In contrast to the other LCR hypersensitive sites (HS2, HS3 and β A/ ϵ), HS1 does not have independent enhancing activity [50], but is likely to play a role in transcription regulation as it presents the traits of an active enhancer.

Studies on the organization of chicken chromosomes show that microchromosomes are gathered within the nuclear interior, while macrochromosomes are located at the periphery of nuclei in both cycling fibroblast and non-proliferating neurons, suggesting that this radial arrangement may exist in erythrocytes [31]. On the other hand, Hutchison and Weintraub reported that the DNase I-sensitive chromatin was located on the periphery of chromosomal territories, along interchromatin channels in chicken erythrocytes [51]. Regardless of gene chromosomal location, transcriptionally active/poised chromatin domains likely share a similar compartmentalization, looping out of their chromosome territories [51, 52]. The solubility and location of the transcriptionally active chromosomal domains in the nuclear environment ensures their ready access by transcription factors and chromatin modifying and remodeling factors.

Chicken has long been recognized as a suitable model system to study the organization and function of a vertebrate genome [53]. Its genome is almost three times smaller than the human genome, but has about the same number of genes, with 60% of them having a single human orthologue. Moreover, there are long blocks of conserved synteny between the chicken and human genomes [32]. In terms of chromosomal organization of genes, the human genome is closer to the chicken genome than to rodent genome. Additionally, following 310 million years of separate evolution, conserved non-coding sequences are likely to highlight functional elements in both chicken and human genomes [32]. Thus, our studies supply valuable information on the structural and functional organization of the chicken polychromatic

erythrocyte epigenome and may also provide insights into the organization of the human erythrocyte genome.

3.5 Conclusions

One to two percent of the chicken polychromatic erythrocyte epigenome is organized in broad highly acetylated, salt-soluble chromatin domains containing at least one highly expressed gene or in narrow highly acetylated, salt-soluble chromatin regions restricted to the 5' end of moderately or poorly expressed genes. The bulk of the genome is highly compacted and silent. The genomic mapping of salt-soluble chromatin domains will aid in the annotation of genes expressed in erythroid cells.

3.6 Methods

3.6.1 Isolation of chicken erythrocytes

Polychromatic erythrocytes were isolated from anemic female adult white Leghorn chickens as described [22]. Ethical approval was obtained from the University of Manitoba Animal Care Committee. The birds were purchased through Central Animal Care Services, University of Manitoba and were housed under standard conditions. A biological sample consisted of a pool of red blood cells from 11-12 anemic chickens (**Table S3.2**).

3.6.2 Salt fractionation

Chicken polychromatic erythrocyte nuclei were prepared as described [22, 27]. The equivalent of 50 A260 nuclei were incubated with 1.5 unit of micrococcal nuclease (Worthington Biochemical Corporation) for 12 minute at 37°C, and the digestion was stopped by the addition of EGTA to 10 mM. Chromatin fragments soluble in a low ionic strength solution containing 10 mM EDTA were recovered in fraction S_E . Chromatin fraction S_E was made 150mM in NaCl, and chromatin fragments from the salt-soluble fraction (S_{150}) were size-resolved on a Bio-Gel A-1.5m column to isolate the F1 fraction containing polynucleosomes [23].

3.6.3 ChIP-seq assays

ChIP-seq assays, using antibodies against H3K27ac or H3K4me3 from Abcam, were done as previously described [23, 54], except that chicken polychromatic erythrocyte nuclei were treated with 0.5% formaldehyde and chromatin was sheared into 200 bp fragments. See Additional file 8 for details regarding sequencing data.

3.6.4 Sequencing and mapping of data

DNA libraries and strand-specific (100-250 nucleotides) RNA libraries (prepared with the SOLiD Total RNA-Seq kit) were sequenced on the 5500xl SOLiD™ System [54]. Single end sequence reads of 50 bp in length were generated from the SE control sample and two biological replicates of F1 (F1-1 and F1-2) chromatin. 70-80% of these color-space sequence reads were mapped to the chicken reference genome galGal3 using the LifeScope™ Genomic Analysis Software 2.5.1 (Life Technologies). Mismatch penalty of -2 and a minimum mapping quality score of 8 were applied in mapping parameter settings. See Additional file 8 for details about F1 and S_E tracks.

Two biological replicates of cellular RNA-seq generated a total of 120 million paired end (50x35bp) sequence reads, more than 85% of these reads were mapped to the genome. 110 million paired end reads were generated from two nuclear RNA-seq samples. More than 85% of these paired end reads were mapped to the genome. The sense and antisense RNA track data were extracted from BAM files using SAMtools [55]. See **Appendix 4** for details about Transcript (+) and Transcript (-) tracks.

H3K27ac and H3K4me3 ChIP-seq produced approximately 30 and 24 million sequence reads, respectively, and more than 65% of these sequences were mapped to galGal3 with an average mapping quality value of 63. We also generated 32 million sequence reads from the input sample.

The mapped BAM or WIG files were visualized using tools from the Integrative Genome Viewer (IGV), UCSC Genome Browser, or Partek Genomic Suite v6.6. The Genes were annotated using Ensembl transcripts database release-70 or UCSC RefSeq genes.

3.6.5 RNA Isolation and Real-time RT-qPCR Analysis

Total RNA was isolated from polychromatic erythrocyte cells and nuclear RNA was isolated from nuclei using the RNeasy Mini Kit (QIAGEN) according to manufacturer's instructions. Complementary DNA was generated from total RNA (800 ng) using the iScript cDNA synthesis kit (BioRad) following the manufacturer's specifications. SsoAdvanced universal SYBR® Green supermix (BioRad) was used to perform real-time PCR reactions using 5ng of cDNA on a CFX96 Touch™ Real-Time PCR Detection System (BioRad). The primers used for RT-PCR reactions are listed in the Additional file 9. The RNA levels were normalized against 18S rRNA.

3.6.6 Active chromatin detection and genomic distribution

We applied a clustering approach (SICER) [56] for identification of islands of DNA-seq enrichment using F1 DNA-seq mapped BAM files as inputs. The window and gap sizes were chosen to be 1 kb each. The SE DNA-seq data were used for background subtraction. We found a total of 9466 islands with a score >100. The island scores were transformed to z-scores = $(x-m)/\sigma$ where (x) is the island score, (m) is the mean of all island scores and (σ) is the standard deviation of all island scores. The z-scores were plotted to the galGal3 genome using Circos [57].

3.6.7 Chromatin profiling of transcriptionally active genes

Transcriptional levels were detected using the LifeScope whole transcriptome mapping module. We used the reads per kilobase per million (RPKM) to assign gene transcription levels. The cellular RNA-seq duplicates were averaged for each gene and these values were used to classify galGal3 RefSeq genes into five 20 percentile groups. The cis-regulatory element annotation system (CEAS) [58] was used to profile these five gene lists against the F1 DNA-seq data. The profiles for regions spanning 1kb on each side of TSS and TTS were plotted. The F1 DNA-seq data extracted at TSS and TTS regions (-1K to 1K) of ranked genes were displayed per 10-base bin on heatmaps by a R script.

3.7 Data availability

The sequencing data are available from GEO under accession number GSE75955.

3.8 Acknowledgements

This work was supported by a Canada Research Chair (to J.R.D.) and a Research Manitoba award funded by Children's Hospital Research Institute of Manitoba and the Research Institute in Oncology and Hematology (to S.J.). We thank Research Manitoba, University of Manitoba Faculty of Health Sciences, Research Institute in Oncology and Hematology, and Children's Hospital Research Institute of Manitoba for support of the Manitoba Next Generation Sequencing facility.

3.9 References

1. Weintraub H, Groudine M. Chromosomal subunits in active genes have an altered conformation. *Science*. 1976;193:848-56.
2. Wang Z, Zang C, Cui K, Schones DE, Barski A, Peng W, et al. Genome-wide mapping of HATs and HDACs reveals distinct functions in active and inactive genes. *Cell*. 2009;138:1019-31.
3. Roh TY, Cuddapah S, Zhao K. Active chromatin domains are defined by acetylation islands revealed by genome-wide mapping. *Genes Dev*. 2005;19:542-52.
4. Anguita E, Johnson CA, Wood WG, Turner BM, Higgs DR. Identification of a conserved erythroid specific domain of histone acetylation across the alpha-globin gene cluster. *Proc Natl Acad Sci U S A*. 2001;98:12114-9.
5. Forsberg EC, Bresnick EH. Histone acetylation beyond promoters: long-range acetylation patterns in the chromatin world. *Bioessays*. 2001;23:820-30.
6. Litt MD, Simpson M, Recillas-Targa F, Prioleau MN, Felsenfeld G. Transitions in histone acetylation reveal boundaries of three separately regulated neighboring loci. *EMBO J*. 2001;20:2224-35.
7. Myers FA, Evans DR, Clayton AL, Thorne AW, Crane-Robinson C. Targeted and extended acetylation of histones H4 and H3 at active and inactive genes in chicken embryo erythrocytes. *J Biol Chem*. 2001;276:20197-205.
8. Hebbes TR, Clayton AL, Thorne AW, Crane-Robinson C. Core histone hyperacetylation co-maps with generalized DNase I sensitivity in the chicken beta-globin chromosomal domain. *EMBO J*. 1994;13:1823-30.
9. Ridsdale JA, Hendzel MJ, Delcuve GP, Davie JR. Histone acetylation alters the capacity of the H1 histones to condense transcriptionally active/competent chromatin. *J Biol Chem*. 1990;265:5150-6.
10. Zhang DE, Nelson DA. Histone acetylation in chicken erythrocytes. Rates of acetylation and evidence that histones in both active and potentially active chromatin are rapidly modified. *Biochem J*. 1988;250:233-40.
11. Rocha E, Davie JR, van Holde KE, Weintraub H. Differential salt fractionation of active and inactive genomic domains in chicken erythrocyte. *J Biol Chem*. 1984;259:8558-63.
12. Ghirlando R, Giles K, Gowher H, Xiao T, Xu Z, Yao H, et al. Chromatin domains, insulators, and the regulation of gene expression. *Biochim Biophys Acta*. 2012;1819:644-51.
13. Lawson GM, Knoll BJ, March CJ, Woo SL, Tsai MJ, O'Malley BW. Definition of 5' and 3' structural boundaries of the chromatin domain containing the ovalbumin multigene family. *J Biol Chem*. 1982;257:1501-7.
14. Alevy MC, Tsai MJ, O'Malley BW. DNase I sensitive domain of the gene coding for the glycolytic enzyme glyceraldehyde-3-phosphate dehydrogenase. *Biochemistry*. 1984;23:2309-14.
15. Antes TJ, Namciu SJ, Fournier RE, Levy-Wilson B. The 5' boundary of the human apolipoprotein B chromatin domain in intestinal cells. *Biochemistry*. 2001;40:6731-42.

16. Williams AF. DNA synthesis in purified populations of avian erythroid cells. *J Cell Sci.* 1972;10:27-46.
17. Affolter M, Cote J, Renaud J, Ruiz-Carrillo A. Regulation of histone and beta A-globin gene expression during differentiation of chicken erythroid cells. *Mol Cell Biol.* 1987;7:3663-72.
18. Roninson IB, Ingram VM. Expression and partial DNA sequence of the chicken beta H-globin gene. *J Biol Chem.* 1983;258:802-9.
19. Schneider R, Bannister AJ, Myers FA, Thorne AW, Crane-Robinson C, Kouzarides T. Histone H3 lysine 4 methylation patterns in higher eukaryotic genes. *Nat Cell Biol.* 2004;6:73-7.
20. Zhang D, Nelson DA. Histone acetylation in chicken erythrocytes. Estimation of the percentage of sites actively modified. *Biochem J.* 1986;240:857-62.
21. Bates DL, Thomas JO. Histones H1 and H5: one or two molecules per nucleosome? *Nucleic Acids Res.* 1981;9:5883-94.
22. Delcuve GP, Davie JR. Chromatin structure of erythroid-specific genes of immature and mature chicken erythrocytes. *Biochem J.* 1989;263:179-86.
23. Sun JM, Chen HY, Espino PS, Davie JR. Phosphorylated serine 28 of histone H3 is associated with destabilized nucleosomes in transcribed chromatin. *Nucleic Acids Res.* 2007;35:6640-7.
24. Locklear L, Jr., Ridsdale JA, Bazett-Jones DP, Davie JR. Ultrastructure of transcriptionally competent chromatin. *Nucleic Acids Res.* 1990;18:7015-24.
25. Walia H, Chen HY, Sun JM, Holth LT, Davie JR. Histone acetylation is required to maintain the unfolded nucleosome structure associated with transcribing DNA. *J Biol Chem.* 1998;273:14516-22.
26. Allegra P, Sterner R, Clayton DF, Allfrey VG. Affinity chromatographic purification of nucleosomes containing transcriptionally active DNA sequences. *J Mol Biol.* 1987;196:379-88.
27. Ridsdale JA, Rattner JB, Davie JR. Erythroid-specific gene chromatin has an altered association with linker histones. *Nucleic Acids Res.* 1988;16:5915-26.
28. Hendzel MJ, Davie JR. Nucleosomal histones of transcriptionally active/competent chromatin preferentially exchange with newly synthesized histones in quiescent chicken erythrocytes. *Biochem J.* 1990;271:67-73.
29. Li W, Nagaraja S, Delcuve GP, Hendzel MJ, Davie JR. Effects of histone acetylation, ubiquitination and variants on nucleosome stability. *Biochem J.* 1993;296 (Pt 3):737-44.
30. McQueen HA, Siriaco G, Bird AP. Chicken microchromosomes are hyperacetylated, early replicating, and gene rich. *Genome Res.* 1998;8:621-30.
31. Habermann FA, Cremer M, Walter J, Kreth G, von Hase J, Bauer K, et al. Arrangements of macro- and microchromosomes in chicken cells. *Chromosome Res.* 2001;9:569-84.
32. International Chicken Genome Sequencing C. Sequence and comparative analysis of the chicken genome provide unique perspectives on vertebrate evolution. *Nature.* 2004;432:695-716.
33. Masabanda JS, Burt DW, O'Brien PC, Vignal A, Fillon V, Walsh PS, et al. Molecular cytogenetic definition of the chicken genome: the first complete avian karyotype. *Genetics.* 2004;166:1367-73.

34. Smith J, Burt DW. Parameters of the chicken genome (*Gallus gallus*). *Anim Genet*. 1998;29:290-4.
35. Woods CM, Lazarides E. The erythroid membrane skeleton: expression and assembly during erythropoiesis. *Annual review of medicine*. 1988;39:107-22.
36. Sanders MM. Fractionation of nucleosomes by salt elution from micrococcal nuclease-digested nuclei. *J Cell Biol*. 1978;79:97-109.
37. Henikoff S, Henikoff JG, Sakai A, Loeb GB, Ahmad K. Genome-wide profiling of salt fractions maps physical properties of chromatin. *Genome Res*. 2009;19:460-9.
38. Roadmap Epigenomics C, Kundaje A, Meuleman W, Ernst J, Bilenky M, Yen A, et al. Integrative analysis of 111 reference human epigenomes. *Nature*. 2015;518:317-30.
39. Bieberstein NI, Carrillo Oesterreich F, Straube K, Neugebauer KM. First exon length controls active chromatin signatures and transcription. *Cell Rep*. 2012;2:62-8.
40. Davie JR, Xu W, Delcuve GP. Histone H3K4 trimethylation: dynamic interplay with pre-mRNA splicing. *Biochem Cell Biol*. 2015;in press.
41. Saitoh N, Bell AC, Recillas-Targa F, West AG, Simpson M, Pikaart M, et al. Structural and functional conservation at the boundaries of the chicken beta-globin domain. *EMBO J*. 2000;19:2315-22.
42. Myers FA, Chong W, Evans DR, Thorne AW, Crane-Robinson C. Acetylation of histone H2B mirrors that of H4 and H3 at the chicken beta-globin locus but not at housekeeping genes. *J Biol Chem*. 2003;278:36315-22.
43. Natt D, Agnvall B, Jensen P. Large sex differences in chicken behavior and brain gene expression coincide with few differences in promoter DNA-methylation. *PloS one*. 2014;9:e96376.
44. Ayers KL, Davidson NM, Demiyah D, Roeszler KN, Grutzner F, Sinclair AH, et al. RNA sequencing reveals sexually dimorphic gene expression before gonadal differentiation in chicken and allows comprehensive annotation of the W-chromosome. *Genome Biol*. 2013;14:R26.
45. Sjakste N, Iarovaia OV, Razin SV, Linares-Cruz G, Sjakste T, Le Gac V, et al. A novel gene is transcribed in the chicken alpha-globin gene domain in the direction opposite to the globin genes. *Molecular & general genetics : MGG*. 2000;262:1012-21.
46. Wight M, Werner A. The functions of natural antisense transcripts. *Essays Biochem*. 2013;54:91-101.
47. Lai F, Shiekhatar R. Enhancer RNAs: the new molecules of transcription. *Curr Opin Genet Dev*. 2014;25:38-42.
48. Kong S, Bohl D, Li C, Tuan D. Transcription of the HS2 enhancer toward a cis-linked gene is independent of the orientation, position, and distance of the enhancer relative to the gene. *Mol Cell Biol*. 1997;17:3955-65.
49. Ling J, Baibakov B, Pi W, Emerson BM, Tuan D. The HS2 enhancer of the beta-globin locus control region initiates synthesis of non-coding, polyadenylated RNAs independent of a cis-linked globin promoter. *J Mol Biol*. 2005;350:883-96.
50. Abruzzo LV, Reitman M. Enhancer activity of upstream hypersensitive site 2 of the chicken beta-globin cluster is mediated by GATA sites. *J Biol Chem*. 1994;269:32565-71.

51. Hutchison N, Weintraub H. Localization of DNAase I-sensitive sequences to specific regions of interphase nuclei. *Cell*. 1985;43:471-82.
52. Simonis M, Klous P, Splinter E, Moshkin Y, Willemsen R, de Wit E, et al. Nuclear organization of active and inactive chromatin domains uncovered by chromosome conformation capture-on-chip (4C). *Nat Genet*. 2006;38:1348-54.
53. Cogburn LA, Porter TE, Duclos MJ, Simon J, Burgess SC, Zhu JJ, et al. Functional genomics of the chicken--a model organism. *Poult Sci*. 2007;86:2059-94.
54. Khan DH, Gonzalez C, Cooper C, Sun JM, Chen HY, Healy S, et al. RNA-dependent dynamic histone acetylation regulates MCL1 alternative splicing. *Nucleic Acids Res*. 2014;42:1656-70.
55. Li H, Handsaker B, Wysoker A, Fennell T, Ruan J, Homer N, et al. The Sequence Alignment/Map format and SAMtools. *Bioinformatics*. 2009;25:2078-9.
56. Zang C, Schones DE, Zeng C, Cui K, Zhao K, Peng W. A clustering approach for identification of enriched domains from histone modification ChIP-Seq data. *Bioinformatics*. 2009;25:1952-8.
57. Krzywinski M, Schein J, Birol I, Connors J, Gascoyne R, Horsman D, et al. Circos: an information aesthetic for comparative genomics. *Genome Res*. 2009;19:1639-45.
58. Shin H, Liu T, Manrai AK, Liu XS. CEAS: cis-regulatory element annotation system. *Bioinformatics*. 2009;25:2605-6.

3.10 Supporting informations

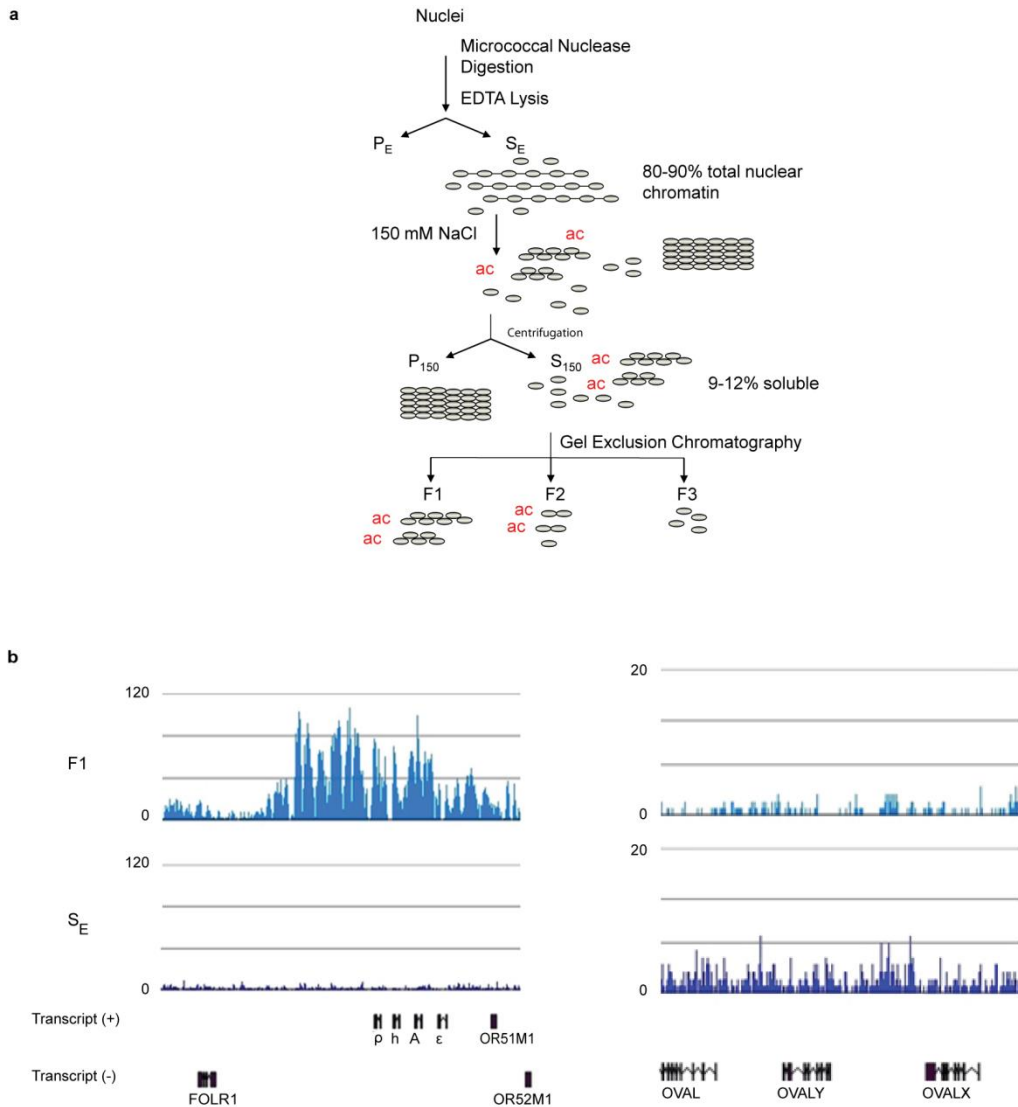


Figure S3.1: a Fractionation of avian erythrocyte chromatin. Chicken polychromatic erythrocyte nuclei were incubated with micrococcal nuclease, and chromatin fragments soluble in a low ionic strength solution containing 10 mM EDTA were recovered in fraction S_E . Chromatin fraction S_E was made 150 mM in NaCl, and chromatin fragments from the salt-soluble fraction (S_{150}) were size-resolved on a Bio-Gel A-1.5 m column to isolate the F1 fraction containing polynucleosomes. b β -globin and ovalbumin F1 and S_E chromatin profiles. The DNA from F1 and S_E chromatin fractions isolated from chicken polychromatic erythrocytes was sequenced. The signal tracks show DNA enrichment for β -globin on chromosome 1 and *OVAL* (ovalbumin) on chromosome 2.

	RPKM from RNA-seq		RNA levels from RT-qPCR				
	Sample s1	Sample s2	Sample s3*			Sample s4	Sample s5
			Repeat 1	Repeat 2	Repeat 3		
HBG2	155,037	169,112	4.327	4.408	4.112	5.170	5.409
FTH1	10,378	10,380	0.266	0.233	0.319	0.272	0.232
CA2	13,205	13,192	0.170	0.266	0.283	0.163	0.146
HDAC2	46	41	0.001	0.001	0.002	0.000	0.000
PRMT7	12	10	0.001	0.001	0.001	0.000	0.000

Table S3.1 Additional file 3: Validation of RNA-seq data by RT-qPCR. Comparison of RPKM values from RNA-seq analyses with RNA levels determined by RT-qPCR assays for specific genes. Transcript levels were normalized to 18S rRNA levels. * Three RT-qPCR assays were done on three different RNA preparations from Sample 3.

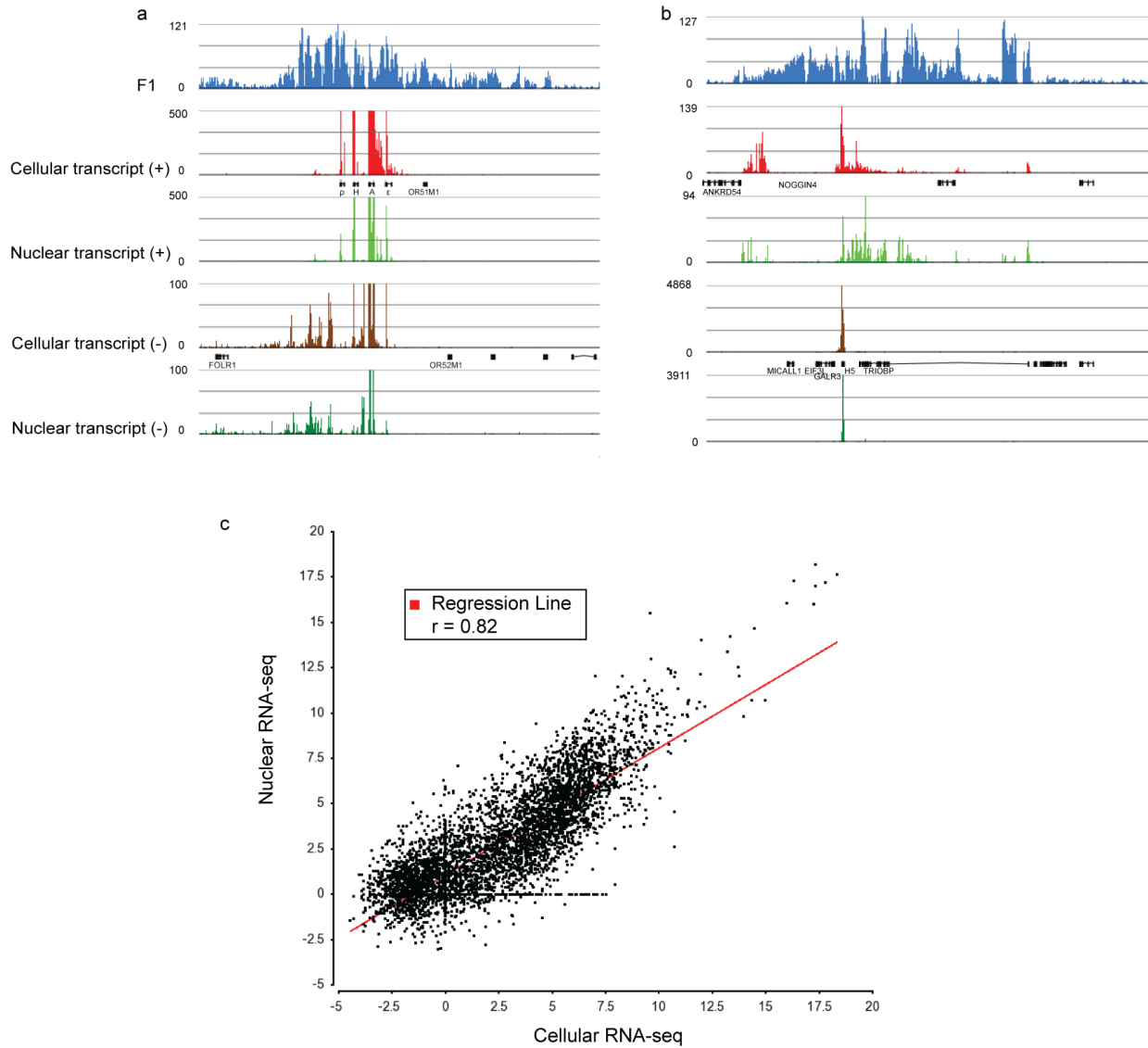


Figure S3.2: Transcriptional activity determination by cellular and nuclear RNA-seq. a Signal tracks showing DNA enrichment in F1 fraction for β -globin (HBB) locus and transcripts on (+) and (-) strands from cellular and nuclear RNA are shown. mRNAs (with exons as black boxes) are shown below their template strand. b Same for H5. c Correlation of the cellular and nuclear RNA-seq data. Unit on both axes is log₂ RPKM, with RPKM being the average of two biological repeats.

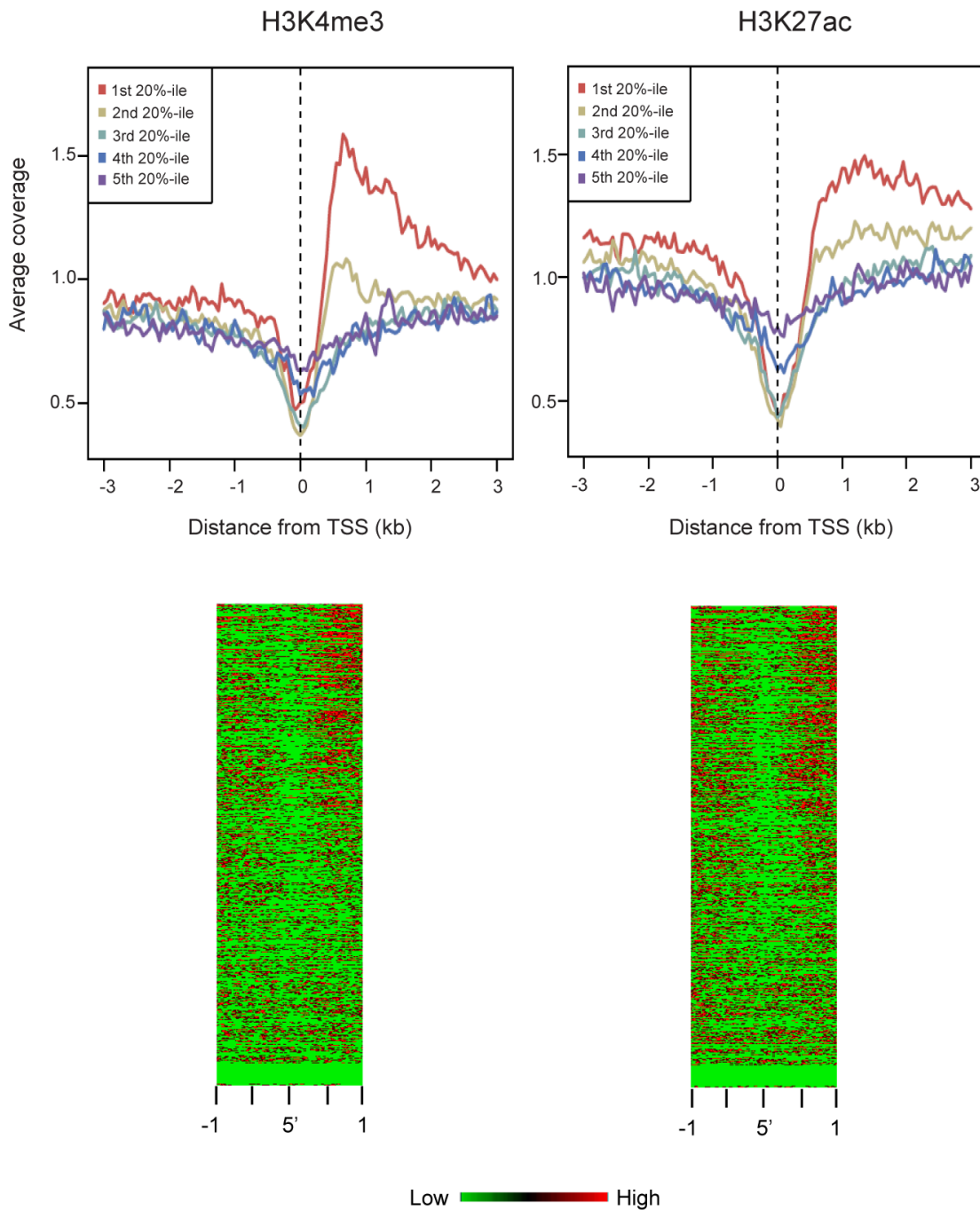


Figure S3.3: H3K4me3 and H3K27ac profiles as a function of gene expression. TSS-centered profiles were divided into quintile classes based on gene expression levels (Additional file 2). Below, heatmap spanning 1 kb on each side of TSS and TTS of all genes ranked from top to bottom, according to their expression levels (Appendix 2).

Source of polychromatic erythrocytes	Experiments	Number of chickens	Age range of chickens	Weight range of chickens
Sample s1	RNA-seq	12	12 months	1.6-2.0 kg
Sample s2	RNA-seq	12	12 months	1.5-1.8 kg
Sample s3	RT-PCR	11	4-7 months	1.2-1.8 kg
Sample s4	RT-PCR	12	5-8 months	1.3-1.8 kg
Sample s5	RT-PCR	12	5-8 months	1.1-1.7 kg
Sample sA	F1-1 DNA-seq	12	5-8 months	1.6-2.0 kg
Sample sB	F1-2 DNA-seq	12	9-10 months	1.4-2.0 kg
Sample sD	H3K4me3 & H3K27ac ChIP	12	12 months	1.6-2.0 kg

Table S3.2: Description of polychromatic erythrocyte sample sources. Each sample consisted of red blood cells collected from 11 to 12 anemic chickens: age and weight ranges

Primers for RT-qPCR assays

Primers	Sequences
HBG2-F	5'-GGCAAGAAAGTGCTCACCTC-3'
HBG2-R	5'-GCTTGTCACAATGCAGTTCG-3'
FTH1-F	5'-ATTTTGACCGGGATGATGTG-3'
FTH1-R	5'-TGGTTTTGCAGCTTCATCAG-3'
CA2-F	5'-AGCCCCTCAGCTTCAGCTAC-3'
CA2-R	5'-ACTTGTCGGAGGAGTCGTCA-3'
HDAC2-F	5'-TATGGACAAGGGCATCCAAT-3'
HDAC2-R	5'-CACGTAAATTTCCATTTTCCTGT-3'
PRMT7-F	5'-TTCTCAACCCAAATCCATCC-3'
PRMT7-R	5'-GCGTGGTTTGCTGAGAGC-3'
18S-F	5'-GTAACCCGTTGAACCCATT-3'
18S-R	5'-CCATCCAATCGGTAGTAGCG-3'

Table S3.3: Primers for RT-qPCR analyses.

CHAPTER IV: TRANSCRIPTION-DEPENDENT ASSOCIATION OF HDAC2 WITH ACTIVE CHROMATIN

4.1 Abstract

Histone deacetylase 2 (HDAC2) catalyzes deacetylation of histones at the promoter and coding regions of transcribed genes and regulates chromatin structure and transcription. To explore the role of HDAC2 and phosphorylated HDAC2 in gene regulation, we studied the location along transcribed genes, the mode of recruitment and the associated proteins with HDAC2 and HDAC2S394ph in chicken polychromatic erythrocytes. We show that HDAC2 and HDAC2S394ph are associated with transcriptionally active chromatin and located in the interchromatin channels. HDAC2S394ph was present primarily at the upstream promoter region of the transcribed *CA2* and *GAS41* genes, while total HDAC2 was also found within the coding region of the *CA2* gene. Recruitment of HDAC2 to these genes was partially dependent upon on-going transcription. Unmodified HDAC2 was associated with RNA binding proteins and interacted with RNA bound to the initiating and elongating forms of RNA polymerase II. HDAC2S394ph was not associated with RNA polymerase II. These results highlight the differential properties of unmodified and phosphorylated HDAC2 and the organization of acetylated transcriptionally active chromatin in the chicken polychromatic erythrocyte.

This collaborative work was published as:

Sanzida Jahan, Jian-Min Sun, Shihua He, James Ronald Davie.

Transcription-Dependent Association of HDAC2 with Active Chromatin.

Journal of Cellular Physiology (2017); doi: 10.1002/jcp.26078.

Sanzida Jahan has generated 50% of the data presented, prepared the figures, drafted and edited the manuscript. Jian-Min Sun performed the CHIP experiments; Shihua He participated in immunofluorescence experiment. JRD conceived of the study, participated in its design and coordination and drafted manuscript. Geneviève P.Delcuve reviewed manuscript.

4.2 Introduction

Histone acetylation is a reversible, dynamic process, which is regulated by lysine acetyltransferases (KATs) and histone deacetylases (HDACs), which add or remove acetyl groups to/from lysine residues within the N-terminal tails of target histones, respectively [423]. The global acetylation level of histones influences chromatin structure and affects the accessibility of transcription factors and effector proteins to the DNA, thereby modulating gene expression. We developed a powerful fractionation protocol which separates transcriptionally active from repressed chromatin of chicken erythrocytes. The two main reasons why this fractionation procedure is operational in chicken erythrocytes are first, the expressed chromatin regions have highly acetylated histones and second, chicken erythrocyte chromatin has a greater level of linker histones, H1 and H5, than most vertebrate cells. The highly acetylated chromatin is required to prevent H1/H5-mediated compaction at physiological ionic strength. We recently demonstrated that the transcriptionally active genes in chicken polychromatic erythrocyte genome were organized into two chromatin structures [285]. Highly expressed genes such as the β -globin genes were organized into highly acetylated chromatin domains, several kb in length that were soluble at physiological ionic strength. Mid- and low-expressing genes (for example, histone deacetylase 2) had highly acetylated region confined to the 5' end of the gene. Although the steady state of histone acetylation is high in these regions, it is important to know that these acetylated histones are being rapidly acetylated and deacetylated [356, 406]. HDAC2 is phosphorylated at S394, S422 and S424 by protein kinase CK2 [163, 167]. The phosphorylation of HDAC2 is essential to form the multiprotein complexes SIN3, NuRD and coREST. Unmodified HDAC2 (human) is not associated with these multiprotein complexes, and is bound to RNA-binding proteins that are involved in processing the primary transcript [165]. We reported that the widely used X-ChIP assay fails to effectively map the distribution of unmodified HDAC2 along the coding regions of genes [163]. With the combination of formaldehyde and DSP dual crosslinking process, it is possible to map both unmodified and phosphorylated HDAC2 [163]. Genome wide mapping of HDACs in human cells was done by dual crosslinking (disuccinimidyl glutarate and formaldehyde) which would track the distribution of the phosphorylated and unmodified HDAC [168]. Under these conditions, HDAC2 was located at the promoter and gene body of active genes. However, gene location of phosphorylated HDAC2 has not been determined. In contrast to our understanding of the mechanisms by which phosphorylated HDAC2, Sin3, and NuRD complexes are recruited to promoters, there is relatively little known as to how unmodified HDAC2 complexes are recruited to transcribed genes in vertebrates.

In this study, using G0-phase non-replicating chicken polychromatic erythrocyte cells, we show that total HDAC2 and HDAC2S394ph are associated with active chromatin. We applied a novel approach to provide evidence that the unmodified HDAC2, which is associated with RNA-binding proteins, is bound to the highly acetylated, active chromatin. Further, we demonstrate that unmodified HDAC2, but not phosphorylated HDAC2, is associated with the initiating and elongating form of RNA polymerase II via the nascent RNA, and that recruitment of HDAC2 to active genes is dependent upon on-going transcription.

4.3 Results

4.3.1 HDAC2 and phosphorylated HDAC2 association with active chromatin

Chicken polychromatic erythrocyte chromatin was fractionated by a method which separates transcriptionally active from repressed chromatin [282, 285]. To determine the efficiency of chromatin fractionation, we monitored the distribution of SRSF1 and H3K36me₃, which are associated with the coding region of transcribed genes [165, 424]. **Figure 4.1** shows that SRSF1 and H3K36me₃ were present in fractions P_E, S₁₅₀ and F1, but not in fraction P₁₅₀ which contains the bulk of repressed chromatin. Next, we determined the distribution of HDAC2 and HDAC2S394ph in the chicken polychromatic erythrocyte chromatin. The mouse monoclonal anti-HDAC2 antibody will detect phosphorylated and non-phosphorylated HDAC2 forms, while the rabbit polyclonal antibody to HDAC2 phosphorylated at S394 will recognize phosphorylated forms of HDAC2 that have this modification. HDAC2 was present in fractions P_E, S₁₅₀, F1 and F2, which contain transcribed chromatin [282]. P₁₅₀, which has repressed chromatin, had very low levels of HDAC2 (**Figure 4.1**). HDAC2S394ph partitioned with the transcriptionally active chromatin containing fractions P_E, S₁₅₀ and F1. The slow-migrating band detected by antibodies against HDAC2S394ph in P_E and F1 is a highly phosphorylated form of HDAC2 [163].

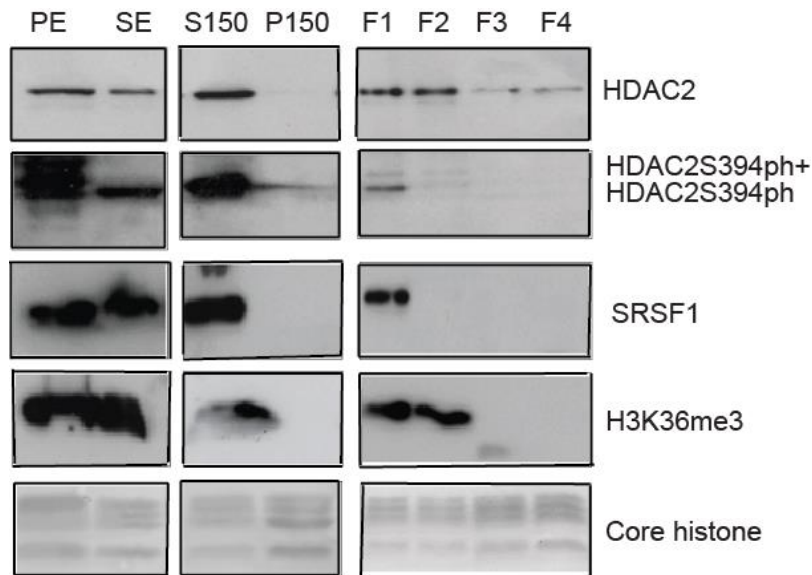


Figure 4.1. HDAC2, HDAC2S394ph, SRSF1 and H3K36me3 are associated with the transcriptionally active chromatin fraction of chicken polychromatic erythrocytes. Chromatin fractions (5 A260) from polychromatic erythrocytes were loaded onto a 10% SDS-polyacrylamide gel, transferred to nitrocellulose membranes, immunochemically stained with anti-HDAC2, anti-HDAC2S394ph, anti-SRSF1 and anti-H3K36me3 antibodies. Ponceau S-stained core histones were used as a loading reference. HDAC2S394ph+ indicates a multi-phosphorylated form of HDAC2 that has S394ph.

4.3.2 HDAC2 co-maps with interchromatin channels of the nuclei

Next, we determined the distribution of HDAC2 in the polychromatic erythrocytes by indirect immunofluorescence. DAPI staining (blue) shows the localization of the condensed chromatin. **Figure 4.2** shows that HDAC2 was located in the inter-chromatin channels, which has previously been shown to contain decondensed, transcriptionally active chromatin [425]. **Figure 4.2A** and **Figure 4.2B** represent two independent experiments.

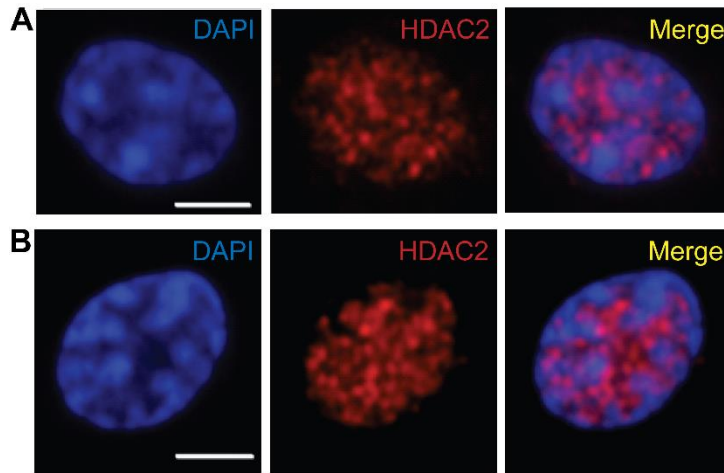


Figure 4.2. Association of HDAC2 with the interchromatin channel of the polychromatic erythrocytes. Indirect immunofluorescence assay for staining was used, nuclei using DAPI was merged with HDAC2. The cells were immunostained with an antibody against HDAC2 and co-stained with DAPI. Spatial distribution was visualized by fluorescence microscopy followed by analyses with AxioVision software. Bar, 5 μ m. Figure panel A and B represent two biological replicates of the experiment.

4.3.3 Phosphorylated HDAC2 binds to regulatory regions of transcribed genes

To further explore the distribution of HDAC2 and HDAC2S394ph across transcriptionally active genes, we determined the location of HDAC2 and HDAC2S394ph across the upstream promoter and coding regions of the *CA2* and *GAS41* genes. The *CA2* (tissue specific) and *GAS41* (housekeeping) are moderately and weakly expressing genes, respectively, in chicken polychromatic erythrocytes [285, 421]. Dual crosslinking ChIP assays (DSP + formaldehyde) were performed for HDAC2 and HDAC2S394ph. HDAC2 was found at the upstream promoter and coding regions (exons 2, 3 and 7) of the *CA2* gene, with exon 3 showing a greater association of HDAC2 than exons 2 and 7 (**Figure 4.3**). In contrast, the greatest HDAC2S394ph enrichment was found with the *CA2* upstream promoter region. In accordance with previous studies [421, 426], acetylated H3 was found at the upstream promoter and 5' end of the *CA2* gene. The *GAS41* housekeeping gene is considerably shorter than the *CA2* gene (2.7 versus 16.2 kb). HDAC2, HDAC2S394ph and H3ac were all polarized towards the upstream promoter region of the *GAS41* gene.

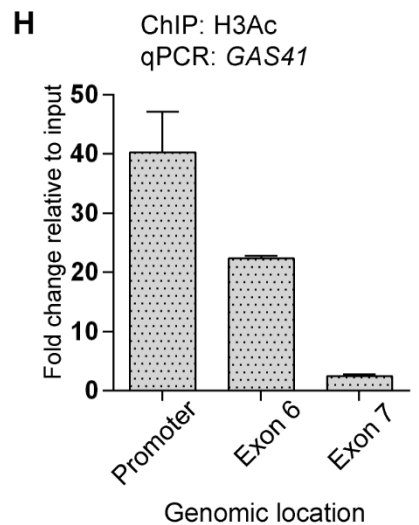
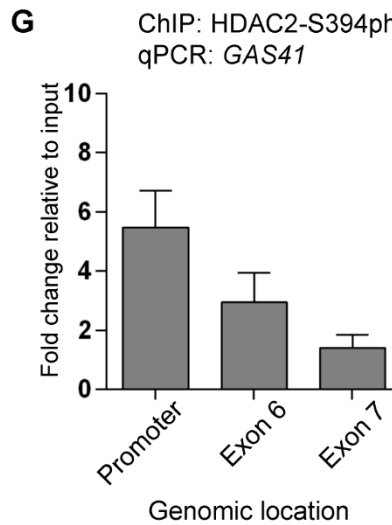
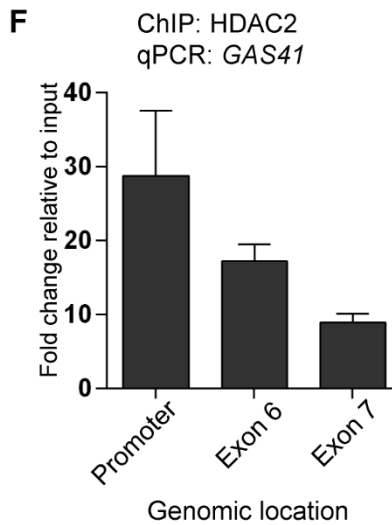
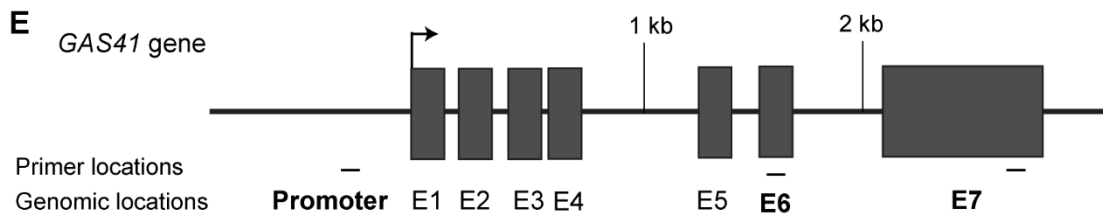
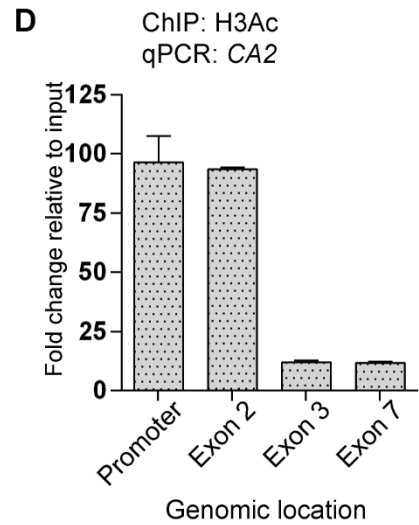
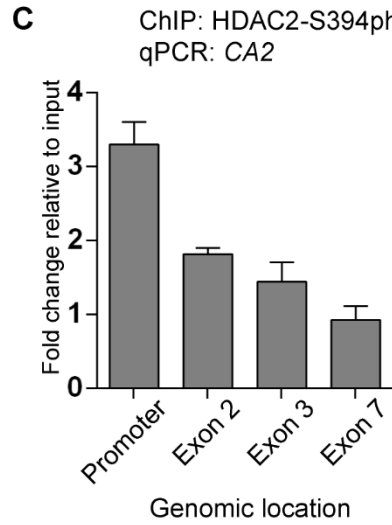
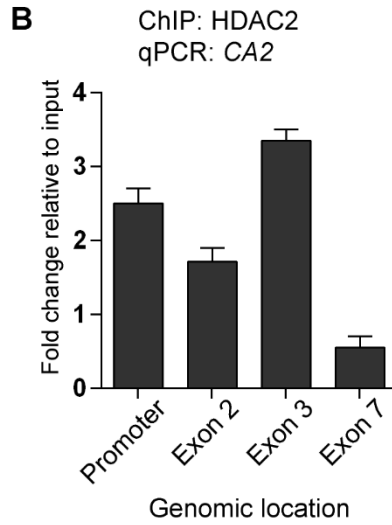
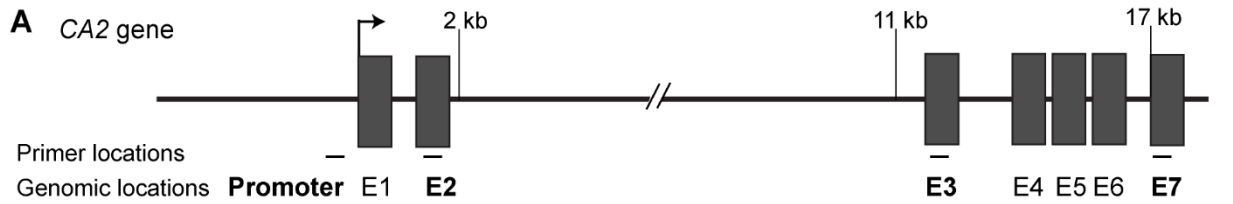


Figure 4.3. Distribution of HDAC2, phosphorylated HDAC2 (HDAC2-S394ph) and acetylated H3 (H3Ac) within the CA2 and GAS41 gene regions. A) Schematic representation of CA2 gene where amplicons are labeled underneath according to the 5' position of the forward primer relative to the transcription start site (arrow). The exons (E1-E7) are represented by the gray boxes. B-D) ChIP assay was performed using antibodies against B) anti-HDAC2, C) anti-HDAC2-S394ph and D) anti-H3Ac on DSP and formaldehyde cross-linked polychromatic erythrocytes. The binding of these proteins and histone modification to CA2 gene regions were determined by qPCR with primers specific for the promoter and coding regions. E) Schematic representation of GAS41 gene. F-H) ChIP-qPCR for F) anti-HDAC2, G) anti-HDAC2-S394ph and H) anti-H3ac within the GAS41 gene promoter and coding regions. Error bars indicate Standard Error of Mean (SEM). N=2.

4.3.4 Recruitment of HDAC2 to promoter and coding region is dependent on transcription

We investigated whether the recruitment of HDAC2 to the promoter and coding regions of the genes was dependent upon on-going transcription. To arrest transcription, chicken polychromatic erythrocytes were incubated with the transcription inhibitor DRB for two hours. These cells were then dual cross-linked with DSP and formaldehyde, followed by the ChIP assay for HDAC2. **Figure 4.4** shows that arresting transcription reduced binding of HDAC2 throughout the promoter and coding regions of the CA2 and GAS41 genes. These observations provide evidence that recruitment of HDAC2 is partially dependent upon transcription.

Dual cross-linked ChIP assay

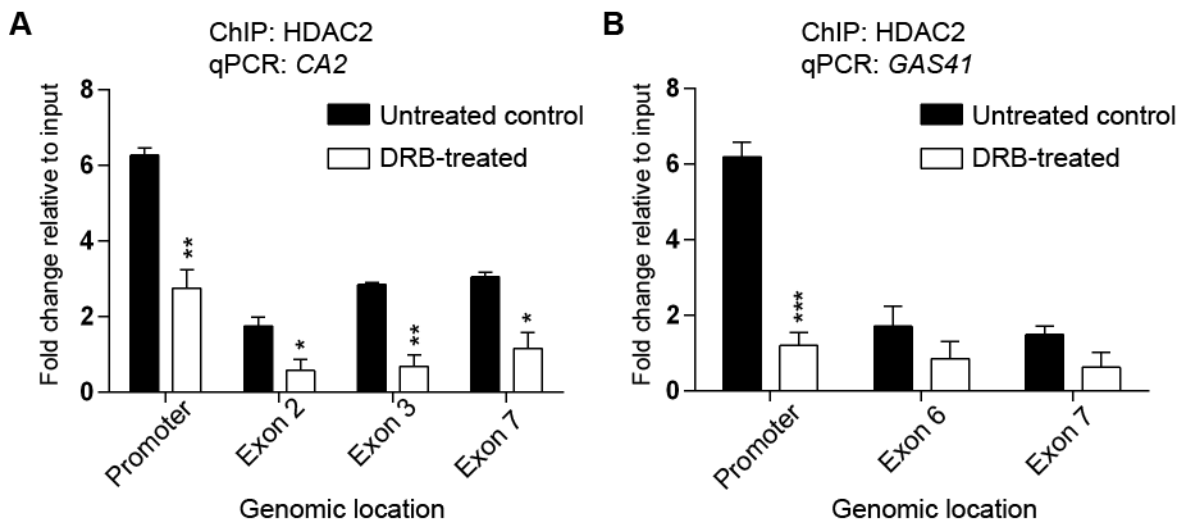


Figure 4.4. Transcription-dependent recruitment of unmodified HDAC2 to *CA2* and *GAS41* gene regions. A) Schematic representation of treatment of polychromatic erythrocytes with transcription inhibitor DRB for two hours. The schematic also shows subsequent experimental setup. B-C) Cells were dual cross-linked with DSP and formaldehyde and treated with DRB. B) ChIP assays with anti-HDAC2 antibodies and qPCR for specific sites along the *CA2* gene (see Figure 4.3 for the position of amplicons). C) ChIP assays with anti-HDAC2 antibodies and qPCR for specific sites along the *GAS41* gene (see Fig. S4.2 for the position of amplicons). Error bars represent the standard error of the mean from three independent experiments. Statistical significance was calculated with respect to the untreated control *P<0.05, **P<0.01, ***P<0.001 or ****P<0.0001.

4.3.5 Chicken erythrocyte HDAC2 associates with RNA splicing factors

The F1 chromatin is associated with phosphorylated and unmodified HDAC2 [163]. We exploited the observation that formaldehyde cross-links unmodified HDAC2 poorly to DNA to design a method to isolate the unmodified HDAC2 complexes from the F1 chromatin [163]. Chromatin fraction F1 was incubated with formaldehyde and then added to hydroxyapatite (HAP) under conditions in which chromatin is bound. The HDAC complexes that were not cross-linked to chromatin were eluted from the column. The formaldehyde cross-links were reversed and the HDAC complexes retrieved. HDAC2 complexes in eluted fractions were isolated by immunoprecipitation with an anti-HDAC2 antibody, and the bound proteins characterized by mass spectrometry. The HDAC2 complexes were devoid of proteins associated with the Sin3, NuRD and CoREST complexes, and contained RNA binding proteins that are involved in pre-RNA splicing (e.g. SRSF1) (Table 4.1). Thus, as with human unmodified HDAC2,

chicken erythrocyte HDAC2 is associated with proteins involved in RNA processing. Further, these results suggest that the unmodified HDAC2 is associated with RNA in chicken polychromatic erythrocytes.

Table 4.I. Protein composition of HAP- unbound HDAC2 complexes in the polynucleosome fraction (F1) of chicken erythrocyte cells

RNA Splicing	SRSF1,6,7,10 SERP1 SNRP70, B, D1,2,3, G, S SNRPEL1 DEK PABPC1 HnRNPR RBMX C20orf119 Sm-D1
--------------	--

4.3.6 Association of HDAC2, but not HDAC2S394ph, with RNAPII

We had previously reported that mammalian HDAC2 was associated with the elongating form of RNAPII (RNAPIIS2ph); an interaction that was dependent upon RNA [165]. To investigate whether chicken erythrocyte HDAC2 and HDAC2S394ph associate with the RNAPII complex, immunoprecipitations of RNAPIIS2ph (transcription elongation-competent) and RNAPIIS5ph (transcription initiation-competent) were performed under low stringency condition from chicken polychromatic erythroid cell lysates treated or not with RNase. Immunoblot analyses show that RNAPIIS2ph and RNAPIIS5ph were efficiently immunoprecipitated from the cell lysates independent of RNase digestion (**Figure 4.5A and 4.5B**). The immunoblot analyses also show that HDAC2 was bound to the two forms of RNAPII but that the interaction was lost when the cell lysate was digested with RNase. In contrast, the majority of the HDAC2S394ph was not bound to RNAPIIS2ph or RNAPIIS5ph (**Figure 5C and D**). The immunoblots also show that the highly phosphorylated HDAC2, which has a reduced mobility on 6% polyacrylamide gels [163] was not associated with RNAPII. These observations provide evidence that unmodified

HDAC2, but not phosphorylated HDAC2, is recruited to transcribed chromatin by associating with the newly formed transcript associated with RNAPII.

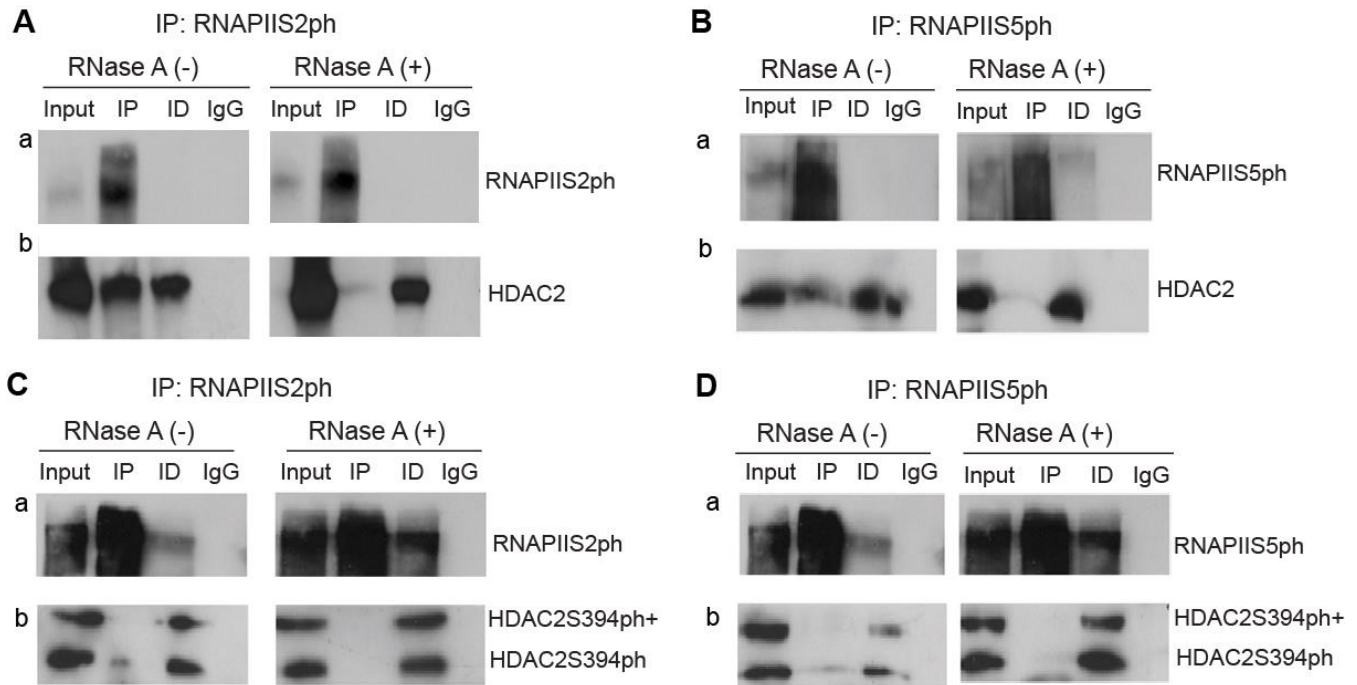


Figure 4.5. Interaction of HDAC2 with transcript bound to RNA polymerase II. Chicken polychromatic erythrocyte lysates treated with or without RNase A were immunoprecipitated with RNAPIIS2ph (A, C) or RNAPIIS5ph (B, D). Immunoblot analyses of the input, immunoprecipitate (IP) and immunodepleted (ID) fraction was done with antibodies against RNAPIIS2ph, RNAPIIS5ph, HDAC2 or HDAC2S394ph. As a control, the immunoprecipitation was done with pre-immune rabbit IgG, and the IP fraction analyzed by immunoblotting with the stated antibody. HDAC2S394ph+ indicates a multi-phosphorylated form of HDAC2 that has S394ph.

4.4 Discussion

Our results show that the unmodified HDAC2 in chicken polychromatic erythrocytes is associated with RNA binding proteins, is associated with the RNA bound to the initiating and elongating forms of RNAPII and is dependent upon transcription to associate with the gene body. These observations provide evidence that in chicken polychromatic erythrocytes as in human cells unmodified HDAC2 is recruited to nascent

transcripts via RNA binding proteins, and it is from the transcript that HDAC2 catalyzes dynamic acetylation of histones bound to the gene body.

To the best of our knowledge, this is the first report showing the location of phosphorylated HDAC2 along transcribed genes. We show that HDAC2S394ph is directed primarily to the upstream promoter region of transcribed genes. The observation that HDAC2S394ph is not associated with RNAPII is consistent with phosphorylated HDAC2 being present in SIN3, NuRD and CoREST [160]: HDAC complexes which are recruited to regulatory regions by a variety of transcription factors.

Dynamic acetylation, catalyzed by KATs and HDACs, plays a major role in the organization and solubility of transcriptionally active chromatin in chicken polychromatic erythrocytes [285]. In these cells, the majority of HDAC2 is bound to transcriptionally active chromatin. The observation that HDAC2 resides in the interchromatin channels between condensed chromatin regions suggests that transcribed chromatin, which has highly acetylated (although dynamic) histones and is soluble at physiological ionic strength, is also located at the boundaries of condensed chromatin. This conclusion is consistent with the report by Hutchison and Weintraub which demonstrated that the DNase sensitive chromatin (a feature of transcriptionally active chromatin) in chicken erythrocytes was located in the interchromatin channels [425]. Super-resolution fluorescence microscopy has shown that transcriptionally active chromatin, RNAPII and nascent RNA are located with the perichromatin region which has decondensed chromatin. The perichromatin region borders on condensed chromatin and interfaces with the interchromatin compartment [427].

In chicken polychromatic erythrocytes, transcribed genes have at least two types of organization. Highly transcribed genes, such as the β -globin gene, are present in chromatin domains several kb in length that have highly acetylated histones, and are DNase I sensitive and soluble at physiological ionic strength. Such gene domains may be entirely present in the perichromatin domain which at the low resolution of our analyses would appear to be in the interchromatin channels. In contrast, mid- to low-expressing genes such as the *CA2* and *GAS41* genes have highly acetylated histones at the 5' end of the gene. Such genes may have their 5' regulatory regions in the perichromatin channel and the remainder of the gene in the condensed chromatin regions [427]. As KAT and HDAC activity are associated with the internal nuclear matrix of polychromatic erythrocytes [281, 428], we speculate that the nuclear matrix structure associated with the perichromatin domain and interchromatin channel is involved in maintaining the differential chromatin organization of high versus mid-/low-expressing gene chromatin structures.

4.5 Materials and Methods

4.5.1 Ethics

All methods involving the use of chickens were approved by and carried out in accordance with the University of Manitoba Animal Care Committee guidelines and regulations. The birds were purchased through Central Animal Care Services, University of Manitoba and were housed under standard conditions.

4.5.2 Chicken erythrocyte chromatin fractionation and HDAC2 isolation

Chicken polychromatic erythrocyte salt-soluble chromatin S₁₅₀ and polynucleosome fraction (F1) were prepared as described previously [282]. The F1 fraction was cross-linked with 1% formaldehyde at room temperature for 10 min, then quenched with glycine. The cross-linked F1 fraction was incubated with hydroxyapatite (HAP) for 1 hr. The unbound fraction, which contains nonphosphorylated HDAC2 complexes, was collected. From this fraction, HDAC2 was immunoprecipitated using an anti-HDAC2 antibody (Thermo Fisher Scientific). Magnetic Dyna beads (Invitrogen, Carlsbad, CA) were used to pull down the immunoprecipitated complex.

4.5.3 Mass Spectrometry

The HDAC2 immunoprecipitated complex was eluted with 1% SDS / 0.1 M NaHCO₃. The eluted fraction was vacuum-dried and washed with 100 mM of NH₄HCO₃ and iodoacetamide. After lyophilization, the sample was incubated with trypsin for over 16 h at 37°C. The nano-liquid chromatography and tandem mass spectrometry were performed as described previously [429]. To identify peptides, the Mass Spectrometry Sequence Database (MSDB), version 20060831 database was searched using the Global Proteome Machine (<http://www.thegpm.org>) search engine as previously described [430].

4.5.4 Immunoblotting

Equal amounts (5.0 A260) from the chicken erythrocyte chromatin fractions were loaded onto the polyacrylamide gel. The blots were immunochemically stained with anti-HDAC2 (Millipore, Billerica, MA), anti-HDAC2S394ph (Abcam, Cambridge, United Kingdom), antiSRSF1 (Santa Cruz, Dallas, TX), and anti-H3K36me3 (Abcam) antibody. The antibodies used and their conditions are listed in Supplementary **Table 4.1**.

4.5.5 Immunofluorescence assay

Indirect immunofluorescence was performed to characterize the distribution of HDAC2 in the chicken erythrocytes as described previously [431]. Briefly, chicken erythrocytes were diluted in PBS and then

smear on poly-lysine coated slides (Sigma). Air-dried blood smears were fixed with 4% formaldehyde and then subjected to immunofluorescence staining using mouse monoclonal antibody against HDAC2 (Millipore) followed by Alexa Fluor 594 donkeys anti-mouse secondary antibody (Molecular Probes, Eugene, OR). The nuclear DNA was stained with 4',6-diamidino-2-phenylindole (DAPI). Fluorescence microscopy was performed using Zeiss Axio Imager Z1 microscope. Digital images were captured using AxioCam (Oberkochen, Germany) HRm camera.

4.5.6 Immunoprecipitation (IP) and co-immunoprecipitation (co-IP) assays

Immunoprecipitation for RNAPIIS2ph and RNAPIIS5ph was performed according to the protocol described [432]. Briefly, cell lysates were prepared by using immunoprecipitation buffer (50 mM Tris-HCl pH 8.0, 150 mM NaCl, 0.5% NP-40, and 1 mM EDTA) with the protease and phosphatase inhibitors added fresh. After brief sonication supernatant was collected and the lysate was precleared with A/G beads (Santa Cruz) for 1 hr at 4°C. For immunoprecipitation 500 µg of cell lysates were incubated with 3 µg 2 | JAHAN ET AL. of RNAPIIS2ph or RNAPIIS5ph antibody (Abcam) overnight at 4°C. Cellular extracts were treated with 400 µg/ml of RNase A for 30 min at 37°C. Next day, 40 µl of protein G beads (Invitrogen) were added and incubated for 3 hr at 4°C. After the beads were washed for four times immunoprecipitated complex was immunochemically stained with HDAC2 (Millipore) or HDAC2S394ph (Abcam) antibodies. The list of antibodies and conditions used in immunoprecipitation and co-immunoprecipitation experiments are listed in **Supplementary Table 4.1**.

4.5.7 Cell Culture and Treatments

Chicken polychromatic erythrocytes were incubated with 0.15 mM 5,6-dichlorobenzimidazole riboside (DRB) for two h.

4.5.8 Chromatin Immunoprecipitation (ChIP) assay

For all studies, dithiobis succinimidyl propionate (DSP) and formaldehyde double cross-linking ChIP assays were performed. Cells were incubated at room temperature with 1 mM DSP for 30 min, and then for 10 min following the addition of formaldehyde to a final concentration of 1%. MNase digestion was optimized to yield an average size of 147 bp fragment [433]. The primers used in ChIP-qPCR experiments are shown in **Supplemental Table 4.2**.

4.5.9 Statistical analysis

Generation of all graphs and statistical analyses were done using GraphPad Prism6.0 version.

4.6 References

1. Delcuve GP, Khan DH, Liyanage VRB, Jahan S, Rastegar M, Kirshenbaum LA, et al. Epigenetics: Chromatin Organization and Function In: Backs J, McKinsey T, editors. Epigenetics in Cardiac Disease. 1 ed. Switzerland: Springer International Publishing 2017. p. 1-35.
2. Jahan S, Xu W, He S, Gonzalez C, Delcuve GP, Davie JR. The chicken erythrocyte epigenome. *Epigenetics Chromatin*. 2016;9:19. doi: 10.1186/s13072-016-0068-2. PubMed PMID: 27226810; PubMed Central PMCID: PMC4879735.
3. Zhang DE, Nelson DA. Histone acetylation in chicken erythrocytes. Rates of deacetylation in immature and mature red blood cells. *Biochem J*. 1988;250(1):241-5. Epub 1988/02/15. PubMed PMID: 3355515; PubMed Central PMCID: PMC1148839.
4. Zhang DE, Nelson DA. Histone acetylation in chicken erythrocytes. Rates of acetylation and evidence that histones in both active and potentially active chromatin are rapidly modified. *Biochem J*. 1988;250(1):233-40. Epub 1988/02/15. PubMed PMID: 2451508; PubMed Central PMCID: PMC1148838.
5. Sun JM, Chen HY, Davie JR. Differential distribution of unmodified and phosphorylated histone deacetylase 2 in chromatin. *J Biol Chem*. 2007;282(45):33227-36. Epub 2007/09/11. doi: 10.1074/jbc.M703549200. PubMed PMID: 17827154.
6. Sun JM, Chen HY, Moniwa M, Litchfield DW, Seto E, Davie JR. The transcriptional repressor Sp3 is associated with CK2-phosphorylated histone deacetylase 2. *J Biol Chem*. 2002;277(39):35783-6. doi: 10.1074/jbc.C200378200. PubMed PMID: 12176973.
7. Khan DH, Gonzalez C, Cooper C, Sun JM, Chen HY, Healy S, et al. RNA-dependent dynamic histone acetylation regulates MCL1 alternative splicing. *Nucleic Acids Res*. 2014;42(3):1656-70. Epub 2013/11/16. doi: 10.1093/nar/gkt1134. PubMed PMID: 24234443; PubMed Central PMCID: PMC3919583.
8. Wang Z, Zang C, Cui K, Schones DE, Barski A, Peng W, et al. Genome-wide mapping of HATs and HDACs reveals distinct functions in active and inactive genes. *Cell*. 2009;138(5):1019-31. doi: 10.1016/j.cell.2009.06.049. PubMed PMID: 19698979; PubMed Central PMCID: PMC2750862.
9. Delcuve GP, Davie JR. Chromatin structure of erythroid-specific genes of immature and mature chicken erythrocytes. *Biochem J*. 1989;263(1):179-86. Epub 1989/10/01. PubMed PMID: 2604693; PubMed Central PMCID: PMC1133406.
10. Li J, Duns G, Westers H, Sijmons R, van den Berg A, Kok K. SETD2: an epigenetic modifier with tumor suppressor functionality. *Oncotarget*. 2016;7(31):50719-34. doi: 10.18632/oncotarget.9368. PubMed PMID: 27191891; PubMed Central PMCID: PMC4879735.
11. Hutchison N, Weintraub H. Localization of DNAase I-sensitive sequences to specific regions of interphase nuclei. *Cell*. 1985;43(2 Pt 1):471-82. PubMed PMID: 4075401.
12. Myers FA, Chong W, Evans DR, Thorne AW, Crane-Robinson C. Acetylation of histone H2B mirrors that of H4 and H3 at the chicken beta-globin locus but not at housekeeping genes. *J Biol Chem*. 2003;278(38):36315-22. Epub 2003/07/17. doi: 10.1074/jbc.M305822200. PubMed PMID: 12865423.

13. Myers FA, Evans DR, Clayton AL, Thorne AW, Crane-Robinson C. Targeted and extended acetylation of histones H4 and H3 at active and inactive genes in chicken embryo erythrocytes. *J Biol Chem.* 2001;276(23):20197-205. Epub 2001/03/29. doi: 10.1074/jbc.M009472200. PubMed PMID: 11274167.
14. Delcuve GP, Khan DH, Davie JR. Targeting class I histone deacetylases in cancer therapy. *Expert Opin Ther Targets.* 2013;17(1):29-41. Epub 2012/10/16. doi: 10.1517/14728222.2013.729042. PubMed PMID: 23062071.
15. Markaki Y, Gunkel M, Schermelleh L, Beichmanis S, Neumann J, Heidemann M, et al. Functional nuclear organization of transcription and DNA replication: a topographical marriage between chromatin domains and the interchromatin compartment. *Cold Spring Harb Symp Quant Biol.* 2010;75:475-92. doi: 10.1101/sqb.2010.75.042. PubMed PMID: 21467142.
16. Hendzel MJ, Sun JM, Chen HY, Rattner JB, Davie JR. Histone acetyltransferase is associated with the nuclear matrix. *J Biol Chem.* 1994;269(36):22894-901. Epub 1994/09/09. PubMed PMID: 8077241.
17. Hendzel MJ, Delcuve GP, Davie JR. Histone deacetylase is a component of the internal nuclear matrix. *J Biol Chem.* 1991;266(32):21936-42. Epub 1991/11/15. PubMed PMID: 1939216.
18. Meng X, Wilkins JA. Compositional characterization of the cytoskeleton of NK-like cells. *Journal of proteome research.* 2005;4(6):2081-7.
19. Fenyö D, Eriksson J, Beavis R. Mass spectrometric protein identification using the global proteome machine. *Computational Biology.* 2010:189-202.
20. He S, Khan DH, Winter S, Seiser C, Davie JR. Dynamic distribution of HDAC1 and HDAC2 during mitosis: association with F-actin. *J Cell Physiol.* 2013;228(7):1525-35. doi: 10.1002/jcp.24311. PubMed PMID: 23280436.
21. Khan DH, Gonzalez C, Cooper C, Sun J-M, Chen HY, Healy S, et al. RNA-dependent dynamic histone acetylation regulates MCL1 alternative splicing. *Nucleic acids research.* 2014;42(3):1656-70.
22. Spencer VA, Sun JM, Li L, Davie JR. Chromatin immunoprecipitation: a tool for studying histone acetylation and transcription factor binding. *Methods.* 2003;31(1):67-75. PubMed PMID: 12893175.

4.7 Supplementary informations

Supplementary Table 4.1. List of antibodies used in immunoblotting (IB) and immunoprecipitation (IP)			
Antibody	Conditions	Description	Company
HDAC2	IP: 5 ug/mL IB: 1:1000	Mouse monoclonal	Thermofisher scientific
HDAC2(phospho S394)	IP: 5ug/mL IB:1:1000	Rabbit polyclonal	Abcam
HDAC2	IB:1:1000	Mouse monoclonal	Millipore
SRSF1	IB: 1:500	Mouse monoclonal	Santa Cruz
Ac-H3	IP: 5ug/mL	Rabbit polyclonal	Millipore
H3K36me3	IB: 1:1000	Rabbit polyclonal	Abcam
RNAPIIS2ph	IP: 5ug/mL IB: 1:1000	Rabbit polyclonal	Abcam
RNAPIIS5ph	IP: 5ug/mL IB: 1:1000	Rabbit polyclonal	Abcam

Supplementary Table 4.2. Primers used in ChIP-qPCR experiments

Gene	Region	Primer sequence
Chicken <i>GAS41</i>	Promoter	FP: GTGTTTCCCGCTTCCTTTCTTAA RP: GCGTTCATGCCGTTTCCATC
	Exon 6	FP: GACACAGCGAGCTTCTCTCGTA RP: CCGTAGCTCTCGTGCAGCTT
	Exon 7	FP: TTGATGGTGCTGTGTATTTTGGT RP: ACGGGACGTCGTTAGCAGTT.
Chicken <i>CA2</i>	Promoter	FP: ACCGCTCTACCTGCCTCCTT RP: GAGGACGCCCTGGTTCT
	Exon 2	FP: GAGAGCAAAGCCAGCCTCACT RP: CAGGGCACTAGCTCACACAAGT
	Exon 3	FP: GGAGCGTGGATGGAGTCTA RP: CCCTGGCCCTCACAGGAT
	Exon 7	FP: GCCCTGGCAACATCTTGTCT RP: TGGCCAAGAGCCTTTCACAT

FP: Forward primer; RP: Reverse primer

CHAPTER V: PRMT1 AND 5 MEDIATED H4R3ME2A AND H3R2ME2S MODIFICATIONS IN TRANSCRIPTIONALLY ACTIVE CHROMATIN

5.1 Abstract

Arginine modifications by protein arginine methyltransferases (PRMTs) can confer both active and repressed chromatin states depending on the type of modifications. Among the different PRMTs, PRMT1 and 5 are the major enzymes responsible for producing asymmetric and symmetric arginine methylation, respectively. Asymmetric dimethylation of H4R3 by PRMT1 is crucial in maintaining histone acetylation across the globin locus as demonstrated in both chicken and mouse erythrocytes [23, 434]. It was demonstrated for the well-characterized chicken erythroid β -globin domain that PRMT1 plays a critical role in establishing and maintaining active histone marks [23]. On the other hand, symmetric dimethylation of H3R2 by PRMT5 is another active histone mark that enhances the binding of WDR5 to the site, thereby establishing a poised chromatin state. Therefore, recruitment of H4R3me2a and H3R2me2s by PRMT1 and 5 to the active chromosomal domains is a critical event in the maintenance of an active chromatin domain structure. However, the distribution of the two active arginine modifications H4R3me2a and H3R2me2s in the genome is not well defined. In this study, using the ChIP-seq assay, it was revealed that both H4R3me2a and H3R2me2s associate with transcriptionally active chromatin. We demonstrated that both H4R3me2a and H3R2me2s mark the distal regulatory region of transcribed genes along with H3K27ac. Moreover, these two modifications are enriched along the gene body of highly transcribed genes in polychromatic erythrocytes. Our analysis showed that both H3K27ac and H4R3me2a mark active promoters, while H3R2me2s and H3K4me3 associate with the 5' end of gene body. Further, co-occupancy of H3R2me2s with H3K4me1 and H3K27ac within a H3 tail establishes that H3R2me2s mark both active and poised enhancers. H3 tail modified with R2me2s contain H3K4me3, and both marks tend to co-localize at the 5' end of expressed genes in polychromatic erythrocytes. PRMT1 and 5 associate with RNAPIIs2ph and the nuclear matrix; this ensures that the role of both enzymes presumably in coupling transcription with posttranscriptional events. The findings from this study provide new insights into the distribution of two active arginine modifications and the signaling events initiated by these modifications. Moreover, these findings provide insights into the role of PRMT1 and 5 in establishing and maintaining the structure of transcriptionally active chromatin.

This collaborative work is in preparation for publication:

Sanzida Jahan performed all of the experiments, Wayne Xu performed the bioinformatics analysis, Aleksandar Ilic prepared the libraries for sequencing.

5.2 Introduction

Histone post-translational modifications contribute to gene activation and repression depending on the type of modifications on the loci [435]. Core histones undergo a variety of reversible post-translational modifications, including acetylation, lysine and arginine methylation, ubiquitination, and phosphorylation [436, 437]. The discovery of new histone PTMs is still ongoing (e.g. H4 lysine propionylation and butyrylation) [438]. Some PTMs (active marks) are associated with transcriptionally active chromatin regions, while others (repressive marks) correlate with silent regions. Histone acetylation usually marks active genes as does di- or tri-methylation of K4 of H3 (H3K4me2, K4me3) whereas H3K9me2 constitutes a repressive mark. Methylation of arginine by PRMTs is a comparatively newly discovered histone modifications which can act both as active or repressed histone modifications in a context-dependent manner, leading to the change of chromatin structure [181, 439]. The mammalian genome encodes eleven PRMTs that transfer a methyl group from S-adenosylmethionine (SAM) to the guanidino nitrogen of arginine. Mono and dimethylation of arginine are catalyzed by two classes of PRMTs enzyme. PRMTs catalyze arginine methylation by using the molecule SAM to form class I/asymmetric (ω -NG, NG-dimethylarginine or ADMA), class II/symmetric (ω -NG, N'G-dimethylarginine or SDMA) or monomethyl arginine (MMA) [181]. The substrates for these enzymes include histones and several nuclear and cytoplasmic proteins. It was demonstrated for the well characterized chicken erythroid β -globin domain, that the histone modifying enzyme PRMT1, which methylates H4 at R3 producing H4R3me2a (asymmetric), plays a critical role in establishing and maintaining active histone marks [H3 dimethylated at K4 (H3K4me2), acetylated histones] at the β -globin domain by recruiting lysine methyltransferase (SET1) and KATs [23]. On the other hand, the class II PRMT, PRMT5, generates H3R2me2s that is recognized by WDR5; WDR5 is a subunit of several co-activator complexes that produce H3K4me3 [217]. PRMT5-driven H3R2me2s is tightly correlated with H3K4me3 at active promoters as demonstrated in human B-cell line [217, 409]. PRMT6 is the major methyltransferase responsible for the genesis of H3R2me2a (inactive) *in vivo*. This H3 PTM antagonizes the MLL1-mediated trimethylation of H3K4, by preventing the recruitment of WDR5, a subunit of the MLL complex [114, 221]. Thus, methylation of histones by PRMTs can provide or block the docking site of other effector molecules. Previously, we mapped all the transcriptionally active chromatin domains in chicken polychromatic erythrocytes using the biochemical fractionation procedure [285]. We showed that highly expressed genes were

associated with H3K4me3 and H3K27ac [285]. H3K4me3 associates primarily with the 5' end of active genes [125]. The H3K27ac is a mark of an active enhancer while H3K4me1 marks both active and poised enhancers [417, 440]. To gain insight into the role of PRMT1 and 5 mediated arginine modifications H4R3me2a and H3R2me2s in the chromosomal domain conformation, ChIP-seq was used in combination with the biochemical fractionation procedure in chicken polychromatic erythrocytes.

In this chapter, we determined the genome wide distribution of arginine modifications, H4R3me2a and H3R2me2s. This is the first time demonstration of the co-localization of H4R3me2a and H3R2me2s at the hypersensitive sites of the chicken β -globin domain and several other distal regulatory regions. H4R3me2a and H3R2me2s are associated with the gene body of the transcribed genes of the polychromatic erythrocytes. The co-localization of H3R2me2s with K4me3 and H3K27 acetylation on the same histone tail suggests that there is a relationship between these modifications to generate an active chromatin locus. Finally, I show the association of PRMT1 and 5 with the nuclear matrix, and the RNAPIIS2ph dependent mechanism of recruitment of these two enzymes to the transcribed gene regions.

5.3 Results

5.3.1 Association of PRMT1, PRMT5 and their products (H4R3me2a and H3R2me2s) with active chromatin fractions

The specificity and cross-reactivity of the antibodies used in the experiments were tested using the peptide dot blot assay (**Supplementary figure S5.1**). Distribution of PRMT1, PRMT5, H4R3me2a, H3R2me2s, H4R3me2s and H3R2me2a was determined using the immunoblot assay on chromatin fractions isolated from chicken erythrocytes by our chromatin fractionation procedure. Immunoblot analysis revealed that PRMT1, PRMT5 and their corresponding arginine methylated products, H3R2me2s and H4R3me2a, were associated with the transcriptionally active chromatin fractions of polychromatic erythrocytes (**Figures 5.1- 5.3**). PRMT1 and 5 were associated with low salt insoluble chromatin fraction P_E, salt soluble polynucleosome chromatin fraction S₁₅₀, F1, and F2 (**Figure 5.1**). PRMT1 mediated H4R3me2a was associated with fractions P_E, S_E, S₁₅₀, F1 and F2 (**Figure 5.2a**). A similar pattern was observed for PRMT5 mediated arginine methylated H3R2me2s (**Figure 5.3a**). Our results demonstrated that H4R3me2s is associated with repressed chromatin fractions P₁₅₀, and distributed across F1-F4 equally (**Figure**

5.2b). However, H3R2me2a was only associated with repressed chromatin fractions P₁₅₀ and F4 (**Figure 5.3b**). A low level of H3R2me2a was observed in S_E chromatin fraction. A similar pattern of distribution was observed for PRMT1, 5, H4R3me2a, H4R3me2s and H3R2me2s in chromatin fractions isolated from mature erythrocytes (**Supplementary figure S5.2-S5.4**). The mature erythrocyte P_E fraction was depleted in H4R3me2a and enriched in H4R3me2s. However, this needs to be tested further as only one biological replicate has been performed. Ponceau S staining of core histones in the blot was used as a loading control in these experiments.

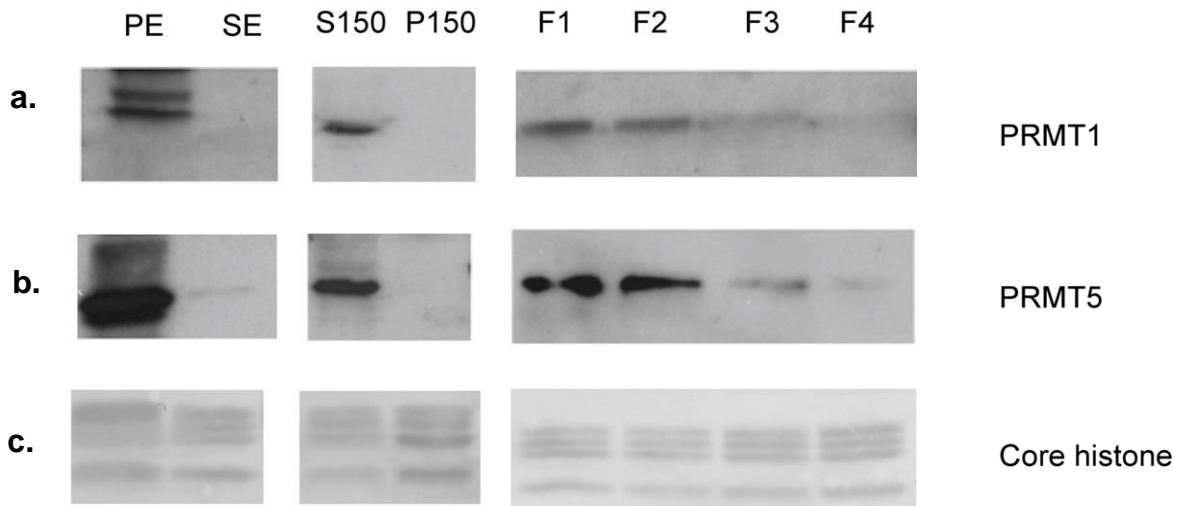


Figure 5.1: PRMT1 and PRMT5 are associated with the transcriptionally active chromatin fractions of chicken polychromatic erythrocytes. Chromatin fractions (5.0 A260) from polychromatic erythrocytes were loaded onto a 10% SDS-polyacrylamide gel, transferred to nitrocellulose membranes, immunochemically stained with a) anti-PRMT1 antibody and b) anti-PRMT5 antibody. c) Ponceau S-stained core histones were used as a loading reference.

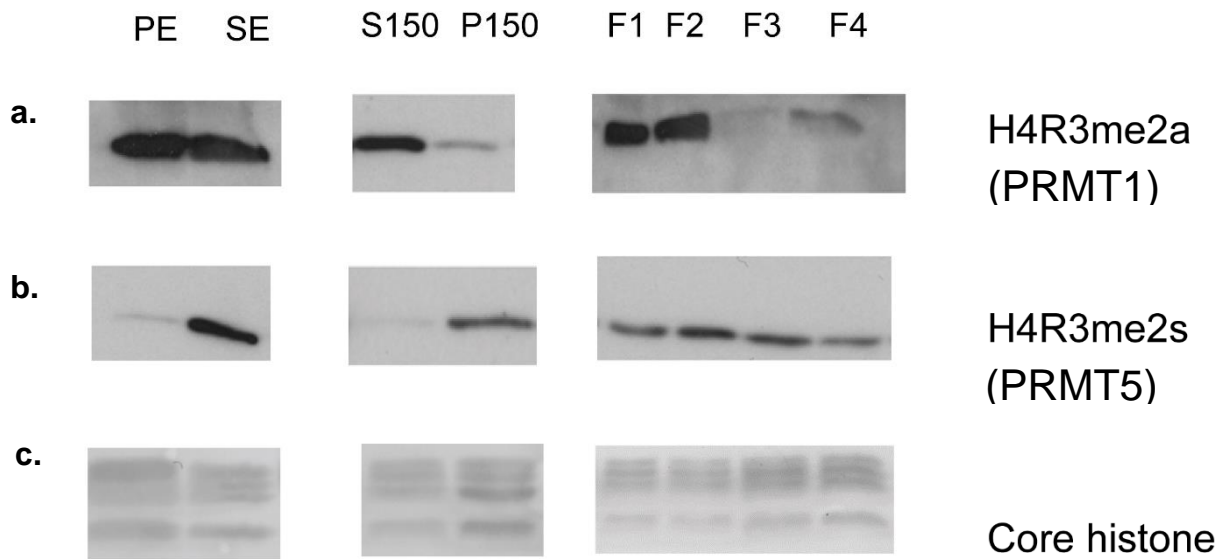


Figure 5.2: Association of H4R3me2a and H4R3me2s arginine modifications with active chromatin fractions. Chromatin fractions (5.0 A260) from polychromatic erythrocytes were loaded onto a 10% SDS-polyacrylamide gel, transferred to nitrocellulose membranes, immunochemically stained with a) anti-H4R3me2a and b) anti-H4R3me2s antibodies. c) Ponceau S-stained core histones were used as a loading reference.

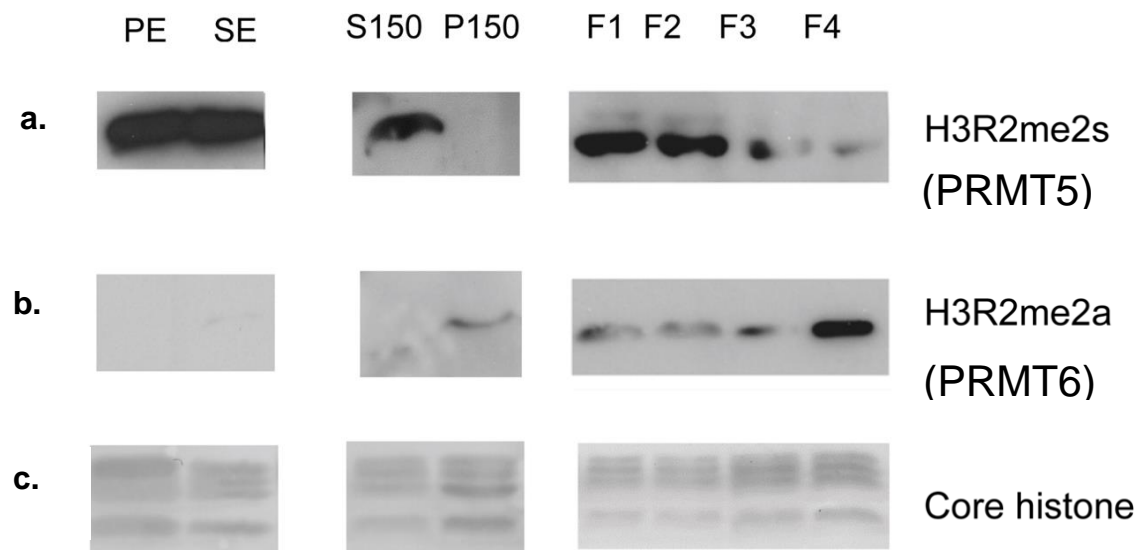


Figure 5.3: Association of H3R2me2s and H3R2me2a arginine modifications with the active chromatin fractions. Chromatin fractions (5.0 A260) from polychromatic erythrocytes were loaded onto a 10% SDS-polyacrylamide gel, transferred to nitrocellulose membranes, immunochemically stained with a) anti-H3R2me2s and b) anti-H3R2me2a antibodies. c) Ponceau S-stained core histones were used as a loading reference.

5.3.2 Correlation of H4R3me2a and H3R2me2s arginine methylation with highly transcribed genes

The genomic distribution of H4R3me2a and H3R2me2s modified histones was further addressed using the ChIP-seq assay. Genome-wide mapping was performed using ChIP-seq assay for the four histone modifications H4R3me2a, H3R2me2s, H3K4me3 and H3K27ac in polychromatic erythrocytes. Previously we reported that H3K4me3 and H3K27ac were associated at the 5' end of the gene body of highly expressed genes in polychromatic erythrocytes.

To determine the H4R3me2a and H3R2me2s profile as a function of gene expression, we first divided the genes from RNA-seq analysis into five 20th percentile groups. The highly expressed genes were grouped as a 1st 20th percentile, genes expressed at a lower level than the first group are in 2nd 20th percentile and so on. H4R3me2a location was determined relative to the transcription start site (TSS) and transcription termination site (TTS) in each of the quintile groups (**Figure 5.4a and 5.4b**). H4R3me2a was significantly enriched at the upstream promoter region and the 5' end of the gene body of highly expressed genes (**Figure 5.4a**). As shown in **Figure 5.4a**, this mark drops sharply at the TSS.

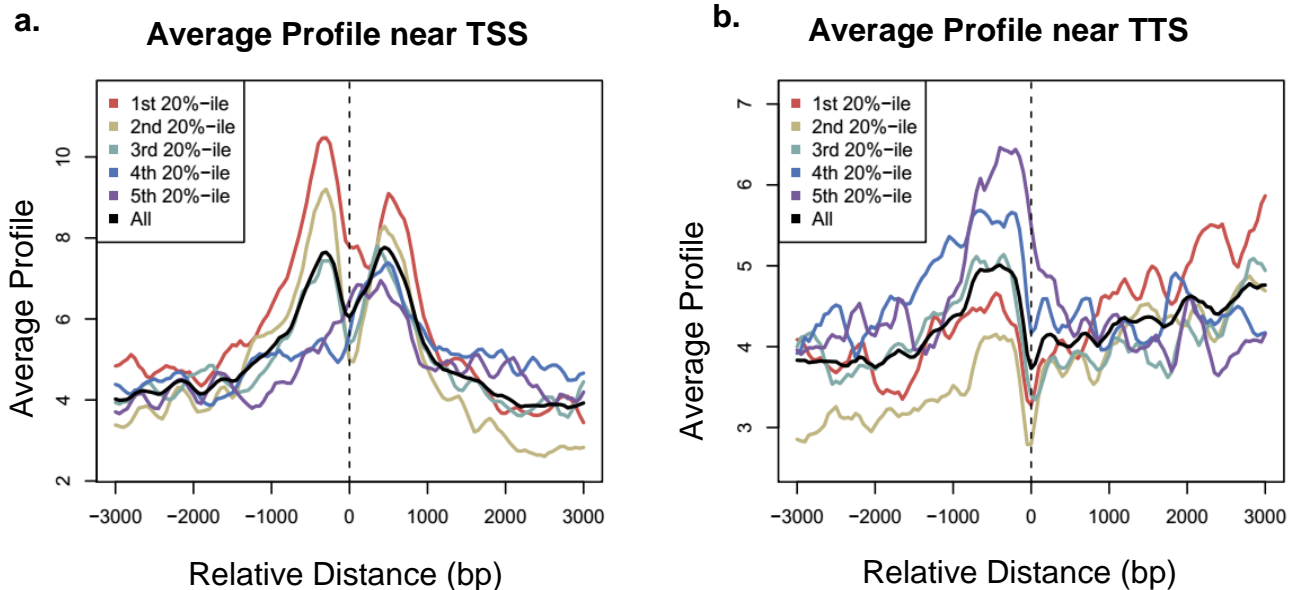


Figure 5.4: Profile of H4R3me2a as a function of gene expression. H4R3me2a was mapped at a) TSS and b) TTS of quintile classes based on gene expression levels. TSS-centered profiles were divided into quintile classes based on gene expression levels (Appendix 2). All 5479 genes from the galGal3 RefSeq database were ranked from top to bottom, according to their level of expression. These genes were profiled for H4R3me2a spanning 3 kb on each side of TSS and TTS (Appendix 2).

A similar analysis was performed for H3R2me2s with the five groups of expressed genes (**Figure 5.5**). Average coverage of H3R2me2s was determined around the TSS and TTS. As shown in **Figure 5.5a**, H3R2me2s was highly enriched at the upstream promoter or promoter proximal region of highly expressed genes. Along the gene body, the profile of H3R2me2s was peaking around 1kb while H4R3me2a peaked at 0.5kb (**Figure 5.4a** and **Figure 5.5a**). At the TTS, H3R2me2s drops sharply (**Figure 5.5b**).

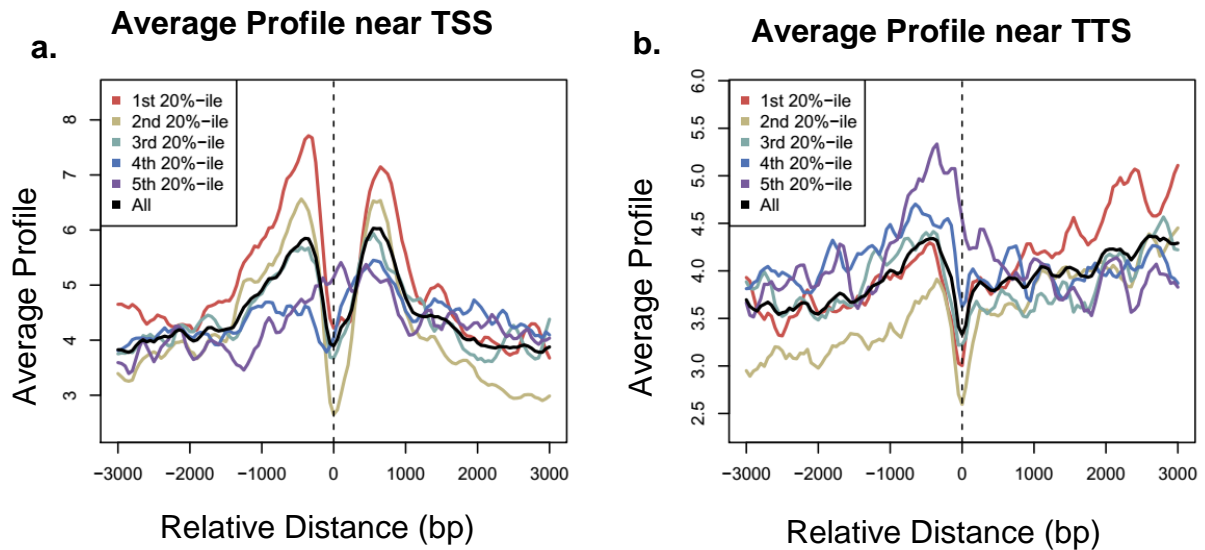


Figure 5.5: Profile of H3R2me2s as a function of gene expression. H3R2me2s was mapped at a) TSS and b) TTS of quintile classes based on gene expression levels. TSS-centered profiles were divided into quintile classes based on gene expression levels (Appendix 2). All 5479 genes from the galGal3 RefSeq database were ranked from top to bottom, according to their level of expression. These genes were profiled for H3R2me2s spanning 3 kb on each side of TSS and TTS (Appendix 2).

5.3.3 Profile of H4R3me2a and H3R2me2s arginine methylation in highly transcribed genes

Further, I studied the distribution of H4R3me2a, H3R2me2s, H3K4me3, and H3K27ac at several genomic loci in chicken polychromatic erythrocytes. At the chicken β -globin locus, H3R2me2s was associated with the HS1, HS2, HS3, HS4, $\beta^{A/\epsilon}$ enhancers and along the second exon-intronic region of β^A globin gene (**Figure 5.6**). H4R3me2a was associated with the HS1, HS2, HS3, HS4, $\beta^{A/\epsilon}$ enhancers, and along the β^A globin gene-body and promoter. These marks co-mapped with H3K27ac at the hypersensitive sites HS1-4 and $\beta^{A/\epsilon}$ enhancers. H4R3me2a co-mapped with H3K27ac at the promoter region of β^A globin gene, providing evidence that H4R3me2a is a mark for an active promoter. H3K4me3 co-mapped with H3R2me2s at the second exon-intronic region of the β^A globin gene.

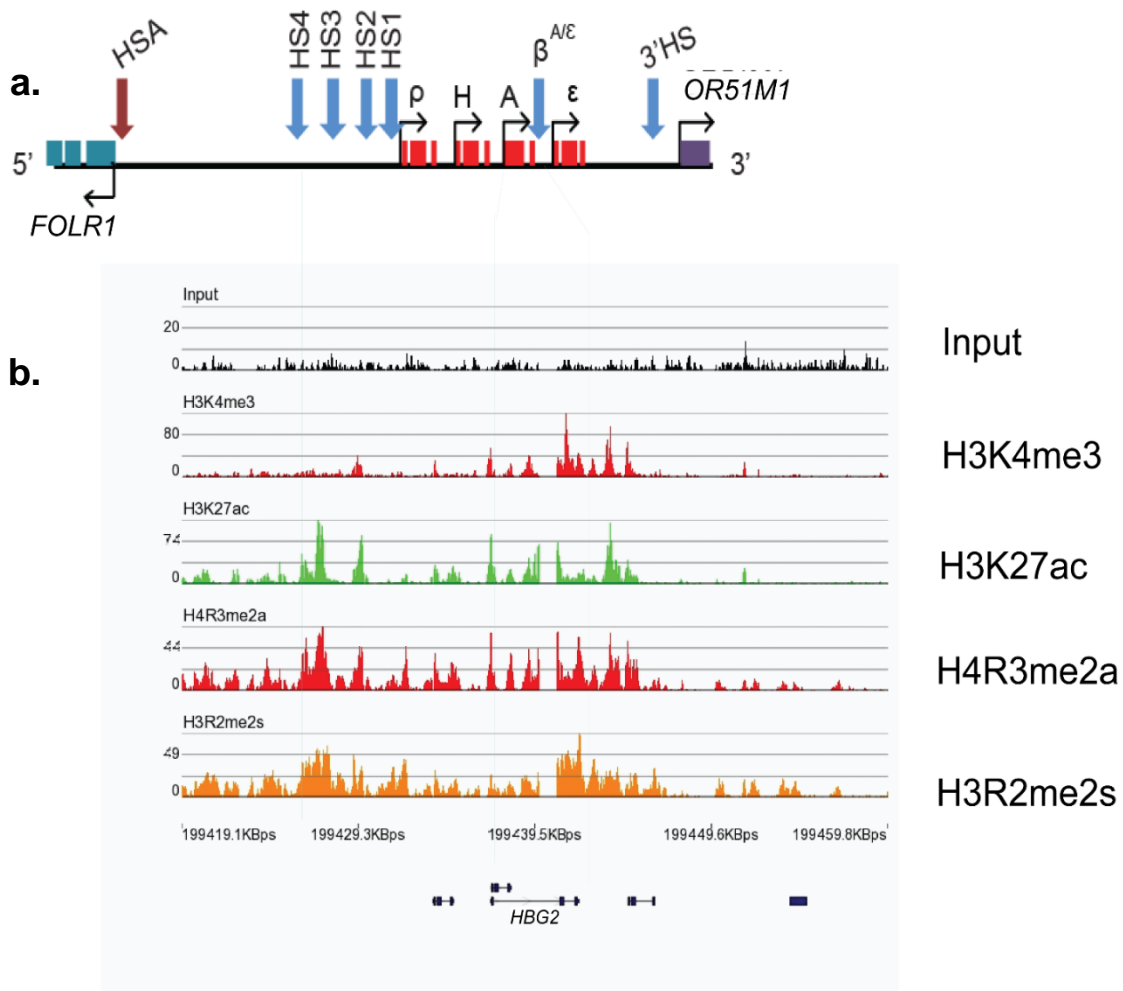


Figure 5.6: Distribution of H3R2me2s and H4R3me2a along the β -globin domain of polychromatic erythrocytes. a) The top panel is the schematic diagram for chicken β -globin domain detailing about the position of genes and hypersensitive sites (HS1-4) within the domain. b) The first track (in black) is the input signal for ChIP-seq, underneath (in red) is the signal track for H3K4me3, distribution of H3K27ac (in green), distribution of H4R3me2a (in red), distribution of H3R2me2s (in orange).

Similarly, other active loci were analyzed in chicken polychromatic erythrocytes. In the α -globin locus, H3R2me2s and H4R3me2a were associated with the transcriptionally active α D and α A globin genes as well as the 3' enhancer, which is located downstream of the α A globin gene (**Figure 5.7**). Association of these two marks was observed for the upstream regulatory regions of α MRE and HS14.9. These marks were absent in the embryonic π gene which is not transcribed in polychromatic erythrocytes.

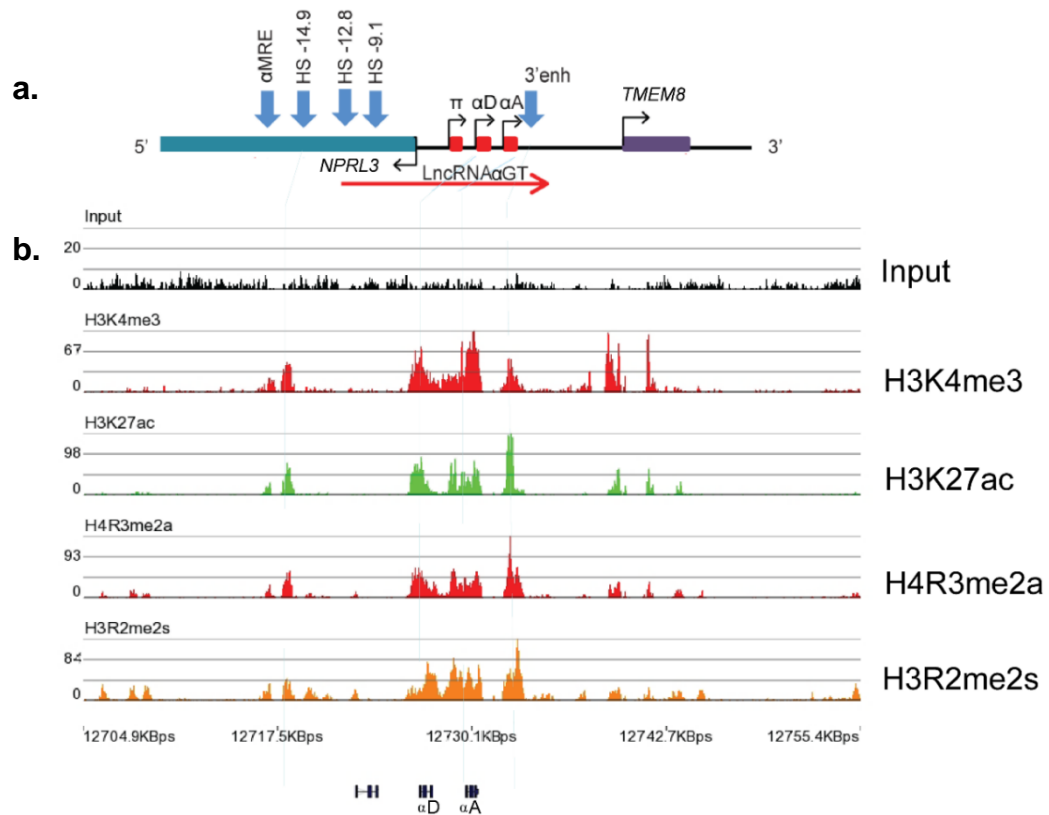
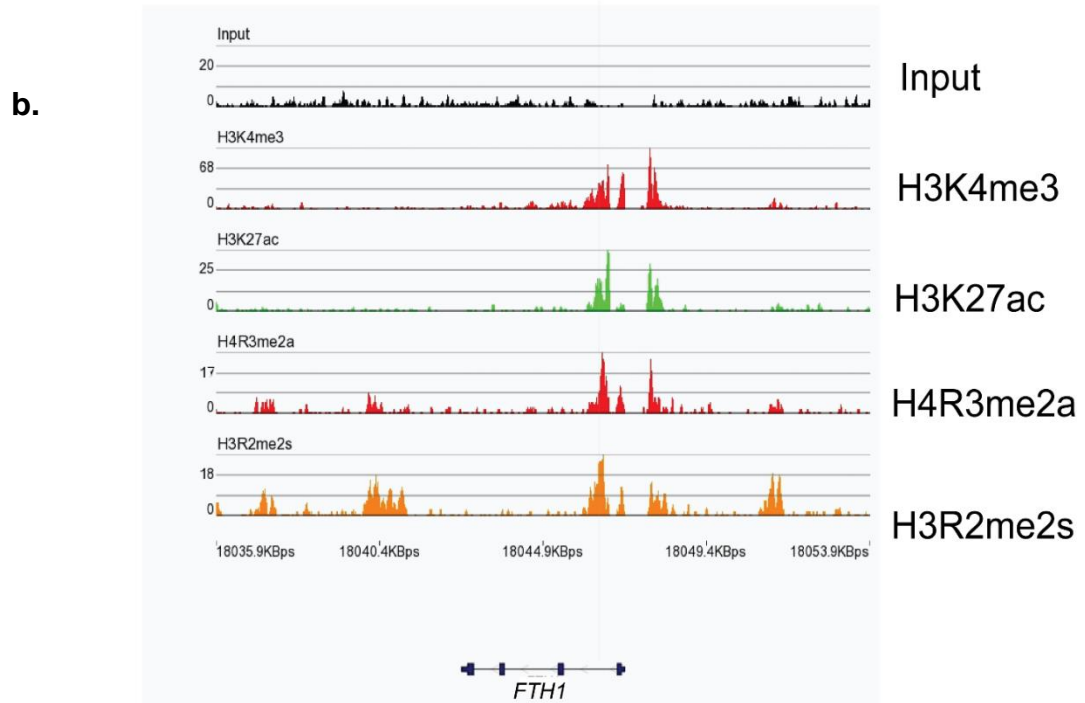
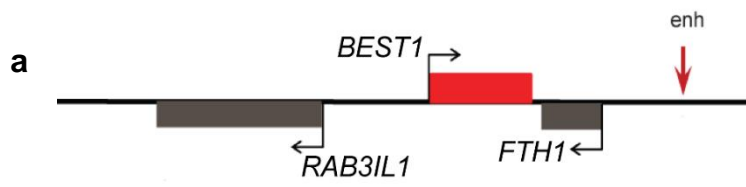


Figure 5.7: Distribution of H3R2me2s and H4R3me2a along expressed genes of polychromatic erythrocytes. a) The top panel is the schematic diagram for chicken α -globin domain detailing about the position of genes and hypersensitive sites within the domain. b) The first track (in black) is the input signal for ChIP-seq, underneath (in red) is the signal track for H3K4me3, distribution of H3K27ac (in green), distribution of H4R3me2a (in red), distribution of H3R2me2s (in orange).

I analyzed two other active chromosomal loci, *FTH1* and *CA2*, which have a moderate expression in polychromatic erythrocytes. In the *FTH1* locus, H3R2me2s and H4R3me2a peaked at the upstream promoter region and the first intronic region of the *FTH1* gene (**Figure 5.8**). These regions were also marked with H3K4me3 and H3K27ac. H3R2me2s and H4R3me2a were associated with the first intron of the *FTH1* gene where they co-mapped with H3K4me3 and H3K27ac. H3R2me2s also peaked at the upstream and downstream of the *FTH1* gene where it marked the location of the putative enhancer. The location of the putative enhancer in the upstream *FTH1* gene was previously reported and also demonstrated in **Chapter III** [285].



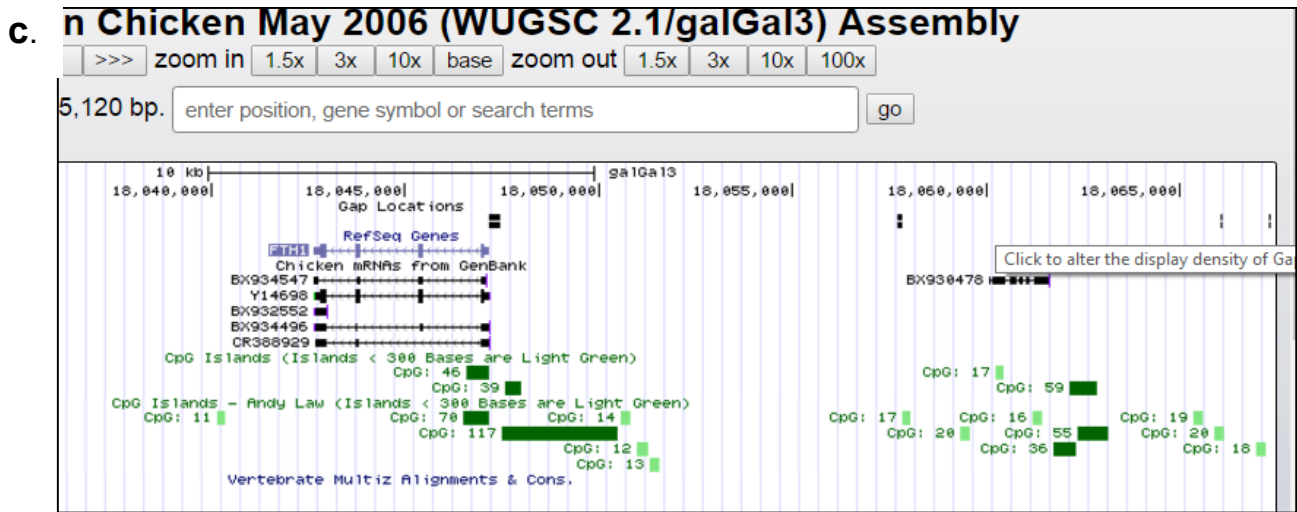
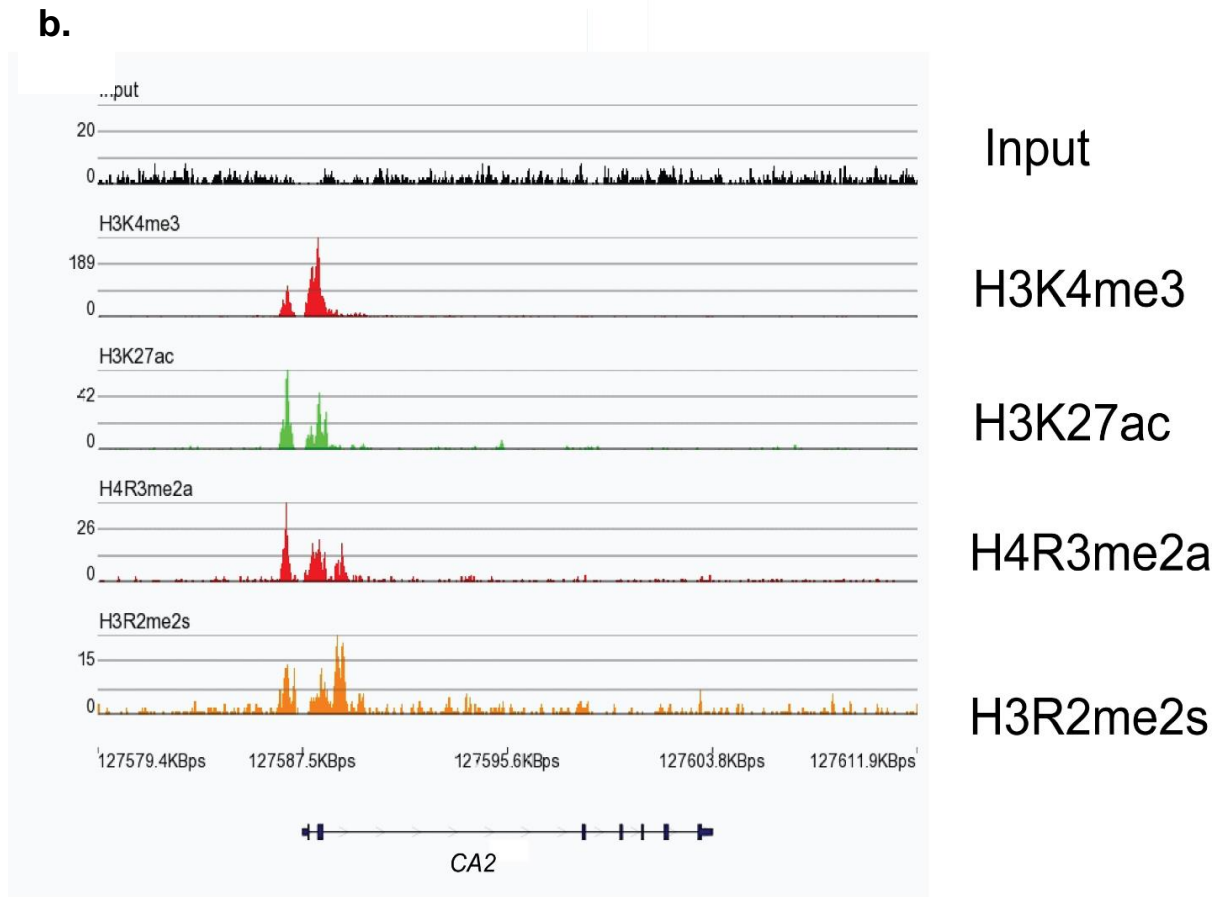


Figure 5.8: Distribution of H3R2me2s and H4R3me2a along *FTH1* gene of polychromatic erythrocytes. a) The top panel is the schematic diagram for chicken *FTH1*-gene domain detailing about the position of genes, a putative enhancer site within the domain. b) The first track (in black) is the input signal for ChIP-seq, underneath (in red) is the signal track for H3K4me3, distribution of H3K27ac (in green), distribution of H4R3me2a (in red), distribution of H3R2me2s (in orange). c) CpG islands were mapped along the *FTH1* gene using galGal3 UCSC genome browser. Green bar under the gene indicates the location of CpG islands.

Similar to the *FTH1* locus, H3R2me2s, and H4R3me2a associated with the upstream promoter region and second exon-intronic region of *CA2* gene (**Figure 5.9**). The location of H4R3me2a and H3R2me2s along the gene body of *CA2* and *FTH1* genes strongly associated with the CpG islands in these regions (**Supplementary figure S5.5**).



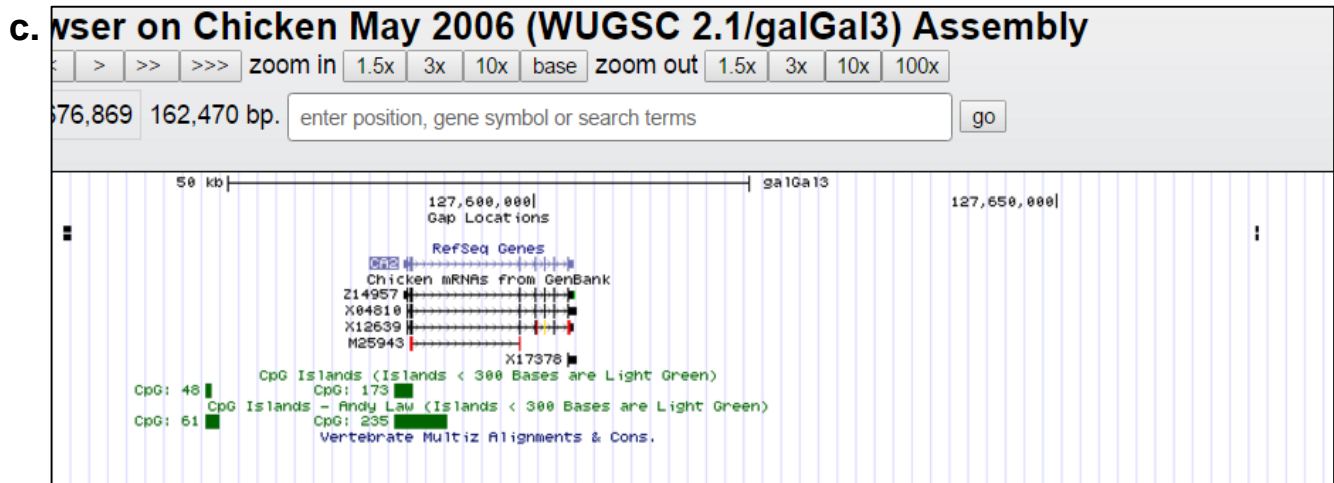


Figure 5.9: Distribution of H3R2me2s and H4R3me2a along CA2 gene of polychromatic erythrocytes. a) The top panel is the schematic diagram for chicken CA2-gene domain detailing about the position of genes, a putative enhancer site within the domain. b) The first track (in black) is the input signal for ChIP-seq, underneath (in red) is the signal track for H3K4me3, distribution of H3K27ac (in green), distribution of H4R3me2a (in red), distribution of H3R2me2s (in orange). c) CpG islands were mapped along the CA2 gene using galGal3 UCSC genome browser. Green bar under the gene indicates the location of CpG islands.

5.3.4 Profile of arginine methylation in lowly expressed genes of polychromatic erythrocyte cells

Lowly expressed genes such as *HDAC2* and *PRMT7* have H3R2me2s and H4R3me2a at the promoter region along with H3K27ac and H3K4me3 (**Figure 5.10, 5.11**). H3R2me2s and H4R3me2a were not found associated with the coding region of these low expressing genes in polychromatic erythrocytes. The ChIP-seq analyses for H4R3me2a and H3R2me2s demonstrated that for all transcribed genes both of these marks were associated with upstream promoter region and the beginning of coding region. Distribution of H3R2me2s and H4R3me2a across the genomic region of several expressed genes were further validated using the ChIP-assay (**Supplementary figure S5.6 and S5.7**).

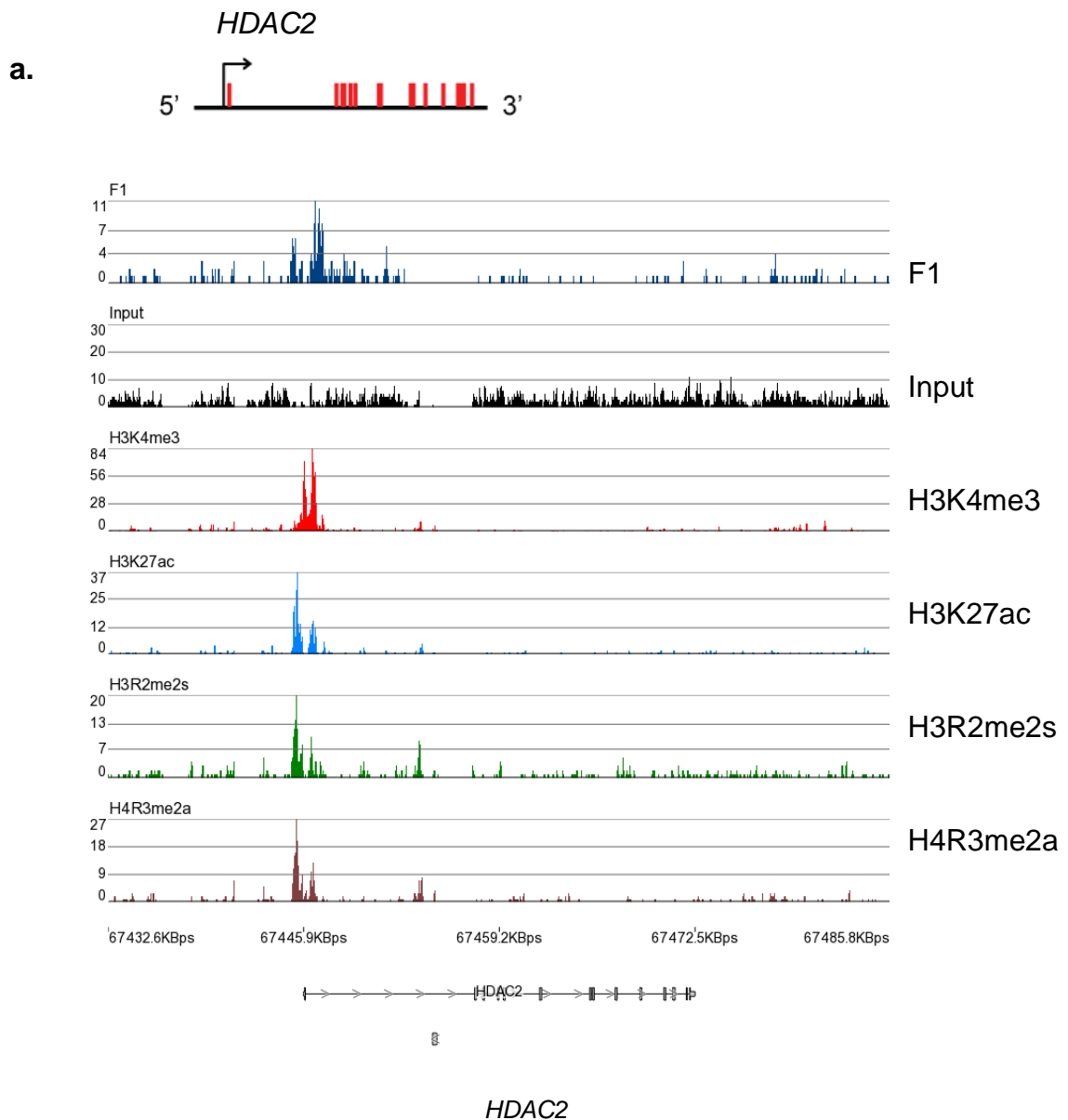


Figure 5.10: Distribution of H3R2me2s and H4R3me2a along *HDAC2* gene of polychromatic erythrocytes. a) The top panel is the schematic diagram for chicken *HDAC2* domain. b) The first track (in black) is the input for ChIP-seq, followed by the signal for H3K4me3 (in red), and the distributions of H3K27ac (in green), H4R3me2a (in red), H3R2me2s (in orange) respectively.

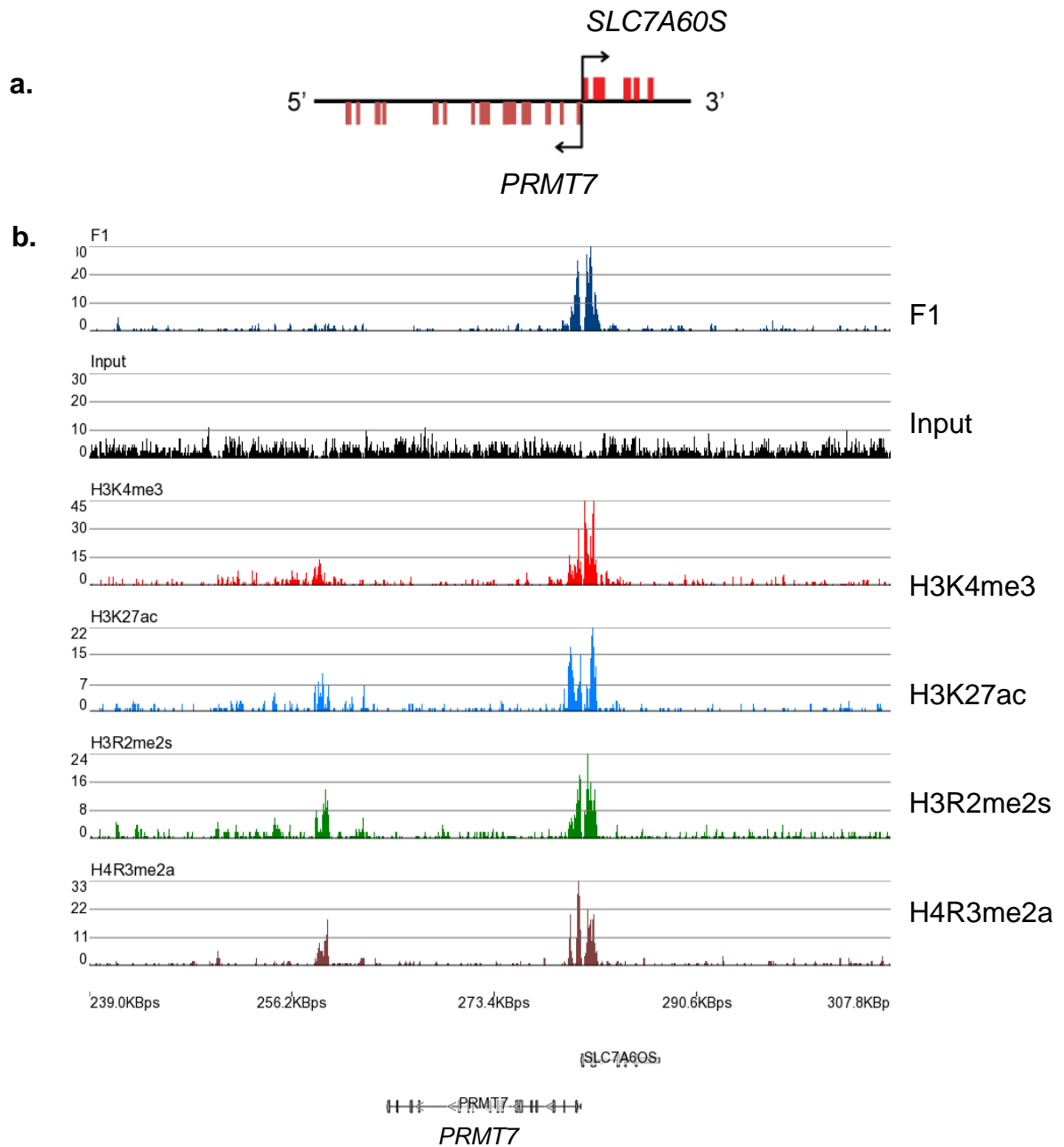


Figure 5.11: Distribution of H3R2me2s and H4R3me2a along the *PRMT7* gene of polychromatic erythrocytes. a) The top figure is the schematic diagram for the chicken *PRMT7* domain. b) The first track (in black) is the input for ChIP-seq, followed (in red) is the signal for H3K4me3; this is followed by the distributions of H3K27ac (in green), H4R3me2a (in red), and H3R2me2s (in orange).

5.3.5 Analysis of correlation between H4R3me2a with H3K27ac ChIP-seq peaks

The correlation between H4R3me2a and H3K27ac binding in the genome was determined by identifying common peaks between the ChIP-seq analysis for H4R3me2a and H3K27ac. As the result shows in **Figure 5.12**, there is a strong correlation (regression value = 0.92) between H4R3me2a and H3K27ac ChIP-seq peaks in the genome of polychromatic erythrocytes. The association of H3R2me2s with H3K27ac was not as strong as it for H4R3me2a (**Supplementary figure S5.8**). However, correlation analysis for H4R3me2a and H3R2me2s ChIP-seq peak shows they co-localize for many regions of the genome (regression value = 0.83) (**Figure 5.13**).

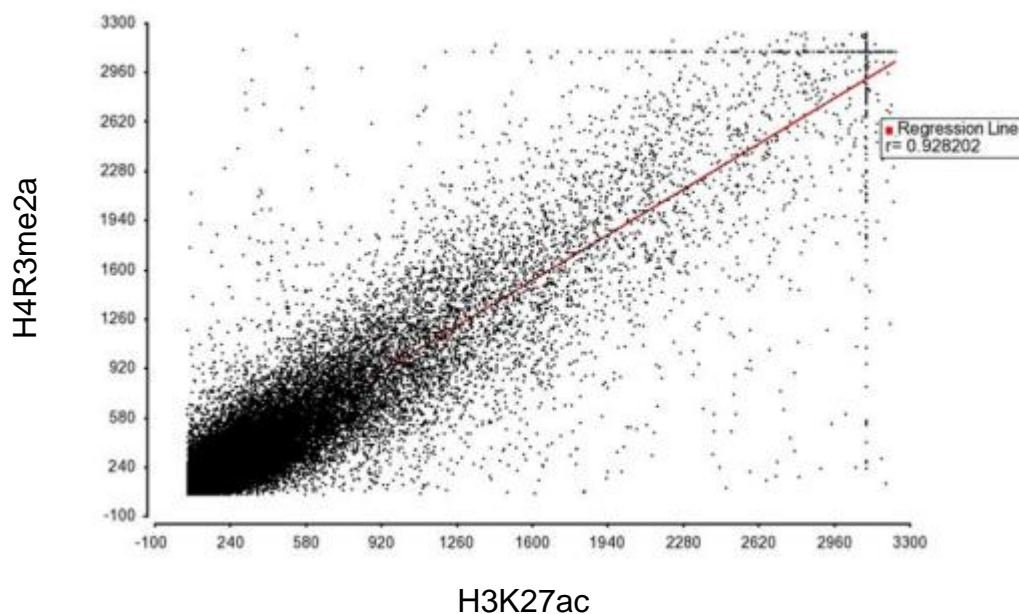


Figure 5.12: Correlation between H4R3me2a and H3K27ac ChIP-seq peaks. The common peak identifiers were generated by detecting overlapping peaks among H4R3me2a and H3K27ac ChIP-seq experiments. Overlapping of peaks within 100 bp were merged by Homer software package. The Pearson correlations were calculated and plotted by Partek software. The calculated regression line is $r=0.92$.

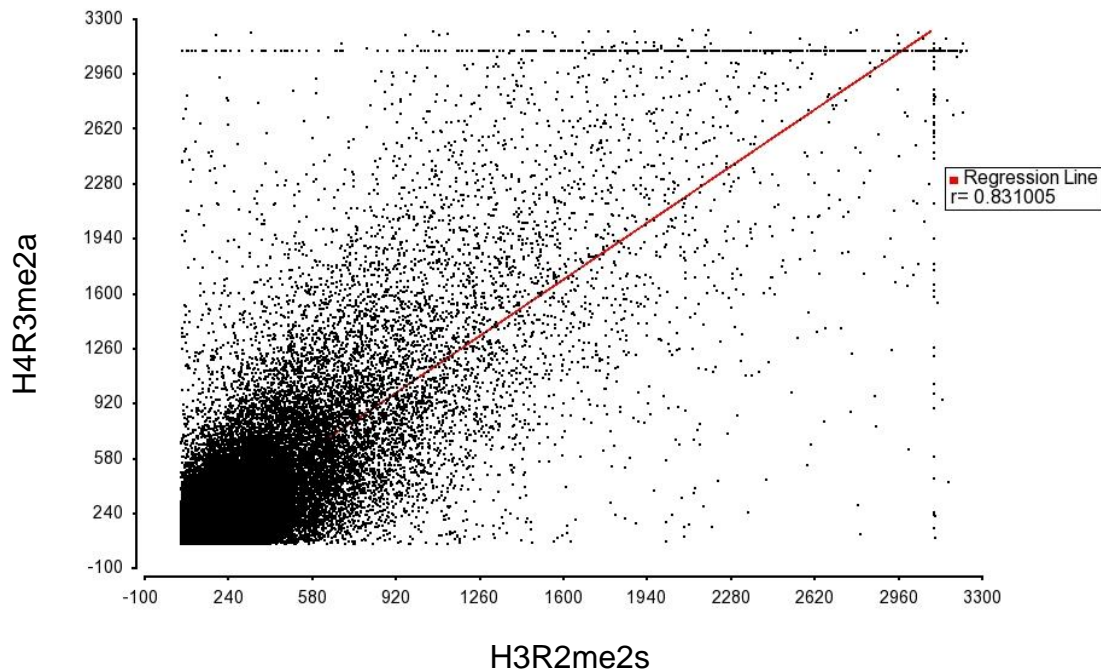


Figure 5.13: Correlation between H4R3me2a and H3R2me2s ChIP-seq peaks. The common peak identifiers were generated by detecting overlapping peaks among H4R3me2a and H3R2me2s ChIP-seq experiments. Overlapping within 100 bp were merged by Homer software package. The Pearson correlations were calculated and plotted by Partek software. The calculated regression line is $r=0.83$.

5.3.6 H3 arginine dimethylation relationship with H3K4me3 and H3K27ac

Co-localization of ChIP-seq peak for H3R2me2s with H3K4me3 and H3K27ac in several genomic regions of polychromatic erythrocytes suggested that R2me2s, K4me3, and K27ac may reside on the same H3 molecule. Therefore, to address whether there is a cross-talk among these marks histone H3 co-IP was performed. H3 tail containing H3R2me2s modification was immunoprecipitated followed by the subsequent immunoblot analyses of immunoprecipitated H3 molecule with several antibodies for modifications on this tail. I included H3K27ac and H3K4me1 in this experiment as H3K27ac tends to mark the active enhancer, while H3K4me1 marks both active and poised enhancers [440]. IP was performed for H3R2me2s followed by immunoblot analysis for each of the modifications H3R2me2s, H3K4me3, H3K27ac and H3K4me1. IP for H3R2me2s followed by immunoblot for the same mark served as an experimental control to demonstrate the efficiency of IP. As shown in the result, H3R2me2s reside on the same H3 histone tail with H3K4me1 or H3K4me3 or H3K27ac (**Figure 5.14b-d**). Under these conditions where

nucleosomes were dissociated in the presence of SDS, H4 was not expected to be associated with H3 molecule. This was further established by the IP of H3R2me2s followed by immunoblot analysis for H4R3me2a which showed negative results under these conditions (**Figure 5.14e**).

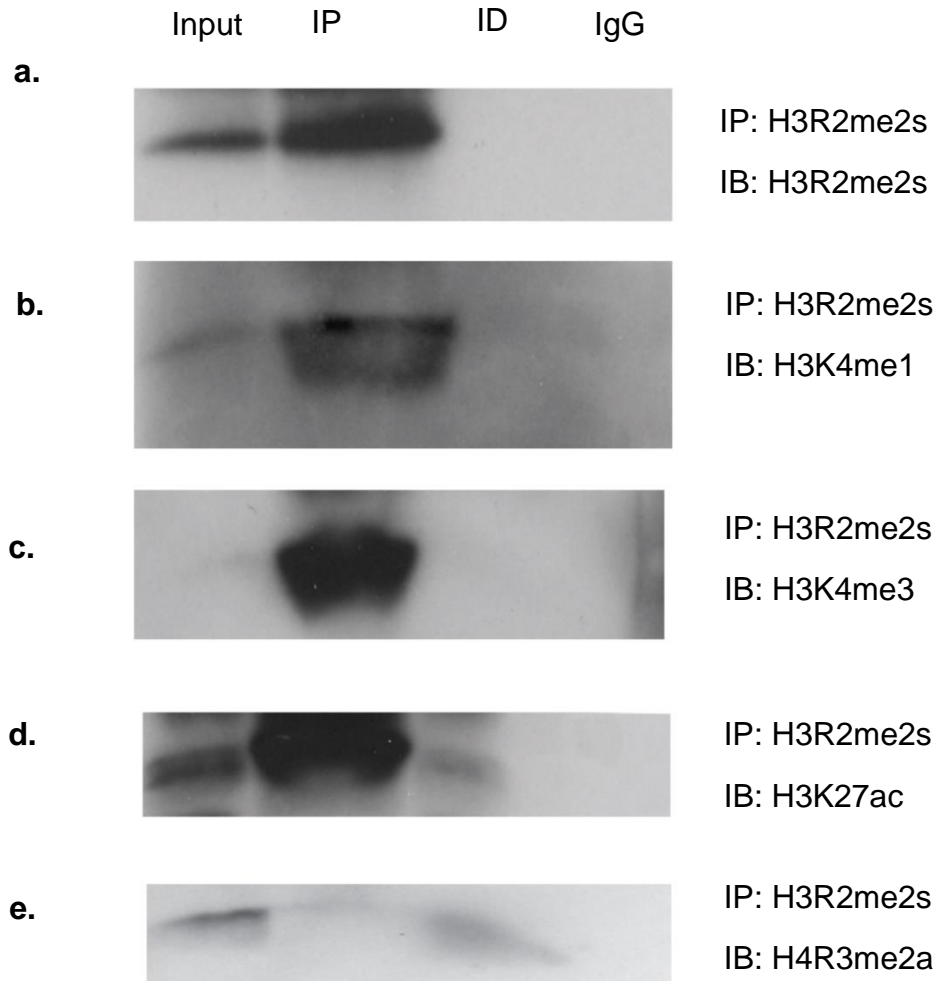


Figure 5.14: Co-occupancy of H3R2me2s arginine methylation with lysine methylation and acetylation. Approximately 5.0 A260 of nuclear lysate was immunoprecipitated with 5 ug of an anti-H3R2me2s antibody or nonspecific IgG antibodies. Immunoprecipitated complex was immunochemically stained with indicated antibodies. IP= Immunoprecipitated complex, ID= Immunodepleted complex.

5.3.7 RNAPIIS2ph dependent recruitment of PRMT1 and 5 to transcribed gene regions

Previous studies report that PRMT1 is recruited to regulatory regions by transcription factors such as USF1 but how PRMTs are recruited to the coding region of transcribed genes is not known [45]. One possibility is that PRMT1 and PRMT5 are associated with RNAPII. This interaction with RNAPII could be due to the protein complex or to the transcript attached to RNAPII. The association of PRMT1 or 5 with RNAPIIS2ph was determined in co-immunoprecipitation studies. Immunoprecipitation of RNAPIIS2ph followed by immunoblotting with antibodies against PRMT1 or 5 revealed the association of PRMT1 and 5 with RNAPIIS2ph (**Figure 5.15**). I further investigated whether the association of these enzymes with RNAPIIS2ph is dependent on the transcribed RNA. For this purpose, cell lysates were treated with RNase A before immunoprecipitation. The RNase A treatment did not release PRMT1 and 5 enzymes from RNAPIIS2ph complex indicating a direct association of these enzymes with RNAPIIS2ph (**Figure 5.15**).

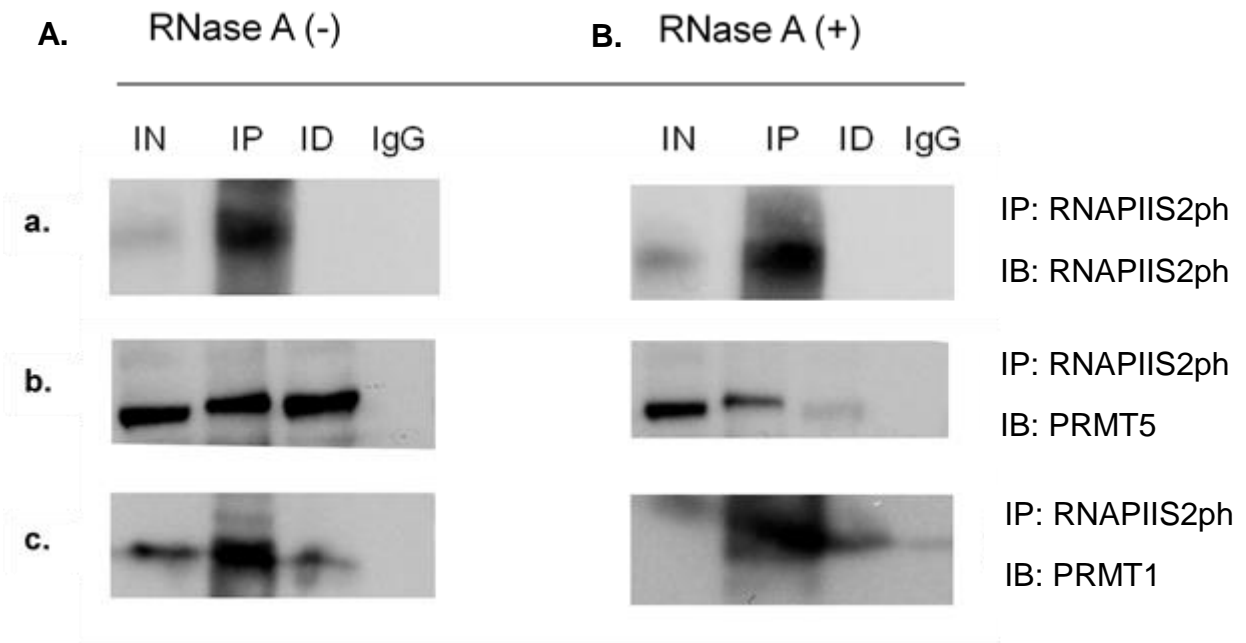


Figure 5.15: PRMT1 and 5 associate with RNAPIIS2ph complex in chicken polychromatic erythrocytes. Cell lysates from polychromatic erythrocytes treated with or without RNaseA. A) Polychromatic erythrocytes not treated with RNaseA, B) Polychromatic erythrocytes treated with 400ug/mL of RNaseA for 30 minute at 37°C. Both non-treated and treated cell lysates were immunoprecipitated with RNAPIIS2ph and subsequently immunoblotted with antibodies against a) RNAPIIS2ph, b) PRMT5 and c) PRMT1.

5.3.8 Association of PRMT1 and 5 with the nuclear matrix

PRMT1 and 5 were enriched in the salt insoluble P_E fraction isolated from polychromatic erythrocytes. Elongating RNAPII (RNAPIIS2ph) associates with the nuclear matrix [441]. Association of PRMT1 and 5 with P_E and RNAPIIS2ph indicated that similar to KATs and HDACs, these enzymes could be attached to the nuclear matrix [281, 428, 441]. The nuclear matrix was isolated using a previously described protocol. Equal amounts of cell lysate, nuclear lysate, nuclear matrix fraction and RNase A treated nuclear matrix fraction were loaded. Ponceau S stained membrane shows the molecular weight ladder (1st lane), isolated total protein (2nd lane), high-salt chromatin extract (3rd lane), the nuclear Matrix fraction (4th lane) and RNase A released protein from nuclear matrix fractions (**Figure 5.16a**). As evident from the results, histones were depleted in nuclear matrix fraction while lamin proteins were predominant in this fraction (**Figure 5.16a**). Immunoblot analyses demonstrated that PRMT1 and 5 were associated with the nuclear matrix. However, the release of these enzymes from the nuclear matrix after RNase A digestion could be due to the solubilization of internal matrix as the internal nuclear matrix is a RNA-protein structure. The result indicated that similar to the KATs and HDACs, PRMT1 and 5 are associated with the nuclear matrix and could have a role in recruiting active gene regions to the nuclear matrix (**Figure 5.16**).

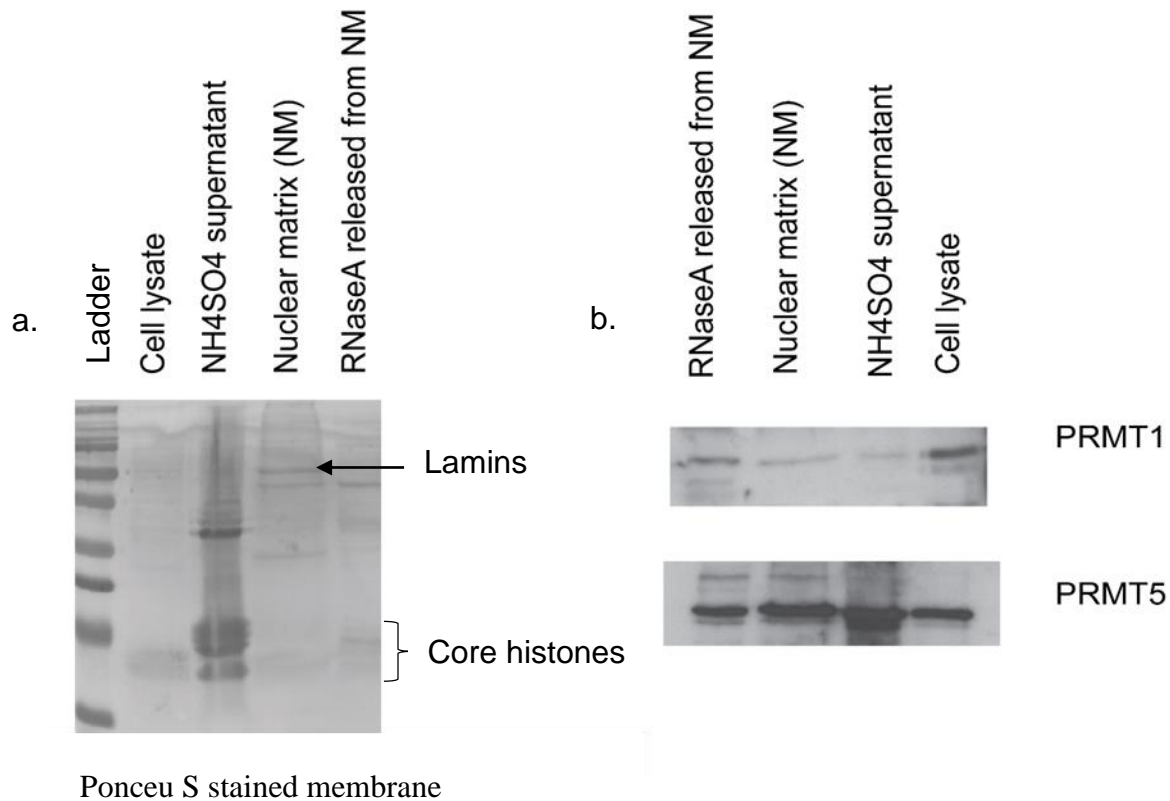


Figure 5.16: Interaction of PRMT1 and PRMT5 with the nuclear matrix. Proteins were extracted from each fraction produced during the isolation of the nuclear matrix. Equal amounts of proteins (10 ug) from each fraction were loaded on an 8% SDS-polyacrylamide gel, transferred to nitrocellulose membrane and Ponceau stained. a) 1st lane to the right is the molecular weight ladder, the sample loaded to each lane is indicated above the lane. On the left Ponceau S-stained core histones were used as a loading reference. b) Blots were immunochemically stained with anti-PRMT1 and anti-PRMT5 antibodies.

5.4 Discussion

5.4.1 PRMT1 and 5 associate with active chromatin

PRMT1 and 5 mediated arginine modifications, H4R3me2a and H4R3me2s, respectively were reported as active and repressed chromatin marks [23, 181]. Similarly, PRMT5 and 6 generates H3R2me2s and H3R2me2a, which are associated with active or repressed chromatin, respectively [217, 221]. Changes in the chemical structure between symmetric or asymmetric orientation could contribute to the preference of binding of specific molecules. H3R2me2a by PRMT6 antagonizes the MLL1 (mixed lineage leukemia1)-mediated trimethylation of H3K4, by preventing the recruitment of WDR5, a subunit of the MLL complex [221]. On the contrary, H3R2me2s recruits

WDR5 which is a subunit of several coactivator complexes that produce H3K4me3 [217]. With the aid of a chromatin fractionation procedure, we previously established that the transcriptionally active genes are associated with both low salt-insoluble (P_E) and salt soluble chromatin (S_{150} , F1, and F2) in chicken polychromatic erythrocytes [21]. By combining the chromatin fractionation procedure with Next-generation DNA sequencing of salt soluble polynucleosome chromatin fraction F1, we identified that F1 chromatin contains at least two classes of transcribed chromatin organization [13]. In this study, using the same chromatin fractionation process we demonstrated for the first time that PRMT1/5 and their corresponding arginine modifications H4R3me2a and H3R2me2s preferentially associate with the transcriptionally active chromatin fractions P_E , S_{150} , F1, and F2. It is to be noted that PRMT5 produces both H3R2me2s and H4R3me2s. However, the chromatin distribution of PRMT5 suggests that the activity of this enzyme is more involved in catalyzing the active mark, H3R2me2s. Thus, the association of PRMT1 and PRMT5 and their corresponding arginine modifications with F1 polynucleosome indicate that they preferentially associate with active/poised genes in chicken polychromatic erythrocytes.

5.4.2 H4R3me2a associate with promoters of transcriptionally active genes

There is very limited information available regarding the distribution of H4R3me2a due to the lack of ChIP-grade quality antibodies. H4R3me2a was reported to facilitate the subsequent acetylation of H4 at Lys 8 and 12 by p300, and therefore H4R3me2a can be considered as a active mark that recruit p300 [220]. It was reported that PRMT1 could not dimethylate R3 when H4 was hyperacetylated [220]. However, it should be noted that the antibody used in that study was not specific towards symmetric or asymmetric methylation of H4R3. PRMT5 mediated H4R3me2s was reported to be associated with silencing function in the mouse LCR and γ -gene promoter [249]. Moreover, our ongoing study revealed that prior acetylation did not affect the level of H4R3me2a in chicken polychromatic or mature erythrocytes (data not shown). PRMT1 mediated H4R3me2a was demonstrated to be crucial in maintaining the active chromosomal locus as loss of PRMT1 was associated with loss of H3K9/14, H4K5 and H4K12 acetylation, leading to heterochromatinization of the globin locus. However, the mechanism as to how H4R3me2a sustains the active chromatin structure remains poorly understood [23]. The USF1/2 heterodimer recruits PRMT1 producing H4R3me2a at the HS4. When the binding of USF1 to this site is prevented, there is a failure of chromatin modifying enzymes to bind to this site and loss of barrier function [45].

In this study, I explored the genomic distribution of H4R3me2a and H3R2me2s by using the ChIP-seq assay. This is the first time that the genomic location of H4R3me2a has been demonstrated and the first time that H3R2me2s and H4R3me2a have been analyzed together. Consistent with the previous findings, our analysis revealed that H4R3me2a associates with the HS4 site at the β -globin locus. Further extending the analysis, we are the first to demonstrate that H4R3me2a is the mark of an active promoter which is also associated with H3K27ac in chicken polychromatic erythrocytes. We showed that H4R3me2a is present at the HS1-HS4 and distal regulatory region of several highly transcribed genes, such as HS14.9 of the α -globin locus. These hypersensitive sites are associated with H3K27ac produced by lysine acetyltransferases p300/CBP [285]. As shown previously, prior methylation of H4R3 stimulates acetylation by p300/CBP. My results are consistent with the idea that p300/CBP is as a reader of H4R3me2a [23]. We next sought to determine whether H4R3me2a co-localizes with H3K27ac. The strong co-localization of these two modifications further supports the effector function of PRMT1 mediated H4R3me2a. Moreover, the ubiquitous distribution of H4R3me2a across the chicken β and α globin domain suggests that this modification plays a crucial role in maintaining domain confirmation and is key in recruiting acetyltransferases to these genomic regions. It is conceivable that PRMT1 and KATs are recruited as a complex to these regions. However, prior acetylation is not a prerequisite for PRMT1 to facilitate H4 arginine methylation [220].

5.4.3 H4R3me2a co-localize with H3R2me2s at the hypersensitive sites HS1-HS4 and other distal regulatory region of transcriptionally active genes

Next, we characterized the distribution of H3R2me2s and its genomic distribution relative to H4R3me2a. Intriguingly, we found that the two active arginine modifications H4R3me2a and H3R2me2s are co-localized at the hypersensitive sites of the chicken α and β globin domain. These data indicate that these active marks are both present at distal regulatory regions of highly transcribing genes. It is possible that H4R3me2a and H3R2me2s reside on the same nucleosome. This can be confirmed by performing sequential ChIP assay for H4R3me2a and H3R2me2s. Moreover, PRMT1 and 5 could be in the same complex and this can be addressed by performing the sequential ChIP for PRMT1 and 5.

5.4.4 H3R2me2s co-localize with H3K4me3 at the 5' end of the gene body of highly expressed genes

Upon further analysis of the distribution of H3R2me2s, we found that this mark co-localizes with the H3K4me3 at the second exon-intronic boundary region of highly expressed genes (such as β^A globin gene, αA and αD globin gene, *CA2* gene). For moderately expressing genes, such as *FTH1*, these two modifications are aligned at the first exon-intron boundary region, co-localize with CpG island at the site. I observed a strong association of CpG islands with the placement of H4R3me2a and H3R2me2s for several genes such as *CA2* and *FTH1*. It is possible that the placement of the H3R2me2s or H4R4me2a marks in the coding region is directed by the presence of the CpG island. Colocalization of H4R3me2a and H3R2me2s at several genomic regions supports the finding from previous studies that H3K4me3 is tightly correlated with H3R2me2s [217, 409]. I extended the findings by establishing that these two modifications are more enriched at the 5' end of gene body where presumably H3R2me2s mark the 5' splice-site selection region similar to the H3K4me3 [442]. These findings were further validated by the histone co-immunoprecipitation experiments, which demonstrated directly that an H3 histone tail that is modified at R2me2s also contain H3K4me3.

5.4.5 H3 modified at R2me2s has K4me1 and H3K27ac

Consistent with the previous findings, I determined that H3R2me2s is a mark of the distal regulatory regions [217]. I showed that H3K4me1 and H3K27ac, which are marks of an active enhancer, co-occupy an H3 tail with H3R2me2s. It is important to note that H3K27ac is the mark for the active enhancer while H3K4me1 is associated with both active and poised enhancers [440, 443, 444]. Therefore, I concluded from this study that some H3 molecules might have R2me2s, K27ac, and/or K4me3 or K4me1. However, this needs to be addressed by sequential ChIP or sequential IP experiments.

5.4.6 PRMT1 and 5 recruited through RNAPIIS2ph

Studies have shown that both PRMT1 and 5 regulate the splicing event by modifying splicing protein and in doing so regulate their nuclear-cytoplasmic shuttling [256, 445-448]. Interaction of PRMT1 and 5 with a broad range of RNA associated proteins indicates the involvement of these enzymes in a splicing-associated events possibly through interaction with RNA. Using the 'interactome capture' analysis to define the mRNA interactome in proliferating HeLa cells,

Hentze's group reported PRMT1 as being one of the candidate RNA-binding proteins [410]. With the ChIP-seq analysis, we found that the association of H4R3me2a and H3R2me2s, which are produced by PRMT1 and 5, respectively along the gene bodies of highly transcribed genes. I sought to determine the mechanism of how these two enzymes move along the gene body and whether the mechanism is coupled to its interaction with the transcript. Co-immunoprecipitation/immunoblot studies demonstrated that both PRMT1 and 5 associate with RNAPIIS2ph. Under low stringency immunoprecipitation conditions, treatment of the cellular lysate with RNaseA did not release the proteins from RNAPIIS2ph. This result indicates that unlike SR proteins and HDAC2, the association of PRMT1 and 5 with RNAPIIS2ph is not mediated through RNA [165].

5.4.7 PRMT1 and 5 binds to the nuclear matrix

Association of PRMT1 and 5 with the low salt insoluble nuclear material (P_E) which contains the nuclear matrix suggested that PRMT1 and 5 associated with the nuclear matrix. The nuclear matrix, which is composed of ribonucleoprotein, serves as the foundation/platform for several nuclear processes. Enzymes regulating chromatin organization such as KATs and HDACs are associated with P_E and nuclear matrix complex [281]. These enzymes are involved in coupling transcription with pre-mRNA processing [165, 449]. Our findings show that PRMT1 and 5 associate with the nuclear matrix. Future studies will be required to address whether PRMT1 and 5 are in the same complex with KATs or HDACs.

The findings of this study hold promise in providing novel insights into the mechanisms as to how chromatin-modifying enzymes can regulate the complex regulatory network of gene expression. PRMT1 and 5 mediated arginine methylation have been linked to metastasis and cancer progression in breast and lung cancer [450, 451]. PRMT1 mediated H4R3me2a is a pioneer mark that establishes other active marks. Active chromatin marks, such as H3K9/K14ac and H4ac, located along the entire chicken globin domain will not be present when PRMT1 is knocked down [23]. The a consequence of the loss of PRMT1 activity, repressive marks such as H3K9me2, H3K27me3 that are associated with heterochromatin are formed in the globin domain [23]. PRMT1 recruited to the chicken HS4 region contain transcription factor USF2, lysine acetyltransferases PCAF and SRC1 in the complex [45]. In this current study, I observed a strong co-localization of H4R3me2a with H3K27ac, which indicate the binding of p300/CBP. Also, my

study is the first to demonstrate a connection between the two active arginine methylation marks, H3R2me2s and H4R3me2a, and their association with H3K27ac, H3K4me3, H3K4me1 marks. These results suggest that the effector enzymes, p300/CBP, MLL1/2 and SETD7, for these marks (H3K27ac, H3K4me3, H3K4me1) bind to the PRMT1 and 5 binding sites. I observed the presence of arginine marks at the several regulatory regions of polychromatic erythrocytes, while other active marks were absent. This observation further supports the role of PRMT1 and 5 mediated arginine modifications as pioneering mark to set up other active marks. Intriguingly, I found that the localization of CpG island plays a crucial role in placing H4R3me2a and H3R2me2s. It is possible that CpG island binding protein such as CXXC1 could be acting as a recruiter for PRMT1 and 5 to these sites [452].

Findings from the current study contribute to novel insights regarding two major asymmetric and symmetric arginine modifying enzymes, which are already under consideration as therapeutic targets in cancer [129]. PRMT1 and 5 enzymes are aberrantly expressed and associated with poor prognosis in several types of cancer [129]. More specifically, H4R3me2a and H3R2me2s by PRMT1 and 5 were shown to be linked to the regulation of the expression of several genes involved in metastasis and epithelial to mesenchymal transition in cancer [450, 451]. Therefore, understanding the role of PRMT1 and 5 in the regulation of transcription and in maintaining higher order chromatin structures will provide further insights in future studies that use inhibitors of these enzymes in cancer therapy.

5.5 Methods

5.5.1 Chromatin fractionation

Chromatin fractionation was performed on polychromatic and mature erythrocytes according to the protocol described previously and included in detail in the method section of **Chapter II**.

5.5.2 Immunoblotting

Proteins in each chromatin fraction (F1-F4) (5.0 A260) were resolved on SDS-PAGE and immunoblotted with antibodies against PRMT1 (Millipore), PRMT5 (Millipore), H4R3me2a (Active motif), and H3R2me2s (Millipore).

5.5.3 Dot-blot assay

Peptide dot blot assays were performed according to the procedures described in **Chapter II**. Briefly, nitrocellulose membrane was labelled to specify the location of the peptides for H4R3me2a, H4R3me2s, H3R2me2a, H3R2me2s, H3K4me1, and H3K4me2. Two ug of each of the peptides were directly added onto the membrane and allowed to dry at 65° C for 15 minute. Membrane was incubated with blocking solution (5.0 % skim milk-0.05% TTBS) for 1 hour at room temperature. Membrane was then incubated with H4R3me2a or H3R2me2s antibody solution overnight. After three washes with 0.05% TTBS, the membrane was incubated with isotype specific secondary antibody solution (diluted in blocking solution) for 1 hour at room temperature with rotation. Finally, membrane was incubated for 3 minute with the chemiluminescent ECL, the film was developed.

5.5.4 Co-association of modification on H3 tail

Histone H3 IP was performed according to the protocol described before [452]. Briefly, cells were lysed using cell lysis buffer (5 mM PIPES [pHed with KOH to 8.0], 85 mM KCl, 0.5% NP-40) buffer with the incubation at 4°C. Supernatant was discarded after centrifugation for 10 minute at 10,000 rpm using microcentrifuge (Hettich Mikro 20 Centrifuge). The nuclear pellet was resuspended in MNase Digestion Buffer (10 mM Tris-HCl pH 7.5, 0.25 M sucrose, 75 mM NaCl) plus phosphatase/protease inhibitors. CaCl₂ was added to the samples to a final concentration of 3 mM and incubated at 37°C for 10 minute. MNase was added to a concentration of 4.5 U/mL and incubated for 20 minute. MNase condition was optimized to get mononucleosome size fragments. Reaction was stopped by adding EDTA pH 8.0 to a final concentration of 5 mM. Nuclei was lysed with SDS (0.5% final concentration) by rotating at room temperature for 1 hour. Insoluble material was separated by centrifugation (10k rpm, 5 minute) (Sorvall Legend Micro 17) and discarded. Nuclear lysate was diluted with RIPA buffer (10 mM Tris-HCl pH 8.0, 1% Triton-X-100, 0.1% SDS, 0.1% sodium deoxycholate-SDC) plus phosphatase/protease inhibitors added freshly. Lysate was pre-cleared with protein A/G agarose (Santa Cruz) beads (40 µl per mL of lysate) for 1 hour at 4°C. Beads were pelleted by centrifugation by using microcentrifuge (Hettich Mikro 20 Centrifuge) for 2-3 minute at 1200 rpm. Supernatant was transferred to new tubes. After measuring the A260, 1 ug of each H3R2me2s antibody was added per A260 of lysate. It was allowed to incubate overnight at 4°C with rotation. Next day, Dynabeads Protein G (Invitrogen) were added and incubated for 2 hours with rotation at 4°C. Beads were washed with RIPA buffer 4 times at

room temperature for 5 minutes with rotation. One A260 of was collected from immunodepleted (ID) fraction. Immunoprecipitant (IP) was eluted from the beads by adding the appropriate volume (usually 40 uL) of SDS loading buffer to the beads. Equal amounts of input and ID (usually 0.2 A260) and 1.0 A260 IP were loaded onto a gel for immunoblot blot analyses with antibodies against H3R2me2s/H3K4me3/H3K27ac/H3K4me1 or H4R3me2a.

5.5.5 Chromatin immunoprecipitation (ChIP) assay and ChIP-seq assay

ChIP-seq and ChIP assays were performed according to a previously described protocol and included in **Chapter II** in detail [285]. Briefly, cells were cross-linked with 0.5% formaldehyde for 10 minutes. Nuclei were lysed and chromatin was sheared to 250 bp using ultrasonic dismembrator (Fisher). ChIP assays were performed with anti-H3K4me3 (Abcam), anti-H3K27ac (Abcam), anti-H3R2me2s (Millipore), and anti-H4R3me2a (Active motif) antibodies. As a control, isotype specific non-related IgG was used in the ChIP assay. ChIP and input DNA were further processed, purified and quantitated using a Qubit® 2.0 fluorometer (Life Technologies). Input and ChIP DNA quality was analyzed using 2000 Bioanalyzer (Agilent). Enrichment values were compared using a previously described calculation with equal amounts of input and immunoprecipitated DNA (1.0 ng). Primers are described in Supplementary **Table S5.1**. The error bars indicate standard deviation (N = 3). ChIP-seq for the above-mentioned histone PTMs were performed similarly as the ChIP assay (N=2).

5.5.6 Immunoprecipitation and co-IP

Immunoprecipitation for RNAPII was performed according to a previously described protocol [165]. Briefly, the cell lysate was prepared by using an IP buffer (50 mM Tris-HCl [pH 8.0], 150 mM NaCl, 0.5% NP-40, 1 mM EDTA) with freshly added protease and phosphatase inhibitors (Promega). After brief sonication (twice at power 2 for 2-three times for 12 sec each, with 1 min interval on ice at power 2), the supernatant was collected and lysate was pre-cleared with A/G beads (Santa Cruz) for 1 hour at 4°C. Approximately 500 ug of cell lysate was incubated overnight at 4°C with 3 ug of RNAPIIs2ph antibody. For RNase A treatment, half of the cellular extracts were treated with 400 µg/mL of RNase A for 30 min at 37°C. Next day, 40 uL of protein G beads (Invitrogen) were added and incubated for 3 h at 4°C. Beads were washed, and the immunoprecipitated complex was loaded onto 8% SDS gel. After transferring the protein complex

into nitrocellulose membrane, the blot was immunochemically stained with RNAPIIs2ph (Abcam) or PRMT1 (Millipore) or PRMT5 (Millipore) antibodies.

5.5.7 Isolation of nuclear matrix

The nuclear matrix from chicken polychromatic erythrocytes was isolated according to the previously described protocol [453]. Cells were lysed by CSK buffer [100 mM KCl, 3 mM MgCl₂, 10 mM Pipes (pH 6.8), 1 mM EGTA, 0.3 M sucrose, 0.5% (v/v) thiodiglycol, 1 mM PMSF, 0.25% Triton X-100] with protease and phosphatase inhibitors. Nuclei were collected by centrifugation for 10 minutes. Nuclei were re-suspended in digestion buffer [10 mM Pipes (pH 6.8), 50 mM NaCl, 300 mM sucrose, 3 mM MgCl₂, 1mM EGTA, 0.5% v/v Triton X-100] at 20 A260/mL. The nuclei were incubated with DNase I (Sigma) at a final concentration of 100 ug/mL for 60 minutes at room temperature. Approximately, 4 M (NH₄)₂SO₄ was added drop wise to get a final concentration of 0.25 M. The nuclear matrices were collected by centrifugation and resuspended in 8 M urea. The supernatant was stored to compare this fraction containing digested chromatin with the nuclear matrix. Half of the nuclear matrix fraction was resuspended with urea and subsequently dialyzed against ddH₂O to get rid of urea. The remainder half of the nuclear matrix fraction was treated with RNaseA at concentration of 10 ug/mL for 30 minutes at 37°C. Equal protein amounts (10 ug) from the cell lysate, (NH₄)₂SO₄ supernatant, protein released from nuclear matrix fraction, and RNase A released protein from the nuclear matrix complex were loaded onto SDS polyacrylamide gels. The fractions were loaded onto 8% SDS polyacrylamide gel. Proteins were transferred onto nitrocellulose membrane and immunochemically stained with PRMT1 (Millipore) and PRMT5 (Millipore) antibodies.

5.5.8 Bioinformatics analysis

5.5.8.1 RNA-seq and ChIP-seq analysis

Bioinformatics analysis for RNA-seq and ChIP-seq analysis was performed according to the process described in **Chapter II** in the method section.

5.5.8.2 ChIP-seq peak distribution

The ChIP-seq peak profiling around TTS and TTS were generated and displayed using the CEAS program. These profiles were grouped based on 5 percentiles of cellular RNA-seq expression level.

5.5.8.3 ChIP-seq peak Correlation

The common peak identifiers were generated by detecting overlapping peaks among different ChIP-seq experiments. Overlapping within 100 bp were merged by Homer software package. The Pearson correlations were calculated and plotted by Partek software.

5.6 References

1. Li X, Hu X, Patel B, Zhou Z, Liang S, Ybarra R, et al. H4R3 methylation facilitates beta-globin transcription by regulating histone acetyltransferase binding and H3 acetylation. *Blood*. 2010;115(10):2028-37. doi: 10.1182/blood-2009-07-236059. PubMed PMID: 20068219; PubMed Central PMCID: PMC2837319.
2. Huang S, Litt M, Felsenfeld G. Methylation of histone H4 by arginine methyltransferase PRMT1 is essential in vivo for many subsequent histone modifications. *Genes Dev*. 2005;19(16):1885-93. doi: 10.1101/gad.1333905. PubMed PMID: 16103216; PubMed Central PMCID: PMC1186188.
3. Kouzarides T. Chromatin modifications and their function. *Cell*. 2007;128(4):693-705. doi: 10.1016/j.cell.2007.02.005. PubMed PMID: 17320507.
4. Rothbart SB, Strahl BD. Interpreting the language of histone and DNA modifications. *Biochim Biophys Acta*. 2014;1839(8):627-43. doi: 10.1016/j.bbagr.2014.03.001. PubMed PMID: 24631868; PubMed Central PMCID: PMC4099259.
5. Bannister AJ, Kouzarides T. Regulation of chromatin by histone modifications. *Cell Res*. 2011;21(3):381-95. doi: 10.1038/cr.2011.22. PubMed PMID: 21321607; PubMed Central PMCID: PMC3193420.
6. Chen Y, Sprung R, Tang Y, Ball H, Sangras B, Kim SC, et al. Lysine propionylation and butyrylation are novel post-translational modifications in histones. *Mol Cell Proteomics*. 2007;6(5):812-9. doi: 10.1074/mcp.M700021-MCP200. PubMed PMID: 17267393; PubMed Central PMCID: PMC2911958.
7. Litt M, Qiu Y, Huang S. Histone arginine methylations: their roles in chromatin dynamics and transcriptional regulation. *Biosci Rep*. 2009;29(2):131-41. doi: 10.1042/BSR20080176. PubMed PMID: 19220199.
8. Jahan S, Davie JR. Protein arginine methyltransferases (PRMTs): role in chromatin organization. *Adv Biol Regul*. 2015;57:173-84. doi: 10.1016/j.jbior.2014.09.003. PubMed PMID: 25263650.
9. Migliori V, Muller J, Phalke S, Low D, Bezzi M, Mok WC, et al. Symmetric dimethylation of H3R2 is a newly identified histone mark that supports euchromatin maintenance. *Nat Struct Mol Biol*. 2012;19(2):136-44. doi: 10.1038/nsmb.2209. PubMed PMID: 22231400.
10. Yuan CC, Matthews AG, Jin Y, Chen CF, Chapman BA, Ohsumi TK, et al. Histone H3R2 symmetric dimethylation and histone H3K4 trimethylation are tightly correlated in eukaryotic genomes. *Cell Rep*. 2012;1(2):83-90. doi: 10.1016/j.celrep.2011.12.008. PubMed PMID: 22720264; PubMed Central PMCID: PMC3377377.
11. Guccione E, Bassi C, Casadio F, Martinato F, Cesaroni M, Schuchlantz H, et al. Methylation of histone H3R2 by PRMT6 and H3K4 by an MLL complex are mutually exclusive. *Nature*. 2007;449(7164):933-7. doi: 10.1038/nature06166. PubMed PMID: 17898714.
12. Hyllus D, Stein C, Schnabel K, Schiltz E, Imhof A, Dou Y, et al. PRMT6-mediated methylation of R2 in histone H3 antagonizes H3 K4 trimethylation. *Genes Dev*.

2007;21(24):3369-80. doi: 10.1101/gad.447007. PubMed PMID: 18079182; PubMed Central PMCID: PMCPMC2113036.

13. Jahan S, Xu W, He S, Gonzalez C, Delcuve GP, Davie JR. The chicken erythrocyte epigenome. *Epigenetics Chromatin*. 2016;9:19. doi: 10.1186/s13072-016-0068-2. PubMed PMID: 27226810; PubMed Central PMCID: PMCPMC4879735.

14. Schneider R, Bannister AJ, Myers FA, Thorne AW, Crane-Robinson C, Kouzarides T. Histone H3 lysine 4 methylation patterns in higher eukaryotic genes. *Nat Cell Biol*. 2004;6(1):73-7. doi: 10.1038/ncb1076. PubMed PMID: 14661024.

15. Roadmap Epigenomics C, Kundaje A, Meuleman W, Ernst J, Bilenky M, Yen A, et al. Integrative analysis of 111 reference human epigenomes. *Nature*. 2015;518(7539):317-30. doi: 10.1038/nature14248. PubMed PMID: 25693563; PubMed Central PMCID: PMCPMC4530010.

16. Creighton MP, Cheng AW, Welstead GG, Kooistra T, Carey BW, Steine EJ, et al. Histone H3K27ac separates active from poised enhancers and predicts developmental state. *Proc Natl Acad Sci U S A*. 2010;107(50):21931-6. doi: 10.1073/pnas.1016071107. PubMed PMID: 21106759; PubMed Central PMCID: PMCPMC3003124.

17. Huang S, Li X, Yusufzai TM, Qiu Y, Felsenfeld G. USF1 recruits histone modification complexes and is critical for maintenance of a chromatin barrier. *Mol Cell Biol*. 2007;27(22):7991-8002. doi: 10.1128/MCB.01326-07. PubMed PMID: 17846119; PubMed Central PMCID: PMCPMC2169148.

18. Patturajan M, Wei X, Berezney R, Corden JL. A nuclear matrix protein interacts with the phosphorylated C-terminal domain of RNA polymerase II. *Mol Cell Biol*. 1998;18(4):2406-15. PubMed PMID: 9528809; PubMed Central PMCID: PMCPMC121500.

19. Hendzel MJ, Sun JM, Chen HY, Rattner JB, Davie JR. Histone acetyltransferase is associated with the nuclear matrix. *J Biol Chem*. 1994;269(36):22894-901. PubMed PMID: 8077241.

20. Hendzel MJ, Delcuve GP, Davie JR. Histone deacetylase is a component of the internal nuclear matrix. *J Biol Chem*. 1991;266(32):21936-42. PubMed PMID: 1939216.

21. Wang H, Huang ZQ, Xia L, Feng Q, Erdjument-Bromage H, Strahl BD, et al. Methylation of histone H4 at arginine 3 facilitating transcriptional activation by nuclear hormone receptor. *Science*. 2001;293(5531):853-7. doi: 10.1126/science.1060781. PubMed PMID: 11387442.

22. Rank G, Cerruti L, Simpson RJ, Moritz RL, Jane SM, Zhao Q. Identification of a PRMT5-dependent repressor complex linked to silencing of human fetal globin gene expression. *Blood*. 2010;116(9):1585-92. doi: 10.1182/blood-2009-10-251116. PubMed PMID: 20495075; PubMed Central PMCID: PMCPMC2938845.

23. Davie JR, Xu W, Delcuve GP. Histone H3K4 trimethylation: dynamic interplay with pre-mRNA splicing. *Biochem Cell Biol*. 2016;94(1):1-11. doi: 10.1139/bcb-2015-0065. PubMed PMID: 26352678.

24. Heinz S, Romanoski CE, Benner C, Glass CK. The selection and function of cell type-specific enhancers. *Nat Rev Mol Cell Biol*. 2015;16(3):144-54. doi: 10.1038/nrm3949. PubMed PMID: 25650801; PubMed Central PMCID: PMCPMC4517609.

25. Shlyueva D, Stampfel G, Stark A. Transcriptional enhancers: from properties to genome-wide predictions. *Nat Rev Genet.* 2014;15(4):272-86. doi: 10.1038/nrg3682. PubMed PMID: 24614317.
26. Zhang L, Tran NT, Su H, Wang R, Lu Y, Tang H, et al. Cross-talk between PRMT1-mediated methylation and ubiquitylation on RBM15 controls RNA splicing. *Elife.* 2015;4. doi: 10.7554/eLife.07938. PubMed PMID: 26575292; PubMed Central PMCID: PMCPMC4775220.
27. Zou L, Zhang H, Du C, Liu X, Zhu S, Zhang W, et al. Correlation of SRSF1 and PRMT1 expression with clinical status of pediatric acute lymphoblastic leukemia. *J Hematol Oncol.* 2012;5:42. doi: 10.1186/1756-8722-5-42. PubMed PMID: 22839530; PubMed Central PMCID: PMCPMC3459738.
28. Koh CM, Bezzi M, Low DH, Ang WX, Teo SX, Gay FP, et al. MYC regulates the core pre-mRNA splicing machinery as an essential step in lymphomagenesis. *Nature.* 2015;523(7558):96-100. doi: 10.1038/nature14351. PubMed PMID: 25970242.
29. Bezzi M, Teo SX, Muller J, Mok WC, Sahu SK, Vardy LA, et al. Regulation of constitutive and alternative splicing by PRMT5 reveals a role for Mdm4 pre-mRNA in sensing defects in the spliceosomal machinery. *Genes Dev.* 2013;27(17):1903-16. doi: 10.1101/gad.219899.113. PubMed PMID: 24013503; PubMed Central PMCID: PMCPMC3778243.
30. Yu MC. The Role of Protein Arginine Methylation in mRNP Dynamics. *Mol Biol Int.* 2011;2011:163827. doi: 10.4061/2011/163827. PubMed PMID: 22091396; PubMed Central PMCID: PMCPMC3195771.
31. Castello A, Fischer B, Eichelbaum K, Horos R, Beckmann BM, Strein C, et al. Insights into RNA biology from an atlas of mammalian mRNA-binding proteins. *Cell.* 2012;149(6):1393-406. doi: 10.1016/j.cell.2012.04.031. PubMed PMID: 22658674.
32. Khan DH, Gonzalez C, Cooper C, Sun JM, Chen HY, Healy S, et al. RNA-dependent dynamic histone acetylation regulates MCL1 alternative splicing. *Nucleic Acids Res.* 2014;42(3):1656-70. doi: 10.1093/nar/gkt1134. PubMed PMID: 24234443; PubMed Central PMCID: PMCPMC3919583.
33. Khan DH, Gonzalez C, Tailor N, Hamedani MK, Leygue E, Davie JR. Dynamic Histone Acetylation of H3K4me3 Nucleosome Regulates MCL1 Pre-mRNA Splicing. *J Cell Physiol.* 2016;231(10):2196-204. doi: 10.1002/jcp.25337. PubMed PMID: 26864447.
34. Chen H, Lorton B, Gupta V, Shechter D. A TGFbeta-PRMT5-MEP50 axis regulates cancer cell invasion through histone H3 and H4 arginine methylation coupled transcriptional activation and repression. *Oncogene.* 2017;36(3):373-86. doi: 10.1038/onc.2016.205. PubMed PMID: 27270440; PubMed Central PMCID: PMCPMC5140780.
35. Gao Y, Zhao Y, Zhang J, Lu Y, Liu X, Geng P, et al. The dual function of PRMT1 in modulating epithelial-mesenchymal transition and cellular senescence in breast cancer cells through regulation of ZEB1. *Sci Rep.* 2016;6:19874. doi: 10.1038/srep19874. PubMed PMID: 26813495; PubMed Central PMCID: PMCPMC4728496.
36. Yang Y, Bedford MT. Protein arginine methyltransferases and cancer. *Nat Rev Cancer.* 2013;13(1):37-50. doi: 10.1038/nrc3409. PubMed PMID: 23235912.

37. Khan DH, Healy S, He S, Lichtensztejn D, Klewes L, Sharma KL, et al. Mitogen-induced distinct epialleles are phosphorylated at either H3S10 or H3S28, depending on H3K27 acetylation. *Mol Biol Cell*. 2017;28(6):817-24. doi: 10.1091/mbc.E16-08-0618. PubMed PMID: 28077620; PubMed Central PMCID: PMC5349788.
38. Chen HY, Sun JM, Hendzel MJ, Rattner JB, Davie JR. Changes in the nuclear matrix of chicken erythrocytes that accompany maturation. *Biochem J*. 1996;320 (Pt 1):257-65. PubMed PMID: 8947496; PubMed Central PMCID: PMC1217926.

5.7 Supporting informations

5.7.1 Supporting figures

5.7.1.1 Determining antibody specificity and cross reactivity

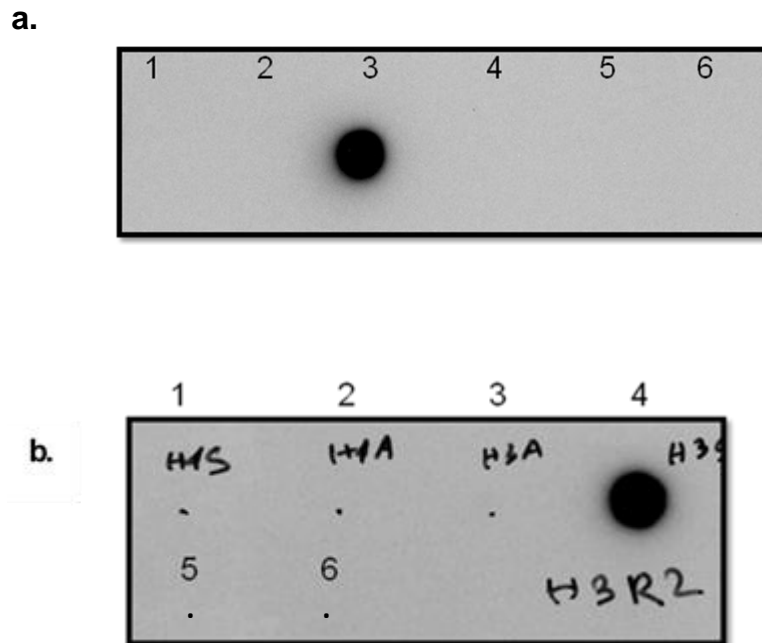


Figure S5.1: Peptide dot-blot assay for determining antibody specificity and cross reactivity.

a) Two ug of each of the peptide 1.H3R2me2s, 2. H3R2me2a, 3. H4R3me2a, 4.H4R3me2s, 5. H3K4me2 and 6. H3K4me3 were placed on nitrocellulose membrane, immunochemically analyzed with anti-H4R3me2a antibody. b) 2.0 ug of each of the peptide 1. H4R3me2s, 2. H4R3me2a, 3. H3R2me2a, 4. H3R2me2s, 5. H3K4me3, 6. H3K4me2 were placed on nitrocellulose membrane and immunochemically analyzed with anti-H3R2me2s antibody.

5.7.1.2 Association of PRMT1, PRMT5 and H3 and H4 arginine methylation with transcriptionally active chromatin

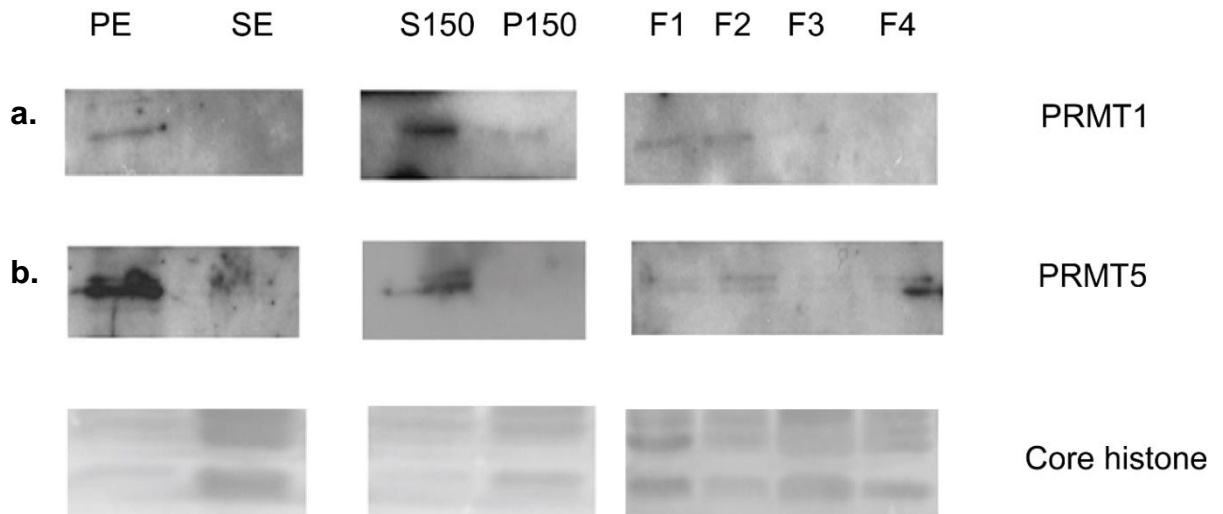


Figure S5.2: PRMT1 and PRMT5 are associated with the transcriptionally active chromatin fraction of chicken mature erythrocytes. Chromatin fractions (5.0 A260) from polychromatic erythrocytes were loaded onto a 10% SDS-polyacrylamide gel, transferred to nitrocellulose membranes, immunochemically stained with a) anti-PRMT1 antibody and b) anti-PRMT5 antibody. c) Ponceau S-stained core histones were used as a loading reference.

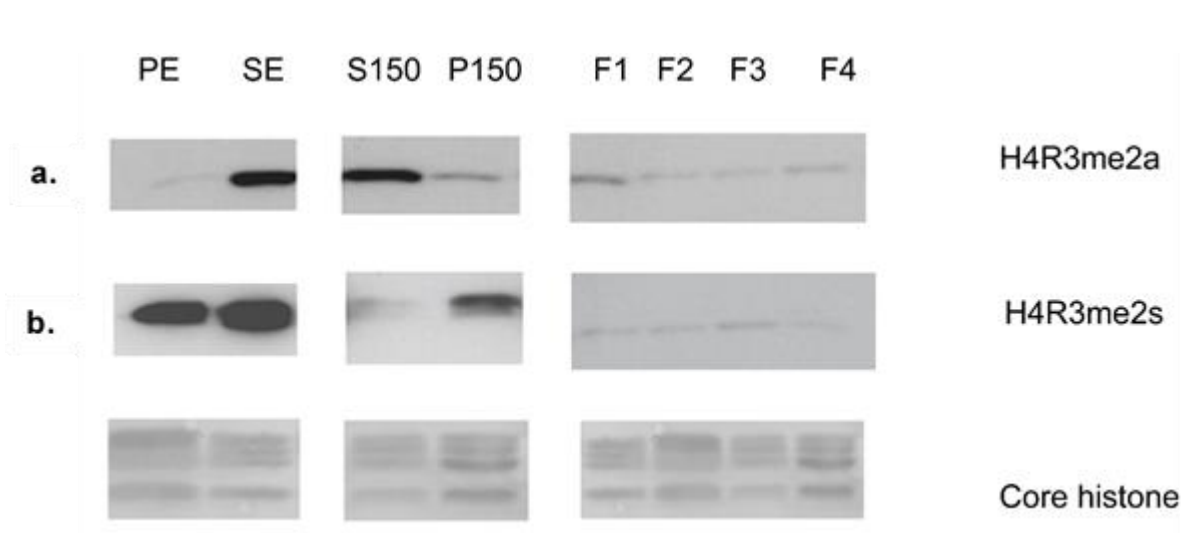


Figure S5.3: Distribution of H4R3me2a and H4R3me2s in mature erythrocyte chromatin fractions. Chromatin fractions (5.0 A260) from polychromatic erythrocytes were loaded onto a 15% SDS-polyacrylamide gel, transferred to nitrocellulose membranes, immunochemically

stained with a. anti-H3R2me2s and b. anti-H3R2me2a antibodies. c. Ponceau S-stained core histone from the blot was used as loading control.

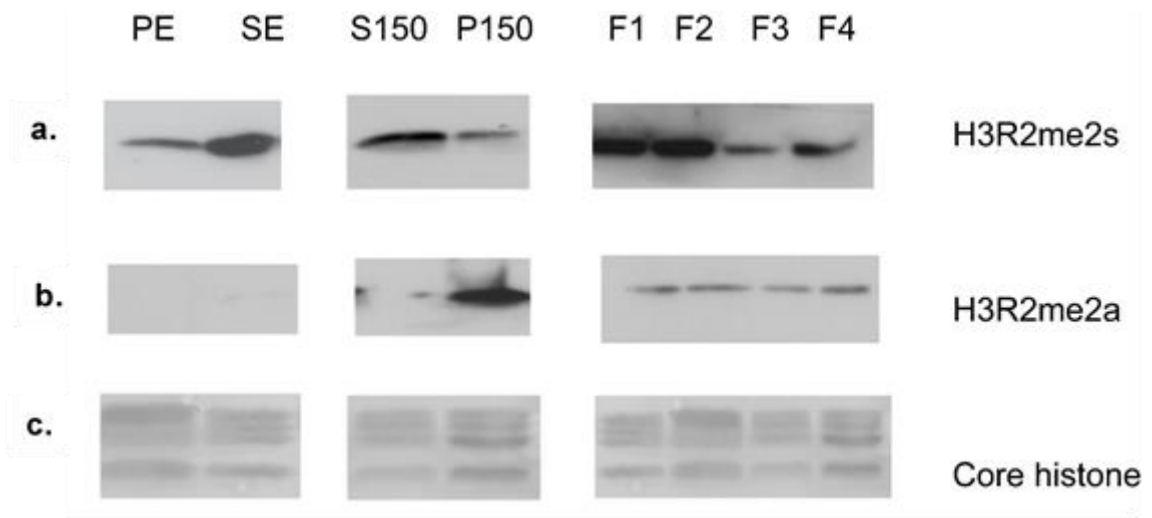


Figure S5.4: Distribution of H3R2me2s and H3R2me2a in mature erythrocyte cellular and chromatin fractions. Chromatin fractions (5.0 A260) from polychromatic erythrocytes were loaded onto a 15% SDS-polyacrylamide gel, transferred to nitrocellulose membranes, immunochemically stained with a) anti-H3R2me2s and b) anti-H3R2me2a. c. Ponceau S-stained core histones were used as a loading reference.

5.7.1.3 ChIP assay for H3R2me2s and H4R3me2a for highly transcribing genes of polychromatic erythrocyte cells.

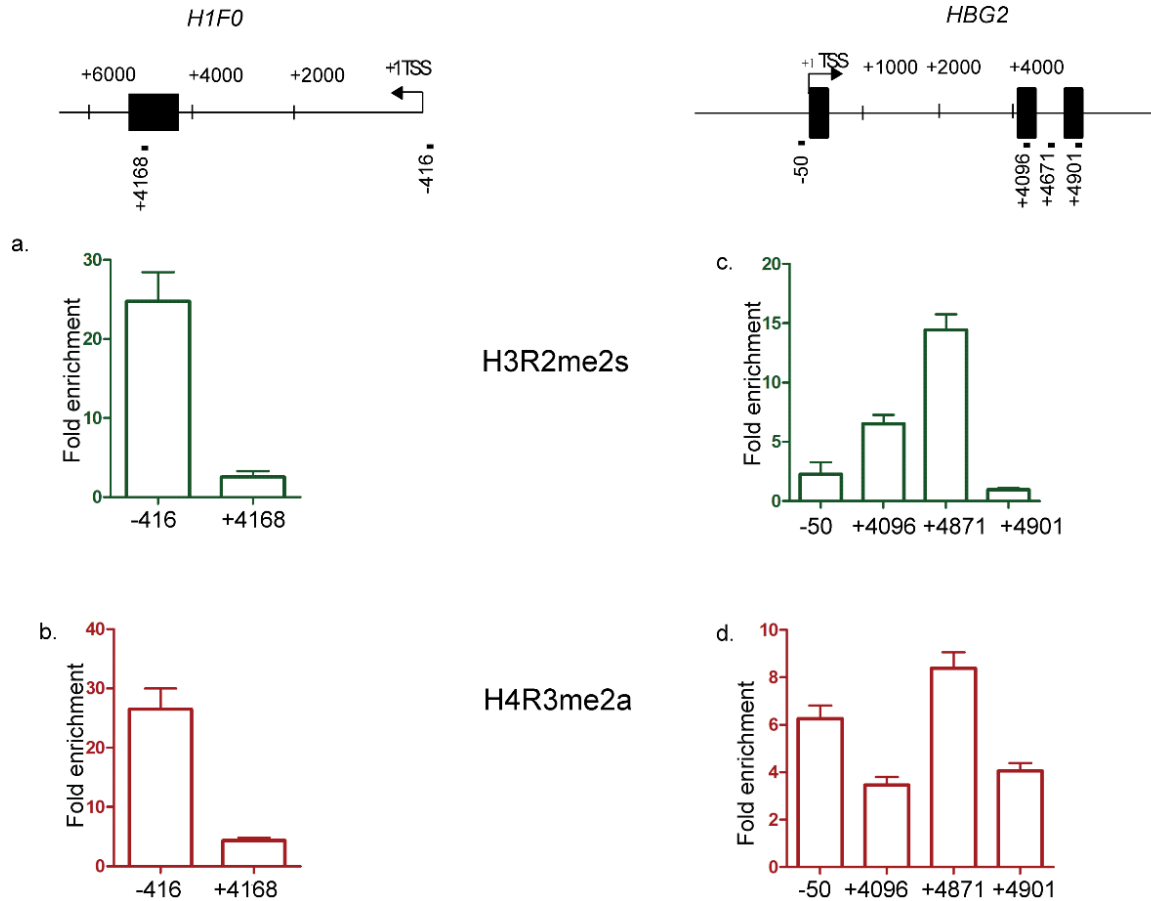


Figure S5.5: H3R2me2s and H4R3me2a distribution along expressed genes. A schematic representation of the amplicons generated by PCR analyses of immunoprecipitated DNA is shown for H5 (H1F0) and β A-globin (HBG2) gene (black lines below the map). Each amplicon is labeled according to the 5' position of the forward primer relative to the transcription start site. Exons are represented by boxes. ChIP assays were performed on formaldehyde-crosslinked sheared chromatin prepared from chicken polychromatic erythrocyte cells. Equal amounts of input and immunoprecipitated DNA were quantified by real-time quantitative PCR. Enrichment values are the mean of three biological repeats, and the error bars represent the standard deviation.

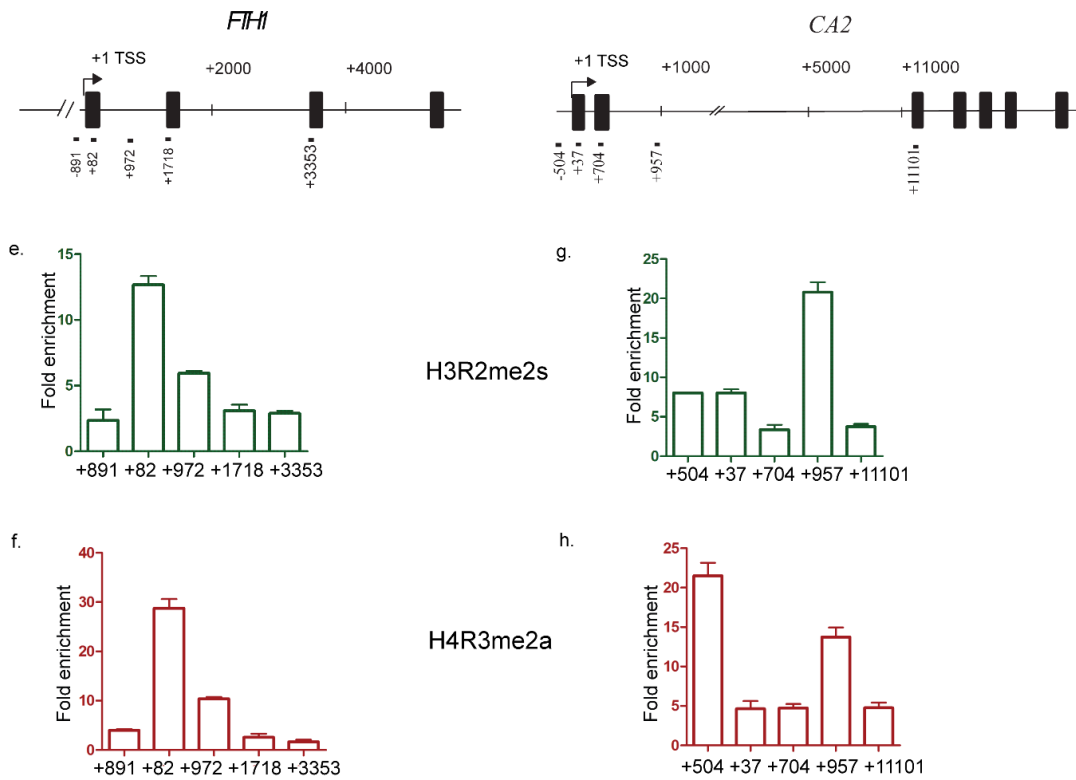


Figure S5.6: H3R2me2s and H4R3me2a distribution along expressed genes. A schematic representation of the amplicons generated by PCR analyses of immunoprecipitated DNA is shown for *FTH1* and *CA2* genes (black lines below the map). Each amplicon is labeled according to the 5' position of the forward primer relative to the transcription start site. Exons are represented by boxes. ChIP assays were performed on formaldehyde-crosslinked sheared chromatin prepared from chicken polychromatic erythrocyte nuclei. Equal amounts of input and immunoprecipitated DNA were quantified by real-time quantitative PCR. Enrichment values are the mean of three biological repeats, and the error bars represent the standard deviation.

5.7.2 Supporting table

Table S5.1: Primers used for ChIP qPCR

Primers	Sequences (5' to 3')
HBG2-Exon1-F	5'- CGGATAAAAAGTGGGGACACA-3'
HBG2-Exon1-R	5'- GTGGCAGTTGGAGGGTAGC-3'
HBG2-Exon2-F	5'- GGCAAGAAAGTGCTCACCTC-3'
HBG2-Exon2-R	5'- GCTTGTCACAATGCAGTTCG-3'
HBG2-Intron2-F	5'-CACATTGCGCATTTTGATGT-3'
HBG2-Intron2-R	5'-GCACCAGGGAAAGATTCCTA-3'
HBG2-Exon3-F	5'- CAGCAAGGACTTCACTCCTGA-3'
HBG2-Exon3-R	5'- TTTGGTGCTGGTGCTTAGTG-3'
FTH1-Promoter-F	5'- CAGCACAGTGCAGCTCTCTT-3'
FTH1-Promoter-R	5'- TGCGTTTGTTCCTAAAAGC-3'
FTH1-Intron1-F	5'-TTATCCACCAGGCAAGAACC-3'
FTH1-Intron1-R	5'-GAACGCAGCTGTTGGTGATA-3'
FTH1-Exon1-F	5'- CCACCGCATCTCTCTTTTC-3'
FTH1-Exon1-R	5'- GCGTACAGCTCCAGGTTGAT-3'
FTH1-Exon2-F	5'- ATTTTGACCGGGATGATGTG-3'
FTH1-Exon2-R	5'- TGGTTTTGCAGCTTCATCAG-3'
FTH1-Exon3-F	5'- TCGTGATGACTGGGAGAATG-3'
FTH1-Exon3-R	5'- TGCCAATTTGTGCAGCTCTA-3'
H5-Promoter-F	5'- AGGTGCGCTCAGAGAGAGAG-3'
H5-Promoter-R	5'- AATTGCTGATGCTGTTGCAC-3'
H5-Exon-F	5'- AGGAAGGCCAGGAAGAAGTC -3'
H5-Exon-R	5'- GACCGCTTCACCTTCTTGG -3'
CA2-Promoter-F	5'- CGCGTTTCCTACAAGGTGAG -3'
CA2-Promoter-R	5'- GACGCCCTGGTTCTTACTT -3'

CA2-Exon1-F	5'- AAGCGGACCTCTCTCTCC-3'
CA2-Exon1-R	5'- GAACTCCATGCCCTTCTCC -3'
CA2-Exon2-F	5'- AGCCCCTCAGCTTCAGCTAC -3'
CA2-Exon2-R	5'- ACTTGTCGGAGGAGTCGTCA -3'
CA2-Intron2-F	5'- GCCTGAGCTGCCCTACTCTA-3'
CA2-Intron2-R	5'- CCTTCTTCCTCCTTCCCATC -3'
CA2-Exon3-F	5'- CGCTGGATGGAGTCTACAGG -3'
CA2-Exon3-R	5'- GCATCGTACTTCACGCCATC -3'
HDAC2-Promoter-F	5'- GTGTGGAGGGTGTTCGTCT -3'
HDAC2-Promoter-R	5'- CCCTCTTGTCCCTTGCTGTA -3'
HDAC2-Exon1-F	5'- CCCTATGGCGTACAGTCAGG -3'
HDAC2-Exon1-R	5'- GCGGTTACGGCGCTCTAC -3'

CHAPTER VI: EPIGENOMIC LANDSCAPE OF IMMUNE GENES IN CHICKEN ERYTHROCYTES

6.1 Abstract

Background: Chicken polychromatic erythrocytes exhibit cellular functions of transcription and translation similar to other nucleated cells. Studies have reported the expression of Toll-like receptors (TLRs) and several cytokines in response to the immune stimulation in chicken mature erythrocytes. These studies have demonstrated a possible novel function of nucleated erythrocytes other than oxygen transport.

Method: In this study, RNA-Seq was used to analyze the expression of several innate immune genes in polychromatic erythrocytes under non-stimulated conditions. With the combination of a biochemical fractionation procedure and ChIP-sequencing, epigenomic features of salt-soluble chromatin of immune genes were characterized in chicken polychromatic erythrocytes.

Result: Here I demonstrate that chicken polychromatic erythrocytes express several immune genes under steady state conditions. The chromatin of these genes associate with active histone modifications and is enriched in the active chromatin fractions. Similar to the other genes in chicken polychromatic erythrocytes, the chromatin of highly expressed immune genes have salt solubility along the gene, while the chromatin of low expressing ones have a salt solubility only at the promoter region. However, in contrast to other genes, the chromatin of immune genes with a low level of transcription exhibit salt solubility and active histone modifications, which categorize them as unique genes in these cells. Therefore, it indicates that immune genes in chicken erythrocytes possess a unique epigenomic feature suggesting that they are poised to be expressed. Finally, poly I:C-mediated induction of several cytokines and TLRs in polychromatic erythrocytes establishes the function of these cells in the innate immune response.

Conclusion: This study demonstrates the distinct epigenomic features of immune genes in chicken polychromatic erythrocytes, which are crucial to the understanding of the underlying mechanisms of immune defense systems against invading organism in nucleated erythrocytes. Thus, epigenetic features of immune genes explored in this study that could be the underlying mechanism to regulate the immune genes in erythroid cells will be able to contribute to the current knowledge regarding epigenome mediated immune defense mechanisms in vertebrate.

This collaborative work is under preparation for publication:

Sanzida Jahan performed all the experiments, Wayne Xu performed the bioinformatics analysis, Aleksandar Ilic prepared the library for sequencing.

6.2 Introduction

Erythrocyte and lymphocyte cells are generated from a common myeloid progenitor cell, the hemocytoblast [454]. The major function of erythrocytes is to carry oxygen through the circulation from lungs to tissues of the body. In mammals, erythrocytes are enucleated at the terminal stage. However non-mammalian vertebrates such as avian, fish, amphibians and reptiles contain a nucleus at the mature erythrocyte stage [351]. The nucleated erythrocytes in non-mammalian vertebrates are transcriptionally active and possess functions other than gas transportation such as modulation of immunity [351, 359]. The RNA-content is inversely correlated with cellular differentiation along with a decreasing RNA content with red blood cell maturity. Though there is variation in erythrocyte morphology and longevity, erythrocytes are highly conserved across vertebrate species [455]. The functions of nucleated erythrocytes are thus not restricted to simply gas exchange and are extended to other physiological processes such as immune defense mechanism against invading microorganisms.

Several studies reported that nucleated erythrocytes from salmon, trout and chicken show immune responses [322, 358, 359]. Innate immune response initiates through the pattern recognition receptors (PRRs) by the recognition of a variety of pathogen-associated molecular patterns (PAMPs). Toll-like receptors (TLRs) are type I transmembrane proteins and serve as the major component of PRR. TLR mediated signal leads to the activation of nuclear factor κ B (NF- κ B) and the mitogen-activated protein kinase signaling cascade. The TLR mediated signaling event leads to release of cytokines and interferon molecules from the infected cells [456].

The first suggestion regarding the role of erythrocytes in immune response came from the study by Nelson in 1953. This study showed that erythrocytes were crucial in enhancing the phagocytic capacity. Erythrocytes act as an opsonic agent to attach the bacteria on the surface and making it a signal for phagocytes to kill the organism [457]. Human erythroid nuclear cells (erythroblast antigen+ and glycophorin A+ cells from human bone marrow) were shown to produce several cytokines and immune regulatory molecules under non-stimulated conditions which includes (IL)-1 β , IL-2, IL-4, IL-6, interferon (IFN)- γ , transforming growth factor (TGF)- β 1, tumor necrosis factor (TNF)- α and IL-10 [357]. In another study, fish erythrocytes were shown to clear pathogens by forming a rosette with macrophages [458]. Following that study, chicken erythrocytes were shown to have similar phenomena where they were able to enhance phagocytic activity in response

to *Candida albicans* [362]. A study conducted on trout and chicken erythrocytes showed that these cells were capable of responding to an immune stimulant such as polyinosinic:polycytidylic acid (poly I:C) [358]. Poly I:C, which mimics dsRNA virus, was able to induce TLR3 and IFN- α transcripts in trout and chicken erythrocytes [358]. To determine the repertoire of TLRs and immune components expressed in chicken erythrocytes, two different concentrations of poly I:C and CpG oligodeoxynucleotides (CpG ODN) were used [322]. Poly I:C produces a TLR3 mediated immune response, while CpG ODN which is a short, single-stranded synthetic DNA molecule, can activate a TLR21 mediated pathway in chickens [307, 331]. Treatment of chicken erythrocytes results in an upregulation in the expression of type I interferon IFN α and β , interleukin IL8 and a low level of induction of MHC II and CD80 molecule. On the other hand, unstimulated erythrocytes were found to differentially express several immune genes such as *TLRs 2, 3, 4, 5, and 21* [322]. Findings from these studies suggest that chicken erythrocytes can respond to various ligand-mediated immune responses and thus contribute to defense against invading organisms.

To gain further insight into the role of immune genes in chicken erythrocytes, we investigated the epigenomic profile of the immune gene chromatin in this study using chicken polychromatic erythrocytes. Chicken polychromatic erythrocyte cells are non-replicating G0 phase cells isolated from anemic chickens [285]. Also, we did transcriptome analysis in chicken polychromatic erythrocytes and at the same time we analyzed the gene expression profile in 6C2 cells. 6C2 cell is a transformed chicken erythroleukemia cell. I did that to confirm that chicken erythrocytes did express immune genes. I hypothesize that chicken polychromatic erythrocytes express immune genes with the distinct epigenomic feature. We previously mapped all of the transcriptionally active chromatin domains in chicken polychromatic erythrocytes. Combining a biochemical fractionation process with next-generation DNA sequencing, we isolated and characterized 150 mM NaCl soluble polynucleosome chromatin fraction (F1 chromatin fraction) [285]. In our previous study, we demonstrated that active genes were organized into two classes of domains. The first class consisted of genes with a high level of expression, antisense transcripts and associated with H3K4me3 and H3K27ac at the 5' end of the gene along with eRNA marking the enhancer nearby. This class of genes had salt solubility along the entire domain. The second class has a low level of expression with no detectable eRNA, association with H3K4me3 and H3K27ac, and the 5' end of the gene is enriched in F1 (described in **Chapter V**) [285].

Here we used the same approach to characterize the features of immune genes in chicken polychromatic erythrocytes. We characterized the salt soluble feature of immune genes, their expression profile and distribution of H3K4me3, H3K27ac, H3R2me2s and H4R3me2a with these genes. We found novel and distinct epigenomic features of immune genes in our study. The results from this study suggest that immune genes are marked with H3K4me3, H3K27ac, H3R2me2s, and H4R3me2a, suggesting that these genes are in a poised configuration ready to be rapidly induced.

6.3 Results

6.3.1 Circos plot for immune genes enrichment in F1

To characterize the salt solubility feature of immune genes in chicken erythrocytes, salt soluble polynucleosome chromatin fraction F1 was sequenced using the SOLiD 5500xl sequencer. As shown in **Figure 6.1**, several of the immune genes in polychromatic erythrocytes were enriched in the F1 salt soluble chromatin fraction. Some of the genes were soluble along the whole gene body, while others show solubility only at the proximal promoter region. To show the genomic distribution of these genes, a Circos plot was generated. As the figure illustrate, the outside of the Circos map was marked with the chromosome number represented with a color for each chromosome in the circle. Approximately 9466 domain islands were mapped to the galGal3 genome using Circos3 (version 0.62.1) with 5 Mb spacing on each chromosome. The blue vertical bars inside is the level of F1 enrichment for the particular gene within the chromosome. Some of the immune genes enriched in F1 are *TLR3*, *TLR21*, *TLR7*, *TLR6*, *TLR15*, *TLR2*, *TLR4*, *TLR5*, *TLR16*, *TRAFD1*, *TRAF7*, *TRAF5*, *Myd88*, *IRAK2*, *IRAK4*, *IRF1*, *IRF2*, *IRF5*, *IRF7*, *IRF8*, *IRF10*, *IRF4*, *NFKB1*, *NFKB2*, *TRAM1*, *IFNB* and *TAB*. As the Circos plot illustrates, salt-soluble immune genes were distributed equally across the entire chicken erythrocyte genome. Chromosomes 3 and 4 contain most of the TLRs and chromosome Z contained the type I interferon.

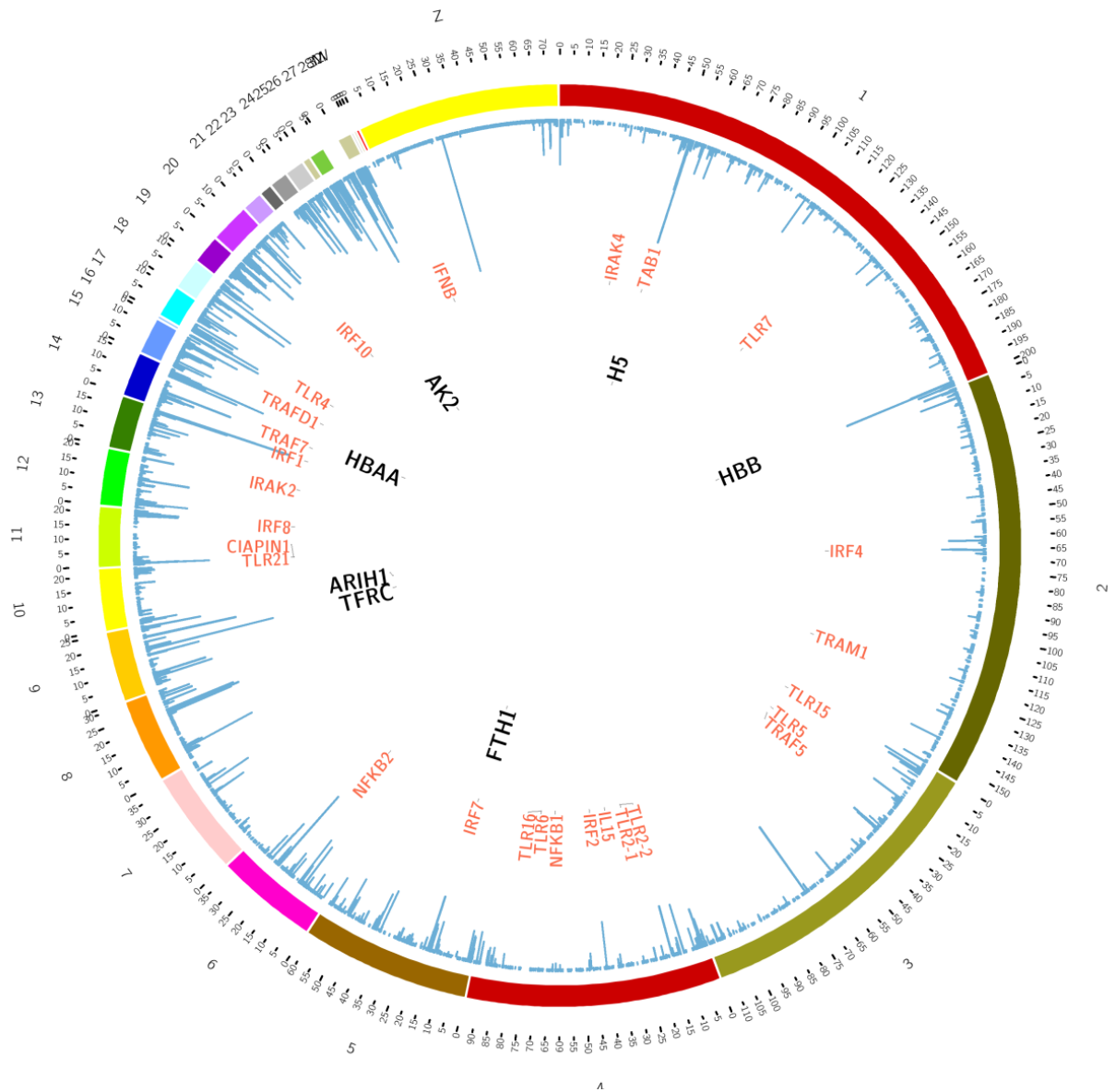


Figure 6.1: Distribution of salt soluble immune genes in chicken erythrocyte genome. Circos plot of DNA sequence enrichment in fraction F1 polynucleosomes (inner vertical blue line). The outer ring represents the chicken chromosomes and numbered according to chromosome number outside of the ring. The interior ring details the mapping and peak intensity of F1 DNA-seq reads. Some of the most enriched immune genes are shown.

6.3.2 Transcriptome profile of immune genes in polychromatic erythrocytes and 6C2 cells

The increased salt solubility of the transcriptionally active chromosomal domains correlates with the acetylation of the enriched genes [285]. We determined the transcriptional activity of the immune genes analyzed in F1-DNA seq. RNA-seq analyses from polychromatic erythrocytes and 6C2 cells were performed on total RNA isolated from these cells. Transcriptome analysis revealed differential expression of several immune genes in chicken erythrocytes under non-induced conditions. **Figure 6.2a** shows that the *TLR3* gene is expressed at low levels from the forward strand in both polychromatic erythrocytes and 6C2 cells. **Figure 6.2b** shows the expression profile of the *TLR21* gene in chicken polychromatic erythrocytes and 6C2 cells. *TLR21* was expressed lowly in polychromatic erythrocytes, and at a low level in 6C2 cells.

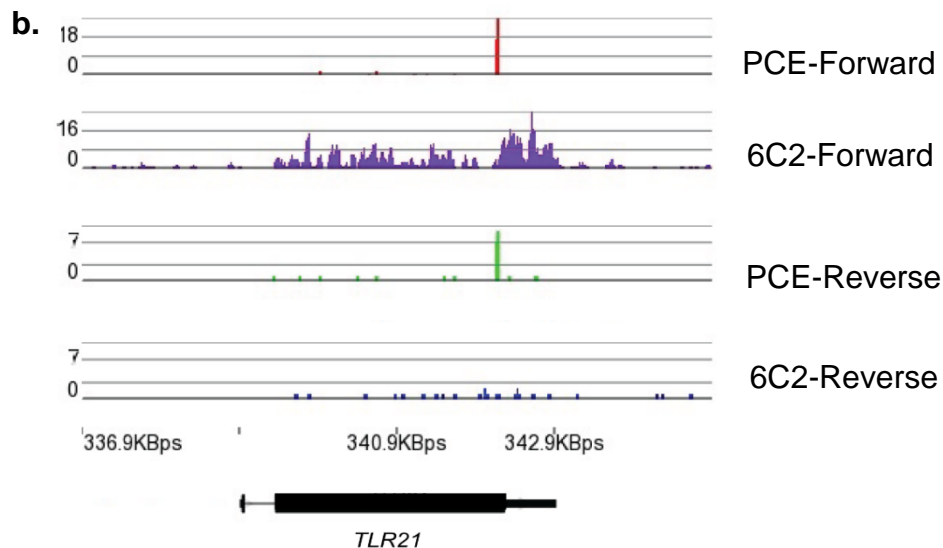
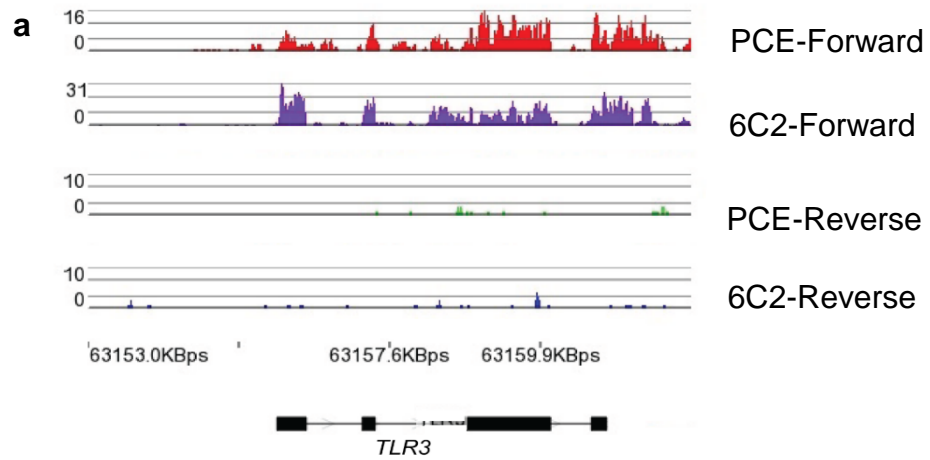


Figure 6.2. Transcriptional activity of a) *TLR3* and b) *TLR21* gene in chicken erythrocytes. a) First track in red is the transcript from forward strand of chicken polychromatic erythrocytes *TLR3* gene, blue track below is the transcript from forward strand from chicken erythrocyt leukemia 6C2 RNA-seq. The bottom two tracks are the transcripts from the reverse strand from polychromatic erythrocytes and 6C2 cells, respectively. b) Forward and reverse transcript from *TLR21* gene in chicken polychromatic erythrocytes and 6C2 cells. **PCE:** polychromatic erythrocytes, **6C2:** chicken erythrocyt leukemia cell line, **Forward:** Forward strand of the transcript, **Reverse:** reverse strand of the transcript.

The *TLR6* gene had a low level of expression in the forward strand in 6C2 cells, but the expression was higher than in polychromatic erythrocytes (**Figure 6.3**). *TLR6* had a low degree of salt solubility at the 5' end of the gene.

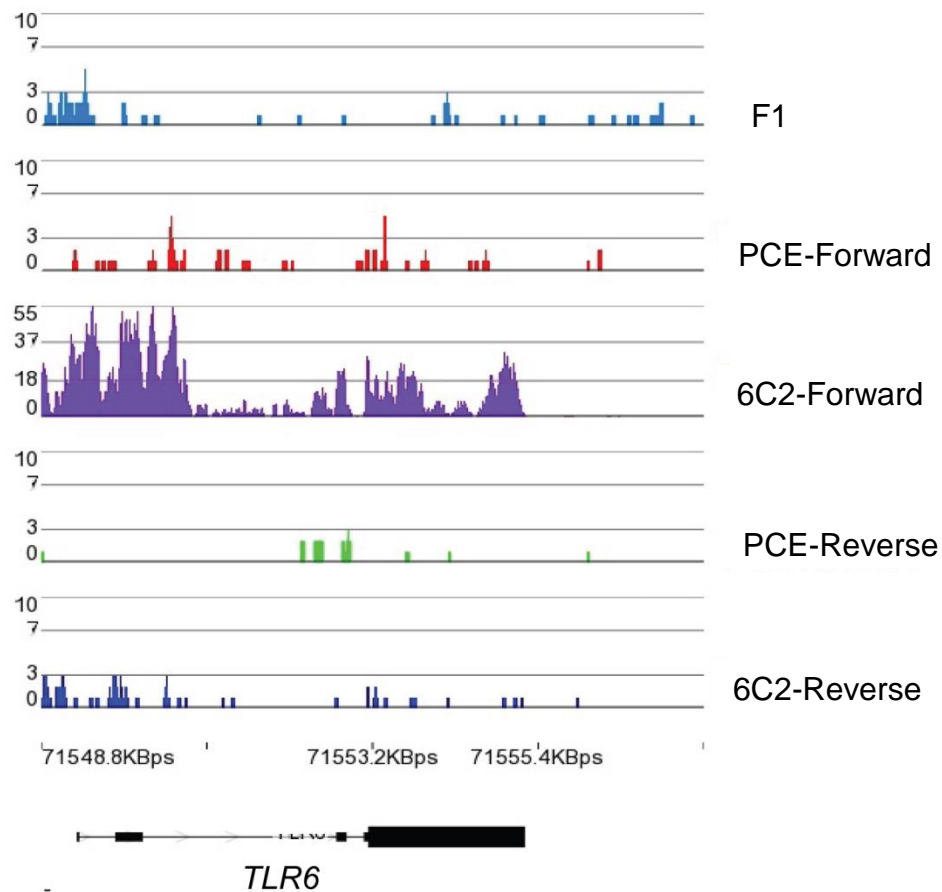


Figure 6.3. Transcriptional activity of *TLR6* in chicken erythrocytes. The first track in blue represents the salt solubility of the *TLR6* gene in F1 polynucleosome chromatin fraction. Undeneath in red is the track for forward transcript from polychromatic erythrocytes *TLR6* gene, blue track below is the forward transcript for *TLR6* in 6C2 chicken erythrocyt leukemia cell. The last two tracks are the transcripts from the reverse strand from polychromatic erythrocytes and 6C2

cells, respectively. **PCE**: polychromatic erythrocytes, **6C2**: chicken erythroleukemia cell line, **Forward**: Forward strand of the transcript, **Reverse**: reverse strand of the transcript.

Figure 6.4 shows *IFNA3* and *IFNW1* have a low level of expression in polychromatic erythrocytes and 6C2 cells. A transcript was produced from the reverse strand, the level of which was considerably higher than the amounts of transcript from the sense (forward strand). This transcript, which is named as *LOC407092* in the galGal3 reference genome, encodes for the ubiquitin associated protein 2.

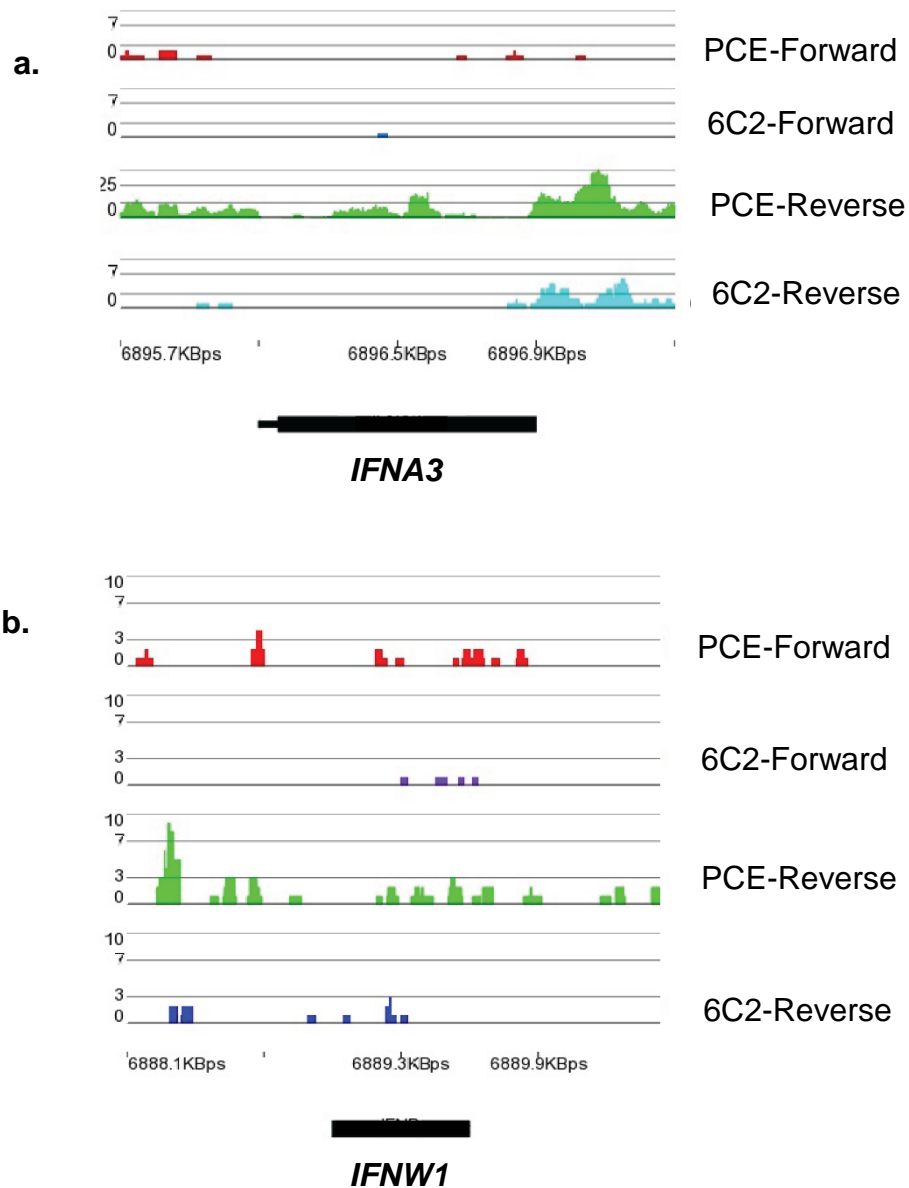
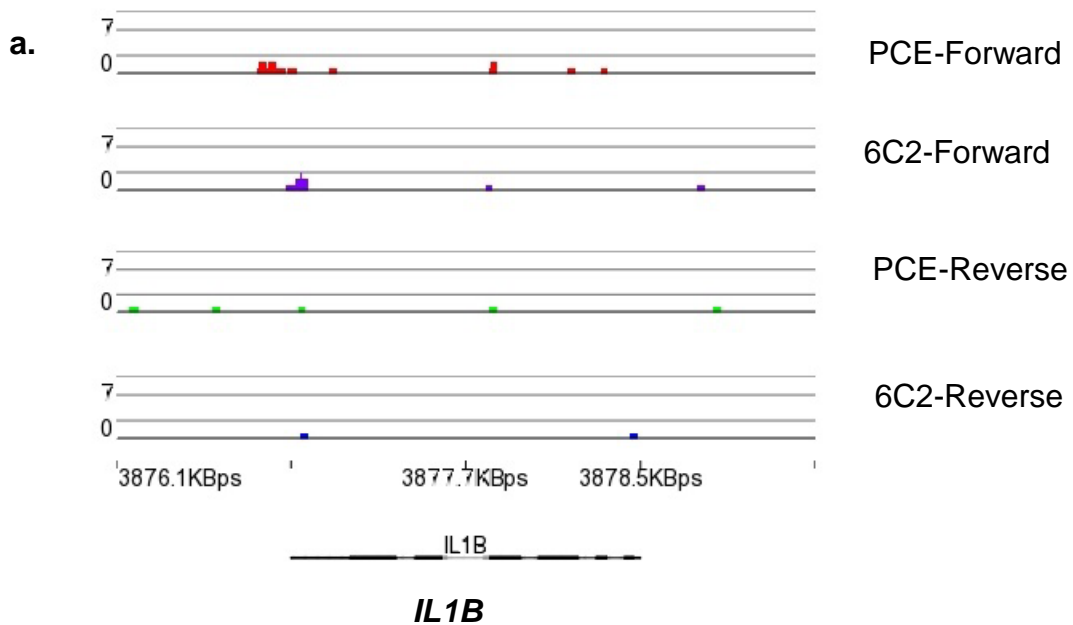


Figure 6.4: Transcriptional activity of a) *IFNA3* and b) *IFNW1* gene in chicken polychromatic erythrocytes. a) The first track in red is the forward transcript from *IFNA3* gene in chicken polychromatic erythrocytes; the blue track below is the forward transcript from 6C2 chicken erythroleukemia cells. The last two tracks are the transcripts from the reverse strand from polychromatic erythrocytes and 6C2 cell line, respectively. b) Forward and reverse transcripts from *IFNW1* gene in chicken polychromatic erythrocytes and 6C2 cells. **PCE:** polychromatic erythrocyte cells, **6C2:** chicken erythroleukemia cell line, **Forward:** Forward strand of the transcript, **Reverse:** reverse strand of the transcript.

Similarly, **Figure 6.5** shows *IL1B* has a very low expression in both cell types, while *IL15* has a moderate level of expression in chicken polychromatic erythrocytes.



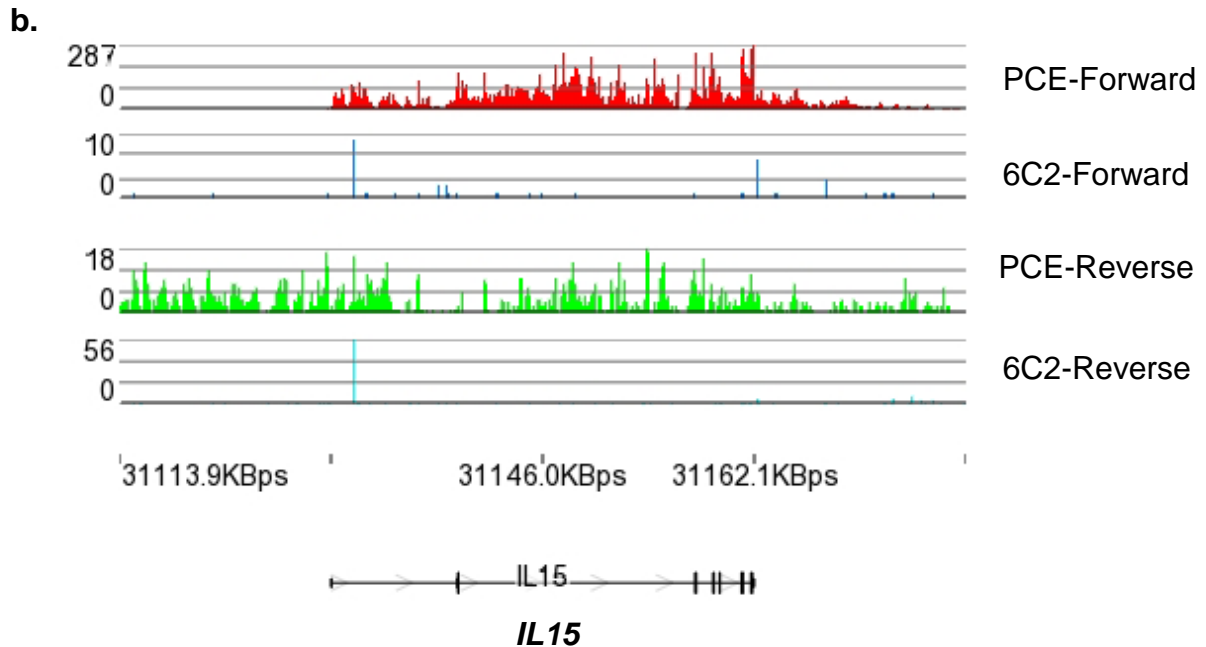


Figure 6.5: Transcriptional activity of a. *IL1B* and b. *IL15* gene in chicken polychromatic erythrocytes. a) The first track in red is the forward transcript from *IL1B* gene in chicken polychromatic erythrocyte cells; the blue track below is the forward transcript from 6C2 chicken erythrocyte leukemia cells. Last two tracks are the transcripts from the reverse strand from polychromatic erythrocytes and 6C2 cell line, respectively. b) Forward and reverse transcript from *IL15* gene in chicken polychromatic erythrocytes and 6C2 cells. **PCE**: polychromatic erythrocyte cells, **6C2**: chicken erythrocyte leukemia cell line, **Forward**: Forward strand of the transcript, **Reverse**: reverse strand of the transcript.

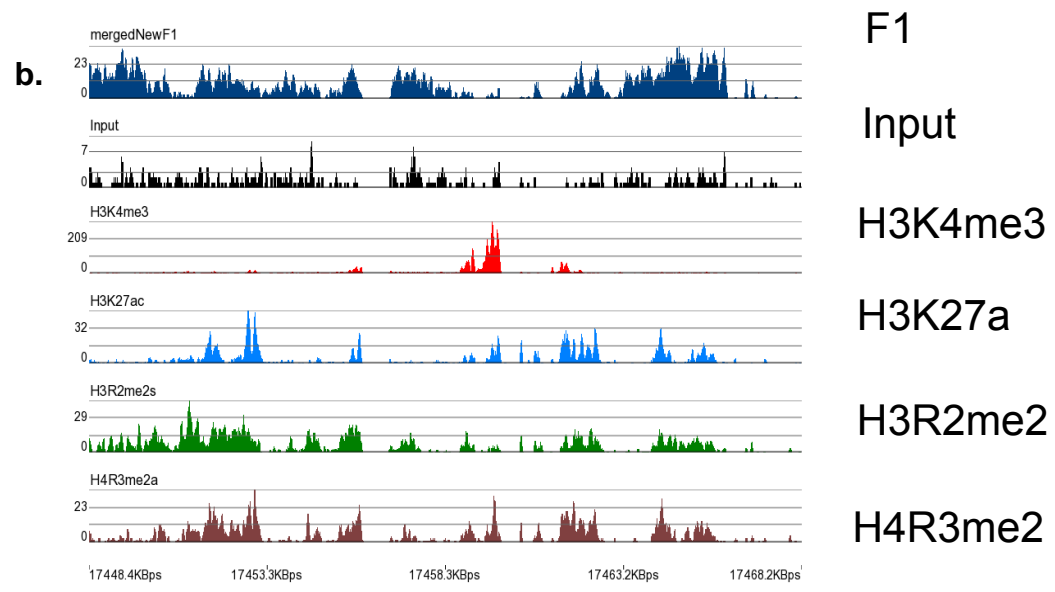
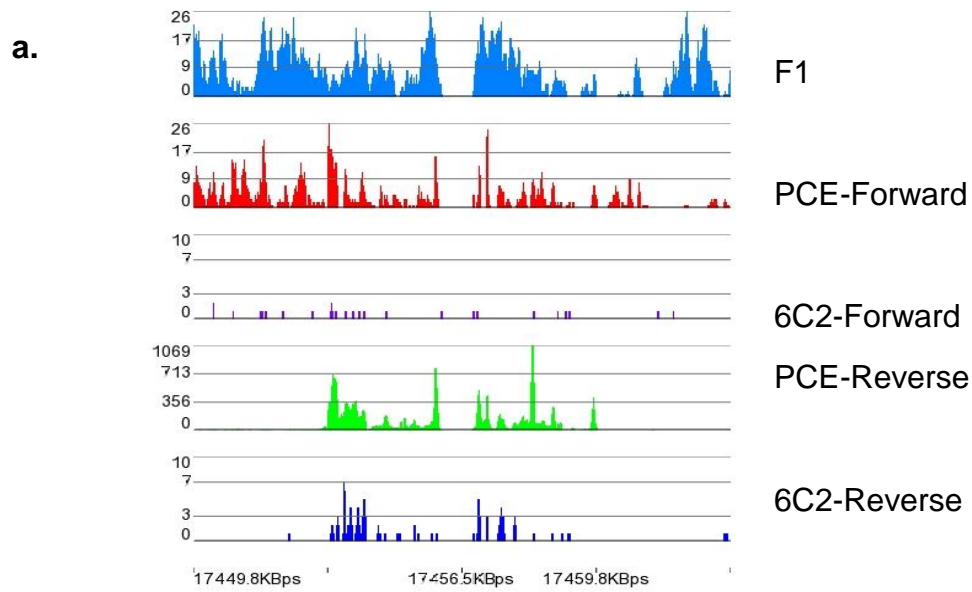
Figures S6.1, S6.2, and S6.4 (Supplementary material) further demonstrate the expression of several immune components such as *IRF7*, *IRF8*, and *TRAFD1* in chicken polychromatic erythrocytes and 6C2 cells. The expression of several other genes was also summarized. **Table 6.1** lists the immune genes that were found to be expressed in chicken polychromatic erythrocytes and 6C2 cells. The list includes several of the cytokines, chemokines, and interferon regulatory genes that are differentially expressed in both cell types.

Table 1: Expression of immune components in chicken polychromatic erythrocytes and chicken erythroleukemia cell (6C2) cells. ‘+’ indicates a low, ‘++’ moderate and ‘+++’ denotes a high level of expression.

Type of cells	TLRs	Adaptor protein	Interleukins	Chemokines	Interferon and Interferon regulatory factors
Polychromatic erythrocytes	TLR3+ TLR2+ TLR4+ TLR5+ TLR6+ TLR7+ TLR21+ TLR15+	MYD88+ TIRAP+ TRAM1+ TICAM1+	IL1B+ IL2+ IL3+ IL5+ IL7+ IL8+ IL9+ IL10+ IL16+ IL18+ IL22+ IL15+++	CCL1+ CCL4+ CCL5+ CCL20 + CXCL12+ CXCL14+	Type I interferon: IFNA3+ and IFNB+ Type II interferon: IFNG Interferon regulatory factors: IRF1 +++ IRF2 ++ IRF7++ IRF4+ IRF8+ IRF10+
6C2 cells	TLR3+ TLR2+ TLR4+ TLR5+ TLR6+ TLR7+ TLR15+ TLR21+	MYD88+ TIRAP+ TRAM1+ TICAM1+	IL1B+ IL1R1+ IL5+ IL12B+ IL28B+ IL22RA1+ IL28RA ++ IL17RD+ IL2RG+ IL11RA+ IL13RA1+ IL4R++ IL21R+ IL8+ IL9+ IL16+ IL13+ IL18++ IL22+ IL17RA+ + IL20RA+ IL10R2++	CCL1+ CCL4+ CCL10+ CCL17+ CCL18+ CXCL12+ CXCL13L2+ CXCL12+	Type I interferon: IFNA+ IFNAR1+ IFNAR2+ IFNB+ Type II interferon: IFNGR1+ IFNGR2+ IFNG+ Interferon regulatory factors: IRF1+ IRF2+ IRF2BPL+ IRF4+ IRF6+ IRF7+ IRF8++ IRF10++

6.3.3 Chromatin profile of highly expressed immune genes

In contrast to those genes presented above, some immune genes showed higher levels of expression in chicken polychromatic erythrocytes, and one such gene was the interferon regulatory factor 1 or *IRF1*. Chromatin profile of the *IRF1* gene was analyzed by combining F1 chromatin profiling and ChIP-seq analyses for H3K4me3, H3K27ac, H3R2me2s and H4R3me2a (**Figure 6.6a and 6.6b**). In **Figure 6.6a**, the first track shows the gene's F1 profile which demonstrates that the entire *IRF1* gene was enriched in the salt soluble chromatin fraction. The gene was highly transcribed (**Figure 6.6a**). There was a low level of antisense transcripts as observed from the forward strand. H3K4me3, H3K27ac, and H4R3me2a were associated with the 5' end of the *IRF1* gene as demonstrated in **Figure 6.6b**. ChIP-seq analysis also showed that H3K27ac, H3R2me2s, and H4R2me2a distributed along the body of *IRF1* gene. The upstream promoter region and downstream of *IRF1* gene were associated with H3K27ac, H3R2me2s and H4R2me2a along with eRNA indicating the presence of a putative enhancer at these sites. Similarly, the distribution of H3K4me3, H3K27ac, H3R2me2s, and H4R2me2a was analyzed for *IRF7* and *IRF8* genes (**Figure S6.5 and S6.6**). Entire chromatin region including the promoter, coding and regulatory region of both genes were enriched in F1 fraction. *IRF7* and *IRF8* had H3K4me3, H3K27ac, H3R2me2s and H4R2me2a at the 5'upstream, 5' end and 3' end of the genes. As H3K4me3 is often found localizing with CpG islands at the 5' end of the genebody, we looked further into the distribution of H4R3me2a and H3R2me2s with CpG islands [459-462]. H3K4me3, H3K27ac, H3R2me2s, and H4R2me2a were mapped with CpG islands along the genebody of *IRF1*, *IRF7* and *IRF8* genes (**Figure 6.6c**).



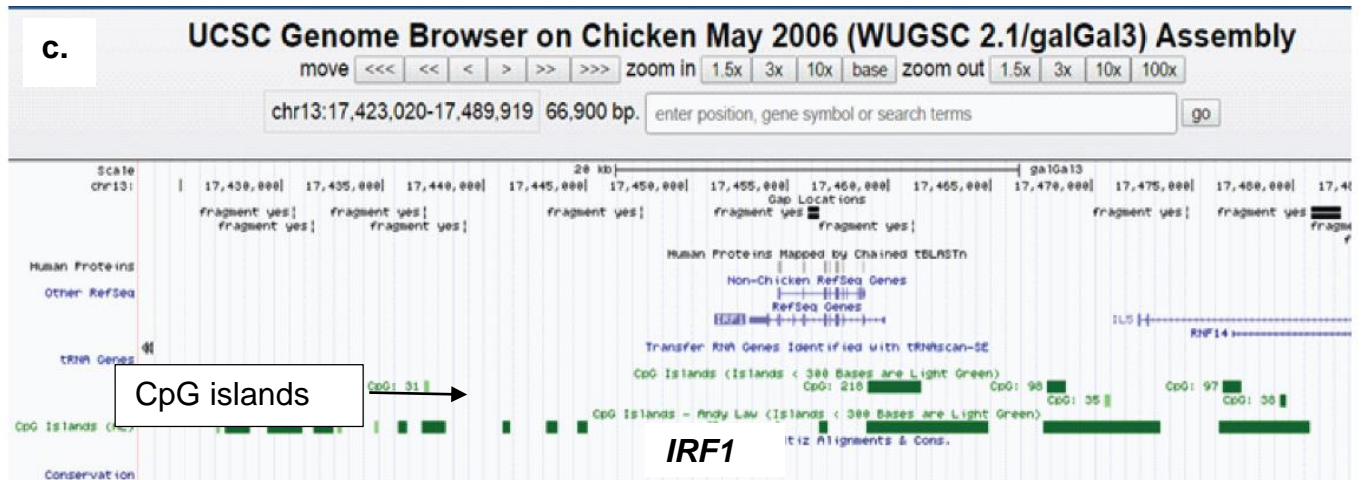
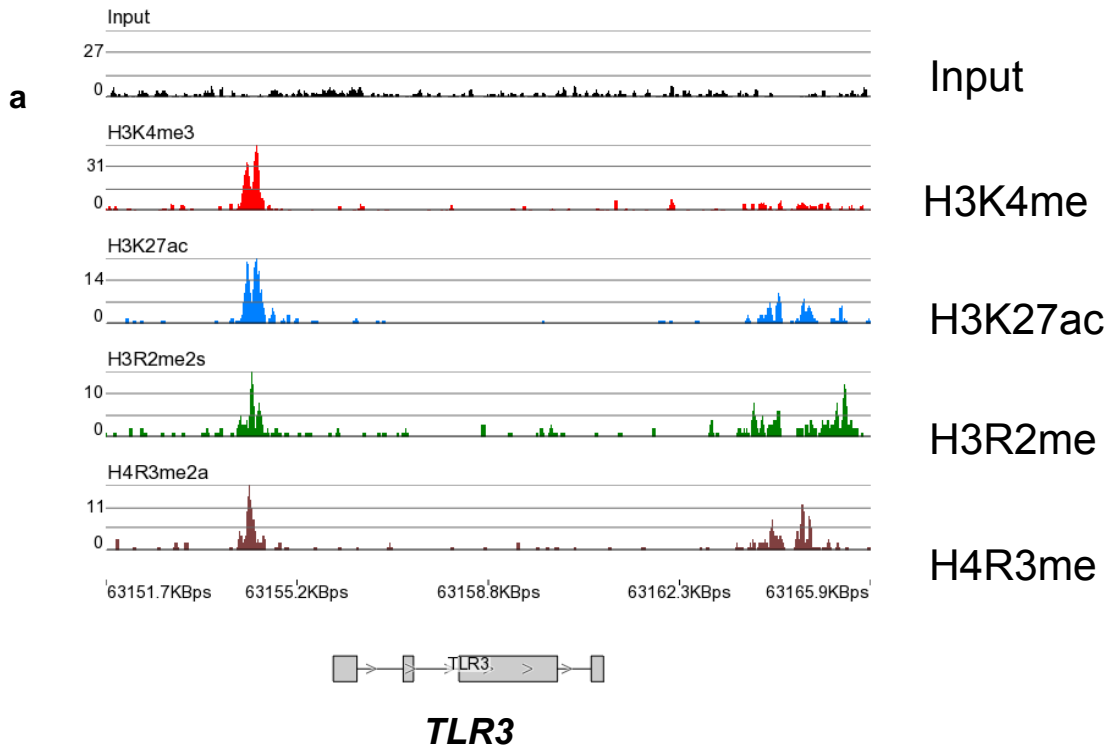


Figure 6.6. Chromatin profile and transcriptional activity of *IRF1* gene. a) Signal tracks showing DNA enrichment in F1 fraction (blue), transcripts on (+) and (-) strands, H3K4me3 track (in purple) and H3K27ac (in light blue) modifications. b) Signal tracks showing DNA enrichment in F1 fraction (blue), H3K4me3 track (red), H3K27ac (blue), H3R2me2s (green) and H4R3me2a (brown) arginine modifications. PCE: polychromatic erythrocyte cells, 6C2: chicken erythrocyte cells, Forward: Forward strand of the transcript, Reverse: reverse strand of the transcript. c) CpG islands were mapped along the *TLR3* gene using galGal3 UCSC genome browser. The green bar underneath the gene indicates the location of CpG islands.

6.3.4 Chromatin profile of low expressed immune genes

Next, we analyzed the chromatin profile of poorly expressed immune genes in chicken polychromatic erythrocytes. **Figure 6.7a** shows the chromatin profile of *TLR3* where the salt solubility or F1 enrichment was restricted to the upstream promoter region (UPR) of the gene. The *TLR3* gene was associated with H3K4me3, H3K27ac, H3R2me2s, and H4R3me2a at the gene's UPR aligning with F1 enrichment. Downstream of the 3' end of the gene, it was associated with H3K27ac, H3R2me2s, and H4R3me2a indicating the presence of a putative enhancer at this site (**Figure 6.7a**). Intriguingly, this region overlapped with the underlying CpG islands at this site as confirmed from UCSC galGal3 genome browser (**Figure 6.7b**). We analyzed the chromatin profile of the *TLR21* gene (**Figure S6.7**). This gene has one exon and had low levels of F1 enrichment

along the gene. *TLR21* was associated with H3K4me3, H3K27ac, H3R2me2s, and H4R3me2a along the gene body (**Figure S6.7**). Next, we determined the distribution of H3K4me3, H3K27ac, H3R2me2s and H4R3me2a along the Toll-Interleukin 1 Receptor (TIR) Domain-Containing Adaptor or *TIRAP* gene (**Figure S6.8**). The gene was moderately transcribed in 6C2 cells and poorly transcribed in polychromatic erythrocytes. *TIRAP* gene contained F1 enrichment in the entire gene body and association with H3K4me3, H3K27ac, H3R2me2s and H4R3me2a at the upstream promoter region (**Figure S6.3, S6.8**). H3R2me2s was distributed along the gene body while H3K27ac and H4R3me2a peaked at the 3' end of the gene. At the 3' downstream of *TIRAP* gene, there was a strong peak for H3K4me3 aligning with H3R2me2s, CpG island and low levels of H3K27ac and H4R3me2a marking putative regulatory region at this site (**Figure S6.3, S6.8**).



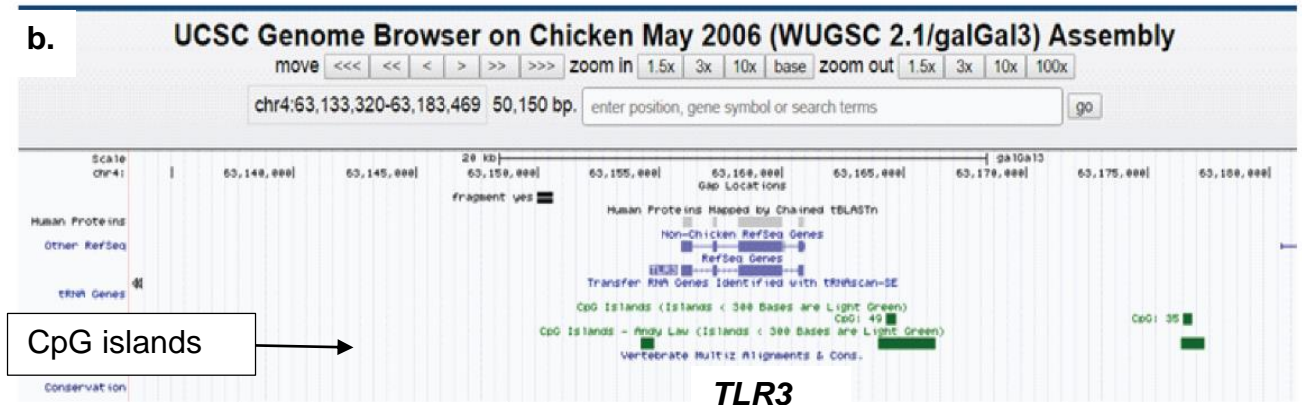


Figure 6.7: Chromatin profile and transcriptional activity of *TLR3* gene. a) Signal tracks are showing DNA enrichment in F1 fraction (blue vertical line), H3K4me3 track (red), H3K27ac (blue), H3R2me2s (green) and H4R3me2a (brown) arginine modifications. b) CpG islands were mapped along the *TLR3* gene using galGal3 UCSC genome browser. The green bar underneath the gene indicates the location of CpG islands.

Figure 6.8 demonstrates the chromatin profile of *IL1B* gene. *IL1B* gene was associated with acetylation or had salt solubility at the 5' end of the gene. This chromatin region is also associated with H3K27ac, H3R2me2s, and H4R3me2a. Also, H3K27ac and H3R2me2s were distributed at a low level along the gene body of *IL1B*. Five prime upstream of the gene there was a F1 peak associated with H3K27ac, H3R2me2s and H4R3me2a, possibly marking a putative enhancer or regulatory region to that site. Downstream of the gene there was strong a peak for H3K4me3 that aligned with H3K27ac, suggestive of an active promoter. However, in the reference genome, there was no gene annotated for that location, suggesting the presence of a putative noncoding gene.

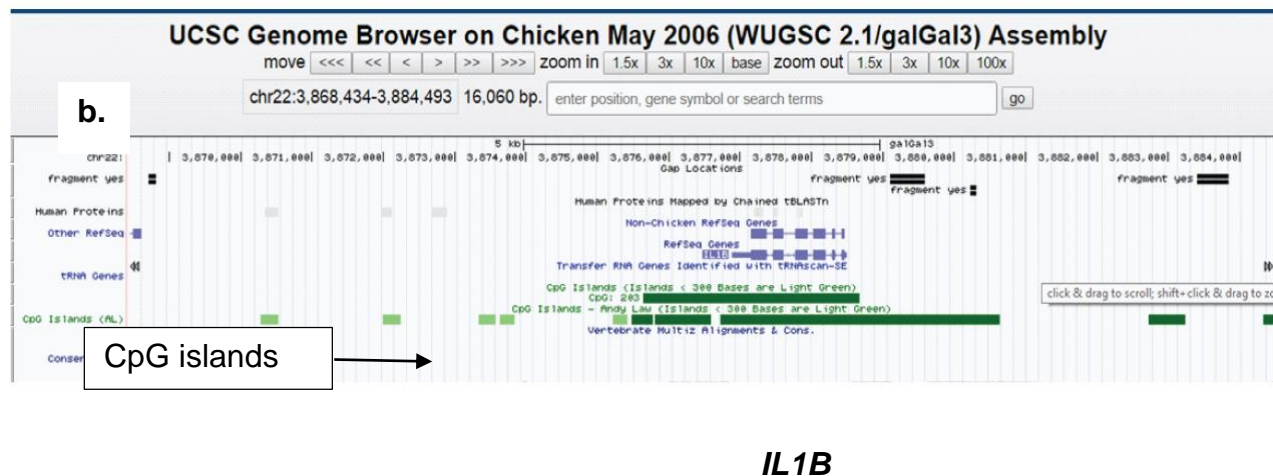
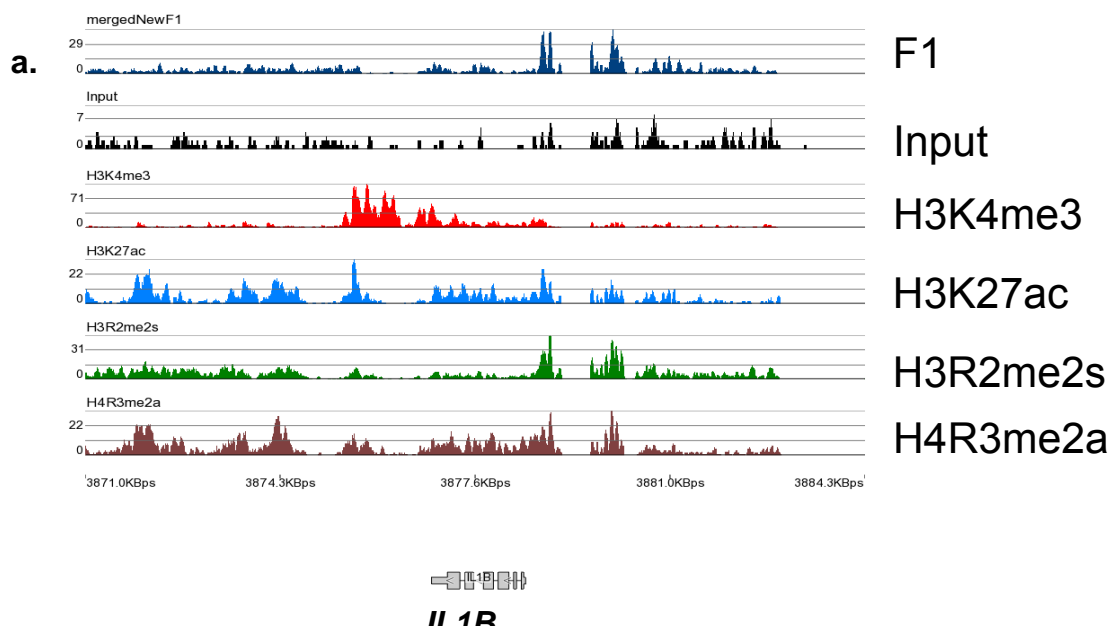
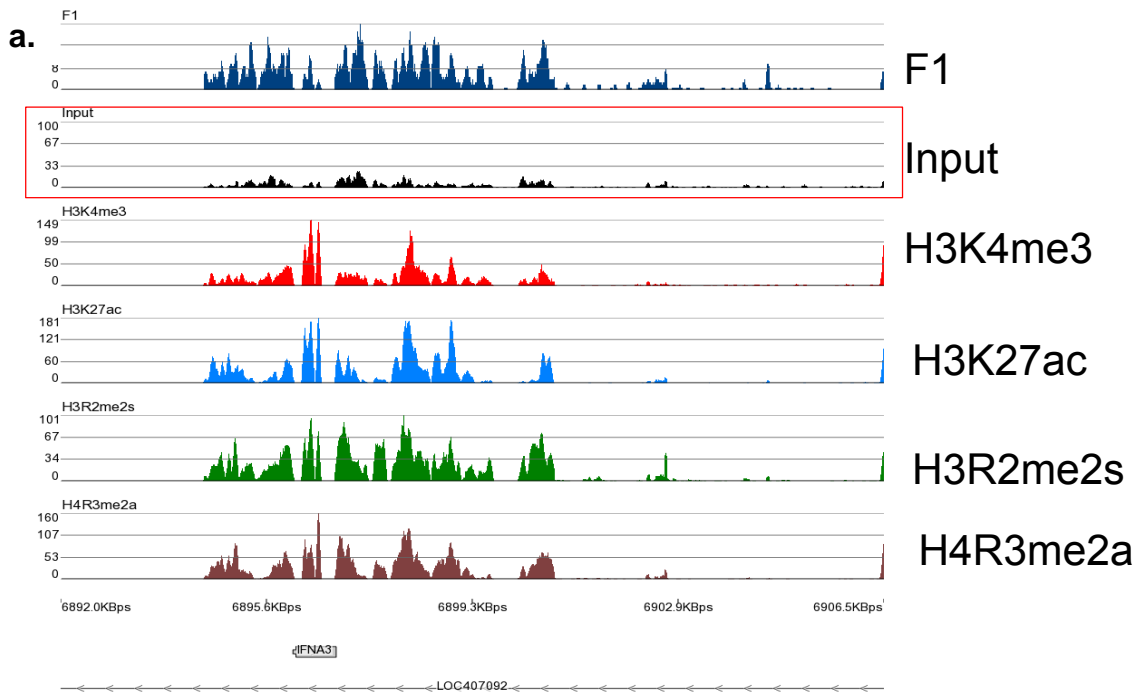


Figure 6.8: Chromatin profile and transcriptional activity of *IL1B* gene. a) Signal tracks showing DNA enrichment in F1 fraction (blue), H3K4me3 (red), H3K27ac (blue), H3R2me2s (green) and H4R3me2a (brown) arginine modifications. b) CpG islands were mapped along the *IL1B* gene using galGal3 UCSC genome browser. The green bar underneath the gene indicates the location of CpG islands.

However, the *IL15* gene, which is moderately expressed in polychromatic erythrocytes, had a low level of F1 enrichment at the 5' end of the gene and low levels of H3K4me3, H3K27ac, H3R2me2s and H4R3me2a at the 3' end of the second intron of the gene (**Figure S6.9a**). The gene did not

map with any CpG islands (**Figure S6.9b**). We also analyzed the negative feedback gene for the innate immunity gene, *TRAFD1* (**Figure S6.4 and S6.11**). *TRAFD1* had moderate expression level in both 6C2 and polychromatic erythrocytes. F1 enrichment peaked only at the 5' end, and the gene had an association with CpG islands, H3K4me3, H3K27ac, H3R2me2s and H4R3me2a (**Figure S6.11**). *NFKB2* (Nuclear Factor Kappa B Subunit 2), which is involved in the production of inflammatory cytokines, had F1 enrichment, and associated with a CpG island and all tested active histone modifications along the gene body (**Figure S6.12**).



IFNA3

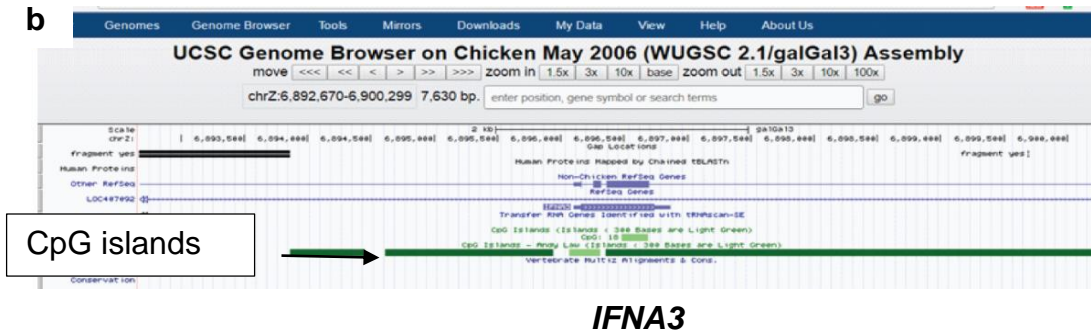


Figure 6.9: Chromatin profile and transcriptional activity of *IFNA3* gene. a) Signal tracks showing DNA enrichment in F1 fraction (blue), H3K4me3 (red), H3K27ac (blue), H3R2me2s (green) and H4R3me2a (brown) arginine modifications. b) CpG islands were mapped along the *IFNA3* and *IFNW1* gene using galGal3 UCSC genome browser. The green bar underneath the gene indicates the location of CpG islands.

Similarly, we characterized the association of H3K4me3, H3K27ac, H3R2me2s, and H4R3me2a with the *IFNW1* gene. This gene was enriched in F1 fraction along the entire gene, low level of enrichment for H3K27ac and strong enrichment for H3R2me2s and H4R3me2a. Upstream of the *IFNW1* gene, there was a strong peak for F1, H3K4me3, H3K27ac, H3R2me2s, and H4R3me2a (**Figure S6.10**). We also observed that a long gene was transcribing from the antisense strand (sense to the *IFN* genes) covering the entire *IFNA3* and *IFNW1* loci (**Figure 6.9 and S6.10**). Moreover, a CpG island was mapped along the *IFNA3* and the *IFNW1* loci (**Figure 6.9b, S6.10**). Strikingly, we observed peaks in the input DNA along *IFNA3* gene body (**Figure 6.9 a**). it should be noted that there is evidence that mechanical shearing of DNA unbiased towards DNA sequence. This observation suggest that there is a feature of chromatin susceptible of breakage at this region, indicating that the chromatin in this region is unstable, contain labile nucleosome.

6.3.5 Induction of immune genes in polychromatic cells

We determined whether the immune genes analyzed for their chromatin profile could be induced by using an immune stimulant. For this purpose, gene expression was analyzed using total RNA isolated from poly I:C treated polychromatic erythrocytes (**Figure 6.10**). First, we separated erythrocytes from white blood cells using centrifugation steps and performed microscopy to confirm proper separation (**Figure S6.13**). Similar caution was maintained for other experiments in this study. Gene expression was normalized with the reference gene *18srRNA*. Poly I:C is a synthetic analog for double-stranded RNA virus and stimulates innate immunity via the TLR3

mediated pathway. Changes in gene expression was calculated by comparing with the expression level of the gene in untreated samples collected from each time point (**Figure 6.10**). At 3 hours of post-treatment, *IL1B* shows highest fold change, at 6 hour *TLR3*, at 12 hour *IRF1* and 24 hour *IL15*, *TLR21*, *CIAPIN*, and *TIRAP1*.

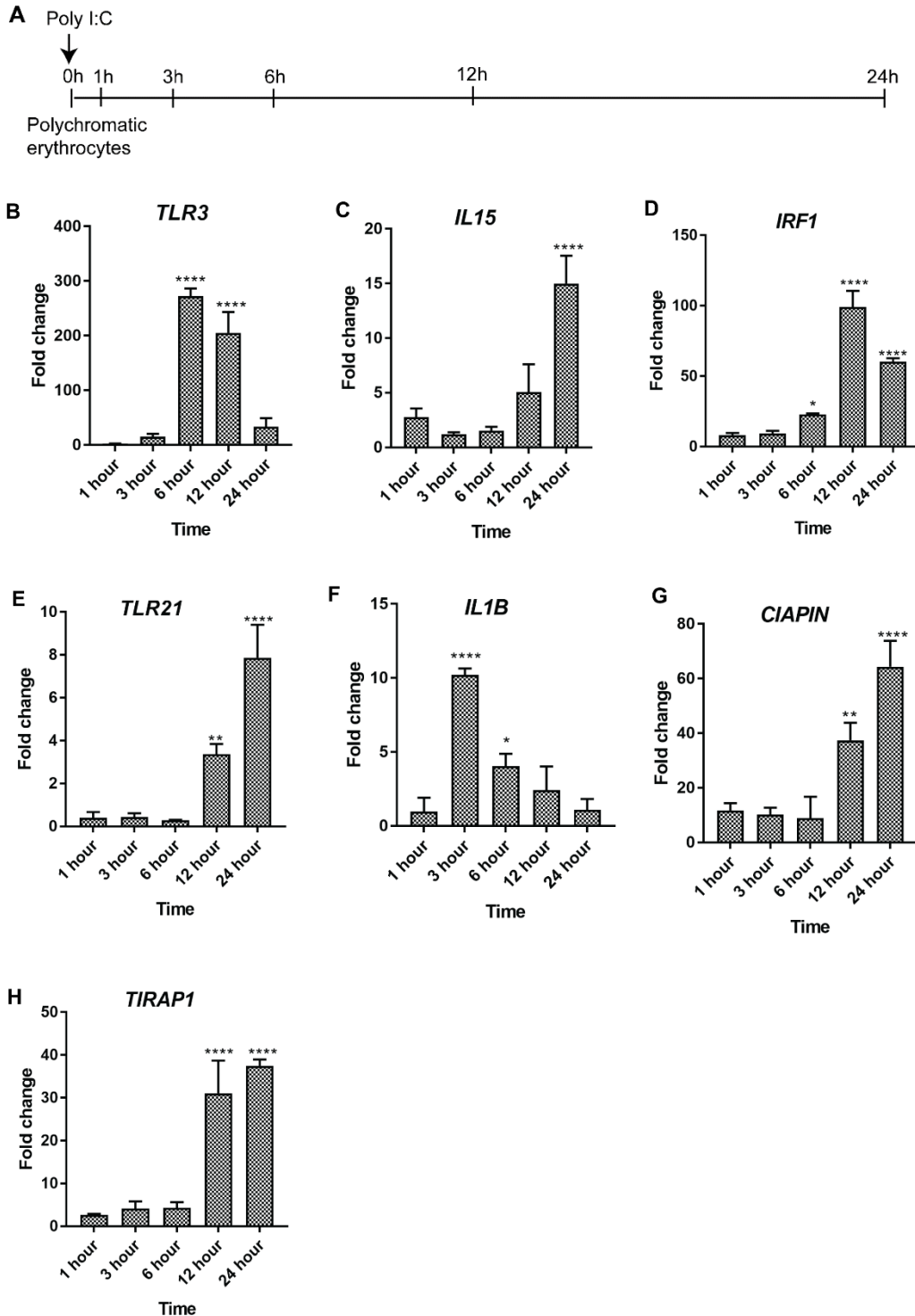


Figure 6.10: Poly I:C mediated induction of immune genes in chicken polychromatic erythrocytes. Gene expression was normalized with *18sRNA* for each gene. Fold change was calculated by comparing with untreated samples for each time point. Error bars represent the standard error of the mean from three independent experiments. Statistical significance was calculated in reference to the 1 hour treatment using One-way ANOVA * $P < 0.05$, ** $P < 0.01$, *** $P < 0.001$ or **** $P < 0.0001$.

6.4 Discussion

Several components of the immune modulatory pathway regulate innate immunity at multiple layers in response to invading microorganisms. We presented here a possible mechanism where epigenetic modifications such as H3K4me, H3K27ac, H4R3me2a, and H3R2me2s could be responsible for the rapid induction of innate immune genes upon infection in chicken polychromatic erythrocytes. We found several of the immune genes are poorly expressed, while others are highly expressed under unstimulated condition. Further, it could be assumed that these low expressing genes may have been induced earlier after the exposure of chickens to some infectious agents and then went back to a low steady-state level of expression.

Chicken erythrocytes express several immune genes that are mostly involved in the innate immune regulation. In the current study, RNA-seq analysis revealed the low-level expression of *TLR3*, *TLR2*, *TLR4*, *TLR5*, *TLR6*, *TLR7*, *TLR21*, *TLR15*, and this was observed in chicken polychromatic erythrocytes and 6C2 cells. This finding is consistent with two previous reports where constitutive expression of *TLR2*, *TLR3*, *TLR4*, *TLR5*, and *TLR21* was observed in chicken mature erythrocytes [322, 358]. These studies utilized a rigorous procedure to isolate approximately >99% pure erythrocytes to reduce the possibility of mixing with white blood cells.

There is a high degree of homology between chicken *TLR* genes 1, 3, 5, 6, 7 and 10 with their human orthologues along with several components in the TLR pathway [463]. Expression of *TLRs* is mostly found within immunological cells. However, several reports have shown that the expression of *TLRs* in chicken fibroblasts and epithelial cells as well [463, 464]. Toll-like receptors mainly function by recognizing different patterns from infectious agents and signal to activate innate and adaptive immunity. Expression of these receptors, other than in immune cells, extends the possibility of these receptors play a role in innate immune defense mechanisms. In the chicken

polychromatic erythrocytes, a wide range of *TLR* family gene expression indicates that erythrocytes can play a role in recognizing the bacterial or viral antigen.

In chicken polychromatic erythrocytes, we found a low level of expression of several interleukins such as *IL1B*, *IL2*, *IL3*, *IL5*, *IL7*, *IL8*, *IL9*, *IL10*, *IL16*, *IL18*, and *IL22*. Moderate to high level of expression was observed for interleukin 15. *IL1B* is a classical pro-inflammatory cytokine secreted from macrophages only after stimulation by a bacterial antigen. After the activation through TLR and MDA5 mediated pathway, IL1B secretion occurs; this can act as a signal amplifier to signal for macrophages to accumulate in the inflammation site [465]. Similar to *IL1B*, *IL18* is interleukin 1 superfamily pro-inflammatory cytokine that is activated by TLRs. On the other hand, *IL10* is an anti-inflammatory cytokine as it downregulates the production of Th1 mediated cytokine production [466]. *IL22* is a member of *IL10* superfamily, and it is involved in the generation of innate immune defense in epithelial cells such as respiratory and gut epithelial cells [467]. *IL3* participates in the regulation of hematopoiesis and differentiation of myeloid progenitor cells. In combination with *IL7*, *IL3* regulates the differentiation of multipotent stem cell into lymphoid progenitor cells [468]. Cytokine *IL5* is involved in immunoglobulin secretion and B-cell differentiation [469]. *IL8* is a chemokine that induces the target cell to migrate to the infection site [470]. Thus, *IL8* is an important modulator of the innate immune defense system. Similar to *IL8*, *IL16* acts as a chemoattractant for the cell containing CD4 surface molecule and therefore attracts activated T-cells to the site [471]. *IL15* is expressed in a wide range of tissues including nerve cell, fibroblast, dendritic cell, macrophages, and monocytes. This cytokine stimulates the production of T-cell and Natural Killer cells upon viral infection [472]. In CD8⁺T cells *IL15* enhances the antitumor immunity, which has made it a promising therapeutic tool in pre-clinical trials [473]. In the current study, we found moderate expression of this interleukin, which led us to consider that the chickens might have had a prior viral infection. Future studies will require characterizing the induction pattern of *IL15* in erythrocytes further.

Chemokines such as *CCL1*, *4*, *5*, *20*, *CXCL12* and *CXCL14* were present in low levels in polychromatic erythrocytes. Among the type I interferons, *IFNA3* and IFN β and type II interferon *IFNG* were found to be expressed in polychromatic erythrocytes. We found the immune adaptor protein *TIRAP* gene had moderate expression. High level of expression of interferon regulatory transcription factor *IRF1* and a moderate level of expression of *IRF2* and *IRF7* was observed.

Conversely, a low degree of expression was observed for *IRF4*, *IRF8*, and *IRF10*. Expression of interferon and interferon regulatory factors under unstimulated conditions could be explained by the fact that these chickens may have encountered prior exposure to an infection. Moreover, our record shows that a sporting event took place in the stadium near the animal house and the noise from the game agitated the chickens. It has been previously demonstrated that stress could potentially lead to a differential immune response [474-476].

Further, we addressed the epigenomic features of the immune genes observed in chicken polychromatic erythrocytes using ChIP-seq assays. We included low, moderately and highly expressed immune genes to determine the relationship between levels and location of H3K4me3, H3K27ac, H3R2me2s and H4R3me2a with transcription levels. Based on the features, we identified three different chromatin types for the immune genes. Type I chromatin include highly and moderately expressed immune genes such as *IRF1* and *IRF7*. Chromatin of this group of genes has salt solubility distributed along the entire gene as well as expanded in the nearby regulatory region. The 5' end of these genes is associated with H3K4me3, H3K27ac, H4R3me2a and H3R2me2s which align with accessible chromatin region and CpG island (compared with UCSC galGAL3 genome browser). These genes harbour nearby putative enhancers that associated with eRNA, H3K27ac, H3R2me2s, and H4R3me2a. Type II chromatin, which includes low expressing gene in polychromatic erythrocyte cells such as *TLR3* and *TLR21*, has a salt solubility at the upstream promoter region, associated with CpG islands along the binding of H3K4me3, H3K27ac, H3R2me2s and H4R3me2a to the site and nearby putative enhancer associated with H3K27ac, H3R2me2s, and H4R3me2a.

Type IV chromatin include some immune genes that show low levels of transcripts but have a strong peak for active histone PTMs. We looked at two interleukins, *IL1B* and *IL15*; these are very low and moderately expressing genes in chicken polychromatic erythrocytes, respectively. *IL1B* is aligned along with CpG islands along the gene and 3' downstream of the gene. This gene has salt-solubility at the promoter region, which is associated with H3K27ac, H3R2me2s, and H4R3me2a. Antisense transcript for the gene was detected from the positive strand of the *IL1B* gene. We identified F1 enrichment upstream of the 5' end of the gene, which was associated with H3K27ac, H3R2me2s, and H4R3me2a. Antisense and bidirectional transcript for *IL1B* have been reported earlier, emphasizing its role in chromatin structure modulation in murine macrophage cell

line RAW 264.7 [477]. Downstream of *IL1B* gene, there is a CpG island, which aligned with H3K4me3, H3K27ac and low level of H4R3me2a. This could signify the location of an active promoter. This needs to be explored further as it may address crucial details regarding the regulation of innate immune genes and the involvement of non-coding RNA and chromatin modifications. On the other hand, *IL15* has a moderate level of gene expression and has a salt solubility at the 5' end of the gene. No CpG island is detected for this gene region in the genome browser. Low level of H3K4me3, H3K27ac, H3R2me2s, and H4R3me2a was present at the 3' end of second intron-exonic region.

Later, we compared these modifications in interferon genes such as *IFNA3* and *IFNWI*. Both genes are lowly expressed in polychromatic erythrocytes. *IFNA3* gene as well as regions upstream and downstream of the gene is salt-soluble. *IFNA3* gene region is probably organized with destabilized nucleosome making the region prone to sonication [478]. This is evident from the enrichment of peak for Formaldehyde-Assisted Isolation of Regulatory Elements (FAIRE-seq) for this region (data not shown). CpG islands lie across the entire genomic region and are associated with H3K4me3, H3K27ac, H3R2me2s, and H4R3me2a. The *IFNWI* gene, which lies upstream of the *IFNA3* gene, shows low salt-solubility along the gene body with low levels of enrichment for H3K27ac, H3R2me2s, and H4R3me2a. Upstream of the *IFNWI* gene, antisense transcripts co-localize with F1 enrichment, H3K4me3, H3K27ac, H3R2me2s, and H4R3me2a. This co-localization indicates the presence of putative regulatory elements at this region. We observed antisense transcripts spanning across both *IFNA3* and *IFNWI* gene that could be involved in regulating the expression of this gene.

In this study, we found a strong correlation of placement of the histone marks H3K4me, H3K27ac, H3R2me2s, and H4R3me2a with CpG islands. A CpG mediated mechanism is a possible recruitment system for these modifications along the gene body. We observed that genes lacking CpG islands in the gene body such as *IL15*, *TRAFD1*, *TLR3*, *IRF8* do not contain the broad distribution of H3K4me, H3K27ac, H3R2me2s and H4R3me2a along the gene body. Previously it was reported that H3K4me3 has a bias towards unmethylated CpG islands [442, 460]. It was reported that CXXC1, which is a component of SETD1A/B complex, could recognize and bind to unmethylated CpG island [479]. Thus, this is one of the possible mechanisms of recruitment of H3K4me3 to CpG sites. Furthermore, WDR5, a component of SETD1A/B complex, can recognize

H3R2me2s and therefore H3K4me3 co-localize with H3R2me2s [480]. This could be one of the possible routes by which both H3R2me2s and H3K4me3 co-localize with CpG islands. However, the mechanism of how H4R3me2a binds to the CpG sites remains elusive.

The literature on immune genes in chicken erythrocytes reported that these genes could be stimulated by various immune modulators [322, 358]. One of the stimulants used was poly I:C, which effectively induced the expression of several immune genes in chicken mature erythrocytes [322, 358]. We provided evidence in our study that using poly I:C, immune components such as *TLR3*, *TLR21*, *IL15*, *IL1B*, *IRF1*, *CIAPIN*, and *TIRAP1* are induced at different time points. Interestingly, consistent with previous findings, poly I:C of varying lengths stimulates varying repertoire of TLRs in chicken polychromatic erythrocytes (Data not shown) [389]. However, it needs more investigation to conclude regarding the length of poly I:C and its associated immune response in chicken erythrocytes. In future, it will be interesting to include gene expression levels from samples collected at zero hour time point as it will provide the information regarding the initial status/basal level of gene expression. Comparison of gene expression from treated and untreated group made the analysis more interesting as changes in gene expression due to nutrients or environmental factor was comparable from poly I:C induced changes. Finally, it will be important to determine whether with the distribution of epigenetic marks analyzed in the current study can change as well with the induction of the gene.

In conclusion, we not only demonstrated that chicken polychromatic erythrocytes constitutively express innate immune components under the unstimulated condition, but these genes have unique epigenomic features. These epigenetic modifications are tightly associated with CpG islands. We have demonstrated for the first time the epigenomic features of innate immune genes in chicken polychromatic erythrocytes and speculate that altogether this could be a mechanism of regulating the expression of these genes in these cells.

6.5 Methods

6.5.1 Cell culture and Treatment

Chicken polychromatic erythrocytes and 6C2 cells were used in the study. Chicken polychromatic erythrocytes were collected from the anemic chicken as described in Chapter II. 6C2 cells are chicken erythroleukemia line representing a colony-forming unit stage of erythroid development

[481]. Polychromatic cells were treated with 50ug/ml of poly I:C (Polyinosinic: polycytidylic acid) for either 1, 3, 6, 12 and 24 hours.

6.5.2 RNA extraction and RT-PCR

RNA from polychromatic erythrocytes was isolated using RNeasy Plus mini kit (Qiagen) following manufacturer's instructions. DNase (Promega) digestion was performed to remove any genomic DNA in the purified RNA. For qPCR analysis, complementary DNA (cDNA) was generated from purified total RNA (400 ng) using M-MLV reverse transcriptase and Oligo dT primers (Invitrogen). Quantitative real-time PCR was performed with F1 DNA (1.0 ng) and cDNA (2.0 ng) on SYBR Green real-time PCR on iCycler IQ5 (BioRad) in accordance with the conditions described in method section (**Chapter II**). Primers for the regions analyzed are described in Supplementary **Table S6.1**.

6.5.3 ChIP-seq on selected immune genes

ChIP-seq was performed according to the previously described protocol [285]. Briefly, nuclei were lysed after cross-linking of cells with 0.5% formaldehyde for 10 minutes, and chromatin was sheared to 250 bp using ultrasonic dismembrator (Fisher). The ChIP assays were performed with anti-H3K4me3 (Abcam), anti-H3R2me2s (Millipore), anti-H4R3me2a (Active motif) antibodies. Isotype-specific nonrelated IgG was used as a negative control for each ChIP assay. ChIP and input DNA was further processed, purified and quantitated using Qubit® 2.0 fluorometer (Life Technologies). Input and ChIP DNA quality was analyzed using 2000 Bioanalyzer (Agilent). ChIP-seq with chicken polychromatic erythrocytes was performed in two biological replicates using the same protocol (N=2).

6.5.3 Statistical analysis

All graphs and statistical analyses were performed using GraphPad Prism (version 6.0).

6.6 References

1. Palis J, Segel GB. Developmental biology of erythropoiesis. *Blood Rev.* 1998;12(2):106-14. PubMed PMID: 9661799.
2. Claver JA, Quaglia AI. Comparative morphology, development, and function of blood cells in nonmammalian vertebrates. *Journal of Exotic Pet Medicine.* 2009;18(2):87-97.
3. Morera D, MacKenzie SA. Is there a direct role for erythrocytes in the immune response? *Vet Res.* 2011;42:89. doi: 10.1186/1297-9716-42-89. PubMed PMID: 21801407; PubMed Central PMCID: PMC3199785.
4. Evans CJ, Hartenstein V, Banerjee U. Thicker than blood: conserved mechanisms in *Drosophila* and vertebrate hematopoiesis. *Dev Cell.* 2003;5(5):673-90. PubMed PMID: 14602069.
5. St Paul M, Paolucci S, Barjesteh N, Wood RD, Sharif S. Chicken erythrocytes respond to Toll-like receptor ligands by up-regulating cytokine transcripts. *Res Vet Sci.* 2013;95(1):87-91. doi: 10.1016/j.rvsc.2013.01.024. PubMed PMID: 23433682.
6. Morera D, Roher N, Ribas L, Balasch JC, Donate C, Callol A, et al. RNA-Seq reveals an integrated immune response in nucleated erythrocytes. *PLoS One.* 2011;6(10):e26998. doi: 10.1371/journal.pone.0026998. PubMed PMID: 22046430; PubMed Central PMCID: PMC3203173.
7. Medzhitov R. Recognition of microorganisms and activation of the immune response. *Nature.* 2007;449(7164):819-26. doi: 10.1038/nature06246. PubMed PMID: 17943118.
8. Nelson RA, Jr. The immune-adherence phenomenon; an immunologically specific reaction between microorganisms and erythrocytes leading to enhanced phagocytosis. *Science.* 1953;118(3077):733-7. PubMed PMID: 13122009.
9. Sennikov SV, Injelevskaya TV, Krysov SV, Silkov AN, Kovinev IB, Dyachkova NJ, et al. Production of hemo- and immunoregulatory cytokines by erythroblast antigen+ and glycoprotein A+ cells from human bone marrow. *BMC Cell Biol.* 2004;5(1):39. doi: 10.1186/1471-2121-5-39. PubMed PMID: 15488155; PubMed Central PMCID: PMC524510.
10. Passantino L, Altamura M, Cianciotta A, Patrino R, Tafaro A, Jirillo E, et al. Fish immunology. I. Binding and engulfment of *Candida albicans* by erythrocytes of rainbow trout (*Salmo gairdneri* Richardson). *Immunopharmacol Immunotoxicol.* 2002;24(4):665-78. doi: 10.1081/IPH-120016050. PubMed PMID: 12510797.
11. Passantino L, Massaro MA, Jirillo F, Di Modugno D, Ribaud MR, Modugno GD, et al. Antigenically activated avian erythrocytes release cytokine-like factors: a conserved phylogenetic function discovered in fish. *Immunopharmacol Immunotoxicol.* 2007;29(1):141-52. doi: 10.1080/08923970701284664. PubMed PMID: 17464774.
12. Akira S, Takeda K, Kaisho T. Toll-like receptors: critical proteins linking innate and acquired immunity. *Nat Immunol.* 2001;2(8):675-80. doi: 10.1038/90609. PubMed PMID: 11477402.
13. Keestra AM, de Zoete MR, Bouwman LI, van Putten JP. Chicken TLR21 is an innate CpG DNA receptor distinct from mammalian TLR9. *J Immunol.* 2010;185(1):460-7. doi: 10.4049/jimmunol.0901921. PubMed PMID: 20498358.

14. Jahan S, Xu W, He S, Gonzalez C, Delcuve GP, Davie JR. The chicken erythrocyte epigenome. *Epigenetics Chromatin*. 2016;9:19. doi: 10.1186/s13072-016-0068-2. PubMed PMID: 27226810; PubMed Central PMCID: PMC4879735.
15. Chen RA, Stempor P, Down TA, Zeiser E, Feuer SK, Ahringer J. Extreme HOT regions are CpG-dense promoters in *C. elegans* and humans. *Genome Res*. 2014;24(7):1138-46. doi: 10.1101/gr.161992.113. PubMed PMID: 24653213; PubMed Central PMCID: PMC4079969.
16. Barrera LO, Li Z, Smith AD, Arden KC, Cavenee WK, Zhang MQ, et al. Genome-wide mapping and analysis of active promoters in mouse embryonic stem cells and adult organs. *Genome Res*. 2008;18(1):46-59. doi: 10.1101/gr.6654808. PubMed PMID: 18042645; PubMed Central PMCID: PMC2134779.
17. Maunakea AK, Nagarajan RP, Bilenky M, Ballinger TJ, D'Souza C, Fouse SD, et al. Conserved role of intragenic DNA methylation in regulating alternative promoters. *Nature*. 2010;466(7303):253-7. doi: 10.1038/nature09165. PubMed PMID: 20613842; PubMed Central PMCID: PMC3998662.
18. Pal S, Gupta R, Kim H, Wickramasinghe P, Baubet V, Showe LC, et al. Alternative transcription exceeds alternative splicing in generating the transcriptome diversity of cerebellar development. *Genome Res*. 2011;21(8):1260-72. doi: 10.1101/gr.120535.111. PubMed PMID: 21712398; PubMed Central PMCID: PMC3149493.
19. Iqbal M, Philbin VJ, Smith AL. Expression patterns of chicken Toll-like receptor mRNA in tissues, immune cell subsets and cell lines. *Vet Immunol Immunopathol*. 2005;104(1-2):117-27. doi: 10.1016/j.vetimm.2004.11.003. PubMed PMID: 15661337.
20. Esnault E, Bonsergent C, Larcher T, Bed'hom B, Vautherot JF, Delaleu B, et al. A novel chicken lung epithelial cell line: characterization and response to low pathogenicity avian influenza virus. *Virus Res*. 2011;159(1):32-42. doi: 10.1016/j.virusres.2011.04.022. PubMed PMID: 21557972.
21. Rider P, Carmi Y, Guttman O, Braiman A, Cohen I, Voronov E, et al. IL-1alpha and IL-1beta recruit different myeloid cells and promote different stages of sterile inflammation. *J Immunol*. 2011;187(9):4835-43. doi: 10.4049/jimmunol.1102048. PubMed PMID: 21930960.
22. de Waal Malefyt R, Abrams J, Bennett B, Figdor CG, de Vries JE. Interleukin 10(IL-10) inhibits cytokine synthesis by human monocytes: an autoregulatory role of IL-10 produced by monocytes. *J Exp Med*. 1991;174(5):1209-20. PubMed PMID: 1940799; PubMed Central PMCID: PMC2119001.
23. Pestka S, Krause CD, Sarkar D, Walter MR, Shi Y, Fisher PB. Interleukin-10 and related cytokines and receptors. *Annu Rev Immunol*. 2004;22:929-79. doi: 10.1146/annurev.immunol.22.012703.104622. PubMed PMID: 15032600.
24. Ihle JN, Pepersack L, Rebar L. Regulation of T cell differentiation: in vitro induction of 20 alpha-hydroxysteroid dehydrogenase in splenic lymphocytes from athymic mice by a unique lymphokine. *J Immunol*. 1981;126(6):2184-9. PubMed PMID: 6971890.

25. Milburn MV, Hassell AM, Lambert MH, Jordan SR, Proudfoot AE, Graber P, et al. A novel dimer configuration revealed by the crystal structure at 2.4 Å resolution of human interleukin-5. *Nature*. 1993;363(6425):172-6. doi: 10.1038/363172a0. PubMed PMID: 8483502.
26. Hedges JC, Singer CA, Gerthoffer WT. Mitogen-activated protein kinases regulate cytokine gene expression in human airway myocytes. *Am J Respir Cell Mol Biol*. 2000;23(1):86-94. doi: 10.1165/ajrcmb.23.1.4014. PubMed PMID: 10873157.
27. Cruikshank W, Center DM. Modulation of lymphocyte migration by human lymphokines. II. Purification of a lymphotactic factor (LCF). *J Immunol*. 1982;128(6):2569-74. PubMed PMID: 7042841.
28. Steel JC, Waldmann TA, Morris JC. Interleukin-15 biology and its therapeutic implications in cancer. *Trends Pharmacol Sci*. 2012;33(1):35-41. doi: 10.1016/j.tips.2011.09.004. PubMed PMID: 22032984; PubMed Central PMCID: PMC3327885.
29. Klebanoff CA, Finkelstein SE, Surman DR, Lichtman MK, Gattinoni L, Theoret MR, et al. IL-15 enhances the in vivo antitumor activity of tumor-reactive CD8⁺ T cells. *Proc Natl Acad Sci U S A*. 2004;101(7):1969-74. doi: 10.1073/pnas.0307298101. PubMed PMID: 14762166; PubMed Central PMCID: PMC357036.
30. Dhabhar FS. Effects of stress on immune function: the good, the bad, and the beautiful. *Immunol Res*. 2014;58(2-3):193-210. doi: 10.1007/s12026-014-8517-0. PubMed PMID: 24798553.
31. Muralidharan S, Mandrekar P. Cellular stress response and innate immune signaling: integrating pathways in host defense and inflammation. *J Leukoc Biol*. 2013;94(6):1167-84. doi: 10.1189/jlb.0313153. PubMed PMID: 23990626; PubMed Central PMCID: PMC3828604.
32. Priyadarshini S, Aich P. Effects of psychological stress on innate immunity and metabolism in humans: a systematic analysis. *PLoS One*. 2012;7(9):e43232. doi: 10.1371/journal.pone.0043232. PubMed PMID: 23028447; PubMed Central PMCID: PMC3446986.
33. Lu J, Wu X, Hong M, Tobias P, Han J. A potential suppressive effect of natural antisense IL-1β RNA on lipopolysaccharide-induced IL-1β expression. *J Immunol*. 2013;190(12):6570-8. doi: 10.4049/jimmunol.1102487. PubMed PMID: 23677478; PubMed Central PMCID: PMC3690360.
34. Tsompana M, Buck MJ. Chromatin accessibility: a window into the genome. *Epigenetics Chromatin*. 2014;7(1):33. doi: 10.1186/1756-8935-7-33. PubMed PMID: 25473421; PubMed Central PMCID: PMC34253006.
35. Davie JR, Xu W, Delcuve GP. Histone H3K4 trimethylation: dynamic interplay with pre-mRNA splicing. *Biochem Cell Biol*. 2016;94(1):1-11. doi: 10.1139/bcb-2015-0065. PubMed PMID: 26352678.
36. Tate CM, Lee JH, Skalnik DG. CXXC finger protein 1 restricts the Setd1A histone H3K4 methyltransferase complex to euchromatin. *FEBS J*. 2010;277(1):210-23. doi: 10.1111/j.1742-4658.2009.07475.x. PubMed PMID: 19951360; PubMed Central PMCID: PMC2806598.

37. Binda O. On your histone mark, SET, methylate! *Epigenetics*. 2013;8(5):457-63. doi: 10.4161/epi.24451. PubMed PMID: 23625014; PubMed Central PMCID: PMC3741215.
38. Mian MF, Ahmed AN, Rad M, Babaian A, Bowdish D, Ashkar AA. Length of dsRNA (poly I:C) drives distinct innate immune responses, depending on the cell type. *J Leukoc Biol*. 2013;94(5):1025-36. doi: 10.1189/jlb.0312125. PubMed PMID: 23911868.
39. Jin C, Felsenfeld G. Distribution of histone H3.3 in hematopoietic cell lineages. *Proc Natl Acad Sci U S A*. 2006;103(3):574-9. doi: 10.1073/pnas.0509974103. PubMed PMID: 16407103; PubMed Central PMCID: PMC1334668.

6.7 Supporting informations

6.7 Supporting informations

6.7.1 Supporting figures

6.7.1.1 Transcriptome profile of several immune genes

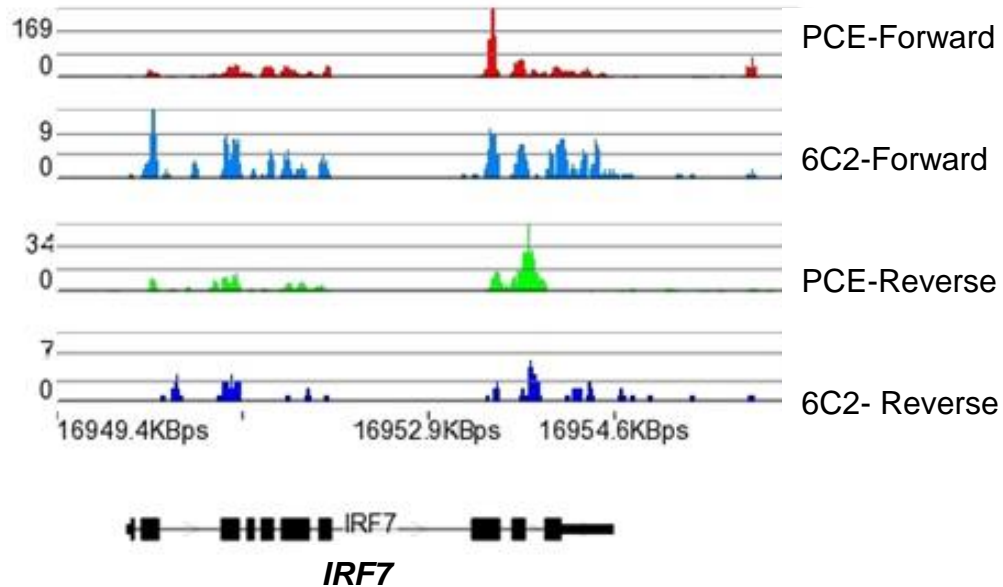


Figure S6.1. Transcriptional activity of *IRF7* in chicken erythrocytes. First track in red is the forward strand from RNA-seq performed in polychromatic erythrocyte cells, blue track below is the forward strand from RNA-seq performed in 6C2 chicken erythrocyte cell line. The last two tracks are the transcript from reverse strand from polychromatic erythrocytes and 6C2 cell line respectively. **PCE:** polychromatic erythrocytes, **6C2:**chicken erythrocyte cell line, **Forward:** forward strand of transcript, **Reverse:** reverse strand of transcript.

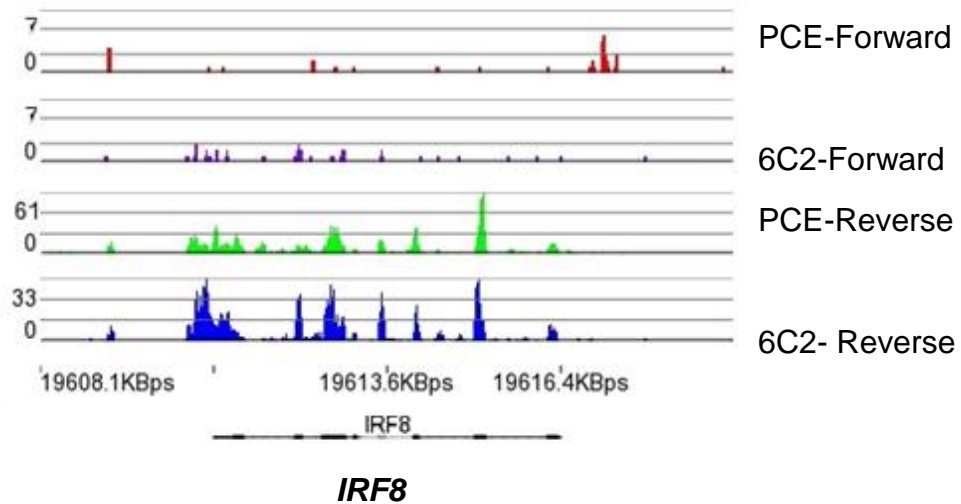


Figure S6.2. Transcriptional activity of *IRF8* in chicken erythrocytes. First track in red is the forward strand from RNA-seq performed in polychromatic erythrocytes, blue track below is the forward strand from RNA-seq performed in 6C2 chicken erythrocyte leukemia cell line. The last two tracks are the transcript from reverse strand from polychromatic erythrocyte cells and 6C2 cell line respectively. **PCE:** polychromatic erythrocytes, **6C2:** chicken erythrocyte leukemia cell line, **Forward:** forward strand of transcript, **Reverse:** reverse strand of transcript.

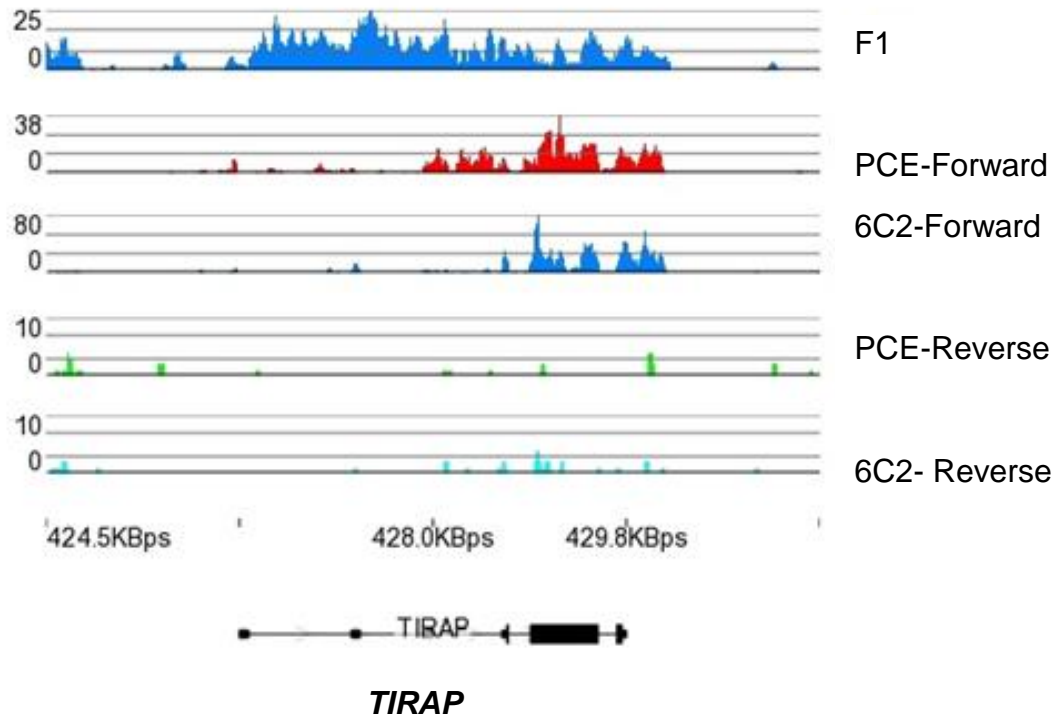


Figure S6.3. Transcriptional activity of *TIRAP* in chicken erythrocytes. First track in blue is the F1 enrichment for *TIRAP* gene. Beneath red is the forward strand from RNA-seq performed in polychromatic erythrocyte cells, blue track below is the forward strand from RNA-seq performed in 6C2 chicken erythrocyt leukemia cell line. The last two tracks are the transcript from reverse strand from polychromatic erythrocytes and 6C2 cell line respectively. **PCE**: polychromatic erythrocyte cells, **6C2**: chicken erythrocyt leukemia cell line, **Forward**: forward strand of transcript, **Reverse**: reverse strand of transcript.

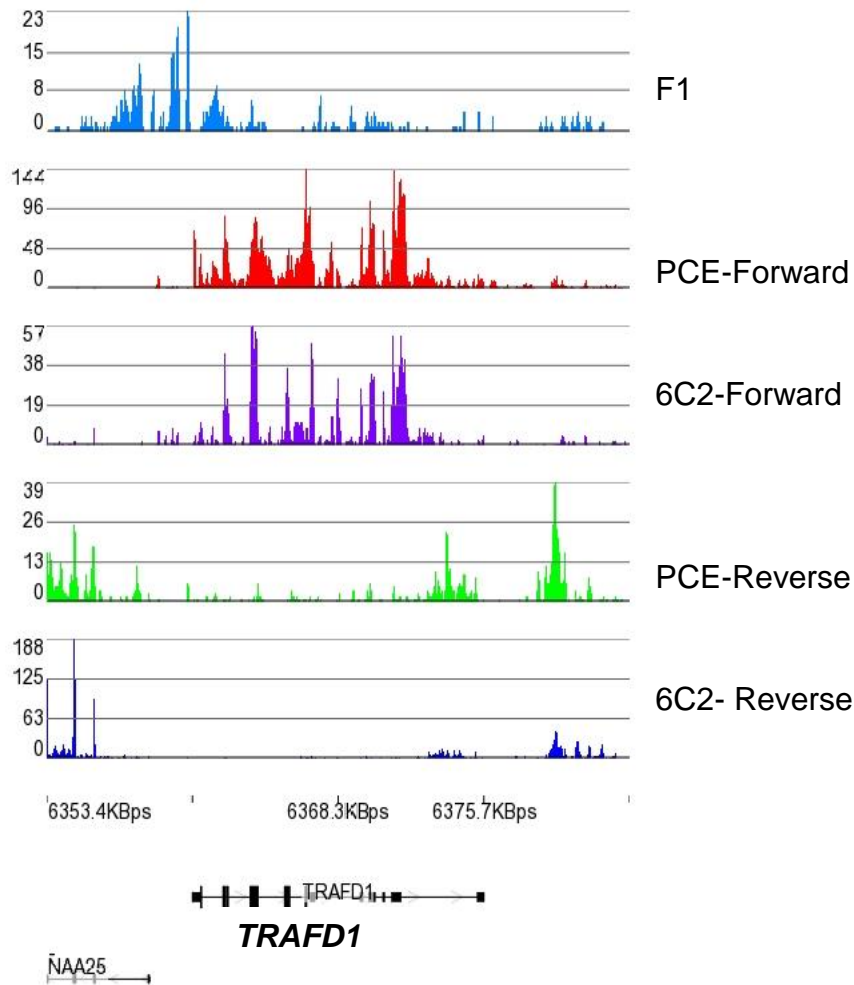


Figure S6.4. Transcriptional activity of *TRAFD1* in chicken erythrocytes. First track in red is the forward strand from RNA-seq performed in polychromatic erythrocyte cells, blue track below is the forward strand from RNA-seq performed in 6C2 chicken erythrocyte cell line. The last two tracks are the transcript from reverse strand from polychromatic erythrocyte cells and 6C2 cell line respectively. **PCE**: Polychromatic erythrocytes, **6C2**: chicken erythrocyte cell line, **Forward**: forward strand of transcript, **Reverse**: reverse strand of transcript.

6.7.1.2 Chromatin profile of several immune genes in polychromatic erythrocytes

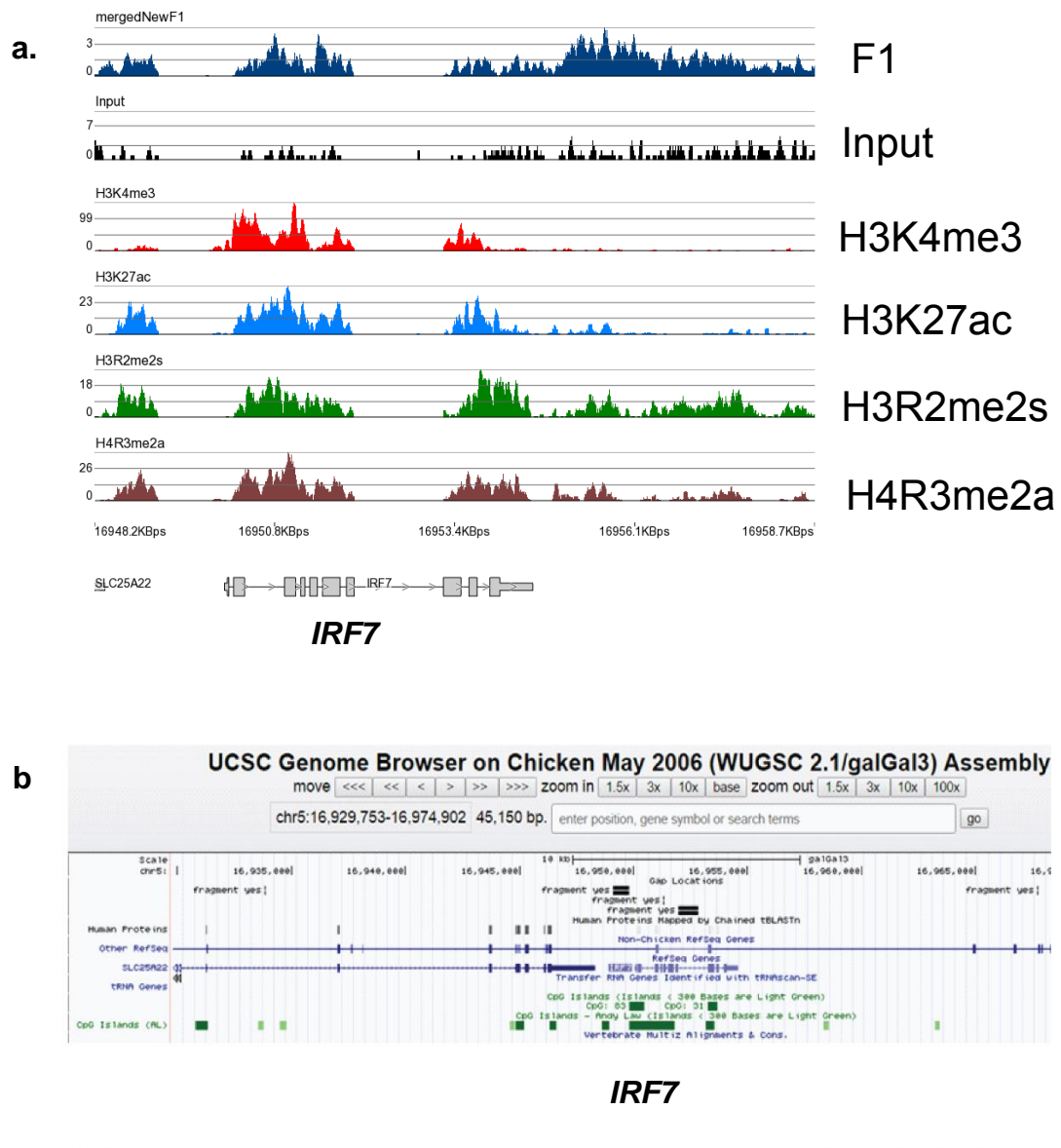


Figure S6.5. Chromatin profile and transcriptional activity of IRF7 gene. **a)** Signal tracks showing DNA enrichment in F1 fraction (blue), H3K4me3 (red), H3K27ac (blue), H3R2me2s (green) and H4R3me2a (brown) arginine modifications. **b)** CpG island was mapped with IRF7 gene using galGal3 UCSC genome browser. Green bar under the gene indicate CpG island.

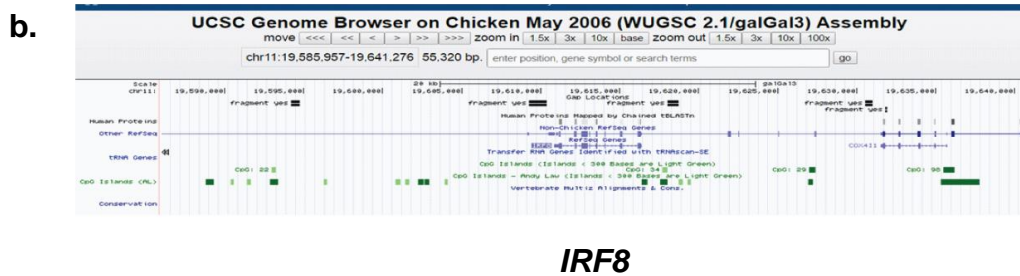
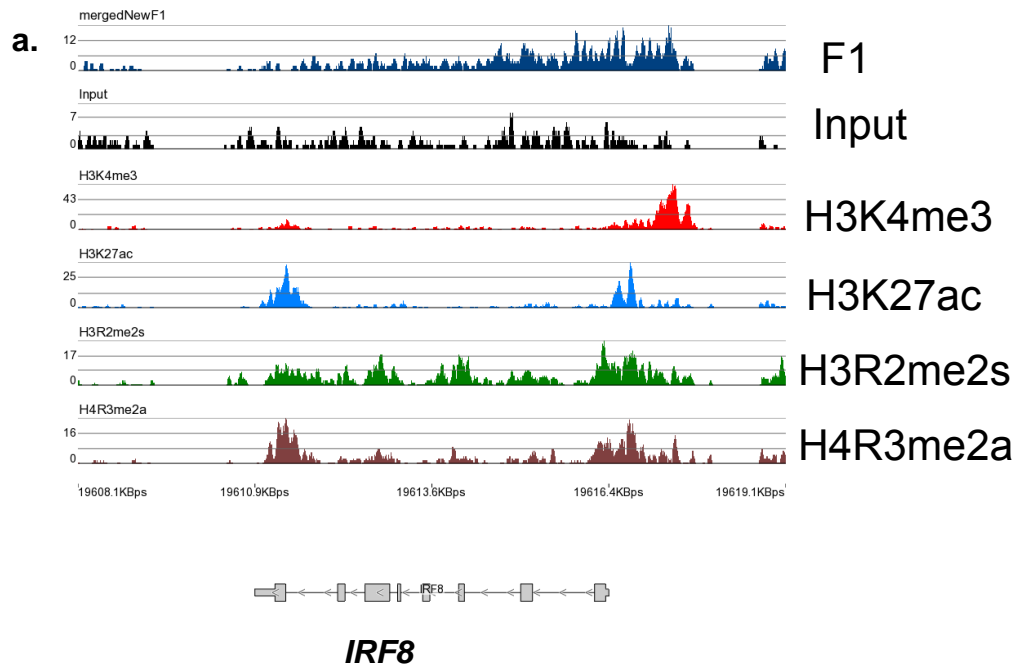


Figure S6.6. Chromatin profile and transcriptional activity of *IRF8* gene. a) Signal tracks showing DNA enrichment in F1 fraction (blue), H3K4me3 (red), H3K27ac (blue), H3R2me2s (green) and H4R3me2a (brown) arginine modifications. b) CpG island was mapped with *IRF8* gene using galGal3 UCSC genome browser. Green bar under the gene indicate CpG island.

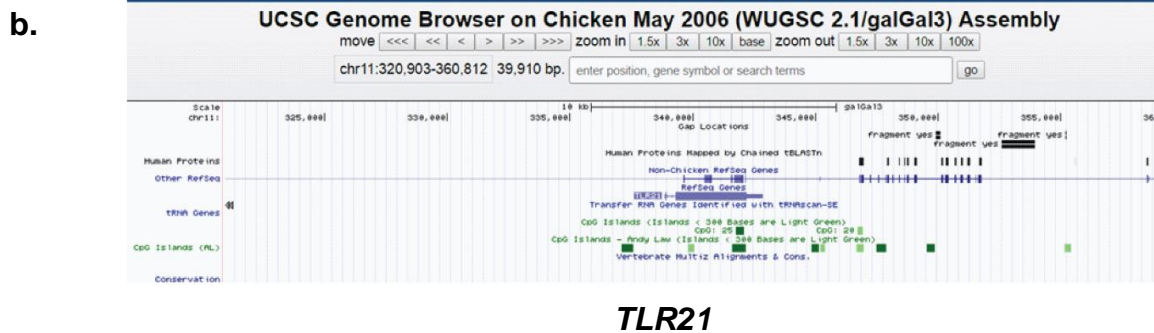
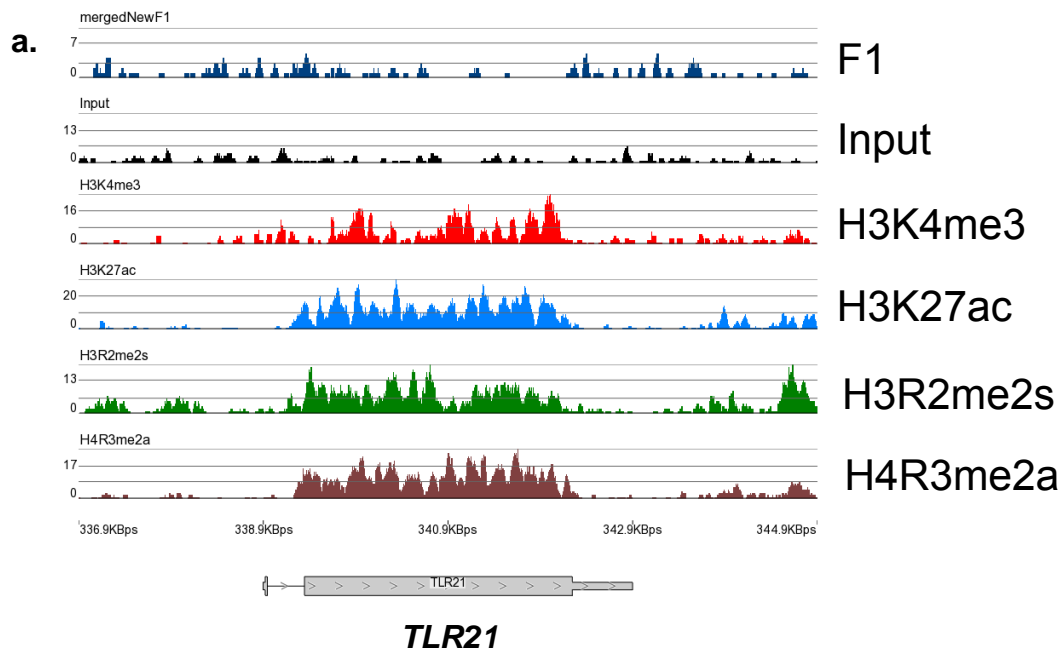


Figure S6.7. Chromatin profile and transcriptional activity of *TLR21* gene. **a)** Signal tracks showing DNA enrichment in F1 fraction (blue), H3K4me3 (red), H3K27ac (blue), H3R2me2s (green) and H4R3me2a (brown) arginine modifications. **b)** CpG island was mapped with *TLR21* gene using galGal3 UCSC genome browser. Green bar under the gene indicate CpG island.

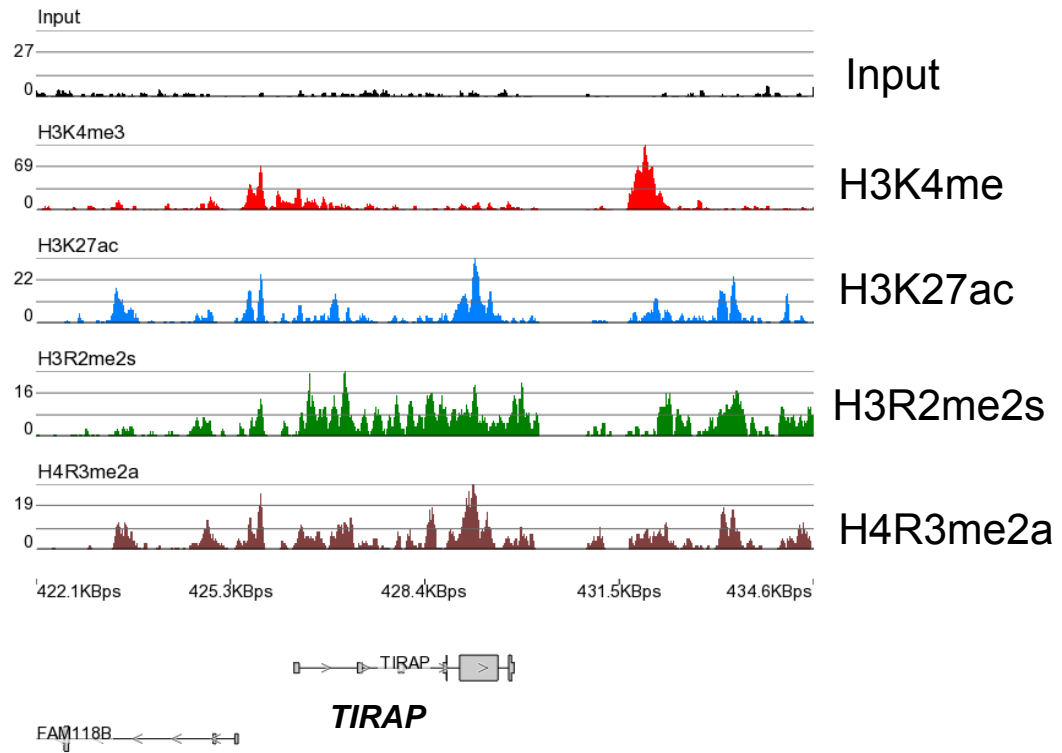


Figure S6.8. Chromatin profile and transcriptional activity of *TIRAP* gene. Signal tracks showing DNA enrichment in F1 fraction (blue), H3K4me3 (red), H3K27ac (blue), H3R2me2s (green) and H4R3me2a (brown) arginine modifications.

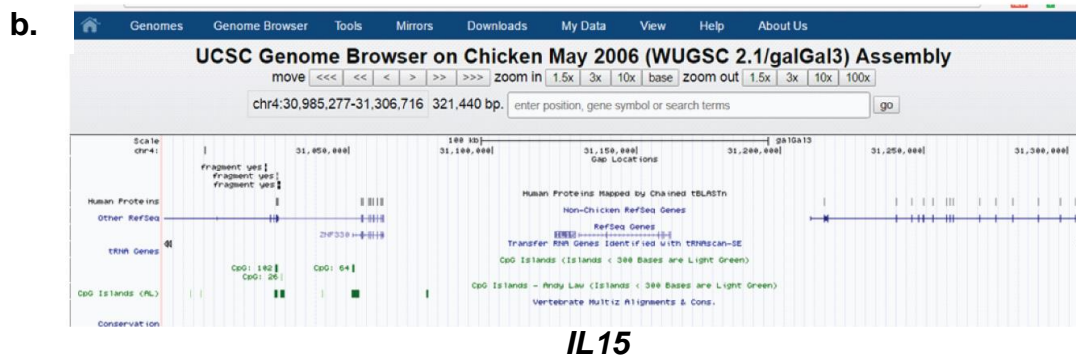
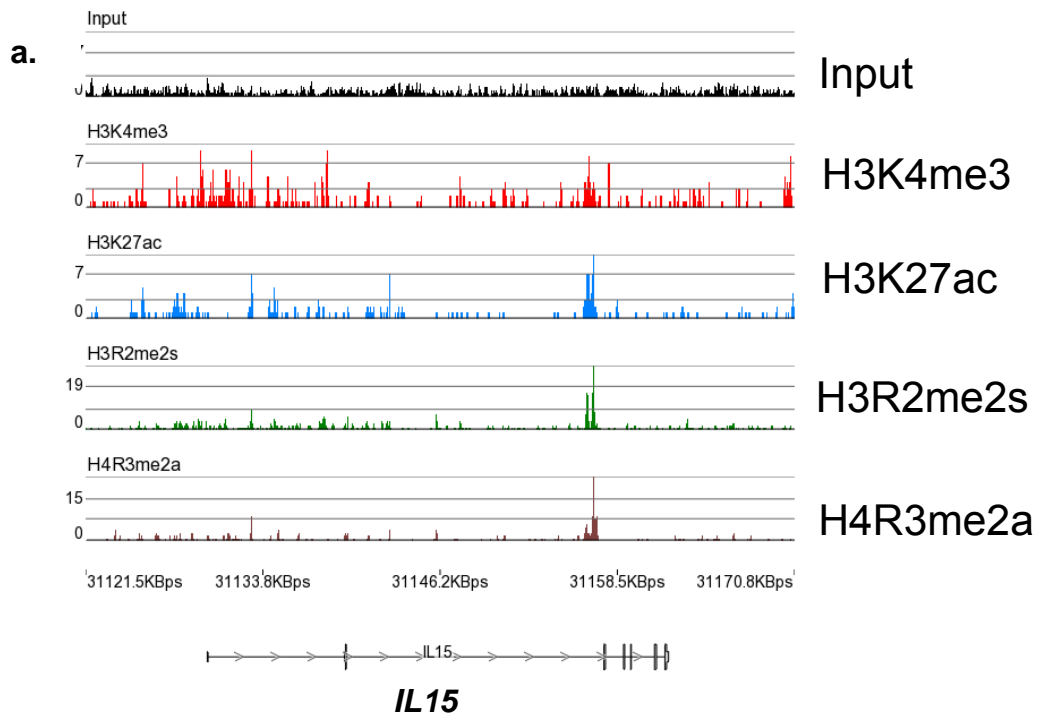


Figure S6.9. Chromatin profile and transcriptional activity of *IL15* gene. **a)** Signal tracks showing DNA enrichment in F1 fraction (blue), H3K4me3 (red), H3K27ac (blue), H3R2me2s (green) and H4R3me2a (brown) arginine modifications. **b)** CpG island was mapped with *IL15* gene using galGal3 UCSC genome browser. Green bar under the gene indicate CpG island.

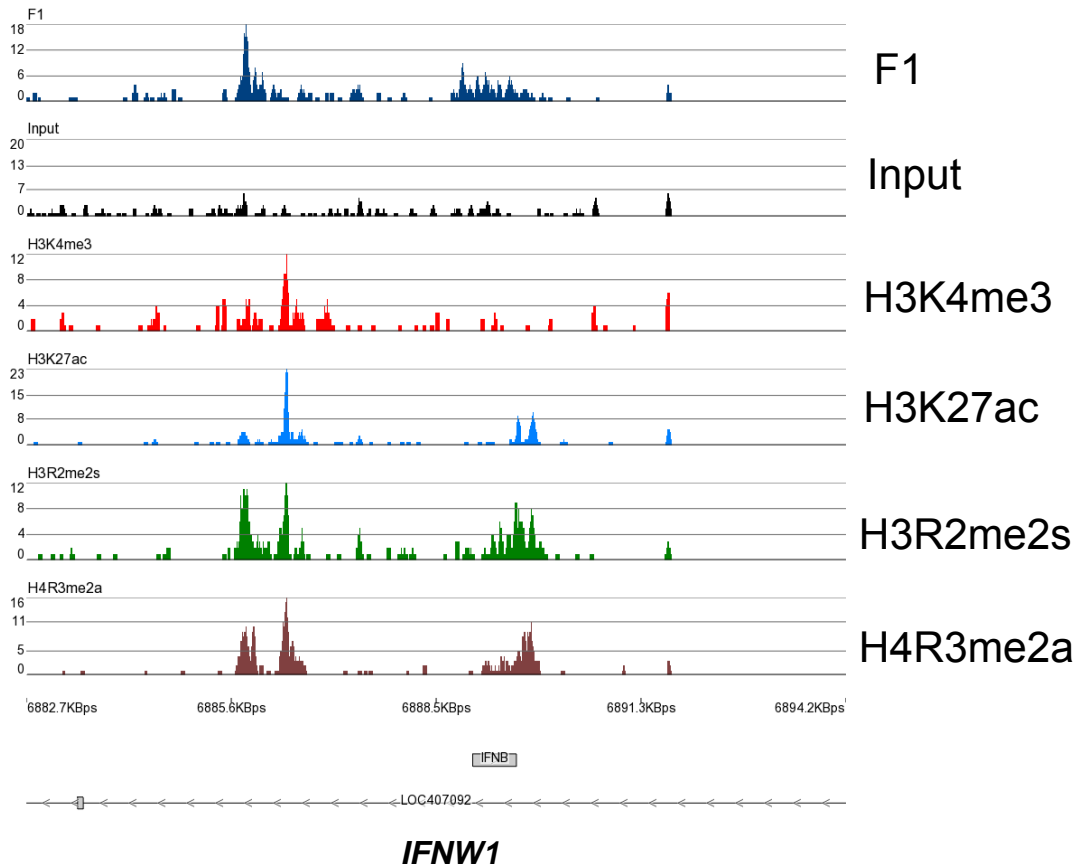


Figure S6.10. Chromatin profile and transcriptional activity of *IFNW1* gene. Signal tracks showing DNA enrichment in F1 fraction (blue), H3K4me3 (red), H3K27ac (blue), H3R2me2s (green) and H4R3me2a (brown) arginine modifications.

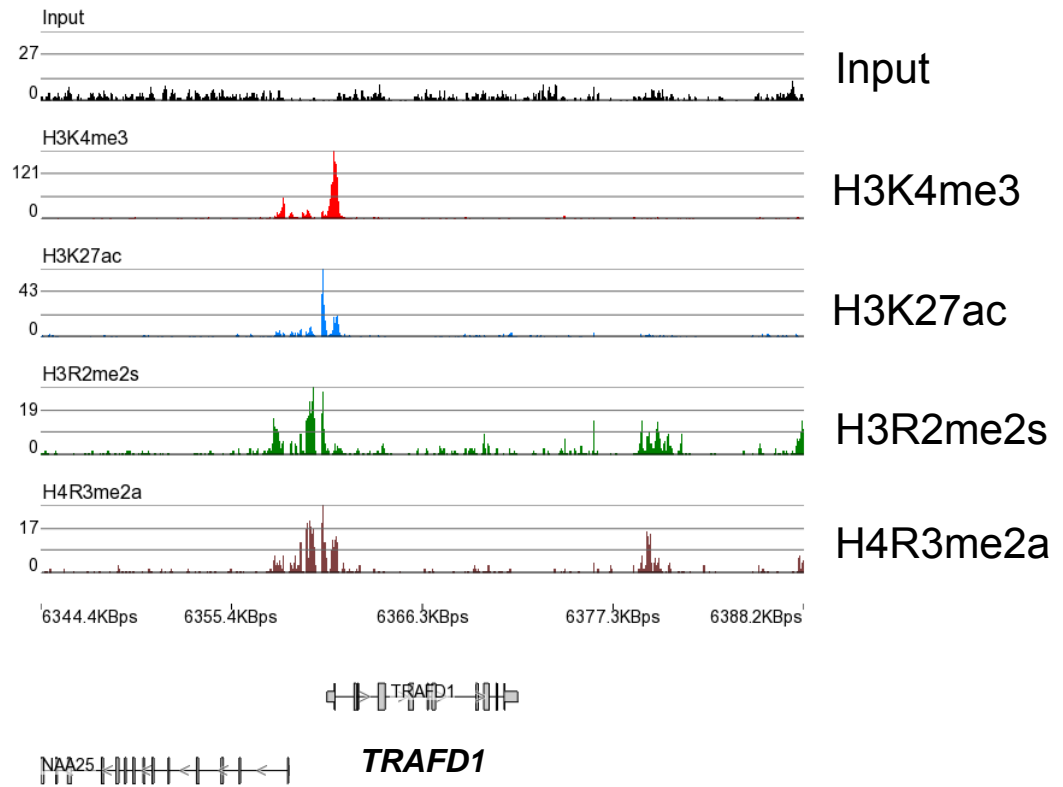


Figure S6.11. Chromatin profile and transcriptional activity of *TRAFD1* gene. Signal tracks showing DNA enrichment in F1 fraction (blue), H3K4me3 (red), H3K27ac (blue), H3R2me2s (green) and H4R3me2a (brown) arginine modifications.

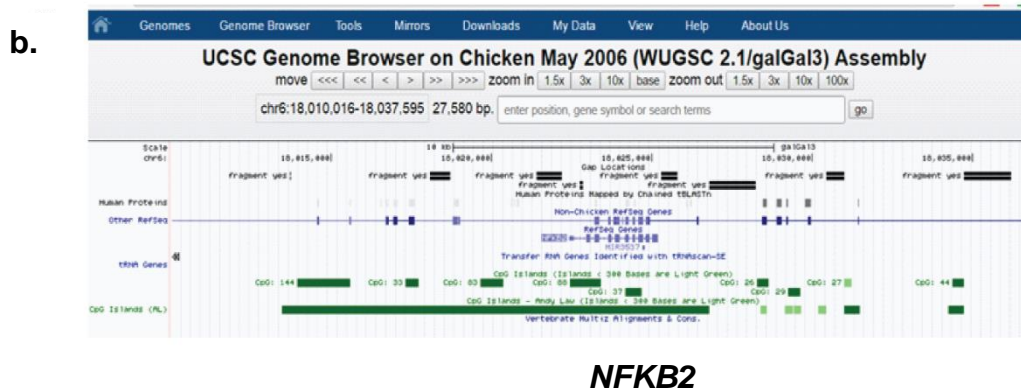
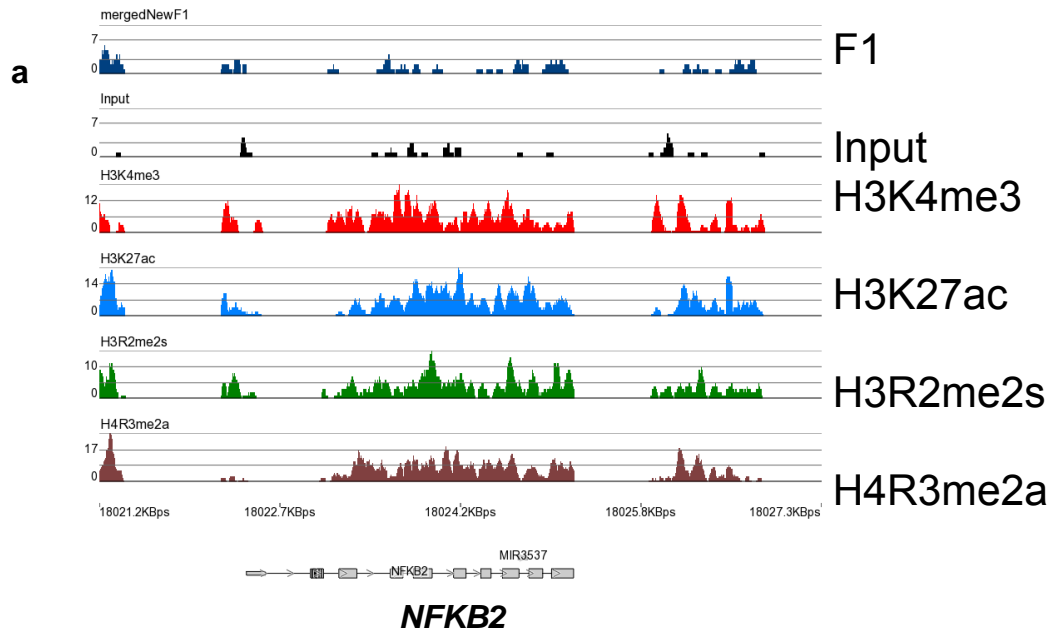


Figure S6.12. Chromatin profile and transcriptional activity of *NFKB2* gene. a) Signal tracks showing DNA enrichment in F1 fraction (blue), H3K4me3 (red), H3K27ac (blue), H3R2me2s (green) and H4R3me2a (brown) arginine modifications. **b)** CpG island was mapped with *NFKB2* gene using galGal3 UCSC genome browser. Green bar under the gene indicate CpG island.

6.7.1.3 Microscopy for polychromatic erythrocytes

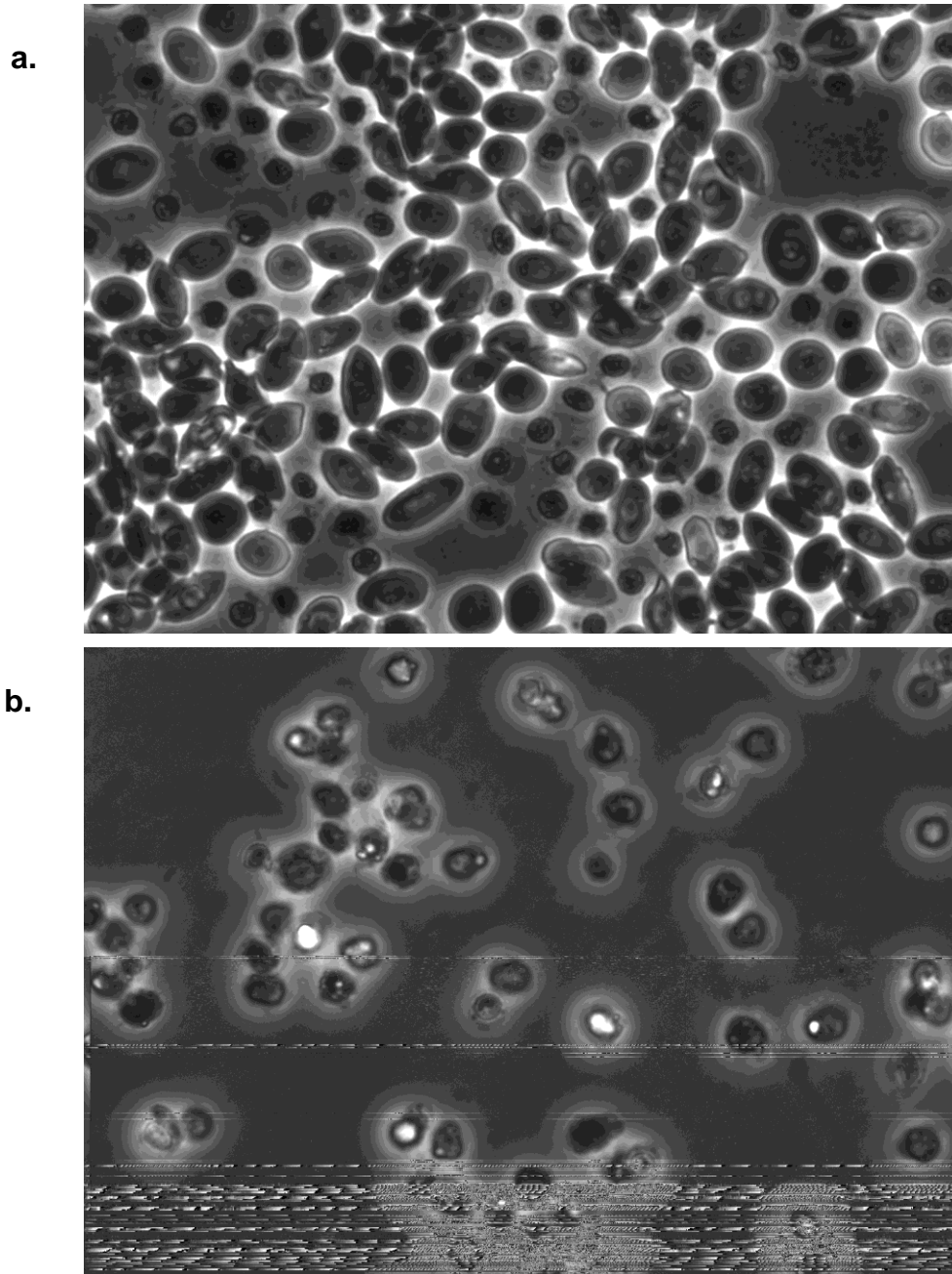


Figure S6.13: Microscopy for red and white blood cells from chicken polychromatic erythrocytes. Chicken polychromatic erythrocytes were separated from white blood cells, smeared on microscopic slide, and imaged with brightfield microscopy at 40 X magnification.

6.7.2 Supporting tables

Table S 6.1: Primers used for RT-PCR of immune gene study

Primer	Sequences
TLR3-F	5'-CCCTGATGGAGTGTTTGCTT-3'
TLR3-R	5'-CCAGGGTTTTGAAAGGATCA-3'
TLR21-F	5'-AAAGGAGAAAGCGGCTGAG-3'
TLR21-R	5'-GACAAGGACAGGGACAGAGC-3'
IL1B-F	5'-CTGAGCACACCACAGTGG-3'
IL1B-R	5'-GCAGCAGTTTGGTCATGG-3'
IRF-1-F	5'-TCATCTCATCTCGTCTCATCTCA-3'
IRF-1-R	5'-CTGTGCTGTGCTGTGTTGTG-3'
TIRAP-1-F	5'-CAGCCCCACCTCAGACAC-3'
TIRAP-1-R	5'-GGTGGAAAGGCTGGAATC-3'
CIAPIN1-F	5'-CTGTGAGATTGGCGTGGAC-3'
CIAPIN1-R	5'-GAGCGGGATAGAGGTGAGAG-3'
IL-15-F	5'-GCAATGTATTTCCCGATCCA-3'
IL-15-R	5'-CTCCGGCAGAGTTTTGTGTT-3'
18S-F	5'-GTAACCCGTTGAACCCATT-3'
18S-R	5'-CCATCCAATCGGTAGTAGCG-3'

CHAPTER VII: DISCUSSION AND FUTURE PERSPECTIVE

7.1 Summary

In this study, I identified four groups of chromatin with distinct features:

Group	Example gene	Properties
Group I	Globin, <i>H5</i> , <i>CA2</i> , <i>IRF1</i> , <i>IRF7</i> , <i>IRF8</i>	<ul style="list-style-type: none"> ➤ Broad salt solubility ➤ Associated with acetylation ➤ Associated with H3K4me3, H3K27ac, H3R2me2s, H4R3me2a ➤ Associated with PRMT1/5, HDAC2/pHDAC2
Group II	<i>HDAC2</i> , <i>PRMT7</i> , <i>GAS41</i>	<ul style="list-style-type: none"> ➤ Salt solubility at the 5' end of the gene ➤ Associated with acetylation ➤ Associated with H3K4me3, H3K27ac, H3R2me2s, H4R3me2a at the 5' end of gene ➤ Associated with PRMT1/5, HDAC2/pHDAC2
Group III	Ovalbumin, Vitellogenin	<ul style="list-style-type: none"> ➤ Not salt soluble ➤ Not acetylated ➤ Not associated with PTMs studied ➤ Not associated with PRMT1/5, HDAC2/pHDAC2
Group IV	<i>TLR3</i> , <i>TLR21</i> , <i>IFNa</i> , <i>IFNb</i>	This group of genes represents features of Group I and II chromatin.

7.2 Insight and perspectives from the studies

7.2.1 Insights and perspectives from the study-1 “Chicken erythrocyte epigenome”:

In this study, we demonstrated and mapped all transcriptionally active chromatin domains based on the salt soluble features of active gene chromatin. We showed that highly expressed genes were located in broad dynamically acetylated salt soluble chromatin domains [285]. Approximately 1000 novel domains have been reported from our study. There are only few that are β -globin like (β -globin, α -globin, *H5*, *FTH1*, *ARIH1*, *AK2*, and *TFRC*) multi-gene chromosomal domains. We identified the functional organization of these domains in polychromatic erythrocytes. Epigenetic marks H3K4me3/H3K27ac, the presence of low levels of anti-sense RNA and association with eRNA are common features of transcriptionally active chromatin domains/regions in chicken polychromatic erythrocytes. However, the role of antisense RNA and eRNA near the highly expressed genes remains unclear. Antisense RNA has been described before for chicken α and β globin genes [426, 482]. Alternative strategies such as strand-specific RT-PCR, global run-on

sequencing (GRO-seq) and native elongating transcript sequencing (NET-seq) can be applied to confirm further and explore the structure of the anti-sense transcripts identified in our study [483]. Moreover, comparative genomic analysis can be performed to address whether these non-coding regions are conserved across other vertebrates and mammals [484]. This type of analysis will be able to contribute crucial information regarding regulation of erythroid-specific functionally important regulators in human. Moreover, we have identified several putative enhancers based on the criteria of presence of eRNA, the presence of H3K27ac and F1 enrichment aligning together. Additional tools such as FAIRE-seq and Assay for Transposase-Accessible Chromatin (ATAC-seq) can be applied to map chromatin accessible and regulatory regions [478]. Techniques such as these will be able to identify the location of factor binding sites and enhancer regions for the novel chromatin domains identified in Study-1. It will be interesting to use Hi-C to identify genome-wide chromatin interaction to confirm the chromatin territories and spatial organization [485]. Finally, knockdown of eRNA located near the locus control region such as in the case of β -globin domain region will be able to answer the functional role of these RNAs in mediating chromatin interaction, if any.

7.2.2 Insights and perspectives from the study-2 “Transcription-Dependent Association of HDAC2 with Active Chromatin.”

In this study, our mass spectrometry analyses revealed the composition of the un-phosphorylated HDAC2 complex in F1 chromatin fraction. However, total HDAC2 from the F1 fraction contains corepressor complexes. Our result complements the previous findings from our lab in mammalian cells in which we demonstrated that HDAC2 mutated at the three phosphorylation sites (Flp-In 293 expressing HDAC2-3S/A-V5) were not associated with the corepressor HDAC complexes [165]. We show here for the first time that HDAC2-S394ph locates with chromatin fraction F1 and is associated with transcriptionally active chromatin regions in chicken polychromatic erythrocytes. Indirect immunofluorescence further shows that HDAC2 is located in interchromatin channels, a location where DNase sensitive chromatin is distributed [425]. Dr. Thomas Cremer and his group demonstrated that perichromatin regions contained decondensed chromatin and are located at the periphery of the interchromatin channels [427]. Therefore, localization of HDAC2 within the interchromatin channel indicate that salt-soluble transcriptionally active genes in F1 chromatin are located in a perichromatin region that interfaces with the interchromatin channel.

We found that total HDAC2 is distributed in the promoter region and along the gene body. However, HDAC2-S394ph is associated with the upstream promoter region of transcribed genes. Total HDAC2 and HDAC2-S394ph are associated with the dynamically acetylated chromatin regions in chicken polychromatic erythrocytes in a transcription-dependent manner. We reported earlier that reduced HDAC activity is inversely correlated with KAT2B, H3 and H4 acetylation on MCL1 exon 2 which has H3K4me3 in human colon cancer cell line [165]. H3K4me3 recruits KAT2B and KAT7, which acetylate proteins in this region. From our observation in studies 1 and 2, it was found that H3K4me3 and H3K27ac align with HDAC2-S394ph at the CA2 promoter region [285]. It will be interesting to address whether HDAC2-S394ph is involved in regulating the local level of H3K4me3 at the transcribed gene region as ING1/2 protein, which is a reader for H3K4me3, is a component of SIN3 corepressor complex [486, 487]. Enrichment of unmodified HDAC2 along the exonic region of *GAS41* and *CA2* indicate its possible role as a transcription pause for the latter nucleosome. Co-mapping of HDAC2-S394ph with H3ac, H3K4me3, and H3K27ac at the promoter region of active genes demonstrated that phosphorylated HDAC2 participate in dynamic histone acetylation with KATs by removing acetylation at the site and reset chromatin state [168]. Moreover, it would be important to know whether other phosphorylated forms of HDAC2 (HDAC2-S422,424ph) show a similar distribution pattern to HDAC2-S394ph.

7.2.3 Insights and perspectives from the study-3 “PRMT1 and 5 mediated H4R3me2a and H3R2me2s modifications in transcriptionally active chromatin”

In this study, we explored the genome-wide distribution of PRMT1 and 5 mediated arginine methylation H4R3me2a and H3R2me2s, respectively, in chicken polychromatic erythrocytes. Our findings show the unique distribution of these two modifications in transcriptionally active genes. I found that H4R3me2a along with H3K27ac mark the transcriptionally active promoter and enhancer. Moreover, regression curve analysis revealed that H4R3me2a and H3K27ac are located together. Enhancer regions are also found associated with H3R2me2s, aligning with H4R3me2a. However, these two arginine methylations are not always correlated as shown from the regression analysis. Furthermore, co-localization of both H3R2me2s and H4R3me2a at the β -globin LCR regions led us to the question whether PRMT1 and 5 are in the same complex. However, low stringency PRMT5 immunoprecipitation followed by PRMT1 immunoblot provide evidence that these two enzymes are not in the same complex (data not shown). Furthermore, using sequential IP and ChIP with the dual crosslinking, we could address whether the co-localization of PRMT1

and 5 occurs indirectly. Although PRMT5 is responsible for both active and repressive histone modifications, we show for the first time that PRMT1 and 5 associate with active chromatin regions in chicken polychromatic erythrocytes. PRMT1 and 5 were enriched at low salt insoluble chromatin fraction P_E and salt soluble poly and oligonucleosomes. The strong location of these enzymes with P_E is similar to what we found for HDAC1/2 (chapter IV) [428]. Moreover, genome-wide mapping of PRMT1 and 5 has not been done yet, and it will be necessary to map the genomic locations of these two enzymes in polychromatic erythrocytes.

Chicken mature erythrocytes are presumably transcriptionally silent while maintaining potentially active gene features [406]. However, dynamic histone acetylation exists in mature erythrocytes but differs from polychromatic erythrocytes in that two rates of acetylation are observed [406]. Therefore, it will be interesting to characterize the distribution of H3R2me2s and H4R3me2a in chicken mature erythrocytes. Furthermore, it was shown that prior acetylation at the H4 tail inhibits methylation of H4R3me2a by PRMT1 [220]. Both polychromatic and mature erythrocytes can be treated with or without HDAC inhibitor butyrate to investigate any change in arginine methylation due to a change in acetylation.

We demonstrated that both PRMT1 and 5 are associated with the elongating form of RNAPII to be recruited to the coding region of transcribed genes. The investigation can be extended to assess the association of PRMT1 and 5 with the initiating form of RNAPII.

In study-3, we identified the co-localization of H4R3me2a with H3K27ac and H3R2me2s. Sequential ChIP with one histone mark followed by the second one will address whether H4R3me2a co-occupy on the same genomic site with other histone marks observed in the study.

7.2.4 Insights and perspectives from the study-4

In this study “Epigenomic features of immune genes in polychromatic erythrocyte cells,” we demonstrated the transcriptome profile of several innate immune genes, and the distribution of H3K4me3, H3K27ac, H3R2me2s and H4R3me2a along these genes. Furthermore, we demonstrated the poly I:C mediated induction of several innate immune genes in chicken polychromatic erythrocytes. The length of polyI:C affects the time of induction for some gene groups as well as different TLR receptors in polychromatic erythrocytes. Therefore, it will be interesting in future studies to investigate different poly I:C to simulate the repertoires of immune genes. We do not know if the increase of immune gene expression is due to increased transcription

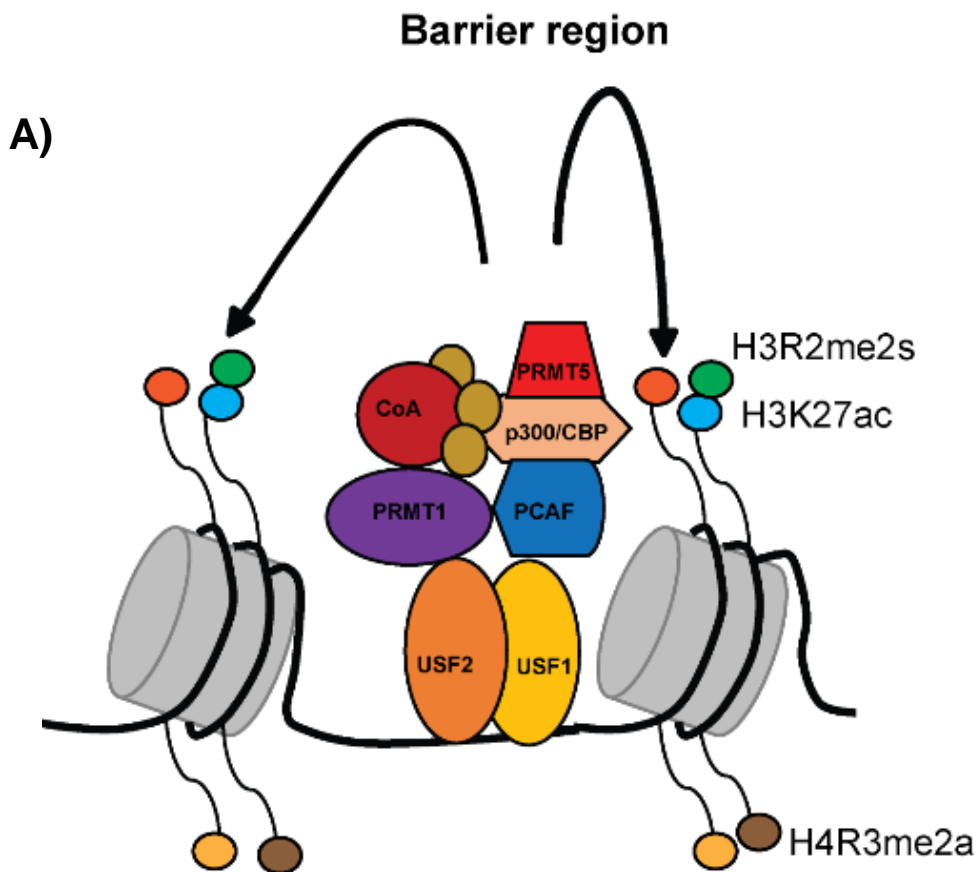
or increased RNA stability. Subsequently, we need to characterize the mRNA stability of the immune genes induced in the study as described in a different study [488]. For this purpose, transcription inhibitors can be added to the cells before poly I:C treatment to check whether the gene induction is mediated through transcription. Moreover, antisense RNA has been demonstrated to regulate the expression of innate immune gene sense transcript as demonstrated for *IL1B* [477]. Overexpression of *IL1B* antisense transcript was shown to be the mechanism for reduced H3K4me3 level and therefore lowering the RNAPII binding at the sense *IL1B* promoter. We found the presence of noncoding RNA, eRNA near several of the immune genes described in chapter-3. Future studies could demonstrate the functional role of these RNAs in regulating the expression of the sense genes. We observed that in immune genes the association of H3K4me3, H3K27ac, H3R2me2s, and H4R3me2a with differentially expressed genes. The association of the active marks with the low expressing immune genes suggests that these genes may have already been induced and returned to steady state level or are in a poised state ready to be expressed. Mapping of these histone modifications using ChIP or ChIP-seq will address whether in an induced state, these modifications have a different distribution along the gene. There exists a strong correlation between the location of CpG islands and the position of H3R2me2s and H4R3me2a with the genes investigated in chapters-3 and 4. Our results suggest that H3R2me2s and H4R3me2a are recruited along the gene body or coding regions of genes in a CpG dependent manner. Thus, it will be necessary to determine the protein components that are involved in CpG mediated recruitment of the enzymes catalyzing these two arginine modifications.

7.3 Conclusion, significance and study limitations

Studies presented in this thesis highlighted the features of transcriptionally active polynucleosome chromatin fraction F1 isolated from chicken polychromatic erythrocytes. We demonstrated that salt solubility of genes in F1 co-map with acetylation for the region. For highly transcribing genes, salt solubility expands as chromatin domain. Drop in acetylation at the chromatin boundary coincides with the loss of salt solubility for the region. Low expressing genes differ in epigenomic features as compared to highly expressing genes regarding salt solubility, the presence of antisense transcripts, association with H3K4me3, H3K27ac, and eRNA.

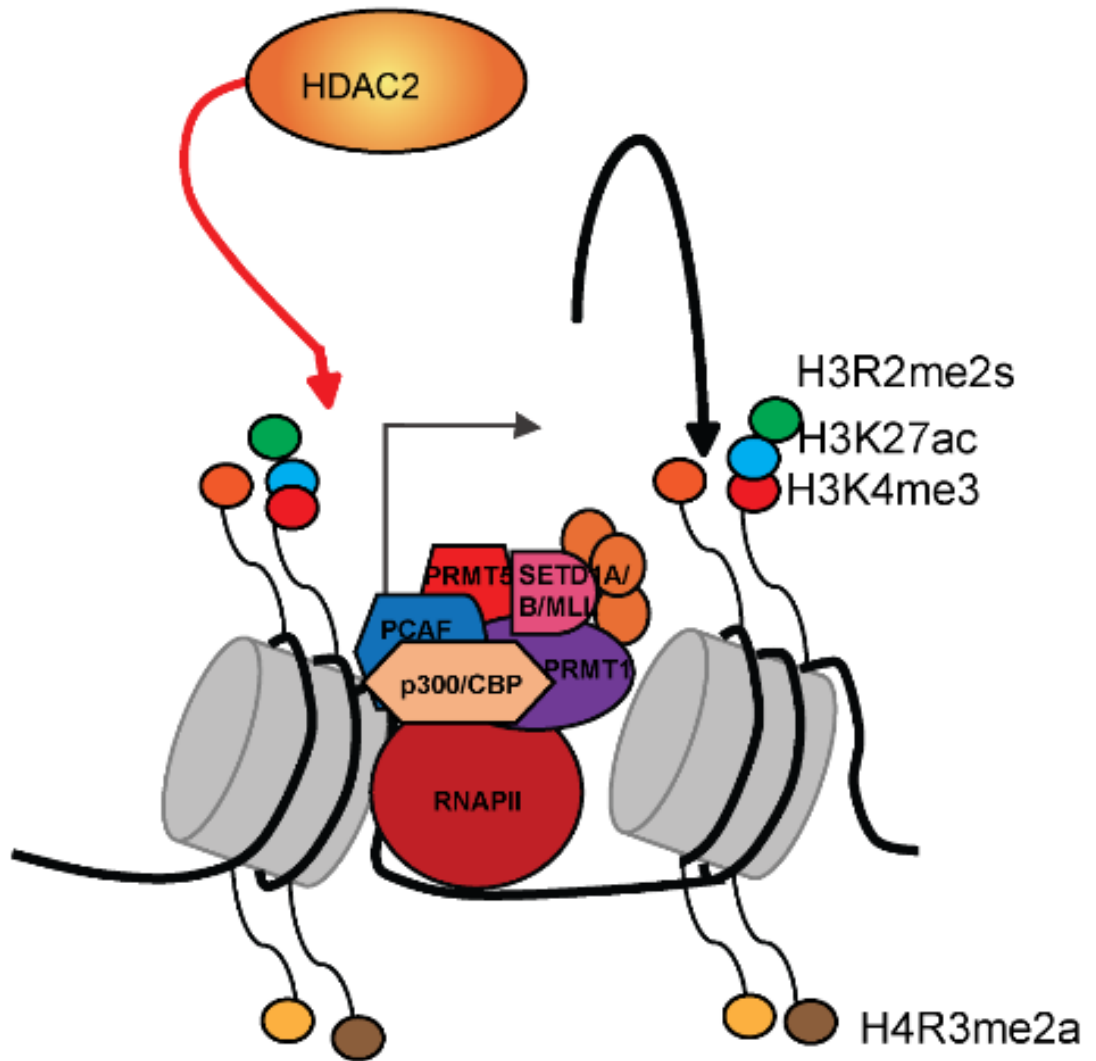
Furthermore, we demonstrated that total HDAC2 and HDAC2-S394ph are distributed along the transcriptionally active genes in polychromatic erythrocytes. We characterized the phosphorylated and unmodified HDAC2 complex in F1 chromatin.

We characterized the distribution of PRMT1 and 5 and their corresponding products H4R3me2a and H3R2me2s along transcriptionally active chromatin fractions. Association of H4R3me2a and H3R2me2s with transcriptionally active genes are distinct depending on several factors. H4R3me2a preferentially associates with active promoters together with H3K27ac. Therefore, it indicates that PRMT1 is associated with p300/CBP. We found that distal regulatory regions are associated with H4R3me2a, H3R2me2s and H3K27ac linking the binding of PRMT1, PRMT5, and p300/CBP to these regions. The findings of my studies revealed that an H3 molecule with R2me2s also has K27ac, K4me1 and/or K4Me3. PRMT5 mediated R2me2s is therefore recognized by writers such as p300/CBP, SETD1A/SETD1B or the MLL complex. The interplay between arginine methylation, lysine methylation and lysine acetylation suggests they play a crucial role in maintaining a transcriptionally active domain conformation in F1.



Transcription start site

B)



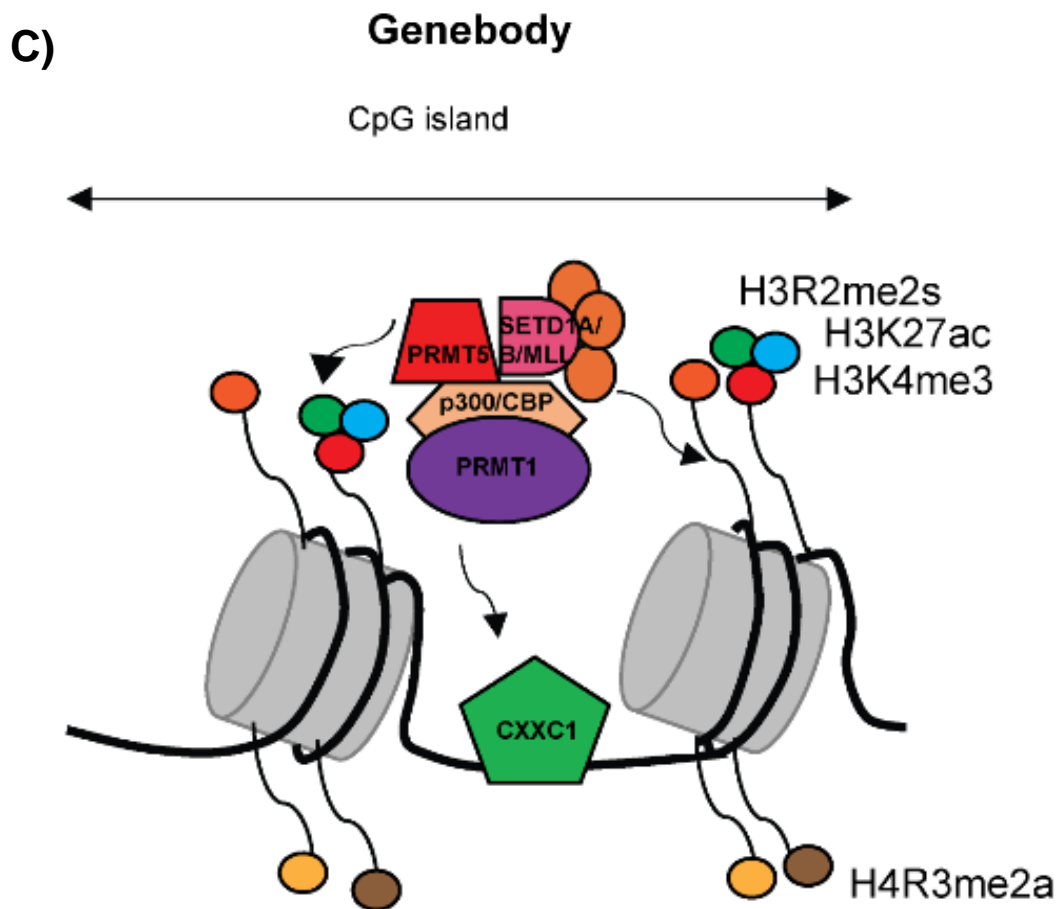


Figure 7.1: Interplay between arginine methylation and lysine methylation and acetylation in transcriptionally chromosomal location. PRMT1 is recruited to A) barrier regions by transcription factors (USF1/USF2), HDAC2, B) PRMT1/5 complexes recruited in a RNAPII-transcription-dependent manner to the gene body of transcribed genes. PRMT1/5 bind to the regulatory regions as a single complex or separately and involved in the recruitment of SETD1A/B, PCAF, p300/CBP, KATs and other modifying enzymes. C) CXXC1 in SETD1A/B complex or possibly in PRMT1/5 complex target these enzymes to unmethylated CpG island along the gene body.

Finally, we demonstrated that immune genes enriched in F1 have distinct epigenetic features. We showed that chicken polychromatic erythrocytes differentially express several immune regulatory genes. These immune genes are associated with H3K4me3, H3K27ac, H3R2me2s, and H4R3me2a. Moreover, chicken polychromatic erythrocytes actively participate in immune-

mediated response as demonstrated by the induction of several immune genes in response to poly I:C.

In this thesis, using a non-replicating cell system, we addressed the inter-relationship between transcription and histone acetylation, deacetylation, methylation, non-coding RNA and chromatin structure. We showed that HDAC2, but not PRMT1/5, bind to RNAPIIS2ph in a RNA-dependent manner. We demonstrated that H3K4me3, H3K27ac, H4R3me2a, and H3R2me2s are located in important active gene regions such as upstream promoter regions, enhancers, and LCRs. The localization of these active PTMs in these regions indicate that they play a critical role in maintaining the active chromatin structure. However, due to the short lifespan of the polychromatic erythrocytes *in vitro*, it was not possible to do stable knockdown in these cells to address the functional significance of the histone modifying enzymes investigated in this thesis.

My study presents mechanisms of how histone acetylation and arginine methylation contribute to the open conformation of erythroid-expressed genes. Thomas Cremer and colleagues reported that decondensed active chromatin, called perichromatin, surrounded condensed chromatin domains. Further, they showed that the perichromatin interfaced with the interchromatin channels [427]. My findings support a model in which highly acetylated, DNase I sensitive multi-gene chromatin regions are located entirely within the perichromatin region. At low resolution, we observed that HDAC2, which is bound to transcribed chromatin, was located in the interchromatin channels. However, based on Thomas Cremer's work, I propose that HDAC2 is bound to the acetylated, salt-soluble chromatin in perichromatin. The highly acetylated, salt-soluble chromatin regions have active marks and CpG islands at the promoter region and gene body (**Figure 7.2**). Moreover, these active chromatin regions have enhancers that are associated with eRNA, H3K27ac, H3R2me2s, and H4R3me2a which would be required to drive gene expression. On the other hand, I propose that mid- to low-expressing genes such as the *CA2* and *GAS41* genes have their 5' regulatory regions in the perichromatin space, and the remainder of the gene is in the condensed chromatin regions. CpG islands and active histone marks are located at the 5' end of this second type of chromatin (**Figure 7.2**). Repressed genes, such as ovalbumin and vitellogenin, lack CpG islands as well as any active histone modification. These genes would be entirely in the condensed chromatin space.

I speculate that the underlying DNA sequence containing the CpG island is a crucial player in the genesis of the active chromatin configuration. CpG island binding proteins such as CXXC1 or transcription factors would bind to the CpG island and recruit histone modifying enzymes PRMT1 and 5 (**Figure 7.1**). The strong association of H3 and H4 arginine modifications with CpG island found in the current study support this notion. Further, the strong correlation of H4R3me2a with H3K27ac suggests that PRMT1 recruits p300/CBP and/or the H4R3me2a mark is read by p300/CBP to facilitate acetylation of this region (**Figure 7.1**). In parallel, PRMT5 is known to recruit lysine methyltransferases and KATs to establish other active marks such as H3K4me3 and acetylated H3 (**Figure 7.1**). Together these signaling events lead to an open conformation of chromatin.

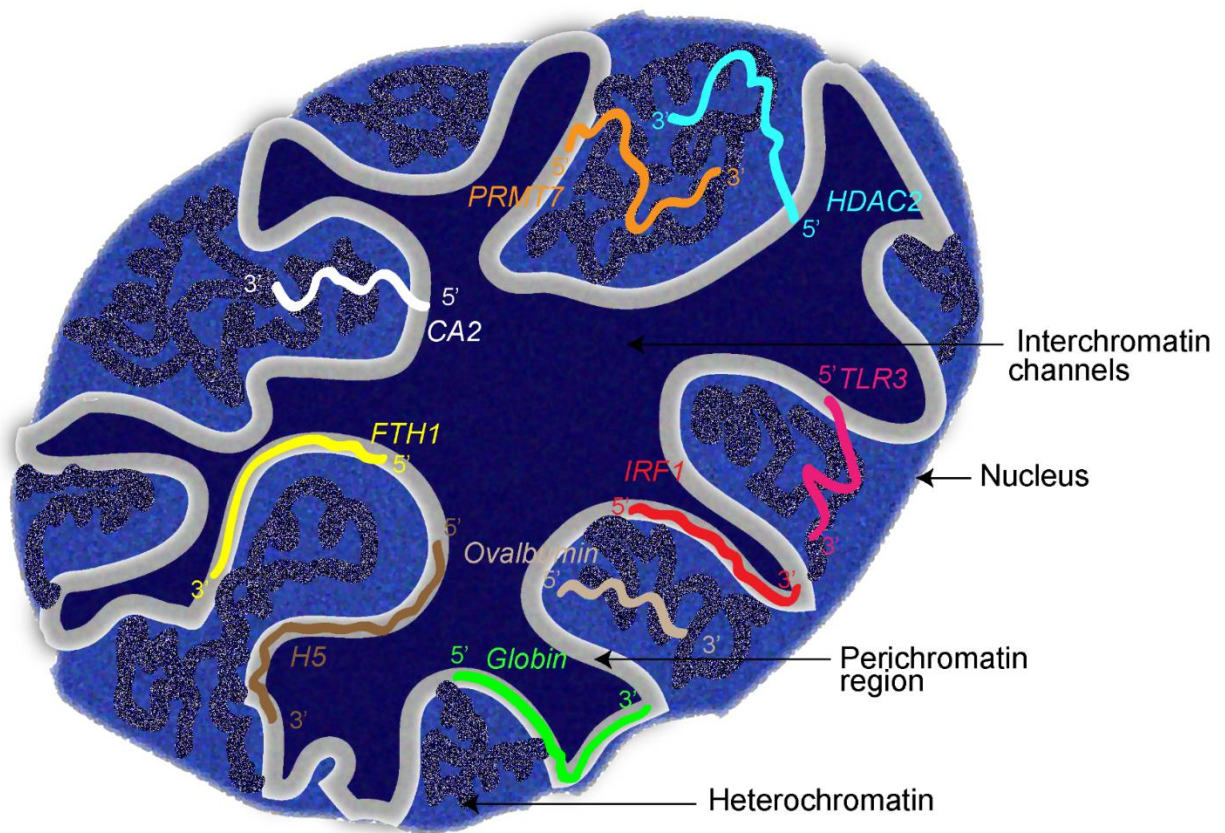


Figure 7.2: Chromatin organization in chicken erythrocyte nuclei.

The chicken genome is one-third in size compared to the human and represents a significantly lower amount of gene duplication, pseudogenes and repeat content. Both chicken and human

genomes share long blocks of conserved synteny and highly conserved sequences in the non-coding region [489]. The classes of non-coding RNAs that highlight conserved synteny between humans and chickens are mostly micro-RNAs and small nucleolar RNAs (snoRNAs) [489]. Therefore, the current study is valuable regarding the information on these functionally important elements in the human genome. Thus, our studies supply useful information on the structural and functional organization of the chicken polychromatic erythrocyte epigenome and may provide insights into the human erythrocyte genome organization.

7.4 References

1. Luger, K., et al., *Crystal structure of the nucleosome core particle at 2.8 Å resolution*. Nature, 1997. **389**(6648): p. 251-60.
2. Tropberger, P. and R. Schneider, *Going global: novel histone modifications in the globular domain of H3*. Epigenetics, 2010. **5**(2): p. 112-7.
3. Cosgrove, M.S., J.D. Boeke, and C. Wolberger, *Regulated nucleosome mobility and the histone code*. Nat Struct Mol Biol, 2004. **11**(11): p. 1037-43.
4. Allan, J., et al., *Roles of H1 domains in determining higher order chromatin structure and H1 location*. J Mol Biol, 1986. **187**(4): p. 591-601.
5. Izzo, A., K. Kamieniarz, and R. Schneider, *The histone H1 family: specific members, specific functions?* Biol Chem, 2008. **389**(4): p. 333-43.
6. Horn, P.J. and C.L. Peterson, *Molecular biology. Chromatin higher order folding--wrapping up transcription*. Science, 2002. **297**(5588): p. 1824-7.
7. International Human Genome Sequencing, C., *Finishing the euchromatic sequence of the human genome*. Nature, 2004. **431**(7011): p. 931-45.

8. Cavalli, G. and T. Misteli, *Functional implications of genome topology*. Nat Struct Mol Biol, 2013. **20**(3): p. 290-9.
9. Lanctot, C., et al., *Dynamic genome architecture in the nuclear space: regulation of gene expression in three dimensions*. Nat Rev Genet, 2007. **8**(2): p. 104-15.
10. Albiez, H., et al., *Chromatin domains and the interchromatin compartment form structurally defined and functionally interacting nuclear networks*. Chromosome Res, 2006. **14**(7): p. 707-33.
11. Osborne, C.S., et al., *Active genes dynamically colocalize to shared sites of ongoing transcription*. Nat Genet, 2004. **36**(10): p. 1065-71.
12. Wei, G.H., D.P. Liu, and C.C. Liang, *Chromatin domain boundaries: insulators and beyond*. Cell Res, 2005. **15**(4): p. 292-300.
13. de Wit, E., et al., *Global chromatin domain organization of the Drosophila genome*. PLoS Genet, 2008. **4**(3): p. e1000045.
14. Goldman, M.A., *The chromatin domain as a unit of gene regulation*. Bioessays, 1988. **9**(2-3): p. 50-5.
15. Oki, M. and R.T. Kamakaka, *Blockers and barriers to transcription: competing activities?* Curr Opin Cell Biol, 2002. **14**(3): p. 299-304.
16. Barkess, G. and A.G. West, *Chromatin insulator elements: establishing barriers to set heterochromatin boundaries*. Epigenomics, 2012. **4**(1): p. 67-80.
17. Geyer, P.K. and V.G. Corces, *DNA position-specific repression of transcription by a Drosophila zinc finger protein*. Genes Dev, 1992. **6**(10): p. 1865-73.
18. Kellum, R. and P. Schedl, *A position-effect assay for boundaries of higher order chromosomal domains*. Cell, 1991. **64**(5): p. 941-50.

19. Sun, F.L. and S.C. Elgin, *Putting boundaries on silence*. Cell, 1999. **99**(5): p. 459-62.
20. West, A.G., M. Gaszner, and G. Felsenfeld, *Insulators: many functions, many mechanisms*. Genes Dev, 2002. **16**(3): p. 271-88.
21. Yang, J. and V.G. Corces, *Chromatin insulators: a role in nuclear organization and gene expression*. Adv Cancer Res, 2011. **110**: p. 43-76.
22. Ghirlando, R., et al., *Chromatin domains, insulators, and the regulation of gene expression*. Biochim Biophys Acta, 2012. **1819**(7): p. 644-51.
23. Huang, S., M. Litt, and G. Felsenfeld, *Methylation of histone H4 by arginine methyltransferase PRMT1 is essential in vivo for many subsequent histone modifications*. Genes Dev, 2005. **19**(16): p. 1885-93.
24. Bell, A.C., A.G. West, and G. Felsenfeld, *Insulators and boundaries: versatile regulatory elements in the eukaryotic genome*. Science, 2001. **291**(5503): p. 447-50.
25. Bell, A.C., A.G. West, and G. Felsenfeld, *The protein CTCF is required for the enhancer blocking activity of vertebrate insulators*. Cell, 1999. **98**(3): p. 387-96.
26. Litt, M.D., et al., *Correlation between histone lysine methylation and developmental changes at the chicken beta-globin locus*. Science, 2001. **293**(5539): p. 2453-5.
27. Lunyak, V.V., *Boundaries. Boundaries...Boundaries???* Curr Opin Cell Biol, 2008. **20**(3): p. 281-7.
28. Bushey, A.M., E.R. Dorman, and V.G. Corces, *Chromatin insulators: regulatory mechanisms and epigenetic inheritance*. Mol Cell, 2008. **32**(1): p. 1-9.
29. Maeda, R.K. and F. Karch, *Making connections: boundaries and insulators in Drosophila*. Curr Opin Genet Dev, 2007. **17**(5): p. 394-9.

30. Raab, J.R. and R.T. Kamakaka, *Insulators and promoters: closer than we think*. Nat Rev Genet, 2010. **11**(6): p. 439-46.
31. Raab, J.R., et al., *Human tRNA genes function as chromatin insulators*. EMBO J, 2012. **31**(2): p. 330-50.
32. Wang, J., V.V. Lunyak, and I.K. Jordan, *Genome-wide prediction and analysis of human chromatin boundary elements*. Nucleic Acids Res, 2012. **40**(2): p. 511-29.
33. Yocum, A.O., et al., *A tissue-specific chromatin loop activates the erythroid ankyrin-1 promoter*. Blood, 2012. **120**(17): p. 3586-93.
34. Zhou, J. and S.L. Berger, *Good fences make good neighbors: barrier elements and genomic regulation*. Mol Cell, 2004. **16**(4): p. 500-2.
35. Filippova, G.N., et al., *An exceptionally conserved transcriptional repressor, CTCF, employs different combinations of zinc fingers to bind diverged promoter sequences of avian and mammalian c-myc oncogenes*. Mol Cell Biol, 1996. **16**(6): p. 2802-13.
36. Rubio, E.D., et al., *CTCF physically links cohesin to chromatin*. Proc Natl Acad Sci U S A, 2008. **105**(24): p. 8309-14.
37. Lobanekov, V.V., et al., *A novel sequence-specific DNA binding protein which interacts with three regularly spaced direct repeats of the CCCTC-motif in the 5'-flanking sequence of the chicken c-myc gene*. Oncogene, 1990. **5**(12): p. 1743-53.
38. Ohlsson, R., R. Renkawitz, and V. Lobanekov, *CTCF is a uniquely versatile transcription regulator linked to epigenetics and disease*. Trends Genet, 2001. **17**(9): p. 520-7.
39. Phillips, J.E. and V.G. Corces, *CTCF: master weaver of the genome*. Cell, 2009. **137**(7): p. 1194-211.

40. Groenen, P.M., et al., *Structure, sequence, and chromosome 19 localization of human USF2 and its rearrangement in a patient with multicystic renal dysplasia*. Genomics, 1996. **38**(2): p. 141-8.
41. Shieh, B.H., et al., *Localization of the gene-encoding upstream stimulatory factor (USF) to human chromosome 1q22-q23*. Genomics, 1993. **16**(1): p. 266-8.
42. West, A.G., et al., *Recruitment of histone modifications by USF proteins at a vertebrate barrier element*. Mol Cell, 2004. **16**(3): p. 453-63.
43. Bresnick, E.H. and G. Felsenfeld, *Evidence that the transcription factor USF is a component of the human beta-globin locus control region heteromeric protein complex*. J Biol Chem, 1993. **268**(25): p. 18824-34.
44. Leach, K.M., et al., *Characterization of the human beta-globin downstream promoter region*. Nucleic Acids Res, 2003. **31**(4): p. 1292-301.
45. Huang, S., et al., *USF1 recruits histone modification complexes and is critical for maintenance of a chromatin barrier*. Mol Cell Biol, 2007. **27**(22): p. 7991-8002.
46. Dickson, J., et al., *VEZF1 elements mediate protection from DNA methylation*. PLoS Genet, 2010. **6**(1): p. e1000804.
47. Simms, T.A., et al., *TFIIIC binding sites function as both heterochromatin barriers and chromatin insulators in Saccharomyces cerevisiae*. Eukaryot Cell, 2008. **7**(12): p. 2078-86.
48. Oettel, S., I. Kober, and K.H. Seifart, *The activity binding to the termination region of several pol III genes represents a separate entity and is distinct from a novel component enhancing U6 snRNA transcription*. Nucleic Acids Res, 1998. **26**(19): p. 4324-31.

49. Nakao, M. and H. Sasaki, *Genomic imprinting: significance in development and diseases and the molecular mechanisms*. J Biochem, 1996. **120**(3): p. 467-73.
50. Banerjee, S. and A. Smallwood, *A chromatin model of IGF2/H19 imprinting*. Nat Genet, 1995. **11**(3): p. 237-8.
51. Brenton, J.D., et al., *A silencer element identified in Drosophila is required for imprinting of H19 reporter transgenes in mice*. Proc Natl Acad Sci U S A, 1999. **96**(16): p. 9242-7.
52. Kanduri, C., et al., *The 5' flank of mouse H19 in an unusual chromatin conformation unidirectionally blocks enhancer-promoter communication*. Curr Biol, 2000. **10**(8): p. 449-57.
53. Bell, A.C. and G. Felsenfeld, *Methylation of a CTCF-dependent boundary controls imprinted expression of the Igf2 gene*. Nature, 2000. **405**(6785): p. 482-5.
54. Hark, A.T., et al., *CTCF mediates methylation-sensitive enhancer-blocking activity at the H19/Igf2 locus*. Nature, 2000. **405**(6785): p. 486-9.
55. Szabo, P., et al., *Maternal-specific footprints at putative CTCF sites in the H19 imprinting control region give evidence for insulator function*. Curr Biol, 2000. **10**(10): p. 607-10.
56. Kanduri, C., et al., *Functional association of CTCF with the insulator upstream of the H19 gene is parent of origin-specific and methylation-sensitive*. Curr Biol, 2000. **10**(14): p. 853-6.
57. Holmgren, C., et al., *CpG methylation regulates the Igf2/H19 insulator*. Curr Biol, 2001. **11**(14): p. 1128-30.

58. Eden, S., et al., *An upstream repressor element plays a role in Igf2 imprinting*. EMBO J, 2001. **20**(13): p. 3518-25.
59. Constancia, M., et al., *Deletion of a silencer element in Igf2 results in loss of imprinting independent of H19*. Nat Genet, 2000. **26**(2): p. 203-6.
60. Murrell, A., et al., *An intragenic methylated region in the imprinted Igf2 gene augments transcription*. EMBO Rep, 2001. **2**(12): p. 1101-6.
61. Pant, V., et al., *Mutation of a single CTCF target site within the H19 imprinting control region leads to loss of Igf2 imprinting and complex patterns of de novo methylation upon maternal inheritance*. Mol Cell Biol, 2004. **24**(8): p. 3497-504.
62. Pant, V., et al., *The nucleotides responsible for the direct physical contact between the chromatin insulator protein CTCF and the H19 imprinting control region manifest parent of origin-specific long-distance insulation and methylation-free domains*. Genes Dev, 2003. **17**(5): p. 586-90.
63. Schoenherr, C.J., J.M. LeVorse, and S.M. Tilghman, *CTCF maintains differential methylation at the Igf2/H19 locus*. Nat Genet, 2003. **33**(1): p. 66-9.
64. Rand, E., et al., *CTCF elements direct allele-specific undermethylation at the imprinted H19 locus*. Curr Biol, 2004. **14**(11): p. 1007-12.
65. Chao, W., et al., *CTCF, a candidate trans-acting factor for X-inactivation choice*. Science, 2002. **295**(5553): p. 345-7.
66. Chung, J.H., M. Whiteley, and G. Felsenfeld, *A 5' element of the chicken beta-globin domain serves as an insulator in human erythroid cells and protects against position effect in Drosophila*. Cell, 1993. **74**(3): p. 505-14.

67. Pikaart, M.J., F. Recillas-Targa, and G. Felsenfeld, *Loss of transcriptional activity of a transgene is accompanied by DNA methylation and histone deacetylation and is prevented by insulators*. Genes Dev, 1998. **12**(18): p. 2852-62.
68. Recillas-Targa, F., et al., *Position-effect protection and enhancer blocking by the chicken beta-globin insulator are separable activities*. Proc Natl Acad Sci U S A, 2002. **99**(10): p. 6883-8.
69. Rincon-Arano, H., M. Furlan-Magaril, and F. Recillas-Targa, *Protection against telomeric position effects by the chicken cHS4 beta-globin insulator*. Proc Natl Acad Sci U S A, 2007. **104**(35): p. 14044-9.
70. Prioleau, M.N., et al., *An insulator element and condensed chromatin region separate the chicken beta-globin locus from an independently regulated erythroid-specific folate receptor gene*. EMBO J, 1999. **18**(14): p. 4035-48.
71. Saitoh, N., et al., *Structural and functional conservation at the boundaries of the chicken beta-globin domain*. EMBO J, 2000. **19**(10): p. 2315-22.
72. Li, X., et al., *Chromatin boundaries require functional collaboration between the hSET1 and NURF complexes*. Blood, 2011. **118**(5): p. 1386-94.
73. Amouyal, M., *Gene insulation. Part II: natural strategies in vertebrates*. Biochem Cell Biol, 2010. **88**(6): p. 885-98.
74. Farrell, C.M., et al., *A large upstream region is not necessary for gene expression or hypersensitive site formation at the mouse beta -globin locus*. Proc Natl Acad Sci U S A, 2000. **97**(26): p. 14554-9.

75. Li, Q., et al., *Evidence that DNase I hypersensitive site 5 of the human beta-globin locus control region functions as a chromosomal insulator in transgenic mice*. Nucleic Acids Res, 2002. **30**(11): p. 2484-91.
76. Driscoll, M.C., C.S. Dobkin, and B.P. Alter, *Gamma delta beta-thalassemia due to a de novo mutation deleting the 5' beta-globin gene activation-region hypersensitive sites*. Proc Natl Acad Sci U S A, 1989. **86**(19): p. 7470-4.
77. Bulger, M., et al., *A complex chromatin landscape revealed by patterns of nuclease sensitivity and histone modification within the mouse beta-globin locus*. Mol Cell Biol, 2003. **23**(15): p. 5234-44.
78. Bender, M.A., et al., *Flanking HS-62.5 and 3' HS1, and regions upstream of the LCR, are not required for beta-globin transcription*. Blood, 2006. **108**(4): p. 1395-401.
79. Bulger, M., et al., *Conservation of sequence and structure flanking the mouse and human beta-globin loci: the beta-globin genes are embedded within an array of odorant receptor genes*. Proc Natl Acad Sci U S A, 1999. **96**(9): p. 5129-34.
80. Farrell, C.M., A.G. West, and G. Felsenfeld, *Conserved CTCF insulator elements flank the mouse and human beta-globin loci*. Mol Cell Biol, 2002. **22**(11): p. 3820-31.
81. Mishiro, T., et al., *Architectural roles of multiple chromatin insulators at the human apolipoprotein gene cluster*. EMBO J, 2009. **28**(9): p. 1234-45.
82. Lai, C.Q., L.D. Parnell, and J.M. Ordovas, *The APOA1/C3/A4/A5 gene cluster, lipid metabolism and cardiovascular disease risk*. Curr Opin Lipidol, 2005. **16**(2): p. 153-66.
83. Dieci, G., et al., *The expanding RNA polymerase III transcriptome*. Trends Genet, 2007. **23**(12): p. 614-22.

84. Geiduschek, E.P. and G.A. Kassavetis, *The RNA polymerase III transcription apparatus*. J Mol Biol, 2001. **310**(1): p. 1-26.
85. Schramm, L. and N. Hernandez, *Recruitment of RNA polymerase III to its target promoters*. Genes Dev, 2002. **16**(20): p. 2593-620.
86. Donze, D. and R.T. Kamakaka, *RNA polymerase III and RNA polymerase II promoter complexes are heterochromatin barriers in Saccharomyces cerevisiae*. EMBO J, 2001. **20**(3): p. 520-31.
87. Noma, K., et al., *A role for TFIIIC transcription factor complex in genome organization*. Cell, 2006. **125**(5): p. 859-72.
88. Biswas, M., et al., *Limiting the extent of the RDN1 heterochromatin domain by a silencing barrier and Sir2 protein levels in Saccharomyces cerevisiae*. Mol Cell Biol, 2009. **29**(10): p. 2889-98.
89. Lunyak, V.V., et al., *Developmentally regulated activation of a SINE B2 repeat as a domain boundary in organogenesis*. Science, 2007. **317**(5835): p. 248-51.
90. Scott, K.C., S.L. Merrett, and H.F. Willard, *A heterochromatin barrier partitions the fission yeast centromere into discrete chromatin domains*. Curr Biol, 2006. **16**(2): p. 119-29.
91. McNairn, A.J. and J.L. Gerton, *The chromosome glue gets a little stickier*. Trends Genet, 2008. **24**(8): p. 382-9.
92. Hoeffler, W.K. and R.G. Roeder, *Enhancement of RNA polymerase III transcription by the E1A gene product of adenovirus*. Cell, 1985. **41**(3): p. 955-63.
93. Felton-Edkins, Z.A., et al., *Direct regulation of RNA polymerase III transcription by RB, p53 and c-Myc*. Cell Cycle, 2003. **2**(3): p. 181-4.

94. Oler, A.J., et al., *Human RNA polymerase III transcriptomes and relationships to Pol II promoter chromatin and enhancer-binding factors*. Nat Struct Mol Biol, 2010. **17**(5): p. 620-8.
95. Woiwode, A., et al., *PTEN represses RNA polymerase III-dependent transcription by targeting the TFIIIB complex*. Mol Cell Biol, 2008. **28**(12): p. 4204-14.
96. Blau, C.A. and G. Stamatoyannopoulos, *Hemoglobin switching and its clinical implications*. Curr Opin Hematol, 1994. **1**(2): p. 136-42.
97. Curtin, P., et al., *A distant gene deletion affects beta-globin gene function in an atypical gamma delta beta-thalassemia*. J Clin Invest, 1985. **76**(4): p. 1554-8.
98. Forrester, W.C., et al., *A deletion of the human beta-globin locus activation region causes a major alteration in chromatin structure and replication across the entire beta-globin locus*. Genes Dev, 1990. **4**(10): p. 1637-49.
99. Taramelli, R., et al., *Gamma delta beta-thalassaemias 1 and 2 are the result of a 100 kbp deletion in the human beta-globin cluster*. Nucleic Acids Res, 1986. **14**(17): p. 7017-29.
100. Eber, S. and S.E. Lux, *Hereditary spherocytosis--defects in proteins that connect the membrane skeleton to the lipid bilayer*. Semin Hematol, 2004. **41**(2): p. 118-41.
101. Perrotta, S., P.G. Gallagher, and N. Mohandas, *Hereditary spherocytosis*. Lancet, 2008. **372**(9647): p. 1411-26.
102. Gallagher, P.G., *Hematologically important mutations: ankyrin variants in hereditary spherocytosis*. Blood Cells Mol Dis, 2005. **35**(3): p. 345-7.
103. Gallagher, P.G., et al., *Mutation of a barrier insulator in the human ankyrin-1 gene is associated with hereditary spherocytosis*. J Clin Invest, 2010. **120**(12): p. 4453-65.

104. Vostrov, A.A. and W.W. Quitschke, *The zinc finger protein CTCF binds to the APBbeta domain of the amyloid beta-protein precursor promoter. Evidence for a role in transcriptional activation.* J Biol Chem, 1997. **272**(52): p. 33353-9.
105. Qi, C.F., et al., *CTCF functions as a critical regulator of cell-cycle arrest and death after ligation of the B cell receptor on immature B cells.* Proc Natl Acad Sci U S A, 2003. **100**(2): p. 633-8.
106. Aulmann, S., et al., *CTCF gene mutations in invasive ductal breast cancer.* Breast Cancer Res Treat, 2003. **80**(3): p. 347-52.
107. Docquier, F., et al., *Heightened expression of CTCF in breast cancer cells is associated with resistance to apoptosis.* Cancer Res, 2005. **65**(12): p. 5112-22.
108. Li, B., M. Carey, and J.L. Workman, *The role of chromatin during transcription.* Cell, 2007. **128**(4): p. 707-19.
109. Musselman, C.A., et al., *Perceiving the epigenetic landscape through histone readers.* Nat Struct Mol Biol, 2012. **19**(12): p. 1218-27.
110. Tarakhovsky, A., *Tools and landscapes of epigenetics.* Nat Immunol, 2010. **11**(7): p. 565-8.
111. Lee, J.S., E. Smith, and A. Shilatifard, *The language of histone crosstalk.* Cell, 2010. **142**(5): p. 682-5.
112. Zhang, T., S. Cooper, and N. Brockdorff, *The interplay of histone modifications - writers that read.* EMBO Rep, 2015. **16**(11): p. 1467-81.
113. Cheung, P., et al., *Synergistic coupling of histone H3 phosphorylation and acetylation in response to epidermal growth factor stimulation.* Mol Cell, 2000. **5**(6): p. 905-15.

114. Guccione, E., et al., *Methylation of histone H3R2 by PRMT6 and H3K4 by an MLL complex are mutually exclusive*. Nature, 2007. **449**(7164): p. 933-7.
115. Zamudio, N.M., S. Chong, and M.K. O'Bryan, *Epigenetic regulation in male germ cells*. Reproduction, 2008. **136**(2): p. 131-46.
116. Allfrey, V., R. Faulkner, and A. Mirsky, *Acetylation and methylation of histones and their possible role in the regulation of RNA synthesis*. Proceedings of the National Academy of Sciences, 1964. **51**(5): p. 786-794.
117. Candido, E.P., R. Reeves, and J.R. Davie, *Sodium butyrate inhibits histone deacetylation in cultured cells*. Cell, 1978. **14**(1): p. 105-13.
118. Vidali, G., et al., *Butyrate suppression of histone deacetylation leads to accumulation of multiacetylated forms of histones H3 and H4 and increased DNase I sensitivity of the associated DNA sequences*. Proc Natl Acad Sci U S A, 1978. **75**(5): p. 2239-43.
119. Hebbes, T.R., A.W. Thorne, and C. Crane-Robinson, *A direct link between core histone acetylation and transcriptionally active chromatin*. EMBO J, 1988. **7**(5): p. 1395-402.
120. Brownell, J.E. and C.D. Allis, *An activity gel assay detects a single, catalytically active histone acetyltransferase subunit in Tetrahymena macronuclei*. Proc Natl Acad Sci U S A, 1995. **92**(14): p. 6364-8.
121. Davie, J.R. and D.N. Chadee, *Regulation and regulatory parameters of histone modifications*. J Cell Biochem Suppl, 1998. **30-31**: p. 203-13.
122. Davie, J.R. and V.A. Spencer, *Control of histone modifications*. J Cell Biochem, 1999. **Suppl 32-33**: p. 141-8.
123. Spencer, V.A. and J.R. Davie, *Role of covalent modifications of histones in regulating gene expression*. Gene, 1999. **240**(1): p. 1-12.

124. Ridsdale, J.A., et al., *Histone acetylation alters the capacity of the H1 histones to condense transcriptionally active/competent chromatin*. J Biol Chem, 1990. **265**(9): p. 5150-6.
125. Schneider, R., et al., *Histone H3 lysine 4 methylation patterns in higher eukaryotic genes*. Nat Cell Biol, 2004. **6**(1): p. 73-7.
126. Jackson, J.P., et al., *Dimethylation of histone H3 lysine 9 is a critical mark for DNA methylation and gene silencing in Arabidopsis thaliana*. Chromosoma, 2004. **112**(6): p. 308-15.
127. Zhang, K. and S.Y. Dent, *Histone modifying enzymes and cancer: going beyond histones*. J Cell Biochem, 2005. **96**(6): p. 1137-48.
128. Wu, S.C. and Y. Zhang, *Minireview: role of protein methylation and demethylation in nuclear hormone signaling*. Mol Endocrinol, 2009. **23**(9): p. 1323-34.
129. Yang, Y. and M.T. Bedford, *Protein arginine methyltransferases and cancer*. Nat Rev Cancer, 2013. **13**(1): p. 37-50.
130. Feng, Q., et al., *Methylation of H3-lysine 79 is mediated by a new family of HMTases without a SET domain*. Curr Biol, 2002. **12**(12): p. 1052-8.
131. Helin, K. and D. Dhanak, *Chromatin proteins and modifications as drug targets*. Nature, 2013. **502**(7472): p. 480-8.
132. Chen, D., et al., *Regulation of transcription by a protein methyltransferase*. Science, 1999. **284**(5423): p. 2174-7.
133. Vossenaar, E.R., et al., *PAD, a growing family of citrullinating enzymes: genes, features and involvement in disease*. Bioessays, 2003. **25**(11): p. 1106-18.

134. Witalison, E.E., P.R. Thompson, and L.J. Hofseth, *Protein Arginine Deiminases and Associated Citrullination: Physiological Functions and Diseases Associated with Dysregulation*. *Curr Drug Targets*, 2015. **16**(7): p. 700-10.
135. Zhang, X., et al., *Peptidylarginine deiminase 2-catalyzed histone H3 arginine 26 citrullination facilitates estrogen receptor alpha target gene activation*. *Proc Natl Acad Sci U S A*, 2012. **109**(33): p. 13331-6.
136. Wang, Y., et al., *Human PAD4 regulates histone arginine methylation levels via demethylination*. *Science*, 2004. **306**(5694): p. 279-83.
137. Chang, B., et al., *JMJD6 is a histone arginine demethylase*. *Science*, 2007. **318**(5849): p. 444-7.
138. Liu, W., et al., *Brd4 and JMJD6-associated anti-pause enhancers in regulation of transcriptional pause release*. *Cell*, 2013. **155**(7): p. 1581-95.
139. Rossetto, D., N. Avvakumov, and J. Cote, *Histone phosphorylation: a chromatin modification involved in diverse nuclear events*. *Epigenetics*, 2012. **7**(10): p. 1098-108.
140. van Attikum, H. and S.M. Gasser, *The histone code at DNA breaks: a guide to repair?* *Nat Rev Mol Cell Biol*, 2005. **6**(10): p. 757-65.
141. Choi, H.S., et al., *Phosphorylation of histone H3 at serine 10 is indispensable for neoplastic cell transformation*. *Cancer Res*, 2005. **65**(13): p. 5818-27.
142. Wei, Y., et al., *Phosphorylation of histone H3 at serine 10 is correlated with chromosome condensation during mitosis and meiosis in Tetrahymena*. *Proc Natl Acad Sci U S A*, 1998. **95**(13): p. 7480-4.
143. Ajiro, K., *Histone H2B phosphorylation in mammalian apoptotic cells. An association with DNA fragmentation*. *J Biol Chem*, 2000. **275**(1): p. 439-43.

144. Clayton, A.L. and L.C. Mahadevan, *MAP kinase-mediated phosphoacetylation of histone H3 and inducible gene regulation*. FEBS Lett, 2003. **546**(1): p. 51-8.
145. Cerutti, H. and J.A. Casas-Mollano, *Histone H3 phosphorylation: universal code or lineage specific dialects?* Epigenetics, 2009. **4**(2): p. 71-5.
146. Fischle, W., Y. Wang, and C.D. Allis, *Histone and chromatin cross-talk*. Curr Opin Cell Biol, 2003. **15**(2): p. 172-83.
147. Lo, W.S., et al., *Phosphorylation of serine 10 in histone H3 is functionally linked in vitro and in vivo to Gcn5-mediated acetylation at lysine 14*. Mol Cell, 2000. **5**(6): p. 917-26.
148. Cao, J. and Q. Yan, *Histone ubiquitination and deubiquitination in transcription, DNA damage response, and cancer*. Front Oncol, 2012. **2**: p. 26.
149. Cao, R., Y. Tsukada, and Y. Zhang, *Role of Bmi-1 and Ring1A in H2A ubiquitylation and Hox gene silencing*. Mol Cell, 2005. **20**(6): p. 845-54.
150. Gearhart, M.D., et al., *Polycomb group and SCF ubiquitin ligases are found in a novel BCOR complex that is recruited to BCL6 targets*. Mol Cell Biol, 2006. **26**(18): p. 6880-9.
151. Kim, J., S.B. Hake, and R.G. Roeder, *The human homolog of yeast BRE1 functions as a transcriptional coactivator through direct activator interactions*. Mol Cell, 2005. **20**(5): p. 759-70.
152. Shio, Y. and R.N. Eisenman, *Histone sumoylation is associated with transcriptional repression*. Proc Natl Acad Sci U S A, 2003. **100**(23): p. 13225-30.
153. Gregoret, I.V., Y.M. Lee, and H.V. Goodson, *Molecular evolution of the histone deacetylase family: functional implications of phylogenetic analysis*. J Mol Biol, 2004. **338**(1): p. 17-31.

154. de Ruijter, A.J., et al., *Histone deacetylases (HDACs): characterization of the classical HDAC family*. *Biochem J*, 2003. **370**(Pt 3): p. 737-49.
155. Hayakawa, T. and J. Nakayama, *Physiological roles of class I HDAC complex and histone demethylase*. *J Biomed Biotechnol*, 2011. **2011**: p. 129383.
156. Denslow, S.A. and P.A. Wade, *The human Mi-2/NuRD complex and gene regulation*. *Oncogene*, 2007. **26**(37): p. 5433-8.
157. Wang, Y., et al., *LSD1 is a subunit of the NuRD complex and targets the metastasis programs in breast cancer*. *Cell*, 2009. **138**(4): p. 660-72.
158. Liang, J., et al., *Nanog and Oct4 associate with unique transcriptional repression complexes in embryonic stem cells*. *Nat Cell Biol*, 2008. **10**(6): p. 731-9.
159. Lee, M.G., et al., *An essential role for CoREST in nucleosomal histone 3 lysine 4 demethylation*. *Nature*, 2005. **437**(7057): p. 432-5.
160. Delcuve, G.P., D.H. Khan, and J.R. Davie, *Targeting class I histone deacetylases in cancer therapy*. *Expert Opin Ther Targets*, 2013. **17**(1): p. 29-41.
161. Segre, C.V. and S. Chiocca, *Regulating the regulators: the post-translational code of class I HDAC1 and HDAC2*. *J Biomed Biotechnol*, 2011. **2011**: p. 690848.
162. Tsai, S.C. and E. Seto, *Regulation of histone deacetylase 2 by protein kinase CK2*. *J Biol Chem*, 2002. **277**(35): p. 31826-33.
163. Sun, J.M., H.Y. Chen, and J.R. Davie, *Differential distribution of unmodified and phosphorylated histone deacetylase 2 in chromatin*. *J Biol Chem*, 2007. **282**(45): p. 33227-36.
164. Pflum, M.K., et al., *Histone deacetylase 1 phosphorylation promotes enzymatic activity and complex formation*. *J Biol Chem*, 2001. **276**(50): p. 47733-41.

165. Khan, D.H., et al., *RNA-dependent dynamic histone acetylation regulates MCL1 alternative splicing*. Nucleic Acids Res, 2014. **42**(3): p. 1656-70.
166. Delcuve, G.P., D.H. Khan, and J.R. Davie, *Roles of histone deacetylases in epigenetic regulation: emerging paradigms from studies with inhibitors*. Clin Epigenetics, 2012. **4**(1): p. 5.
167. Sun, J.M., et al., *The transcriptional repressor Sp3 is associated with CK2-phosphorylated histone deacetylase 2*. J Biol Chem, 2002. **277**(39): p. 35783-6.
168. Wang, Z., et al., *Genome-wide mapping of HATs and HDACs reveals distinct functions in active and inactive genes*. Cell, 2009. **138**(5): p. 1019-31.
169. Bedford, M.T. and S.G. Clarke, *Protein arginine methylation in mammals: who, what, and why*. Mol Cell, 2009. **33**(1): p. 1-13.
170. Migliori, V., et al., *Arginine/lysine-methyl/methyl switches: biochemical role of histone arginine methylation in transcriptional regulation*. Epigenomics, 2010. **2**(1): p. 119-37.
171. Di Lorenzo, A. and M.T. Bedford, *Histone arginine methylation*. FEBS Lett, 2011. **585**(13): p. 2024-31.
172. Zurita-Lopez, C.I., et al., *Human protein arginine methyltransferase 7 (PRMT7) is a type III enzyme forming omega-NG-monomethylated arginine residues*. J Biol Chem, 2012. **287**(11): p. 7859-70.
173. Wolf, S.S., *The protein arginine methyltransferase family: an update about function, new perspectives and the physiological role in humans*. Cell Mol Life Sci, 2009. **66**(13): p. 2109-21.

174. Krause, C.D., et al., *Protein arginine methyltransferases: evolution and assessment of their pharmacological and therapeutic potential*. *Pharmacol Ther*, 2007. **113**(1): p. 50-87.
175. Pahlich, S., R.P. Zakaryan, and H. Gehring, *Protein arginine methylation: Cellular functions and methods of analysis*. *Biochim Biophys Acta*, 2006. **1764**(12): p. 1890-903.
176. Wei, H., et al., *Protein arginine methylation of non-histone proteins and its role in diseases*. *Cell Cycle*, 2014. **13**(1): p. 32-41.
177. Boisvert, F.M., C.A. Chenard, and S. Richard, *Protein interfaces in signaling regulated by arginine methylation*. *Sci STKE*, 2005. **2005**(271): p. re2.
178. Cheung, N., et al., *Protein arginine-methyltransferase-dependent oncogenesis*. *Nat Cell Biol*, 2007. **9**(10): p. 1208-15.
179. Sugai, M., et al., *Asymmetric dimethylarginine (ADMA) in the aqueous humor of diabetic patients*. *Endocr J*, 2007. **54**(2): p. 303-9.
180. Valkonen, V.P., T.P. Tuomainen, and R. Laaksonen, *DDAH gene and cardiovascular risk*. *Vasc Med*, 2005. **10 Suppl 1**: p. S45-8.
181. Jahan, S. and J.R. Davie, *Protein arginine methyltransferases (PRMTs): role in chromatin organization*. *Adv Biol Regul*, 2015. **57**: p. 173-84.
182. Lin, W.J., et al., *The mammalian immediate-early TIS21 protein and the leukemia-associated BTG1 protein interact with a protein-arginine N-methyltransferase*. *J Biol Chem*, 1996. **271**(25): p. 15034-44.
183. Tang, J., et al., *PRMT 3, a type I protein arginine N-methyltransferase that differs from PRMT1 in its oligomerization, subcellular localization, substrate specificity, and regulation*. *J Biol Chem*, 1998. **273**(27): p. 16935-45.

184. Lee, J. and M.T. Bedford, *PABP1 identified as an arginine methyltransferase substrate using high-density protein arrays*. EMBO Rep, 2002. **3**(3): p. 268-73.
185. Zhang, X. and X. Cheng, *Structure of the predominant protein arginine methyltransferase PRMT1 and analysis of its binding to substrate peptides*. Structure, 2003. **11**(5): p. 509-20.
186. Gayatri, S. and M.T. Bedford, *Readers of histone methylarginine marks*. Biochim Biophys Acta, 2014. **1839**(8): p. 702-10.
187. Sayegh, J., et al., *Regulation of protein arginine methyltransferase 8 (PRMT8) activity by its N-terminal domain*. J Biol Chem, 2007. **282**(50): p. 36444-53.
188. Ganesh, L., et al., *Protein methyltransferase 2 inhibits NF-kappaB function and promotes apoptosis*. Mol Cell Biol, 2006. **26**(10): p. 3864-74.
189. Blythe, S.A., et al., *beta-Catenin primes organizer gene expression by recruiting a histone H3 arginine 8 methyltransferase, Prmt2*. Dev Cell, 2010. **19**(2): p. 220-31.
190. Su, X., et al., *Molecular basis underlying histone H3 lysine-arginine methylation pattern readout by Spin/Ssty repeats of Spindlin1*. Genes Dev, 2014. **28**(6): p. 622-36.
191. Swiercz, R., et al., *Ribosomal protein rpS2 is hypomethylated in PRMT3-deficient mice*. J Biol Chem, 2007. **282**(23): p. 16917-23.
192. Yadav, N., et al., *Specific protein methylation defects and gene expression perturbations in coactivator-associated arginine methyltransferase 1-deficient mice*. Proc Natl Acad Sci U S A, 2003. **100**(11): p. 6464-8.
193. Kim, J., et al., *Loss of CARM1 results in hypomethylation of thymocyte cyclic AMP-regulated phosphoprotein and deregulated early T cell development*. J Biol Chem, 2004. **279**(24): p. 25339-44.

194. Ito, T., et al., *Arginine methyltransferase CARM1/PRMT4 regulates endochondral ossification*. BMC Dev Biol, 2009. **9**: p. 47.
195. O'Brien, K.B., et al., *CARM1 is required for proper control of proliferation and differentiation of pulmonary epithelial cells*. Development, 2010. **137**(13): p. 2147-56.
196. Wu, J., et al., *A role for CARM1-mediated histone H3 arginine methylation in protecting histone acetylation by releasing corepressors from chromatin*. PLoS One, 2012. **7**(6): p. e34692.
197. Casadio, F., et al., *H3R42me2a is a histone modification with positive transcriptional effects*. Proc Natl Acad Sci U S A, 2013. **110**(37): p. 14894-9.
198. Pollack, B.P., et al., *The human homologue of the yeast proteins Skb1 and Hsl7p interacts with Jak kinases and contains protein methyltransferase activity*. J Biol Chem, 1999. **274**(44): p. 31531-42.
199. Zhou, Z., et al., *PRMT5 regulates Golgi apparatus structure through methylation of the golgin GM130*. Cell Res, 2010. **20**(9): p. 1023-33.
200. Neuenkirchen, N., A. Chari, and U. Fischer, *Deciphering the assembly pathway of Sm-class U snRNPs*. FEBS Lett, 2008. **582**(14): p. 1997-2003.
201. Dacwag, C.S., et al., *The protein arginine methyltransferase Prmt5 is required for myogenesis because it facilitates ATP-dependent chromatin remodeling*. Mol Cell Biol, 2007. **27**(1): p. 384-94.
202. Lacroix, M., et al., *The histone-binding protein COPR5 is required for nuclear functions of the protein arginine methyltransferase PRMT5*. EMBO Rep, 2008. **9**(5): p. 452-8.

203. Wang, L., S. Pal, and S. Sif, *Protein arginine methyltransferase 5 suppresses the transcription of the RB family of tumor suppressors in leukemia and lymphoma cells.* Mol Cell Biol, 2008. **28**(20): p. 6262-77.
204. Di Lorenzo, A., et al., *A gain-of-function mouse model identifies PRMT6 as a NF-kappaB coactivator.* Nucleic Acids Res, 2014. **42**(13): p. 8297-309.
205. Stein, C., et al., *The arginine methyltransferase PRMT6 regulates cell proliferation and senescence through transcriptional repression of tumor suppressor genes.* Nucleic Acids Res, 2012. **40**(19): p. 9522-33.
206. Lakowski, T.M. and A. Frankel, *A kinetic study of human protein arginine N-methyltransferase 6 reveals a distributive mechanism.* J Biol Chem, 2008. **283**(15): p. 10015-25.
207. Lee, J.H., et al., *PRMT7, a new protein arginine methyltransferase that synthesizes symmetric dimethylarginine.* J Biol Chem, 2005. **280**(5): p. 3656-64.
208. Gonsalvez, G.B., et al., *Two distinct arginine methyltransferases are required for biogenesis of Sm-class ribonucleoproteins.* J Cell Biol, 2007. **178**(5): p. 733-40.
209. Zheng, Z., et al., *A Mendelian locus on chromosome 16 determines susceptibility to doxorubicin nephropathy in the mouse.* Proc Natl Acad Sci U S A, 2005. **102**(7): p. 2502-7.
210. Gros, L., et al., *Identification of new drug sensitivity genes using genetic suppressor elements: protein arginine N-methyltransferase mediates cell sensitivity to DNA-damaging agents.* Cancer Res, 2003. **63**(1): p. 164-71.
211. Bleibel, W.K., et al., *Identification of genomic regions contributing to etoposide-induced cytotoxicity.* Hum Genet, 2009. **125**(2): p. 173-80.

212. Buhr, N., et al., *Nuclear proteome analysis of undifferentiated mouse embryonic stem and germ cells*. Electrophoresis, 2008. **29**(11): p. 2381-90.
213. Lee, J., et al., *PRMT8, a new membrane-bound tissue-specific member of the protein arginine methyltransferase family*. J Biol Chem, 2005. **280**(38): p. 32890-6.
214. Scaramuzzino, C., et al., *Protein arginine methyltransferase 1 and 8 interact with FUS to modify its sub-cellular distribution and toxicity in vitro and in vivo*. PLoS One, 2013. **8**(4): p. e61576.
215. Andrade, M.A., C. Perez-Iratxeta, and C.P. Ponting, *Protein repeats: structures, functions, and evolution*. J Struct Biol, 2001. **134**(2-3): p. 117-31.
216. Hardisty-Hughes, R.E., et al., *A mutation in the F-box gene, Fbxo11, causes otitis media in the Jeff mouse*. Hum Mol Genet, 2006. **15**(22): p. 3273-9.
217. Migliori, V., et al., *Symmetric dimethylation of H3R2 is a newly identified histone mark that supports euchromatin maintenance*. Nat Struct Mol Biol, 2012. **19**(2): p. 136-44.
218. Schurter, B.T., et al., *Methylation of histone H3 by coactivator-associated arginine methyltransferase 1*. Biochemistry, 2001. **40**(19): p. 5747-56.
219. El Messaoudi, S., et al., *Coactivator-associated arginine methyltransferase 1 (CARM1) is a positive regulator of the Cyclin E1 gene*. Proc Natl Acad Sci U S A, 2006. **103**(36): p. 13351-6.
220. Wang, H., et al., *Methylation of histone H4 at arginine 3 facilitating transcriptional activation by nuclear hormone receptor*. Science, 2001. **293**(5531): p. 853-7.
221. Hyllus, D., et al., *PRMT6-mediated methylation of R2 in histone H3 antagonizes H3 K4 trimethylation*. Genes Dev, 2007. **21**(24): p. 3369-80.

222. Iberg, A.N., et al., *Arginine methylation of the histone H3 tail impedes effector binding*. J Biol Chem, 2008. **283**(6): p. 3006-10.
223. Pal, S., et al., *Human SWI/SNF-associated PRMT5 methylates histone H3 arginine 8 and negatively regulates expression of ST7 and NM23 tumor suppressor genes*. Mol Cell Biol, 2004. **24**(21): p. 9630-45.
224. Zhao, Q., et al., *PRMT5-mediated methylation of histone H4R3 recruits DNMT3A, coupling histone and DNA methylation in gene silencing*. Nat Struct Mol Biol, 2009. **16**(3): p. 304-11.
225. Waldmann, T., et al., *Methylation of H2AR29 is a novel repressive PRMT6 target*. Epigenetics Chromatin, 2011. **4**: p. 11.
226. Aravind, L., S. Abhiman, and L.M. Iyer, *Natural history of the eukaryotic chromatin protein methylation system*. Prog Mol Biol Transl Sci, 2011. **101**: p. 105-76.
227. Pal, S. and S. Sif, *Interplay between chromatin remodelers and protein arginine methyltransferases*. J Cell Physiol, 2007. **213**(2): p. 306-15.
228. Cheng, X., R.E. Collins, and X. Zhang, *Structural and sequence motifs of protein (histone) methylation enzymes*. Annu Rev Biophys Biomol Struct, 2005. **34**: p. 267-94.
229. Selvi, B.R., et al., *Identification of a novel inhibitor of coactivator-associated arginine methyltransferase 1 (CARM1)-mediated methylation of histone H3 Arg-17*. J Biol Chem, 2010. **285**(10): p. 7143-52.
230. Daujat, S., et al., *Crosstalk between CARM1 methylation and CBP acetylation on histone H3*. Curr Biol, 2002. **12**(24): p. 2090-7.

231. Molina-Serrano, D., V. Schiza, and A. Kirmizis, *Cross-talk among epigenetic modifications: lessons from histone arginine methylation*. *Biochem Soc Trans*, 2013. **41**(3): p. 751-9.
232. An, W., J. Kim, and R.G. Roeder, *Ordered cooperative functions of PRMT1, p300, and CARM1 in transcriptional activation by p53*. *Cell*, 2004. **117**(6): p. 735-48.
233. Yue, W.W., et al., *Insights into histone code syntax from structural and biochemical studies of CARM1 methyltransferase*. *EMBO J*, 2007. **26**(20): p. 4402-12.
234. Metivier, R., et al., *Estrogen receptor-alpha directs ordered, cyclical, and combinatorial recruitment of cofactors on a natural target promoter*. *Cell*, 2003. **115**(6): p. 751-63.
235. Sakabe, K. and G.W. Hart, *O-GlcNAc transferase regulates mitotic chromatin dynamics*. *J Biol Chem*, 2010. **285**(45): p. 34460-8.
236. Lupien, M., et al., *Coactivator function defines the active estrogen receptor alpha cistrome*. *Mol Cell Biol*, 2009. **29**(12): p. 3413-23.
237. Bauer, U.M., et al., *Methylation at arginine 17 of histone H3 is linked to gene activation*. *EMBO Rep*, 2002. **3**(1): p. 39-44.
238. Margueron, R., et al., *Role of the polycomb protein EED in the propagation of repressive histone marks*. *Nature*, 2009. **461**(7265): p. 762-7.
239. Guccione, E., et al., *Myc-binding-site recognition in the human genome is determined by chromatin context*. *Nat Cell Biol*, 2006. **8**(7): p. 764-70.
240. Rosenfeld, J.A., et al., *Determination of enriched histone modifications in non-genic portions of the human genome*. *BMC Genomics*, 2009. **10**: p. 143.
241. Barski, A., et al., *High-resolution profiling of histone methylations in the human genome*. *Cell*, 2007. **129**(4): p. 823-37.

242. Denis, H., et al., *Functional connection between deimination and deacetylation of histones*. Mol Cell Biol, 2009. **29**(18): p. 4982-93.
243. Kleinschmidt, M.A., et al., *The protein arginine methyltransferases CARM1 and PRMT1 cooperate in gene regulation*. Nucleic Acids Res, 2008. **36**(10): p. 3202-13.
244. Xie, Y., et al., *Epigenetic regulation of transcriptional activity of pregnane X receptor by protein arginine methyltransferase I*. J Biol Chem, 2009. **284**(14): p. 9199-205.
245. Pesavento, J.J., et al., *Combinatorial modification of human histone H4 quantitated by two-dimensional liquid chromatography coupled with top down mass spectrometry*. J Biol Chem, 2008. **283**(22): p. 14927-37.
246. Phanstiel, D., et al., *Mass spectrometry identifies and quantifies 74 unique histone H4 isoforms in differentiating human embryonic stem cells*. Proc Natl Acad Sci U S A, 2008. **105**(11): p. 4093-8.
247. Girardot, M., et al., *PRMT5-mediated histone H4 arginine-3 symmetrical dimethylation marks chromatin at G + C-rich regions of the mouse genome*. Nucleic Acids Res, 2014. **42**(1): p. 235-48.
248. Jelinic, P., J.C. Stehle, and P. Shaw, *The testis-specific factor CTCFL cooperates with the protein methyltransferase PRMT7 in H19 imprinting control region methylation*. PLoS Biol, 2006. **4**(11): p. e355.
249. Rank, G., et al., *Identification of a PRMT5-dependent repressor complex linked to silencing of human fetal globin gene expression*. Blood, 2010. **116**(9): p. 1585-92.
250. Hou, Z., et al., *The LIM protein AJUBA recruits protein arginine methyltransferase 5 to mediate SNAIL-dependent transcriptional repression*. Mol Cell Biol, 2008. **28**(10): p. 3198-207.

251. Cesaro, E., et al., *The Kruppel-like zinc finger protein ZNF224 recruits the arginine methyltransferase PRMT5 on the transcriptional repressor complex of the aldolase A gene*. J Biol Chem, 2009. **284**(47): p. 32321-30.
252. Tabata, T., et al., *Ski co-repressor complexes maintain the basal repressed state of the TGF-beta target gene, SMAD7, via HDAC3 and PRMT5*. Genes Cells, 2009. **14**(1): p. 17-28.
253. Tae, S., et al., *Bromodomain protein 7 interacts with PRMT5 and PRC2, and is involved in transcriptional repression of their target genes*. Nucleic Acids Res, 2011. **39**(13): p. 5424-38.
254. Rathert, P., et al., *Protein lysine methyltransferase G9a acts on non-histone targets*. Nat Chem Biol, 2008. **4**(6): p. 344-6.
255. Kuhn, P. and W. Xu, *Protein arginine methyltransferases: nuclear receptor coregulators and beyond*. Prog Mol Biol Transl Sci, 2009. **87**: p. 299-342.
256. Bezzi, M., et al., *Regulation of constitutive and alternative splicing by PRMT5 reveals a role for Mdm4 pre-mRNA in sensing defects in the spliceosomal machinery*. Genes Dev, 2013. **27**(17): p. 1903-16.
257. Karkhanis, V., et al., *Versatility of PRMT5-induced methylation in growth control and development*. Trends Biochem Sci, 2011. **36**(12): p. 633-41.
258. Bedford, M.T. and S. Richard, *Arginine methylation an emerging regulator of protein function*. Mol Cell, 2005. **18**(3): p. 263-72.
259. Zhao, X., et al., *Methylation of RUNX1 by PRMT1 abrogates SIN3A binding and potentiates its transcriptional activity*. Genes Dev, 2008. **22**(5): p. 640-53.

260. Le Guezennec, X., et al., *MBD2/NuRD and MBD3/NuRD, two distinct complexes with different biochemical and functional properties*. Mol Cell Biol, 2006. **26**(3): p. 843-51.
261. Ma, M.K., et al., *Histone crosstalk directed by H2B ubiquitination is required for chromatin boundary integrity*. PLoS.Genet., 2011. **7**(7): p. e1002175.
262. Yuan, C.C., et al., *Histone H3R2 symmetric dimethylation and histone H3K4 trimethylation are tightly correlated in eukaryotic genomes*. Cell Rep., 2012. **1**(2): p. 83-90.
263. Baldwin, R.M., A. Morettin, and J. Cote, *Role of PRMTs in cancer: Could minor isoforms be leaving a mark?* World J Biol Chem, 2014. **5**(2): p. 115-29.
264. Van Rechem, C. and J.R. Whetstine, *Examining the impact of gene variants on histone lysine methylation*. Biochim Biophys Acta, 2014. **1839**(12): p. 1463-76.
265. Wang, J., et al., *Pharmacophore-based virtual screening and biological evaluation of small molecule inhibitors for protein arginine methylation*. J Med Chem, 2012. **55**(18): p. 7978-87.
266. Yang, Y., et al., *TDRD3 is an effector molecule for arginine-methylated histone marks*. Mol Cell, 2010. **40**(6): p. 1016-23.
267. Majumder, S., et al., *Involvement of arginine methyltransferase CARM1 in androgen receptor function and prostate cancer cell viability*. Prostate, 2006. **66**(12): p. 1292-301.
268. Yager, J.D. and N.E. Davidson, *Estrogen carcinogenesis in breast cancer*. N Engl J Med, 2006. **354**(3): p. 270-82.
269. Ou, C.Y., et al., *A coactivator role of CARM1 in the dysregulation of beta-catenin activity in colorectal cancer cell growth and gene expression*. Mol Cancer Res, 2011. **9**(5): p. 660-70.

270. Kim, Y.R., et al., *Differential CARM1 expression in prostate and colorectal cancers*. BMC Cancer, 2010. **10**: p. 197.
271. Chung, J., et al., *Protein arginine methyltransferase 5 (PRMT5) inhibition induces lymphoma cell death through reactivation of the retinoblastoma tumor suppressor pathway and polycomb repressor complex 2 (PRC2) silencing*. J Biol Chem, 2013. **288**(49): p. 35534-47.
272. Yoshimatsu, M., et al., *Dysregulation of PRMT1 and PRMT6, Type I arginine methyltransferases, is involved in various types of human cancers*. Int J Cancer, 2011. **128**(3): p. 562-73.
273. Wei, T.Y., et al., *Protein arginine methyltransferase 5 is a potential oncoprotein that upregulates G1 cyclins/cyclin-dependent kinases and the phosphoinositide 3-kinase/AKT signaling cascade*. Cancer Sci, 2012. **103**(9): p. 1640-50.
274. Kooistra, S.M. and K. Helin, *Molecular mechanisms and potential functions of histone demethylases*. Nat Rev Mol Cell Biol, 2012. **13**(5): p. 297-311.
275. Cuthbert, G.L., et al., *Histone deimination antagonizes arginine methylation*. Cell, 2004. **118**(5): p. 545-53.
276. Robin-Lespinnasse, Y., et al., *hCAF1, a new regulator of PRMT1-dependent arginine methylation*. J Cell Sci, 2007. **120**(Pt 4): p. 638-47.
277. Singh, V., et al., *DAL-1/4.1B tumor suppressor interacts with protein arginine N-methyltransferase 3 (PRMT3) and inhibits its ability to methylate substrates in vitro and in vivo*. Oncogene, 2004. **23**(47): p. 7761-71.
278. Cha, B. and E.H. Jho, *Protein arginine methyltransferases (PRMTs) as therapeutic targets*. Expert Opin Ther Targets, 2012. **16**(7): p. 651-64.

279. Sanders, M.M., *Fractionation of nucleosomes by salt elution from micrococcal nuclease-digested nuclei*. J Cell Biol, 1978. **79**(1): p. 97-109.
280. Henikoff, S., et al., *Genome-wide profiling of salt fractions maps physical properties of chromatin*. Genome Res, 2009. **19**(3): p. 460-9.
281. Hendzel, M.J., et al., *Histone acetyltransferase is associated with the nuclear matrix*. J Biol Chem, 1994. **269**(36): p. 22894-901.
282. Delcuve, G.P. and J.R. Davie, *Chromatin structure of erythroid-specific genes of immature and mature chicken erythrocytes*. Biochem J, 1989. **263**(1): p. 179-86.
283. Hebbes, T.R. and S.C. Allen, *Multiple histone acetyltransferases are associated with a chicken erythrocyte chromatin fraction enriched in active genes*. J Biol Chem, 2000. **275**(40): p. 31347-52.
284. Bates, D.L. and J.O. Thomas, *Histones H1 and H5: one or two molecules per nucleosome?* Nucleic Acids Res, 1981. **9**(22): p. 5883-94.
285. Jahan, S., et al., *The chicken erythrocyte epigenome*. Epigenetics Chromatin, 2016. **9**: p. 19.
286. Williams, A.F., *DNA synthesis in purified populations of avian erythroid cells*. J Cell Sci, 1972. **10**(1): p. 27-46.
287. Ridsdale, J.A. and J.R. Davie, *Chicken erythrocyte polynucleosomes which are soluble at physiological ionic strength and contain linker histones are highly enriched in beta-globin gene sequences*. Nucleic Acids Res, 1987. **15**(3): p. 1081-96.
288. Shogren-Knaak, M., et al., *Histone H4-K16 acetylation controls chromatin structure and protein interactions*. Science, 2006. **311**(5762): p. 844-7.

289. Ridsdale, J.A., J.B. Rattner, and J.R. Davie, *Erythroid-specific gene chromatin has an altered association with linker histones*. Nucleic Acids Res, 1988. **16**(13): p. 5915-26.
290. Locklear, L., Jr., et al., *Ultrastructure of transcriptionally competent chromatin*. Nucleic Acids Res, 1990. **18**(23): p. 7015-24.
291. Sun, J.M., et al., *Phosphorylated serine 28 of histone H3 is associated with destabilized nucleosomes in transcribed chromatin*. Nucleic Acids Res, 2007. **35**(19): p. 6640-7.
292. Clark, R. and T. Kupper, *Old meets new: the interaction between innate and adaptive immunity*. J Invest Dermatol, 2005. **125**(4): p. 629-37.
293. Chen, S., A. Cheng, and M. Wang, *Innate sensing of viruses by pattern recognition receptors in birds*. Vet Res, 2013. **44**: p. 82.
294. Kaiser, P., *Advances in avian immunology--prospects for disease control: a review*. Avian Pathol, 2010. **39**(5): p. 309-24.
295. Temperley, N.D., et al., *Evolution of the chicken Toll-like receptor gene family: a story of gene gain and gene loss*. BMC Genomics, 2008. **9**: p. 62.
296. Boyd, A., V.J. Philbin, and A.L. Smith, *Conserved and distinct aspects of the avian Toll-like receptor (TLR) system: implications for transmission and control of bird-borne zoonoses*. Biochem Soc Trans, 2007. **35**(Pt 6): p. 1504-7.
297. Lynn, D.J., et al., *Avian beta-defensin nomenclature: a community proposed update*. Immunol Lett, 2007. **110**(1): p. 86-9.
298. Kaiser, P., et al., *A genomic analysis of chicken cytokines and chemokines*. J Interferon Cytokine Res, 2005. **25**(8): p. 467-84.
299. Kaiser, P., *The avian immune genome--a glass half-full or half-empty?* Cytogenet Genome Res, 2007. **117**(1-4): p. 221-30.

300. Petrilli, V., et al., *The inflammasome: a danger sensing complex triggering innate immunity*. *Curr Opin Immunol*, 2007. **19**(6): p. 615-22.
301. Takeuchi, O. and S. Akira, *Innate immunity to virus infection*. *Immunol Rev*, 2009. **227**(1): p. 75-86.
302. Fukui, A., et al., *Molecular cloning and functional characterization of chicken toll-like receptors. A single chicken toll covers multiple molecular patterns*. *J Biol Chem*, 2001. **276**(50): p. 47143-9.
303. Kogut, M.H., et al., *Expression and function of Toll-like receptors in chicken heterophils*. *Dev Comp Immunol*, 2005. **29**(9): p. 791-807.
304. Schwarz, H., et al., *Chicken toll-like receptor 3 recognizes its cognate ligand when ectopically expressed in human cells*. *J Interferon Cytokine Res*, 2007. **27**(2): p. 97-101.
305. He, H., et al., *Profile of Toll-like receptor expressions and induction of nitric oxide synthesis by Toll-like receptor agonists in chicken monocytes*. *Mol Immunol*, 2006. **43**(7): p. 783-9.
306. Kawai, T. and S. Akira, *The role of pattern-recognition receptors in innate immunity: update on Toll-like receptors*. *Nat Immunol*, 2010. **11**(5): p. 373-84.
307. Akira, S., K. Takeda, and T. Kaisho, *Toll-like receptors: critical proteins linking innate and acquired immunity*. *Nat Immunol*, 2001. **2**(8): p. 675-80.
308. Akira, S., S. Uematsu, and O. Takeuchi, *Pathogen recognition and innate immunity*. *Cell*, 2006. **124**(4): p. 783-801.
309. Kawai, T. and S. Akira, *Innate immune recognition of viral infection*. *Nat Immunol*, 2006. **7**(2): p. 131-7.

310. Barbalat, R., et al., *Toll-like receptor 2 on inflammatory monocytes induces type I interferon in response to viral but not bacterial ligands*. Nat Immunol, 2009. **10**(11): p. 1200-7.
311. Brownlie, R. and B. Allan, *Avian toll-like receptors*. Cell Tissue Res, 2011. **343**(1): p. 121-30.
312. Keesstra, A.M., et al., *The central leucine-rich repeat region of chicken TLR16 dictates unique ligand specificity and species-specific interaction with TLR2*. J Immunol, 2007. **178**(11): p. 7110-9.
313. Higuchi, M., et al., *Combinational recognition of bacterial lipoproteins and peptidoglycan by chicken Toll-like receptor 2 subfamily*. Dev Comp Immunol, 2008. **32**(2): p. 147-55.
314. Ruan, W., Y. Wu, and S.J. Zheng, *Different genetic patterns in avian Toll-like receptor (TLR)5 genes*. Mol Biol Rep, 2012. **39**(4): p. 3419-26.
315. Bieback, K., et al., *Hemagglutinin protein of wild-type measles virus activates toll-like receptor 2 signaling*. J Virol, 2002. **76**(17): p. 8729-36.
316. Compton, T., et al., *Human cytomegalovirus activates inflammatory cytokine responses via CD14 and Toll-like receptor 2*. J Virol, 2003. **77**(8): p. 4588-96.
317. Wang, J.P., et al., *Varicella-zoster virus activates inflammatory cytokines in human monocytes and macrophages via Toll-like receptor 2*. J Virol, 2005. **79**(20): p. 12658-66.
318. Kurt-Jones, E.A., et al., *Herpes simplex virus 1 interaction with Toll-like receptor 2 contributes to lethal encephalitis*. Proc Natl Acad Sci U S A, 2004. **101**(5): p. 1315-20.
319. Kurt-Jones, E.A., et al., *Pattern recognition receptors TLR4 and CD14 mediate response to respiratory syncytial virus*. Nat Immunol, 2000. **1**(5): p. 398-401.

320. Courreges, M.C., et al., *Critical role of dendritic cells in mouse mammary tumor virus in vivo infection*. J Virol, 2007. **81**(8): p. 3769-77.
321. St Paul, M., et al., *Toll-like receptor ligands induce the expression of interferon-gamma and interleukin-17 in chicken CD4+ T cells*. BMC Res Notes, 2012. **5**: p. 616.
322. St Paul, M., et al., *Chicken erythrocytes respond to Toll-like receptor ligands by up-regulating cytokine transcripts*. Res Vet Sci, 2013. **95**(1): p. 87-91.
323. Philbin, V.J., et al., *Identification and characterization of a functional, alternatively spliced Toll-like receptor 7 (TLR7) and genomic disruption of TLR8 in chickens*. Immunology, 2005. **114**(4): p. 507-21.
324. Vleugels, B., C. Ververken, and B.M. Goddeeris, *Stimulatory effect of CpG sequences on humoral response in chickens*. Poult Sci, 2002. **81**(9): p. 1317-21.
325. Higgs, R., et al., *Induction of a novel chicken Toll-like receptor following Salmonella enterica serovar Typhimurium infection*. Infect Immun, 2006. **74**(3): p. 1692-8.
326. Ramasamy, K.T., et al., *Expression analysis of turkey (Meleagris gallopavo) toll-like receptors and molecular characterization of avian specific TLR15*. Mol Biol Rep, 2012. **39**(8): p. 8539-49.
327. Ciraci, C. and S.J. Lamont, *Avian-specific TLRs and downstream effector responses to CpG-induction in chicken macrophages*. Dev Comp Immunol, 2011. **35**(3): p. 392-8.
328. Heidari, M., et al., *Marek's disease virus-induced immunosuppression: array analysis of chicken immune response gene expression profiling*. Viral Immunol, 2010. **23**(3): p. 309-19.
329. Roach, J.C., et al., *The evolution of vertebrate Toll-like receptors*. Proc Natl Acad Sci U S A, 2005. **102**(27): p. 9577-82.

330. Brownlie, R., et al., *Chicken TLR21 acts as a functional homologue to mammalian TLR9 in the recognition of CpG oligodeoxynucleotides*. Mol Immunol, 2009. **46**(15): p. 3163-70.
331. Kestra, A.M., et al., *Chicken TLR21 is an innate CpG DNA receptor distinct from mammalian TLR9*. J Immunol, 2010. **185**(1): p. 460-7.
332. Brisbin, J.T., P. Parvizi, and S. Sharif, *Differential cytokine expression in T-cell subsets of chicken caecal tonsils co-cultured with three species of Lactobacillus*. Benef Microbes, 2012. **3**(3): p. 205-10.
333. Yoneyama, M. and T. Fujita, *RNA recognition and signal transduction by RIG-I-like receptors*. Immunol Rev, 2009. **227**(1): p. 54-65.
334. Zou, J., et al., *Origin and evolution of the RIG-I like RNA helicase gene family*. BMC Evol Biol, 2009. **9**: p. 85.
335. Pichlmair, A., et al., *RIG-I-mediated antiviral responses to single-stranded RNA bearing 5'-phosphates*. Science, 2006. **314**(5801): p. 997-1001.
336. Matsumiya, T. and D.M. Stafforini, *Function and regulation of retinoic acid-inducible gene-I*. Crit Rev Immunol, 2010. **30**(6): p. 489-513.
337. Samanta, M., et al., *EB virus-encoded RNAs are recognized by RIG-I and activate signaling to induce type I IFN*. EMBO J, 2006. **25**(18): p. 4207-14.
338. Hornung, V., et al., *5'-Triphosphate RNA is the ligand for RIG-I*. Science, 2006. **314**(5801): p. 994-7.
339. Karpala, A.J., et al., *Characterization of chicken Mda5 activity: regulation of IFN-beta in the absence of RIG-I functionality*. J Immunol, 2011. **186**(9): p. 5397-405.

340. Kato, H., et al., *Length-dependent recognition of double-stranded ribonucleic acids by retinoic acid-inducible gene-I and melanoma differentiation-associated gene 5*. J Exp Med, 2008. **205**(7): p. 1601-10.
341. Lee, C.C., C.C. Wu, and T.L. Lin, *Characterization of chicken melanoma differentiation-associated gene 5 (MDA5) from alternative translation initiation*. Comp Immunol Microbiol Infect Dis, 2012. **35**(4): p. 335-43.
342. Liniger, M., A. Summerfield, and N. Ruggli, *MDA5 can be exploited as efficacious genetic adjuvant for DNA vaccination against lethal H5N1 influenza virus infection in chickens*. PLoS One, 2012. **7**(12): p. e49952.
343. Childs, K., et al., *mda-5, but not RIG-I, is a common target for paramyxovirus V proteins*. Virology, 2007. **359**(1): p. 190-200.
344. Liniger, M., et al., *Chicken cells sense influenza A virus infection through MDA5 and CARDIF signaling involving LGP2*. J Virol, 2012. **86**(2): p. 705-17.
345. Franchi, L., et al., *The inflammasome: a caspase-1-activation platform that regulates immune responses and disease pathogenesis*. Nat Immunol, 2009. **10**(3): p. 241-7.
346. Muruve, D.A., et al., *The inflammasome recognizes cytosolic microbial and host DNA and triggers an innate immune response*. Nature, 2008. **452**(7183): p. 103-7.
347. Inohara, et al., *NOD-LRR proteins: role in host-microbial interactions and inflammatory disease*. Annu Rev Biochem, 2005. **74**: p. 355-83.
348. Lian, L., et al., *NLRC5 knockdown in chicken macrophages alters response to LPS and poly (I:C) stimulation*. BMC Vet Res, 2012. **8**: p. 23.
349. Ciraci, C., et al., *Unique genome-wide transcriptome profiles of chicken macrophages exposed to Salmonella-derived endotoxin*. BMC Genomics, 2010. **11**: p. 545.

350. Kaufman, J., et al., *The chicken B locus is a minimal essential major histocompatibility complex*. Nature, 1999. **401**(6756): p. 923-5.
351. Claver, J.A. and A.I. Quaglia, *Comparative Morphology, Development, and Function of Blood Cells in Nonmammalian Vertebrates*. Journal of Exotic Pet Medicine, 2009. **18**(2): p. 87-97.
352. Hawkey, C.M., et al., *Erythrocyte size, number and haemoglobin content in vertebrates*. Br J Haematol, 1991. **77**(3): p. 392-7.
353. Avery, E.H., et al., *Bile pigments in gallbladder and freshly-secreted hepatic duct bile from fed and fasted rainbow trout, *Oncorhynchus mykiss**. Comp Biochem Physiol Comp Physiol, 1992. **101**(4): p. 857-61.
354. O'Malley, B., *Clinical anatomy and physiology of exotic species*. 2005: WB Saunders Company.
355. Davies, A.J. and M.R. Johnston, *The biology of some intraerythrocytic parasites of fishes, amphibia and reptiles*. Adv Parasitol, 2000. **45**: p. 1-107.
356. Zhang, D.E. and D.A. Nelson, *Histone acetylation in chicken erythrocytes. Rates of deacetylation in immature and mature red blood cells*. Biochem J, 1988. **250**(1): p. 241-5.
357. Sennikov, S.V., et al., *Production of hemo- and immunoregulatory cytokines by erythroblast antigen+ and glycophorin A+ cells from human bone marrow*. BMC Cell Biol, 2004. **5**(1): p. 39.
358. Morera, D., et al., *RNA-Seq reveals an integrated immune response in nucleated erythrocytes*. PLoS One, 2011. **6**(10): p. e26998.

359. Morera, D. and S.A. MacKenzie, *Is there a direct role for erythrocytes in the immune response?* Vet Res, 2011. **42**: p. 89.
360. Workenhe, S.T., et al., *Infectious salmon anaemia virus replication and induction of alpha interferon in Atlantic salmon erythrocytes.* Virol J, 2008. **5**: p. 36.
361. Passantino, L., et al., *Maturation of fish erythrocytes coincides with changes in their morphology, enhanced ability to interact with Candida albicans and release of cytokine-like factors active upon autologous macrophages.* Immunopharmacol Immunotoxicol, 2004. **26**(4): p. 573-85.
362. Passantino, L., et al., *Antigenically activated avian erythrocytes release cytokine-like factors: a conserved phylogenetic function discovered in fish.* Immunopharmacol Immunotoxicol, 2007. **29**(1): p. 141-52.
363. Nikinmaa, M., *Oxygen and carbon dioxide transport in vertebrate erythrocytes: an evolutionary change in the role of membrane transport.* J Exp Biol, 1997. **200**(Pt 2): p. 369-80.
364. Montel-Hagen, A., M. Sitbon, and N. Taylor, *Erythroid glucose transporters.* Curr Opin Hematol, 2009. **16**(3): p. 165-72.
365. Perez-Gordones, M.C., et al., *Diacylglycerol regulates the plasma membrane calcium pump from human erythrocytes by direct interaction.* Arch Biochem Biophys, 2009. **489**(1-2): p. 55-61.
366. Tsantes, A.E., et al., *Redox imbalance, macrocytosis, and RBC homeostasis.* Antioxid Redox Signal, 2006. **8**(7-8): p. 1205-16.

367. Fonseca, A.M., et al., *Red blood cells promote survival and cell cycle progression of human peripheral blood T cells independently of CD58/LFA-3 and heme compounds*. Cell Immunol, 2003. **224**(1): p. 17-28.
368. Gershon, H., *The anti-inflammatory role of the erythrocyte: impairment in the elderly*. Arch Gerontol Geriatr, 1997. **24**(2): p. 157-65.
369. Jiang, N., et al., *Respiratory protein-generated reactive oxygen species as an antimicrobial strategy*. Nat Immunol, 2007. **8**(10): p. 1114-22.
370. Liepke, C., et al., *Human hemoglobin-derived peptides exhibit antimicrobial activity: a class of host defense peptides*. J Chromatogr B Analyt Technol Biomed Life Sci, 2003. **791**(1-2): p. 345-56.
371. Morariu, A.M., et al., *Acute isovolemic hemodilution triggers proinflammatory and procoagulatory endothelial activation in vital organs: role of erythrocyte aggregation*. Microcirculation, 2006. **13**(5): p. 397-409.
372. Pesquero, J., et al., *Glucose metabolism by trout (*Salmo trutta*) red blood cells*. J Comp Physiol B, 1992. **162**(5): p. 448-54.
373. Orlov, S.N., S.L. Aksentsev, and S.V. Kotelevtsev, *Extracellular calcium is required for the maintenance of plasma membrane integrity in nucleated cells*. Cell Calcium, 2005. **38**(1): p. 53-7.
374. Jensen, F.B., *The role of nitrite in nitric oxide homeostasis: a comparative perspective*. Biochim Biophys Acta, 2009. **1787**(7): p. 841-8.
375. Schraml, B., M.A. Baker, and B.D. Reilly, *A complement receptor for opsonized immune complexes on erythrocytes from *Oncorhynchus mykiss* but not *Ictalurus punctatus**. Mol Immunol, 2006. **43**(10): p. 1595-603.

376. Fedeli, D., M. Carloni, and G. Falcioni, *Oxidative damage in trout erythrocyte in response to "in vitro" copper exposure*. Mar Environ Res, 2010. **69**(3): p. 172-7.
377. Ullal, A.J., R.W. Litaker, and E.J. Noga, *Antimicrobial peptides derived from hemoglobin are expressed in epithelium of channel catfish (*Ictalurus punctatus*, *Rafinesque*)*. Dev Comp Immunol, 2008. **32**(11): p. 1301-12.
378. Fernandes, J.M. and V.J. Smith, *Partial purification of antibacterial proteinaceous factors from erythrocytes of *Oncorhynchus mykiss**. Fish Shellfish Immunol, 2004. **16**(1): p. 1-9.
379. Kaloyianni, M. and I. Doukakis, *Effect of adrenaline on glucose transport in red cells of *Rana balcanica**. Gen Physiol Biophys, 2003. **22**(1): p. 69-80.
380. Light, D.B., et al., *Cell swelling increases intracellular calcium in *Necturus erythrocytes**. J Cell Sci, 2003. **116**(Pt 1): p. 101-9.
381. Mauro, N.A. and R.E. Isaacks, *Examination of reptilian erythrocytes as models of the progenitor of mammalian red blood cells*. Comp Biochem Physiol A Physiol, 1997. **116**(4): p. 323-7.
382. Bagnaresi, P., M.T. Rodrigues, and C.R. Garcia, *Calcium signaling in lizard red blood cells*. Comp Biochem Physiol A Mol Integr Physiol, 2007. **147**(3): p. 779-87.
383. Torsoni, M.A. and S.H. Ogo, *Hemoglobin-sulfhydryls from tortoise (*Geochelone carbonaria*) can reduce oxidative damage induced by organic hydroperoxide in erythrocyte membrane*. Comp Biochem Physiol B Biochem Mol Biol, 2000. **126**(4): p. 571-7.
384. Parish, C.A., et al., *Broad-spectrum antimicrobial activity of hemoglobin*. Bioorg Med Chem, 2001. **9**(2): p. 377-82.

385. Braun, E.J. and K.L. Sweazea, *Glucose regulation in birds*. Comp Biochem Physiol B Biochem Mol Biol, 2008. **151**(1): p. 1-9.
386. Alves-Ferreira, M., H.M. Scofano, and A. Ferreira-Pereira, *Ca(2+)-ATPase from chicken (Gallus domesticus) erythrocyte plasma membrane: effects of calmodulin and taurine on the Ca(2+)-dependent ATPase activity and Ca²⁺ uptake*. Comp Biochem Physiol B Biochem Mol Biol, 1999. **122**(3): p. 269-76.
387. Di Simplicio, P., et al., *Role of protein -SH groups in redox homeostasis--the erythrocyte as a model system*. Arch Biochem Biophys, 1998. **355**(2): p. 145-52.
388. Bertram, E.M., A.R. Jilbert, and I. Kotlarski, *Optimization of an in vitro assay which measures the proliferation of duck T lymphocytes from peripheral blood in response to stimulation with PHA and ConA*. Dev Comp Immunol, 1997. **21**(3): p. 299-310.
389. Mian, M.F., et al., *Length of dsRNA (poly I:C) drives distinct innate immune responses, depending on the cell type*. J Leukoc Biol, 2013. **94**(5): p. 1025-36.
390. Brat, D.J., A.C. Bellail, and E.G. Van Meir, *The role of interleukin-8 and its receptors in gliomagenesis and tumoral angiogenesis*. Neuro-oncology, 2005. **7**(2): p. 122-133.
391. Fortier, M.E., et al., *The viral mimic, polyinosinic:polycytidylic acid, induces fever in rats via an interleukin-1-dependent mechanism*. Am J Physiol Regul Integr Comp Physiol, 2004. **287**(4): p. R759-66.
392. DeWitte-Orr, S.J., et al., *Long double-stranded RNA induces an antiviral response independent of IFN regulatory factor 3, IFN-beta promoter stimulator 1, and IFN*. J Immunol, 2009. **183**(10): p. 6545-53.
393. Poltorak, A., et al., *Defective LPS signaling in C3H/HeJ and C57BL/10ScCr mice: mutations in Tlr4 gene*. Science, 1998. **282**(5396): p. 2085-8.

394. Shimazu, R., et al., *MD-2, a molecule that confers lipopolysaccharide responsiveness on Toll-like receptor 4*. J Exp Med, 1999. **189**(11): p. 1777-82.
395. Netea, M.G., et al., *Does the shape of lipid A determine the interaction of LPS with Toll-like receptors?* Trends Immunol, 2002. **23**(3): p. 135-9.
396. Kawai, T., et al., *Lipopolysaccharide stimulates the MyD88-independent pathway and results in activation of IFN-regulatory factor 3 and the expression of a subset of lipopolysaccharide-inducible genes*. J Immunol, 2001. **167**(10): p. 5887-94.
397. Shah, S.M., et al., *Differential Expression of Th1- and Th2- Type Cytokines in Peripheral Blood Mononuclear Cells of Murrah Buffalo (Bubalus Bubalis) on TLR2 Induction by B. Subtilis Peptidoglycan*. Asian-Australas J Anim Sci, 2012. **25**(7): p. 1021-8.
398. Schwandner, R., et al., *Peptidoglycan- and lipoteichoic acid-induced cell activation is mediated by toll-like receptor 2*. J Biol Chem, 1999. **274**(25): p. 17406-9.
399. Takeuchi, O., et al., *Differential roles of TLR2 and TLR4 in recognition of gram-negative and gram-positive bacterial cell wall components*. Immunity, 1999. **11**(4): p. 443-51.
400. Chamailard, M., et al., *An essential role for NOD1 in host recognition of bacterial peptidoglycan containing diaminopimelic acid*. Nat Immunol, 2003. **4**(7): p. 702-7.
401. Girardin, S.E., et al., *Nod1 detects a unique muropeptide from gram-negative bacterial peptidoglycan*. Science, 2003. **300**(5625): p. 1584-7.
402. Girardin, S.E., et al., *Nod2 is a general sensor of peptidoglycan through muramyl dipeptide (MDP) detection*. J Biol Chem, 2003. **278**(11): p. 8869-72.
403. Bauer, S. and H. Wagner, *Bacterial CpG-DNA licenses TLR9*. Curr Top Microbiol Immunol, 2002. **270**: p. 145-54.

404. Rothenfusser, S., et al., *Plasmacytoid dendritic cells: the key to CpG*. Hum Immunol, 2002. **63**(12): p. 1111-9.
405. Vollmer, J. and A.M. Krieg, *Immunotherapeutic applications of CpG oligodeoxynucleotide TLR9 agonists*. Adv Drug Deliv Rev, 2009. **61**(3): p. 195-204.
406. Zhang, D.E. and D.A. Nelson, *Histone acetylation in chicken erythrocytes. Rates of acetylation and evidence that histones in both active and potentially active chromatin are rapidly modified*. Biochem J, 1988. **250**(1): p. 233-40.
407. Rocha, E., et al., *Differential salt fractionation of active and inactive genomic domains in chicken erythrocyte*. J Biol Chem, 1984. **259**(13): p. 8558-63.
408. Spencer, V.A. and J.R. Davie, *Dynamically acetylated histone association with transcriptionally active and competent genes in the avian adult beta-globin gene domain*. J Biol Chem, 2001. **276**(37): p. 34810-5.
409. Yuan, C.C., et al., *Histone H3R2 symmetric dimethylation and histone H3K4 trimethylation are tightly correlated in eukaryotic genomes*. Cell Rep, 2012. **1**(2): p. 83-90.
410. Castello, A., et al., *Insights into RNA biology from an atlas of mammalian mRNA-binding proteins*. Cell, 2012. **149**(6): p. 1393-406.
411. Beug, H., et al., *Chicken hematopoietic cells transformed by seven strains of defective avian leukemia viruses display three distinct phenotypes of differentiation*. Cell, 1979. **18**(2): p. 375-90.
412. Laemmli, U.K., *Cleavage of structural proteins during the assembly of the head of bacteriophage T4*. Nature, 1970. **227**(5259): p. 680-5.

413. Zang, C., et al., *A clustering approach for identification of enriched domains from histone modification ChIP-Seq data*. *Bioinformatics*, 2009. **25**(15): p. 1952-8.
414. Krzywinski, M., et al., *Circos: an information aesthetic for comparative genomics*. *Genome Res*, 2009. **19**(9): p. 1639-45.
415. Li, H., et al., *The Sequence Alignment/Map format and SAMtools*. *Bioinformatics*, 2009. **25**(16): p. 2078-9.
416. Shin, H., et al., *CEAS: cis-regulatory element annotation system*. *Bioinformatics*, 2009. **25**(19): p. 2605-6.
417. Roadmap Epigenomics, C., et al., *Integrative analysis of 111 reference human epigenomes*. *Nature*, 2015. **518**(7539): p. 317-30.
418. Bieberstein, N.I., et al., *First exon length controls active chromatin signatures and transcription*. *Cell Rep*, 2012. **2**(1): p. 62-8.
419. Davie, J.R., W. Xu, and G.P. Delcuve, *Histone H3K4 trimethylation: dynamic interplay with pre-mRNA splicing*. *Biochem Cell Biol*, 2015. **in press**.
420. Litt, M.D., et al., *Transitions in histone acetylation reveal boundaries of three separately regulated neighboring loci*. *EMBO J*, 2001. **20**(9): p. 2224-35.
421. Myers, F.A., et al., *Acetylation of histone H2B mirrors that of H4 and H3 at the chicken beta-globin locus but not at housekeeping genes*. *J Biol Chem*, 2003. **278**(38): p. 36315-22.
422. Anguita, E., et al., *Identification of a conserved erythroid specific domain of histone acetylation across the alpha-globin gene cluster*. *Proc Natl Acad Sci U S A*, 2001. **98**(21): p. 12114-9.

423. Delcuve, G.P., et al., *Epigenetics: Chromatin Organization and Function in Epigenetics in Cardiac Disease*, J. Backs and T. McKinsey, Editors. 2017, Springer International Publishing Switzerland. p. 1-35.
424. Li, J., et al., *SETD2: an epigenetic modifier with tumor suppressor functionality*. *Oncotarget*, 2016. **7**(31): p. 50719-50734.
425. Hutchison, N. and H. Weintraub, *Localization of DNAase I-sensitive sequences to specific regions of interphase nuclei*. *Cell*, 1985. **43**(2 Pt 1): p. 471-82.
426. Myers, F.A., et al., *Targeted and extended acetylation of histones H4 and H3 at active and inactive genes in chicken embryo erythrocytes*. *J Biol Chem*, 2001. **276**(23): p. 20197-205.
427. Markaki, Y., et al., *Functional nuclear organization of transcription and DNA replication: a topographical marriage between chromatin domains and the interchromatin compartment*. *Cold Spring Harb Symp Quant Biol*, 2010. **75**: p. 475-92.
428. Hendzel, M.J., G.P. Delcuve, and J.R. Davie, *Histone deacetylase is a component of the internal nuclear matrix*. *J Biol Chem*, 1991. **266**(32): p. 21936-42.
429. Meng, X. and J.A. Wilkins, *Compositional characterization of the cytoskeleton of NK-like cells*. *Journal of proteome research*, 2005. **4**(6): p. 2081-2087.
430. Fenyő, D., J. Eriksson, and R. Beavis, *Mass spectrometric protein identification using the global proteome machine*. *Computational Biology*, 2010: p. 189-202.
431. He, S., et al., *Dynamic distribution of HDAC1 and HDAC2 during mitosis: association with F-actin*. *J Cell Physiol*, 2013. **228**(7): p. 1525-35.
432. Khan, D.H., et al., *RNA-dependent dynamic histone acetylation regulates MCL1 alternative splicing*. *Nucleic acids research*, 2014. **42**(3): p. 1656-1670.

433. Spencer, V.A., et al., *Chromatin immunoprecipitation: a tool for studying histone acetylation and transcription factor binding*. *Methods*, 2003. **31**(1): p. 67-75.
434. Li, X., et al., *H4R3 methylation facilitates beta-globin transcription by regulating histone acetyltransferase binding and H3 acetylation*. *Blood*, 2010. **115**(10): p. 2028-37.
435. Kouzarides, T., *Chromatin modifications and their function*. *Cell*, 2007. **128**(4): p. 693-705.
436. Rothbart, S.B. and B.D. Strahl, *Interpreting the language of histone and DNA modifications*. *Biochim Biophys Acta*, 2014. **1839**(8): p. 627-43.
437. Bannister, A.J. and T. Kouzarides, *Regulation of chromatin by histone modifications*. *Cell Res*, 2011. **21**(3): p. 381-95.
438. Chen, Y., et al., *Lysine propionylation and butyrylation are novel post-translational modifications in histones*. *Mol Cell Proteomics*, 2007. **6**(5): p. 812-9.
439. Litt, M., Y. Qiu, and S. Huang, *Histone arginine methylations: their roles in chromatin dynamics and transcriptional regulation*. *Biosci Rep*, 2009. **29**(2): p. 131-41.
440. Creighton, M.P., et al., *Histone H3K27ac separates active from poised enhancers and predicts developmental state*. *Proc Natl Acad Sci U S A*, 2010. **107**(50): p. 21931-6.
441. Patturajan, M., et al., *A nuclear matrix protein interacts with the phosphorylated C-terminal domain of RNA polymerase II*. *Mol Cell Biol*, 1998. **18**(4): p. 2406-15.
442. Davie, J.R., W. Xu, and G.P. Delcuve, *Histone H3K4 trimethylation: dynamic interplay with pre-mRNA splicing*. *Biochem Cell Biol*, 2016. **94**(1): p. 1-11.
443. Heinz, S., et al., *The selection and function of cell type-specific enhancers*. *Nat Rev Mol Cell Biol*, 2015. **16**(3): p. 144-54.

444. Shlyueva, D., G. Stampfel, and A. Stark, *Transcriptional enhancers: from properties to genome-wide predictions*. Nat Rev Genet, 2014. **15**(4): p. 272-86.
445. Zhang, L., et al., *Cross-talk between PRMT1-mediated methylation and ubiquitylation on RBM15 controls RNA splicing*. Elife, 2015. **4**.
446. Zou, L., et al., *Correlation of SRSF1 and PRMT1 expression with clinical status of pediatric acute lymphoblastic leukemia*. J Hematol Oncol, 2012. **5**: p. 42.
447. Koh, C.M., et al., *MYC regulates the core pre-mRNA splicing machinery as an essential step in lymphomagenesis*. Nature, 2015. **523**(7558): p. 96-100.
448. Yu, M.C., *The Role of Protein Arginine Methylation in mRNP Dynamics*. Mol Biol Int, 2011. **2011**: p. 163827.
449. Khan, D.H., et al., *Dynamic Histone Acetylation of H3K4me3 Nucleosome Regulates MCL1 Pre-mRNA Splicing*. J Cell Physiol, 2016. **231**(10): p. 2196-204.
450. Chen, H., et al., *A TGFbeta-PRMT5-MEP50 axis regulates cancer cell invasion through histone H3 and H4 arginine methylation coupled transcriptional activation and repression*. Oncogene, 2017. **36**(3): p. 373-386.
451. Gao, Y., et al., *The dual function of PRMT1 in modulating epithelial-mesenchymal transition and cellular senescence in breast cancer cells through regulation of ZEB1*. Sci Rep, 2016. **6**: p. 19874.
452. Khan, D.H., et al., *Mitogen-induced distinct epialleles are phosphorylated at either H3S10 or H3S28, depending on H3K27 acetylation*. Mol Biol Cell, 2017. **28**(6): p. 817-824.
453. Chen, H.Y., et al., *Changes in the nuclear matrix of chicken erythrocytes that accompany maturation*. Biochem J, 1996. **320** (Pt 1): p. 257-65.

454. Palis, J. and G.B. Segel, *Developmental biology of erythropoiesis*. Blood Rev, 1998. **12**(2): p. 106-14.
455. Evans, C.J., V. Hartenstein, and U. Banerjee, *Thicker than blood: conserved mechanisms in Drosophila and vertebrate hematopoiesis*. Dev Cell, 2003. **5**(5): p. 673-90.
456. Medzhitov, R., *Recognition of microorganisms and activation of the immune response*. Nature, 2007. **449**(7164): p. 819-26.
457. Nelson, R.A., Jr., *The immune-adherence phenomenon; an immunologically specific reaction between microorganisms and erythrocytes leading to enhanced phagocytosis*. Science, 1953. **118**(3077): p. 733-7.
458. Passantino, L., et al., *Fish immunology. I. Binding and engulfment of Candida albicans by erythrocytes of rainbow trout (Salmo gairdneri Richardson)*. Immunopharmacol Immunotoxicol, 2002. **24**(4): p. 665-78.
459. Chen, R.A., et al., *Extreme HOT regions are CpG-dense promoters in C. elegans and humans*. Genome Res, 2014. **24**(7): p. 1138-46.
460. Barrera, L.O., et al., *Genome-wide mapping and analysis of active promoters in mouse embryonic stem cells and adult organs*. Genome Res, 2008. **18**(1): p. 46-59.
461. Maunakea, A.K., et al., *Conserved role of intragenic DNA methylation in regulating alternative promoters*. Nature, 2010. **466**(7303): p. 253-7.
462. Pal, S., et al., *Alternative transcription exceeds alternative splicing in generating the transcriptome diversity of cerebellar development*. Genome Res, 2011. **21**(8): p. 1260-72.
463. Iqbal, M., V.J. Philbin, and A.L. Smith, *Expression patterns of chicken Toll-like receptor mRNA in tissues, immune cell subsets and cell lines*. Vet Immunol Immunopathol, 2005. **104**(1-2): p. 117-27.

464. Esnault, E., et al., *A novel chicken lung epithelial cell line: characterization and response to low pathogenicity avian influenza virus*. *Virus Res*, 2011. **159**(1): p. 32-42.
465. Rider, P., et al., *IL-1alpha and IL-1beta recruit different myeloid cells and promote different stages of sterile inflammation*. *J Immunol*, 2011. **187**(9): p. 4835-43.
466. de Waal Malefyt, R., et al., *Interleukin 10(IL-10) inhibits cytokine synthesis by human monocytes: an autoregulatory role of IL-10 produced by monocytes*. *J Exp Med*, 1991. **174**(5): p. 1209-20.
467. Pestka, S., et al., *Interleukin-10 and related cytokines and receptors*. *Annu Rev Immunol*, 2004. **22**: p. 929-79.
468. Ihle, J.N., L. Pepersack, and L. Rebar, *Regulation of T cell differentiation: in vitro induction of 20 alpha-hydroxysteroid dehydrogenase in splenic lymphocytes from athymic mice by a unique lymphokine*. *J Immunol*, 1981. **126**(6): p. 2184-9.
469. Milburn, M.V., et al., *A novel dimer configuration revealed by the crystal structure at 2.4 A resolution of human interleukin-5*. *Nature*, 1993. **363**(6425): p. 172-6.
470. Hedges, J.C., C.A. Singer, and W.T. Gerthoffer, *Mitogen-activated protein kinases regulate cytokine gene expression in human airway myocytes*. *Am J Respir Cell Mol Biol*, 2000. **23**(1): p. 86-94.
471. Cruikshank, W. and D.M. Center, *Modulation of lymphocyte migration by human lymphokines. II. Purification of a lymphotactic factor (LCF)*. *J Immunol*, 1982. **128**(6): p. 2569-74.
472. Steel, J.C., T.A. Waldmann, and J.C. Morris, *Interleukin-15 biology and its therapeutic implications in cancer*. *Trends Pharmacol Sci*, 2012. **33**(1): p. 35-41.

473. Klebanoff, C.A., et al., *IL-15 enhances the in vivo antitumor activity of tumor-reactive CD8+ T cells*. Proc Natl Acad Sci U S A, 2004. **101**(7): p. 1969-74.
474. Dhabhar, F.S., *Effects of stress on immune function: the good, the bad, and the beautiful*. Immunol Res, 2014. **58**(2-3): p. 193-210.
475. Muralidharan, S. and P. Mandrekar, *Cellular stress response and innate immune signaling: integrating pathways in host defense and inflammation*. J Leukoc Biol, 2013. **94**(6): p. 1167-84.
476. Priyadarshini, S. and P. Aich, *Effects of psychological stress on innate immunity and metabolism in humans: a systematic analysis*. PLoS One, 2012. **7**(9): p. e43232.
477. Lu, J., et al., *A potential suppressive effect of natural antisense IL-1beta RNA on lipopolysaccharide-induced IL-1beta expression*. J Immunol, 2013. **190**(12): p. 6570-8.
478. Tsompana, M. and M.J. Buck, *Chromatin accessibility: a window into the genome*. Epigenetics Chromatin, 2014. **7**(1): p. 33.
479. Tate, C.M., J.H. Lee, and D.G. Skalnik, *CXXC finger protein 1 restricts the Setd1A histone H3K4 methyltransferase complex to euchromatin*. FEBS J, 2010. **277**(1): p. 210-23.
480. Binda, O., *On your histone mark, SET, methylate!* Epigenetics, 2013. **8**(5): p. 457-63.
481. Jin, C. and G. Felsenfeld, *Distribution of histone H3.3 in hematopoietic cell lineages*. Proc Natl Acad Sci U S A, 2006. **103**(3): p. 574-9.
482. Sjakste, N., et al., *A novel gene is transcribed in the chicken alpha-globin gene domain in the direction opposite to the globin genes*. Mol Gen Genet, 2000. **262**(6): p. 1012-21.
483. Pelechano, V. and L.M. Steinmetz, *Gene regulation by antisense transcription*. Nat Rev Genet, 2013. **14**(12): p. 880-93.

484. Guttman, M., et al., *Chromatin signature reveals over a thousand highly conserved large non-coding RNAs in mammals*. Nature, 2009. **458**(7235): p. 223-7.
485. Lieberman-Aiden, E., et al., *Comprehensive mapping of long-range interactions reveals folding principles of the human genome*. Science, 2009. **326**(5950): p. 289-93.
486. Hurst, D.R., *Metastasis suppression by BRMS1 associated with SIN3 chromatin remodeling complexes*. Cancer Metastasis Rev, 2012. **31**(3-4): p. 641-51.
487. Eberl, H.C., et al., *A map of general and specialized chromatin readers in mouse tissues generated by label-free interaction proteomics*. Mol Cell, 2013. **49**(2): p. 368-78.
488. Hao, S. and D. Baltimore, *The stability of mRNA influences the temporal order of the induction of genes encoding inflammatory molecules*. Nat Immunol, 2009. **10**(3): p. 281-8.
489. International Chicken Genome Sequencing, C., *Sequence and comparative analysis of the chicken genome provide unique perspectives on vertebrate evolution*. Nature, 2004. **432**(7018): p. 695-716.

APPENDICES

Appendix 1: List of antibodies

Appendix 2: Gene ranking according to expression levels in chicken polychromatic erythrocytes

Appendix 3: Sense and antisense transcript reads for the 1095 genes from the galGal3 RefSeq database belonging to the first 20th-percentile

Appendix 4: Table with information regarding all sequencing tracks shown in this study

Appendix 1: List of antibodies

Antibodies

Protein target	Source	Type
H3K4me3	Abcam	Rabbit polyclonal
H3K4me2	Abcam	Rabbit polyclonal
H3K4me1	Abcam	Rabbit polyclonal
H3K36me3	Abcam	Rabbit polyclonal
H3K27ac	Abcam	Rabbit polyclonal
H3K9ac	Abcam	Rabbit polyclonal
H4K5ac	Millipore	Rabbit polyclonal
H4K8ac	Millipore	Rabbit polyclonal
H3R2me2a	Epigentek	Rabbit polyclonal
H3R2me2s	Millipore	Rabbit polyclonal
H4R3me2a	Active motif	Rabbit polyclonal
H4R3me2s	Active motif	Rabbit polyclonal
PRMT1	Millipore	Rabbit polyclonal
PRMT5	Millipore	Rabbit polyclonal
HDAC2	Millipore	Mouse monoclonal
HDAC2	Thermofisher	Rabbit polyclonal
pHDAC2	Abcam	Rabbit polyclonal
H3K36me3	Abcam	Rabbit polyclonal
SFRS1	Santacruz	Mouse monoclonal
RNAPII	Millipore	Mouse monoclonal
RNAPIIs2ph	Abcam	Rabbit polyclonal
RNAPIIs5ph	Abcam	Rabbit polyclonal

Appendix 2: Gene ranking according to expression levels in chicken polychromatic erythrocytes. All 5479 genes from the galGal3 RefSeq database were placed in order of their level of expression (mean RPKM from two biological samples) and were then divided into five 20th-percentile classes in relation to expression level. First 20 %-ile (*red filled*), second 20 %-ile (*green filled*), third 20 %-ile (*blue filled*), fourth 20 %-ile (*dark blue filled*) and fifth 20 %-ile (*violet filled*).

Gene	Chr	Strand	Start	End	RPKM
HBAA	chr14	+	12,729,708	12,730,496	333,077
HBM	chr14	+	12,726,702	12,727,536	225,893
MIR3528	chr17	+	8,404,342	8,404,438	162,885
HBG2	chr1	+	199,436,906	199,442,000	162,074
MIR1563	chr12	+	738,668	738,738	155,249
MIR3538-2	chr1	+	52,608,155	52,608,229	82,358
MIR3535	chr9	-	16,372,628	16,372,709	64,425
MIR1434	chr28	+	1,055,204	1,055,280	31,661
MIR3536	chr25	+	1,478,485	1,478,562	22,667
MIR193B	chr14	+	759,453	759,535	20,977
MIR451	chr19	-	5,823,968	5,824,036	15,843
MIR2188	chr22	-	2,684,926	2,685,094	13,649
CA2	chr2	+	127,587,512	127,603,758	13,199
FTH1	chr5	-	18,042,642	18,047,153	10,379
MIR3540	chr10	+	12,751,614	12,751,675	9,451
RPS3A	chr4	+	34,368,754	34,372,136	4,572
HSPA2	chr5	-	55,409,841	55,412,160	4,007
SAT1	chr1	-	121,771,899	121,775,847	3,958
HBE1	chr1	+	199,436,938	199,438,083	3,847
ITM2A	chr4	-	1,454,025	1,463,005	3,552
IFRD1	chr1	-	28,722,344	28,732,937	2,693
TPT1	chr1	-	172,044,505	172,048,430	2,653
NCOA4	chr6	+	3,761,446	3,770,224	2,648
RHAG	chr3	+	111,573,999	111,585,157	2,624
EIF5	chr5	+	52,729,413	52,736,425	2,499
BNIP3L	chr22	-	528,198	542,276	2,392
ISG12-2	chr2	+	92,043,572	92,046,962	2,165
SPTAN1	chr17	+	5,766,712	5,812,561	1,872
BF2_dup2	chr16	-	50,368	51,875	1,742
MIR92	chr1	-	152,248,070	152,248,147	1,694
HSP90AA1	chr5	-	51,983,680	51,988,436	1,694
MIR1454	chr3	-	58,701,686	58,701,785	1,682

MIRLET7G	chr12	-	2,809,078	2,809,160	1,660
SKP1	chr13	+	16,355,077	16,363,289	1,562
EEF1A1	chr3	+	84,252,817	84,257,460	1,556
IFI27L2	chr23	+	4,664,702	4,665,614	1,512
TUBB1	chr20	-	10,839,422	10,844,439	1,504
HNRNPH1	chr13	+	13,660,042	13,675,749	1,502
NT5C3	chr2	+	48,041,581	48,053,721	1,496
SLC38A2	chr1	-	32,777,741	32,793,469	1,429
NFE2L2	chr7	+	16,905,967	16,922,637	1,400
BTG1	chr1	-	46,282,645	46,285,175	1,362
BF1	chr16	-	50,515	51,875	1,356
DDX3X	chr1	-	115,609,206	115,627,183	1,355
WBP4	chr1	+	170,109,127	170,131,041	1,337
PNRC1	chr3	-	78,545,062	78,547,319	1,316
SGK1	chr3	+	58,129,917	58,135,484	1,267
H3F3C	chr3	-	18,256,332	18,259,608	1,193
IRF1	chr13	-	17,453,125	17,459,814	1,107
LOC422090	chr18	+	9,824,613	9,825,618	1,104
TFRC	chr9	+	16,044,796	16,053,740	1,075
UBE2D3	chr4	-	62,741,266	62,764,553	1,055
ATF4	chr1	-	52,501,043	52,503,978	1,049
PPP1CB	chr3	-	28,415,919	28,446,283	988
FXR1	chr9	-	18,236,607	18,259,966	985
EPAS1	chr3	+	27,794,886	27,826,490	974
SRSF5	chr5	-	30,163,796	30,168,433	970
MCL1	chr25	+	1,660,135	1,662,330	955
TXN	chrZ	-	65,067,561	65,073,529	947
H3F3C	chr18	+	4,698,469	4,700,927	940
PHOSPHO1	chr27	+	3,378,978	3,382,733	893
MIR3526	chr3	+	16,500,330	16,500,444	881
B-G_dup1	chr16	+	84,813	89,079	872
MXI1	chr6	+	27,285,986	27,328,967	843
VIM	chr2	-	19,728,508	19,735,564	840
RDX	chr1	+	183,923,286	183,950,291	835
CTSD	chr5	+	15,225,774	15,236,942	828
TAL1	chr8	-	22,631,613	22,638,449	824
RPS8	chr8	+	21,479,964	21,484,357	822
BRD2	chr16	-	72,223	81,200	790
CYB5A	chr2	+	94,287,667	94,298,980	777
ITPK1	chr5	-	47,359,141	47,492,853	764
HSP25	chr27	+	4,486,394	4,487,253	758

RPLP1	chr2	+	151,341,217	151,342,368	753
PSAP	chr6	-	13,023,612	13,044,767	716
EPB41	chr23	+	2,908,245	2,969,177	694
MIR181A-1	chr8	+	2,001,561	2,001,664	691
MIR1783	chr12	+	9,044,610	9,044,710	684
TRNAU1AP	chr2	-	63,224,188	63,234,661	680
TCP11L2	chr1	-	55,927,383	55,938,688	680
LAPTM4A	chr3	-	104,330,537	104,343,340	680
RPSA	chr2	-	44,378,630	44,383,377	677
KPNA4	chr9	+	23,677,941	23,701,604	668
OAZ1	chr28	-	1,566,531	1,568,098	666
MIR15B	chr9	-	23,742,966	23,743,056	665
RPS4X	chr4	+	1,862,595	1,865,074	664
RPL11	chr23	+	5,837,003	5,839,342	663
SBNO1	chr15	+	5,047,036	5,076,553	662
EEF2	chr28	+	1,051,728	1,059,663	657
HSPA8	chr24	+	3,111,092	3,116,502	648
TXNRD1	chr1	-	56,627,718	56,653,900	647
MBNL1	chr9	-	24,950,163	24,980,528	639
RPL39	chr4	+	16,633,043	16,635,306	631
ITGB1BP3	chr10	-	12,391,572	12,394,023	630
MIR103-2	chr4	-	91,906,889	91,906,971	630
TMEM183A	chr26	-	905,314	917,068	614
MORC3	chr1	+	110,089,174	110,116,965	603
BSG	chr28	+	2,166,723	2,175,357	602
PCMTD1	chr2	-	112,942,520	112,988,563	592
B-G_dup2	chr16	-	230,388	250,501	589
TACC3	chr4	-	86,906,002	86,921,633	585
MIR30C-1	chr23	+	5,249,637	5,249,725	584
EIF1	chr27	+	4,298,436	4,300,249	582
RPLP0	chr15	+	9,699,637	9,702,332	573
C26H6orf106	chr26	+	4,144,092	4,175,943	568
EIF4A2	chr9	+	17,295,318	17,302,173	567
ITPKA	chr5	+	26,826,565	26,860,645	561
SYNM	chr10	+	18,889,794	18,924,663	560
SLC6A6	chr12	+	11,251,619	11,301,059	552
MIR365-1	chr14	+	764,271	764,355	544
C4BPA_dup2	chr26	+	2,498,399	2,509,349	539
KIAA1191	chr13	+	10,487,314	10,495,069	530
RPL4	chr10	-	20,668,331	20,673,652	526
MIR1661	chr2	-	19,733,987	19,734,047	503

LAMP1_dup2	chr1	-	141,725,552	141,743,181	500
UBE2H	chr1	-	722,841	742,683	490
RPS27A	chr3	+	12,687	14,950	488
DDX5	chr18	-	6,896,656	6,904,115	486
HNRNPAB	chr13	-	14,482,748	14,505,745	484
MYOD1	chr5	+	13,283,712	13,286,804	483
MIR1787	chr12	+	8,996,102	8,996,191	477
ACTB	chr14	-	4,187,366	4,188,052	466
MIR140	chr11	+	21,030,641	21,030,735	464
RPS3	chr1	-	200,048,855	200,055,870	450
ARIH1	chr10	+	1,012,292	1,061,448	449
XBP1	chr15	-	7,957,483	7,960,608	449
TRIM59	chr9	+	23,706,346	23,713,670	448
ADA	chr20	+	5,320,188	5,332,822	439
H1FO	chr1	-	53,073,884	53,079,989	437
TMSB4X	chr1	-	126,774,228	126,774,748	434
BF2_dup1	chr16	+	40,458	41,102	432
HEBP1	chr1	-	50,117,980	50,125,098	432
DNAJB9	chr1	-	30,213,368	30,221,863	429
HERC2	chr1	+	134,617,867	134,722,450	428
EIF3E	chr2	-	137,431,312	137,452,249	423
RPL37A	chr7	-	24,873,706	24,875,755	421
YME1L1	chr2	-	15,827,679	15,844,651	419
CSDA	chr1	+	81,463,345	81,503,689	419
JAK2	chrZ	+	28,062,563	28,146,011	419
EDF1	chr17	+	932,046	935,223	416
RPL19	chr27	+	4,012,008	4,015,020	411
MIRLET7F	chr12	-	6,302,497	6,302,583	408
LPIN2	chr2	+	104,103,022	104,152,635	408
MIR181A-2	chr17	+	10,218,497	10,218,587	408
TBX22	chr4	+	1,492,764	1,497,990	405
YY1	chr5	+	50,999,598	51,022,607	404
HBP1	chr1	+	15,534,402	15,546,735	403
TCF12	chr10	-	8,404,986	8,517,607	403
GHITM	chr6	-	4,108,925	4,113,570	397
PNPLA2	chr5	-	16,838,465	16,868,661	386
BIRC2	chr1	-	186,919,506	186,929,678	385
NFS1	chr20	+	1,028,203	1,040,388	385
TRIM27_dup1	chr16	+	122,459	126,409	383
IL15	chr4	+	31,129,925	31,162,068	379
TLX3	chrZ	+	967,141	968,404	379

LOC768701	chr15	+	7,188,399	7,209,605	377
MIR22	chr19	-	5,352,096	5,352,195	377
MIR1571	chr11	+	20,363,859	20,363,956	374
ITM2B	chr1	+	173,006,061	173,031,338	373
GSTA3_dup1	chr3	+	91,190,846	91,198,881	370
CISH	chr12	-	1,736,930	1,741,989	369
SOD1	chr1	+	108,112,866	108,117,305	368
FOS	chr5	+	40,634,392	40,635,384	368
RPL13	chr11	+	20,693,001	20,697,255	366
HAGH	chr14	-	6,070,463	6,075,474	365
MST4	chr4	+	3,420,719	3,448,119	364
ADAL	chr10	+	7,202,557	7,212,097	363
TUBB2C	chr17	-	2,276,961	2,279,058	360
RPL22	chr21	+	599,514	601,779	357
API5_dup1	chr5	+	20,399,077	20,403,021	357
17.5	chr1	+	34,420,435	34,444,453	354
CD93	chr3	+	3,257,363	3,259,729	348
HAGHL	chr14	-	6,064,649	6,069,153	344
TMEM184B	chr1	+	52,894,656	52,919,170	344
MIR147-1	chr10	+	12,334,922	12,334,991	339
MIR144	chr19	-	5,824,123	5,824,207	339
EIF4G2	chr5	+	9,709,026	9,720,898	337
MXD1	chr22	+	2,860,586	2,866,188	336
SRSF1	chr19	+	8,667,064	8,671,119	336
MIR16C	chr4	-	4,048,689	4,048,759	335
NUCB2	chr5	+	12,912,558	12,938,199	332
MIR16-1	chr1	-	173,700,351	173,700,434	332
OSTC	chr4	-	39,013,810	39,018,520	330
RPS15	chr28	+	2,552,982	2,554,253	330
RPL5	chr8	-	14,745,906	14,752,218	328
ARGLU1	chr1	+	145,236,646	145,246,855	327
CD69	chr1	+	13,752	20,858	327
ST6GAL2	chr1	-	139,929,513	139,951,719	326
RPL7A	chr17	+	7,532,204	7,535,326	326
CD99	chr1	-	132,661,354	132,685,301	309
TAP2	chr16	-	42,106	45,339	308
RPS10	chr26	+	4,209,892	4,216,177	305
GLRX5	chr5	+	48,537,539	48,543,879	304
RBM5	chr12	+	2,956,104	2,971,523	304
PUM2	chr3	-	104,495,277	104,538,316	303
HNRNPA2B1	chr2	-	32,117,297	32,127,841	296

RHD	chr23	+	2,670,491	2,686,228	294
PSMA4	chr10	-	4,589,004	4,594,111	292
AMPD3	chr5	-	9,877,376	9,902,985	292
CDKN1B_dup1	chr1	+	74,441,100	74,447,141	291
AP2A2	chr5	-	16,149,935	16,192,834	289
RPL7	chr2	-	122,516,736	122,523,351	281
RMND5A	chr4	+	88,868,905	88,890,117	277
RNF103	chr4	-	88,846,293	88,863,778	270
SAP18	chr1	-	182,921,714	182,924,013	267
HMOX1	chr1	-	54,136,215	54,141,675	266
PABPC1	chr2	-	133,697,039	133,743,323	266
TAX1BP1	chr2	+	32,879,735	32,930,845	263
BSDC1	chr23	-	5,452,429	5,458,843	260
RPL32	chr12	-	20,121,794	20,124,538	259
BAG5	chr5	-	52,919,484	52,924,438	257
MIR223	chr4	+	232,949	233,048	256
RPS6	chrZ	-	33,519,934	33,523,885	255
CCPG1	chr10	+	9,083,002	9,102,123	254
RBM24	chr2	+	63,053,768	63,064,867	254
SLC25A6	chr1	+	133,256,379	133,259,778	253
LAMP1_dup1	chr1	-	141,725,018	141,725,446	250
ATP5B	chrE22C19W28_E50C23	+	894,183	895,115	250
TBC1D15	chr1	+	38,343,471	38,371,483	248
UBE2A	chr4	-	16,676,640	16,683,718	247
C6H10orf46	chr6	-	31,297,394	31,337,386	247
KPNA6	chr23	-	5,433,441	5,449,501	247
ZC3H11A	chr26	+	479,574	493,561	247
RBL2	chr11	-	5,083,249	5,103,344	246
PON2	chr2	-	23,807,426	23,827,637	245
CCNL2	chr21	+	2,196,317	2,204,643	245
MIRLET7I	chr1	+	34,895,687	34,895,770	244
CLTC	chr19	+	7,239,507	7,261,769	243
ELF1	chr1	-	170,022,658	170,108,996	243
GNB2L1	chr16	+	110,334	113,797	243
SRSF6	chr20	-	69,284	74,352	242
ACOT9	chr1	+	121,778,560	121,800,278	241
CST3	chr3	+	16,498,156	16,500,491	240
VCP	chrZ	-	7,931,929	7,954,971	240
RPL37	chrZ	-	12,331,789	12,334,419	239
GMPR	chr2	+	62,658,093	62,689,291	238
MIR24	chrZ	+	41,158,175	41,158,242	237

SLC46A3	chr1	+	180,062,318	180,076,085	235
MLX	chr27	+	4,613,604	4,616,680	234
CR1L	chr26	+	2,469,319	2,475,028	234
FAM126A	chr2	-	30,925,910	30,963,487	234
CSDE1	chr26	-	3,742,619	3,760,175	233
TOP2B	chr2	-	37,832,496	37,894,040	231
ASB6	chr17	-	6,201,185	6,206,196	229
VCIPI1	chr2	-	119,530,680	119,544,005	229
ERAL1	chr19	-	5,819,257	5,823,279	228
USP48	chr21	+	6,717,021	6,741,576	226
AP2M1	chr9	+	16,927,767	16,950,469	226
RPL9	chr4	+	71,289,541	71,295,690	225
ADRM1	chr20	+	7,803,913	7,810,847	224
SELT	chr9	-	25,208,762	25,214,435	222
MAP1LC3B	chr11	+	19,752,538	19,764,116	222
EDEM1	chr12	+	19,253,532	19,263,549	221
COX4I1	chr11	-	19,631,521	19,635,731	219
SOD2	chr3	+	47,509,331	47,516,570	218
PCNA	chr22	+	341,131	343,721	216
IRF2	chr4	+	40,941,772	40,965,995	215
MIR142	chr19	-	496,983	497,070	215
NFIA	chr8	+	27,824,188	28,056,676	214
HPGDS	chr4	-	38,364,189	38,391,036	212
RABGAP1L	chr8	-	7,438,681	7,625,323	212
RPL35	chr17	-	10,244,733	10,246,059	209
DNAJA2	chr11	+	8,266,732	8,277,667	209
GFI1B	chr17	+	7,406,092	7,414,965	208
UBE2R2	chrZ	+	6,817,155	6,872,776	208
IREB2	chr10	-	4,602,943	4,622,738	208
EPS15	chr8	-	24,801,109	24,843,408	207
JAK1	chr8	-	28,989,755	29,042,651	207
RPL30	chr2	-	132,392,734	132,395,801	206
APBB1IP	chr2	-	16,054,537	16,112,353	206
API5_dup2	chr5	+	23,342,215	23,349,112	206
LMO2	chr5	-	19,808,366	19,811,908	206
PDE3B	chr5	+	11,409,886	11,484,468	205
PIAS1	chr10	+	21,271,905	21,300,780	205
USP4	chr12	-	2,637,963	2,667,530	205
HIGD1A	chr2	-	1,969,110	1,974,509	205
PSMD9	chr15	+	5,740,925	5,743,647	205
UBE2L3	chr15	+	348,584	356,664	204

BG2	chr16	-	194,396	235,950	203
RNF114	chr20	-	13,850,753	13,855,844	201
FLOT2	chr19	-	5,826,441	5,838,008	200
STAT1	chr7	-	8,878,637	8,898,622	200
CNBP	chr12	+	5,253,629	5,262,898	198
RNF11	chr8	+	24,721,977	24,749,502	198
PSME4	chr3	+	2,876,710	2,935,391	197
FBXO18	chr1	-	891,750	914,134	194
MIR29B-2	chr26	-	2,512,569	2,512,648	194
FBXO32	chr2	-	143,695,679	143,720,333	192
USP47	chr5	-	9,110,885	9,164,482	191
LSM14A	chr11	+	11,670,872	11,689,997	191
TMEM59	chr8	-	25,881,136	25,889,363	191
FTL	chr5	+	13,275,441	13,278,776	186
GTF2H5	chr3	+	53,785,644	53,790,123	185
BTBD9	chr3	+	30,738,005	30,848,938	184
MIR30D	chr2	-	148,337,263	148,337,326	184
ZNF593	chr23	-	213,355	214,554	182
IFIH1	chr7	+	22,606,882	22,635,561	182
NDEL1	chr18	+	1,663,249	1,686,261	181
IFNGR1	chr3	+	56,734,307	56,753,051	181
TP53INP1	chr2	-	131,156,615	131,167,500	180
TNFRSF10B	chr22	+	1,282,714	1,285,576	180
CALM	chr3	-	28,337,191	28,349,438	178
CAST	chrZ	-	55,902,661	55,957,486	178
CHMP7	chr22	-	1,265,636	1,274,713	177
EIF3H	chr2	-	140,871,171	140,953,283	176
SSBP3	chr8	-	25,924,361	25,974,662	175
PSMA3	chr5	-	57,844,569	57,853,136	175
TAPT1	chr4	+	79,379,462	79,419,015	174
RPL3	chr1	+	52,599,799	52,610,317	174
WIPI2	chr14	+	4,065,857	4,086,668	174
NR3C1	chr13	-	17,984,148	18,034,839	173
MIR106	chr4	-	3,970,359	3,970,439	173
SUMO2	chr18	-	10,640,127	10,646,794	173
MAP2K3	chr14	-	4,509,005	4,522,146	173
RPL29	chr12	+	531,576	534,472	171
NRD1	chr8	-	24,917,941	24,941,754	169
FAM177A1	chr5	+	38,473,642	38,488,336	168
LOC772071	chr4	-	14,328,607	14,352,886	168
E2F1	chr20	+	2,167,958	2,170,027	168

ACTG1	chr10	+	1,891,946	1,893,482	167
METAP2	chr1	+	47,433,955	47,448,737	167
PDK3	chr1	-	121,541,231	121,591,416	166
CD47	chr1	-	90,711,199	90,730,204	166
PAPOLA	chr5	+	48,952,742	48,992,572	165
MIR30E	chr23	+	5,248,414	5,248,509	165
RAB18	chr2	-	15,707,879	15,720,957	165
IGF2R	chr3	-	47,356,789	47,411,223	165
PDCD10	chr9	+	22,157,191	22,168,715	163
DNAJB6	chr2	+	8,603,660	8,653,381	162
TAOK3	chr15	+	10,089,280	10,157,868	162
PSMB7	chr17	-	10,091,692	10,111,466	162
RAB5A	chr2	+	35,783,173	35,800,927	161
HBXIP	chr26	-	1,220,032	1,222,791	161
TRDMT1	chr2	+	19,749,600	19,778,353	160
C1H11orf75	chr1	+	190,167,836	190,196,632	160
RFFL	chr19	+	4,449,792	4,474,760	160
ATP6V0A1	chr27	+	4,585,404	4,607,653	159
SLC25A3	chr1	+	48,554,809	48,563,005	159
PIP5K1B	chrZ	+	34,139,950	34,236,768	158
IRF7	chr5	+	16,950,071	16,954,585	158
GNB1	chr21	+	1,907,993	1,941,797	158
PSMD5	chr17	-	8,970,660	8,977,372	157
PPP2CA	chr13	+	16,330,227	16,346,270	157
RPS14	chr13	+	13,218,570	13,223,073	156
ARNT	chr25	-	1,796,213	1,818,277	156
SLC35B1	chr27	+	3,026,828	3,029,939	155
RNF13	chr9	-	25,338,076	25,367,113	155
RPL27	chr27	+	4,737,558	4,739,819	154
CSNK1A1	chr13	-	8,389,986	8,421,793	154
CDC2L1	chr21	+	1,995,302	2,007,412	154
STRBP	chr17	-	9,612,507	9,664,360	153
LBR	chr3	+	18,522,831	18,537,601	152
LY75	chr7	+	23,470,581	23,509,171	152
RHOA	chr12	-	2,673,483	2,679,747	151
MEMO1	chr3	+	34,923,723	34,949,296	150
PAIP2	chr13	-	2,192,057	2,200,948	150
CZH5orf43	chrZ	-	18,387,604	18,390,589	150
PLAG1	chr2	-	114,921,756	114,927,794	149
DDX6	chr24	-	5,696,272	5,710,164	149
ZMAT2	chr13	-	809,253	819,126	149

HNRPD1	chr4	+	47,862,704	47,867,639	149
WWP1	chr2	+	127,795,815	127,856,103	149
MATR3	chr13	-	2,204,320	2,229,263	148
EIF3I	chr23	-	5,408,790	5,412,911	148
WSB1	chr19	+	9,063,618	9,071,030	148
HSPA4L	chr4	+	35,438,536	35,461,570	148
QKI	chr3	-	45,968,564	46,105,064	147
MGAT3	chr1	-	52,533,243	52,539,549	146
ABCC4	chr1	+	150,346,326	150,485,168	146
PANK4	chr21	+	1,411,024	1,432,841	146
CDKN1B_dup2	chr1	+	76,856,513	76,857,389	146
HBE	chr1	+	199,444,835	199,446,373	146
ODC1	chr3	-	99,660,021	99,668,084	145
DSTN	chr3	-	16,459,873	16,473,343	144
DYRK1A	chr1	+	110,615,543	110,636,267	144
YTHDC1	chr4	+	53,261,192	53,275,913	143
ATG9A	chr7	+	23,779,167	23,787,140	143
YPEL5	chr3	-	8,031,083	8,041,009	143
MGEA5	chr6	+	24,104,165	24,128,093	142
TRAFD1	chr15	+	6,360,834	6,375,710	141
SLC48A1	chrE22C19W28_E50C23	-	421,424	423,642	141
FYTTD1	chr9	+	16,130,916	16,144,309	141
SP3	chr7	+	18,334,642	18,355,198	141
LUC7L3	chr18	-	10,074,576	10,087,770	139
MIRLET7D	chr12	-	6,301,452	6,301,554	139
PSMA2	chr2	-	51,287,876	51,293,729	139
HBG1	chr1	+	199,433,573	199,434,763	139
CUL2	chr2	+	12,951,480	12,998,820	139
ABCA1	chrZ	-	53,602,291	53,696,883	138
MIR20B	chr4	-	3,970,047	3,970,131	137
XPO7	chr22	-	1,337,149	1,369,517	137
CCT4	chr3	+	16,246,822	16,253,836	136
PSMC3	chr5	+	25,021,826	25,027,459	136
C5H11orf58	chr5	+	12,600,786	12,607,591	135
CCDC101	chr8	+	30,633,592	30,638,227	135
RPS11	chr1	-	199,344,202	199,346,749	135
MKLN1	chr1	-	2,942,940	3,042,345	135
RPRD1B	chr20	-	10,336,682	10,357,495	134
USP7	chr14	+	10,166,845	10,207,418	134
CYTH1	chr18	+	9,707,540	9,743,135	133
MIRLET7B	chr1	+	73,422,101	73,422,185	132

SRSF3	chr26	+	1,382,511	1,388,447	132
TOB2	chr1	+	51,523,189	51,530,050	132
DNAJA1	chrZ	+	68,670,992	68,678,723	131
UBE2G1	chr19	+	3,109,009	3,133,901	131
ADCY9	chr14	-	13,294,823	13,353,192	131
MIR130B	chr15	-	398,720	398,796	130
STK11	chr28	+	2,464,516	2,497,354	129
MARCH5	chr6	-	22,006,366	22,048,011	129
KAT2A	chr27	-	4,475,249	4,483,332	128
PPM1B	chr3	+	26,603,843	26,665,123	128
PNPLA8	chr1	+	30,303,463	30,338,086	128
NUTF2	chr11	+	881,677	901,274	126
SERINC3	chr20	+	5,362,845	5,370,316	126
APLP2	chr24	-	1,463,163	1,486,156	126
PSPC1	chr1	+	183,460,882	183,501,932	125
SERINC1	chr3	+	63,939,043	63,956,707	125
PSMA1	chr5	-	11,382,981	11,390,098	125
REEP3	chr6	-	8,869,448	8,904,159	124
CHMP1B	chr4	-	1,509,850	1,516,407	124
TRAM1	chr2	-	121,362,691	121,380,275	124
TOB1	chr18	+	10,032,791	10,034,619	123
XK	chr1	-	116,756,833	116,772,882	123
CD36	chr1	-	12,076,054	12,119,368	123
FNIP1	chr13	-	17,077,127	17,127,285	122
C20H20orf111	chr20	+	5,459,213	5,466,311	122
CTBP1	chr4	+	87,707,985	87,871,088	122
PSMD12	chr18	+	7,146,343	7,154,351	122
ADD1	chr4	-	85,307,319	85,365,225	122
NFKBIA	chr5	-	38,574,318	38,577,820	122
ELAVL1	chr28	-	910,806	928,361	121
CHMP2B	chr1	-	96,228,950	96,240,484	121
MIR19B	chr1	-	152,248,183	152,248,269	121
PSMD4	chr25	+	1,870,586	1,875,204	121
JUN	chr8	-	27,141,993	27,143,699	121
KLHDC2	chr5	+	60,230,350	60,242,062	121
PM20D1	chr26	-	2,117,141	2,128,322	120
MYLIP	chr2	+	62,607,108	62,620,388	120
MKRN1	chr1	-	58,845,921	58,867,710	120
AKIRIN2	chr3	+	79,076,095	79,093,538	119
SGMS1	chr6	+	10,810,570	10,888,759	119
PLEKHA3	chr7	-	16,484,453	16,499,738	119

ITGAV	chr7	-	1,310,026	1,353,721	118
MIR1808	chr5	-	996,847	996,937	118
BDH1	chr9	-	13,732,797	13,746,997	118
PBX1	chr8	-	5,416,453	5,539,116	118
MORF4L1	chr10	-	21,824,774	21,842,564	117
SIRT1	chr6	-	7,709,369	7,730,940	117
YWHAZ	chr2	-	133,774,465	133,802,441	117
TPD52L2	chr20	-	9,516,723	9,532,937	117
PSMC2	chr1	+	13,964,561	13,972,128	117
EIF5A2	chr9	+	21,259,954	21,264,260	116
SSR2	chr25	+	1,783,704	1,786,531	116
MAFG	chr18	-	9,917,051	9,918,754	115
PSMB1	chr3	+	42,604,006	42,609,973	115
PPP6R3	chr5	+	17,727,724	17,779,993	115
KIAA0907	chr25	-	1,588,126	1,596,958	115
CHP1	chr5	+	26,686,560	26,703,514	115
CLTB	chr13	+	10,472,832	10,479,753	114
INCENP	chr5	+	18,267,636	18,286,122	114
SRF	chr3	+	4,344,745	4,354,015	114
PSME3	chr27	+	4,698,668	4,705,374	114
DBR1	chr9	-	1,580,792	1,588,690	114
TOP1	chr20	+	4,813,649	4,848,503	113
MFAP1	chr3	-	98,153,608	98,154,600	113
HMGCL	chr23	-	5,868,333	5,871,956	113
SELO	chr1	+	21,693,534	21,707,297	113
MRPS17	chr19	+	4,814,821	4,817,499	113
HMGB3	chr4	-	17,789,154	17,789,969	113
ARPC4	chr12	+	11,779,567	11,780,625	113
CLIC2	chr4	-	1,799,818	1,804,668	113
PSMD1	chr9	+	16,231,315	16,292,763	111
CREM	chr2	-	12,911,102	12,916,911	111
LDB1	chr6	+	23,947,775	23,954,279	111
RAB11A	chr10	+	20,307,423	20,323,546	111
TRA2A	chr2	-	31,208,403	31,232,818	111
GYG1	chr9	-	25,525,176	25,540,189	111
SPTY2D1	chr5	-	13,681,871	13,693,835	110
ADIPOR2	chr1	+	63,061,148	63,101,540	110
JARID2	chr2	+	62,187,577	62,395,650	110
C20H20orf43	chr20	-	11,933,110	11,953,582	110
STAM2_dup2	chr7	-	37,033,429	37,052,765	110
ATF7IP	chr1	+	50,722,219	50,783,365	109

TARDBP	chr21	+	4,066,167	4,071,800	109
EIF2AK2	chr3	+	33,243,191	33,261,816	108
SEMA3D	chr1	+	8,884,476	9,046,660	108
TLN1	chrZ	+	8,512,627	8,542,651	108
AKTIP	chr11	+	5,066,544	5,078,837	108
SUMO1	chr7	-	12,824,475	12,830,281	108
IFNAR1	chr1	+	108,723,811	108,741,081	107
RPS17L	chr10	-	707,283	710,012	107
TAPBP	chr16	+	64,557	68,919	107
STAT3	chr27	-	4,551,674	4,560,466	107
SLC9A8	chr20	-	13,879,567	13,902,229	107
CEBPG	chr11	+	11,012,915	11,017,409	107
RREB1	chr2	-	65,833,919	65,954,776	107
MYH9	chr1	+	53,762,688	53,824,830	106
MOV10	chr26	+	3,370,713	3,377,196	106
RPL7L1	chr4	-	56,083,848	56,087,514	106
CHCHD2	chr19	-	4,868,202	4,870,357	106
PFN2	chr9	+	25,214,090	25,333,955	105
MIR1813-1	chr2	+	136,620,145	136,620,230	105
COPS7A	chr1	+	80,303,031	80,306,162	105
ABTB1	chr12	-	9,927,378	9,954,542	104
COPS8	chr7	-	4,916,703	4,925,942	104
RPL6	chr15	-	6,479,461	6,482,828	104
RAB10	chr3	+	107,710,115	107,748,991	104
SMAP2	chr23	+	5,200,788	5,212,986	104
LZIC	chr21	-	3,561,368	3,570,113	104
TCF3	chr28	+	1,893,174	1,942,138	104
INO80	chr5	-	26,607,439	26,668,923	103
HSPA5	chr17	-	10,313,902	10,317,954	103
EIF3M	chr5	+	5,583,345	5,597,652	103
UBE3C	chr2	+	8,533,448	8,597,209	103
GARNL3	chr17	+	11,137,384	11,173,293	103
SELK	chr12	-	7,468,694	7,472,754	102
PSMC1	chr5	+	46,255,522	46,263,820	102
THAP5	chr1	+	30,222,079	30,228,501	101
CNOT7	chr4	+	64,995,115	65,015,117	101
RGS18	chr8	-	3,673,804	3,681,426	101
TRPC4AP	chr20	+	2,550,660	2,583,822	100
PNRC2	chr23	+	5,884,445	5,888,553	100
N4BP1	chr11	+	7,834,473	7,853,942	100
MEAF6	chr23	+	4,060,052	4,065,575	100

TBCA	chrZ	+	22,531,890	22,564,379	100
PPHLN1	chr1	+	31,361,499	31,430,263	99
CDC14A	chr8	+	12,454,644	12,512,078	99
NDUFA9	chr1	+	75,728,373	75,748,020	99
DDX1	chr3	+	101,837,291	101,859,295	98
RNF4	chr4	-	85,588,098	85,604,151	98
GTF2H1	chr5	+	13,606,056	13,624,127	98
VPS35	chr11	+	8,380,737	8,402,603	98
CLINT1	chr13	+	11,300,313	11,347,903	98
SNX5	chr3	+	16,380,104	16,396,110	98
PNISR	chr3	+	74,160,603	74,186,259	98
ZFYVE1	chr5	+	28,604,842	28,627,820	98
LOC420411	chr2	+	3,951,762	3,953,857	98
MDM2	chr1	+	37,168,660	37,179,856	97
ACTA1	chr3	-	41,876,220	41,877,744	97
BCL2L1	chr20	-	9,968,507	9,985,476	97
CTSB	chr3	-	110,174,375	110,178,814	97
SPG7	chr11	+	20,661,096	20,691,619	97
TNRC15	chr9	+	1,930,976	1,992,786	97
VEZF1	chr19	+	8,683,796	8,690,204	97
SLMAP	chr12	+	8,996,448	9,071,053	97
STAT5B	chr27	-	4,528,597	4,540,040	96
ASXL2	chr3	-	107,596,219	107,681,931	96
SEC24B	chr4	-	38,491,204	38,535,024	96
ANXA11	chr6	-	6,239,813	6,259,084	96
SLC25A36	chr9	-	7,815,632	7,846,099	96
MIR107	chr6	-	20,487,964	20,488,044	96
MOSPD2	chr1	-	125,735,611	125,770,056	96
MIR125B	chr1	+	102,457,647	102,457,736	96
TMEM66	chr4	-	50,706,688	50,714,393	96
SPINZ	chrZ	+	42,620,886	42,648,541	95
BRAF	chr1	-	58,998,631	59,068,933	95
STRAP	chr1	+	65,247,566	65,256,698	95
MAPRE2	chr2	+	110,793,551	110,830,488	94
GLYR1	chr14	+	15,143,260	15,166,898	94
EIF4H	chr19	-	2,837,001	2,847,590	94
CDC42	chr21	-	6,541,980	6,563,829	94
DGCR6	chr15	-	10,343,881	10,351,106	94
SBDS	chr19	-	782,449	787,469	94
ACADL	chr7	-	2,734,813	2,748,502	94
USP15	chr1	+	34,739,762	34,804,126	94

FURIN	chr10	-	22,267,941	22,278,031	93
MED22	chr17	-	7,530,579	7,531,569	93
SOX4	chr2	-	60,045,744	60,046,084	93
TIMP3	chr1	-	55,131,913	55,164,377	93
HNRNPR	chr23	+	1,514,336	1,536,736	93
VPS29	chr15	-	5,991,969	5,997,067	92
N4BP2L2	chr1	+	178,778,533	178,802,746	92
GSTA3_dup2	chr3	+	91,203,986	91,209,669	92
LUC7L2	chr1	+	51,011,943	51,034,857	92
EIF5B	chr1	+	136,685,917	136,717,114	92
SLU7	chr13	+	7,581,222	7,592,262	92
C13H5orf15	chr13	+	16,499,846	16,505,639	91
ATP6V1A	chr1	-	82,403,569	82,420,821	91
NXT2	chr4	-	13,910,733	13,917,011	91
IK	chr13	-	844,737	852,961	91
MMADHC	chr7	-	36,552,506	36,565,155	91
ATP6V0E1	chr13	+	9,075,834	9,090,633	90
CWC22	chr7	+	15,874,911	15,902,827	90
ARF1	chr2	-	2,259,658	2,271,703	90
MIER1	chr8	+	29,391,389	29,408,800	90
SEPT2	chr15	+	722,287	746,859	90
CNPPD1	chr7	+	23,807,714	23,814,416	90
WAPAL	chr6	-	3,245,581	3,303,391	90
EIF2S3	chr1	-	121,677,748	121,690,599	90
XPO1	chr3	-	2,327,705	2,367,043	89
ZNF326	chr8	-	15,655,783	15,677,052	89
KLHL7	chr2	+	30,984,848	31,008,406	89
DFFB	chr21	-	885,300	887,853	89
EXD2	chr5	-	30,402,424	30,411,906	89
SNX14	chr3	+	79,638,623	79,685,853	89
PSMC6	chr5	+	60,799,896	60,811,594	89
ARIH2	chr12	-	11,943,756	11,972,625	89
KARS	chr11	+	21,838,578	21,850,742	89
CASC4	chr10	-	21,995,104	22,015,835	89
FXYD6	chr24	-	5,521,959	5,529,319	89
TRIM27_dup2	chr16	+	174,778	179,640	88
BRD1	chr1	-	20,001,459	20,064,756	88
COBRA1	chr17	+	2,302,414	2,313,550	88
BZW1	chr7	+	12,346,390	12,356,067	88
ENTPD1	chr6	+	23,437,687	23,445,435	88
CHMP4B	chr20	-	2,109,507	2,131,052	88

HDLBP	chr9	-	5,995,259	6,015,325	88
KDM5B	chr26	+	537,102	565,572	88
MIR130C	chr19	-	7,145,027	7,145,120	88
MIR30B	chr2	-	148,331,598	148,331,684	87
DERL1	chr2	-	143,531,400	143,546,528	87
SERBP1	chr8	-	29,461,803	29,474,561	87
HMG1	chr1	-	111,448,474	111,454,689	87
IRF8	chr11	-	19,610,851	19,616,382	87
CTSL2	chrZ	+	40,910,613	40,916,034	87
TGM2	chr20	+	10,324,566	10,332,891	87
TNFSF13B	chr1	-	144,362,666	144,376,034	87
MRPS26	chr4	+	92,044,252	92,049,642	87
ANGEL1	chr5	-	41,300,799	41,309,445	87
MIR1768	chr2	+	14,046,710	14,046,786	86
MYST2	chr27	-	2,986,851	2,998,323	86
TPM3	chr25	-	1,442,149	1,452,874	86
SH3GLB1	chr8	-	16,640,781	16,657,740	86
MIR18B	chr4	-	3,970,228	3,970,311	86
ZBTB7A	chr28	+	1,029,152	1,029,935	86
MIR1692	chr9	+	23,692,587	23,692,675	86
ATP5A1	chrZ	+	1,938,128	1,946,380	86
HINT1	chrZ	+	44,169,888	44,173,884	86
RAD21	chr2	-	140,994,059	141,017,985	86
PDIA3	chr10	-	22,286,276	22,295,652	85
THOC7	chr12	-	13,818,986	13,826,733	85
VMA21	chr4	-	17,648,228	17,653,101	85
COPS3	chr14	-	4,762,723	4,773,286	84
CCT5	chr2	-	80,497,729	80,505,714	84
G3BP1	chr13	-	12,954,067	12,977,536	84
PAFAH1B1	chr19	+	9,411,438	9,440,942	83
BOK	chr9	+	6,144,952	6,157,556	83
FAM133	chr2	-	22,633,584	22,649,970	83
VAMP3	chr21	-	282,366	286,131	83
PUF60	chr2	-	154,841,395	154,866,396	83
ANP32E	chr25	+	26,015	41,148	83
ASB9	chr1	+	125,552,596	125,565,916	83
NRBF2	chr6	-	9,076,991	9,091,109	82
GRB2	chr18	-	10,708,465	10,742,722	82
MIR181B-1	chr8	+	2,001,750	2,001,838	82
BTBD1	chr10	-	12,886,231	12,899,515	82
WASH1	chr1	-	62,071,951	62,111,156	82

MIR17	chr1	-	152,248,781	152,248,865	82
VPS4B	chr2	+	69,002,727	69,022,330	82
BECN1	chr27	-	4,693,710	4,698,493	81
LIG3	chr19	-	4,475,316	4,490,521	81
CCND3	chr26	-	4,838,546	4,850,970	81
MCAM	chr24	+	4,242,127	4,247,822	81
LOC422249	chr4	+	4,437,213	4,464,292	81
GLS	chr7	+	8,822,033	8,874,561	81
EAPP	chr5	-	38,286,796	38,292,050	80
WDR82	chr12	-	2,801,271	2,815,488	80
DTD1	chr3	-	16,266,215	16,279,558	80
SEP15	chr8	+	16,611,247	16,630,840	80
TMEM57	chr23	-	2,652,360	2,668,245	80
TGFBR1	chr2	+	57,071,509	57,104,459	80
TIA1	chr6	-	31,733,525	31,751,360	80
PPP1R21	chr3	+	8,870,959	8,900,393	80
CIAPIN1	chr11	+	566,342	572,320	79
ASNS	chr2	-	24,628,019	24,641,745	79
PCID2	chr1	+	141,785,076	141,793,889	79
MYL12A	chr2	-	103,992,059	103,999,219	79
CEP63	chr9	+	4,690,853	4,710,324	79
PDHA1	chr1	-	123,735,124	123,747,111	79
PDPK1	chr14	+	7,390,286	7,420,767	78
JAZF1	chr2	-	32,931,596	33,106,531	78
UBE2E3	chr7	-	15,611,716	15,667,519	78
VDAC2	chr6	-	15,928,302	15,938,058	78
ING5	chr9	-	5,815,396	5,821,513	78
LOC416354	chr13	+	18,741,153	18,752,277	78
COPA	chr25	-	1,302,811	1,322,473	78
TMED10	chr5	-	40,600,059	40,614,965	78
BCAP29	chr1	+	15,746,082	15,769,526	78
PDCD4	chr6	+	27,602,767	27,614,874	77
HMGCR	chrZ	-	23,472,984	23,487,423	77
PSMA7	chr20	-	7,715,038	7,719,215	77
PCYT2	chr18	-	9,899,434	9,914,135	77
PRKAR1A	chr18	+	7,869,231	7,886,087	77
MAFK	chr14	+	2,615,829	2,617,746	77
PTBP1	chr28	+	2,286,248	2,313,581	77
GATAD2A	chr28	-	2,575,646	2,599,508	76
RAB3IL1	chr5	-	18,012,549	18,026,336	76
CLASP2	chr2	-	44,703,447	44,837,679	76

SRSF5A	chr5	+	30,595,571	30,612,642	76
IFNGR2	chr1	+	108,757,200	108,765,661	76
GPR126	chr3	-	54,785,457	54,892,785	75
MCMBP	chr6	-	31,843,146	31,857,279	75
SRSF11	chr8	+	29,804,110	29,821,717	75
ARCN1	chr24	-	5,620,605	5,628,657	75
ACTR1A	chr6	-	24,598,315	24,611,559	75
RPS6KB1	chr19	+	7,337,424	7,349,748	75
CDC73	chr8	-	3,416,974	3,512,154	74
PDCD6IP	chr2	+	44,861,686	44,894,525	74
THRAP3	chr23	-	4,372,000	4,736,196	74
DNM1L	chr1	-	61,047,537	61,082,459	74
NADK	chr21	+	1,954,904	1,975,308	74
FGFR10P2	chr1	+	70,147,467	70,158,775	73
UBE4A	chr24	-	4,430,684	4,445,126	73
HN1	chr18	-	10,622,961	10,633,727	73
SNX3	chr3	+	70,113,236	70,132,157	73
TRIM41	chr16	-	115,281	120,779	73
COX7A2	chr3	+	83,533,751	83,537,087	73
PPP4R2	chr12	+	17,132,529	17,159,021	73
CBWD1	chrZ	-	26,477,353	26,497,485	73
UBL7	chr10	+	1,894,367	1,899,511	73
TST	chr1	+	53,491,343	53,498,516	73
GABPA	chr1	+	105,994,350	106,024,089	73
ZNF335	chr20	-	10,510,165	10,518,382	73
PTPN2	chr2	+	99,313,301	99,347,213	72
MBLAC2	chrZ	+	58,545,658	58,553,723	72
HNRNPD	chr4	+	47,870,194	47,876,422	72
TPRA1	chr12	+	10,007,989	10,023,859	72
IFNAR2	chr1	+	108,690,430	108,701,716	72
ITGB3	chr27	+	2,207,680	2,225,804	72
MIR1611	chr10	+	16,350,472	16,350,560	72
DEGS1	chr3	-	18,724,022	18,728,435	72
PRELID1	chr13	-	10,282,356	10,283,490	72
POLR2F	chr1	-	53,012,621	53,016,755	71
RNASEH1	chr3	-	96,571,135	96,577,099	71
C22H2orf42	chr22	-	2,867,064	2,873,684	71
MIR146C-1	chr4	-	92,169,271	92,169,399	71
PLEK	chr3	+	11,260,981	11,276,064	71
NRBP1	chr3	-	107,320,783	107,346,140	71
H2AFZ	chr4	-	61,795,246	61,799,527	71

PPP2CB	chr4	-	35,774,451	35,786,884	71
MED20	chr26	-	4,828,535	4,833,077	71
PRDX6	chr8	-	4,336,640	4,344,270	71
ZFAND5	chrZ	-	35,431,236	35,446,144	71
EXOC7	chr18	+	4,498,582	4,518,894	71
TMX4	chr3	+	15,529,452	15,555,198	71
MAGOH	chr8	-	25,398,769	25,400,444	70
CAT	chr5	+	20,130,953	20,144,867	70
XRN2	chr3	-	3,462,639	3,508,431	70
CARS	chr5	+	14,172,351	14,199,645	70
SRPR	chr24	+	408,949	417,184	70
NUCKS1	chr26	-	2,070,405	2,084,478	70
IKKBK	chr22	+	2,772,157	2,784,185	69
ADAM17	chr3	-	99,084,972	99,117,779	69
MIR138-1	chr2	-	40,745,148	40,745,243	69
FOXO1	chr1	+	174,856,600	174,920,095	69
YIPF4	chr3	-	32,917,781	32,931,289	69
GFPT1	chr22	+	113,818	142,466	69
ZRANB2	chr8	-	29,907,377	29,919,164	69
IL2RG	chr4	+	2,374,517	2,377,288	69
KDM3A	chr4	+	88,810,655	88,838,178	69
MLF2	chr1	-	80,317,268	80,324,389	69
NANP	chr3	-	33,238,736	33,242,498	69
DHX15	chr4	+	76,221,629	76,266,689	68
CLPX	chr10	+	19,877,021	19,896,763	68
CLP1	chr5	-	18,181,915	18,184,159	68
MIR128-2	chr2	+	45,549,176	45,549,259	68
CELF1	chr5	+	24,948,679	24,996,338	68
EXOC5	chr5	+	58,150,743	58,177,169	68
GOLGA7	chr22	+	2,633,839	2,638,217	68
GOSR1	chr19	+	6,212,728	6,234,979	68
TERF2IP	chr11	-	21,835,912	21,838,905	68
POLDIP3	chr1	+	51,064,506	51,078,398	68
CCZ1	chr14	-	1,003,310	1,017,143	67
NCOA7	chr3	-	62,183,626	62,268,174	67
LLPH	chr1	-	36,235,469	36,238,092	67
EIF2S1	chr5	-	31,257,050	31,266,870	67
CYBASC3	chr5	+	318,934	321,397	67
ADD3	chr6	+	27,211,689	27,268,533	67
DIAPH1	chr4	-	5,829,143	5,989,365	66
ANKHD1	chr13	+	1,443,501	1,544,365	66

C20H20orf11	chr20	+	8,419,225	8,425,693	66
FECH	chrZ	+	267,107	278,253	66
PPP1R12A	chr1	-	41,440,938	41,565,256	66
TTC14	chr9	-	18,336,606	18,345,725	66
C1H2orf49	chr1	+	139,399,187	139,413,865	66
RPRD1A	chr2	+	85,793,669	85,811,105	66
MKKS	chr3	+	14,515,684	14,522,518	66
HSP90B1	chr1	-	56,757,644	56,767,490	65
FEM1B	chr10	+	21,322,283	21,325,906	65
FLII	chr14	-	5,085,599	5,094,200	65
DPY30	chr3	+	34,912,973	34,917,499	65
TOLLIP	chr5	+	15,766,715	15,791,784	65
SNX2	chrZ	+	73,831,465	73,865,549	65
SNX12	chr4	+	2,403,867	2,408,572	65
RIT1	chr25	-	1,581,877	1,587,989	65
ASH2L	chr22	+	2,296,454	2,304,664	65
CTCF	chr11	-	1,048,387	1,078,408	64
MTPN	chr1	+	60,292,823	60,332,330	64
SLC25A46	chrZ	-	46,002,375	46,016,365	64
PPP2R5C	chr5	+	51,877,530	51,925,026	64
PPP3R1	chr3	-	11,187,652	11,221,444	64
ADAM10	chr10	+	7,909,620	7,949,767	64
RANGAP1	chr1	+	51,620,377	51,639,710	64
CTDSPL	chr2	+	4,407,693	4,474,618	64
SNAP29	chr15	-	79,006	88,074	64
LBH	chr3	-	8,000,279	8,010,947	64
PSMD2	chr9	+	16,997,432	17,002,138	64
BAP1	chr12	-	2,932,160	2,944,742	64
HARS	chr13	+	825,160	836,801	64
NARS	chrZ	+	252,567	263,886	63
NDUFV3	chr1	+	113,023,006	113,030,847	63
MAPK1	chr15	+	520,665	531,340	63
HDAC1	chr23	-	5,381,210	5,394,541	63
COPS4	chr4	-	47,731,200	47,739,644	63
OPTN	chr1	+	6,939,350	6,962,537	63
NUMA1	chr1	-	199,117,932	199,128,258	63
AP1G1	chr11	+	21,724,444	21,766,175	63
CEPT1	chr26	-	1,024,607	1,047,756	63
IP6K2	chr12	+	9,219,609	9,227,211	63
B4GALT1	chrZ	-	68,711,927	68,722,880	62
TMEM30A	chr3	+	83,515,837	83,529,332	62

ANKRD27	chr11	-	10,541,149	10,580,352	62
OPA1	chr9	-	14,131,770	14,181,442	62
C25H1orf43	chr25	-	1,460,502	1,464,165	62
UBXN2A	chr3	+	106,980,080	106,997,115	62
RAP2C	chr4	-	3,472,761	3,475,173	62
ABCE1	chr4	+	32,136,106	32,146,233	62
ABCC1	chr14	+	7,697,009	7,753,424	62
MX1	chr1	+	112,367,798	112,388,566	62
MIR26A	chr2	+	4,467,516	4,467,592	62
RIC8A	chr5	-	1,653,805	1,665,443	62
FAM53A	chr4	+	86,995,652	87,062,905	62
CUTC	chr6	-	23,518,199	23,522,571	61
SETD1B	chr15	+	5,689,047	5,730,283	61
TCEB1	chr2	-	122,808,414	122,822,177	61
TBL1XR1	chr9	+	19,274,720	19,390,085	61
MXD4	chr4	+	85,853,956	85,891,029	61
ARFGAP2	chr5	+	25,349,098	25,358,464	61
TIRAP	chr24	+	426,283	429,814	61
CRIP1	chr3	+	27,956,254	27,961,670	61
DYM	chrZ	+	981,731	1,104,226	61
LAMP2	chr4	+	16,551,749	16,568,477	61
WHSC2	chr4	+	86,186,526	86,209,821	61
ING3	chr1	-	25,215,322	25,229,309	61
REV1	chr1	-	136,719,317	136,759,179	60
KLHL15	chr1	+	121,691,485	121,714,115	60
PIP4K2A	chr2	+	17,516,262	17,566,832	60
DNAJC18	chr13	+	2,171,372	2,183,026	60
GTF2A1	chr5	-	43,260,868	43,280,567	60
EIF3J	chr10	-	21,935,533	21,944,864	60
NAP1L4	chr5	+	14,203,337	14,228,991	60
RBMX	chr4	-	4,422,127	4,432,978	60
FBXO9	chr3	-	91,134,810	91,152,294	60
USP34	chr3	-	2,177,964	2,321,017	60
PAK1IP1	chr2	+	63,234,706	63,244,325	60
ACTR3	chr7	-	31,216,916	31,242,468	60
IKZF1	chr2	+	82,955,360	83,013,898	59
SMU1	chrZ	-	68,683,599	68,694,813	59
HSPH1	chr1	+	179,284,226	179,306,848	59
SRSF2	chr18	+	4,230,354	4,233,815	59
TRAPPC2	chr1	+	126,388,987	126,394,653	59
PDHB	chr12	-	12,099,060	12,102,799	59

U2AF1	chr1	-	113,163,827	113,180,262	59
DNAJB14	chr4	-	61,758,031	61,794,289	59
HDAC3	chr13	-	1,666,159	1,679,123	59
RAB9A	chr1	-	126,395,772	126,403,906	58
VPS18	chr5	+	26,447,463	26,456,315	58
P2RY1	chr9	-	24,936,264	24,937,581	58
PHF20L1	chr2	+	147,372,810	147,420,656	58
MIRLET7J	chr26	-	1,442,697	1,442,779	58
SPCS1	chr12	+	749,082	751,370	58
OAT	chr6	-	33,693,678	33,707,776	58
ARPP19	chr10	+	9,974,336	9,978,124	58
ZBTB8B	chr23	+	5,458,920	5,460,145	58
HBZ	chr14	+	12,722,558	12,723,991	58
AARS	chr11	+	1,131,020	1,143,395	58
ATXN3	chr5	-	47,024,940	47,036,575	58
MIR130A	chr15	-	408,399	408,481	58
CPNE1	chr20	+	1,045,115	1,089,526	58
SEC62	chr9	-	21,421,066	21,436,760	57
CNDP2	chr2	-	94,202,656	94,216,929	57
DDX19B	chr21	-	4,911,508	4,918,720	57
SPTLC2	chr5	-	41,683,215	41,742,510	57
DAZAP1	chr28	+	2,530,892	2,551,006	57
STRADA	chr27	-	2,696,785	2,707,899	57
CHMP1A	chr11	-	20,711,846	20,716,257	57
LOC424740	chr9	+	1,878,394	1,883,589	57
CHUK	chr6	+	10,408,241	10,431,602	57
BRAP	chr15	-	6,233,740	6,269,146	57
C14H17orf103	chr14	+	4,530,216	4,536,572	57
SNRK	chr2	-	41,033,908	41,058,027	57
DDB1	chr5	+	327,010	340,161	57
MRPL23	chr5	-	15,100,230	15,111,062	57
NDUFS1	chr7	+	13,645,222	13,658,989	57
PSMF1	chr20	-	9,832,124	9,838,437	57
SRRM1	chr23	-	2,831,993	2,848,706	57
SLC2A3	chr1	+	78,956,011	78,965,357	56
AKAP9	chr2	+	22,341,790	22,440,966	56
GNS	chr1	-	35,636,504	35,657,053	56
GALNT1	chr2	-	86,081,814	86,136,442	56
MIR1451	chr3	+	78,710,207	78,710,316	56
RAB2A	chr2	+	116,781,915	116,815,997	56
NUP85	chr18	+	10,652,712	10,664,532	56

RNF166	chr11	-	20,398,122	20,403,954	56
MAVS	chr4	-	91,915,662	91,923,618	56
EIF2S2	chr20	+	1,657,968	1,669,727	56
TFIP11	chr15	-	7,381,278	7,389,078	56
MIR1764	chr15	+	5,834,671	5,834,773	56
ATP6AP2	chr1	-	115,861,428	115,870,576	55
PHB2	chr1	-	80,507,661	80,514,142	55
MIR16-2	chr9	-	23,742,791	23,742,884	55
MIRLET7A-1	chr12	-	6,302,911	6,303,000	55
SNAP23	chr5	+	27,881,677	27,896,698	55
C5H14orf166	chr5	+	60,668,508	60,681,162	55
TMEM111	chr12	+	2,630,388	2,634,232	55
YIPF3	chr3	+	32,154,710	32,160,417	55
NFYA	chr26	+	4,548,212	4,559,974	55
NDUFB1	chr5	-	47,037,143	47,039,156	55
YBX1	chr21	-	6,593,435	6,601,770	55
FAM125B	chr17	+	10,690,052	10,738,803	55
CRK	chr19	+	5,132,386	5,145,043	55
MORN4	chr6	+	23,737,926	23,740,400	55
DNAJC3	chr1	-	150,158,271	150,190,313	55
RNF126	chr28	-	2,214,538	2,223,356	55
FYCO1	chr2	+	42,764,578	42,788,947	55
C11H16orf70	chr11	+	2,379,021	2,408,689	55
ITGB1	chr2	+	13,960,079	14,001,480	55
OGDH	chr22	+	3,902,816	3,920,575	55
FKBP4	chr1	-	78,821,649	78,835,770	55
LYSMD3	chrZ	+	58,515,030	58,519,009	54
ZNF706	chr2	-	133,884,186	133,893,722	54
RNF141	chr5	+	9,860,107	9,871,441	54
PPP3CB	chr6	+	17,232,001	17,275,231	54
USP12P1	chr4	+	12,342,373	12,370,624	54
NR1H3	chr5	-	25,261,732	25,273,218	54
EIF4A3	chr3	+	17,373,450	17,380,533	54
UFD1L	chr15	-	670,413	676,394	54
COPS5	chr2	-	119,185,987	119,682,639	54
STUB1	chr14	+	13,902,163	13,905,791	54
YAF2	chr1	-	31,291,663	31,318,641	54
HPSE	chr4	-	47,901,448	47,905,868	54
CNOT2	chr1	+	37,653,493	37,692,933	53
SRP14	chr5	+	31,773,540	31,777,290	53
SUDS3	chr15	-	10,063,148	10,085,836	53

RNF220	chr8	+	21,280,859	21,441,677	53
POLK	chrZ	-	23,353,996	23,384,115	53
SNX13	chr2	-	28,977,658	29,039,187	53
BAG1	chr2	-	87,930,593	87,939,818	53
SDC4	chr20	+	5,090,512	5,105,057	53
AKAP17A	chr1	-	133,141,898	133,150,205	53
ALDH3A2	chr19	+	6,791,277	6,797,362	53
DNAJB12	chr6	+	12,516,742	12,531,929	52
BTF3L4	chr8	+	25,006,516	25,016,746	52
MTF1	chr23	+	3,845,313	3,857,757	52
SUMO3	chr9	+	6,218,677	6,220,916	52
ENSA_dup2	chr25	-	1,635,854	1,640,120	52
PAM16	chr14	-	13,386,833	13,388,630	52
LMBRD1	chr3	+	85,866,375	85,932,384	52
SNX27	chr25	+	2,000,555	2,017,679	52
SEPP1	chrZ	-	13,006,180	13,014,828	52
NDUFA5	chr1	+	24,083,294	24,088,344	52
SMC3	chr6	+	27,453,001	27,474,815	52
ZCCHC8	chr15	-	5,934,216	5,946,247	52
CDC27	chr27	+	2,752,685	2,780,063	52
C26H6orf89	chr26	+	1,406,906	1,428,443	52
MEF2A	chr10	+	19,050,788	19,146,397	52
RER1	chr21	-	1,535,967	1,543,193	52
AHCYL1	chr26	+	1,122,297	1,132,596	52
ING4	chr1	-	80,221,384	80,236,134	51
HSPA9	chr13	+	2,514,354	2,535,959	51
RBM25	chr5	-	28,566,665	28,601,373	51
GSPT1	chr14	-	106,663	132,178	51
CAPZB	chr21	-	4,697,472	4,761,850	51
POLR2B	chr4	-	50,651,533	50,671,637	51
SDF4	chr21	+	2,518,154	2,530,954	51
VAPB	chr20	-	11,136,269	11,163,770	51
GGA3	chr18	-	10,664,861	10,683,765	51
SPPL2A	chr10	+	12,415,548	12,447,107	51
YWHAG	chr19	+	4,212,583	4,215,681	51
RAP1B	chr1	+	37,085,902	37,119,298	51
YWHAE	chr19	+	5,150,960	5,171,219	51
PRKAB2	chr8	-	4,307,852	4,313,941	51
LPP	chr9	-	15,438,435	15,751,182	51
TRAPPC11	chr4	-	41,155,867	41,180,887	51
LOC422426	chr4	+	26,033,719	26,041,568	51

TMEM11	chr14	+	4,547,530	4,548,436	51
MVP	chr28	+	29,828	39,820	50
CFLAR	chr7	+	12,459,576	12,478,640	50
CLK2	chr25	+	1,643,831	1,652,303	50
RLIM	chr4	-	12,438,000	12,451,072	50
LMBR1	chr2	-	8,381,575	8,431,415	50
UBN1	chr14	+	13,994,226	14,018,716	50
FAM86A	chr14	-	14,150,469	14,154,900	50
MAPT	chr27	-	2,857,111	2,885,074	50
TTC7B	chr5	-	46,439,395	46,560,128	50
ELOVL1	chr8	-	20,388,515	20,398,577	50
INTS2	chr19	+	7,424,422	7,439,447	50
ST3GAL6	chr1	+	87,546,775	87,588,888	50
THOC5	chr15	+	11,442,445	11,453,986	50
RB1	chr1	+	173,042,817	173,121,034	50
COPS2	chr10	-	11,987,106	12,012,839	49
CCT2	chr1	+	37,378,166	37,390,588	49
SLMO2	chr20	+	10,824,109	10,829,841	49
NUBP2	chr14	-	13,967,402	13,971,932	49
GAPDH	chr1	+	80,089,632	80,094,155	49
ATE1	chr6	-	32,509,113	32,579,286	49
PTP4A1	chr3	-	88,427,250	88,442,861	49
UBQLN4	chr25	-	149,994	159,319	49
RALGAPB	chr20	-	730,979	787,784	49
FAM116A	chr12	-	8,970,131	8,987,510	49
SLC23A2	chr22	+	386,157	413,238	49
GPR107	chr17	+	6,405,364	6,440,400	49
LETM1	chr4	+	86,330,939	86,354,064	49
RBM22	chr13	+	13,155,188	13,162,288	49
RAP1GAP2	chr19	+	9,501,624	9,544,974	49
CASP3	chr4	+	40,901,656	40,912,361	48
ABHD13	chr1	-	144,385,544	144,393,523	48
CZH5orf44	chrZ	+	20,018,730	20,043,196	48
SLC26A5	chr1	-	13,975,834	14,009,190	48
LOC769174	chr1	-	81,611,549	81,618,856	48
YPEL2	chr19	+	7,176,002	7,207,404	48
TFEB	chr26	-	4,730,395	4,744,364	48
E2F6	chr3	-	100,165,714	100,176,147	48
CTDSPL2	chr10	-	21,949,302	21,986,002	48
LIN7C	chr5	-	3,731,016	3,743,533	47
LOC395787	chr22	+	2,638,457	2,646,802	47

VPS39	chr5	-	27,747,030	27,771,210	47
TNKS	chr4	-	50,855,020	50,962,543	47
CORO1C	chr15	-	6,659,066	6,695,339	47
KLHL24	chr9	+	3,547,586	3,561,734	47
TPH1	chr5	-	13,546,048	13,556,600	47
SMARCA2	chrZ	+	27,123,348	27,225,427	47
LAMTOR3	chr4	-	61,753,676	61,757,657	47
SASS6	chr8	+	12,617,089	12,629,520	47
SATB1	chr2	-	35,135,980	35,226,779	47
P2RX5	chr19	+	6,568,782	6,581,636	47
CDC40	chr3	-	69,262,140	69,298,612	47
USO1	chr4	-	46,222,803	46,250,387	47
BCAS2	chr26	-	3,698,351	3,701,362	46
C3H6orf120	chr3	-	43,032,629	43,035,344	46
XPOT	chr1	+	35,468,803	35,494,595	46
ARID4A	chr5	-	57,790,580	57,834,535	46
UBE2I	chr14	+	7,459,608	7,467,790	46
SRSF10	chr23	-	5,891,178	5,899,591	46
COG1	chr18	+	9,005,096	9,013,817	46
LYRM4	chr2	+	66,635,447	66,721,931	46
FAM104A	chr18	-	9,012,404	9,021,769	46
HACE1	chr3	+	71,670,626	71,715,651	46
POLR3F	chr3	-	16,301,156	16,308,732	46
TSC22D1	chr1	-	171,694,280	171,775,796	46
ARID3B	chr10	-	1,866,343	1,888,166	46
XIAP	chr4	-	15,780,147	15,797,496	46
MEF2BNB	chr28	+	2,674,289	2,683,211	46
SF3A2_dup1	chr28	-	1,600,319	1,601,558	46
TOR1A	chr17	-	6,256,659	6,260,292	46
TSSC1	chr3	-	96,443,537	96,508,213	45
RAB35	chr15	+	9,747,823	9,763,717	45
TSN	chr7	+	27,825,439	27,829,858	45
HNRNPM	chr28	-	487,437	514,001	45
TAP1	chr16	+	45,895	50,004	45
YTHDF3	chr2	+	118,024,711	118,047,381	45
GPS1	chr18	-	4,962,416	4,971,803	45
NR2C1	chr1	-	47,221,127	47,266,528	45
LY6E	chr2	-	154,010,621	154,016,715	45
ZYX	chr1	-	80,670,674	80,682,092	45
WWP2	chr11	+	21,000,439	21,035,828	45
PCSK7	chr24	-	5,350,723	5,366,019	45

KATNA1	chr3	-	50,050,996	50,064,594	45
DSTYK	chr26	-	1,823,408	1,843,085	45
SELS	chr10	-	19,757,218	19,764,194	45
SPCS3	chr4	+	45,830,036	45,834,675	45
NKAP	chr4	+	16,552,523	16,619,065	45
ARL6IP4	chr15	-	5,247,424	5,251,466	45
UBE2F	chr7	+	4,562,111	4,625,545	45
RAB11B	chr28	-	821,035	833,898	45
YARS	chr23	-	5,526,570	5,531,378	45
NCDN	chr23	-	4,626,824	4,630,807	45
DDX27	chr20	-	10,704,389	10,710,342	45
SAR1B	chr13	+	16,148,767	16,160,344	44
LDHA	chr5	+	13,644,502	13,650,253	44
MTERFD1	chr2	-	131,591,988	131,608,602	44
KPNA1	chr1	-	79,912,901	79,987,339	44
CBR1	chr1	+	110,028,120	110,033,603	44
SLC30A7	chr8	-	12,421,452	12,443,095	44
MAP2K1	chr10	+	20,632,188	20,664,054	44
TCEB3	chr23	+	5,842,345	5,855,501	44
FBXW5	chr17	+	897,253	910,707	44
HIAT1	chr8	-	12,630,191	12,645,931	44
RNF25	chr7	+	24,014,677	24,018,367	44
HDAC2	chr3	+	67,445,902	67,472,523	44
NFU1	chr22	+	97,923	109,820	44
FAM76A	chr23	+	2,406,871	2,422,840	44
SEC23B	chr3	-	16,281,636	16,298,248	44
PPP6C	chr17	-	10,306,425	10,310,144	44
ZC3HAV1	chr1	-	73,639,563	73,671,158	44
MFAP3	chr13	-	12,334,925	12,344,934	44
ASNSD1	chr7	-	299,833	306,511	43
PDS5A	chr4	+	70,992,115	71,065,118	43
PPP2R2A	chr22	-	548,038	581,717	43
SF3A1	chr15	+	11,157,975	11,171,451	43
MIR128-1	chr7	+	32,228,150	32,228,231	43
CAPN1	chr3	-	31,550,244	31,560,627	43
FBXO7	chr1	-	55,265,519	55,279,129	43
C26H6orf130	chr26	-	4,541,749	4,544,997	43
SPG21	chr10	-	19,864,525	19,875,307	43
MIRLET7A-2	chr24	+	3,380,993	3,381,064	43
ABHD5	chr2	-	40,864,579	40,893,158	43
KIAA1279	chr6	+	11,901,700	11,910,480	43

TRA2B	chr9	+	5,425,339	5,443,595	43
XPA	chrZ	+	68,836,470	68,837,258	43
EIF3L	chr1	-	53,042,946	53,052,560	42
PCNP	chr1	+	88,658,518	88,668,071	42
CBX3	chr2	+	32,127,948	32,141,074	42
PTDSS1	chr2	+	131,608,773	131,638,394	42
KIAA0913	chr6	-	16,914,973	16,976,096	42
EIF2AK1	chr14	+	957,169	973,389	42
RRAGC	chr23	+	3,558,522	3,567,932	42
DDX42	chr27	+	2,718,320	2,734,738	42
NUDT3	chr26	+	4,218,029	4,238,067	42
NRF1	chr1	+	668,691	716,284	42
PLIN2	chrZ	-	33,390,846	33,398,608	42
HEXA	chr10	-	994,574	1,003,828	42
WDR1	chr4	+	81,264,301	81,283,770	42
HCN2	chr28	+	2,142,777	2,151,682	42
MON2	chr1	+	34,818,513	34,889,144	42
ZC3H15	chr7	-	1,361,283	1,373,924	42
NGLY1	chr2	-	37,908,743	37,928,089	42
TBK1	chr1	+	35,504,629	35,527,612	41
OSBPL2	chr20	+	7,772,485	7,801,406	41
CHD1	chrZ	+	50,156,877	50,204,555	41
COX6C	chr2	-	133,393,631	133,400,584	41
NOL11	chr18	-	7,059,771	7,070,837	41
KLHL6	chr9	-	3,518,624	3,537,038	41
C5H11orf2	chr5	-	1,670,992	1,679,870	41
RBBP4	chr23	+	5,487,802	5,494,839	41
SUFU	chr6	+	24,612,158	24,693,312	41
MIR15A	chr1	-	173,700,493	173,700,575	41
WDR48	chr2	-	5,199,024	5,222,620	41
IMPG2	chr1	-	88,553,513	88,604,100	41
DCAF12	chrZ	-	6,997,339	7,028,390	41
BRP44L	chr3	+	44,699,197	44,709,848	41
TMEM170A	chr11	+	2,010,968	2,015,102	41
MYSM1	chr8	-	27,105,409	27,120,348	41
TAPBPL	chr1	+	80,009,262	80,018,520	41
NSFL1C	chr20	+	9,777,523	9,783,837	41
PCM1	chr4	-	64,649,652	64,687,502	41
RNF7	chr9	+	11,342,193	11,348,613	41
FAM18B1	chr18	+	2,207,083	2,213,899	41
DHX30	chr2	-	610,014	635,155	41

EXOC4	chr1	-	1,298,022	1,721,003	40
SPATA2	chr20	+	13,856,109	13,862,740	40
NSA2	chrZ	-	23,675,939	23,679,787	40
RQCD1	chr7	-	24,043,569	24,055,174	40
RSU1	chr2	+	19,935,290	20,032,633	40
CNOT10	chr2	+	40,515,089	40,544,285	40
NBN	chr2	-	129,112,204	129,133,674	40
BLMH	chr19	-	6,165,521	6,180,883	40
EFTUD2	chr27	-	1,243,459	1,259,114	40
ZNF384	chr1	-	80,242,136	80,267,074	40
MFSD1	chr9	-	23,966,320	23,976,937	40
TMEM189	chr20	+	13,775,889	13,789,248	40
PDCL3	chr1	+	137,296,850	137,302,515	40
MIR1740	chr3	+	3,714,988	3,715,089	40
PHAX	chrZ	+	55,049,254	55,058,194	40
NKIRAS2	chr27	+	4,406,901	4,409,025	40
USP45	chr3	+	74,102,771	74,156,225	40
USP10	chr11	+	18,779,565	18,830,243	40
CCM2	chr2	-	3,927,091	3,951,546	39
PMPCB	chr1	+	13,936,176	13,947,140	39
OAZ2	chr10	+	504,522	515,575	39
C5H14orf129	chr5	+	48,927,532	48,931,113	39
RABEP1	chr19	-	3,408,203	3,448,370	39
ATP2B1	chr1	-	45,275,391	45,306,012	39
SUGT1	chr1	-	169,998,190	170,020,746	39
FNDC3A	chr1	+	173,294,978	173,407,273	39
ELL	chr28	+	2,996,935	3,029,184	39
MIR29C	chr26	-	2,511,658	2,511,746	39
EPRS	chr3	+	19,948,116	19,985,400	39
TPST2	chr15	-	7,389,269	7,400,656	39
CXCR7	chr7	-	5,015,527	5,017,479	39
TOP3B	chr15	+	453,410	467,189	39
CCT6A	chr19	+	4,851,113	4,857,341	39
ATP5J2	chr14	-	4,408,183	4,409,242	39
SIRT6	chr28	+	2,096,154	2,102,129	39
CDK9	chr17	-	5,523,530	5,530,125	39
MUTED	chr2	+	65,481,301	65,494,813	39
RCHY1	chr4	+	35,741,445	35,747,161	39
MIR15C	chr4	-	4,049,055	4,049,130	39
ST7L	chr26	-	3,339,754	3,358,863	38
E2F4	chr11	+	981,694	994,129	38

SMYD4	chr19	-	5,386,354	5,395,265	38
GTF2A2	chr10	+	6,353,125	6,356,500	38
NF2	chr15	-	11,397,274	11,438,825	38
SH3BGRL	chr4	-	9,416,982	9,448,069	38
HSPD1	chr7	-	11,216,067	11,227,992	38
STK3	chr2	-	132,610,455	132,783,669	38
MR1	chr16	+	366,615	368,647	38
ATF2	chr7	+	17,790,934	17,851,252	38
ZC3H3	chr2	-	154,334,250	154,491,378	38
GLG1	chr11	-	1,779,863	1,835,894	38
LOC768350	chr16	+	366,615	368,647	38
APPBP2	chr19	+	7,929,007	7,946,974	38
PLA2R1	chr7	+	23,416,555	23,452,323	38
PIK3CA	chr9	-	18,774,941	18,800,202	38
TTL	chr3	+	16,915,420	16,930,755	38
CCNC	chr3	+	74,078,102	74,095,953	38
RNF20	chrZ	-	63,651,116	63,671,625	38
VCL	chr6	-	16,483,843	16,537,808	38
RAB40C	chr14	+	14,295,240	14,317,455	38
EXOC3	chr2	+	91,222,769	91,240,807	38
PPIB	chr10	+	677,469	678,763	38
RPS6KA5	chr5	-	46,575,361	46,638,246	38
CSK	chr10	-	1,794,490	1,798,042	38
RAB5C	chr27	-	4,489,016	4,492,769	38
NANS	chrZ	-	50,920,778	50,930,436	37
ZNF692	chr16	-	181,148	187,797	37
VDAC1	chr13	+	16,484,123	16,498,884	37
EDC3	chr10	+	1,826,922	1,849,735	37
LIN52	chr5	+	40,146,283	40,189,315	37
MIRLET7C	chr1	+	102,425,086	102,425,169	37
ERCC5	chr1	-	146,967,527	146,982,578	37
ARMC8	chr9	-	1,515,846	1,575,946	37
SCAF11	chr1	-	32,656,364	32,687,366	37
TDG	chr1	-	56,741,664	56,752,171	37
MRPL48	chr1	+	200,512,787	200,521,458	37
NCL	chr9	-	16,370,197	16,377,722	37
HNRNPH3	chr6	+	11,672,562	11,679,500	37
THOC3	chr13	+	10,503,957	10,507,477	37
MAGT1	chr4	-	12,984,309	12,998,136	37
RBM12	chr20	+	1,045,134	1,055,599	37
CDCA4	chr5	-	54,471,596	54,473,589	37

RBBP5	chr26	-	1,811,043	1,820,368	37
SDHB	chr21	+	174,094	182,465	37
FAM214A	chr10	+	9,931,326	9,968,081	36
MIR103-1	chr13	+	4,449,242	4,449,319	36
COPE	chr28	+	2,828,392	2,833,187	36
WDR91	chr1	+	49,778,906	49,793,909	36
ARFIP1	chr4	+	35,021,760	35,062,469	36
DICER1	chr5	-	48,298,826	48,334,651	36
RAF1	chr12	-	5,155,148	5,183,083	36
RAB14	chr17	-	9,082,024	9,097,439	36
ASAH1	chr4	+	64,617,883	64,633,404	36
P4HB	chr18	-	9,868,868	9,875,309	36
PUM1	chr23	-	438,323	508,294	36
MMP11	chr15	+	8,245,766	8,255,722	36
ZFYVE27	chr6	-	23,721,315	23,726,499	36
MPHOSPH8	chr1	-	183,526,965	183,546,926	36
UCHL5	chr8	+	3,533,310	3,546,011	36
MIR99A	chr1	+	102,424,333	102,424,413	36
MAPKAPK5	chr15	+	6,269,798	6,289,762	36
TMEM188	chr11	-	7,041,387	7,047,235	36
SCOC	chr4	+	30,762,727	30,766,289	36
COMMD5	chr4	-	16,846,723	16,866,842	35
TOMM7	chr2	-	30,904,640	30,908,666	35
DRG1	chr15	-	9,258,636	9,263,136	35
CNOT4	chr1	+	49,647,318	49,717,601	35
C11H16orf80	chr11	+	426,238	432,752	35
HP1BP3	chr21	+	6,881,433	6,895,647	35
MRPL38	chr18	+	4,609,670	4,614,452	35
CALM1	chr5	+	46,321,178	46,329,340	35
PPME1	chr1	+	200,611,703	200,642,465	35
NUP50	chr1	+	72,387,869	72,403,912	35
CCDC132	chr2	+	22,899,725	22,968,879	35
YIPF5	chr13	-	18,144,055	18,151,153	35
TIA1	chr22	-	2,875,036	2,887,913	35
DLST	chr5	+	40,503,983	40,519,025	35
RPIA	chr4	+	89,350,452	89,365,852	35
YFV	chr16	+	289,047	368,647	35
TMEM16E	chr5	+	2,770,253	2,802,692	35
AURKAIP1	chr21	+	2,218,649	2,221,229	35
REL	chr3	+	2,007,403	2,041,347	35
FAM46A	chr3	+	81,189,258	81,193,854	35

UBE2J1	chr3	+	78,396,171	78,419,659	35
SNX10	chr2	+	32,150,649	32,184,070	35
GNAQ	chrZ	-	37,357,851	37,477,114	35
EGR1	chr13	+	18,848,294	18,851,096	34
SMC4	chr9	-	23,715,844	23,747,112	34
EIF2C4	chr23	-	4,528,583	4,539,847	34
ARPC1A	chr14	+	4,360,144	4,375,242	34
SRP72	chr4	+	50,719,580	50,734,207	34
RBM6	chr12	+	2,425,320	2,476,542	34
MTG1	chr6	-	10,499,182	10,502,277	34
RAB6A	chr1	-	200,443,596	200,502,643	34
SURF6	chr17	-	7,520,042	7,522,770	34
BTK	chr4	+	2,009,589	2,020,513	34
COPG	chr12	+	9,350,912	9,369,955	34
RPL36	chr28	+	656,891	660,417	34
TRAPPC4	chr24	+	5,783,338	5,785,937	34
B4GALT2	chr8	+	21,087,257	21,094,576	34
CNOT8	chr13	-	12,104,519	12,110,304	34
PPP2R4	chr17	+	6,066,242	6,090,870	34
UVRAG	chr1	-	198,996,194	199,064,133	34
ABCF2	chr2	+	131,031	143,837	34
STX2	chr15	+	2,944,420	3,235,979	34
FRS2	chr1	+	37,322,047	37,369,318	34
ERCC3	chr7	+	25,171,773	25,188,953	34
C1H21orf59	chr1	-	108,461,450	108,468,775	34
ARL6IP5	chr12	+	15,756,683	15,769,490	34
SSU72	chr21	+	2,099,380	2,121,397	34
SLC7A5	chr11	-	19,928,909	19,962,052	34
TSPAN3	chr10	+	4,049,702	4,075,319	34
MIR1772	chr6	-	11,560,478	11,560,546	34
RAN	chr15	-	3,213,189	3,217,742	34
TBPL1	chr3	-	58,196,459	58,203,023	34
PSMD14	chr7	-	22,963,974	23,009,387	34
STXBP3	chr8	+	1,275,518	1,300,327	33
BANP	chr11	+	19,999,129	20,118,675	33
EPN2	chr14	+	5,218,226	5,241,873	33
PRPF19	chr5	+	364,546	365,242	33
MTMR9	chr3	+	109,935,098	109,958,445	33
GCLM	chr8	+	14,456,927	14,467,159	33
DDX55	chr15	-	4,991,481	4,998,054	33
TMEM106B	chr2	+	26,557,233	26,571,834	33

POFUT1	chr20	+	10,099,701	10,104,490	33
CDV3	chr2	+	42,641,655	42,648,137	33
AHCTF1	chr3	+	35,028,495	35,082,206	33
SLC35C2	chr20	-	10,675,954	10,681,837	33
DYNC1I2	chr7	-	19,388,693	19,412,865	33
TADA1L	chr8	+	4,344,411	4,354,170	33
CLCN7	chr14	-	12,934,459	12,958,134	33
NAGA	chr1	+	51,312,497	51,316,803	33
RNF111	chr10	-	7,796,854	7,839,019	33
FBXW11	chr13	+	2,574,566	2,640,561	33
GLRX	chrZ	+	56,240,543	56,249,418	33
DPM2	chr17	+	5,501,067	5,503,545	33
GRPEL1	chr4	-	82,912,799	82,919,205	33
SRSF7	chr3	+	17,533,877	17,542,302	33
VRK1	chr5	+	49,088,188	49,120,694	32
SCAF4	chr1	-	108,120,637	108,164,831	32
ST8SIA4	chrZ	+	49,620,546	49,676,370	32
RBM7	chr24	+	4,600,811	4,604,745	32
PAAF1	chr1	+	200,524,228	200,539,149	32
SYNCRIP	chr3	+	79,601,699	79,624,545	32
CPSF2	chr5	+	47,039,362	47,052,874	32
NOS2	chr19	-	9,162,701	9,181,875	32
CKAP5	chr5	+	25,549,034	25,585,874	32
NME2	chr18	+	5,062,096	5,064,054	32
ATG5	chr3	+	70,885,393	70,957,641	32
NUDT7	chr11	+	15,310,340	15,313,332	32
RFNG	chr18	+	4,972,110	4,979,646	32
ARL6IP1	chr14	-	8,517,375	8,526,531	32
COG4	chr11	+	1,727,384	1,742,042	32
MIR1306	chr15	+	1,296,916	1,296,984	32
FKBP8	chr28	+	2,989,234	2,996,336	32
FBXO22	chr10	-	4,433,990	4,440,640	32
ACOX1	chr18	+	4,575,743	4,593,733	31
CLDND1	chr1	-	86,278,285	86,508,666	31
STX8	chr18	-	2,043,803	2,121,408	31
UBE2W	chr2	-	122,768,086	122,800,358	31
TOM1	chr1	-	54,149,022	54,169,699	31
TH1L	chr20	-	10,853,911	10,862,700	31
FAM48A	chr1	+	176,577,373	176,610,956	31
STK4	chr20	-	5,148,653	5,188,836	31
DHX38	chr11	-	21,678,371	21,689,124	31

HSP90AB1	chr3	-	31,508,313	31,514,151	31
C3H6orf72	chr3	+	50,030,407	50,047,028	31
C5H15orf57	chr5	-	916,872	924,049	31
LEPROT	chr8	+	29,108,000	29,113,841	31
TAF12	chr23	+	2,543,019	2,548,976	31
ZBTB33	chr4	-	16,607,060	16,609,125	31
ST13	chr1	+	51,793,994	51,813,785	31
PDIA4	chr2	-	55,512,348	55,524,177	31
CAPZA2	chr1	-	26,663,733	26,693,460	31
NHLRC2	chr6	+	29,028,367	29,059,462	31
TAF3	chr1	+	4,190,718	4,308,360	31
RPRD2	chr25	-	1,621,159	1,668,259	31
PHB	chr27	+	3,312,565	3,321,761	31
UCHL3	chr1	-	159,089,889	159,130,249	31
ARSK	chrZ	-	56,304,346	56,315,471	30
GCH1	chr5	+	58,923,105	58,939,912	30
MIR148A	chr2	-	32,053,543	32,053,610	30
CLPTM1L	chr2	-	88,089,575	88,119,806	30
ACTC1	chr5	+	34,611,409	34,616,220	30
MOB4	chr7	+	11,240,055	11,250,151	30
LGALS8	chr3	-	39,245,438	39,261,045	30
TCP1	chr3	+	47,459,245	47,467,504	30
SSRP1	chr5	+	18,212,450	18,220,609	30
CIR1	chr7	+	18,113,107	18,117,273	30
CLOCK	chr4	+	66,957,224	66,979,525	30
NRAS	chr26	-	3,735,644	3,742,472	30
NAA50	chr1	+	82,436,933	82,459,860	30
ROMO1	chr20	-	1,026,215	1,028,189	30
SUPT4H1	chr19	-	504,579	507,444	30
NECAB3	chr20	+	2,172,148	2,198,337	30
ATP2A3	chr19	+	3,239,928	3,264,151	30
DCUN1D1	chr9	+	17,519,565	17,529,291	30
GCC1	chr1	+	475,203	479,606	30
BID	chr1	-	63,990,398	64,008,993	30
ARFGAP3	chr1	-	70,535,311	70,568,803	30
ACTA2	chr6	-	20,317,354	20,323,139	30
PHF21A	chr5	+	25,929,775	26,050,993	29
SHISA5	chr12	-	3,482,411	3,493,568	29
CHERP	chr28	+	3,877,970	3,889,448	29
QRICH1	chr12	+	11,875,101	11,896,303	29
F13A1	chr2	+	66,208,504	66,267,841	29

KLF6	chr2	-	11,709,660	11,718,622	29
DENND1A	chr17	-	9,814,830	9,912,496	29
TRIM2	chr4	+	20,911,647	20,948,893	29
INTS9	chr3	-	108,814,038	108,882,147	29
SDHD	chr24	-	6,297,760	6,300,662	29
HSD17B4	chrZ	-	69,621,727	69,678,081	29
SPAST	chr3	-	34,877,604	34,909,837	29
POU2F1	chr1	-	94,998,986	95,046,447	29
SERPINI1	chr9	-	22,117,952	22,156,946	29
RASA2	chr9	+	11,293,295	11,335,484	29
GGNBP2	chr19	+	8,103,164	8,120,006	29
KCTD2	chr18	+	10,592,320	10,599,410	29
VPS37C	chr5	+	357,474	361,477	29
RASA3	chr1	+	141,237,656	141,365,818	29
SEMA7A	chr10	+	1,910,158	1,932,505	29
ATP6V0A2	chr15	-	4,956,424	4,971,999	29
MIR1560	chr11	-	20,587,341	20,587,444	29
INSIG2	chr7	-	30,432,497	30,437,656	29
RAB8A	chr28	-	3,983,232	3,996,027	29
RPN2	chr20	+	4,976,613	4,997,503	29
BCL6	chr9	+	15,885,283	15,902,356	29
TIMM17A	chr26	-	1,096,567	1,104,751	29
RHOT2	chr14	+	13,882,539	13,893,370	28
CPSF3L	chr21	+	2,325,524	2,332,854	28
AP3S1	chrZ	-	71,017,177	71,044,186	28
SLC25A13	chr2	-	24,089,486	24,184,138	28
RNF139	chr2	+	144,106,561	144,108,611	28
SKIV2L2	chrZ	+	16,102,170	16,145,323	28
PPT1	chr23	-	5,832,208	5,836,864	28
TARS	chrZ	+	9,466,482	9,482,356	28
FAM102A	chr17	+	5,464,678	5,496,217	28
CD74	chr13	+	13,225,806	13,229,327	28
PDLIM5	chr4	+	59,769,827	59,887,046	28
SOCS1	chr14	+	9,162,464	9,163,172	28
ZNF410	chr5	+	40,071,383	40,087,920	28
DROSHA	chr2	+	70,380,481	70,449,443	28
TBP	chr3	-	42,592,959	42,601,778	28
ILK	chr1	-	199,266,976	199,272,722	28
UBA2	chr11	-	11,950,282	11,971,243	28
QARS	chr12	+	11,870,310	11,873,220	28
CCDC127	chr2	+	87,982,791	87,987,031	28

EMC1	chr21	-	4,668,954	4,679,730	27
DLD	chr1	+	15,844,353	15,858,104	27
VPS33B	chr10	+	22,223,081	22,232,367	27
KCTD9	chr22	+	825,699	833,764	27
TLR3	chr4	+	63,155,888	63,160,902	27
MTA1	chr8	-	4,033,977	4,100,550	27
PTPN11	chr15	+	6,487,260	6,515,631	27
SUGP1	chr28	+	2,635,130	2,652,865	27
TMCO3	chr1	-	141,584,980	141,616,309	27
TUBB3	chr11	+	20,805,307	20,805,967	27
VAV3	chr8	-	991,739	1,114,280	27
SLC25A14	chr4	-	1,545,933	1,553,342	27
UQCR11	chr28	+	1,949,046	1,950,949	27
ZBTB34	chr17	+	10,986,600	10,995,118	27
Sep-05	chr15	+	778,379	787,714	27
HADHA	chr3	-	107,758,663	107,781,352	27
PBRM1	chr12	-	674,549	731,322	27
EIF2A	chr9	-	25,214,674	25,227,136	27
MYO1C	chr19	-	5,173,534	5,226,072	27
CSNK2A1	chr20	+	9,883,195	9,905,429	27
AARS2	chr3	+	31,433,965	31,450,362	27
ZC3H6	chr3	+	3,163,591	3,192,965	27
GPR89B	chr1	+	95,846,504	95,870,303	27
TMEM229B	chr5	-	31,043,832	31,048,546	27
GATA2	chr12	+	9,445,136	9,462,559	27
UBE2V2	chr2	+	111,281,455	111,326,698	27
PAFAH1B2	chr24	+	5,330,193	5,338,417	27
CAMK2D	chr4	+	58,100,029	58,259,686	27
SCYL2	chr1	+	49,116,308	49,147,265	27
PPIL2	chr15	-	578,501	635,624	27
ADIPOR1	chr26	+	1,090,461	1,096,137	27
CCT8	chr1	-	107,461,737	107,472,447	27
MRPS5	chr3	-	17,022,234	17,069,081	27
FLI1	chr24	+	1,009,741	1,082,004	27
BRD7	chr11	+	6,849,419	6,880,597	27
IRF10	chr20	-	10,018,363	10,021,470	27
GET4	chr14	+	2,181,209	2,190,575	26
NDUFB8	chr6	+	18,495,025	18,497,910	26
RPS13	chr5	-	12,841,867	12,845,611	26
DNAJC16	chr21	-	4,978,204	4,987,858	26
JMJD1C	chr6	+	8,922,004	9,069,790	26

TMEM104	chr18	+	10,413,485	10,455,019	26
GABPB1	chr10	+	12,549,483	12,563,099	26
ATG4B	chr9	-	5,830,264	5,843,089	26
HIRA	chr15	-	637,897	665,388	26
WDR24	chr14	-	13,908,477	13,914,236	26
PPP1R2	chr9	+	13,776,741	13,789,544	26
WDSUB1	chr7	-	38,161,552	38,186,050	26
EXOSC9	chr4	-	55,481,792	55,487,095	26
BRD8	chr13	+	10,153,055	10,173,957	26
HERC3	chr4	+	36,199,494	36,244,426	26
UBE2D1	chr6	-	6,298,140	6,313,874	26
PMPCA	chr17	-	8,573,203	8,578,774	26
DCTN5	chr14	+	6,928,939	6,936,129	26
SUB1	chrZ	+	9,152,663	9,168,444	26
SHFM1	chr2	-	24,284,949	24,291,484	26
PRKAA1	chrZ	-	12,305,637	12,326,800	26
MIR18A	chr1	-	152,248,626	152,248,718	26
UBIAD1	chr21	+	4,196,588	4,201,907	26
CD81	chr5	-	14,722,996	14,745,258	26
MAPK9	chr13	+	14,089,879	14,110,002	26
INTS8	chr2	+	131,110,546	131,136,239	26
KIFC1	chr16	-	190,172	193,482	26
TMED5	chr8	+	14,675,887	14,683,614	26
TBC1D23	chr1	+	88,163,771	88,194,919	26
RGP1	chrZ	-	8,454,996	8,462,638	26
ALAS1	chr12	+	2,762,833	2,768,435	26
ANKH	chr2	+	77,989,746	78,092,623	26
ARMC1	chr2	-	119,063,537	119,106,336	26
MAFF	chr1	-	52,919,674	52,922,631	25
SMAD5	chr13	-	15,432,571	15,439,754	25
SRGAP3	chr12	-	19,984,521	20,046,884	25
TMEM180	chr6	+	24,582,088	24,596,399	25
TNKS2	chr6	-	20,973,678	21,005,681	25
RFXANK	chr28	-	2,669,210	2,674,255	25
ENOX2	chr4	-	1,517,346	1,541,093	25
KRR1	chr1	-	39,674,272	39,679,739	25
TMED2	chr15	-	4,998,384	5,004,357	25
TMEM60	chr1	+	13,468,266	13,472,492	25
SEC22B	chr8	+	4,170,654	4,179,655	25
FBXW2	chr17	-	11,104,040	11,113,606	25
CRABP1	chr10	-	4,640,028	4,652,924	25

FIG4	chr3	-	69,426,542	69,487,101	25
PSEN1	chr5	-	28,543,833	28,564,776	25
IARS2	chr3	-	19,909,213	19,933,854	25
GOSR2	chr27	-	1,040,317	1,046,533	25
PER2	chr9	-	6,540,251	6,563,407	25
DNAJC2	chr1	-	13,947,076	13,964,307	25
CHIC1	chr4	+	12,213,208	12,232,434	25
CHRNA5	chr10	-	4,572,039	4,583,033	25
SYK	chrZ	+	43,329,249	43,382,289	25
TAF5	chr6	+	25,031,579	25,042,738	25
GPR137B	chr3	-	39,338,427	39,379,411	25
TMEM41B	chr5	+	10,375,348	10,382,984	25
TRIM37	chr19	-	7,117,941	7,139,276	25
RHOT1	chr18	+	6,657,451	6,680,705	25
BUD13	chr24	-	5,218,628	5,224,589	25
RAC2	chr1	+	53,381,298	53,391,120	25
PSEN2	chr3	-	13,392,743	13,403,970	25
MED17	chr1	-	190,068,503	190,082,536	25
C12H3orf19	chr12	+	11,545,538	11,556,881	25
HRAS	chr5	+	17,163,410	17,173,485	25
ACTR6	chr1	+	49,106,103	49,115,094	24
RFC1	chr4	+	71,317,529	71,355,917	24
TRMT6	chr3	-	18,014,325	18,026,648	24
SPRYD7	chr1	-	173,656,820	173,665,613	24
HSBP1	chr11	-	18,457,856	18,459,684	24
ACAD9	chr12	-	5,426,114	5,452,360	24
LARP4	chrE22C19W28_E50C23	-	190,048	210,411	24
RAE1	chr20	-	11,600,843	11,606,001	24
ELOVL5	chr3	+	91,059,746	91,097,551	24
ARL1	chr1	-	49,579,238	49,584,701	24
NSF	chr27	-	1,121,299	1,178,779	24
MAPKAP1	chr17	-	10,363,741	10,448,514	24
FAM96A	chr10	-	21,902,475	21,906,994	24
XRCC6BP1	chr1	+	33,237,905	33,245,085	24
PTK2	chr2	-	151,344,628	151,491,588	24
PLS1	chr9	+	11,576,028	11,614,246	24
KLHL13	chr4	-	3,190,283	3,258,449	24
PPP1CC	chr15	-	6,050,256	6,065,466	24
SCRN3	chr7	-	18,103,832	18,112,426	24
INTS10	chr4	+	35,263,989	35,282,592	24
SHOC2	chr6	+	27,626,795	27,682,433	24

KIF2A	chrZ	+	18,823,680	18,861,645	24
COPB1	chr5	-	11,366,129	11,382,585	24
JMJD6	chr18	+	4,235,848	4,246,974	24
DDOST	chr21	+	6,919,709	6,925,335	24
UFM1	chr1	-	175,863,970	175,874,257	24
KIAA1143	chr2	+	43,237,008	43,242,904	24
USMG5	chr6	-	25,042,673	25,046,481	24
STK40	chr23	+	4,352,425	4,367,594	24
FOCAD	chrZ	+	33,964,855	34,065,268	23
FBXO34	chr5	-	58,782,530	58,819,617	23
MIR1562	chr8	+	24,908,387	24,908,488	23
PLA2G6	chr1	+	52,923,153	52,941,071	23
PPIL3	chr7	-	12,364,301	12,371,388	23
SMARCE1	chr27	-	4,136,997	4,151,539	23
MAN2C1	chr10	-	3,507,358	3,518,977	23
MYEF2	chr10	-	11,529,044	11,550,274	23
ATP6V1E1	chr1	-	63,935,887	63,945,483	23
H2B-V	chr1	+	50,045,032	50,045,412	23
GSN	chr17	+	9,115,188	9,128,186	23
LRRC28	chr10	+	18,946,018	18,994,746	23
VPS53	chr19	+	6,885,947	6,935,255	23
LCLAT1	chr3	-	7,822,875	7,930,821	23
YTHDF1	chr20	-	8,691,045	8,704,254	23
C5H11orf46	chr5	+	4,611,128	4,618,349	23
AXIN1	chr14	+	12,791,896	12,866,694	23
C1D	chr3	-	11,151,314	11,164,912	23
SC4MOL	chr4	+	24,970,616	24,976,867	23
ZEB1	chr2	-	14,295,360	14,404,723	23
CANX	chr13	-	13,622,864	13,635,959	23
DARS	chr7	-	32,297,229	32,333,237	23
PGS1	chr18	-	9,768,925	9,786,289	23
MRPS7	chr18	+	10,683,794	10,689,210	23
CD80	chr1	+	95,614,908	95,639,138	23
BRE	chr3	-	28,621,367	28,785,081	23
BET1L	chr5	+	1,665,558	1,669,893	23
MAEA	chr4	-	87,545,899	87,594,789	23
AVEN	chr5	+	32,386,603	32,471,520	23
COMMD10	chrZ	-	70,838,334	70,934,606	23
REPS1	chr3	+	56,050,145	56,097,236	23
TDRD3	chr1	-	166,407,688	166,510,209	23
DNAJC7	chr27	-	4,385,481	4,406,077	23

GXYLT1	chr1	-	31,247,486	31,278,504	23
RARS	chr13	-	4,497,005	4,511,853	22
NFAT5	chr11	+	20,929,366	20,989,823	22
MIR1786	chr14	+	7,801,714	7,801,822	22
ACYP1	chr5	-	40,563,085	40,564,044	22
SLBP	chr4	+	86,952,893	86,959,644	22
FAM3C	chr1	+	24,998,230	25,026,790	22
WRB	chr1	+	111,455,657	111,462,126	22
WDR43	chr3	-	8,519,212	8,540,817	22
DNASE1L3	chr12	-	9,173,236	9,177,695	22
PITPNB	chr15	-	7,771,363	7,788,016	22
ACBD3	chr3	+	18,227,128	18,244,980	22
DCTN3	chrZ	-	7,400,105	7,404,679	22
MIR1767	chr3	+	44,732,913	44,732,971	22
UFSP2	chr4	+	40,643,754	40,655,328	22
PTPN1	chr20	-	13,593,741	13,632,610	22
SET	chr17	+	5,834,463	5,844,114	22
USE1	chr28	-	3,709,992	3,714,211	22
FOXN2	chr3	+	8,844,465	8,860,023	22
MIR7-1	chrZ	-	39,554,766	39,554,874	22
CPT1A	chr5	-	17,858,573	17,889,380	22
NUDC	chr23	+	1,773,548	1,782,434	22
CCNK	chr5	+	50,489,844	50,502,543	22
ARFGAP1	chr20	+	8,775,796	8,792,555	22
TAF13	chr1	-	86,727,706	86,730,020	22
GIT2	chr15	-	7,059,792	7,089,031	22
MIR221	chr1	+	114,218,926	114,219,024	22
RAB3GAP2	chr3	+	19,868,638	19,909,037	22
C3H2orf43	chr3	-	104,835,015	104,944,902	22
AP1M1	chr28	-	3,968,535	3,976,303	22
TXN2	chr1	+	53,732,631	53,740,685	22
CAPRIN1	chr5	+	19,864,632	19,905,071	22
YKT6	chr22	-	3,887,944	3,890,850	22
WDR59	chr11	-	1,878,951	1,927,727	22
ACTN1	chr5	+	30,507,697	30,590,666	22
PHKB	chr11	-	8,060,122	8,127,805	22
KIAA1467	chr1	+	50,140,009	50,162,406	22
NSL1	chr3	+	22,948,537	22,960,413	22
DYNC1LI2	chr11	+	12,220,591	12,245,255	22
NCBP2	chr4	-	2,426,113	2,428,867	21
IL10RB	chr1	+	108,704,304	108,714,263	21

FBXL18	chr14	-	4,164,498	4,183,099	21
HOOK1	chr8	+	27,420,810	27,444,339	21
RAB22A	chr20	-	11,170,371	11,186,100	21
WDR92	chr3	-	11,176,752	11,182,613	21
PHLDA2	chr5	+	14,242,801	14,244,264	21
SS18	chr2	-	107,239,097	107,282,251	21
CLN8	chr3	-	93,821,689	93,828,283	21
SLC30A5	chrZ	+	21,302,705	21,323,827	21
MRPL53	chr2	+	126,069,174	126,073,225	21
AIP	chr5	-	392,047	393,034	21
CEBPZ	chr3	-	34,767,876	34,783,840	21
COQ9	chr11	-	560,077	566,300	21
KDEL2	chr14	+	9,008,512	9,020,535	21
SMN	chrZ	-	71,153,568	71,157,771	21
MIR1643	chr11	-	1,919,446	1,919,540	21
RBX1	chr1	-	51,747,944	51,758,977	21
SEPT6	chr4	+	16,638,499	16,662,022	21
IFT52	chr20	-	3,617,948	3,628,547	21
MIR1736	chr1	-	143,453,192	143,453,290	21
Fam175b	chr6	+	33,884,802	33,907,727	21
PIP5K1A	chr25	+	1,851,591	1,868,762	21
CLK3	chr10	-	1,854,152	1,862,281	21
WEE1	chr5	-	10,277,282	10,286,470	21
NCSTN	chr25	+	1,322,551	1,333,421	21
DDX49	chr28	-	2,822,081	2,828,235	21
C20H20orf108	chr20	-	11,990,475	11,993,924	21
PGAM1	chr6	-	23,772,831	23,774,828	21
VAMP7	chr4	+	11,274,034	11,289,156	20
SDCBP	chr2	+	115,848,932	115,866,259	20
ACBD5	chr2	-	15,870,318	15,897,420	20
STX17	chr2	-	91,626,576	91,658,317	20
GTF3C6	chr3	-	68,940,807	68,946,226	20
MESDC2	chr10	+	13,930,467	13,936,343	20
SLC17A5	chr3	+	84,208,788	84,234,510	20
PTPRC	chr8	-	2,034,798	2,092,242	20
DUSP10	chr3	+	19,447,982	19,470,254	20
CYR61	chr8	-	16,906,547	16,908,610	20
VLDLR	chrZ	+	27,352,766	27,367,737	20
SF3A2_dup2	chr28	-	1,605,529	1,608,833	20
CCDC12	chr2	-	3,737,749	3,771,177	20
LMBRD2	chrZ	-	10,285,617	10,327,766	20

SSR1	chr2	+	65,808,875	65,818,550	20
CBL	chr24	-	4,256,546	4,282,304	20
KLHL18	chr2	+	3,872,651	3,895,329	20
SOCS5	chr3	+	28,033,834	28,039,372	20
RPAP3	chr1	-	33,222,808	33,237,737	20
CBLL1	chr1	+	15,799,755	15,806,217	20
PCMT1	chr3	+	50,108,445	50,144,213	20
MIR365-2	chr18	+	6,437,296	6,437,391	20
MRPL28	chr14	+	12,762,115	12,766,787	20
ZW10	chr24	+	5,606,082	5,614,953	20
RNF34	chr15	+	5,512,942	5,520,955	20
HAUS2	chr5	+	27,906,119	27,910,806	20
WDR45L	chr18	+	3,363,620	3,377,967	20
SUCLA2	chr1	-	172,941,354	172,955,443	20
TRPC1	chr9	+	11,615,421	11,636,162	20
TAB1	chr1	-	52,567,546	52,575,977	20
RIPK1	chr2	-	67,527,226	67,547,158	20
LPL	chrZ	-	53,399,698	53,408,327	20
KIF3A	chr13	-	17,537,580	17,556,539	20
MIR1626	chr1	+	5,735,270	5,735,359	20
BCL10	chr8	+	16,997,294	17,005,134	19
METTL14	chr4	-	56,527,530	56,551,595	19
ETV6	chr1	+	73,725,630	73,888,489	19
STK25	chr9	-	6,120,720	6,137,449	19
PARK7	chr21	-	235,472	244,119	19
EXOC8	chr3	+	41,621,910	41,624,848	19
C21H1orf144	chr21	+	4,369,762	4,382,207	19
LOC429115	chr8	+	29,563,271	29,574,625	19
STX16	chr20	-	11,027,894	11,038,403	19
ACO2	chr1	-	51,491,244	51,512,148	19
MIR3523	chr13	-	8,968,882	8,969,047	19
SNRPE	chr26	+	1,472,138	1,474,003	19
NDUFA10	chr7	-	6,517,417	6,557,988	19
NUP188	chr17	+	5,959,250	5,986,375	19
WBSCR16	chr19	-	2,594,454	2,608,735	19
SNRPD3	chr15	-	8,682,515	8,685,991	19
C3H20orf7	chr3	-	13,482,778	13,488,070	19
ARL6IP4	chr3	+	11,289,351	11,294,947	19
EIF1AY	chr1	+	123,267,782	123,275,986	19
RFK	chrZ	+	34,085,695	34,089,769	19
PRPF3	chr25	-	1,670,097	1,686,926	19

CRLF3	chr18	-	6,614,874	6,628,012	19
MIR1778	chr13	-	12,212,334	12,212,406	19
HMGB1	chr1	+	179,435,631	179,440,901	19
ACP2	chr5	+	25,292,554	25,298,648	19
IBA57	chr2	-	2,196,445	2,200,899	19
CNP	chr27	+	4,377,953	4,382,889	19
TMEM38A	chr28	-	3,838,793	3,843,157	19
TBC1D24	chr14	-	14,675,971	14,700,099	19
ERH	chr5	+	30,312,547	30,319,569	19
NECAP2	chr21	+	4,382,720	4,389,439	19
ANP32B	chr28	+	1,324,070	1,333,276	19
CSNK2A2	chr11	+	401,655	422,346	19
NT5C3L	chr27	-	4,327,919	4,332,617	19
LIMS1	chr1	+	140,543,193	140,556,647	19
NFIL3	chrZ	-	43,619,445	43,621,029	18
MAPRE1	chr20	+	10,214,067	10,222,090	18
ZDHHC5	chr5	-	18,165,280	18,174,477	18
HMGN3	chr3	+	82,198,940	82,223,275	18
FKBP1A	chr20	+	9,797,567	9,797,698	18
GANC	chr5	+	27,796,886	27,816,407	18
CISD1	chr6	+	6,314,180	6,323,759	18
FBXO8	chr4	-	45,136,921	45,153,740	18
RMI2	chr14	-	9,135,906	9,137,531	18
FOPNL	chr14	-	7,688,258	7,693,246	18
RAC1	chr14	-	9,036,810	9,050,145	18
MIR20A	chr1	-	152,248,306	152,248,403	18
FAM108B1	chrZ	-	35,299,232	35,316,913	18
SEPT9	chr18	+	3,763,496	3,812,282	18
MIB2	chr21	-	2,025,268	2,058,322	18
AP3M1	chr6	+	16,462,816	16,479,520	18
ENAH	chr3	+	18,409,106	18,495,981	18
ADAT1	chr11	+	21,850,830	21,872,623	18
CDKN3	chr5	-	59,060,988	59,067,001	18
PLA2G7	chr3	-	112,655,573	112,669,249	18
PSPH	chr19	-	4,836,254	4,846,979	18
VAMP1	chr1	-	80,050,790	80,053,646	18
C1H22orf40	chr1	-	73,513,796	73,539,478	18
LYPLA2	chr23	+	5,859,724	5,863,558	18
VPS45	chr25	-	95,861	123,031	18
HMG20A	chr10	-	3,842,481	3,903,256	18
HMG2	chr23	-	132,496	135,894	18

MKRN2	chr12	+	5,141,751	5,151,454	18
ADSL	chr1	-	51,977,354	51,993,080	18
KIAA1704	chr1	+	171,909,504	171,924,291	18
WDR61	chr10	+	4,671,958	4,679,647	18
SEPT7	chr2	-	46,956,494	47,011,997	18
NKRF	chr4	+	16,664,299	16,672,586	18
FDX1	chr1	-	183,880,120	183,896,597	18
UTP6	chr18	-	6,575,494	6,585,267	18
C1H21orf91	chr1	-	102,781,813	102,798,496	18
DCAF13	chr2	+	134,874,886	134,898,052	18
VKORC1L1	chr19	+	4,871,770	4,881,893	18
ACVR1	chr7	-	37,894,083	37,907,942	18
SPPL2B	chr28	+	546,414	582,728	18
SLA	chr2	-	147,512,270	147,526,348	18
ZBED4	chr1	+	20,100,925	20,105,376	17
PNPLA7	chr17	+	1,984,126	2,099,421	17
SMAD2	chrZ	+	1,290,967	1,331,005	17
TCP11L1	chr5	+	5,795,337	5,812,334	17
ANGEL2	chr3	+	22,876,187	22,888,226	17
ACSL1	chr4	+	40,834,173	40,871,803	17
YOD1	chr26	-	2,425,842	2,429,413	17
C1H21orf33	chr1	+	113,827,940	113,834,954	17
VPS41	chr2	-	49,377,949	49,485,343	17
HEATR3	chr11	-	7,018,121	7,039,103	17
CHM	chr4	+	8,622,348	8,681,696	17
WDR70	chrZ	+	10,937,170	11,080,945	17
RUNX1	chr1	-	109,473,589	109,621,192	17
EXOC2	chr2	-	67,705,749	67,835,174	17
DMTF1	chr1	-	7,909,052	7,937,944	17
PELI1	chr3	-	9,549,138	9,567,020	17
USPL1	chr1	-	179,371,081	179,384,218	17
SLC2A8	chr17	+	11,113,792	11,122,569	17
SAP130	chr9	-	2,432,412	2,453,527	17
SCFD1	chr5	+	36,524,468	36,569,134	17
RNF113A	chr27	+	2,689,831	2,695,878	17
PIK3CD	chr21	+	3,457,205	3,480,868	17
CCDC43	chr27	-	1,202,328	1,210,569	17
MIR1596	chr1	+	5,887,350	5,887,439	17
OSTM1	chr3	+	70,177,177	70,188,138	17
FLNB	chr12	+	9,089,762	9,170,226	17
TCF7L2	chr6	+	28,510,784	28,683,593	17

MIR21	chr19	+	7,322,072	7,322,168	17
MIR1705	chr17	-	9,510,405	9,510,494	17
TRAPPC6B	chr5	-	39,998,572	40,002,391	17
ARHGDI1A	chr18	-	9,880,302	9,889,500	17
TESC	chr15	+	11,653,004	11,655,419	17
CFDP1	chr11	-	1,959,809	2,010,716	17
C6H10orf57	chr6	+	6,180,971	6,186,094	17
MCTS1	chr4	-	16,513,180	16,521,219	17
GOT2	chr11	-	1,452,057	1,460,789	17
KATNB1	chr11	-	483,523	501,372	17
USP6NL	chr1	-	6,146,734	6,295,357	17
CLIP1	chr15	-	5,866,253	5,918,580	17
NEMF	chr5	-	60,242,485	60,262,819	17
TEF	chr1	-	51,548,177	51,563,882	17
EWSR1	chr15	-	11,488,354	11,510,884	16
AMD1	chr3	-	68,963,476	68,980,706	16
ANKRD16	chr1	+	916,987	933,442	16
SEC11A	chr10	+	365,105	374,270	16
ITFG1	chr11	+	8,131,082	8,202,251	16
C4H4orf29	chr4	+	35,507,647	35,530,357	16
SLC30A6	chr3	-	34,858,807	34,871,560	16
NRP1	chr2	+	13,799,693	13,905,996	16
MRPL21	chr5	-	1,452,105	1,469,268	16
SDR16C5	chr2	-	114,998,137	115,011,843	16
PPP2R2D	chr6	+	36,781,779	36,808,868	16
HSPA13	chr1	-	101,477,457	101,485,065	16
G2E3	chr5	+	36,500,735	36,520,664	16
ANKMY2	chr2	-	28,465,050	28,486,016	16
NUBP1	chr14	-	9,338,546	9,343,256	16
GPATCH3	chr23	-	1,763,493	1,768,603	16
FAM105A	chr2	-	78,140,484	78,164,589	16
CAMLG	chr13	-	16,118,438	16,121,456	16
RAD17	chrZ	+	62,774,071	62,789,979	16
E2F5	chr2	+	127,428,845	127,441,383	16
TSPAN14	chr6	-	5,415,003	5,437,470	16
SRRD	chr15	+	7,380,018	7,381,793	16
HIST1H1C	chr1	+	50,042,930	50,043,699	16
NAA25	chr15	-	6,319,717	6,358,654	16
RWDD1	chr3	-	66,426,667	66,435,740	16
MIR1729	chr15	+	769,596	769,666	16
MBNL3	chr4	-	3,485,812	3,544,306	16

TAF11	chr26	+	4,104,911	4,108,376	16
MIR1673	chr15	+	756,494	756,593	16
TUBGCP2	chr6	-	10,462,517	10,487,523	16
NCBP1	chrZ	-	68,812,310	68,847,098	16
BIVM	chr1	-	146,983,796	147,000,433	16
NDUFS3	chr5	-	24,930,135	24,934,914	16
MICALL1	chr1	-	53,021,170	53,039,327	16
CKB	chr5	-	52,833,368	52,841,007	16
C1H11orf73	chr1	-	195,064,951	195,073,858	16
NREP	chrZ	+	45,606,429	45,625,270	16
AAMP	chr7	+	24,110,112	24,114,536	16
SCPEP1	chr18	+	6,299,672	6,310,410	16
ARF6	chr5	+	60,273,584	60,274,061	16
CYB5B	chr11	+	20,907,933	20,921,353	16
GMPS	chr9	-	24,497,164	24,518,333	16
PSIP1	chrZ	-	31,672,682	31,708,353	16
MIR1804	chr4	+	47,863,649	47,863,731	15
PTPLAD1	chr10	+	20,200,032	20,209,676	15
CD247	chr1	+	94,935,255	94,985,510	15
DR1	chr8	-	14,625,124	14,637,597	15
MRPL45	chr27	+	3,860,703	3,864,374	15
MIR1717	chr3	+	35,031,812	35,031,912	15
WDR5	chr17	+	7,878,391	7,890,170	15
RHOG	chr4	-	2,231,929	2,243,539	15
CD200R1_dup2	chr1	+	86,766,575	86,787,098	15
TSEN2	chr12	+	5,127,298	5,137,435	15
PHKG1	chr19	-	4,862,449	4,867,367	15
ELP3	chr3	-	108,485,799	108,570,070	15
FUBP1	chr8	+	19,591,030	19,612,139	15
UBLCP1	chr13	-	10,671,222	10,684,036	15
FAM98A	chr3	+	32,284,639	32,300,514	15
DTNBP1	chr2	-	62,397,299	62,465,995	15
RNF170	chrZ	-	52,557,396	52,570,420	15
INVS	chr2	-	91,490,448	91,576,378	15
SRP68	chr18	+	4,528,117	4,541,596	15
ACTR5	chr20	+	3,726,027	3,736,301	15
MRPS18C	chr4	+	47,924,877	47,927,045	15
TASP1	chr3	+	13,522,409	13,594,438	15
C1H12orf73	chr1	+	56,752,368	56,753,648	15
SMPDL3B	chr23	+	1,424,651	1,430,420	15
TAF8	chr26	+	4,876,560	4,884,910	15

UQCRFS1	chr11	-	8,669,418	8,672,771	15
ARRDC1	chr17	+	2,361,839	2,388,459	15
PEX13	chr3	+	2,078,126	2,085,296	15
SH3GL1	chr28	-	2,006,349	2,031,964	15
KIAA0776	chr3	-	75,492,426	75,514,053	15
POMT1	chr17	+	6,847,998	6,861,461	15
KLHL20	chr8	+	5,809,822	5,832,789	15
PGK1	chr4	+	13,036,098	13,046,979	15
ZNF341	chr20	-	2,135,304	2,150,010	15
CAPZA1	chr26	+	3,359,017	3,368,964	15
SUCLG1	chr4	+	89,378,315	89,393,808	15
RNF185	chr15	-	9,342,136	9,351,582	15
MIR1689	chr19	-	9,363,453	9,363,556	15
RCAN3	chr23	+	6,028,731	6,036,037	15
C19H17orf63	chr19	-	5,789,798	5,818,026	15
GATA3	chr1	+	4,344,480	4,367,560	15
NFYB	chr1	+	56,685,115	56,691,879	15
MIR23B	chrZ	+	41,157,406	41,157,491	15
UBE2K	chr4	-	71,078,890	71,141,749	15
NDE1	chr14	+	7,608,539	7,620,641	15
TNFAIP1	chr19	+	9,273,471	9,285,500	15
LSG1	chr9	+	13,919,709	13,931,640	15
ACAP2	chr9	+	13,790,330	13,847,996	15
NAIF1	chr17	+	5,455,509	5,458,662	15
MIR1685	chr2	+	24,751,266	24,751,360	15
GEMIN4	chr19	+	6,873,179	6,880,315	15
UBE2N	chr1	-	46,728,774	46,750,488	14
SRP9	chr3	-	18,369,190	18,377,483	14
METAP1	chr4	+	61,512,267	61,536,257	14
TBL1X	chr1	-	129,005,342	129,166,042	14
GBE	chr1	-	51,039,513	51,043,445	14
YWHAQ	chr3	-	99,139,517	99,165,554	14
PDE4B	chr8	+	29,305,327	29,315,124	14
TRIM39	chr16	+	137,058	141,079	14
MRPS11	chr10	-	14,861,337	14,864,868	14
MTMR8	chr4	+	11,716,305	11,740,319	14
ZCCHC17	chr23	+	550,946	564,043	14
VAPA	chr2	-	100,936,925	100,967,393	14
EPHA5	chr4	-	52,562,733	52,762,923	14
LANCL1	chr7	-	2,789,268	2,804,935	14
ICMT	chr21	+	588,694	592,500	14

TPM2	chrZ	+	8,550,287	8,553,846	14
KBTBD4	chr5	+	24,938,267	24,943,705	14
LSM7	chr28	-	540,993	546,348	14
CELF2	chr1	+	5,927,617	6,073,060	14
TMLHE	chr4	-	11,092,946	11,110,808	14
DRG2	chr14	+	5,020,758	5,029,252	14
CPSF6	chr1	+	37,256,467	37,282,365	14
STIM1	chr1	-	199,574,924	199,580,277	14
TSNAX	chr3	-	41,489,935	41,506,277	14
LRRC45	chr18	-	4,991,013	5,000,508	14
OXNAD1	chr2	+	34,251,529	34,270,804	14
PQLC2	chr21	+	4,686,372	4,692,899	14
MPL	chr8	+	20,376,338	20,380,285	14
PLEKHJ1	chr28	+	1,604,050	1,613,894	14
EXOSC10	chr21	-	4,118,846	4,132,959	14
EBAG9	chr2	+	137,879,498	137,898,721	14
CALCRL	chr7	+	1,108,694	1,135,271	14
FOXP1	chr12	-	16,478,421	16,653,728	14
PMS1	chr7	-	239,919	281,469	14
KRIT1	chr2	-	22,460,367	22,480,714	14
SOCS6	chr2	-	95,938,797	95,942,000	14
GORASP2	chr7	-	19,629,974	19,637,107	14
HIST2H2AC_dup2	chr1	-	50,044,294	50,044,681	14
MTF2	chr8	-	14,689,878	14,713,292	14
NFRKB	chr24	+	1,563,539	1,580,761	14
LOC693265	chr12	-	811,981	813,866	14
MRPS33	chr1	-	59,082,645	59,087,543	14
MIR1781	chr14	-	3,330,762	3,330,854	14
MIR456	chr3	-	32,679,710	32,679,821	13
TRIM8	chr6	+	24,706,987	24,725,664	13
MED6	chr5	+	29,702,647	29,711,185	13
PIK3CG	chr1	+	15,390,286	15,418,411	13
GARS	chr2	-	4,262,091	4,285,376	13
HS2ST1	chr8	-	16,540,396	16,610,554	13
ENO1	chr21	-	3,197,152	3,209,544	13
FANCD2	chr12	-	2,583,819	2,629,840	13
DERL3	chr15	-	8,257,576	8,262,050	13
TMEM68	chr2	-	114,645,704	114,665,389	13
WBSCR22	chr19	+	73,358	78,108	13
VGLL4	chr12	-	4,695,253	4,741,075	13
PRR5	chr1	+	71,888,375	71,975,018	13

TMC7	chr14	-	8,695,807	8,712,942	13
MIR1578	chr5	-	57,724,751	57,724,817	13
RUFY1	chr13	-	13,676,786	13,697,319	13
ROCK1	chr2	-	105,321,687	105,399,548	13
NRG1	chrZ	-	52,836,616	52,938,466	13
UBL3	chr1	+	179,612,550	179,669,473	13
ARHGAP25	chr22	-	299,045	315,601	13
FAS	chr6	+	20,340,538	20,352,851	13
YWHAB	chr20	-	5,206,921	5,219,910	13
MIR2129	chr14	+	4,018,489	4,018,572	13
NONO	chr4	-	2,255,310	2,269,715	13
ATG7	chr12	+	4,585,676	4,674,522	13
CMPK1	chr8	+	22,661,517	22,674,010	13
MID1IP1	chr1	-	116,300,244	116,301,246	13
GDI2	chr1	+	941,252	949,319	13
ADCK3	chr3	-	13,349,537	13,381,377	13
POLD3	chr1	-	200,758,968	200,790,002	13
NADSYN1	chr5	-	1,680,061	1,697,704	13
TBC1D14	chr4	+	82,869,181	82,897,943	13
CCDC61	chr9	-	4,456,690	4,460,953	13
CHST10	chr1	-	137,240,246	137,256,719	13
ETFA	chr10	+	4,298,859	4,330,531	13
SETD3	chr5	-	50,436,085	50,489,422	13
CYCS	chr2	-	31,693,796	31,694,280	13
SERPINE2	chr9	-	9,384,818	9,409,408	13
NEIL1	chr10	+	3,502,248	3,507,190	13
NOC2L	chr21	+	2,871,079	2,904,474	13
LRRC57	chr5	-	27,901,335	27,906,066	13
CHORDC1	chr1	+	191,849,848	191,862,268	13
EIF2C3	chr23	-	4,478,187	4,499,985	13
POLH	chr3	-	32,113,336	32,121,563	13
MIR29A	chr1	+	3,236,329	3,236,417	13
PUS10	chr3	-	2,043,413	2,077,790	13
SUGP2	chr28	+	2,764,650	2,775,181	13
PSMG1	chr1	-	111,382,068	111,390,997	13
ENSA_dup1	chr25	+	1,618,799	1,619,952	13
DAD1	chr27	+	71,909	74,671	13
EHD3	chr3	-	7,615,214	7,640,401	13
NR13	chr10	+	10,154,230	10,156,837	13
ATP6AP1	chr1	+	24,118,922	24,173,200	13
ABCD3	chr8	-	14,241,828	14,268,200	12

SCYL3	chr8	+	5,252,301	5,265,377	12
SURF1	chr17	-	7,535,553	7,539,173	12
MTX3	chrZ	+	21,479,268	21,489,546	12
PLEKHM1	chr27	-	1,491,229	1,505,933	12
BEST3	chr1	-	37,409,023	37,425,512	12
TRAPPC3	chr23	+	4,412,456	4,418,168	12
LOC420860	chr2	-	64,400,643	64,404,161	12
MIR1737	chr10	+	19,149,635	19,149,727	12
GLIPR1	chr1	+	39,662,655	39,670,286	12
TGS1	chr2	+	114,722,854	114,757,201	12
MIR1765	chr18	+	5,840,573	5,840,677	12
BLB1	chr16	+	69,850	71,202	12
DCAF7	chr27	+	2,612,006	2,629,022	12
DEK	chr2	+	61,435,724	61,453,184	12
CNIH	chr5	+	59,054,176	59,059,960	12
REEP5	chrZ	+	45,143,651	45,162,810	12
TLE4	chrZ	+	38,049,188	38,146,664	12
AZIN1	chr2	-	134,626,073	134,655,219	12
CDK10	chr11	+	20,717,746	20,721,824	12
BLB2	chr16	+	69,833	71,214	12
BET1	chr2	-	23,354,136	23,360,050	12
XYLT2	chr18	-	10,358,357	10,370,856	12
C5H14orf109	chr5	+	47,506,516	47,509,592	12
TTC35	chr2	+	137,539,917	137,577,287	12
CASP18	chr7	+	12,495,350	12,503,503	12
KLHDC4	chr11	-	19,883,479	19,912,894	12
NDUFA12	chr1	-	47,205,599	47,213,077	12
ZBTB2	chr3	-	50,759,332	50,766,723	12
NPM1	chr13	-	3,025,462	3,038,578	12
ALG6	chr8	+	28,569,495	28,589,852	12
UBAC2	chr1	-	148,754,443	148,854,244	12
MIR1598	chr3	-	24,011,306	24,011,380	12
MSN	chr4	+	113,862	153,722	12
SYNGR3	chr14	+	6,211,506	6,231,037	12
CRYGN	chr2	-	6,187,400	6,191,956	12
NCK2	chr1	+	139,551,605	139,634,106	12
PIGA	chr1	+	125,514,501	125,523,793	12
RGS9BP	chr11	+	10,582,411	10,586,663	12
PTCH1	chrZ	-	41,285,006	41,326,491	12
ADSS	chr3	+	36,034,617	36,055,236	12
ARL8A	chr26	-	350,402	355,252	12

MIR1697	chr19	+	7,194,813	7,194,891	12
JMJD4	chr2	+	3,131,740	3,140,137	12
MIR1572	chr12	-	9,668,820	9,668,914	12
MDH1	chr3	+	9,433,097	9,443,585	12
BAHD1	chr5	+	858,461	875,952	12
NAA35	chrZ	+	40,227,899	40,255,293	12
SIRT3	chr5	+	1,647,530	1,651,663	12
CSTF3	chr5	-	5,812,326	5,855,932	12
TMPO	chr1	+	48,528,636	48,550,811	12
MIR454	chr15	-	399,833	399,953	12
PPARD	chr26	-	3,920,818	3,937,442	12
YWHAH	chr15	-	9,078,613	9,086,941	12
LYRM1	chr14	+	15,681,960	15,692,935	12
LYN	chr2	+	114,794,179	114,852,930	12
RBPMS2	chr10	-	463,456	477,042	12
PACSIN2	chr1	-	70,575,138	70,638,490	12
ZDHC13	chr5	+	1,709,431	1,722,711	11
ZC3H14	chr5	+	45,577,801	45,598,674	11
DYNC1L1	chr2	-	40,470,970	40,493,460	11
ORC3	chr3	-	79,098,223	79,135,817	11
LCP2	chr13	+	3,611,380	3,640,695	11
CYBB	chr1	-	116,720,613	116,740,692	11
PEX10	chr21	+	1,529,724	1,533,314	11
CSNK1G1	chr10	+	585,589	672,427	11
L3MBTL2	chr1	-	51,645,263	51,659,859	11
NPC2	chr5	+	40,335,903	40,338,081	11
LMF2	chr1	+	411,338	412,252	11
PEX5	chr1	+	80,595,698	80,604,778	11
SNRPB	chr20	+	10,700,969	10,703,720	11
MIR1683	chr1	-	51,777,702	51,777,802	11
GRK4	chr4	-	85,226,136	85,256,866	11
MAP2K5	chr10	+	21,102,233	21,225,084	11
MIRLET7A-3	chr1	+	73,421,272	73,421,347	11
SLMO1	chr2	-	99,535,762	99,546,151	11
GTPBP1	chr1	-	52,747,171	52,765,452	11
PLS3	chr4	+	2,968,317	2,985,740	11
CSTF2	chr4	-	5,171,533	5,178,083	11
MTIF2	chr3	-	16,094	27,025	11
GATA6	chr2	+	105,796,446	105,809,517	11
TRAF7	chr14	+	6,455,088	6,484,390	11
FYB	chrZ	-	11,668,114	11,730,690	11

NDUFB5	chr9	-	18,632,069	18,635,615	11
MIR100	chr24	+	3,372,894	3,372,973	11
EHMT1	chr17	+	2,391,254	2,490,316	11
CITED4	chr23	+	1,356,990	1,359,206	11
EIF6	chr20	+	1,331,588	1,338,505	11
FARSB	chr9	-	9,053,427	9,087,768	11
TCOF1	chr13	-	13,229,988	13,247,660	11
PRMT7	chr11	-	264,296	280,738	11
MYLK	chr7	-	28,762,752	28,891,615	11
PLK1S1	chr3	-	3,516,288	3,557,015	11
UBE2V1	chr20	+	13,792,902	13,806,856	11
CMTM7	chr2	+	40,416,466	40,444,193	11
KIAA0586	chr5	-	57,712,712	57,777,125	11
PRKAB1	chr15	-	9,906,778	9,912,314	11
MAL	chr3	+	17,014,726	17,018,636	11
TRPC3	chr4	+	55,418,007	55,457,288	11
PRRC1	chrZ	+	55,327,762	55,356,283	11
FUT10	chrZ	+	52,746,118	52,754,676	11
MPP5	chr5	-	31,278,497	31,324,781	11
PPPDE1	chr3	-	35,977,109	35,991,779	11
CZH9orf80	chrZ	+	64,463,219	64,474,293	11
MIRLET7K	chr26	-	1,442,897	1,442,979	11
TSPAN13	chr2	+	28,553,447	28,570,281	11
ARHGAP26	chr13	+	17,892,826	17,974,138	11
SLC9A3R1	chr18	+	10,398,845	10,406,721	11
SNRPA1	chr10	-	19,764,376	19,769,991	11
USP40	chr7	+	5,867,405	5,896,714	11
STK17B	chr7	-	10,771,838	10,791,099	11
CLTA	chrZ	+	50,949,593	50,965,045	11
RRP1B	chr1	+	113,488,192	113,516,743	11
ARL2BP	chr11	+	740,722	750,277	11
HMGCS1	chrZ	-	13,067,038	13,077,340	11
SNX24	chrZ	+	73,868,018	73,944,711	11
C5H15orf29	chr5	+	32,325,752	32,341,242	10
IMPDH2	chr12	+	11,901,651	11,913,806	10
C5H11orf10	chr5	+	164,323	166,195	10
CLDN5	chr15	-	706,766	708,358	10
MGAT4C	chr26	-	897,459	902,049	10
DAGLB	chr14	+	9,024,022	9,034,907	10
NDFIP2	chr1	-	157,097,423	157,143,918	10
ERLIN1	chr6	+	10,431,747	10,447,937	10

STK38L	chr1	+	70,241,342	70,283,239	10
PIAS2	chrZ	+	1,560,806	1,590,560	10
PKM2	chr10	-	955,304	973,190	10
MIR222-1_dup1	chr1	+	114,216,027	114,216,124	10
MIR222-2_dup1	chr1	+	114,216,027	114,216,124	10
MIR222-1_dup2	chr1	+	114,218,422	114,218,519	10
MIR222-2_dup2	chr1	+	114,218,422	114,218,519	10
MPPE1	chr2	+	99,672,871	99,704,461	10
ANO3	chr5	+	3,289,298	3,411,373	10
PGRMC2	chr4	-	35,574,430	35,588,230	10
ALKBH1	chr5	-	41,762,805	41,775,668	10
MIR133A-2	chr20	+	8,119,054	8,119,149	10
ARHGEF3	chr12	-	8,665,324	8,697,330	10
BRMS1L	chr5	+	38,735,855	38,755,295	10
CASP2	chr1	-	80,809,182	80,835,922	10
BUB3	chr6	+	33,088,914	33,110,830	10
MBNL2	chr1	-	149,545,243	149,617,725	10
PTPRJ	chr5	+	13,950,233	13,975,462	10
KIF3B	chr20	+	10,104,697	10,113,465	10
KIAA0020	chrZ	-	27,426,487	27,451,167	10
P4HA1	chr6	+	12,270,435	12,298,790	10
CFL2	chr5	-	38,341,895	38,344,696	10
CCDC18	chr8	-	14,648,281	14,675,682	10
WRAP73	chr21	+	945,213	958,706	10
MYBL1	chr2	-	119,492,641	119,512,112	10
SLC6A4	chr19	-	6,143,364	6,155,492	10
MTO1	chr3	-	84,269,491	84,277,130	10
CPPED1	chr14	-	253,496	293,421	10
PRKD1	chr5	-	36,190,046	36,300,945	10
CYP4V2	chr4	+	63,195,452	63,208,385	10
SEC22A	chr7	+	28,515,212	28,529,130	10
TBL3	chr14	+	6,175,759	6,186,661	10
CHADL	chr1	+	51,640,818	51,644,428	10
TTLL12	chr1	-	70,704,344	70,724,520	10
LEPRE1	chr21	+	6,571,369	6,577,882	10
SMS	chr1	-	122,454,859	122,500,047	10
HACL1	chr2	-	33,950,471	33,969,248	10
MCF2L	chr1	-	141,847,271	141,993,130	10
RRM1	chr1	-	199,540,617	199,560,670	10
SIKE1	chr26	-	3,760,759	3,765,368	10
IGHMBP2	chr5	+	1,469,278	1,504,623	10

MIR301	chr15	-	406,313	406,405	10
LOC427896	chr1	-	50,050,495	50,051,237	10
TSSC4	chr5	-	14,711,560	14,715,908	10
AATF	chr19	+	8,358,942	8,400,355	10
RFT1	chr12	-	1,126,017	1,137,009	10
C20H20orf4	chr20	+	214,338	220,403	10
MIR1551	chr14	+	5,233,361	5,233,450	10
EIF2B2	chr5	+	40,537,707	40,543,467	10
CCDC6	chr6	+	10,189,724	10,235,182	10
EI24	chr24	-	396,853	404,921	10
GADD45A	chr8	+	29,485,018	29,485,191	10
ADI1	chr3	-	96,561,730	96,569,149	10
EXOC6	chr6	-	21,728,562	21,820,767	9
SMAD6	chr10	+	20,839,626	20,868,401	9
PIGK	chr8	+	19,884,729	19,948,555	9
LOC100502566	chr4	+	1,962,058	1,962,591	9
ZBTB48	chr21	-	550,986	557,453	9
C17H9orf16	chr17	-	5,725,458	5,728,736	9
NUFIP1	chr1	-	171,884,365	171,909,411	9
RBM19	chr15	+	12,771,340	12,815,668	9
SLC39A9	chr5	-	30,295,075	30,312,305	9
SERTAD2	chr3	-	9,728,597	9,747,533	9
IDH3A	chr10	-	4,719,965	4,730,704	9
IRAK4	chr1	+	31,853,699	31,865,151	9
MIR1456	chrZ	-	44,167,486	44,167,595	9
NUDT16L1	chr14	-	13,013,418	13,014,062	9
XPO4	chr1	+	183,035,679	183,085,288	9
SSB	chr7	-	20,038,498	20,046,560	9
ARID5B	chr6	-	9,380,311	9,477,788	9
MRPL50	chrZ	+	63,710,372	63,711,147	9
LRIG3	chr1	-	33,519,694	33,563,467	9
ANAPC10	chr4	-	32,097,854	32,132,648	9
ITGA6	chr7	-	19,091,250	19,134,525	9
NVL	chr3	+	18,689,418	18,718,949	9
PRMT3	chr5	+	2,161,167	2,215,964	9
ARPC5	chr8	-	7,941,224	7,944,726	9
OLFML3	chr26	+	3,629,576	3,631,171	9
NTHL1	chr14	-	6,298,136	6,303,054	9
MENT-1	chr2	-	68,879,734	68,886,128	9
ACTR2	chr3	+	9,927,966	9,942,328	9
F10	chr1	-	141,819,206	141,833,119	9

STT3B	chr2	+	40,165,731	40,193,184	9
LIMD2	chr27	-	2,678,993	2,683,693	9
MIR1719	chr12	-	842,924	843,012	9
FN1	chr7	-	4,361,938	4,411,021	9
EIF2B3	chr8	-	21,535,370	21,620,843	9
CCR5	chr2	-	42,682,320	42,683,186	9
DNPEP	chr7	+	23,739,243	23,744,544	9
ZDHC17	chr1	+	40,040,080	40,105,985	9
PUS7	chr1	+	14,958,659	14,977,855	9
LRRC16A	chr2	-	92,247,368	92,422,574	9
RECQL	chr1	-	67,475,071	67,494,287	9
TMEM230	chr22	+	346,000	361,504	9
PRKCA	chr18	-	7,328,232	7,441,502	9
BST1	chr4	-	79,579,990	79,594,314	9
TFDP2	chr9	-	11,417,806	11,461,895	9
ZNF622	chr2	+	77,430,792	77,437,336	9
ACADS	chr15	-	9,436,932	9,444,505	9
SUPV3L1	chr6	+	11,931,239	11,944,752	9
ERGIC2	chr1	+	15,956,570	15,979,596	9
PDLIM7	chr13	-	10,249,091	10,260,687	9
MIR1653	chr9	-	15,430,499	15,430,602	9
C1H7orf60	chr1	+	28,585,254	28,607,518	9
MIR181B-2	chr17	+	10,220,137	10,220,221	9
DENR	chr15	-	5,313,473	5,319,599	9
STXBP1	chr17	+	2,826,756	2,831,035	9
PRC1	chr10	+	22,232,700	22,240,596	9
MIR1453	chr20	-	1,396,012	1,396,085	9
FAM45A	chr6	+	31,488,971	31,497,974	9
BLNK	chr6	-	22,326,702	22,383,448	9
LONP2	chr11	-	7,929,181	7,968,448	9
H2AFJ	chr1	-	49,975,825	49,976,214	9
RSL1D1	chr14	-	95,711	101,074	9
EAF2	chr7	+	27,896,671	27,910,346	9
OTUD6B	chr2	+	129,518,738	129,527,575	8
TMEM70	chr2	+	122,822,859	122,826,873	8
ADPRHL2	chr23	-	4,457,041	4,462,263	8
OSTF1	chrZ	+	36,405,661	36,418,207	8
GMNN	chr2	-	92,550,070	92,555,455	8
MIR1668	chrE22C19W28_E50C23	-	187,325	187,414	8
FEN1	chr5	-	161,536	164,220	8
ADAM9	chr22	+	2,471,858	2,486,630	8

MRPL37	chr8	+	25,916,522	25,919,946	8
HMHA1	chr28	+	2,386,861	2,400,191	8
TCEANC2	chr8	+	25,889,508	25,893,502	8
ERI1	chr4	+	50,990,601	50,999,467	8
UBA5	chr2	+	42,338,542	42,346,089	8
RBM48	chr2	+	22,624,461	22,629,769	8
GMFB	chr5	+	59,037,259	59,046,770	8
MIR34A	chr21	-	3,251,514	3,251,622	8
SIP1	chr5	+	39,989,260	39,998,552	8
LOC421792	chr3	-	74,098,462	74,101,342	8
SPATS2L	chr7	+	12,172,016	12,230,785	8
TCEA1	chr2	-	113,842,514	113,863,088	8
IMMT	chr4	-	88,714,414	88,727,264	8
DDX52	chr19	-	8,592,481	8,599,656	8
RBMS1	chr7	+	23,214,270	23,352,271	8
AP4B1	chr26	-	3,590,933	3,597,509	8
LIN9	chr3	+	18,177,622	18,205,556	8
ALG10	chr1	-	16,869,598	16,878,150	8
MIR1559	chr7	-	1,330,064	1,330,139	8
MIR101-2	chr8	-	29,051,918	29,051,993	8
RPA1	chr19	+	5,395,396	5,416,895	8
STAU1	chr20	+	6,402,495	6,425,940	8
C1GALT1	chr2	+	24,660,239	24,668,494	8
NAPRT1	chr2	-	154,533,071	154,536,966	8
TBCD	chr18	-	3,204,948	3,314,150	8
PREP	chr3	+	71,361,735	71,456,583	8
CCRN4L	chr4	+	30,325,194	30,327,003	8
FAM210A	chr2	+	98,894,852	98,912,137	8
CST7	chr3	+	16,732,014	16,737,299	8
AKAP2	chrZ	+	64,373,955	64,393,969	8
TMEM167A	chrZ	+	61,618,462	61,640,758	8
KCNMA1	chr6	+	14,425,381	14,862,328	8
ACTR10	chr5	-	57,854,784	57,863,404	8
LCP1	chr1	-	172,312,438	172,341,057	8
CYP51A1	chr2	-	22,441,416	22,455,200	8
CCND2	chr1	-	75,501,156	75,542,025	8
TBC1D22A	chr1	+	17,232,848	17,422,620	8
MBD4	chr12	-	20,124,716	20,127,100	8
CCT7	chr4	-	93,250,452	93,259,186	8
RBM12B	chr2	-	130,603,264	130,610,114	8
SLC22A4	chr13	+	17,375,374	17,390,206	8

CHCHD4	chr12	-	11,058,989	11,067,559	8
SLC25A32	chr2	-	134,852,324	134,872,006	8
ABHD12	chr3	-	4,134,986	4,162,800	8
APOOL	chr4	-	8,784,187	8,797,286	8
EXOSC7	chr2	-	43,123,114	43,142,601	8
CHMP6	chr18	-	9,334,367	9,340,258	8
HTR1B	chr3	+	82,820,824	82,821,989	8
MATN3	chr3	-	104,310,042	104,325,904	8
RRBP1	chr3	+	16,430,700	16,456,808	8
ASB7	chr10	+	19,461,813	19,491,480	8
HDAC7_dup2	chrE22C19W28_E50C23	+	401,100	402,286	7
TPM1	chr10	-	5,108,291	5,126,986	7
EMB	chrZ	-	14,147,214	14,166,737	7
IKZF5	chr6	-	32,997,686	33,024,228	7
UMPS	chr7	+	29,451,779	29,457,619	7
HS6ST1	chr9	-	2,514,084	2,680,845	7
BPGM	chr1	+	64,321,920	64,339,522	7
DUSP1	chr13	-	8,966,505	8,969,110	7
MIR1696	chr19	-	5,566,318	5,566,387	7
ST6GALNAC1	chr18	+	4,284,273	4,295,750	7
C15H12orf65	chr15	-	5,105,859	5,107,184	7
SLC40A1	chr7	+	335,942	350,381	7
PHF14	chr2	+	26,016,194	26,170,958	7
GBAS	chr19	+	4,818,142	4,832,175	7
BRIP1	chr19	+	7,440,974	7,487,928	7
APIP	chr5	-	20,346,948	20,370,905	7
CHAC1	chr5	+	26,595,622	26,597,739	7
MIR1754	chr9	-	25,014,275	25,014,342	7
OLA1	chr7	+	18,153,750	18,275,722	7
BMP2R2	chr7	+	12,933,358	12,979,052	7
MIR1624	chr6	-	16,899,106	16,899,180	7
YEATS4	chr1	+	37,302,348	37,305,118	7
MIR30C-2	chr3	+	85,126,853	85,126,924	7
BTC	chr4	+	35,763,316	35,768,653	7
MIR1640	chr15	+	10,242,915	10,243,005	7
FAM175A	chr4	-	47,928,155	47,934,703	7
URM1	chr17	-	5,578,669	5,597,771	7
RPS19BP1	chr1	+	52,487,150	52,489,272	7
NAMPT	chr1	-	15,209,063	15,235,365	7
SLC38A1	chr1	-	32,729,088	32,753,599	7
SLC16A8	chr1	+	52,952,426	52,960,092	7

AIFM1	chr4	+	1,565,973	1,578,338	7
MRPS6	chr1	+	109,140,293	109,152,968	7
HPRT1	chr4	+	4,031,842	4,046,316	7
ORAOV1	chr5	-	18,734,841	18,741,403	7
ACAA2	chrZ	+	864,204	877,739	7
C19H17orf85	chr19	-	5,113,307	5,128,479	7
PLDN	chr10	+	12,363,491	12,371,815	7
SLC10A7	chr4	-	32,523,115	32,675,326	7
CTSA	chr20	+	10,487,795	10,491,692	7
GCHFR	chr5	+	1,016,759	1,024,439	7
RALBP1	chr2	-	101,171,597	101,217,582	7
RABL3	chr1	+	83,089,794	83,102,751	7
KPNA3	chr1	-	173,577,370	173,612,626	7
PDHX	chr5	+	20,371,028	20,444,823	7
INSIG1	chr2	+	7,777,320	7,783,968	7
MIR1739	chr5	+	41,656,800	41,656,892	7
MIR1815	chr6	+	29,566,734	29,566,810	7
TULP1	chr26	-	57,467	61,594	7
HIBCH	chr7	+	139,173	171,757	7
ANAPC5	chr15	-	5,498,421	5,510,605	7
MIR1674	chr6	+	24,237,813	24,237,908	7
RAC3	chr18	-	4,985,369	4,990,238	7
RAP1GDS1	chr4	+	61,277,434	61,367,145	7
SIK1	chr1	-	113,342,607	113,355,363	7
FAM122A	chr4	+	4,086,051	4,101,723	7
MSANTD2	chr24	+	270,378	290,889	7
TMED8	chr5	-	41,619,662	41,625,283	7
ADH5	chr4	-	61,539,235	61,546,853	7
DCLRE1B	chr26	+	3,597,232	3,600,802	7
MGST1	chr1	+	65,427,632	65,434,126	7
PACSIN3	chr5	+	25,316,286	25,337,465	7
CREB1	chr7	-	13,252,997	13,288,892	7
IVD	chr5	+	789,732	811,092	7
SNX16	chr2	-	126,242,474	126,266,110	7
KIF18A	chr5	-	3,897,708	3,940,064	7
ADAM23	chr7	-	13,526,229	13,584,488	7
MEIS1	chr3	+	10,411,919	10,486,821	7
BRPF1	chr12	+	11,758,524	11,769,333	7
HHATL	chr2	-	1,921,544	1,933,694	7
MFN1	chr9	-	18,725,672	18,758,191	7
LOC419429	chr21	-	2,664,591	2,684,797	6

HPCAL1	chr3	+	99,600,903	99,652,757	6
COX19	chr14	-	2,240,655	2,242,633	6
MIR1794	chr10	+	1,926,428	1,926,525	6
FAM172A	chrZ	+	56,992,247	57,259,079	6
FASN	chr18	+	4,906,223	4,943,362	6
IRX4	chr2	-	88,351,998	88,361,079	6
LRRC40	chr8	-	29,786,080	29,801,935	6
NAPB	chr3	+	3,203,701	3,210,509	6
TPX2	chr20	+	9,989,995	9,999,061	6
GTPBP4	chr2	+	10,315,411	10,326,679	6
MIR458	chr13	-	8,034,158	8,034,273	6
ORAI2	chr19	+	4,103,711	4,112,993	6
TGFBR2	chr2	+	39,810,472	39,873,236	6
CD320	chr28	+	872,990	876,349	6
BRIX1	chrZ	+	9,918,985	9,922,559	6
RANBP1	chr15	+	1,318,631	1,326,000	6
CHAF1A	chr28	+	2,033,047	2,047,545	6
DKC1	chr4	+	2,098,487	2,107,184	6
EIF2D	chr26	-	2,315,294	2,325,130	6
HN1L	chr14	-	14,432,683	14,437,756	6
MIR1715	chr14	-	15,041,201	15,041,302	6
ACADSB	chr6	+	33,024,247	33,043,374	6
BMS1	chr6	-	6,144,879	6,166,037	6
TMEM184C	chr4	+	33,083,785	33,094,344	6
GTF3C3	chr7	-	10,985,163	11,005,202	6
PGD	chr21	+	3,707,882	3,718,203	6
PEX11G	chr28	+	3,608,473	3,610,620	6
MRPL51	chr1	-	80,054,953	80,056,507	6
TALDO1	chr5	-	447,025	448,078	6
ANKRD10	chr1	-	143,495,595	143,530,482	6
SKI	chr21	-	1,657,220	1,747,412	6
CXCR4	chr7	-	32,376,681	32,379,364	6
SNUPN	chr10	-	3,553,531	3,563,564	6
C4H4orf52	chr4	-	75,817,808	75,821,763	6
MCM5	chr1	-	54,126,110	54,134,367	6
MIR1785	chr11	-	20,641,236	20,641,337	6
TAGLN	chr24	+	5,347,431	5,350,373	6
FTSJ3	chr27	-	1,600,050	1,607,179	6
LOC396380	chr3	+	91,174,655	91,180,826	6
NAE1	chr11	+	12,187,425	12,199,965	6
NDUFAF2	chrZ	+	18,338,353	18,386,917	6

PCBD2	chr13	-	16,050,712	16,071,727	6
MAP2K2	chr28	+	2,108,066	2,117,006	6
TNFAIP8L1	chr28	-	4,498,846	4,505,740	6
SLC37A3	chr1	-	58,816,380	58,837,119	6
POLR3A	chr6	+	14,217,316	14,248,771	6
DNAJC12	chr6	+	7,734,940	7,743,969	6
MIR34B	chr24	+	5,684,900	5,684,983	6
DZANK1	chr3	+	16,308,937	16,329,064	6
TWF2	chr12	-	2,770,687	2,783,687	6
LOC770433	chr2	-	64,183,131	64,283,522	6
IL1R1	chr1	+	138,002,937	138,026,152	6
ZSWIM7	chr19	-	6,390,842	6,400,724	6
PDZD11	chr4	-	1,247,334	1,250,584	6
MIR19A	chr1	-	152,248,492	152,248,572	6
C20H20orf24	chr20	+	453,329	457,685	6
PEX2	chr2	-	124,294,436	124,318,200	6
SYF2	chr23	-	2,701,068	2,703,624	6
PPP1R8	chr23	+	1,387,807	1,405,845	6
AGA	chr4	+	43,642,111	43,654,042	6
GPI	chr11	+	11,776,935	11,798,311	6
SGK3	chr2	+	119,560,164	119,617,334	6
CKAP2	chr1	-	174,680,950	174,690,386	6
FN3KRP	chr18	-	3,326,206	3,332,532	6
ZC3HC1	chr1	-	767,671	776,655	6
MIR138-2	chr11	-	2,023,954	2,024,036	6
COG5	chr1	-	15,547,472	15,731,429	6
LRRC59	chr18	+	10,336,996	10,341,290	6
NUPL2	chr2	+	31,009,734	31,016,473	6
FAM118B	chr24	-	417,302	425,384	6
PWP1	chr1	-	55,381,603	55,395,966	6
SQLE	chr2	+	144,320,583	144,334,934	6
RAB27A	chr10	+	9,114,418	9,148,498	6
MIR1459	chrZ	+	64,993,986	64,994,070	6
BTBD10	chr5	+	8,487,714	8,501,280	6
BZW2	chr2	+	28,486,318	28,538,316	6
NEK6	chr17	+	10,044,636	10,090,953	6
SMYD5	chr4	-	93,262,798	93,270,905	6
TMOD3	chr10	-	10,297,871	10,324,021	6
ECD	chr6	-	6,266,209	6,274,526	6
SNRNP40	chr23	-	539,930	550,685	6
ANXA1	chrZ	+	35,731,215	35,745,297	6

WDR3	chr1	-	82,297,150	82,322,476	6
CBFA2T3	chr11	-	20,494,668	20,516,485	6
UQCC	chr20	+	1,246,846	1,299,512	6
ABI1	chr2	+	15,921,868	16,005,231	6
ACSL5	chr6	+	28,167,020	28,184,196	6
HDAC7_dup1	chrE22C19W28_E50C23	+	360,495	400,216	6
NEK7	chr8	-	2,182,279	2,239,873	6
QSER1	chr5	+	5,690,409	5,710,969	6
FHOD1	chr11	+	1,319,217	1,334,287	6
ACO1	chrZ	+	69,043,752	69,081,426	6
WIPF1	chr7	+	17,997,859	18,048,854	6
SH3BP5	chr2	+	41,451,064	41,492,500	5
DCT	chr1	+	150,688,697	150,710,210	5
TXNRD3	chr12	+	10,676,015	10,695,740	5
TNFRSF1B	chr21	-	5,630,366	5,645,565	5
FKBP3	chr5	+	61,386,077	61,389,492	5
STX18	chr4	-	81,562,234	81,617,264	5
ATP1B1	chr1	-	87,105,202	87,119,232	5
IPO13	chr8	+	21,051,279	21,075,499	5
LOC395772	chrE22C19W28_E50C23	-	689,595	703,948	5
MTFR1	chr2	+	119,107,207	119,147,289	5
ATP1B3	chr9	+	11,387,002	11,409,578	5
CRYBB3	chr15	+	7,210,748	7,212,427	5
RNH1	chr5	+	17,266,724	17,274,919	5
PIK3AP1	chr6	-	17,803,696	17,845,376	5
DNAJC27	chr3	+	108,219,632	108,225,863	5
NFKBIZ	chr1	+	88,744,250	88,760,603	5
MIR1564	chr14	-	12,896,507	12,896,577	5
MIR1758	chr24	-	25,236	25,306	5
FAM20B	chr8	-	6,555,540	6,577,582	5
C15H12orf49	chr15	+	11,746,650	11,752,193	5
C8H1orf27	chr8	-	10,161,674	10,182,843	5
BLM	chr10	-	22,082,199	22,098,242	5
TK2	chr11	+	12,324,437	12,338,930	5
DERA	chr1	+	65,258,314	65,312,770	5
CENPQ	chr3	-	111,606,643	111,612,127	5
PYGL	chr5	-	60,544,252	60,554,702	5
CAB39L	chr1	-	173,442,770	173,503,468	5
XKR8	chr23	+	1,430,459	1,432,622	5
GLT8D1	chr12	-	743,037	748,312	5
MCFD2	chr3	-	28,134,438	28,138,463	5

RHOB	chr3	+	104,599,205	104,601,532	5
RASD1	chr14	-	4,804,542	4,806,388	5
DNA2	chr6	-	11,706,921	11,721,474	5
AP3S2	chr10	-	22,181,275	22,185,642	5
RHOF	chr15	-	5,666,312	5,674,128	5
OIP5	chr5	-	26,722,857	26,725,770	5
PDGFB	chr1	+	52,640,169	52,651,753	5
LOC427001	chr14	+	15,641,475	15,655,617	5
RXRG	chr8	+	5,341,403	5,358,242	5
PRLHR	chr6	-	31,242,680	31,243,785	5
PRKAG3	chr7	-	23,974,428	23,978,557	5
TES	chr1	-	26,969,630	26,994,486	5
MIR1634	chr11	+	12,200,275	12,200,370	5
PARP1	chr3	+	18,133,803	18,163,615	5
TPI1	chr1	+	80,431,223	80,434,223	5
RABEPK	chr17	+	10,311,435	10,313,008	5
CDHR1	chr6	-	4,050,310	4,083,792	5
FDFT1	chr3	+	110,161,011	110,172,705	5
STX6	chr8	+	6,119,192	6,133,187	5
SEC31A	chr4	+	47,785,537	47,818,566	5
LIG4	chr1	+	144,394,049	144,397,685	5
METTL2A	chr27	+	2,238,733	2,251,624	5
MYD88	chr2	+	4,730,082	4,742,683	5
SLC35A3	chr8	-	12,651,536	12,669,918	5
DPYSL2	chr22	-	464,443	505,520	5
TWSG1	chr2	-	101,221,763	101,242,615	5
NUMB	chr5	+	28,378,441	28,472,458	5
CCR7	chr27	-	4,121,045	4,129,775	5
CKM	chr5	+	53,555,290	53,555,574	5
SPECC1L	chr15	-	8,772,287	8,828,286	5
PBX3	chr17	+	10,451,482	10,547,885	5
SMC5	chrZ	+	34,629,093	34,685,406	5
C9H21orf2	chr9	-	5,418,475	5,424,475	5
SNAPC5	chr10	-	20,664,686	20,667,113	5
TERF1	chr2	+	122,411,877	122,434,645	5
LSS	chr7	-	6,878,402	6,888,484	5
EXOSC2	chr17	+	6,556,737	6,563,309	5
PTRH2	chr19	-	7,263,328	7,264,488	5
P20K	chr17	-	881,082	883,995	5
ALDH4A1	chr21	-	4,535,470	4,543,531	5
ACP1	chr3	+	94,770,314	94,791,112	5

USP1	chr8	+	28,268,821	28,277,869	5
TMEM123	chr1	+	186,896,582	186,913,664	5
BTN1A1	chr28	-	788,958	794,489	5
ERNI	chr5	-	56,151,623	56,155,476	5
NFKB2	chr6	+	18,022,427	18,025,184	5
DIEXF	chr3	-	23,989,827	24,004,793	5
PLEKHB2	chr9	-	3,184,527	3,198,749	5
TMEM18	chr3	-	94,980,667	94,985,354	5
TRMT11	chr3	-	62,136,036	62,165,338	5
HIBADH	chr2	-	32,780,837	32,863,086	5
RGS19	chr20	+	9,332,180	9,345,346	5
CSRP2	chr1	-	40,109,491	40,117,264	5
MYH10	chr18	-	1,687,410	1,767,912	5
FAM108C1	chr10	-	14,049,731	14,080,413	5
MYB	chr3	-	57,630,244	57,651,656	5
GTF3C5	chr17	+	7,440,436	7,447,358	5
MRPS30	chrZ	+	13,609,765	13,870,783	5
LASP1	chr27	+	3,965,132	3,979,222	5
AMH	chr28	-	1,592,776	1,598,113	5
ADPRH	chr1	-	95,594,733	95,599,726	5
IRAK2	chr12	+	20,078,601	20,092,031	5
SREBF1	chr14	-	4,933,060	4,934,925	5
PRKCI	chr9	-	21,354,557	21,377,507	5
PLEKHO1	chr25	-	70,297	86,511	5
PLCXD1	chr1	-	134,185,341	134,203,509	5
SLC7A1	chr1	+	179,733,883	179,752,465	5
MAD2L2	chr21	+	5,847,481	5,851,517	5
GTF2A1L	chr3	-	7,540,671	7,552,022	5
ZDHHC18	chr23	+	1,744,621	1,751,702	5
KRAS	chr1	-	69,357,722	69,378,607	5
C28H19orf10	chr28	+	4,492,164	4,497,047	5
MAPK6	chr10	-	10,179,566	10,212,658	5
TUBB2B	chr2	+	67,483,545	67,486,745	5
MRE11A	chr1	+	189,912,122	189,930,816	5
FET1	chr4	-	64,948,286	64,951,559	5
CHAF1B	chr1	+	110,117,275	110,134,825	5
KCNIP2	chr6	+	24,098,682	24,101,560	5
PAPD7	chr2	-	81,993,472	82,032,084	4
ZNF767	chr2	+	414,957	429,876	4
APEH	chr12	-	2,315,966	2,319,577	4
CRTAP	chr2	+	44,501,250	44,522,633	4

PDCD2	chr3	+	42,588,095	42,591,707	4
BAK1	chr26	+	4,498,992	4,730,550	4
PRPS2	chr1	-	126,836,914	126,861,017	4
XRCC3	chr5	-	52,988,342	52,997,049	4
TWIST1	chr2	-	29,581,433	29,583,668	4
ABCD2	chr1	+	16,351,567	16,403,175	4
MIR1734	chr3	+	48,111,389	48,111,472	4
CCL20	chr9	+	10,616,596	10,618,706	4
BRI3BP	chr15	+	4,517,994	4,520,819	4
HYDIN	chr11	+	1,519,238	1,625,770	4
LOC770922	chr13	-	13,661,037	13,666,425	4
HK1	chr6	+	11,979,962	12,004,711	4
PKIA	chr2	+	125,040,194	125,045,100	4
FAR1	chr5	-	8,387,722	8,429,007	4
CDC20	chr8	+	20,380,552	20,385,951	4
GORASP1	chr2	+	5,190,729	5,197,455	4
HMGB2	chr4	-	44,739,576	44,741,233	4
ETFDH	chr4	+	23,003,717	23,021,116	4
RIOK2	chrZ	+	50,427,860	50,439,885	4
BCL11A	chr3	-	1,826,670	1,883,382	4
BMA1	chr16	-	59,095	61,304	4
PPDPF	chr20	-	9,012,685	9,014,992	4
PLCB4	chr3	-	14,858,397	14,949,892	4
LMAN1	chrZ	-	819,542	839,127	4
ACLY	chr27	-	4,344,211	4,368,712	4
EXT2	chr5	+	23,700,234	23,795,920	4
SCD	chr6	-	18,573,466	18,589,084	4
CRMP1	chr4	-	82,175,812	82,218,120	4
CSRP2BP	chr3	-	16,332,317	16,350,828	4
NCOA1	chr3	-	108,258,014	108,365,176	4
FANCC	chrZ	-	41,169,261	41,261,459	4
COX10	chr18	-	2,562,675	2,659,453	4
SBF2	chr5	+	9,948,204	10,182,404	4
MIR1628	chr4	+	1,891,993	1,892,089	4
EED	chr1	+	195,039,453	195,055,430	4
SURF2	chr17	+	7,539,272	7,542,301	4
NHP2	chr13	+	10,182,910	10,184,725	4
HAT1	chr7	-	19,315,513	19,333,876	4
NSUN2	chr2	+	82,065,202	82,082,133	4
UBAC1	chr17	+	8,848,588	8,864,762	4
MIR301B	chr19	-	7,144,739	7,144,828	4

C12H3orf37	chr12	+	9,370,027	9,373,777	4
ENS-1	chr5	-	56,151,616	56,156,062	4
PDDC1	chr5	+	425,889	436,226	4
ACACA	chr19	-	8,405,762	8,504,836	4
GPX3	chr13	-	13,133,782	13,135,761	4
VAC14	chr11	+	1,626,448	1,679,788	4
WDR18	chr28	+	2,357,720	2,361,649	4
SYNGR1	chr1	-	52,587,042	52,598,000	4
PCDHGC3	chr13	+	1,624,022	1,633,968	4
MMD	chr18	-	5,950,023	5,963,316	4
CTTN	chr5	+	19,134,498	19,168,723	4
ATP1A1	chr1	-	83,570,075	83,592,637	4
RNASSET2	chr3	+	44,377,351	44,398,551	4
PPM1M	chr12	+	2,790,935	2,798,124	4
AGPAT9	chr4	+	47,976,455	47,987,052	4
GDF3	chr28	+	2,847,298	2,849,389	4
MBOAT1	chr2	+	60,674,402	60,718,687	4
NIPA2	chr1	-	134,558,392	134,562,340	4
FASLG	chr8	-	4,518,173	4,521,188	4
AACS	chr15	-	4,476,203	4,515,355	4
DHODH	chr11	-	21,690,487	21,693,968	4
MIR204-2	chr10	+	6,651,274	6,651,374	4
ITGB2	chr7	-	7,142,970	7,154,552	4
VEGFA	chr3	-	31,888,801	31,910,241	4
IL9	chr13	-	15,573,175	15,575,874	4
SNAP91	chr3	+	80,365,703	80,436,691	4
CACNB4	chr7	-	36,952,806	36,977,983	4
TMEM39B	chr23	+	5,358,827	5,364,856	4
CASP8	chr7	+	12,508,765	12,514,867	4
TRIM27.2	chr16	-	131,861	134,916	4
HMGA2	chr1	+	36,072,025	36,177,364	4
HIPK3	chr5	+	5,856,077	5,948,515	4
MIR155	chr1	+	105,930,213	105,930,275	4
GPATCH2	chr3	+	20,869,306	20,973,825	4
GJA3	chr1	+	183,285,774	183,287,309	4
FANCG	chrZ	-	7,956,394	7,961,598	4
SDK1	chr14	+	3,540,926	3,896,082	4
ODF2	chr17	+	5,736,216	5,755,270	4
CCDC93	chr7	+	30,475,755	30,508,074	4
FUT11	chr6	-	17,020,568	17,026,867	4
PARN	chr14	-	788,981	823,635	4

PPIF	chr6	-	13,304,080	13,312,011	4
MPP1	chr4	-	2,107,568	2,122,122	4
GK5	chr9	-	11,477,070	11,498,192	4
MIR375	chr7	+	23,901,124	23,901,188	4
ACAT2	chr3	-	47,467,515	47,475,456	4
OR51M1	chr1	+	199,454,179	199,455,138	4
USP28	chr24	-	4,456,825	4,479,109	4
DAPP1	chr4	+	61,725,599	61,752,727	4
LY86	chr2	-	66,078,677	66,102,261	4
MND1	chr4	+	20,955,848	20,995,059	4
SOCS3	chr18	+	9,788,132	9,790,163	4
QSOX1	chr8	-	6,288,365	6,293,472	4
NFKB1	chr4	+	62,616,899	62,673,940	4
LFNG	chr14	+	3,240,614	3,245,342	4
MAP3K14	chr27	-	1,353,335	1,366,543	4
DGKZ	chr5	-	25,805,247	25,844,008	4
RBM45	chr7	-	16,630,757	16,641,825	4
TBCK	chr4	+	39,818,858	39,911,554	4
KPNA2	chr18	-	6,990,201	6,995,846	4
DDX10	chr1	-	184,304,061	184,468,319	4
SLC9A1	chr23	-	1,821,934	1,828,213	4
RPA2	chr23	-	1,420,616	1,424,414	4
TMEM208	chr11	+	1,005,631	1,011,435	4
FUBP3	chr17	+	6,500,207	6,542,963	4
PFKP	chr2	+	11,326,475	11,368,025	4
CLU	chr3	+	107,997,679	108,001,887	4
MIR1464	chr15	+	11,747,272	11,747,381	4
SMAD3	chr10	+	20,954,584	21,015,136	4
RAMP3	chr2	+	55,590,677	55,641,843	4
THPO	chr9	+	17,033,203	17,034,207	4
AHSA2	chr3	+	2,166,476	2,174,715	4
PLA2G4A	chr8	-	9,953,816	10,016,608	4
MIR146B	chr6	+	24,570,060	24,570,164	4
CLSTN1	chr21	-	3,481,011	3,515,674	4
DTYMK	chr9	+	5,821,691	5,827,103	4
EREG	chr4	+	46,163,379	46,171,251	4
DUT	chr10	+	11,638,192	11,650,228	4
PLEKHF2	chr2	+	131,210,451	131,226,678	4
CCNE2	chr2	-	131,136,116	131,146,334	4
MXRA8	chr21	+	2,233,556	2,248,314	4
ZDHHC21	chrZ	-	31,352,289	31,397,437	4

ESF1	chr3	-	4,442,630	4,453,487	4
UCP3	chr1	-	200,544,391	200,547,326	4
TIPIN	chr10	-	20,621,245	20,628,648	4
ARHGEF6	chr4	-	4,386,282	4,415,638	4
ST6GALNAC4	chr17	+	5,506,250	5,507,408	3
C10H15orf44	chr10	-	20,209,856	20,219,711	3
ARNTL	chr5	-	8,502,153	8,522,873	3
TRIM7	chr16	+	149,561	159,548	3
GHRL	chr12	-	20,094,804	20,097,504	3
CRY1	chr1	-	55,632,379	55,667,623	3
SWAP70	chr5	-	10,238,478	10,266,274	3
GSTK1	chr1	-	80,901,822	80,911,455	3
MPDZ	chrZ	-	30,735,443	30,824,383	3
ST6GAL1	chr9	+	6,298,123	6,329,524	3
CTNNB1	chr2	+	43,458,954	43,480,408	3
MIR1701	chr4	-	82,234,261	82,234,337	3
ADAM33	chr4	-	93,121,724	93,145,342	3
MIR1463	chr5	-	11,171,642	11,171,751	3
MIR1465	chr17	+	8,862,951	8,863,060	3
MIR211	chr28	+	1,784,394	1,784,467	3
ARPC1B	chr14	+	4,377,765	4,382,357	3
TMEM129	chr4	+	86,928,868	86,936,813	3
ACAD11	chr2	-	42,309,933	42,338,078	3
RASSF2	chr22	+	421,091	433,359	3
GNRH1	chr22	+	836,307	839,634	3
FANCB	chr1	+	125,770,228	125,784,524	3
TLR7	chr1	-	126,823,955	126,830,698	3
HSF2	chr3	-	63,957,842	63,986,035	3
ID2	chr3	+	98,724,872	98,726,620	3
LACTB	chr10	-	5,091,732	5,099,040	3
UGP2	chr3	+	9,465,775	9,488,932	3
LDHB	chr1	+	69,204,377	69,214,070	3
CCDC111	chr4	-	40,884,900	40,900,904	3
NEURL	chr6	+	25,159,822	25,236,369	3
RCSD1	chr1	-	94,857,039	94,868,398	3
NUPL1	chr1	-	181,349,014	181,386,220	3
AKT1	chr5	-	54,122,987	54,193,913	3
INTS7	chr3	+	23,195,862	23,216,263	3
PNO1	chr3	+	11,182,639	11,186,187	3
CDH20	chr2	-	69,809,205	69,921,434	3
ZFP64	chr20	+	13,035,003	13,045,929	3

C3H2orf94	chr3	-	14,440,421	14,515,532	3
PTPLB	chr7	-	28,739,236	28,758,916	3
OPN1LW	chr19	+	6,999,227	7,002,022	3
GATA5	chr20	-	8,002,370	8,012,087	3
MCCC1	chr9	+	17,489,040	17,504,955	3
MIR1795	chr21	+	2,359,869	2,359,946	3
STARD4	chrZ	+	45,677,856	45,686,318	3
VIL1	chr7	-	24,088,185	24,094,194	3
CD151	chr5	-	16,730,519	16,772,760	3
LGALS1	chr1	-	53,130,081	53,133,213	3
T	chr3	+	44,800,690	44,808,591	3
GNAL	chr2	-	99,708,734	99,837,282	3
RDH10	chr2	+	122,524,322	122,549,063	3
HCLS1	chr1	+	69,104	83,498	3
CD40	chr20	+	10,567,354	10,571,036	3
PHC1	chr1	+	79,288,028	79,307,973	3
CETP	chr11	+	611,151	616,778	3
KIAA1524	chr1	-	90,843,678	90,879,004	3
COX15	chr6	+	23,522,630	23,526,598	3
C7H2orf69	chr7	+	12,069,633	12,074,668	3
FAM206A	chr2	-	90,872,181	90,874,278	3
RPS6KA1	chr23	-	89,601	120,259	3
BTD	chr2	+	33,969,521	33,980,190	3
BCS1L	chr7	-	24,020,667	24,025,961	3
RRP12	chr6	+	23,776,016	23,784,357	3
METTL16	chr1	+	82,691,395	82,705,808	3
SIGIRR	chr5	+	1,574,070	1,578,869	3
HIST1H2BO	chr1	+	49,963,488	49,963,868	3
WDR36	chrZ	-	45,899,205	45,932,568	3
STK11IP	chr7	+	23,619,802	23,636,113	3
ATM	chr1	-	184,572,899	184,633,830	3
CZH9orf100	chrZ	+	8,622,960	8,637,358	3
QDPR	chr4	+	78,889,056	78,889,863	3
CENPH	chrZ	+	21,329,358	21,335,530	3
TEC	chr4	+	68,388,642	68,430,421	3
HAO1	chr3	+	15,560,506	15,588,058	3
TMOD1	chrZ	-	68,867,406	68,883,882	3
DCK	chr4	+	51,630,307	51,641,697	3
CCNB2	chr10	-	7,788,365	7,795,441	3
MIR126	chr17	-	8,431,742	8,431,825	3
FYN	chr3	+	68,609,250	68,646,283	3

SLC22A5	chr13	+	17,398,703	17,422,331	3
MICAL1	chr26	+	19,282	27,136	3
POPDC2	chr1	+	83,483,259	83,493,025	3
PLOD1	chr21	-	5,699,791	5,716,917	3
AP1S2	chr1	+	125,276,203	125,310,091	3
SLC35E3	chr1	+	37,147,150	37,152,691	3
NT5C2	chr6	-	24,939,429	24,995,767	3
FAM129A	chr8	-	8,277,780	8,336,769	3
MIR1644	chr14	+	8,284,308	8,284,393	3
MIR1648	chr20	+	13,872,249	13,872,334	3
STK24	chr1	+	149,053,929	149,110,086	3
LOC425215	chrZ	-	62,769,972	62,774,012	3
FGL2	chr1	+	13,742,634	13,748,631	3
SEPSECS	chr4	+	76,012,821	76,036,621	3
COL9A3	chr20	+	8,327,716	8,359,507	3
MYO1G	chr2	+	3,954,615	3,964,435	3
S100A11	chr25	+	1,300,645	1,302,364	3
HIP1R	chr15	-	5,296,593	5,306,747	3
NKX2-6	chr22	+	1,146,844	1,147,743	3
MIR1788	chr7	+	23,909,930	23,910,017	3
CD3D	chr24	-	5,602,408	5,604,885	3
HAUS6	chrZ	-	33,363,340	33,382,892	3
DLX1	chr7	-	19,237,519	19,245,061	3
SHISA2	chr1	-	181,339,929	181,343,736	3
CSF3R	chr23	+	4,327,802	4,332,968	3
PDK4	chr2	-	23,865,491	23,874,871	3
MIR1617	chr5	+	30,615,451	30,615,539	3
MIR1744	chr10	+	11,373,903	11,373,991	3
MIR2131	chrZ	-	68,816,728	68,816,816	3
SEPHS1	chr1	-	7,026,657	7,051,787	3
GNPDA1	chr13	-	17,758,122	17,763,082	3
ANXA6	chr13	+	13,107,547	13,119,259	3
ZNF250	chr18	+	28,823	33,468	3
SRC	chr20	+	5,036,233	5,044,178	3
NRP2	chr7	-	13,735,459	13,807,916	3
MTSS1	chr2	-	144,128,117	144,247,668	3
TMEM194B	chr7	+	86,041	99,717	3
COQ5	chr15	+	9,543,635	9,549,352	3
DCXR	chr18	+	4,980,897	4,984,413	3
SUV39H2	chr1	+	7,865,913	7,875,672	3
CRIM1	chr3	-	33,530,905	33,693,731	3

MSRB3	chr1	+	35,852,484	35,932,633	3
SASH3	chr4	-	1,622,391	1,626,549	3
RNASEL	chr8	+	5,893,272	5,901,070	3
FAM46C	chr1	-	82,383,496	82,388,056	3
SPI1	chr5	+	25,094,320	25,115,278	3
THADA	chr3	-	26,173,900	26,326,300	3
TICAM1	chr28	+	4,419,724	4,422,751	3
MIR1615	chr14	+	6,745,553	6,745,645	3
LOC421975	chr3	-	107,038,798	107,046,427	3
LOC396318	chr4	-	17,749,666	17,776,315	3
TRAP1	chr14	-	13,176,989	13,195,178	3
MIR199-1	chr17	+	5,667,150	5,667,243	3
RBBP7	chr1	+	124,845,757	124,853,982	3
PEBP1	chr15	-	10,160,874	10,162,373	3
GTDC1	chr7	-	34,737,548	34,901,715	3
LTA4H	chr1	-	47,605,162	47,619,805	3
MIR7-3	chr28	-	4,436,025	4,436,119	3
AUH	chrZ	-	43,474,404	43,588,754	3
POGLUT1	chr1	-	95,647,990	95,665,653	3
GTSE1	chr1	+	16,895,124	16,905,537	3
GLT1D1	chr15	-	3,741,935	3,784,737	3
SURF4	chr17	-	7,542,580	7,559,677	3
TSPAN12	chr1	+	25,256,683	25,302,249	3
BBS5	chr7	-	20,134,395	20,145,260	3
HCCS	chr8	-	14,021,789	14,029,846	3
PIGH	chr5	-	31,154,390	31,159,637	3
KIAA1328	chrZ	-	6,461,916	6,623,963	3
KDSR	chr2	+	69,033,784	69,051,547	3
MRPL3	chr2	-	41,883,889	41,912,183	3
CCND1	chr5	+	18,709,552	18,721,847	3
YES1	chr2	+	105,030,221	105,079,363	3
LOC770371	chr18	-	4,782,310	4,793,363	3
MIR1586	chr4	-	1,226,474	1,226,570	3
NACC2	chr17	+	8,780,039	8,833,001	3
ALG11	chr1	+	174,637,993	174,641,833	3
MIR1550	chr12	+	13,130,851	13,130,948	2
HOPX	chr4	-	50,745,585	50,748,881	2
RBFA	chr2	-	57,227,612	57,242,704	2
DCLRE1C	chr1	-	7,875,942	7,886,518	2
NR1D2	chr2	+	37,194,558	37,218,099	2
RIMBP2	chr15	+	3,253,013	3,356,590	2

C4	chr16	-	29,325	39,848	2
C4H8orf40	chr4	+	35,304,390	35,306,722	2
CTSS	chr25	-	1,787,277	1,789,851	2
ANXA2	chr10	+	6,040,844	6,063,439	2
MRPL15	chr2	+	113,879,083	113,889,583	2
PDP1	chr2	+	130,665,950	130,673,077	2
DEAF1	chr5	+	502,521	523,902	2
EZR	chr3	-	54,025,356	54,064,610	2
PRKDC	chr2	-	111,118,345	111,233,804	2
SETD4	chr1	-	110,017,664	110,027,973	2
LPGAT1	chr3	+	23,235,088	23,291,141	2
LMNB2	chr28	-	621,786	648,172	2
MYBPH	chr26	-	993,815	1,003,847	2
RAD18	chr12	-	19,938,710	19,974,905	2
SLC6A9	chr8	-	21,095,032	21,100,978	2
APOD	chr9	+	13,772,027	13,774,955	2
DCLRE1A	chr6	-	29,013,573	29,027,601	2
PXN	chr15	+	9,657,831	9,698,034	2
DTWD2	chrZ	+	69,842,757	69,921,079	2
IL6ST	chrZ	-	16,366,576	16,391,591	2
LSP1	chr5	-	15,156,515	15,194,898	2
GNAI3	chr11	+	2,186,811	2,187,048	2
ARL5B	chr2	-	19,006,274	19,022,328	2
GALR3	chr1	-	53,062,872	53,064,706	2
CEL	chr17	+	7,428,217	7,438,519	2
ATP6V1H	chr2	-	113,738,174	113,783,083	2
DHCR7	chr5	+	1,698,078	1,704,646	2
TECTA	chr24	-	3,565,142	3,588,338	2
FAM65B	chr2	+	92,497,452	92,532,478	2
CDK2AP1	chr15	+	5,087,628	5,104,705	2
SLC11A1	chr7	-	24,097,183	24,102,479	2
CD3E	chr24	+	5,595,448	5,600,351	2
TREML2	chr26	-	4,578,267	4,580,646	2
PCDHGA2	chr13	+	1,586,628	1,633,946	2
CRYL1	chr1	+	183,160,410	183,211,647	2
TREM-B2V2	chr26	-	4,578,267	4,580,647	2
NCAPD2	chr1	+	80,056,621	80,080,557	2
BPNT1	chr3	+	19,933,925	19,944,743	2
CHID1	chr5	+	16,197,970	16,302,326	2
THRB_dup2	chr2	-	37,252,739	37,300,833	2
LRPAP1	chr4	+	84,861,416	84,870,479	2

OXCT1	chrZ	-	12,594,282	12,682,178	2
LTF	chr9	-	5,631,644	5,643,602	2
GPHN	chr5	-	31,351,870	31,537,335	2
DNAL4	chr1	+	52,722,932	52,727,176	2
DIO3	chr5	+	51,792,772	51,794,156	2
TNNI2	chr5	-	15,196,413	15,199,144	2
SCLY	chr9	-	1,872,487	1,878,094	2
SFRP1	chr22	-	2,610,998	2,623,172	2
H2AFY	chr13	+	15,791,504	15,839,163	2
STMN1	chr23	+	3,540,034	3,543,336	2
SGOL1	chr2	-	35,856,966	35,862,273	2
HSPE1	chr7	+	11,228,223	11,236,177	2
HHEX	chr6	-	21,872,189	21,876,787	2
PDCD2L	chr11	-	11,979,955	11,988,140	2
APITD1	chr21	+	3,719,287	3,723,404	2
ORC1	chr8	-	25,124,175	25,139,401	2
MIR1458	chr9	+	11,743,528	11,743,637	2
B-NK	chr16	+	76,419	76,786	2
TNFAIP8	chrZ	-	69,691,802	69,695,252	2
LGI1	chr6	-	21,390,603	21,404,830	2
STAR	chr22	-	2,304,611	2,307,538	2
GUSB	chr19	-	4,887,302	4,898,518	2
APOA1	chr24	-	5,236,963	5,238,063	2
TNNC1	chr12	-	540,262	545,700	2
PRPSAP2	chr14	+	5,137,448	5,152,076	2
ZNF365	chr6	-	9,294,684	9,310,423	2
KIF4A	chr4	+	1,250,810	1,267,876	2
ATRIP	chr12	-	3,496,909	3,508,510	2
TNFRSF8	chr21	-	5,648,619	5,661,727	2
OGDHL	chr6	+	3,866,748	3,916,959	2
CD300A	chr18	-	10,372,516	10,376,182	2
RHOC	chr26	-	3,377,656	3,382,628	2
KCNAB1	chr9	-	24,453,477	24,482,116	2
KCNN2	chrZ	-	71,360,075	71,432,785	2
BRCA2	chr1	-	178,837,300	178,874,033	2
DPH1	chr19	+	5,474,195	5,486,992	2
MPZL3	chr24	-	5,581,005	5,586,833	2
CCR2	chr2	-	42,699,264	42,700,328	2
EPM2A	chr3	-	48,362,871	48,403,456	2
GNG2	chr5	+	60,664,179	60,667,675	2
ADCK1	chr5	+	41,801,154	41,878,712	2

MMP2	chr11	-	3,680,956	3,716,302	2
GFOD2	chr11	+	579,758	585,261	2
MCM3	chr3	+	110,345,698	110,355,156	2
COLEC12	chr2	+	105,165,420	105,260,653	2
MCM2	chr12	-	9,995,142	10,006,470	2
GNB1L	chr15	-	949,693	985,648	2
RAPSN	chr5	+	25,007,430	25,016,826	2
THY1	chr24	+	4,207,541	4,210,159	2
GOT1	chr6	+	23,563,160	23,566,302	2
WDFY2	chr1	+	174,429,981	174,496,675	2
P2RX1	chr19	+	3,271,135	3,278,486	2
ACYP2	chr3	-	2,805,097	2,851,521	2
CTPS2	chr1	+	124,901,293	124,958,096	2
METTL15	chr5	+	3,942,075	4,049,153	2
CGNRH-R	chr10	+	19,960,362	19,963,079	2
MINA	chr1	-	94,563,143	94,577,439	2
STX7	chr3	+	58,817,177	58,860,821	2
NET1	chr1	-	1,011,481	1,022,893	2
H2B-VII_dup1	chr1	-	49,947,771	49,948,151	2
ZFYVE19	chr5	+	26,379,210	26,388,054	2
DBI	chr7	-	29,977,990	29,981,332	2
PALM	chr28	+	2,247,577	2,258,792	2
C5H15orf23	chr5	+	782,013	789,548	2
MITF	chr12	+	16,011,883	16,049,372	2
ATPBD4	chr5	+	34,320,247	34,501,388	2
SPTBN1	chr3	-	2,616,864	2,708,942	2
B-MA2	chr16	-	53,461	56,396	2
POLE2	chr5	-	60,179,765	60,198,936	2
DOLPP1	chr17	+	6,033,307	6,046,089	2
EFHD1	chr9	+	1,898,762	1,913,293	2
TFAM	chr6	-	6,292,549	6,297,550	2
CD44	chr5	+	20,527,998	20,591,037	2
C3H20orf3	chr3	-	16,742,098	16,755,103	2
FOLR1	chr1	-	199,402,555	199,405,661	2
PTPN6	chr1	+	80,498,126	80,507,551	2
SGCB	chr4	+	68,043,979	68,048,929	2
TNFRSF1A	chr1	+	82,676,769	82,689,708	2
KIAA1841	chr3	+	2,086,134	2,109,350	2
HEP21	chr16	+	147,024	148,531	2
CALB2	chr11	-	1,461,760	1,463,637	2
ASB3	chr3	+	2,965,073	2,991,072	2

IFNB	chrZ	+	6,888,979	6,889,590	2
SLC41A2	chr1	+	56,371,513	56,420,570	2
DENND2C	chr26	-	3,701,378	3,715,857	2
ARHGAP15	chr7	+	34,330,973	34,650,293	2
UCKL1	chr20	+	9,443,260	9,467,691	2
TNIP1	chr24	-	897,099	936,958	2
BMF	chr5	+	31,700,785	31,715,509	2
ACCN2	chrE22C19W28_E50C23	-	283,041	300,911	2
SALL1	chr11	+	6,198,098	6,213,605	2
DYX1C1	chr10	+	9,068,382	9,078,711	2
MIR30A	chr3	+	85,102,239	85,102,310	2
PTGR1	chrZ	+	65,036,603	65,055,863	2
RASSF5	chr26	+	2,305,309	2,315,138	2
SKIL	chr9	-	21,338,223	21,349,351	2
IGF2BP3	chr2	-	31,082,194	31,189,901	2
HJURP	chr1	-	90,952,626	90,966,985	2
POT1	chr1	+	23,426,399	23,504,940	2
ARHGAP29	chr8	+	14,293,294	14,344,514	2
BIN1	chr7	+	25,228,473	25,316,212	2
GJA4	chr23	-	4,768,999	4,771,881	2
SPRED1	chr5	-	33,059,387	33,115,278	2
HDAC4	chr7	-	6,177,293	6,396,498	2
RRAS2	chr5	-	11,300,112	11,334,838	2
HBEGF	chr13	-	1,412,890	1,419,352	2
MIR135B	chr3	+	38,893,084	38,893,150	2
MYBL2	chr20	-	3,598,030	3,613,744	2
MIR2126	chr1	-	15,746,036	15,746,181	2
DIO2	chr5	-	42,977,042	42,994,457	2
TGFBI	chr13	-	15,498,990	15,525,592	2
FGF12	chr9	+	14,525,119	14,610,608	2
PDK1	chr7	-	19,075,186	19,085,006	2
CEND1	chr5	+	401,352	413,658	2
MIR1568	chr5	-	9,074,445	9,074,512	2
GNE	chrZ	-	50,968,852	51,009,155	2
CHEK2	chr15	-	7,922,055	7,934,746	2
RTBDN	chr8	-	21,960,860	21,971,812	2
NMRAL1	chr14	-	13,438,985	13,443,917	2
OPN4-1	chr4	+	38,452,534	38,473,581	2
PEAK1	chr10	+	3,998,079	4,026,578	2
PCDH1	chr13	+	1,786,861	1,796,819	2
MIR33	chr1	-	51,372,282	51,372,350	2

GNAI1	chr1	-	12,296,098	12,333,986	2
PDS5B	chr1	-	178,669,984	178,768,220	2
ELK3	chr1	+	47,660,643	47,695,089	2
ANKRD44	chr7	-	11,050,443	11,121,169	2
C2H18orf1	chr2	-	98,929,300	98,943,413	2
IGF1R	chr10	-	18,686,958	18,845,584	2
CRK	chr8	+	12,428,026	12,428,396	2
KIF11	chr6	-	21,900,390	21,922,891	2
ST7	chr1	-	26,513,689	26,651,714	2
BSX	chr24	+	3,135,533	3,137,466	2
ORC2	chr7	-	12,380,788	12,397,183	2
MIR1747	chr2	-	62,758,708	62,758,784	2
MIR122B	chr4	-	60,285,286	60,285,362	2
LAT2	chr19	-	2,823,176	2,827,710	2
MARCKS_dup1	chr3	-	67,454,672	67,454,965	2
RTTN	chr2	+	96,000,823	96,083,131	2
RIPK2	chr2	+	129,010,266	129,029,220	2
GAL7	chr3	+	110,245,138	110,246,743	2
MST1	chr12	+	2,306,413	2,310,891	2
MTMR2	chr1	+	189,479,849	189,512,354	2
TRABD	chr1	+	21,614,774	21,653,462	2
PRNP	chr22	-	439,397	443,886	2
PTK7	chr3	+	4,315,260	4,342,247	2
NTPCR	chr3	-	40,764,733	40,777,843	2
TRPM7	chr10	+	12,459,087	12,512,285	2
ENS-3	chr2	+	72,996,486	73,002,095	2
PGP	chr14	-	6,534,841	6,537,814	2
TRAIP	chr12	-	2,379,435	2,397,156	2
LOC395991	chr12	+	11,935,385	11,938,739	2
UGDH	chr4	+	71,210,031	71,273,388	2
PAICS	chr4	-	66,600,964	66,608,317	2
MAT1A	chr6	+	5,503,525	5,520,194	2
C14H16orf59	chr14	+	14,983,217	14,989,783	2
FSTL4	chr13	+	16,695,010	16,874,067	2
ZFP161	chr2	+	103,254,148	103,256,179	2
K123	chr1	+	3,268,812	3,278,839	2
SIX1	chr5	+	56,938,944	56,965,303	2
SLC38A4	chr1	-	32,894,668	32,915,219	2
PEMT	chr14	-	4,812,245	4,850,575	2
CENPP	chr12	-	3,551,075	3,667,932	2
MIR184	chr10	+	22,146,245	22,146,318	2

MIR34C	chr24	+	5,685,637	5,685,710	2
PLK1	chr14	+	6,936,894	6,943,202	2
RUVBL1	chr12	+	9,764,314	9,782,019	2
NRK	chr4	+	17,338,667	17,434,059	2
ORC5	chr1	-	14,319,463	14,388,326	2
CYP46A1	chr5	+	50,655,757	50,671,085	2
LYVE1	chr5	+	9,847,788	9,858,393	2
C5H11orf96	chr5	+	23,627,925	23,628,909	2
SP5	chr7	-	19,714,659	19,715,756	2
TXNRD2	chr15	-	1,005,660	1,040,040	2
SLC39A13	chr5	-	25,043,450	25,062,047	2
HIF1A	chr5	-	56,522,429	56,553,597	2
LEPR	chr8	+	29,125,599	29,156,553	2
TNFRSF21	chr3	-	112,760,764	112,790,192	2
CRYZ	chr8	-	30,434,763	30,441,226	2
CBFA2T2	chr20	-	2,199,584	2,247,145	2
HSF4	chr11	+	2,444,540	2,459,224	2
MIR1565	chr28	+	2,707,379	2,707,460	2
CENPF	chr3	-	22,160,392	22,195,531	2
CANT1	chr18	+	9,721,792	9,723,269	2
LPAR6	chr1	-	173,087,768	173,089,200	2
NOTCH2	chr8	+	4,186,605	4,266,540	2
ARL6	chr1	+	94,459,233	94,464,114	2
NOX1	chr4	+	5,166,311	5,170,233	2
TWISTNB	chr2	-	29,769,961	29,773,234	2
MIR3537	chr6	+	18,024,717	18,024,793	2
MIR1612	chr9	+	6,031,748	6,031,831	2
MIR193A	chr18	+	6,423,770	6,423,846	2
FTO	chr11	-	4,674,142	4,943,138	2
LCMT1	chr14	+	6,649,617	6,669,072	2
ECHDC3	chr1	+	6,317,403	6,322,151	2
RHOQ	chr3	+	27,920,853	27,937,062	2
GPR39	chr7	+	31,310,373	31,374,650	2
MNX1	chr2	-	8,487,360	8,490,376	2
GNG10	chrZ	-	64,932,054	64,938,692	2
ANXA13	chr2	-	143,761,645	143,785,065	2
PPP1R16B	chr20	+	3,754,443	3,800,226	2
MIR1750	chr4	+	10,640,690	10,640,774	2
MIR1558	chr20	-	964,319	964,403	2
MIR1452	chrZ	+	64,990,795	64,990,872	2
FAM60A	chr1	+	61,674,910	61,691,016	2

CD200R1_dup1	chr1	+	86,739,137	86,758,372	2
ARHGAP11A	chr5	-	32,935,357	32,946,910	2
TOP2A	chr27	-	4,074,315	4,092,016	2
PREPL	chr3	-	26,686,985	26,704,143	2
ESRRG	chr3	+	21,102,220	21,466,404	2
CSTB	chr1	+	79,861,287	79,865,647	2
MYL1	chr7	-	2,758,508	2,766,334	2
MLNR	chr1	+	173,409,564	173,413,406	2
MIR216C	chr3	+	288,216	288,301	2
WNT11B	chr4	+	1,181,759	1,183,797	2
MIR1745-1_dup1	chr24	-	5,271,413	5,271,499	2
MIR1745-2_dup1	chr24	-	5,271,413	5,271,499	2
FH	chr2	-	87,950,231	87,965,401	2
CDK6	chr2	-	22,666,125	22,784,572	2
ITGA1	chrZ	+	15,099,448	15,161,382	2
FBF1	chr18	+	4,595,460	4,609,236	2
NUSAP1	chr5	+	26,726,089	26,740,000	2
MIR1761	chr8	-	17,523,212	17,523,292	2
MIR1748	chr18	+	734,584	734,664	2
CBFB	chr11	+	2,331,063	2,368,850	2
NUF2	chr8	-	5,723,318	5,739,034	2
DNASE2B	chr8	-	17,320,339	17,329,536	2
INHA	chr7	-	23,643,750	23,645,964	2
PGM1	chr8	+	28,644,938	28,665,889	2
PEPD	chr11	-	11,020,879	11,171,964	1
DYRK2	chr1	+	36,769,946	36,780,041	1
SSTR3	chr1	+	53,394,935	53,399,325	1
MAFA	chr2	-	154,329,488	154,331,050	1
KCNA3	chr26	-	1,289,092	1,290,386	1
LPAR1	chrZ	-	65,373,552	65,415,900	1
MOS	chr2	-	114,899,053	114,902,785	1
HVCN1	chr15	-	6,037,278	6,046,816	1
DAP	chr2	+	80,172,659	80,218,073	1
GYPC	chr7	-	25,575,240	25,601,901	1
PTPRG	chr12	+	13,003,771	13,378,851	1
GLCCI1	chr2	+	24,861,127	24,913,048	1
RUNDC3B	chr2	+	20,714,164	20,734,777	1
CCNE1	chr11	+	9,086,731	9,102,670	1
G0S2	chr26	+	2,961,383	2,962,268	1
XDH	chr3	+	4,394,692	4,435,263	1
AGMAT	chr21	+	4,975,103	4,977,437	1

MIR1650	chr2	-	22,663,909	22,664,001	1
TSGA14	chr1	-	840,172	848,472	1
TNFRSF18	chr21	+	2,545,741	2,552,051	1
MIR455	chr17	+	5,339,701	5,339,786	1
MIR1616	chr11	-	1,243,998	1,244,091	1
MYH11	chr14	-	7,623,241	7,682,699	1
PAK1	chr1	+	198,012,637	198,057,088	1
EPT1	chr3	+	107,819,505	107,839,009	1
KTN1	chr5	-	58,674,620	58,744,944	1
MYO1F	chr28	-	1,340,718	1,353,861	1
PTGER4	chrZ	+	12,251,057	12,262,553	1
YAP1	chr1	-	186,969,786	187,051,550	1
ORAI1	chr15	+	5,627,884	5,637,744	1
BAZ2B	chr7	-	38,189,619	38,269,262	1
C15H22orf25	chr15	+	1,272,257	1,288,928	1
DDB2	chr5	-	25,298,580	25,312,307	1
C5H14orf169	chr5	-	28,369,878	28,371,746	1
GART	chr1	-	108,807,618	108,840,814	1
SEPN1	chr23	-	2,564,018	2,577,618	1
FGFRL1	chr4	-	88,229,000	88,434,067	1
MAPK11	chr1	-	21,806,994	21,828,380	1
MIR137	chr8	+	13,210,193	13,210,288	1
EVL	chr5	+	50,903,043	50,969,098	1
MYOM1	chr2	+	104,021,928	104,095,796	1
C4BPA_dup1	chr26	+	2,445,711	2,453,125	1
DEPDC1	chr8	-	29,582,597	29,592,933	1
ZNF277	chr1	-	28,774,298	28,828,812	1
MIR1622	chr2	-	40,218,775	40,218,871	1
XRCC6	chr1	-	51,436,175	51,450,748	1
BRSK2	chr5	-	15,432,139	15,729,650	1
ARHGAP21	chr2	+	16,711,041	16,849,596	1
NME5	chr13	+	14,516,714	14,526,014	1
IL7	chr2	-	125,117,020	125,123,266	1
MIR1686	chr3	-	78,289,128	78,289,225	1
ASF1A	chr3	-	65,437,366	65,447,518	1
MIR460A	chr2	+	3,583,690	3,583,779	1
MIR1666	chr19	-	5,527,608	5,527,697	1
MCM6	chr7	-	32,279,983	32,293,245	1
DHRS11	chr19	+	8,121,385	8,142,581	1
CHAT1	chr3	+	17,837,664	17,838,507	1
LOH12CR1	chr1	+	74,168,800	74,188,818	1

POR	chr19	-	4,276,440	4,292,808	1
ZMYND19	chr17	+	1,962,494	1,967,586	1
SRGAP1	chr1	+	35,299,480	35,440,951	1
COLEC11	chr3	+	96,613,135	96,632,502	1
OTOR	chr3	+	5,584,686	5,589,682	1
MIR146A	chr13	-	7,555,593	7,555,691	1
LRRN1	chr12	+	18,898,800	18,915,529	1
RAD51	chr5	+	963,990	971,046	1
MIR1738	chr1	+	108,216,426	108,216,516	1
MIR1755	chr9	-	16,721,831	16,721,921	1
CENPK	chrZ	-	19,960,479	19,980,158	1
TBCCD1	chr9	-	5,381,115	5,389,493	1
EDARADD	chr3	-	39,269,396	39,280,617	1
SERPINB6	chr2	-	68,854,260	68,863,717	1
SULT1C3	chr1	+	140,446,503	140,452,154	1
SLC20A2	chr4	+	35,306,945	35,364,637	1
CRADD	chr1	+	46,794,800	46,870,620	1
RMI1	chrZ	+	39,572,878	39,576,734	1
ECE1	chr21	+	6,756,941	6,761,579	1
TLR6_dup1	chr4	+	71,549,952	71,555,092	1
LMNB1	chrZ	+	55,080,956	55,104,222	1
LHX8	chr8	+	30,510,076	30,521,624	1
HOXA11	chr2	-	32,599,373	32,603,906	1
CAPN3	chr5	+	27,818,851	27,842,861	1
GPR174	chr4	+	1,439,060	1,444,915	1
TMEM128	chr4	-	81,479,384	81,485,137	1
MARCKS_dup2	chr3	-	67,518,372	67,518,660	1
MIR1708	chr1	-	200,158,576	200,158,669	1
MIR196-2	chr2	-	32,586,149	32,586,242	1
MIR449B	chrZ	-	16,040,763	16,040,856	1
CHRNA10_dup1	chr1	+	199,644,965	199,648,218	1
ASS1	chr17	+	6,472,178	6,490,062	1
FOXG1	chr5	+	35,889,059	35,891,197	1
MIR2127	chr1	+	170,154,815	170,154,918	1
TJP2	chrZ	+	34,256,633	34,321,404	1
PNPLA4	chr1	+	130,120,480	130,133,843	1
DDX47	chr1	+	50,074,589	50,083,738	1
CXCL12	chr6	-	20,112,185	20,120,138	1
FAM49A	chr3	-	102,477,352	102,530,842	1
MIR1553	chr7	+	25,293,057	25,293,161	1
TK1	chr18	+	9,813,042	9,815,009	1

UBXN2B	chr2	+	115,751,997	115,789,259	1
REPS2	chr1	-	124,723,087	124,817,474	1
PYGB	chr3	+	4,118,368	4,134,571	1
TEX10	chr2	+	91,440,785	91,490,874	1
EEF1A1	chr13	+	13,356,595	13,365,446	1
NPL	chr8	+	7,749,184	7,758,425	1
MIR1770	chr2	+	151,547,087	151,547,183	1
BUB1B	chr5	+	562,263	585,857	1
LOC429451	chr28	-	949,669	951,389	1
ITGB3BP	chr8	-	28,594,829	28,613,676	1
BRCA1	chr27	-	4,789,797	4,810,155	1
SH3GLB2	chr17	-	5,988,133	6,013,191	1
MIR1647	chr28	+	1,817,973	1,818,079	1
PARP4	chr1	-	183,547,378	183,590,987	1
HAVCR1	chr13	+	11,525,689	11,535,057	1
GINS1	chr3	+	17,346,728	17,349,654	1
LOC422926	chr4	+	89,102,054	89,111,266	1
OGN	chr12	+	3,642,004	3,652,066	1
ADAM20	chr15	+	6,295,082	6,296,476	1
H4	chr1	+	49,971,396	49,971,707	1
H4-VII	chr1	+	49,971,396	49,971,707	1
MIR199-2	chr8	+	4,732,773	4,732,880	1
WDR51B	chr1	-	45,210,134	45,254,068	1
CMTM3	chr11	-	12,299,064	12,321,332	1
MYL3	chr2	-	3,342,134	3,378,274	1
LUZP2	chr5	-	1,122,019	1,291,076	1
COX16	chr5	+	29,828,588	29,867,397	1
LGALS1	chr4	+	51,219,237	51,220,230	1
LGALS3	chr5	-	58,849,111	58,850,842	1
APCDD1	chr2	+	100,876,208	100,920,319	1
MIS12	chr19	-	3,374,748	3,375,380	1
RNASEH2B	chr1	+	174,171,388	174,215,701	1
IGFBP3	chr2	-	56,056,029	56,071,640	1
MIR214	chr8	+	4,739,550	4,739,659	1
NPPC	chr21	+	5,753,368	5,755,105	1
PRIM2	chr3	-	89,435,408	89,520,703	1
PGM2	chr4	-	71,875,329	71,893,775	1
SLC26A6	chr12	+	9,295,051	9,300,810	1
RAP1GAP	chr1	+	80,853,213	80,893,905	1
MIR1693	chr1	-	21,990,299	21,990,400	1
MIR1731	chr12	-	10,938,255	10,938,356	1

VCAN	chrZ	-	61,308,618	61,409,263	1
CDC16	chr1	-	141,165,100	141,184,277	1
THYN1	chr24	-	2,587,751	2,592,845	1
SLC8A1	chr3	+	17,263,368	17,337,674	1
CENPC1	chr4	-	53,083,975	53,115,873	1
VIP	chr3	+	51,388,589	51,395,840	1
CSNK1E	chr1	+	52,878,359	52,892,175	1
MIR1769	chr15	+	2,251,403	2,251,505	1
CDH1	chr11	+	20,827,085	20,836,079	1
CCNA2	chr4	+	55,473,246	55,479,346	1
CEBPA	chr11	-	10,986,725	10,988,384	1
CYTH4	chr1	-	53,353,099	53,372,372	1
CDCA7L	chr2	-	30,586,865	30,625,547	1
PIGM	chr3	-	37,140,388	37,142,316	1
SOX14	chr9	-	5,233,805	5,234,353	1
MIR1816	chr2	+	90,603,851	90,603,955	1
TLL5	chr5	+	40,741,504	40,860,232	1
P2RY8	chr1	+	133,187,192	133,213,127	1
RGS2	chr8	-	3,589,875	3,592,669	1
NEDD1	chr1	+	47,926,747	47,951,593	1
CD8A_dup1	chr4	-	88,894,668	88,906,709	1
TREM2	chr26	-	4,571,685	4,576,072	1
RFTN1	chr2	-	34,275,134	34,369,674	1
DHCR24	chr8	-	26,011,324	26,019,531	1
ANXA5	chr4	+	55,512,723	55,534,713	1
NRXN1	chr3	+	6,458,891	7,107,993	1
SOX2	chr9	-	17,990,091	17,991,429	1
MIR1698	chr19	-	625,967	626,073	1
RAB33B	chr4	+	30,437,373	30,444,389	1
ACVR2A	chr7	+	36,127,982	36,182,504	1
SULT1B1	chr4	-	53,309,682	53,311,964	1
BARD1	chr7	-	4,181,053	4,223,665	1
AKR1A1	chr8	+	21,870,044	21,887,967	1
SERPINF1	chr19	+	5,379,025	5,385,857	1
CECR2	chr1	+	63,875,622	63,922,210	1
RFC3	chr1	-	178,159,174	178,172,945	1
SKP2	chrZ	+	10,327,865	10,338,425	1
PTHLH	chr1	-	74,765,553	74,776,935	1
CSRP1	chr26	+	537,251	760,479	1
STT3A	chr24	-	387,072	388,439	1
HYOU1	chr24	-	5,795,672	5,809,063	1

EDN2	chr23	+	932,556	937,876	1
DMRT1	chrZ	+	26,739,124	26,742,050	1
CD1C	chr16	+	1,374	11,714	1
BARX1	chr12	+	6,352,209	6,354,408	1
DAAM1	chr5	-	57,386,859	57,457,053	1
LIMK2	chr15	-	9,310,510	9,341,763	1
ADARB1	chr7	+	7,223,739	7,300,792	1
FANCL	chr3	-	891,587	920,584	1
TNIP2	chr4	+	85,454,419	85,461,579	1
KDR	chr4	+	67,056,278	67,083,945	1
NAT10	chr5	+	19,911,846	19,939,613	1
TRIB2	chr3	+	100,743,468	100,765,216	1
SLC9A9	chr9	-	11,801,450	11,976,639	1
LRP5	chr5	+	17,555,890	17,711,686	1
TRPV1	chr19	+	6,605,208	6,616,453	1
PRTG	chr10	+	8,959,034	9,039,736	1
STAU2	chr2	-	122,687,009	122,735,468	1
CHRNA4	chr20	-	8,862,693	8,881,295	1
LEAP2	chr13	+	17,658,818	17,660,565	1
ITPR1	chr12	+	19,042,283	19,182,580	1
BMP15	chr4	+	1,832,440	1,835,869	1
ENG	chr17	+	5,509,400	5,517,845	1
SAMHD1	chr20	-	590,236	616,845	1
CDC25A	chr2	+	471,911	484,805	1
GJC1	chr27	-	1,228,980	1,232,266	1
DPF3	chr5	+	28,669,155	28,827,246	1
FPGT	chr8	+	30,360,412	30,365,471	1
CERK	chr1	-	17,154,694	17,195,915	1
UNC5B	chr6	+	12,842,667	12,871,574	1
FAM190B	chr6	+	1,961,741	2,015,099	1
ZP3	chr10	+	3,496,411	3,498,806	1
CDA	chr21	+	4,951,471	4,955,042	1
NDC80	chr2	-	104,305,855	104,324,772	1
SMC2	chrZ	-	65,014,194	65,036,306	1
FAP	chr7	+	22,640,008	22,679,487	1
BFSP1	chr3	+	11,408,315	11,426,963	1
NUDT14	chr5	-	54,739,263	54,790,063	1
FRZB	chr7	+	2,296,057	2,312,214	1
CORO7	chr14	-	13,388,823	13,425,396	1
TRIM14	chrZ	+	50,910,991	50,919,003	1
MLF1IP	chr4	+	40,874,753	40,884,606	1

AVP	chr4	-	92,053,878	92,058,295	1
MYH2	chr18	-	482,485	500,775	1
CRELD2	chr1	+	20,135,877	20,147,497	1
SEC16B	chr8	+	6,926,277	6,937,584	1
EEF1A2	chr20	-	8,992,658	9,006,441	1
NR0B2	chr23	-	1,769,697	1,772,151	1
GHR	chrZ	+	12,905,426	12,988,509	1
PLTP	chr20	-	10,492,172	10,495,427	1
ALPL	chr21	-	6,748,718	6,754,529	1
CD40LG	chr4	+	4,377,155	4,379,974	1
IRF4	chr2	+	67,667,008	67,679,940	1
AQP12	chr9	-	5,669,259	5,671,109	1
WASL	chr1	+	23,984,371	24,034,762	1
LOC769357	chr2	+	103,270,322	103,288,979	1
DPH2	chr8	-	21,075,980	21,078,352	1
WNT7B	chr1	-	72,939,329	73,031,977	1
RASSF3	chr1	+	35,579,692	35,630,340	1
F7	chr1	-	141,835,984	141,844,253	1
LOC421212	chr3	+	27,176	28,299	1
NOX5	chr10	+	21,451,802	21,457,658	1
CSPG5	chr2	+	727,837	731,083	1
HMX1	chr4	-	84,420,384	84,423,043	1
NTSR1	chr20	+	8,211,995	8,258,960	1
CARD11	chr14	-	3,443,607	3,482,893	1
TTC27	chr3	-	32,610,033	32,712,377	1
IRG1	chr1	-	158,569,918	158,577,428	1
SDSL	chr15	-	12,890,724	12,893,215	1
TLR21	chr11	+	338,863	342,853	1
MGAT4A	chr1	-	136,440,074	136,516,957	1
ST6GALNAC2	chr18	+	4,299,294	4,305,335	1
C12H3orf64	chr12	-	15,684,244	15,706,080	1
MYOG	chr26	-	960,210	964,268	1
NKX3-2	chr4	+	80,371,236	80,372,133	1
NMB	chr10	+	384,408	387,683	1
DPP4	chr7	+	22,713,219	22,757,360	1
SPRY2	chr1	+	156,881,808	156,890,287	1
HAPLN1	chrZ	+	61,186,909	61,273,055	1
RAX	chr28	+	946,749	949,704	1
KCTD4	chr1	-	171,976,250	171,977,589	1
ID1	chr20	+	9,955,625	9,956,740	1
MTR	chr3	-	39,040,628	39,102,191	1

CENPM	chr1	+	51,348,432	51,353,117	1
KCNMB4	chr1	+	37,699,395	37,710,916	1
TCF15	chr20	+	9,877,468	9,877,893	1
POLE3	chr17	+	1,832,350	1,836,568	1
LAMB2	chr12	+	11,830,508	11,846,159	1
TTBK1	chr3	+	16,812,632	16,889,632	1
PAK7	chr3	+	14,797,277	14,841,045	1
KIT	chr4	-	67,140,610	67,193,203	1
PIK3R5	chr18	-	1,938,527	1,987,805	1
ITGB5	chr7	-	29,462,560	29,503,485	1
NCF4	chr1	-	53,569,059	53,579,617	1
LOC396260	chrZ	+	8,501,239	8,502,411	1
CHRNA	chr9	+	16,709,968	16,714,344	1
RP2	chr1	-	134,314,099	134,332,287	1
MCPH1	chr3	-	91,368,533	91,490,547	1
CPZ	chr4	+	84,149,787	84,188,441	1
ACE	chr27	+	2,567,619	2,583,871	1
IL28B	chr7	+	4,546,939	4,548,447	1
BUB1	chr3	+	3,029,831	3,049,593	1
IL10RA	chr24	+	5,544,340	5,547,618	1
ENO2	chr1	+	80,444,835	80,454,069	1
PECR	chr7	+	25,110,164	25,122,516	1
CD1B	chr16	+	5,443	7,734	1
GALR2	chr18	-	4,524,209	4,526,246	1
MDM1	chr1	-	36,985,648	37,009,791	1
BCL2	chr2	+	69,060,893	69,147,814	1
IGF2BP1	chr27	-	3,408,157	3,435,193	1
BETA3	chr2	+	118,603,261	118,603,830	1
ACSBG2	chr28	+	1,242,765	1,259,040	1
SAMSN1	chr1	-	101,512,833	101,547,418	1
PPARA	chr1	+	73,468,062	73,505,210	1
FOXC2	chr2	+	77,048,231	77,050,759	1
AVR2	chrZ	-	8,482,168	8,483,208	1
LOC417536	chr19	-	4,779,221	4,779,920	1
PTDSS2	chr5	-	1,517,340	1,552,919	1
ASMT	chr1	-	133,127,530	133,133,572	1
HABP4	chrZ	+	41,679,704	41,701,612	1
GNRHR	chr10	-	22,162,439	22,164,225	1
PTGER3	chr8	-	29,898,485	29,906,502	1
RUNX2	chr3	+	112,112,912	112,258,054	1
TPD52	chr2	-	125,600,211	125,635,083	1

BAMBI	chr2	-	15,232,262	15,236,102	1
TNS1	chr7	+	24,141,081	24,180,704	1
LIMK1	chr19	+	748,964	755,711	1
RGS4	chr8	+	3,702,499	3,707,852	1
THBS1	chr5	-	31,927,624	31,943,257	1
LSAMP	chr1	+	85,271,704	85,558,083	1
TGIF1	chr2	-	103,921,071	103,929,324	1
SNAI1	chr20	-	13,845,737	13,848,433	1
SLC16A3	chr18	-	4,859,464	4,863,225	1
BARX2	chr24	+	1,366,889	1,393,022	1
MST1R	chr12	-	2,407,515	2,415,443	1
MYO6	chr3	-	83,191,279	83,264,234	1
LCORL	chr4	+	78,711,367	78,739,476	1
CNTN1	chr1	+	30,689,196	30,775,124	1
RHOBTB1	chr6	+	9,774,999	9,797,309	1
GATM	chr10	+	12,588,264	12,601,291	1
KLF11	chr3	+	99,365,067	99,372,871	1
WNT6	chr7	-	23,961,932	23,965,019	1
LHX2	chr17	+	9,938,895	9,959,105	1
RALGPS2	chr8	-	6,605,648	6,717,274	1
LIN28A	chr23	-	148,876	160,182	1
EXOSC3	chr6	-	5,481,078	5,484,751	1
CAMP	chr2	-	3,899,980	3,903,251	1
NES	chr25	-	870,594	878,150	1
KIF23	chr10	+	21,512,826	21,531,258	1
KIF18B	chr27	-	1,272,001	1,279,347	1
TLR15	chr3	-	2,945,856	2,948,462	1
SERPINB14B	chr2	-	68,923,804	68,930,456	1
TFAP2A	chr2	+	64,442,590	64,456,081	1
APOA4	chr24	-	5,232,979	5,234,448	1
SPINK7	chr13	+	10,633,892	10,639,342	1
HCRT	chr27	-	4,507,696	4,509,553	1
ADORA3	chr26	-	3,047,965	3,050,306	1
NHLH2	chr1	+	83,744,915	83,745,819	1
MEF2D	chr25	-	966,730	982,620	1
WDFY1	chr9	-	9,355,927	9,373,068	1
CDH5	chr11	-	12,423,010	12,452,265	1
CBX4	chr18	+	9,596,948	9,599,727	1
ART7B	chr1	-	199,089,494	199,090,741	1
B3GNT5	chr9	-	17,399,052	17,403,530	1
SAMD13	chr8	-	17,343,421	17,355,216	1

JUP	chr27	-	4,311,393	4,318,989	1
PRKCD	chr12	-	1,448,409	1,480,179	1
KBP	chr21	-	1,432,231	1,443,126	1
NHLH1	chr25	+	1,347,056	1,348,927	1
GALK2	chr10	+	12,024,099	12,105,719	1
DBX1	chr5	-	2,077,300	2,080,999	1
HCRTR2	chr3	-	90,392,818	90,428,151	1
UPRT	chr4	+	12,653,347	12,665,228	1
UNG	chr15	+	6,807,153	6,812,467	1
LMOD2	chr1	-	24,053,297	24,059,448	1
SLC24A5	chr10	+	11,522,317	11,530,284	1
MAFB_dup1	chr20	-	4,642,415	4,643,995	1
PAQR7	chr23	+	3,545,569	3,549,373	1
CLSPN	chr23	+	4,541,895	4,555,424	1
APP	chr1	-	106,057,664	106,223,263	1
MMACHC	chr8	+	21,848,763	21,854,441	1
RARRES1	chr9	+	23,996,321	24,003,806	1
AMACR	chrZ	-	9,721,335	9,743,363	1
CD79B	chr27	-	1,528,905	1,533,332	1
C6H10orf58	chr6	-	5,460,901	5,469,226	1
ALDH1A3	chr10	+	19,570,926	19,612,701	1
CHST3	chr6	+	13,056,513	13,059,902	1
SMAD1	chr4	+	32,259,341	32,283,620	1
FAM213A	chr6	-	5,460,901	5,472,174	1
SH3BP2	chr4	-	85,371,525	85,407,779	1
BORA	chr1	-	160,346,462	160,365,991	1
C1S	chr1	+	80,541,033	80,550,138	1
SP8	chr2	-	30,186,079	30,189,430	1
LOC417954	chr1	+	50,026,207	50,026,866	1
SLC16A1	chr26	-	3,439,842	3,454,783	1
EVC2	chr4	-	82,054,940	82,118,333	1
SOCS4	chr5	-	58,880,484	58,888,640	1
SOX8	chr14	-	5,769,583	5,772,973	1
CRISPLD1	chr2	+	123,275,092	123,312,565	1
NEK2	chr3	+	23,314,595	23,321,271	1
SNX6	chr5	-	38,293,630	38,317,696	1
ARR3	chr4	+	1,220,625	1,226,329	1
CENPO	chr3	-	108,243,762	108,250,454	1
TPRXL	chr8	+	19,334,544	19,377,181	1
SLC34A2	chr4	-	75,884,660	75,905,255	1
PTGFR	chr8	-	19,436,328	19,453,239	1

TOP3A	chr14	-	5,099,948	5,111,853	1
SLC12A7	chr2	+	56,586,378	56,661,035	1
LGALS1	chr3	+	9,642,946	9,650,160	1
FMOD	chr26	-	4,946,736	4,952,662	1
SNCA	chr4	-	36,527,377	36,594,328	1
GAL	chr5	+	17,807,042	17,815,004	1
ATIC	chr7	+	4,341,051	4,358,775	1
PITX2	chr4	+	59,365,938	59,368,567	1
DMD	chr1	+	118,069,256	119,072,610	1
EPCAM	chr3	+	8,563,774	8,569,412	1
GAL9	chr3	+	110,236,007	110,239,064	1
SCCPDH	chr3	-	35,104,610	35,114,605	1
RAD51D	chr19	+	4,444,287	4,448,307	1
TNR	chr8	+	7,319,619	7,369,216	1
PAQR8	chr3	-	110,329,384	110,341,599	1
STAT4	chr7	-	8,903,301	8,940,899	1
SIRPA	chr20	+	9,775,303	9,777,070	1
EBF1	chr13	+	10,746,339	11,007,624	1
DCTD	chr4	+	41,410,071	41,430,379	1
DYDC1	chr6	+	5,484,900	5,488,579	1
MARCKSL1	chr23	+	5,377,330	5,379,581	1
LPHN2	chr8	-	18,117,645	18,244,423	1
DCX	chr4	+	13,329,701	13,403,237	1
STMN3	chr20	+	9,675,253	9,686,654	1
FABP3	chr23	-	565,195	568,772	1
GLB1	chr2	-	44,469,156	44,498,750	1
PTRF	chr27	-	4,567,082	4,582,516	1
PHTF2	chr1	-	13,406,544	13,467,892	1
EPGN	chr4	+	46,138,927	46,147,650	1
SIX6	chr5	-	56,988,925	56,992,323	1
CRYBB2	chr15	+	7,214,430	7,216,380	1
PDE6H	chr1	-	49,844,283	49,850,106	1
CHPT1	chr1	-	57,620,832	57,640,178	1
STK17A	chr2	+	51,638,044	51,664,946	1
RHO	chr26	-	4,375,372	4,380,959	1
IL7R	chrZ	+	10,231,994	10,245,667	1
FZD7	chr7	+	12,741,968	12,745,019	1
PTGDS	chr17	-	888,782	890,795	1
FZD4	chr1	+	193,006,476	193,011,392	1
RGS3	chr17	-	1,759,420	1,810,990	1
LOC427470	chrZ	-	41,879,084	41,887,640	1

MTAP	chrZ	+	71,968,346	71,996,017	1
FNDC3B	chr9	-	20,861,425	20,981,264	1
COL6A2	chr7	+	6,754,924	6,780,959	1
CCNRC01	chr13	-	621,963	693,839	1
NRG4	chr10	+	4,407,762	4,430,998	1
KCNMB1	chr13	+	3,543,730	3,550,735	1
TNC	chr17	-	3,035,604	3,102,206	1
EPHA3	chr1	+	92,450,603	92,669,803	1
EPHX2	chr3	+	107,888,809	107,898,004	1
CD5	chr5	-	361,450	364,255	1
SOX11	chr3	+	97,427,132	97,428,590	1
AHR	chr2	+	28,771,608	28,825,146	1
PLEKHB1	chr1	+	200,147,920	200,438,473	1
SETD6	chr11	+	1,384,081	1,386,765	1
IFNG_dup2	chr1	+	87,329,807	87,333,781	1
SYT12	chr5	-	1,505,740	1,512,671	1
PPFIBP1	chr1	+	70,419,134	70,459,959	1
ATP13A2	chr21	-	4,408,250	4,412,854	1
SFTP1A1	chr6	-	5,550,705	5,556,235	1
MT3	chr11	-	2,102,932	2,103,780	1
FABP7	chr3	-	63,843,220	63,846,573	1
HAUS1	chrZ	-	1,925,177	1,934,125	1
HES1	chr21	+	2,786,967	2,788,401	1
H2B-VII_dup2	chr1	+	49,976,548	49,976,928	1
BBS2	chr11	+	2,109,631	2,125,140	1
SOX3	chr4	+	10,594,559	10,596,382	1
METTL9	chr14	+	8,948,508	8,966,683	1
ELMO1	chr2	+	46,430,133	46,695,791	1
SLC25A4	chr4	-	40,757,647	40,760,469	1
ZAR1L	chr1	+	178,876,173	178,877,989	1
RAMP2	chr27	+	4,667,600	4,669,023	1
SLC2A1	chr21	-	6,659,188	6,667,015	1
KHDRBS1	chr23	+	5,336,071	5,352,090	1
TNFRSF13C	chr1	+	51,363,876	51,365,483	1
HAS2	chr2	-	142,977,906	142,996,607	1
CBLN2	chr2	+	94,978,728	94,984,780	1
TTC7A	chr3	+	28,138,626	28,267,673	1
IGFBP2	chr7	-	24,797,527	24,802,623	1
MC1R	chr11	+	20,802,676	20,805,060	1
NGFR	chr27	-	3,124,981	3,125,340	1
PPAP2B	chr8	-	26,467,556	26,511,431	1

HDAC9	chr2	+	29,265,256	29,536,269	1
ANKRD1	chr6	-	20,728,953	20,737,641	1
TXNDC5	chr2	+	65,520,413	65,541,151	1
TCIRG1	chr5	+	93,185	98,885	1
CNTFR	chrZ	+	7,663,412	7,781,120	1
CHAC2	chr3	-	2,968,683	2,979,580	1
ANKRD40	chr18	+	10,088,501	10,095,153	1
DACT1	chr5	-	57,671,526	57,680,212	1
CCR8	chr2	+	44,399,478	44,402,795	1
LOC395933	chr3	-	43,679,679	43,688,238	1
BCKDHB	chr3	-	81,766,270	81,876,676	1
MAGI3	chr26	+	3,516,479	3,545,774	1
ZDHC23	chr1	-	86,357,970	86,364,627	1
WFDC1	chr11	+	18,603,213	18,615,568	1
ANGPTL3	chr8	+	28,325,071	28,331,554	1
PMEPA1	chr20	+	11,483,057	11,488,191	1
OTX2_dup2	chr5	+	58,374,938	58,375,137	1
SOX1	chr1	+	144,077,931	144,079,326	1
CD82	chr5	+	24,004,510	24,049,142	1
C18H17orf106	chr18	-	4,571,745	4,574,345	1
CAMK4	chr28	+	2,507,902	2,508,086	1
SLC16A7	chr1	+	33,896,443	33,925,831	1
SDC3	chr23	-	412,667	432,268	1
CCR9	chr2	-	42,795,854	42,797,002	1
CELA2A	chr21	+	5,728,757	5,733,531	1
UTS2	chr21	+	256,327	259,641	1
FOXC1	chr2	+	68,198,571	68,198,953	1
EVI2A	chr19	+	8,992,997	8,996,551	1
CCL4_dup2	chr19	+	373,753	375,322	1
MAFB_dup2	chr20	-	4,645,545	4,646,351	1
TIAM2	chr3	+	52,407,422	52,493,149	1
CAPN2	chr3	-	18,797,911	18,818,133	1
MOXD1	chr3	+	58,885,840	58,943,917	1
CD4	chr1	+	80,360,877	80,373,481	1
RLBP1	chr10	+	14,662,079	14,666,265	1
CD72_dup3	chrZ	-	8,431,936	8,434,952	1
CRYBA2	chr7	+	23,908,411	23,908,977	1
SLC25A15	chr1	-	174,785,297	174,800,876	1
IFNA3	chrZ	+	6,896,104	6,896,866	1
GDPD5	chr1	-	199,808,984	200,003,901	1
ELOVL6	chr4	+	59,493,263	59,560,594	1

ALDH1A1	chrZ	-	35,597,345	35,649,840	1
SH3KBP1	chr1	+	123,425,184	123,649,275	1
CALB1	chr2	-	129,152,181	129,170,055	1
PCDH19	chr4	+	5,230,868	5,281,760	1
SLC47A1	chr19	-	6,805,622	6,813,553	1
CHMP4C	chr2	+	126,220,693	126,234,740	1
THG1L	chr13	-	11,371,697	11,377,007	1
PLEKHA2	chr22	+	2,451,556	2,460,955	1
HOXD12	chr7	-	17,431,436	17,433,113	1
FKBP5	chr26	-	65,801	76,175	1
LOC396454	chrZ	+	52,408,699	52,414,029	1
ARHGAP19	chr6	+	23,786,205	23,805,886	1
TBX5	chr15	+	12,625,657	12,666,982	1
EARS2	chr14	+	6,961,127	6,968,451	1
WNT3A	chr2	-	2,364,220	2,451,014	1
IGF2	chr5	+	14,875,654	14,883,996	1
CDK1	chr6	-	9,821,486	9,829,491	1
HOXB5	chr27	+	3,584,382	3,587,216	1
NTN1	chr18	+	1,994,992	2,040,449	1
TUBB6	chr2	-	99,592,006	99,599,495	1
TCF7	chr13	-	16,365,201	16,427,288	1
COL12A1	chr3	+	83,548,165	83,648,679	1
COL4A2	chr1	+	143,165,551	143,306,844	1
PHYHIPL	chr6	-	1,627,582	1,660,297	1
LINGO1	chr10	+	3,611,236	3,693,726	1
BMP3	chr4	+	46,904,640	46,918,970	1
MYC	chr2	+	145,392,353	145,394,591	1
PRTFDC1	chr2	+	16,665,633	16,710,329	1
PMM2	chr14	-	10,286,394	10,298,414	1
ETS2	chr1	+	111,250,667	111,265,698	1
TUBA8	chr1	+	64,201,157	64,204,707	1
OCC-1	chr1	-	56,225,501	56,242,118	1
HOXB8	chr27	+	3,578,954	3,580,585	1
COTL1	chr11	-	18,699,322	18,756,457	1
IMPG1	chr3	+	83,131,170	83,187,529	1
LRRTM3	chr6	-	7,889,367	7,970,491	1
MERTK	chr3	+	3,125,312	3,146,292	1
SOBP	chr3	-	70,373,573	70,470,073	1
DNAJC9	chr6	-	6,288,998	6,292,116	1
AICDA	chr1	-	79,043,135	79,047,114	1
ALCAM	chr1	+	89,846,135	89,964,052	1

CHAT	chr6	-	3,933,063	3,964,302	1
ITGA8	chr2	+	20,273,104	20,372,007	1
CDR2	chr14	-	8,916,599	8,930,083	1
PRLR	chrZ	-	9,965,748	9,995,834	1
RFC4	chr9	-	17,302,424	17,313,235	1
B4GALT6	chr2	-	109,317,691	109,342,102	1
NRTN	chr28	-	1,114,154	1,117,972	1
PRKAG2	chr2	-	6,231,510	6,254,788	1
NR2E3	chr10	+	769,616	773,299	1
WNT4	chr21	+	6,505,909	6,517,953	1
OSR2	chr2	+	132,808,941	132,811,780	1
RRH	chr4	-	59,673,736	59,684,850	1
GPX7	chr8	+	25,192,158	25,200,735	1
PITX1	chr13	+	16,003,464	16,017,081	1
PROCR	chr9	-	5,408,816	5,410,602	1
POUV	chr17	-	841,824	842,421	1
MEOX2	chr2	-	28,044,157	28,098,985	1
PNAT3	chr11	+	17,481,972	17,493,920	1
QTRTD1	chr1	-	86,322,076	86,334,253	1
HAND2	chr4	-	44,836,109	44,837,250	1
CLEC2D	chr16	-	74,767	75,819	1
NFASC	chr26	+	1,697,227	1,773,801	1
PIK3CB	chr9	-	6,651,427	6,734,668	1
SLCO4A1	chr20	+	8,164,079	8,189,319	1
NPHP1	chr3	-	2,996,918	3,016,335	1
CHRNA9	chr4	-	70,872,474	70,876,958	1
SRL	chr14	-	13,365,668	13,385,943	1
CEBPB	chr20	-	13,765,291	13,766,624	1
SCIN	chr2	+	26,728,953	26,778,500	1
PI4K2B	chr4	-	75,987,346	76,010,046	1
POU2AF1	chr24	-	4,343,749	4,356,189	1
SOX5	chr1	+	68,081,129	68,335,942	1
CASP6	chr4	+	59,717,631	59,726,409	1
VSX2	chr5	+	40,231,661	40,251,161	1
TBX19	chr1	-	87,417,468	87,431,720	1
LPAR3	chr8	+	17,134,950	17,141,445	1
PTGES	chr17	-	6,232,944	6,235,407	1
GFRA2	chr22	+	1,392,362	1,413,351	1
FANCA	chr11	-	20,738,007	20,771,631	1
NKX2-1	chr5	-	39,014,045	39,016,319	1
STXBP6	chr5	-	34,758,974	34,813,703	1

ISL1	chrZ	+	14,559,393	14,572,371	1
ACTN2	chr3	-	39,113,980	39,192,072	1
MEOX1	chr27	+	3,250,187	3,259,338	1
CHRNA2	chr3	-	107,876,061	107,879,433	1
NEUROD1	chr7	+	15,350,165	15,351,974	1
SSTR1	chr5	+	39,747,754	39,749,034	1
MYO5A	chr10	+	9,983,311	10,081,583	1
PLIN1	chr10	+	14,521,307	14,525,500	1
WDR77	chr26	-	3,035,272	3,039,335	1
TOP1MT	chr2	-	154,083,017	154,094,914	1
OAF	chr24	-	3,865,269	3,877,689	1
DNMT3A	chr3	-	107,427,886	107,432,478	1
MBL2	chr6	-	5,569,917	5,578,096	1
NAB1	chr7	-	43,878	62,294	1
NEGR1	chr8	-	29,962,712	30,046,010	1
CIDEA	chr2	-	99,617,678	99,625,865	1
CPS1	chr7	+	2,805,103	2,906,849	1
ACAA1	chr2	-	4,623,536	4,631,610	1
PRRG4	chr5	+	5,661,655	5,668,581	1
GZMA	chrZ	+	15,998,583	16,002,777	1
NAPEPLD	chr1	-	13,894,475	13,915,023	1
EFHC2	chr1	+	114,628,575	114,689,931	1
SSPO	chr2	+	314,863	348,112	1
TERT	chr2	-	88,046,748	88,076,214	1
FSHB	chr5	+	4,580,528	4,583,903	1
HOXA4	chr2	-	32,543,959	32,546,257	1
RPP38	chr2	-	20,555,001	20,557,772	1
HTR6	chr21	+	4,816,488	4,819,994	1
VAX1	chr6	-	30,559,317	30,563,628	1
GUCA1B	chr26	+	2,999,190	3,002,725	1
MYCN	chr3	+	102,114,357	102,117,498	1
TYRP1	chrZ	+	30,550,134	30,561,433	1
HTR1A	chrZ	-	19,383,037	19,384,371	1
ADCYAP1	chr2	-	104,980,384	104,984,705	1
LOC418120	chr1	+	59,102,053	59,317,109	1
HS6ST2	chr4	-	3,590,597	3,692,078	1
NEUROG2	chr4	+	58,692,144	58,692,815	1
NOG	chr18	+	6,194,497	6,195,168	1
DEPDC6	chr2	+	142,282,864	142,357,046	1
IL4I1	chr16	-	163,641	168,435	1
CAV2	chr1	-	26,875,378	26,883,231	1

RGMA	chr10	-	16,396,405	16,399,562	1
DBN1	chr13	-	10,242,876	10,243,579	1
POSTN	chr1	+	176,288,241	176,321,010	1
MYH7	chr19	+	7,167	20,393	1
ENTPD2	chr17	+	784,834	793,345	1
NME1	chr18	-	9,929,821	9,933,360	1
FGF1	chr13	-	17,843,798	17,859,021	1
PARD3	chr2	+	13,046,302	13,484,187	1
GBGT1	chr17	-	7,494,356	7,501,562	1
PHACTR1	chr2	-	63,373,557	63,446,915	1
AREGB	chr4	+	46,181,370	46,187,839	1
DNAJC24	chr5	+	5,051,574	5,083,300	1
LITAF	chr14	+	923,095	929,912	1
TERC	chr9	+	21,505,855	21,506,865	1
TTPAL	chr20	-	5,370,743	5,378,966	1
MAP7	chr3	+	56,993,300	57,101,732	1
CDX1	chr13	-	13,312,550	13,322,789	1
CALD1	chr1	+	64,422,940	64,609,400	1
MFI2	chr9	-	13,556,867	13,573,461	1
TMEM5	chr1	+	35,230,647	35,242,267	1
KIAA1609	chr11	-	18,644,398	18,656,671	1
MLXIPL	chr19	-	157,069	172,107	1
TLR2-1	chr4	+	21,101,227	21,108,624	1
MPZL2	chr24	-	5,587,010	5,592,591	1
CD14	chr13	+	862,594	863,991	1
GJA8	chr1	+	95,836,741	95,837,943	1
GBX2	chr7	+	5,167,462	5,168,418	1
IL18	chr24	+	6,291,980	6,295,249	1
GAL6	chr3	+	110,248,974	110,251,859	1
PTGER2	chr5	+	60,704,352	60,704,581	1
PDE6C	chr6	-	21,453,054	21,481,667	1
RCOR3	chr3	-	23,440,906	23,460,197	1
MAL2	chr2	+	141,929,448	141,946,401	1
SLC7A2	chr4	-	64,871,851	64,887,375	1
SAMD11	chr21	-	2,906,187	2,940,554	1
FOXM1	chr1	+	78,765,155	78,773,787	1
HSPB1	chr19	-	4,218,151	4,220,565	1
RET	chr6	-	5,877,654	5,953,679	1
LECT1	chr1	+	169,981,840	169,993,576	1
PADI3	chr21	-	138,108	144,397	1
ZP4	chr6	-	17,640,935	17,645,446	1

CDX2	chr1	+	180,351,960	180,355,993	1
SS2	chr21	-	4,100,317	4,104,042	1
LBFABP	chr23	-	5,902,057	5,904,572	1
MT4	chr11	-	2,100,369	2,100,601	1
PRKAA2	chr8	+	26,532,235	26,550,853	1
LRP8	chr8	-	25,168,003	25,560,448	1
IGJ	chr4	-	51,507,275	51,513,039	1
RHBG	chr25	+	900,025	904,928	1
RDM1	chr27	-	1,517,261	1,522,082	1
HES5	chr21	+	1,408,372	1,409,775	1
LOC769134	chr1	-	23,834,274	23,864,122	1
GIPR	chr18	+	9,856,833	9,859,769	1
TMC2	chr2	+	44,339,001	44,365,450	1
CHUNK-1	chr1	+	63,114,463	63,116,388	1
CECR1	chr1	-	63,802,135	63,817,469	1
MRAS	chr7	+	26,779,882	26,815,460	1
COL1A2	chr2	+	23,530,766	23,569,737	1
ABCC6	chr14	-	7,763,329	7,787,131	1
PKP4	chr7	+	38,002,476	38,069,371	1
RGL1	chr8	+	7,978,145	8,047,911	1
RELL1	chr4	+	71,914,027	71,946,182	1
VNN1	chr3	+	58,745,712	58,758,867	1
ZIC1	chr9	+	13,009,760	13,014,235	1
ST3GAL2	chr11	+	1,750,551	1,753,440	1
LHFPL5	chr26	+	93,070	97,423	1
SSTR4	chr3	-	3,269,921	3,271,148	1
UCK2	chr8	+	5,787,460	5,804,518	1
NGB	chr5	-	41,556,461	41,558,795	1
NCS1	chr17	+	6,460,932	6,463,784	1
PTGS2	chr8	+	10,059,565	10,067,539	1
IFT81	chr15	-	5,419,557	5,459,044	1
PROX1	chr3	-	22,432,062	22,468,755	1
IL16	chr10	-	13,802,549	13,810,903	1
SSTR2	chr18	+	8,997,369	8,999,654	1
FADS2	chr5	+	17,986,929	18,003,968	1
DDT	chr15	+	8,372,897	8,375,320	1
CHRM4	chr5	+	25,798,570	25,800,042	1
MYH15	chr1	-	90,776,483	90,820,252	0
COL20A1	chr20	+	8,813,122	8,856,913	0
CENPI	chr4	-	2,061,532	2,075,788	0
TADA2A	chr19	+	8,513,748	8,535,824	0

NUDT19	chr11	+	10,593,186	10,597,541	0
TWIST2	chr7	+	6,118,581	6,148,967	0
POMC	chr3	+	108,172,213	108,173,787	0
PLXNB1	chr12	+	11,607,623	11,639,643	0
COL18A1	chr7	+	6,616,327	6,649,907	0
DCBLD2	chr1	+	87,868,803	87,913,653	0
ZFP92	chr1	-	95,221,216	95,226,004	0
DACH2	chr4	-	8,338,908	8,605,684	0
GABRQ	chr4	-	10,736,727	10,801,159	0
SOHO-1	chr4	-	84,410,067	84,413,010	0
HPS1	chr6	+	23,667,520	23,673,180	0
MARCO	chr7	-	30,079,089	30,088,128	0
LHX9	chr8	-	2,288,712	2,299,119	0
MSGN1	chr3	+	103,106,658	103,107,959	0
MYF6	chr1	+	41,882,384	41,884,264	0
FABP1	chr4	-	89,155,943	89,159,670	0
AGRP	chr11	-	1,374,480	1,376,072	0
TRAF5	chr3	-	23,415,555	23,431,689	0
FANCI	chr10	-	14,638,348	14,661,198	0
TMEM175	chrZ	+	52,350,488	52,364,158	0
BMPER	chr2	-	47,574,124	47,724,199	0
SPERT	chr1	+	172,145,197	172,147,839	0
SNCG	chr6	+	3,621,079	3,629,559	0
NAV3	chr1	+	40,545,986	40,802,286	0
C5H15orf41	chr5	-	33,771,167	33,887,960	0
WLS	chr8	-	29,518,977	29,543,121	0
ITIH2	chr1	+	4,126,597	4,157,606	0
FGFR2	chr6	-	32,368,721	32,444,733	0
KCNJ2	chr18	+	8,205,149	8,211,891	0
NBL1	chr21	+	4,801,385	4,813,970	0
KCNA10	chr26	-	1,234,687	1,236,536	0
ST3GAL5	chr4	-	88,608,429	88,633,119	0
GPR37	chr1	+	23,547,150	23,562,166	0
ALG12	chr1	-	20,126,979	20,131,040	0
GAL12	chr3	-	110,205,029	110,205,928	0
EYA2	chr20	+	5,622,656	5,714,913	0
CACNA1D	chr12	+	7,276,290	7,443,143	0
FAM26E	chr3	-	66,454,206	66,462,104	0
GPR158	chr2	-	16,407,548	16,588,807	0
ATP6V0A4	chr1	+	58,384,884	58,407,729	0
SOX9	chr18	+	8,812,548	8,815,458	0

SOX17	chr2	+	114,054,316	114,064,873	0
TNFSF8	chr17	-	2,996,909	3,010,535	0
RS1	chr1	+	123,945,624	123,958,969	0
SERINC2	chr23	+	585,462	589,774	0
SLC25A22	chr5	+	16,899,479	16,948,320	0
SGPL1	chr6	+	12,668,049	12,695,719	0
ATP13A4	chr9	+	14,184,137	14,218,104	0
TMEM120B	chr15	+	5,651,288	5,663,564	0
HSD3B2	chr1	-	81,648,997	81,659,406	0
CNGA3	chr1	-	136,055,881	136,088,433	0
TPH2	chr1	+	38,382,635	38,436,926	0
IGF1	chr1	+	57,327,750	57,376,178	0
ANGPT1	chr2	-	136,942,353	137,132,163	0
GABRB3	chr1	+	135,465,540	135,577,049	0
N6AMT2	chr1	+	183,095,166	183,104,803	0
CDH11	chr11	+	13,166,650	13,257,246	0
KCNA4	chr5	-	4,536,093	4,540,765	0
THBS2	chr3	+	43,230,980	43,260,685	0
C1H12orf23	chr1	-	55,677,010	55,690,450	0
MEPE	chr4	-	47,118,993	47,122,507	0
GSTT1	chr15	+	8,360,841	8,370,443	0
LOC419112	chr1	+	4,029,905	4,064,443	0
IBSP	chr4	-	47,123,221	47,124,441	0
C11H16orf61	chr11	-	16,951,390	16,960,266	0
PGR	chr1	+	187,457,391	187,496,309	0
TLR4	chr17	+	4,062,994	4,068,447	0
GJA5	chr1	-	95,779,772	95,798,673	0
TIMD4	chr13	+	11,536,349	11,551,711	0
MSX2	chr13	+	9,809,286	9,813,858	0
LYG2	chr1	-	136,653,845	136,657,331	0
RGS20	chr2	+	113,829,080	113,838,977	0
HOXA2	chr2	-	32,513,804	32,519,311	0
ENTPD6	chr3	+	16,995,361	17,009,120	0
PIGR	chr26	-	2,390,697	2,401,255	0
TMEM65	chr2	-	144,035,964	144,067,330	0
SLC46A1	chr19	-	5,623,313	5,626,825	0
PPYR1	chr6	+	18,935,941	18,937,074	0
CHD7	chr2	+	116,874,780	116,977,118	0
VAV2	chr17	-	7,725,698	7,829,135	0
LRR17	chr1	+	13,834,883	13,850,912	0
LMX1B	chr17	+	10,784,728	10,879,992	0

GALR1	chr2	-	92,738,617	92,752,932	0
OSR1	chr3	-	103,927,498	103,929,131	0
PRSS2	chr1	-	81,245,628	81,249,404	0
COL4A1	chr1	-	143,054,856	143,165,166	0
FBLN1	chr1	+	72,638,880	72,721,710	0
RNLS	chr6	+	10,547,503	10,612,279	0
TCTN3	chr6	+	37,299,917	37,305,483	0
MTHFD1	chr5	-	55,461,403	55,499,288	0
VSNL1	chr3	+	102,957,139	103,033,061	0
BCMO1	chr11	+	17,085,904	17,101,834	0
SDR42E2	chr14	+	8,847,990	8,857,991	0
KRT5	chrE22C19W28_E50C23	+	642,021	648,330	0
FOSL2	chr3	-	28,588,715	28,594,272	0
ROR1	chr8	+	28,767,095	28,809,797	0
KIF20A	chr13	-	10,143,044	10,152,916	0
FZD1	chr2	+	22,082,221	22,084,539	0
NLGN3	chr4	-	2,307,676	2,324,178	0
SOCS2	chr1	+	46,783,618	46,785,293	0
GPR34	chr1	-	115,480,830	115,481,975	0
CPLX3	chr10	-	1,789,026	1,790,951	0
LCT	chr7	-	32,259,995	32,277,526	0
HOXA3	chr2	-	32,523,840	32,538,638	0
PAX9	chr5	+	39,103,431	39,121,701	0
HESX1	chr12	-	8,835,296	8,837,508	0
MELK	chrZ	-	74,572,577	74,595,002	0
GLP2R	chr18	+	128,433	171,552	0
NTRK1	chr25	-	825,268	832,763	0
TPCN3	chr3	+	3,016,884	3,028,588	0
TNFAIP6	chr7	+	36,757,319	36,770,976	0
CRYBB1	chr15	-	7,401,161	7,403,452	0
ZP1	chr5	-	366,361	366,971	0
MASP1	chr9	+	15,969,363	15,987,093	0
FGFR3	chr4	-	86,423,243	86,476,740	0
GRIA4	chr1	-	185,494,254	185,717,049	0
NR5A1	chr17	-	10,147,290	10,164,771	0
GYLTL1B	chr5	-	26,058,859	26,064,297	0
VGLL2	chr3	-	66,201,243	66,207,330	0
P2RY6	chr1	+	200,242,851	200,244,013	0
CRNN	chr25	+	1,286,861	1,288,137	0
CRYBA1	chr19	+	5,917,521	5,921,901	0
CTTNBP2	chr1	+	26,272,141	26,347,270	0

CX3CL1	chr11	+	760,088	764,369	0
DNAJC6	chr8	+	29,085,892	29,106,841	0
ADIPOQ	chr9	-	6,283,328	6,285,474	0
CBLN4	chr20	+	12,070,718	12,075,259	0
NEBL	chr2	+	18,040,904	18,285,246	0
SEPX1	chr14	-	6,148,709	6,151,643	0
TNNT2	chr26	+	785,618	794,076	0
GFRA1	chr6	-	30,088,281	30,225,382	0
NTRK3	chr10	+	14,944,527	15,091,853	0
COCH	chr5	+	36,604,204	36,620,897	0
WNT5A	chr12	-	8,133,521	8,145,604	0
PDLIM4	chr13	+	17,326,725	17,362,380	0
C6H10orf2	chr6	-	24,509,102	24,509,700	0
GPR149	chr9	+	24,729,009	24,750,207	0
SOUL	chr5	+	61,370,747	61,381,373	0
MIXL1	chr3	-	18,207,458	18,208,488	0
FOXD3	chr8	+	28,563,111	28,563,687	0
ACAN	chr10	-	14,734,434	14,778,815	0
PCDH10	chr4	+	27,987,008	28,020,248	0
CYP2D6	chr1	+	51,291,779	51,300,958	0
PMEL	chrE22C19W28_E50C23	+	485,431	489,564	0
PTPRJ	chr8	+	18,221,427	18,222,331	0
RYR3	chr5	-	32,472,012	32,658,515	0
MAGI2	chr1	+	12,654,450	13,385,728	0
PCK1	chr20	-	11,513,400	11,521,119	0
TEAD4	chr1	-	78,659,066	78,705,705	0
MAB21L2	chr4	+	34,138,908	34,140,097	0
LOC420419	chr2	-	4,632,460	4,701,170	0
RAD54B	chr2	-	130,826,456	130,886,491	0
TMEM164	chr4	-	13,801,067	13,839,245	0
DACH1	chr1	+	160,767,150	161,137,858	0
NR1H4	chr1	+	49,206,988	49,239,779	0
ST3GAL1	chr2	-	147,767,513	147,792,188	0
TWIST3	chrE22C19W28_E50C23	-	402,458	407,970	0
CL2	chr4	-	51,109,366	51,110,407	0
DNMT3B	chr20	+	10,203,706	10,212,614	0
DPYSL3	chr13	-	18,592,795	18,607,856	0
ARHGAP40	chr20	-	3,684,615	3,720,366	0
OGCHI_dup1	chr17	+	5,427,813	5,428,207	0
DUSP6	chr1	-	45,170,088	45,175,062	0
KCNJ3	chr7	+	37,363,206	37,392,741	0

CHIA	chr26	-	4,897,095	4,901,738	0
GPR83	chr1	+	189,935,351	189,938,299	0
SRI	chr2	-	20,925,129	20,933,670	0
MC5R	chr2	-	98,854,016	98,854,993	0
PID1	chr9	-	10,925,171	11,002,436	0
RHO	chr12	+	20,163,800	20,166,318	0
NOG2	chr14	-	14,811,864	14,812,487	0
COL6A3	chr7	+	4,791,165	4,844,414	0
SGK196	chr4	+	35,294,883	35,298,858	0
HAL	chr1	-	47,589,470	47,602,093	0
SERPINB14	chr2	-	68,905,915	68,913,487	0
EDA2R	chr4	-	346,387	355,457	0
TH	chr5	+	14,814,005	14,831,018	0
IL13RA2	chr4	-	2,822,785	2,832,339	0
MBOAT4	chr4	-	51,100,803	51,102,680	0
PDLIM3	chr4	-	62,897,016	62,917,915	0
SPARC	chr13	+	12,997,371	13,000,373	0
SUCLG2	chr12	-	15,049,722	15,151,688	0
N4BP3	chr13	-	10,185,168	10,191,401	0
CHRD1	chr4	+	13,612,341	13,654,186	0
SERPINH1	chr1	+	200,036,710	200,044,182	0
CHRNA6	chrZ	+	52,486,214	52,496,080	0
TYR	chr1	-	192,138,669	192,188,837	0
BPIFB8	chr20	+	10,238,415	10,246,455	0
VIPR2	chr2	-	9,570,163	9,620,910	0
PDGFC	chr4	+	22,269,566	22,387,721	0
KRT14	chr27	-	4,274,002	4,277,832	0
SLC18A3	chr6	-	3,969,228	3,970,513	0
ASB13	chr1	+	990,854	999,128	0
KCNIP4	chr4	+	77,219,895	77,664,123	0
FGF8	chr6	+	24,138,330	24,145,322	0
TLR5	chr3	+	18,975,945	18,978,530	0
FGF19	chr5	-	18,743,574	18,748,511	0
EDNRB	chr1	+	157,998,669	158,012,644	0
ANGPTL5	chr1	+	187,138,002	187,152,068	0
NOV	chr2	+	142,002,874	142,012,301	0
TRIM55	chr2	+	119,298,172	119,336,545	0
BVES	chr3	+	71,505,287	71,531,938	0
PGC	chr26	-	4,751,620	4,755,464	0
MESP2_dup2	chr10	-	22,167,719	22,168,753	0
AKR1B1L	chr1	-	64,279,091	64,287,625	0

LAMP3	chr9	+	17,469,967	17,481,612	0
PPAT	chr4	+	66,608,662	66,649,585	0
TRPV4	chr15	-	7,045,631	7,054,451	0
EBF2	chr22	+	612,347	736,594	0
ABLIM1	chr6	-	29,286,709	29,466,356	0
SLCO2A1	chr9	+	5,597,952	5,622,265	0
KRT75_dup1	chrE22C19W28_E50C23	+	655,421	660,547	0
CYP11A1	chr10	+	1,937,165	1,941,637	0
IFNG_dup1	chr1	-	36,925,485	36,929,632	0
BIRC5	chr3	-	16,329,443	16,330,576	0
TAS2R7	chr3	-	112,675,246	112,676,211	0
CENPN	chr11	+	16,979,515	16,986,438	0
SNCB	chr13	+	10,418,656	10,421,303	0
LOC431251_dup2	chr22	-	2,271,510	2,272,452	0
SLC1A2	chr5	-	20,605,480	20,686,717	0
SOX10	chr1	+	52,999,731	53,009,692	0
DFNA5	chr2	-	31,534,990	31,560,405	0
SDC2	chr2	+	131,690,147	131,750,267	0
AFAP1	chr4	-	83,517,663	83,576,335	0
RTKN2	chr6	+	9,323,573	9,356,305	0
NR5A2	chr8	-	1,599,597	1,674,490	0
LPCAT2	chr11	-	3,628,904	3,657,319	0
RASGRP3	chr3	-	32,306,819	32,345,209	0
CNGA1	chr4	+	68,468,398	68,475,888	0
ADAM12	chr6	-	34,382,443	34,588,731	0
NLGN1	chr9	-	20,187,136	20,523,530	0
ESR1	chr3	+	50,936,183	51,041,281	0
KDELRL3	chr1	-	52,839,529	52,844,641	0
CYP8B1	chr2	+	1,984,108	1,985,753	0
NCF1	chr19	-	2,609,413	2,616,232	0
LIN28B	chr3	-	71,550,790	71,626,325	0
TFAP2D	chr3	-	111,073,658	111,125,063	0
PAX3	chr9	-	8,937,632	9,001,296	0
LOC395159	chr2	+	26,606,953	26,617,355	0
UTS2D	chr9	+	14,792,256	14,799,015	0
SPRY4	chr13	-	17,796,912	17,797,908	0
NUDT1	chr14	+	3,094,127	3,098,133	0
OCM	chr14	-	1,020,597	1,023,986	0
PTPRU	chr23	+	2,732,055	3,110,162	0
TGFBR3	chr8	+	15,046,477	15,153,887	0
DTL	chr3	-	23,173,359	23,195,621	0

SPON1	chr5	+	6,303,749	6,472,110	0
CCDC50	chr9	-	14,746,262	14,783,034	0
AMY2A	chr8	-	38,922	43,343	0
NPY5R	chr4	+	24,480,176	24,481,507	0
ST8SIA3	chrZ	-	317,110	320,474	0
NR1I3	chr25	-	1,775,239	1,778,012	0
NCAM1	chr24	-	5,930,035	6,012,210	0
NR3C2	chr4	-	33,247,975	33,445,576	0
CNTN5	chr1	-	187,746,370	188,354,191	0
BHLHE23	chr20	-	8,473,655	8,477,731	0
GLUL	chr8	+	5,929,460	5,936,023	0
NPAS2	chr1	+	137,452,342	137,500,343	0
PLAU	chr6	-	16,583,890	16,592,063	0
INHBA	chr2	-	50,699,071	50,711,410	0
SFRP2	chr4	-	21,143,631	21,147,274	0
SPINK5	chr13	+	10,614,328	10,624,092	0
MYL9	chr20	-	443,129	449,538	0
FAT3	chr1	-	190,659,663	191,010,324	0
COL3A1	chr7	-	566,176	617,061	0
COL22A1	chr2	-	150,186,477	150,415,758	0
SALL3	chr2	-	58,060,629	58,080,021	0
CHRNA7	chr10	-	7,632,035	7,672,069	0
GPRIN2	chr6	+	3,753,674	3,756,052	0
DNTT	chr6	+	22,471,871	22,572,917	0
LEF1	chr4	+	39,199,281	39,280,607	0
C21H1orf187	chr21	-	5,834,625	5,846,629	0
B3GAT2	chr3	+	85,291,505	85,314,892	0
CD8B	chr4	-	89,093,479	89,098,571	0
FSTL1	chr1	+	83,186,280	83,229,153	0
SLC4A1	chr11	-	3,443,550	3,444,211	0
GTF2H4	chr17	+	2,231,043	2,269,366	0
ESR2	chr5	+	55,537,412	55,579,008	0
TMEM121	chr8	-	3,905,764	3,909,361	0
SGTB	chrZ	-	20,045,073	20,065,739	0
FKBP9	chr2	-	48,059,097	48,074,886	0
IL5RA	chr12	-	18,709,611	18,723,823	0
MBD3	chr28	+	1,954,899	1,970,483	0
HSDL1	chr11	+	2,477,126	2,484,035	0
CPM	chr1	-	37,186,036	37,217,594	0
GJC2	chr2	-	2,204,512	2,211,189	0
CTSO	chr4	-	21,969,334	21,976,936	0

ELMO3	chr11	+	995,085	1,003,876	0
SLCO1C1	chr1	+	67,294,363	67,315,601	0
IL18R1	chr1	+	138,124,785	138,139,652	0
PTH1R	chr2	+	3,487,991	3,596,980	0
ASZ1	chr1	+	26,455,464	26,490,434	0
PKNOX2	chr24	-	139,110	159,912	0
PRLHR2	chr5	-	909,020	910,077	0
FST	chrZ	+	15,391,895	15,398,098	0
LOC693258	chr1	+	53,067,285	53,068,004	0
FGF10	chrZ	-	13,389,594	13,393,980	0
TLR6_dup2	chr4	+	71,561,343	71,566,600	0
METTL22	chr14	-	10,348,924	10,377,128	0
SLIT2	chr4	-	77,708,527	77,974,936	0
MYH7B	chr20	-	2,584,792	2,613,111	0
SIPA1L1	chr5	-	29,139,943	29,210,239	0
ZDHHC8	chr15	+	1,328,701	1,411,144	0
MYOCD	chr18	-	755,983	789,459	0
ARHGAP8	chr1	+	72,015,047	72,092,410	0
AVPR2	chr1	-	30,281,578	30,283,773	0
NR0B1	chr1	+	119,395,075	119,397,112	0
MC2R	chr2	+	98,815,507	98,816,580	0
DUSP4	chr4	+	50,848,022	50,849,488	0
CYP1A1_dup1	chr10	-	1,806,681	1,809,495	0
IL1B	chr22	-	3,876,886	3,878,491	0
TSPAN15	chr6	+	12,016,787	12,028,759	0
VTG2	chr8	+	17,191,849	17,212,554	0
STON1	chr3	-	7,556,559	7,568,203	0
ESRP2	chr11	+	3,224,006	3,267,557	0
B3GNT2	chr3	+	8,984,689	8,996,504	0
LGSN	chr3	+	88,512,911	88,529,716	0
WWOX	chr11	+	15,431,673	15,950,034	0
DAZL	chr2	-	34,385,114	34,398,353	0
TBX18	chr3	+	79,961,977	79,983,214	0
BMPRI1A	chr6	+	3,546,263	3,585,603	0
OLFM4	chr1	-	169,834,840	169,859,044	0
DRD1	chr13	-	10,105,359	10,106,758	0
CRHR1	chr27	+	2,132,525	2,157,408	0
TP53I11	chr5	-	24,245,258	24,275,951	0
NPY6R	chr13	-	14,713,792	14,714,916	0
SH3GL2	chrZ	+	32,741,006	32,832,334	0
MYF5	chr1	+	41,887,465	41,888,684	0

LOC420716	chr2	+	44,006,745	44,016,344	0
IL17D	chr1	-	183,110,468	183,110,818	0
CFTR	chr1	-	26,351,868	26,435,794	0
WNT11	chr1	+	198,826,726	198,854,182	0
BDKRB1	chr5	+	48,856,221	48,857,297	0
ANKS1B	chr1	-	48,616,187	49,031,136	0
CD200	chr1	+	92,004,787	92,017,787	0
DRD4	chr5	-	522,522	530,408	0
ANGPT2	chr3	+	91,425,482	91,449,466	0
MME	chr9	-	24,629,271	24,664,612	0
FOXN4	chr15	-	6,844,360	6,868,887	0
TBX4	chr19	-	7,545,197	7,566,786	0
LEFTY2	chr3	-	18,288,982	18,292,218	0
NR2E1	chr3	-	70,136,117	70,146,734	0
RGR	chr6	-	3,996,226	4,009,959	0
RAP2B	chr18	-	4,049,584	4,050,721	0
CLEC3B	chr2	-	43,107,315	43,113,966	0
ALB	chr4	+	52,344,907	52,357,740	0
DBT	chr8	+	12,585,448	12,598,458	0
SMYD1	chr4	+	89,132,017	89,153,752	0
IL2	chr4	+	55,255,551	55,258,596	0
B4GALT7	chr13	-	10,194,874	10,196,143	0
NGEF	chr9	-	2,001,867	2,024,924	0
PCDH8	chr1	+	169,959,399	169,962,915	0
FGFR1	chr22	-	2,374,132	2,389,918	0
TAF1B	chr3	+	99,273,083	99,318,440	0
NPFRR2	chr4	+	51,919,422	51,933,528	0
ST8SIA2	chr10	+	16,196,088	16,220,722	0
B-LA	chr18	+	10,640,326	10,646,668	0
LOC770548	chrZ	-	41,827,149	41,840,524	0
KCTD7	chr19	+	4,989,014	4,995,784	0
SYT1	chr1	+	41,111,970	41,335,788	0
USP2	chr24	+	4,214,224	4,221,567	0
WNT9A	chr2	+	2,483,585	2,535,827	0
ARG2	chr5	+	31,160,786	31,177,777	0
CHRNA10_dup2	chr1	-	199,663,003	199,664,750	0
GCG	chr7	+	22,692,909	22,707,259	0
OPN4	chr6	+	3,339,623	3,362,569	0
PPP1R12B	chr26	-	662,970	683,066	0
ST8SIA6	chr2	+	19,666,198	19,699,118	0
PMCH	chr1	+	57,419,555	57,420,946	0

THRSP	chr1	+	197,836,616	197,838,038	0
GREM1	chr5	-	32,885,070	32,892,433	0
PVALB	chr14	-	1,038,897	1,043,785	0
CD72_dup2	chrZ	+	8,426,772	8,429,887	0
ATP5I	chrZ	+	52,365,086	52,366,954	0
NBEA	chr1	-	177,296,424	177,772,934	0
ZNF800	chr1	+	22,387,753	22,401,879	0
C1H12orf48	chr1	-	57,417,186	57,465,700	0
ARNTL2	chr1	+	70,297,389	70,333,506	0
ENPP2	chr2	-	142,057,818	142,117,291	0
PPARGC1A	chr4	+	76,629,533	76,695,702	0
TRH	chr12	+	20,356,533	20,361,089	0
OLFM1	chr17	+	8,291,312	8,309,504	0
ENTPD8	chr17	-	1,308,773	1,315,103	0
TNFSF11	chr1	+	170,785,843	170,805,727	0
DLX6	chr2	+	24,407,053	24,410,604	0
WISP1	chr2	+	147,605,421	147,640,602	0
JMJD7	chr5	+	27,300,436	27,306,929	0
DLK1	chr5	+	51,436,882	51,446,497	0
CRYAB	chr24	+	6,366,683	6,370,601	0
BASP1	chr2	-	76,998,659	76,999,486	0
DDAH1	chr8	+	16,977,807	16,990,456	0
IL3	chr13	+	17,245,232	17,250,126	0
LOC395095	chr25	-	1,028,053	1,028,469	0
COL14A1	chr2	+	142,375,665	142,507,966	0
F2RL1	chrZ	-	22,869,448	22,878,650	0
KIAA1274	chr6	+	12,604,477	12,619,586	0
ELAVL4	chr8	+	24,301,112	24,357,708	0
MASP2	chr21	-	4,073,739	4,087,159	0
MANSC1	chr1	-	74,144,657	74,150,842	0
ATP4B	chr1	+	141,527,050	141,532,760	0
ATP6V0D2	chr2	+	127,758,259	127,776,042	0
PTX3	chr9	-	24,281,401	24,286,374	0
CYP3A7	chr14	-	3,939,676	3,949,017	0
GRPR	chr1	-	125,139,798	125,161,235	0
IL8_dup2	chr4	+	52,446,739	52,449,903	0
CXCR5	chr24	+	5,716,658	5,717,838	0
BDNF	chr5	-	3,774,659	3,775,498	0
LOC431251_dup1	chr22	-	2,269,394	2,271,506	0
CNP1	chr1	+	80,085,194	80,086,911	0
TOX	chr2	-	116,029,382	116,236,062	0

TYRO3	chr5	+	27,083,312	27,124,132	0
AOX2P	chr7	+	12,298,760	12,341,341	0
SNTB1	chr2	-	142,564,785	142,692,122	0
CDH8	chr11	+	14,007,063	14,164,292	0
PCDHA1	chr13	-	621,963	775,133	0
KERA	chr1	-	45,851,123	45,859,598	0
TEAD1	chr5	-	8,689,001	8,828,999	0
TCTB	chr6	+	28,134,554	28,142,630	0
GAL8	chr3	-	110,240,053	110,242,722	0
MDK	chr5	-	25,801,826	25,802,506	0
FARP1	chr1	-	149,113,743	149,277,439	0
CACNA2D1	chr1	+	10,956,367	11,365,801	0
ADK	chr6	-	16,186,690	16,461,920	0
LEPREL1	chr9	+	15,075,015	15,128,734	0
CHRM5	chr5	-	32,380,524	32,382,110	0
RHCG	chr10	+	14,558,128	14,566,053	0
LOC418424	chr1	+	91,991,492	91,998,703	0
TRAIL-LIKE	chr4	-	9,669,318	9,672,980	0
CRH	chr2	-	119,337,753	119,338,746	0
PRRX1	chr8	-	4,978,270	5,010,772	0
PCDHAC2	chr13	-	621,963	664,913	0
COL6A1	chr7	+	6,711,897	6,734,653	0
ADCY5	chr7	-	28,535,221	28,732,276	0
SCNN1A	chr1	+	80,034,908	80,045,394	0
DAB1	chr8	-	26,623,165	26,711,757	0
LHCGR	chr3	+	7,517,756	7,537,096	0
PRPH2	chr3	-	24,194,929	24,204,445	0
SLC24A2	chrZ	-	33,575,074	33,680,163	0
CRY2	chr5	-	26,107,903	26,126,820	0
VIPR1	chr2	+	1,662,424	1,729,055	0
DLX5	chr2	-	24,415,562	24,417,819	0
IL8_dup1	chr4	+	52,434,109	52,437,188	0
EFNB1	chr4	-	998,872	1,015,623	0
CAMK4	chrZ	-	45,708,534	45,869,844	0
LOC395160	chr5	-	10,702,444	10,705,102	0
PDE6G	chr18	+	9,170,777	9,171,418	0
SDK2	chr18	-	9,042,699	9,067,560	0
CHN1	chr7	+	17,889,766	17,966,549	0
KCNG2	chr2	-	57,404,673	57,430,172	0
PRSS3	chr1	+	81,289,131	81,292,565	0
ODZ2	chr13	-	4,581,438	5,056,955	0

F2	chr5	-	25,587,956	25,597,861	0
SLC2A2	chr9	+	21,249,522	21,257,228	0
FTCD	chr7	-	6,786,522	6,793,354	0
GJB1	chr4	-	2,304,456	2,305,283	0
LMO4	chr8	-	16,428,692	16,442,421	0
IL5	chr13	-	17,472,321	17,483,539	0
IL13	chr13	+	17,528,677	17,530,347	0
SPHKAP	chr9	-	10,650,332	10,716,323	0
KCNT1	chr17	-	8,907,317	8,935,688	0
VMO1	chr1	+	185,051,415	185,055,405	0
GJB6	chr1	+	183,241,712	183,250,039	0
TBX20	chr2	+	47,288,007	47,320,789	0
LAMB4	chr1	-	15,903,739	15,956,526	0
IFT140	chr14	+	14,486,656	14,564,333	0
AHRR	chr2	-	91,291,773	91,357,658	0
STK32A	chr13	+	18,572,256	18,591,512	0
CMTM8	chr2	+	40,375,562	40,412,312	0
CD28	chr7	-	14,528,349	14,540,564	0
SOX18	chr20	+	9,374,602	9,375,442	0
CAV3	chr12	+	19,919,136	19,921,074	0
CACNA1B	chr17	+	2,509,605	2,763,633	0
PCDH15	chr6	+	7,396,968	7,696,220	0
LOC426385	chr3	+	108,471,725	108,478,791	0
HDX	chr4	+	8,996,604	9,034,897	0
EDNRB2	chr4	+	11,255,609	11,264,791	0
SLC35C1	chr5	-	26,127,657	26,132,018	0
SLC19A1	chr7	-	6,649,708	6,655,619	0
UGT8	chr4	-	57,812,083	57,837,114	0
SLC7A9	chr11	-	10,624,396	10,636,803	0
ARC	chr2	-	153,663,334	153,664,686	0
NKX6-2	chr6	-	37,274,456	37,276,571	0
IL22	chr1	-	36,974,029	36,976,482	0
SPRY3	chr4	+	11,125,289	11,126,179	0
SLC24A1	chr10	+	20,223,387	20,239,716	0
OTC	chr1	-	116,461,325	116,487,231	0
RLN3	chrZ	-	28,156,680	28,159,178	0
CD300L-S1	chr18	-	10,380,703	10,381,433	0
EGFR	chr2	-	51,962,135	52,111,376	0
PTPRO	chr1	+	64,927,901	65,076,426	0
PTCHD2	chr21	-	5,910,772	5,926,237	0
FMN1	chr5	+	32,737,310	32,859,037	0

CYP24A1	chr20	+	12,321,165	12,332,946	0
FZD10	chr15	-	3,445,651	3,447,893	0
FGB	chr4	+	21,391,920	21,398,059	0
RALYL	chr2	+	127,210,608	127,321,031	0
CER1	chrZ	-	31,404,227	31,405,322	0
FABP4	chr2	-	126,157,975	126,161,197	0
IL21	chr4	+	55,218,439	55,223,194	0
HNFA4	chr20	-	5,386,955	5,401,538	0
MYOM2	chr3	-	93,565,396	93,640,512	0
HSPG2	chr21	+	6,705,517	6,714,383	0
RTN1	chr5	+	57,245,010	57,342,339	0
F9	chr4	+	5,025,926	5,038,527	0
NPFPR1	chr6	-	12,592,594	12,596,127	0
NANOG	chr1	-	79,002,735	79,005,518	0
AGR3	chr2	-	28,600,422	28,607,233	0
MYL10	chr19	-	3,715,234	3,736,164	0
GABRA1	chr13	-	6,943,293	6,985,336	0
TRPM8	chr7	+	5,560,894	5,591,300	0
ROR2	chrZ	-	43,747,237	43,906,028	0
GRB10	chr2	-	83,128,775	83,233,991	0
ELOVL4	chr3	+	81,985,005	82,019,408	0
GABRE	chr4	+	10,924,798	10,951,617	0
ADH6	chr4	-	61,555,326	61,566,170	0
DKK3	chr5	+	9,085,495	9,108,292	0
DIO1	chr8	+	25,857,746	25,862,569	0
OR52R1	chr1	-	199,460,248	199,461,195	0
FGFBP2	chr4	+	79,507,017	79,508,866	0
ANG	chr6	-	10,376,968	10,378,404	0
INS	chr5	+	14,845,825	14,850,417	0
ODZ3	chr4	-	41,461,109	41,774,119	0
SLC15A1	chr1	+	149,017,041	149,041,062	0
CCKAR	chr4	+	75,629,864	75,636,710	0
BCHE	chr9	+	22,521,806	22,548,312	0
BMP4	chr5	-	61,149,771	61,153,269	0
OR8D4	chr5	+	126,671	127,669	0
HOXD8	chr7	-	17,401,999	17,404,374	0
PTPRZ1	chr1	-	24,687,424	24,821,140	0
NRCAM	chr1	+	30,434,172	30,496,674	0
ATP12A	chr24	-	2,886,072	2,903,664	0
CDH17	chr2	-	130,738,358	130,764,845	0
TSHR	chr5	+	43,202,356	43,250,961	0

BMP5	chr3	+	90,160,798	90,213,945	0
NFIB	chrZ	-	31,058,166	31,232,124	0
CRYAA	chr1	+	113,199,267	113,202,653	0
HTR7	chr6	-	20,682,868	20,705,248	0
CACNG4	chr18	-	7,250,794	7,286,076	0
CAV1	chr1	-	26,853,774	26,867,447	0
NPY	chr2	+	31,392,138	31,400,047	0
PRIMA1	chr5	-	47,729,350	47,773,300	0
ART4	chr1	+	49,921,700	49,926,293	0
CDH7	chr2	-	97,914,716	97,993,225	0
PCDHA2	chr13	-	621,963	775,133	0
SSX2IP	chr8	+	17,167,270	17,186,796	0
ACVR2B	chr2	-	5,662,067	5,680,476	0
AMY1A	chr8	-	11,738,273	11,744,575	0
BEST4	chr8	-	21,487,010	21,490,204	0
CHRNA3	chr10	+	4,563,691	4,569,508	0
LHX1	chr19	+	8,346,010	8,350,488	0
MALL	chr3	-	2,992,611	2,995,488	0
RNP	chr21	+	5,758,606	5,759,346	0
MYBPC3	chr5	+	25,127,048	25,184,562	0
CCDC80	chr1	+	86,865,488	86,889,078	0
LIFR	chrZ	-	11,395,951	11,438,221	0
EPHA4	chr9	-	8,685,668	8,776,445	0
NTRK2	chrZ	+	39,776,210	39,989,185	0
MBOAT2	chr3	-	98,813,584	98,904,285	0
NEFM	chr22	-	962,612	966,512	0
TMC1	chrZ	+	35,506,627	35,569,325	0
RAD52	chr1	-	62,663,189	62,675,446	0
GAS2	chr5	+	2,990,057	3,072,062	0
VSX1	chr3	-	16,974,235	16,977,265	0
ALDOB	chrZ	+	63,699,750	63,708,702	0
AVPR1A	chr1	-	35,132,311	35,135,463	0
NTF3	chr1	+	76,251,402	76,308,649	0
GAL2	chr3	+	110,256,126	110,258,630	0
ANPEP	chr10	-	22,175,309	22,177,412	0
OGCHI_dup2	chr17	-	5,428,814	5,429,563	0
ARVCF	chr15	-	1,065,939	1,191,278	0
GRIA2	chr4	+	22,493,150	22,582,154	0
NOVA1	chr5	-	35,197,915	35,327,547	0
PLN	chr3	-	65,579,056	65,584,190	0
SUPT3H	chr3	-	111,880,304	112,142,933	0

CASQ2	chr1	+	83,775,773	83,806,506	0
CHRM3	chr3	-	37,731,615	37,921,244	0
TBX6	chr15	+	8,490,757	8,501,676	0
PLD5	chr3	+	36,737,228	36,905,047	0
CHRNA5	chr9	+	16,706,036	16,709,227	0
NKX2-5	chr13	-	9,141,155	9,143,369	0
ELOVL2	chr2	+	64,290,232	64,329,039	0
OSTN	chr9	-	14,802,499	14,813,678	0
ASIP	chr20	-	1,554,843	1,581,567	0
IDUA	chrZ	-	52,416,974	52,464,826	0
GRM5	chr1	+	192,231,217	192,474,227	0
DNAL1	chr5	-	28,327,720	28,341,333	0
EPHB6	chr1	-	81,087,980	81,143,381	0
CDH10	chr2	+	73,523,999	73,621,549	0
CPNE8	chr1	+	16,636,820	16,758,258	0
PPARG	chr12	+	5,069,040	5,089,703	0
FIGF	chr1	+	125,472,478	125,503,664	0
CYP19A1	chr10	-	10,552,822	10,571,874	0
KRT15	chr27	-	4,195,252	4,199,678	0
GPM6B	chr1	+	126,252,311	126,356,974	0
IRX1	chr2	+	89,430,034	89,435,107	0
VSIG1	chr4	-	14,232,514	14,252,966	0
GPM6A	chr4	-	45,581,537	45,683,146	0
CATHL3	chr2	-	3,902,612	3,903,418	0
KK34	chr13	+	17,255,004	17,258,669	0
FSCN1	chr14	+	4,202,389	4,203,741	0
EPHA1	chr1	+	80,635,032	80,665,697	0
SLIT3	chr13	+	3,967,939	4,434,800	0
JAM2	chr1	+	105,955,446	105,989,107	0
IL2RA	chr1	-	3,285,068	3,301,375	0
LOC768251	chr8	-	11,734,769	11,736,107	0
FOXL2	chr9	-	6,759,890	6,761,019	0
ATOH7	chr6	-	11,641,835	11,642,345	0
MESP2_dup1	chr10	-	22,166,076	22,166,594	0
HSPB2	chr24	-	6,363,394	6,364,901	0
AMPH	chr2	-	49,245,233	49,353,284	0
PCDHA5	chr13	-	621,963	775,133	0
POU1F1	chr1	+	96,212,684	96,226,602	0
ADAM19	chr13	+	11,389,085	11,415,847	0
SLC17A9	chr20	+	8,429,334	8,444,285	0
MUSK	chrZ	+	65,272,460	65,322,353	0

BMPR1B	chr4	+	59,924,083	60,161,259	0
DMP1	chr4	-	47,126,504	47,128,807	0
TSPAN8	chr1	-	38,014,522	38,031,644	0
PAX5	chrZ	+	74,379,756	74,488,276	0
CNR1	chr3	+	78,900,801	78,906,231	0
CYP2H1	chr6	-	18,668,468	18,675,791	0
PCDHA7_dup1	chr13	-	621,963	728,785	0
P4HA2	chr13	-	17,268,961	17,297,063	0
TWF1	chr1	-	31,875,034	31,885,537	0
IKZF2	chr7	-	3,627,671	3,727,935	0
WNT8A	chr13	-	14,563,742	14,567,673	0
IL11RA	chrZ	+	7,805,781	7,829,580	0
COPN5L2	chr3	-	111,634,337	111,638,583	0
GIT1	chr19	-	6,020,364	6,021,578	0
GHSR	chr9	+	20,849,601	20,853,770	0
MYH1	chr18	-	352,394	611,284	0
SEMA3C	chr1	+	11,908,401	12,047,268	0
CDC42BPA	chr3	+	13,183,221	13,343,421	0
EPHA7	chr3	+	76,598,799	76,743,927	0
SLC16A9	chr6	+	10,260,320	10,275,212	0
AQP4	chr2	-	107,598,315	107,603,611	0
LAP3	chr4	-	78,865,514	78,880,037	0
IGSF1	chr20	+	22,577	25,635	0
MMP9	chr20	+	10,528,560	10,532,207	0
CCR8-L	chr2	-	42,718,918	42,720,051	0
SPP1	chr4	-	47,107,504	47,110,549	0
GJD2	chr5	+	34,633,413	34,635,060	0
SH3GL3	chr10	+	13,102,065	13,145,325	0
MUSTN1	chr12	-	806,374	809,638	0
TMC3	chr10	+	13,777,625	13,794,954	0
TRIM71	chr2	-	40,552,319	40,562,711	0
C2H3orf39	chr2	+	41,157,713	41,159,446	0
TP63	chr9	-	15,138,525	15,202,322	0
FGF14	chr1	+	147,184,980	147,572,060	0
NRN1	chr2	+	66,306,355	66,313,684	0
OPN5	chr3	+	112,922,113	112,945,367	0
WNT7A	chr12	-	6,244,431	6,277,634	0
AVPR1B	chr26	-	2,175,179	2,177,159	0
XIRP1	chr2	-	4,874,877	4,896,411	0
SALL4	chr20	+	13,146,806	13,155,039	0
FLT1	chr1	+	180,120,509	180,222,373	0

PDGFRA	chr4	-	67,270,550	67,295,073	0
EVC	chr4	+	82,118,411	82,170,325	0
PCDHA3	chr13	-	621,963	775,133	0
C6	chrZ	-	12,379,730	12,403,686	0
LARGE	chr1	+	54,793,761	54,990,691	0
CTGF	chr3	+	59,163,516	59,165,853	0
ENPP4	chr3	+	112,513,145	112,519,087	0
ST8SIA1	chr1	+	68,756,419	68,873,904	0
RGN	chr1	-	134,230,905	134,244,210	0
NEUROG1	chr13	+	15,707,661	15,708,865	0
APOB	chr3	-	105,109,112	105,146,028	0
AGRN	chr21	-	2,693,976	2,753,394	0
LOC396151	chr1	-	79,411,098	79,446,888	0
MET	chr1	-	26,718,630	26,804,814	0
EDNRA	chr4	+	33,032,155	33,062,197	0
C3AR1	chr1	+	68,964,175	68,967,471	0
SLC5A7	chr1	+	140,322,894	140,343,857	0
FUT8	chr5	-	24,711,231	24,756,207	0
SLC35G2	chr9	+	1,865,489	1,871,335	0
LOC396098	chr1	+	95,262,872	95,272,732	0
ART1	chr1	-	199,085,776	199,091,639	0
NPY7R	chr13	-	13,409,351	13,410,508	0
FSCN2	chr18	-	9,202,394	9,206,838	0
GRIN1	chr17	-	1,396,943	1,422,706	0
MYLK2	chr20	+	10,005,230	10,013,044	0
CDH2	chr2	-	107,949,716	108,063,355	0
TNNT3	chr5	-	15,112,245	15,146,407	0
KLHL14	chr2	-	109,750,378	109,810,748	0
IL21R	chr14	+	7,358,207	7,370,966	0
BRS3	chr4	+	4,332,640	4,336,938	0
IFITM5	chr5	+	1,620,244	1,621,813	0
TLX3	chr13	-	3,060,807	3,062,412	0
LAMA1	chr2	+	102,406,289	102,528,030	0
UGGT2	chr1	+	150,076,327	150,155,773	0
MMP16	chr2	-	128,395,307	128,576,249	0
PCDHA9	chr13	-	621,963	775,133	0
IL1RL1	chr1	+	138,087,258	138,115,414	0
PKD2	chr4	-	47,092,908	47,107,295	0
GLDC	chrZ	-	28,557,831	28,588,002	0
DCLK1	chr1	+	177,002,511	177,234,141	0
SYNPR	chr12	+	13,757,574	13,788,792	0

ZP2	chr14	-	15,777,545	15,785,327	0
AMIGO2	chr1	-	33,045,659	33,055,182	0
KAL1	chr1	+	129,616,326	129,753,011	0
FMO6P	chr8	-	4,952,118	4,960,174	0
HNF4beta	chr11	+	18,929,995	18,954,907	0
RGS17	chr3	-	51,528,119	51,595,597	0
SLC35A1	chr3	-	79,169,518	79,185,275	0
MSX1	chr4	+	81,774,811	81,777,300	0
LOC395926	chr26	+	1,229,704	1,232,833	0
MGP	chr1	+	49,904,636	49,909,869	0
HOXA7	chr2	-	32,570,323	32,572,160	0
TXLNB	chr3	+	55,908,535	55,945,501	0
EPHB2	chr21	-	6,152,871	6,250,764	0
IL17RD	chr12	-	8,786,336	8,825,173	0
AXIN2	chr18	+	7,624,732	7,645,904	0
CCDC104	chr3	+	129,666	147,257	0
LOC395824	chr8	-	22,337,292	22,347,424	0
GSTA	chr3	+	91,219,401	91,238,663	0
ZPD	chr11	+	516,649	521,247	0
RFC2	chr19	+	2,812,273	2,818,539	0
RELB	chrZ	-	64,567,072	64,579,447	0
HOXA13	chr2	-	32,621,246	32,621,873	0
GAL10	chr3	+	110,227,859	110,230,475	0
OTX2_dup1	chr5	+	58,372,338	58,372,966	0
CRYGS	chr9	-	5,375,304	5,379,102	0
LOC414835	chr2	+	131,066,517	131,109,919	0
ODZ1	chr4	+	15,414,755	15,646,471	0
ITGA9	chr2	-	48,770,434	48,992,328	0
ADAM22	chr2	+	20,808,363	20,916,892	0
SYPL1	chr1	-	15,174,477	15,180,696	0
CRDS2	chr5	+	28,142,765	28,153,166	0
CPA5	chr1	+	829,380	834,031	0
SCTR	chr7	+	29,949,419	29,963,087	0
CRYBA4	chr15	+	7,405,588	7,406,721	0
ADMP	chr28	-	881,340	881,979	0
PCDHA4	chr13	-	564,611	775,133	0
GAD1	chr7	-	19,662,322	19,687,471	0
PTCHD4	chr3	-	112,992,202	113,076,343	0
LOC396120	chrZ	+	51,644,958	51,707,866	0
LOC428961	chr6	-	21,106,093	21,107,470	0
PROC	chr9	+	2,222,312	2,231,023	0

APOVLDLII	chr1	-	86,530,329	86,533,255	0
TTR	chr2	+	109,301,406	109,308,867	0
ICOS	chr7	-	14,461,414	14,471,438	0
MYH3	chr18	-	384,632	632,507	0
AR	chr4	+	416,134	460,778	0
ERBB4	chr7	-	3,053,248	3,455,878	0
PHEX	chr1	-	122,345,891	122,438,410	0
ADCYAP1R1	chr2	+	1,268,392	1,369,982	0
HOXA3	chr8	+	12,749,704	12,751,191	0
AGTR1	chr9	+	13,475,625	13,496,603	0
AANAT	chr18	-	4,365,293	4,369,118	0
DRD2	chr24	+	5,874,352	5,879,422	0
CCK	chr2	-	43,849,710	43,854,383	0
ROS1	chr3	+	66,116,675	66,189,021	0
CDH13	chr11	+	17,690,483	18,177,684	0
PCDHA12_dup1	chr13	-	621,963	728,785	0
CDH4	chr20	+	7,212,913	7,627,205	0
GALNTL4	chr5	+	9,258,961	9,473,014	0
SATB2	chr7	-	11,851,930	11,975,540	0
PPP1R9B	chr7	+	19,043,230	19,069,585	0
CPA2	chr1	+	821,276	827,664	0
CD86	chr1	+	79,726,248	79,736,929	0
XKR9	chr2	+	121,410,394	121,418,141	0
GLP1R	chr3	-	30,518,671	30,598,577	0
TFAP2B	chr3	-	111,026,378	111,052,692	0
CDX4	chr4	+	12,198,898	12,208,037	0
CHRNA1	chr7	+	17,979,760	17,989,603	0
TNFSF15	chr17	-	2,943,950	2,959,452	0
ASL2	chr19	-	4,899,262	4,906,156	0
MID1	chr1	+	128,309,856	128,427,093	0
CHRN3	chrZ	-	52,500,394	52,510,307	0
SOSTDC1	chr2	-	28,409,774	28,413,555	0
ASL1	chr19	-	4,911,997	4,919,749	0
NIM1	chrZ	+	13,056,791	13,065,650	0
HSBP1L1	chr2	-	57,311,159	57,314,157	0
RAB23	chr3	+	89,542,575	89,551,340	0
GH	chr27	-	1,522,161	1,526,512	0
CTNNA3	chr6	+	7,763,393	8,204,278	0
PTGR2	chr5	-	28,244,413	28,258,662	0
TLL1	chr4	+	25,164,186	25,298,464	0
UNC5C	chr4	-	60,174,910	60,414,602	0

KCND2	chr1	-	25,310,273	25,579,182	0
RPE65	chr8	-	29,574,645	29,579,495	0
QRFPR	chr4	+	55,612,461	55,632,143	0
PCDHA6	chr13	-	621,963	775,133	0
MAP6	chr1	+	199,703,504	199,734,133	0
FSHR	chr3	+	7,353,248	7,430,911	0
RAG1	chr5	+	21,212,793	21,217,470	0
TLR2-2	chr4	+	21,113,342	21,115,936	0
SHH	chr2	-	8,024,867	8,034,924	0
BFSP2	chr2	+	42,621,658	42,637,063	0
CHRN4	chr10	+	4,545,867	4,557,516	0
LL	chr6	-	5,542,218	5,544,682	0
PCDHA8	chr13	-	621,963	775,133	0
COL5A1	chr17	+	8,143,956	8,242,793	0
PCDHA11	chr13	-	621,963	755,210	0
GRIA1	chr13	-	12,397,620	12,505,280	0
PCDHA7_dup2	chr13	-	736,149	775,133	0
PCDHA12_dup2	chr13	-	736,186	775,133	0
ABCB1	chr2	-	20,653,124	20,685,692	0
CNTN2	chr26	+	1,776,432	1,800,083	0
RGS6	chr5	-	28,861,699	29,088,640	0
SLC26A3	chr1	-	15,810,427	15,821,026	0
EPYC	chr1	-	45,805,847	45,828,423	0
CXCL14	chr13	+	15,684,189	15,691,454	0
GPER	chr14	+	2,361,755	2,364,582	0
VTN	chr19	-	5,609,345	5,614,133	0
CKMT2	chrZ	-	62,423,068	62,444,747	0
FGF13	chr4	-	4,765,422	4,977,976	0
SPP2	chr7	+	5,598,780	5,608,915	0
PDGFA	chr14	-	1,995,279	2,016,488	0
NPPB	chr21	+	5,763,169	5,765,788	0
LOC408038	chr25	-	1,187,986	1,189,572	0
SEMA3A	chr1	+	9,427,238	9,612,553	0
TGM4	chr2	-	43,175,396	43,185,867	0
TLR16_dup2	chr4	+	71,563,594	71,565,965	0
MLPH	chr7	-	4,760,204	4,777,914	0
NOX4	chr1	+	192,020,464	192,113,365	0
GCM2	chr2	+	64,359,442	64,364,492	0
GJA1	chr3	-	64,410,058	64,417,555	0
MINPP1	chr6	-	10,772,380	10,791,421	0
PAR6B	chr20	-	13,520,988	13,534,331	0

IAPP	chr1	+	67,422,578	67,426,304	0
PMP2	chr2	-	126,148,066	126,152,515	0
RBP4	chr6	+	21,493,044	21,498,204	0
LIX1	chrZ	+	50,443,148	50,470,019	0
MYH6	chr18	-	384,714	611,296	0
ZPAX	chr3	-	103,114,611	103,125,500	0
PAX2	chr6	-	18,179,336	18,258,551	0
CYP17A1	chr6	-	24,817,997	24,820,474	0
KRT19	chr27	-	4,202,596	4,207,238	0
MZT1	chr1	+	160,366,175	160,370,922	0
STMN2	chr2	+	125,412,754	125,446,134	0
LOC378902	chr5	+	14,153,165	14,159,407	0
CDD	chr19	+	181,980	183,772	0
KIAA1024	chr10	-	14,448,538	14,456,860	0
GNOT1	chr4	-	93,271,995	93,275,468	0
FCRL2	chr25	-	1,706,862	1,712,508	0
TSKU	chr1	-	198,370,509	198,385,013	0
IGFBP1	chr2	+	56,040,113	56,046,347	0
DEPDC7	chr5	+	5,786,132	5,794,435	0
PYGO1	chr10	+	9,051,761	9,059,688	0
CAMK2A	chr13	+	13,271,388	13,292,788	0
TSPAN18	chr5	+	24,178,758	24,236,609	0
PLLP	chr11	-	750,378	752,713	0
GCSH	chr11	-	17,029,995	17,039,195	0
NELL2	chr1	-	32,129,254	32,250,978	0
MAOA	chr1	-	114,866,376	114,910,104	0
SLC6A2	chr11	-	3,543,538	3,607,585	0
DEPDC1B	chrZ	-	18,218,434	18,238,277	0
CYP7A1	chr2	-	115,822,085	115,831,912	0
CD9	chr1	+	76,732,781	76,756,428	0
PRL	chr2	+	59,724,576	59,730,730	0
COLEC10	chr2	+	141,892,126	141,911,878	0
IL12B	chr13	+	7,916,531	7,925,309	0
WIF1	chr1	-	35,746,197	35,788,663	0
TGFB3	chr5	-	40,870,933	40,879,234	0
MC4R	chr2	-	70,267,038	70,268,033	0
NCALD	chr2	-	134,193,541	134,261,470	0
CITED2	chr3	+	55,890,959	55,892,417	0
IL17F	chr3	-	110,369,629	110,371,729	0
CTLA4	chr7	-	14,494,467	14,497,920	0
AP1S3	chr9	-	9,332,581	9,348,334	0

CYP1A1_dup2	chr10	+	1,822,774	1,824,958	0
CD72_dup1	chrZ	-	8,422,983	8,425,424	0
EGF	chr4	-	59,593,971	59,646,098	0
CDH19	chr2	+	97,601,184	97,659,460	0
GRIA3	chr4	-	15,868,385	16,009,119	0
CYP1A4	chr10	+	1,822,773	1,826,204	0
POP4	chr11	+	9,002,232	9,004,845	0
OXTR	chr12	-	19,923,361	19,926,252	0
LECT2	chr13	+	15,543,059	15,547,914	0
ELOVL7	chrZ	-	18,241,724	18,252,966	0
ETV1	chr2	-	27,268,791	27,332,861	0
ATP1B4	chr4	-	16,570,193	16,577,357	0
CRTAM	chr24	-	3,159,075	3,171,541	0
KCND3	chr26	-	3,124,817	3,214,381	0
RORB	chrZ	+	36,092,235	36,226,099	0
NPVF	chr2	-	31,731,797	31,735,364	0
TPD52L1	chr3	-	62,542,675	62,584,800	0
cor7a	chr10	+	109,320	110,291	0
SSTR5	chr14	-	5,640,745	5,641,824	0
FUT7	chr17	+	838,136	839,179	0
BICC1	chr6	-	1,755,769	1,852,005	0
LOC417800	chr1	+	32,320,114	32,323,985	0
C1H12orf32	chr1	-	78,760,759	78,764,941	0
CD38	chr4	-	79,543,247	79,564,958	0
MPPED2	chr5	-	4,652,087	4,746,173	0
LOC415713	chr11	-	3,398,251	3,413,435	0
BEAN1	chr11	-	12,353,008	12,395,560	0
KCNA2	chr26	-	1,265,725	1,267,989	0
FUT4	chr1	-	189,893,301	189,894,356	0
IL6	chr2	+	30,893,617	30,896,305	0
MTNR1A	chr4	-	63,442,645	63,492,251	0
WNT2B	chr26	+	3,320,810	3,331,480	0
WNT3	chr27	+	1,097,512	1,119,374	0
HOXB3	chr27	+	3,615,199	3,617,447	0
PLCZ1	chr1	-	66,341,653	66,385,981	0
MBP	chr2	+	92,901,806	92,919,561	0
RUNX1T1	chr2	-	129,794,089	129,883,550	0
DLL1	chr3	+	42,712,669	42,719,729	0
PTH	chr5	+	8,468,130	8,472,198	0
CYP2C18	chr6	-	18,655,325	18,664,396	0
PNAT10	chr11	+	17,503,003	17,507,517	0

LGI2	chr4	+	76,058,727	76,079,114	0
MTPP	chr4	+	61,628,642	61,673,771	0
ALDH1A2	chr10	+	8,081,716	8,137,462	0
CCR6	chr3	-	44,325,500	44,326,680	0
WNT10A	chr7	-	23,942,411	23,952,798	0
CFC1B	chrZ	-	41,910,326	41,914,991	0
NLGN4X	chr1	+	130,904,688	131,025,946	0
CPA6	chr2	-	119,845,180	119,932,138	0
ICOSLG	chr1	-	113,897,698	113,911,725	0
NPY1R	chr4	-	24,462,147	24,463,425	0
TLR16_dup1	chr4	+	71,553,831	71,555,080	0
ALX4	chr5	-	23,812,602	23,839,873	0
BDKRB2	chr5	+	48,848,958	48,850,103	0
HOXD13	chr7	-	17,437,102	17,439,672	0
GPR151	chr14	-	15,202,136	15,206,380	0
CDK3	chr18	-	4,565,637	4,570,074	0
RBP3	chr6	-	19,065,266	19,079,720	0
SYT13	chr5	-	24,410,419	24,423,752	0
TNNI3K	chr8	+	30,370,450	30,413,156	0
CRHR2	chr2	+	4,118,255	4,213,198	0
PI15	chr2	+	123,175,660	123,198,020	0
PGA	chr5	-	346,128	352,857	0
LHX3	chr17	+	8,735,542	8,741,059	0
GUCA2A	chr21	+	6,029,926	6,034,822	0
ST8SIA5	chrZ	+	1,625,848	1,658,619	0
AOX1	chr7	+	12,258,383	12,294,638	0
CNTNAP5	chr7	-	25,970,551	26,227,278	0
SEMA3E	chr1	+	10,137,709	10,290,778	0
VIT	chr3	-	33,394,432	33,436,950	0
DBC1	chr17	-	4,541,117	4,624,685	0
CHRM2	chr1	-	59,887,754	59,889,154	0
GTF3A	chr1	-	180,557,797	180,562,206	0
TNFRSF19	chr1	-	181,788,510	181,829,082	0
FABP5	chr2	+	126,080,812	126,085,870	0
GEM	chr2	-	130,786,045	130,793,743	0
GFRA4	chr4	-	92,872,932	92,940,953	0
GABRG2	chr13	-	6,808,844	6,851,434	0
GHRHR	chr27	-	1,566,923	1,573,625	0
IRX2	chr2	-	88,921,543	88,925,629	0
CYP2C45_dup1	chr6	+	17,648,419	17,654,233	0
KRT222	chr27	-	4,153,995	4,159,597	0

MDGA1	chr3	+	31,210,013	31,298,271	0
CTNNA2	chr4	-	90,616,390	91,075,785	0
TFEC	chr1	+	27,082,338	27,509,244	0
PAH	chr1	+	57,119,389	57,156,204	0
SMAD9	chr1	+	176,679,640	176,700,537	0
MMP27	chr1	+	186,808,449	186,815,916	0
SPAG6	chr2	-	17,617,010	17,649,527	0
GC	chr4	-	51,903,676	51,909,490	0
MAF	chr11	-	15,949,093	16,144,054	0
GABRA6	chr13	-	7,033,966	7,056,187	0
GDF5	chr20	+	1,226,547	1,229,597	0
GUCA1A	chr26	-	3,006,742	3,011,817	0
PTPRS	chr28	+	4,202,647	4,289,715	0
HGF	chr1	+	11,443,009	11,513,810	0
KITLG	chr1	-	44,855,820	44,909,340	0
PROKR2	chr3	-	11,319,105	11,326,250	0
GDF2	chr6	-	19,091,529	19,094,749	0
LMX1A	chr8	+	5,364,291	5,386,515	0
P2RX4	chr15	+	5,476,617	5,482,563	0
ARSH	chr1	+	132,545,116	132,558,435	0
RGS7	chr3	+	37,173,236	37,435,316	0
ME1	chr3	+	80,492,248	80,649,031	0
GCM1	chr3	+	91,112,648	91,124,918	0
NSG1	chr4	+	81,539,401	81,560,656	0
SLC17A6	chr5	+	2,823,817	2,853,269	0
DDX4	chrZ	+	16,270,672	16,296,823	0
COL9A1	chr3	+	85,586,668	85,653,626	0
RARB	chr2	+	37,509,076	37,831,404	0
PAX6	chr5	-	5,255,555	5,272,960	0
SLC47A2	chr19	-	6,798,819	6,804,842	0
CRTAC1	chr6	+	23,699,775	23,709,858	0
SLC9A4	chr1	+	138,163,437	138,207,449	0
CLDN1	chr9	+	15,032,109	15,042,590	0
PIWIL1	chr15	-	3,361,196	3,377,877	0
MIR1604	chr1	+	312,691	312,787	0
MIR1651	chr1	+	556,211	556,294	0
CPA1	chr1	+	834,915	838,679	0
CALML3	chr1	-	1,007,094	1,007,543	0
MIR205B	chr1	-	1,147,520	1,147,617	0
MIR29B-1	chr1	+	3,235,312	3,235,392	0
MIR1460	chr1	-	7,266,960	7,267,058	0

MIR1645	chr1	-	25,165,359	25,165,422	0
MIR1695	chr1	+	28,529,937	28,530,015	0
LYZ	chr1	+	37,298,048	37,301,735	0
DCN	chr1	-	45,901,761	45,943,552	0
MIR1691	chr1	+	48,126,457	48,126,547	0
MIR135A-2	chr1	+	48,192,659	48,192,758	0
OC3	chr1	+	49,913,469	49,919,391	0
HIST2H2AC_dup1	chr1	-	50,012,001	50,012,390	0
MIR1581	chr1	+	51,158,137	51,158,222	0
PVALB	chr1	+	53,604,472	53,613,774	0
MIR1742	chr1	+	53,732,443	53,732,525	0
MB	chr1	+	54,036,383	54,040,088	0
MIR490	chr1	-	59,948,701	59,948,793	0
MIR1593	chr1	+	61,691,788	61,691,877	0
WNT5B	chr1	+	63,037,405	63,053,051	0
AKR1B10	chr1	-	64,610,739	64,618,852	0
MIR1727-1_dup1	chr1	+	73,750,825	73,750,930	0
MIR1727-2_dup1	chr1	+	73,750,825	73,750,930	0
MIR1727-1_dup2	chr1	+	73,752,485	73,752,590	0
MIR1727-2_dup2	chr1	+	73,752,485	73,752,590	0
MIR3539	chr1	+	84,091,756	84,091,826	0
MIR1690	chr1	+	87,161,021	87,161,124	0
MIR1806	chr1	-	97,200,876	97,200,960	0
ERG	chr1	-	111,025,203	111,090,947	0
MIR1397	chr1	+	130,934,884	130,934,988	0
SHOX	chr1	-	133,843,667	133,851,753	0
MIR1805	chr1	-	135,141,607	135,141,690	0
MIR1656	chr1	+	137,743,231	137,743,296	0
EDAR	chr1	-	140,700,011	140,726,053	0
MIR1700	chr1	+	140,966,218	140,966,317	0
MIR1632	chr1	+	144,114,537	144,114,627	0
EFNB2	chr1	+	145,254,089	145,295,056	0
MIR1555	chr1	-	149,148,336	149,148,421	0
MIR1743	chr1	+	160,786,664	160,786,766	0
MAB21L1	chr1	+	177,444,762	177,445,994	0
MIR1646	chr1	-	179,480,925	179,481,018	0
FGF9	chr1	-	182,656,287	182,687,605	0
MIR1709	chr1	+	185,296,332	185,296,413	0
MMP7	chr1	+	186,865,326	186,869,667	0
MIR1657	chr1	+	192,585,867	192,585,960	0
MIR1664	chr1	-	194,622,059	194,622,155	0

MADPRT	chr1	+	199,097,429	199,098,565	0
MIR1600	chr1	+	199,256,187	199,256,266	0
CCKBR	chr1	-	199,323,533	199,325,913	0
MIR1749	chr2	+	475,530	475,627	0
AQP1	chr2	+	990,641	1,007,803	0
GHRHR	chr2	+	1,041,920	1,060,062	0
MIR1662	chr2	+	1,721,334	1,721,406	0
MIR1639	chr2	-	3,173,520	3,173,591	0
MIR1706	chr2	-	3,751,023	3,751,096	0
MIR153	chr2	-	8,765,687	8,765,773	0
MIR466	chr2	+	21,671,961	21,672,029	0
HSPE1	chr2	-	22,440,843	22,440,964	0
MIR489	chr2	-	23,068,877	23,068,960	0
HOXA6	chr2	-	32,562,059	32,563,594	0
MIR1732	chr2	-	32,584,271	32,584,371	0
THRB_dup1	chr2	+	37,250,922	37,251,469	0
MIR1723	chr2	-	41,377,973	41,378,078	0
XCR1	chr2	+	42,746,061	42,747,068	0
MIR1607	chr2	+	45,452,355	45,452,433	0
ID4	chr2	-	60,841,774	60,843,459	0
MIR1759	chr2	-	63,666,692	63,666,766	0
MIR1782	chr2	+	69,711,200	69,711,298	0
CDH6	chr2	-	70,478,952	70,593,706	0
MIR1766-1	chr2	+	77,319,215	77,319,307	0
MIR1766-2	chr2	+	77,321,253	77,321,345	0
MIR757-1	chr2	-	78,310,844	78,310,925	0
MIR1613-1_dup1	chr2	+	79,848,153	79,848,229	0
MIR1613-2_dup1	chr2	+	79,848,153	79,848,229	0
MIR1613-1_dup2	chr2	+	79,850,282	79,850,358	0
MIR1613-2_dup2	chr2	+	79,850,282	79,850,358	0
MIR187	chr2	+	85,892,470	85,892,555	0
MIR32	chr2	-	86,506,451	86,506,520	0
MIR1803	chr2	+	94,915,366	94,915,454	0
MIR1681	chr2	-	96,361,604	96,361,703	0
MIR133A-1	chr2	-	105,670,357	105,670,443	0
MIR1A-2	chr2	-	105,673,483	105,673,567	0
MIR1597	chr2	-	106,946,894	106,946,964	0
MIR1557	chr2	+	116,867,241	116,867,310	0
MIR124A	chr2	+	118,524,157	118,524,252	0
MIR1714	chr2	+	118,527,168	118,527,243	0
MIR1569-1_dup1	chr2	-	121,223,340	121,223,409	0

MIR1569-2_dup1	chr2	-	121,223,340	121,223,409	0
MIR1569-1_dup2	chr2	-	121,225,097	121,225,166	0
MIR1569-2_dup2	chr2	-	121,225,097	121,225,166	0
MIR1796	chr2	+	122,244,446	122,244,515	0
TRHR	chr2	+	137,806,650	137,827,318	0
MIR1467	chr2	-	141,373,919	141,374,028	0
TNFRSF11B	chr2	-	141,817,105	141,836,944	0
MIR217	chr3	-	280,139	280,245	0
MIR216	chr3	-	282,807	282,912	0
MIR216B	chr3	-	288,214	288,302	0
MIR1792	chr3	+	7,712,006	7,712,104	0
MIR1641	chr3	-	14,173,147	14,173,241	0
SNAP25	chr3	-	14,552,656	14,582,272	0
MIR1756B	chr3	-	15,591,886	15,591,974	0
BMP2	chr3	-	16,010,636	16,013,577	0
SLC22A7	chr3	+	16,899,350	16,913,606	0
MIR194	chr3	+	19,924,487	19,924,561	0
MIR215	chr3	+	19,924,793	19,924,897	0
MIR1649	chr3	+	23,001,998	23,002,095	0
SIX2	chr3	-	27,086,838	27,087,162	0
MIR1784	chr3	+	36,895,820	36,895,922	0
MIR1660	chr3	-	60,428,131	60,428,184	0
MIR199B	chr3	+	65,613,516	65,613,581	0
POPDC3	chr3	+	71,491,799	71,496,138	0
FUT9	chr3	-	75,597,295	75,598,374	0
MIR1677	chr3	+	76,659,763	76,659,835	0
MIR1712	chr3	-	81,937,337	81,937,409	0
MIR1329	chr3	+	99,798,387	99,798,481	0
FKBP1B	chr3	+	107,079,620	107,126,235	0
PNOC	chr3	-	108,461,944	108,465,331	0
GAL13	chr3	-	110,195,466	110,200,074	0
GAL11	chr3	-	110,208,402	110,209,559	0
GAL1	chr3	-	110,260,055	110,262,499	0
DEFB1	chr3	-	110,264,668	110,267,211	0
GAL5	chr3	-	110,270,044	110,271,447	0
GAL4	chr3	-	110,273,739	110,276,282	0
MIR133B	chr3	-	110,384,935	110,385,016	0
MIR206	chr3	-	110,390,439	110,390,514	0
PLP1	chr4	-	1,976,272	1,978,976	0
MIR460B	chr4	+	2,687,396	2,687,485	0
TNMD	chr4	-	5,206,028	5,213,822	0

MIR1462	chr4	-	8,572,345	8,572,454	0
MIR1728	chr4	-	11,023,002	11,023,097	0
MIR1790	chr4	-	11,666,887	11,666,991	0
MIR1573	chr4	-	12,563,649	12,563,721	0
FGF16	chr4	+	12,887,028	12,897,432	0
MIR1606	chr4	-	13,536,589	13,536,657	0
MIR1757	chr4	-	16,712,627	16,712,731	0
FGG	chr4	-	21,416,207	21,421,311	0
NPY2R	chr4	+	21,626,205	21,627,362	0
MIR1575	chr4	-	30,660,577	30,660,680	0
MIR1627	chr4	+	40,379,665	40,379,734	0
MIR1776	chr4	+	45,051,725	45,051,825	0
SPATA4	chr4	-	45,783,932	45,790,676	0
MIR1730	chr4	+	49,672,436	49,672,528	0
MIR1751	chr4	+	51,588,988	51,589,077	0
MIR1679	chr4	-	52,619,171	52,619,258	0
FGF2	chr4	-	55,114,992	55,139,718	0
FABP2	chr4	+	56,264,388	56,266,833	0
MIR302B	chr4	+	58,651,314	58,651,385	0
MIR302C	chr4	+	58,651,576	58,651,640	0
MIR1811	chr4	+	58,651,698	58,651,778	0
MIR302A	chr4	+	58,651,879	58,651,945	0
MIR302D	chr4	+	58,652,214	58,652,282	0
MIR367	chr4	+	58,652,350	58,652,422	0
MIR1814	chr4	+	61,722,590	61,722,663	0
MIR1605	chr4	-	64,895,966	64,896,053	0
MIR383	chr4	+	65,844,695	65,844,767	0
UCHL1	chr4	-	70,548,410	70,552,633	0
MIR218-1	chr4	-	77,774,698	77,774,806	0
LDB2	chr4	+	79,102,123	79,318,311	0
MIR1602	chr4	+	79,189,648	79,189,738	0
ATOH8	chr4	+	88,543,439	88,551,679	0
GNB1	chr4	+	88,608,377	88,633,213	0
CD8A_dup2	chr4	-	88,991,618	88,995,625	0
HTR7	chr4	-	92,298,399	92,307,726	0
MIR1684	chr4	-	92,587,438	92,587,539	0
MIR1654-1	chr4	+	92,718,271	92,718,364	0
CNOT2	chr4	-	93,283,421	93,285,603	0
cor4	chr5	+	151,544	152,482	0
SCT	chr5	+	539,413	542,190	0
COR4	chr5	-	1,046,923	1,047,861	0

COR1	chr5	+	1,064,267	1,065,223	0
cor6	chr5	-	1,404,947	1,405,885	0
CSRP3	chr5	-	1,723,547	1,733,528	0
MIR1775	chr5	+	2,488,503	2,488,591	0
MIR1760	chr5	+	3,878,870	3,878,962	0
WT1	chr5	-	5,499,297	5,530,736	0
MIR1663	chr5	+	16,920,987	16,921,088	0
MIR1802	chr5	-	18,252,173	18,252,252	0
FGF4	chr5	-	18,774,767	18,778,346	0
FGF3	chr5	-	18,804,842	18,809,980	0
MIR1725	chr5	-	25,027,902	25,027,970	0
MIR1710	chr5	+	30,170,145	30,170,224	0
MEIS2	chr5	+	33,556,733	33,721,734	0
MIR1718	chr5	-	33,777,662	33,777,741	0
MIR3532	chr5	-	35,319,907	35,319,990	0
MIR1566	chr5	-	40,282,495	40,282,575	0
MIR1799	chr5	+	42,365,934	42,366,017	0
MIR1800	chr5	+	47,604,931	47,605,006	0
GSC	chr5	-	48,185,200	48,186,500	0
MIR203	chr5	+	53,206,814	53,206,911	0
MIR1771	chr5	-	54,133,078	54,133,163	0
MIR1638	chr5	+	58,712,377	58,712,463	0
TBPL2	chr5	+	58,752,875	58,760,330	0
MIR1676	chr5	-	58,997,736	58,997,835	0
MIR1716	chr5	-	60,283,968	60,284,072	0
MIR1703	chr5	-	60,576,033	60,576,121	0
MIR1579	chr6	+	3,677,284	3,677,350	0
TMEM26	chr6	+	9,630,849	9,645,280	0
BKJ	chr6	+	10,356,291	10,369,903	0
RSFR	chr6	-	10,385,807	10,386,982	0
PCBD1	chr6	-	12,696,495	12,699,023	0
MIR1590	chr6	-	13,488,312	13,488,410	0
DUPD1	chr6	+	16,040,601	16,060,108	0
CYP2C45_dup2	chr6	+	17,658,059	17,660,909	0
CYP26A1	chr6	-	21,717,030	21,719,652	0
MIR202	chr6	+	22,813,068	22,813,156	0
TLX1	chr6	-	24,462,474	24,465,802	0
HMX3	chr6	+	33,072,775	33,073,884	0
MIR1726	chr6	-	34,084,308	34,084,404	0
DPYSL4	chr6	+	36,879,517	36,883,700	0
MSTN	chr7	+	199,294	204,786	0

MIR1812	chr7	-	1,263,807	1,263,894	0
PRLH	chr7	-	4,757,615	4,758,550	0
LOC396419	chr7	+	5,180,824	5,181,055	0
MIR1694	chr7	-	5,419,755	5,419,852	0
MIR1845	chr7	-	6,562,728	6,562,813	0
MIR1603	chr7	-	11,205,574	11,205,660	0
MIR1659	chr7	-	14,764,187	14,764,287	0
MIR1713	chr7	-	17,384,289	17,384,387	0
MIR10B	chr7	-	17,389,048	17,389,157	0
HOXD11	chr7	-	17,425,058	17,426,044	0
MIR1570	chr7	+	17,931,020	17,931,119	0
MIR1733	chr7	-	20,421,062	20,421,145	0
MIR1591	chr7	-	20,783,298	20,783,375	0
MNR2	chr7	+	23,876,551	23,878,036	0
MIR1582	chr7	+	25,245,058	25,245,146	0
MIR1599	chr7	+	25,926,968	25,927,019	0
MIR3530	chr7	+	26,820,146	26,820,234	0
MIR1C	chr7	+	36,625,855	36,625,928	0
STAM2_dup1	chr7	+	37,029,687	37,030,107	0
MIR1801	chr8	-	3,838,453	3,838,555	0
MIR1721	chr8	-	5,165,871	5,165,944	0
MIR1633	chr8	-	5,554,872	5,554,966	0
MIR1618	chr8	+	7,759,515	7,759,593	0
MIR1655	chr8	+	7,813,654	7,813,756	0
MIR1610	chr8	-	12,398,260	12,398,347	0
MIR1589	chr8	-	17,168,146	17,168,224	0
MIR1620	chr8	+	19,191,144	19,191,231	0
MIR1665	chr8	+	20,445,135	20,445,212	0
MIR1595	chr8	-	21,475,759	21,475,823	0
MIR1809	chr8	-	23,417,849	23,417,956	0
MIR1675	chr8	-	25,397,767	25,397,866	0
DMRTB1	chr8	+	25,619,991	25,625,011	0
MIR1630	chr9	+	1,883,593	1,883,648	0
RN5S_dup1	chr9	+	1,892,357	1,892,476	0
RN5S_dup2	chr9	+	1,895,060	1,895,179	0
RN5S_dup3	chr9	+	1,897,240	1,897,359	0
MIR1704	chr9	+	5,933,148	5,933,218	0
MIR1608	chr9	+	6,277,070	6,277,162	0
MIR1577	chr9	+	6,500,392	6,500,476	0
MIR1741	chr9	+	8,226,405	8,226,477	0
MIR1762	chr9	-	14,978,306	14,978,403	0

SST	chr9	+	15,910,976	15,911,496	0
TNFSF10	chr9	+	20,835,853	20,843,107	0
MIR551	chr9	-	21,966,405	21,966,517	0
IL12A	chr9	-	23,817,146	23,818,935	0
MIR1658	chr9	-	24,500,772	24,500,861	0
MIR1793	chr9	-	25,115,521	25,115,617	0
MIR1670	chr10	-	222,478	222,537	0
MIR1688	chr10	-	742,918	742,988	0
LOC415324	chr10	-	763,837	765,957	0
MIR1623	chr10	+	1,395,848	1,395,943	0
MIR2128	chr10	-	1,811,806	1,811,869	0
MIR190	chr10	-	5,209,724	5,209,808	0
MIR1574	chr10	+	6,651,001	6,651,074	0
FGF7	chr10	+	12,161,437	12,193,064	0
BCL2A1	chr10	+	14,334,535	14,336,550	0
MIR1720	chr10	-	14,823,390	14,823,454	0
MIR7-2	chr10	-	14,823,525	14,823,623	0
MIR3529	chr10	+	14,823,529	14,823,619	0
NR2F2	chr10	+	17,662,393	17,662,669	0
MIR1680	chr10	+	17,701,564	17,701,652	0
MIR1813-2	chr10	+	18,568,987	18,569,060	0
MIR1722	chr10	-	20,000,338	20,000,429	0
MIR1642	chr10	+	21,236,745	21,236,818	0
MESP2_dup3	chr10	+	22,173,616	22,174,155	0
CKMT1A	chr10	-	22,299,085	22,307,261	0
MIR1789	chr11	+	9,553,017	9,553,079	0
MIR1791	chr11	+	9,633,722	9,633,806	0
NAT	chr11	+	17,494,829	17,499,267	0
MIR1699	chr11	-	21,458,750	21,458,846	0
MIR1678	chr12	-	2,390,252	2,390,337	0
MIR135A-1	chr12	-	2,830,742	2,830,829	0
SNTN	chr12	+	13,793,228	13,795,152	0
MIR1711	chr12	-	17,010,140	17,010,207	0
MIR1702	chr13	+	1,828,160	1,828,243	0
FGF18	chr13	-	2,952,328	3,016,649	0
MIR218-2	chr13	+	4,322,860	4,322,954	0
HAND1	chr13	+	12,203,949	12,204,061	0
CSF2	chr13	+	17,234,340	17,237,014	0
MIR1609-1_dup1	chr13	+	17,399,772	17,399,865	0
MIR1609-2_dup1	chr13	+	17,399,772	17,399,865	0
MIR1609-1_dup2	chr13	+	17,401,478	17,401,571	0

MIR1609-2_dup2	chr13	+	17,401,478	17,401,571	0
IL4	chr13	+	17,534,726	17,536,462	0
GDF9	chr13	+	17,650,094	17,652,799	0
MIR1576	chr13	+	18,532,632	18,532,726	0
PLA2G10	chr14	-	833,721	844,072	0
TNFRSF13B	chr14	-	4,669,866	4,672,999	0
MIR1682	chr14	+	4,937,108	4,937,180	0
MIR1554	chr14	+	5,817,641	5,817,719	0
CACNG3	chr14	+	6,777,922	6,791,771	0
DNASE1	chr14	-	12,969,952	12,975,758	0
MIR1588	chr14	-	14,876,163	14,876,264	0
MIR1636	chr15	+	4,729,959	4,730,046	0
MIR1671	chr15	+	5,095,750	5,095,809	0
MIR762	chr15	-	5,760,038	5,760,116	0
MIR1625	chr15	-	7,810,092	7,810,171	0
PLA2G1B	chr15	+	9,632,899	9,634,552	0
CYP21A2	chr16	-	28,262	29,196	0
MIR1707	chr17	+	2,228,319	2,228,414	0
MIR2964	chr17	-	5,577,814	5,577,902	0
MIR219	chr17	+	5,577,817	5,577,901	0
MIR1753-1	chr17	+	6,548,914	6,548,992	0
ALC	chr17	-	10,778,875	10,780,068	0
CYGB	chr18	+	4,333,044	4,340,687	0
MIR1561	chr18	+	6,413,289	6,413,373	0
MIR1672	chr18	-	8,798,785	8,798,860	0
MIR1652	chr18	-	9,615,233	9,615,328	0
MIR1637	chr18	-	10,216,005	10,216,069	0
MIR1580	chr18	-	10,554,160	10,554,232	0
GGCL1	chr19	+	355,105	356,043	0
CCL4_dup1	chr19	-	366,643	367,507	0
CCL5	chr19	-	379,525	380,689	0
MIR1567	chr19	-	1,690,727	1,690,815	0
MIR1354	chr19	-	1,776,157	1,776,232	0
MIR1587	chr19	-	1,782,806	1,782,901	0
CCL1	chr19	+	4,761,751	4,762,968	0
ADORA2B	chr19	+	6,380,471	6,389,175	0
MIR1585	chr19	-	8,800,028	8,800,118	0
MIR1592	chr19	-	9,339,013	9,339,079	0
MIR499	chr20	-	2,599,334	2,599,424	0
MIR1614	chr20	+	4,894,122	4,894,203	0
GHRH	chr20	-	5,000,462	5,007,633	0

MIR1A-1	chr20	+	8,107,831	8,107,901	0
MIR1773	chr20	+	8,109,136	8,109,213	0
MIR1746	chr20	-	8,632,244	8,632,343	0
MIR124A-2	chr20	+	8,681,782	8,681,879	0
MIR1798	chr20	-	9,654,914	9,655,009	0
TENP	chr20	-	10,247,698	10,252,184	0
MIR1619	chr20	-	12,664,073	12,664,164	0
MIR1687	chr20	+	13,129,454	13,129,544	0
MIR1635	chr21	-	1,720,026	1,720,132	0
MIR429	chr21	-	2,580,812	2,580,895	0
MIR200A	chr21	-	2,583,317	2,583,403	0
MIR200B	chr21	-	2,585,642	2,585,726	0
PAX7	chr21	+	4,432,725	4,518,485	0
PLA2G2E	chr21	-	4,893,243	4,894,810	0
C21H1orf158	chr21	-	5,385,188	5,388,547	0
TGFA	chr22	-	2,901,857	2,903,363	0
MIR3531	chr23	-	417,154	417,240	0
MIR124B	chr23	+	2,510,331	2,510,423	0
MIR1724	chr23	+	3,067,920	3,068,021	0
MIR1B	chr23	+	4,663,912	4,663,975	0
MIR133C	chr23	+	4,664,051	4,664,129	0
MIR1780	chr23	-	5,325,254	5,325,329	0
NTM	chr24	+	1,893,356	2,143,176	0
MIR1601	chr24	+	2,043,673	2,043,749	0
OPCML	chr24	-	2,150,971	2,164,932	0
MIR1807	chr24	+	3,207,751	3,207,840	0
MIR1466	chr24	+	4,209,057	4,209,166	0
MIR1745-1_dup2	chr24	-	5,273,293	5,273,379	0
MIR1745-2_dup2	chr24	-	5,273,293	5,273,379	0
MIR1667	chr24	-	5,433,864	5,433,950	0
LOC429492	chr25	+	1,095,732	1,096,028	0
F-KER	chr25	+	1,098,603	1,099,722	0
LOC431324	chr25	+	1,105,874	1,106,170	0
MIR1629	chr25	+	1,490,876	1,490,968	0
MIR1752	chr25	+	1,568,659	1,568,740	0
CLPS	chr26	-	91,619	92,166	0
ADORA1	chr26	+	974,224	991,244	0
LOC395100	chr26	-	1,073,551	1,080,033	0
MIR135A-3	chr26	-	1,925,942	1,926,037	0
MIR1797	chr26	-	2,086,591	2,086,691	0
IL10	chr26	-	2,373,246	2,375,480	0

MIR205A	chr26	+	2,896,047	2,896,142	0
MIR1669	chr26	+	3,455,234	3,455,324	0
TSHB	chr26	+	3,809,806	3,812,700	0
OPTC	chr26	+	4,990,766	4,993,729	0
GIP	chr27	+	3,444,186	3,451,841	0
MIR196-1	chr27	+	3,553,097	3,553,191	0
MIR1735	chr27	+	3,899,720	3,899,798	0
RND2	chr27	+	4,765,747	4,779,182	0
MIR1777	chr28	+	2,555,498	2,555,592	0
MIR1621	chr28	+	2,706,112	2,706,182	0
MIR9-1	chr28	+	2,709,362	2,709,449	0
PAPD7	chr2_random	+	51,204	53,430	0
DCTN1	chr4_random	-	174,242	179,122	0
MIR147-1	chr10_random	-	11,894	11,963	0
POU4F3	chr13_random	+	8,533	9,573	0
Y-Lec1	chr16_random	+	136,131	211,969	0
B-LA	chr16_random	-	138,442	138,699	0
B-G	chr16_random	+	142,219	154,963	0
MTHFD2	chr22_random	+	5,798	14,310	0
TACR1	chr22_random	+	116,236	130,977	0
NCAPH	chr22_random	+	145,254	151,188	0
NEUROD4	chrE22C19W28_E50C23	-	472,633	473,744	0
KRT75_dup2	chrE22C19W28_E50C23	+	664,327	668,529	0
KRTAP10-4	chr25_random	-	51,762	52,986	0
MIR1774	chr28_random	-	3,195	3,273	0
HSD11B1L	chr28_random	+	30,539	36,017	0
NCLN	chr28_random	-	77,301	85,617	0
PIT54	chrE64_random	-	113,564	120,203	0
CHIR-B3	chrUn_random	+	176,647	177,127	0
FOXN4	chrUn_random	-	205,290	206,291	0
TCIRG1	chrUn_random	+	317,581	318,660	0
HOXB4_dup1	chrUn_random	-	372,993	377,019	0
MIR10A	chrUn_random	-	379,304	379,377	0
MIR1457	chrUn_random	-	419,967	420,053	0
MYO1A	chrUn_random	-	482,441	616,490	0
GALNT6_dup1	chrUn_random	+	930,471	932,735	0
CELA1	chrUn_random	+	934,340	938,649	0
CIRBP	chrUn_random	-	968,595	972,258	0
PSMD2	chrUn_random	-	1,911,461	1,912,273	0
CHIR-B5_dup1	chrUn_random	-	1,921,705	1,922,040	0
LBX3	chrUn_random	+	2,035,326	2,035,860	0

CHMP2A	chrUn_random	+	2,559,028	2,561,758	0
SCX	chrUn_random	-	2,999,616	3,000,005	0
ADPRH	chrUn_random	-	3,291,134	3,292,348	0
DNAJB14_dup1	chrUn_random	-	3,410,525	3,411,440	0
NFIC	chrUn_random	-	3,622,478	3,623,012	0
PRKAB2	chrUn_random	-	4,312,528	4,314,287	0
PRKAG1	chrUn_random	+	5,489,101	5,492,045	0
GTSE1_dup1	chrUn_random	+	5,614,599	5,623,447	0
CHIR-B5_dup2	chrUn_random	+	5,637,545	5,637,839	0
CDK5RAP3	chrUn_random	+	5,910,999	5,913,273	0
NFE2L1	chrUn_random	+	5,917,855	5,925,495	0
LMO2	chrUn_random	-	6,448,668	6,455,405	0
PTGER2	chrUn_random	+	6,602,152	6,602,390	0
IDH2	chrUn_random	+	6,667,486	6,670,428	0
PLL_P_dup1	chrUn_random	-	6,786,099	6,977,312	0
PRPF19_dup1	chrUn_random	+	7,010,822	7,011,643	0
ZP1_dup1	chrUn_random	-	7,013,694	7,014,522	0
GNAI3	chrUn_random	-	7,126,036	7,132,907	0
CLDN3	chrUn_random	-	7,657,806	7,658,974	0
SNRNP200_dup1	chrUn_random	-	8,424,909	8,440,465	0
SLC4A1	chrUn_random	-	8,759,592	8,764,747	0
YRK	chrUn_random	+	8,949,562	8,951,006	0
CHRD	chrUn_random	+	9,017,692	9,019,927	0
ATP5B	chrUn_random	-	9,509,749	9,510,580	0
MIR1552	chrUn_random	-	9,521,375	9,521,457	0
HK2	chrUn_random	+	10,828,735	10,842,671	0
SEPW1	chrUn_random	+	10,970,514	10,970,791	0
GTSE1_dup2	chrUn_random	+	11,120,642	11,122,088	0
DLX3_dup1	chrUn_random	+	11,131,916	11,132,480	0
SERINC2	chrUn_random	+	11,762,531	11,763,112	0
ANPEP_dup1	chrUn_random	-	11,788,901	11,790,072	0
NDUFC2	chrUn_random	-	11,820,006	11,820,736	0
MIR122-2	chrUn_random	-	12,066,796	12,066,872	0
PCDHGA2_dup1	chrUn_random	+	12,307,784	12,416,340	0
PCK2_dup1	chrUn_random	+	12,315,762	12,324,931	0
NCAPH_dup1	chrUn_random	+	12,791,356	12,796,448	0
LMF2	chrUn_random	-	13,099,422	13,100,246	0
GNAT1	chrUn_random	+	13,257,942	13,258,699	0
GNAI2	chrUn_random	-	13,261,065	13,266,963	0
BIN2	chrUn_random	-	13,913,375	13,913,776	0
RARA	chrUn_random	+	14,253,897	14,254,304	0

DOK3	chrUn_random	+	14,445,395	14,446,110	0
MIR146C-1	chrUn_random	+	14,731,534	14,731,662	0
MTCH2	chrUn_random	+	14,925,240	14,926,385	0
FTSJ3	chrUn_random	+	15,583,868	15,584,939	0
PCDHGA2_dup2	chrUn_random	+	15,873,319	15,874,325	0
PCK2_dup2	chrUn_random	-	15,875,720	15,876,372	0
PLL2_dup2	chrUn_random	-	15,906,207	15,906,846	0
ARPC1B	chrUn_random	-	16,411,682	16,413,391	0
VAMP7	chrUn_random	-	16,536,775	16,537,808	0
ISLR2	chrUn_random	-	16,929,624	16,930,454	0
LOC693257	chrUn_random	-	17,005,848	17,006,497	0
CHAT1_dup1	chrUn_random	+	17,095,915	17,096,169	0
CXCR2	chrUn_random	-	17,433,792	17,434,561	0
CRP	chrUn_random	-	17,526,584	17,527,100	0
FOXD2	chrUn_random	-	17,802,916	18,557,504	0
DNAJB14_dup2	chrUn_random	-	18,322,175	18,323,619	0
TMOD4	chrUn_random	-	18,471,766	18,472,541	0
FOXD3	chrUn_random	-	18,557,186	18,557,669	0
C3	chrUn_random	-	18,863,182	18,881,232	0
IRF5	chrUn_random	+	19,690,743	19,694,138	0
DPF2	chrUn_random	+	19,890,680	19,892,912	0
MRPL45	chrUn_random	-	20,021,426	20,021,998	0
ANPEP_dup2	chrUn_random	-	20,218,411	20,219,390	0
CIP1	chrUn_random	-	20,415,661	20,416,182	0
LOC772096	chrUn_random	+	20,427,549	20,428,182	0
ACTB	chrUn_random	+	20,438,261	20,439,143	0
MIR3533	chrUn_random	+	20,438,961	20,439,044	0
TNNC2	chrUn_random	+	20,732,110	20,732,980	0
PPIA_dup1	chrUn_random	-	21,112,177	21,112,565	0
CCDC81_dup1	chrUn_random	+	21,678,760	21,683,988	0
PPIA_dup2	chrUn_random	+	21,847,044	21,847,237	0
CNTF	chrUn_random	-	22,518,211	22,519,662	0
TSC22D3	chrUn_random	+	23,123,077	23,124,011	0
RAD9A	chrUn_random	+	23,154,091	23,155,741	0
MARS	chrUn_random	+	23,235,472	23,236,276	0
MMP9	chrUn_random	+	23,244,477	23,244,980	0
CHRN2	chrUn_random	-	23,340,725	23,341,293	0
PELO	chrUn_random	-	23,438,777	23,441,290	0
C6H10orf2	chrUn_random	-	23,563,794	23,564,754	0
MARCKS	chrUn_random	-	23,880,744	23,881,380	0
MIR757-1	chrUn_random	-	24,327,424	24,327,505	0

HAGH	chrUn_random	+	25,015,500	25,015,709	0
NCAPH_dup2	chrUn_random	-	25,031,207	25,036,826	0
LOC425113_dup1	chrUn_random	+	25,407,157	25,477,455	0
GPR37	chrUn_random	+	25,490,964	25,491,586	0
CHIR-AB3	chrUn_random	+	25,500,932	25,502,864	0
FOXMI	chrUn_random	+	26,351,946	26,353,712	0
NCAN	chrUn_random	+	26,548,968	26,556,035	0
DNASE1	chrUn_random	+	26,620,940	26,623,176	0
ESF1	chrUn_random	+	26,661,513	26,666,130	0
MIR1654-1	chrUn_random	+	26,716,756	26,716,849	0
ADRBK1	chrUn_random	-	27,605,781	27,611,657	0
MIR196-3	chrUn_random	-	27,776,456	27,776,563	0
BRD4	chrUn_random	-	28,111,572	28,112,681	0
SLC27A1	chrUn_random	-	28,114,128	28,121,701	0
TRMU	chrUn_random	-	28,856,527	28,868,166	0
SLC11A2	chrUn_random	-	28,890,644	28,893,077	0
THRA_dup1	chrUn_random	-	29,435,449	29,438,614	0
MED24	chrUn_random	+	29,439,426	29,456,766	0
PSMD3	chrUn_random	-	29,461,886	29,465,500	0
GSDMA	chrUn_random	-	29,465,958	29,470,728	0
ZBP2	chrUn_random	-	29,488,800	29,494,217	0
IKZF3	chrUn_random	+	29,499,779	29,521,584	0
ERBB2	chrUn_random	-	29,523,662	29,529,367	0
OASL	chrUn_random	+	29,792,247	29,794,335	0
FBXL12	chrUn_random	+	30,261,702	30,262,663	0
FAM125A	chrUn_random	-	30,292,041	30,296,727	0
DSN1	chrUn_random	-	30,298,465	30,302,870	0
LPAR2	chrUn_random	-	30,316,912	30,318,262	0
VDR	chrUn_random	-	31,433,320	31,462,533	0
COL2A1	chrUn_random	-	31,472,525	31,478,827	0
PFKM	chrUn_random	+	31,501,907	31,515,898	0
ASB8	chrUn_random	-	31,516,141	31,519,142	0
ANKRA2	chrUn_random	-	31,620,987	31,628,010	0
UTP15	chrUn_random	+	31,628,123	31,639,030	0
DCTN2	chrUn_random	-	32,349,482	32,349,960	0
MIR3534	chrUn_random	-	32,350,014	32,350,095	0
LOC425534_dup1	chrUn_random	+	33,420,888	33,518,004	0
CHIR-B2_dup1	chrUn_random	+	33,515,419	33,517,103	0
MFAP1	chrUn_random	-	33,580,711	33,581,977	0
NR1I3	chrUn_random	+	35,148,840	35,152,203	0
KLHL20	chrUn_random	+	35,285,407	35,286,155	0

CENPL	chrUn_random	-	35,287,292	35,288,196	0
FAM214A	chrUn_random	+	36,154,531	36,155,594	0
ARPP19	chrUn_random	+	36,157,763	36,158,001	0
CD69	chrUn_random	+	36,186,503	36,187,658	0
SMAD7B	chrUn_random	+	37,181,834	37,184,369	0
SEMA3F	chrUn_random	+	37,251,822	37,262,425	0
TEAD4	chrUn_random	-	37,780,759	37,781,363	0
HNRPK	chrUn_random	+	38,144,125	38,164,862	0
MIR7B	chrUn_random	+	38,163,821	38,163,930	0
SGTA	chrUn_random	-	38,260,894	38,269,485	0
MIR2130	chrUn_random	+	38,326,364	38,326,428	0
SUPT5H	chrUn_random	-	38,509,491	38,517,414	0
ACTN4	chrUn_random	-	38,543,184	38,550,527	0
PFKFB4	chrUn_random	+	38,656,374	38,660,287	0
NDNL2	chrUn_random	-	38,659,046	38,659,797	0
MEF2D	chrUn_random	+	39,432,610	39,436,343	0
ANKRD52	chrUn_random	-	40,245,936	40,261,826	0
ZP1_dup2	chrUn_random	+	40,471,978	40,473,296	0
PRPF19_dup2	chrUn_random	-	40,475,023	40,476,504	0
DHFR	chrUn_random	+	40,656,814	40,674,169	0
SARNP	chrUn_random	-	40,815,588	40,836,834	0
ORMDL2	chrUn_random	+	40,838,034	40,840,316	0
TUBB	chrUn_random	-	41,252,653	41,253,904	0
MBD2	chrUn_random	-	41,557,442	41,557,622	0
FZD2	chrUn_random	-	42,059,627	42,061,237	0
DAPP1	chrUn_random	+	42,119,806	42,121,412	0
SP1	chrUn_random	-	42,169,891	42,170,325	0
NOP56	chrUn_random	+	42,525,364	42,529,417	0
IDH3B	chrUn_random	-	42,531,010	42,538,446	0
TALDO1	chrUn_random	+	42,824,332	42,826,600	0
TLR16	chrUn_random	+	43,919,064	43,920,313	0
MIR3538-1	chrUn_random	-	44,040,736	44,040,810	0
LOC425113_dup2	chrUn_random	-	44,215,006	44,818,482	0
CHIR-AB1	chrUn_random	-	44,217,473	44,818,452	0
DOHH	chrUn_random	-	44,461,239	44,468,276	0
CDH1-A	chrUn_random	+	44,477,942	44,482,767	0
FZR1	chrUn_random	+	44,477,942	44,485,261	0
LOC426385	chrUn_random	+	44,546,300	44,546,857	0
CHAT1_dup2	chrUn_random	-	45,215,608	45,217,275	0
USF1	chrUn_random	-	45,281,595	45,286,459	0
CIR1	chrUn_random	+	45,648,401	45,654,565	0

ACTG2	chrUn_random	+	46,095,518	46,097,035	0
SOX18	chrUn_random	+	46,223,881	46,224,163	0
CHIR-B2_dup2	chrUn_random	-	46,355,427	46,356,875	0
LOC425534_dup2	chrUn_random	-	46,355,427	46,356,908	0
CHIR-A2_dup1	chrUn_random	-	46,625,149	46,626,060	0
TMEM101	chrUn_random	+	46,817,867	46,821,214	0
TAP1	chrUn_random	-	47,329,624	47,332,440	0
TIMMDC1	chrUn_random	-	47,403,023	47,410,226	0
POGLUT1	chrUn_random	-	47,411,044	47,421,813	0
OPN1LW	chrUn_random	-	48,544,375	48,544,710	0
BRD8	chrUn_random	+	48,790,861	48,795,619	0
DLX3_dup2	chrUn_random	+	48,995,413	48,995,608	0
PDHX	chrUn_random	+	49,002,019	49,019,252	0
CCDC81_dup2	chrUn_random	+	49,890,991	49,918,360	0
MIR1753-1	chrUn_random	+	50,031,798	50,031,876	0
CBX1	chrUn_random	+	50,256,202	50,259,307	0
QDPR	chrUn_random	-	50,831,734	50,832,514	0
FOXA2	chrUn_random	-	51,622,967	51,624,232	0
MIR1634	chrUn_random	-	51,902,066	51,902,158	0
RBL2	chrUn_random	-	51,974,678	51,984,765	0
ERBB3	chrUn_random	-	53,383,714	53,391,142	0
NIPBL	chrUn_random	-	55,408,411	55,419,324	0
HOXC8	chrUn_random	-	55,989,694	55,990,116	0
DDA1	chrUn_random	-	56,371,638	56,379,609	0
NDUFV1	chrUn_random	-	57,190,858	57,191,291	0
GALNT6_dup2	chrUn_random	-	57,643,239	57,652,163	0
CHIR-B5_dup3	chrUn_random	-	58,246,588	58,975,460	0
ECE1	chrUn_random	-	58,305,878	58,309,242	0
TFCP2	chrUn_random	-	58,848,517	58,857,993	0
PQLC2	chrUn_random	-	59,438,646	59,440,008	0
SNRNP200_dup2	chrUn_random	-	59,559,777	59,570,023	0
THRA_dup2	chrUn_random	+	59,800,915	59,804,393	0
PAN2	chrUn_random	-	59,912,012	59,921,223	0
CASP14	chrUn_random	+	60,206,804	60,209,974	0
PSMA5	chrUn_random	-	60,239,486	60,245,670	0
PNPLA6	chrUn_random	+	60,649,955	60,661,866	0
S100A6	chrUn_random	+	60,925,970	60,926,167	0
OLIG3	chrUn_random	+	61,044,251	61,044,558	0
IHH	chrUn_random	-	61,160,170	61,163,563	0
GNA11	chrUn_random	+	61,465,148	61,471,798	0
GRK1	chrUn_random	-	62,406,499	62,408,218	0

ARF5	chrUn_random	+	62,656,714	62,656,840	0
JAK3	chrUn_random	-	62,942,606	62,946,604	0
CHIR-A2_dup2	chrUn_random	+	63,034,581	63,035,777	0
CHAT2	chrUn_random	+	63,085,771	63,087,427	0
SARS	chrUn_random	+	63,141,255	63,145,004	0
HOXB4_dup2	chrUn_random	-	63,311,445	63,312,149	0
TREML2	chrUn_random	-	63,814,440	63,815,428	0
TREM-B2V2	chrUn_random	-	63,815,090	63,815,428	0
CHIR-B4	chrUn_random	-	63,827,657	63,829,571	0
CANX	chrUn_random	-	63,853,521	63,854,633	0
GADD45B	chrUn_random	+	63,869,375	63,869,638	0
AKAP8L_dup1	chrW_random	+	1,437	2,499	0
AKAP8L_dup2	chrW_random	+	41,199	49,231	0
SPINW	chrW_random	+	109,492	154,214	0
NIPBL	chrW_random	-	233,926	338,456	0
HINTW	chrW_random	-	581,337	584,838	0
MIR1594	chrZ	+	75,709	75,799	0
MIR122-1	chrZ	+	649,337	649,413	0
SLC45A2	chrZ	-	9,705,134	9,719,945	0
MIR1631	chrZ	+	15,789,429	15,789,502	0
MIR449	chrZ	-	16,040,613	16,040,698	0
MIR449C	chrZ	-	16,041,927	16,041,998	0
MIR1584	chrZ	+	18,238,506	18,238,570	0
MIR101	chrZ	+	28,037,874	28,037,952	0
MIR1779	chrZ	-	32,054,387	32,054,478	0
MIR1556	chrZ	+	34,315,854	34,315,939	0
MIR1416	chrZ	+	34,596,479	34,596,567	0
MIR27B	chrZ	+	41,157,642	41,157,738	0
EFNA5	chrZ	+	47,402,951	47,438,366	0
MIR9-2	chrZ	+	59,286,315	59,286,401	0
MIR1756A	chrZ	-	61,446,154	61,446,243	0
MIR1583	chrZ	-	68,835,650	68,835,747	0
MIR31	chrZ	-	71,882,171	71,882,264	0
CDKN2B	chrZ	-	72,007,551	72,011,966	0
LOX	chrZ	-	73,603,985	73,609,994	0

Appendix 3: Sense and antisense transcript reads for the 1095 genes from the galGal3 RefSeq database belonging to the first 20th-percentile

Gene	Chr	Strand	Sense reads/gene	Antisense reads/gene	Antisense / sense %
HBAA	chr14	+	593,842	5,169	0.9%
HBM	chr14	+	330,154	1,912	0.6%
MIR3528	chr17	+	52,128	42	0.1%
HBG2	chr1	+	336,371	3,280	1.0%
MIR1563	chr12	+	41,973	162	0.4%
MIR3538-2	chr1	?	22,135	11	0.0%
MIR3535	chr9	-	20,324	199	1.0%
MIR1434	chr28	+	6,411	288	4.5%
MIR3536	chr25	+	6,280	84	1.3%
MIR193B	chr14	+	5,849	9	0.1%
MIR451	chr19	-	4,196	24	0.6%
MIR2188	chr22	-	8,526	13	0.2%
CA2	chr2	+	68,630	769	1.1%
FTH1	chr5	-	32,628	200	0.6%
MIR3540	chr10	+	2,205	18	0.8%
RPS3A	chr4	+	14,781	42	0.3%
HSPA2	chr5	-	35,805	267	0.7%
SAT1	chr1	-	14,714	160	1.1%
HBE1	chr1	+	6,320	107	1.7%
ITM2A	chr4	-	23,975	187	0.8%
IFRD1	chr1	-	22,347	200	0.9%
TPT1	chr1	-	8,287	97	1.2%
NCOA4	chr6	+	33,430	321	1.0%
RHAG	chr3	+	14,871	143	1.0%
EIF5	chr5	+	17,249	142	0.8%
BNIP3L	chr22	-	32,134	325	1.0%
ISG12-2	chr2	+	3,553	29	0.8%
SPTAN1	chr17	+	50,646	471	0.9%
BF2_dup2	chr16	-	5,003	51	1.0%
MIR92	chr1	-	120	0	0.0%
HSP90AA1	chr5	-	8,765	89	1.0%
MIR1454	chr3	-	642	5	0.8%
MIRLET7G	chr12	-	195	1	0.3%
SKP1	chr13	+	9,728	126	1.3%
EEF1A1	chr3	+	9,636	76	0.8%
IFI27L2	chr23	+	2,240	25	1.1%

TUBB1	chr20	-	17,568	150	0.9%
HNRNPH1	chr13	+	13,154	99	0.8%
NT5C3	chr2	+	8,916	97	1.1%
SLC38A2	chr1	-	28,349	289	1.0%
NFE2L2	chr7	+	12,993	184	1.4%
BTG1	chr1	-	8,092	62	0.8%
BF1	chr16	-	3,917	40	1.0%
DDX3X	chr1	-	23,181	232	1.0%
WBP4	chr1	+	23,334	331	1.4%
PNRC1	chr3	-	8,620	103	1.2%
SGK1	chr3	+	10,993	138	1.3%
H3F3C	chr3	-	1,266	11	0.8%
IRF1	chr13	-	8,171	78	0.9%
LOC422090	chr18	+	3,347	63	1.9%
TFRC	chr9	+	9,381	74	0.8%
UBE2D3	chr4	-	7,933	80	1.0%
ATF4	chr1	-	5,821	88	1.5%
PPP1CB	chr3	-	4,550	34	0.7%
FXR1	chr9	-	10,358	93	0.9%
EPAS1	chr3	+	8,996	93	1.0%
SRSF5	chr5	-	6,054	87	1.4%
MCL1	chr25	+	4,908	35	0.7%
TXN	chrZ	-	2,232	18	0.8%
H3F3C	chr18	+	3,620	48	1.3%
PHOSPHO1	chr27	+	3,239	25	0.8%
MIR3526	chr3	+	365	7	1.8%
B-G_dup1	chr16	+	2,549	53	2.1%
MXI1	chr6	+	7,229	64	0.9%
VIM	chr2	-	4,408	27	0.6%
RDX	chr1	+	5,791	71	1.2%
CTSD	chr5	+	4,118	37	0.9%
TAL1	chr8	-	4,475	41	0.9%
RPS8	chr8	+	2,100	16	0.8%
BRD2	chr16	-	5,853	42	0.7%
CYB5A	chr2	+	4,312	45	1.0%
ITPK1	chr5	-	20,117	199	1.0%
HSP25	chr27	+	2,326	26	1.1%
RPLP1	chr2	+	1,170	16	1.3%
PSAP	chr6	-	10,556	80	0.8%
EPB41	chr23	+	7,859	80	1.0%
MIR181A-1	chr8	+	285	0	0.0%

MIR1783	chr12	+	261	0	0.0%
TRNAU1AP	chr2	-	3,477	31	0.9%
TCP11L2	chr1	-	5,538	73	1.3%
LAPTM4A	chr3	-	2,252	11	0.5%
RPSA	chr2	-	2,738	18	0.6%
KPNA4	chr9	+	8,639	107	1.2%
OAZ1	chr28	-	2,057	22	1.0%
MIR15B	chr9	-	132	0	0.0%
RPS4X	chr4	+	1,482	12	0.8%
RPL11	chr23	+	1,143	7	0.6%
SBNO1	chr15	+	13,028	156	1.2%
EEF2	chr28	+	7,267	48	0.7%
HSPA8	chr24	+	4,924	32	0.6%
TXNRD1	chr1	-	7,999	94	1.2%
MBNL1	chr9	-	9,191	92	1.0%
RPL39	chr4	+	848	6	0.7%
ITGB1BP3	chr10	-	2,380	27	1.1%
MIR103-2	chr4	-	206	0	0.0%
TMEM183A	chr26	-	3,650	29	0.8%
MORC3	chr1	+	10,617	140	1.3%
BSG	chr28	+	3,890	46	1.2%
PCMTD1	chr2	-	7,938	72	0.9%
B-G_dup2	chr16	-	3,701	60	1.6%
TACC3	chr4	-	6,203	71	1.1%
MIR30C-1	chr23	+	205	0	0.0%
EIF1	chr27	+	2,531	33	1.3%
RPLP0	chr15	+	1,601	11	0.7%
C26H6orf106	chr26	+	9,465	98	1.0%
EIF4A2	chr9	+	3,747	31	0.8%
ITPKA	chr5	+	4,363	52	1.2%
SYNM	chr10	+	16,735	203	1.2%
SLC6A6	chr12	+	4,781	55	1.2%
MIR365-1	chr14	+	177	7	3.7%
C4BPA_dup2	chr26	+	3,378	34	1.0%
KIAA1191	chr13	+	5,327	44	0.8%
RPL4	chr10	-	2,794	19	0.7%
MIR1661	chr2	-	113	3	2.7%
LAMP1_dup2	chr1	-	3,128	29	0.9%
UBE2H	chr1	-	4,824	57	1.2%
RPS27A	chr3	+	904	9	0.9%
DDX5	chr18	-	5,008	58	1.1%

HNRNPAB	chr13	-	2,473	30	1.2%
MYOD1	chr5	+	2,344	21	0.9%
MIR1787	chr12	+	158	5	3.2%
ACTB	chrUn_random	+	1,200	12	1.0%
MIR140	chr11	+	156	0	0.0%
RPS3	chr1	-	1,430	6	0.4%
ARIH1	chr10	+	3,346	37	1.1%
XBP1	chr15	-	2,822	12	0.4%
TRIM59	chr9	+	5,405	54	1.0%
ADA	chr20	+	4,279	39	0.9%
H1FO	chr1	-	10,002	104	1.0%
TMSB4X	chr1	-	354	3	0.8%
BF2_dup1	chr16	-	842	12	1.4%
HEBP1	chr1	-	4,693	38	0.8%
DNAJB9	chr1	-	5,320	48	0.9%
HERC2	chr1	+	23,227	223	1.0%
EIF3E	chr2	-	2,373	21	0.9%
RPL37A	chr7	-	439	7	1.6%
YME1L1	chr2	-	6,037	72	1.2%
CSDA	chr1	+	2,022	28	1.4%
JAK2	chrZ	+	5,265	44	0.8%
EDF1	chr17	+	1,499	17	1.1%
RPL19	chr27	+	977	6	0.6%
MIRLET7F	chr12	-	135	1	0.4%
LPIN2	chr2	+	4,064	48	1.2%
MIR181A-2	chr17	+	146	0	0.0%
TBX22	chr4	+	299	2	0.5%
YY1	chr5	+	2,575	38	1.5%
HBP1	chr1	+	2,390	20	0.8%
TCF12	chr10	-	6,011	61	1.0%
GHITM	chr6	-	2,618	18	0.7%
PNPLA2	chr5	-	2,264	20	0.9%
BIRC2	chr1	-	6,531	62	0.9%
NFS1	chr20	+	4,290	63	1.5%
TRIM27_dup1	chr16	+	2,435	24	1.0%
IL15	chr4	+	1,108	17	1.5%
TLX3	chrZ	+	420	2	0.5%
LOC768701	chr15	+	4,473	55	1.2%
MIR22	chr19	-	41	1	1.2%
MIR1571	chr11	+	139	0	0.0%
ITM2B	chr1	+	1,067	10	0.9%

GSTA3_dup1	chr3	+	1,118	19	1.7%
CISH	chr12	-	1,702	15	0.9%
SOD1	chr1	+	890	10	1.1%
FOS	chr5	+	1,252	11	0.9%
RPL13	chr11	+	903	5	0.5%
HAGH	chrUn_random	+	1,317	6	0.5%
MST4	chr4	+	3,885	58	1.5%
ADAL	chr10	+	2,169	31	1.4%
TUBB2C	chr17	-	2,104	23	1.1%
RPL22	chr21	+	509	9	1.8%
API5_dup1	chr5	+	1,131	8	0.7%
17.5	chr1	+	1,082	10	0.9%
CD93	chr3	+	2,975	26	0.9%
HAGHL	chr14	-	3,315	27	0.8%
TMEM184B	chr1	+	4,497	38	0.8%
MIR147-1	chr10	+	84	2	1.8%
MIR144	chr19	-	100	2	1.5%
EIF4G2	chr5	+	4,962	58	1.2%
MXD1	chr22	+	4,477	56	1.3%
SRSF1	chr19	+	3,117	49	1.6%
MIR16C	chr4	-	37	0	0.0%
NUCB2	chr5	+	2,369	28	1.2%
MIR16-1	chr1	-	92	0	0.0%
OSTC	chr4	-	1,276	14	1.1%
RPS15	chr28	+	537	1	0.2%
RPL5	chr8	-	1,194	9	0.8%
ARGLU1	chr1	+	1,999	34	1.7%
CD69	chrUn_random	+	957	8	0.8%
ST6GAL2	chr1	-	2,845	25	0.9%
RPL7A	chr17	+	950	10	1.0%
CD99	chr1	-	1,010	8	0.8%
TAP2	chr16	-	1,572	12	0.7%
RPS10	chr26	+	612	5	0.8%
GLRX5	chr5	+	2,498	36	1.4%
RBM5	chr12	+	3,345	44	1.3%
PUM2	chr3	-	3,806	42	1.1%
HNRNPA2B1	chr2	-	1,906	37	1.9%
RHD	chr23	+	1,608	20	1.2%
PSMA4	chr10	-	1,280	18	1.4%
AMPD3	chr5	-	2,779	23	0.8%
CDKN1B_dup1	chr1	+	939	12	1.3%

AP2A2	chr5	-	6,093	47	0.8%
RPL7	chr2	-	889	9	1.0%
RMND5A	chr4	+	2,326	32	1.4%
RNF103	chr4	-	2,681	21	0.8%
SAP18	chr1	-	615	2	0.3%
HMOX1	chr1	-	922	5	0.5%
PABPC1	chr2	-	3,957	69	1.7%
TAX1BP1	chr2	+	3,270	41	1.2%
BSDC1	chr23	-	3,116	29	0.9%
RPL32	chr12	-	742	9	1.2%
BAG5	chr5	-	4,623	46	1.0%
MIR223	chr4	+	72	1	1.4%
RPS6	chrZ	-	837	10	1.1%
CCPG1	chr10	+	2,870	44	1.5%
RBM24	chr2	+	2,539	48	1.9%
SLC25A6	chr1	+	1,200	13	1.0%
LAMP1_dup1	chr1	-	398	3	0.6%
ATP5B	chrE22C19W28_E50C23	+	441	2	0.5%
TBC1D15	chr1	+	2,803	36	1.3%
UBE2A	chr4	-	430	5	1.0%
C6H10orf46	chr6	-	2,156	24	1.1%
KPNA6	chr23	-	2,820	23	0.8%
ZC3H11A	chr26	+	2,193	21	1.0%
RBL2	chr11	-	1,752	16	0.9%
PON2	chr2	-	5,260	42	0.8%
CCNL2	chr21	+	2,186	22	1.0%
MIRLET7I	chr1	+	59	1	0.9%
CLTC	chr19	+	5,041	41	0.8%
ELF1	chr1	-	2,963	24	0.8%
GNB2L1	chr16	+	977	8	0.8%
SRSF6	chr20	-	2,063	14	0.7%
ACOT9	chr1	+	3,115	36	1.1%
CST3	chr3	+	703	9	1.3%
VCP	chrZ	-	2,650	18	0.7%
RPL37	chrZ	-	467	2	0.4%
GMPR	chr2	+	1,815	24	1.3%
MIR24	chrZ	+	26	1	2.0%
SLC46A3	chr1	+	3,394	50	1.5%
MLX	chr27	+	1,760	20	1.1%
CR1L	chr26	+	1,467	13	0.9%
FAM126A	chr2	-	3,058	36	1.2%

CSDE1	chr26	-	3,670	41	1.1%
TOP2B	chr2	-	4,749	61	1.3%
ASB6	chr17	-	2,404	15	0.6%
VCPIP1	chr2	-	4,200	30	0.7%
ERAL1	chr19	-	1,417	11	0.8%
USP48	chr21	+	2,710	25	0.9%
AP2M1	chr9	+	1,935	17	0.9%
RPL9	chr4	+	623	3	0.4%
ADRM1	chr20	+	987	9	0.9%
SELT	chr9	-	1,256	3	0.2%
MAP1LC3B	chr11	+	1,660	16	0.9%
EDEM1	chr12	+	1,699	21	1.2%
COX4I1	chr11	-	566	4	0.7%
SOD2	chr3	+	876	9	1.0%
PCNA	chr22	+	625	6	0.9%
IRF2	chr4	+	1,616	20	1.2%
MIR142	chr19	-	72	3	3.5%
NFIA	chr8	+	1,775	23	1.3%
HPGDS	chr4	-	737	8	1.1%
RABGAP1L	chr8	-	2,843	29	1.0%
RPL35	chr17	-	364	8	2.2%
DNAJA2	chr11	+	1,073	8	0.7%
GFI1B	chr17	+	1,039	13	1.2%
UBE2R2	chrZ	+	967	18	1.9%
IREB2	chr10	-	2,529	21	0.8%
EPS15	chr8	-	3,653	46	1.2%
JAK1	chr8	-	2,954	32	1.1%
RPL30	chr2	-	273	4	1.3%
APBB1IP	chr2	-	1,728	15	0.9%
API5_dup2	chr5	+	1,151	13	1.1%
LMO2	chrUn_random	-	768	11	1.4%
PDE3B	chr5	+	2,509	38	1.5%
PIAS1	chr10	+	1,376	11	0.8%
USP4	chr12	-	2,453	19	0.8%
HIGD1A	chr2	-	1,088	11	1.0%
PSMD9	chr15	+	1,035	10	0.9%
UBE2L3	chr15	+	767	10	1.2%
BG2	chr16	-	728	17	2.3%
RNF114	chr20	-	1,943	17	0.9%
FLOT2	chr19	-	1,720	11	0.6%
STAT1	chr7	-	2,903	28	1.0%

CNBP	chr12	+	1,089	15	1.4%
RNF11	chr8	+	1,314	30	2.2%
PSME4	chr3	+	4,080	34	0.8%
FBXO18	chr1	-	2,251	13	0.6%
MIR29B-2	chr26	-	58	1	0.9%
FBXO32	chr2	-	3,361	20	0.6%
USP47	chr5	-	3,953	32	0.8%
LSM14A	chr11	+	1,547	16	1.0%
TMEM59	chr8	-	1,356	9	0.7%
FTL	chr5	+	781	10	1.3%
GTF2H5	chr3	+	802	8	0.9%
BTBD9	chr3	+	1,720	23	1.3%
MIR30D	chr2	-	45	0	0.0%
ZNF593	chr23	-	454	5	1.0%
IFIH1	chr7	+	2,475	36	1.5%
NDEL1	chr18	+	1,083	13	1.2%
IFNGR1	chr3	+	1,395	14	1.0%
TP53INP1	chr2	-	2,887	28	1.0%
TNFRSF10B	chr22	+	657	8	1.2%
CALM	chr3	-	648	6	0.8%
CAST	chrZ	-	1,587	18	1.1%
CHMP7	chr22	-	2,010	18	0.9%
EIF3H	chr2	-	826	9	1.1%
SSBP3	chr8	-	856	7	0.8%
PSMA3	chr5	-	639	6	0.9%
TAPT1	chr4	+	2,265	32	1.4%
RPL3	chr1	+	782	12	1.5%
WIPI2	chr14	+	1,246	12	0.9%
NR3C1	chr13	-	1,689	11	0.6%
MIR106	chr4	-	50	0	0.0%
SUMO2	chr18	-	708	13	1.8%
MAP2K3	chr14	-	960	13	1.4%
RPL29	chr12	+	578	3	0.4%
NRD1	chr8	-	2,218	28	1.2%
FAM177A1	chr5	+	1,654	24	1.5%
LOC772071	chr4	-	2,027	18	0.9%
E2F1	chr20	+	901	4	0.4%
ACTG1	chr10	+	779	19	2.4%
METAP2	chr1	+	1,075	14	1.3%
PDK3	chr1	-	1,496	11	0.7%
CD47	chr1	-	1,064	9	0.8%

PAPOLA	chr5	+	1,797	26	1.4%
MIR30E	chr23	+	51	1	2.0%
RAB18	chr2	-	1,104	8	0.7%
IGF2R	chr3	-	5,512	47	0.9%
PDCD10	chr9	+	760	11	1.4%
DNAJB6	chr2	+	1,534	21	1.4%
TAOK3	chr15	+	1,897	22	1.2%
PSMB7	chr17	-	565	9	1.5%
RAB5A	chr2	+	1,320	15	1.1%
HBXIP	chr26	-	384	3	0.7%
TRDMT1	chr2	+	1,067	11	1.0%
C1H11orf75	chr1	+	622	11	1.7%
RFFL	chr19	+	1,997	23	1.1%
ATP6V0A1	chr27	+	1,399	10	0.7%
SLC25A3	chr1	+	694	10	1.4%
PIP5K1B	chrZ	+	1,481	16	1.0%
IRF7	chr5	+	1,063	7	0.6%
GNB1	chr21	+	1,727	22	1.3%
PSMD5	chr17	-	1,853	15	0.8%
PPP2CA	chr13	+	1,017	11	1.0%
RPS14	chr13	+	1,114	10	0.9%
ARNT	chr25	-	1,640	10	0.6%
SLC35B1	chr27	+	702	8	1.1%
RNF13	chr9	-	1,312	14	1.1%
RPL27	chr27	+	246	6	2.4%
CSNK1A1	chr13	-	643	6	0.9%
CDC2L1	chr21	+	1,242	13	1.0%
STRBP	chr17	-	1,520	19	1.3%
LBR	chr3	+	1,122	15	1.3%
LY75	chr7	+	2,886	31	1.1%
RHOA	chr12	-	970	7	0.7%
MEMO1	chr3	+	804	12	1.5%
PAIP2	chr13	-	898	13	1.4%
CZH5orf43	chrZ	-	1,166	9	0.8%
PLAG1	chr2	-	980	5	0.5%
DDX6	chr24	-	1,911	16	0.8%
ZMAT2	chr13	-	738	8	1.0%
HNRPDL	chr4	+	1,111	19	1.7%
WWP1	chr2	+	2,007	19	0.9%
MATR3	chr13	-	1,926	16	0.8%
EIF3I	chr23	-	769	5	0.7%

WSB1	chr19	+	1,207	17	1.4%
HSPA4L	chr4	+	1,593	21	1.3%
QKI	chr3	-	668	4	0.5%
MGAT3	chr1	-	3,482	32	0.9%
ABCC4	chr1	+	2,384	32	1.3%
PANK4	chr21	+	2,398	32	1.3%
CDKN1B_dup2	chr1	+	424	2	0.5%
HBE	chr1	+	245	1	0.4%
ODC1	chr3	-	1,055	11	1.0%
DSTN	chr3	-	1,042	16	1.5%
DYRK1A	chr1	+	1,202	12	1.0%
YTHDC1	chr4	+	2,483	33	1.3%
ATG9A	chr7	+	2,082	14	0.7%
YPEL5	chr3	-	1,271	18	1.4%
MGEA5	chr6	+	2,657	38	1.4%
TRAFD1	chr15	+	1,481	19	1.2%
SLC48A1	chrE22C19W28_E50C23	-	845	8	0.9%
FYTTD1	chr9	+	1,416	20	1.4%
SP3	chr7	+	1,178	11	0.9%
LUC7L3	chr18	-	1,739	29	1.6%
MIRLET7D	chr12	-	51	1	1.0%
PSMA2	chr2	-	562	10	1.8%
HBG1	chr1	+	285	0	0.0%
CUL2	chr2	+	2,738	34	1.2%
ABCA1	chrZ	-	3,587	36	1.0%
MIR20B	chr4	-	44	0	0.0%
XPO7	chr22	-	1,790	11	0.6%
CCT4	chr3	+	949	7	0.7%
PSMC3	chr5	+	844	8	0.9%
C5H11orf58	chr5	+	329	3	0.9%
CCDC101	chr8	+	680	7	1.0%
RPS11	chr1	-	151	1	0.7%
MKLN1	chr1	-	1,235	12	0.9%
RPRD1B	chr20	-	1,737	18	1.0%
USP7	chr14	+	1,798	20	1.1%
CYTH1	chr18	+	436	5	1.0%
MIRLET7B	chr1	+	36	0	0.0%
SRSF3	chr26	+	672	5	0.7%
TOB2	chr1	+	1,874	26	1.4%
DNAJA1	chrZ	+	1,113	16	1.4%
UBE2G1	chr19	+	953	11	1.2%

ADCY9	chr14	-	2,048	17	0.8%
MIR130B	chr15	-	35	0	0.0%
STK11	chr28	+	618	10	1.5%
MARCH5	chr6	-	1,612	21	1.3%
KAT2A	chr27	-	1,214	12	0.9%
PPM1B	chr3	+	2,116	37	1.7%
PNPLA8	chr1	+	1,118	10	0.9%
NUTF2	chr11	+	424	4	0.9%
SERINC3	chr20	+	1,039	12	1.2%
APLP2	chr24	-	1,735	19	1.1%
PSPC1	chr1	+	836	9	1.0%
SERINC1	chr3	+	1,328	12	0.9%
PSMA1	chr5	-	433	4	0.8%
REEP3	chr6	-	522	6	1.1%
CHMP1B	chr4	-	626	8	1.2%
TRAM1	chr2	-	816	13	1.5%
TOB1	chr18	+	825	9	1.1%
XK	chr1	-	979	11	1.1%
CD36	chr1	-	1,095	12	1.1%
FNIP1	chr13	-	1,624	12	0.7%
C20H20orf111	chr20	+	472	5	1.1%
CTBP1	chr4	+	1,080	20	1.9%
PSMD12	chr18	+	709	9	1.2%
ADD1	chr4	-	1,923	17	0.9%
NFKBIA	chr5	-	800	9	1.1%
ELAVL1	chr28	-	567	3	0.4%
CHMP2B	chr1	-	1,112	11	0.9%
MIR19B	chr1	-	35	0	0.0%
PSMD4	chr25	+	356	5	1.4%
JUN	chr8	-	789	11	1.4%
KLHDC2	chr5	+	909	8	0.8%
PM20D1	chr26	-	1,445	10	0.7%
MYLIP	chr2	+	1,108	17	1.5%
MKRN1	chr1	-	1,268	11	0.8%
AKIRIN2	chr3	+	579	6	1.0%
SGMS1	chr6	+	1,411	12	0.9%
PLEKHA3	chr7	-	1,242	18	1.4%
ITGAV	chr7	-	1,569	11	0.7%
MIR1808	chr5	-	41	1	1.2%
BDH1	chr9	-	1,107	13	1.2%
PBX1	chr8	-	644	9	1.3%

MORF4L1	chr10	-	427	7	1.5%
SIRT1	chr6	-	915	8	0.9%
YWHAZ	chr2	-	772	5	0.6%
TPD52L2	chr20	-	1,025	8	0.8%
PSMC2	chr1	+	603	3	0.5%
EIF5A2	chr9	+	703	11	1.6%
SSR2	chr25	+	363	3	0.7%
MAFG	chr18	-	709	7	1.0%
PSMB1	chr3	+	443	4	0.9%
PPP6R3	chr5	+	1,829	23	1.3%
KIAA0907	chr25	-	1,303	13	1.0%
CHP1	chr5	+	975	15	1.5%
CLTB	chr13	+	1,079	8	0.7%
INCENP	chr5	+	2,039	0	0.0%
SRF	chr3	+	957	6	0.6%
PSME3	chr27	+	1,049	10	1.0%
DBR1	chr9	-	1,190	9	0.7%
TOP1	chr20	+	1,422	22	1.5%
MFAP1	chrUn_random	-	350	1	0.1%
HMGCL	chr23	-	874	7	0.8%
SELO	chr1	+	2,095	24	1.1%
MRPS17	chr19	+	360	3	0.7%
HMGB3	chr4	-	135	2	1.1%
ARPC4	chr12	+	218	2	0.9%
CLIC2	chr4	-	848	7	0.8%
PSMD1	chr9	+	1,226	13	1.1%
CREM	chr2	-	141	0	0.0%
LDB1	chr6	+	467	3	0.6%
RAB11A	chr10	+	940	7	0.7%
TRA2A	chr2	-	832	8	1.0%
GYG1	chr9	-	720	5	0.7%
SPTY2D1	chr5	-	960	17	1.7%
ADIPOR2	chr1	+	772	7	0.8%
JARID2	chr2	+	1,940	29	1.5%
C20H20orf43	chr20	-	481	6	1.1%
STAM2_dup2	chr7	-	573	5	0.8%
ATF7IP	chr1	+	2,178	23	1.0%
TARDBP	chr21	+	1,080	14	1.3%
EIF2AK2	chr3	+	1,163	15	1.2%
SEMA3D	chr1	+	1,045	10	1.0%
TLN1	chrZ	+	2,549	16	0.6%

AKTIP	chr11	+	726	9	1.2%
SUMO1	chr7	-	1,133	13	1.1%
IFNAR1	chr1	+	937	12	1.3%
RPS17L	chr10	-	158	2	1.0%
TAPBP	chr16	+	490	6	1.1%
STAT3	chr27	-	939	5	0.5%
SLC9A8	chr20	-	1,045	12	1.1%
CEBPG	chr11	+	913	11	1.2%
RREB1	chr2	-	2,384	23	0.9%
MYH9	chr1	+	2,132	24	1.1%
MOV10	chr26	+	1,140	12	1.1%
RPL7L1	chr4	-	598	5	0.8%
CHCHD2	chr19	-	304	5	1.6%
PFN2	chr9	+	912	14	1.5%
MIR1813-1	chr2	+	33	0	0.0%
COPS7A	chr1	+	575	8	1.4%
ABTB1	chr12	-	1,969	16	0.8%
COPS8	chr7	-	659	2	0.2%
RPL6	chr15	-	378	1	0.3%
RAB10	chr3	+	1,091	18	1.7%
SMAP2	chr23	+	623	9	1.4%
LZIC	chr21	-	1,348	10	0.7%
TCF3	chr28	+	860	8	0.9%
INO80	chr5	-	2,689	23	0.9%
HSPA5	chr17	-	919	16	1.7%
EIF3M	chr5	+	484	5	1.0%
UBE3C	chr2	+	1,649	25	1.5%
GARNL3	chr17	+	1,309	23	1.8%
SELK	chr12	-	249	4	1.6%
PSMC1	chr5	+	518	4	0.8%
THAP5	chr1	+	675	8	1.2%
CNOT7	chr4	+	931	15	1.6%
RGS18	chr8	-	356	2	0.6%
TRPC4AP	chr20	+	1,542	14	0.9%
PNRC2	chr23	+	987	15	1.5%
N4BP1	chr11	+	1,110	11	1.0%
MEAF6	chr23	+	395	3	0.8%
TBCA	chrZ	+	468	7	1.5%
PPHLN1	chr1	+	1,164	16	1.3%
CDC14A	chr8	+	641	8	1.2%
NDUFA9	chr1	+	435	4	0.9%

DDX1	chr3	+	808	12	1.5%
RNF4	chr4	-	1,227	10	0.8%
GTF2H1	chr5	+	809	7	0.8%
VPS35	chr11	+	1,103	19	1.7%
CLINT1	chr13	+	1,190	19	1.6%
SNX5	chr3	+	418	1	0.2%
PNISR	chr3	+	1,041	14	1.3%
ZFYVE1	chr5	+	1,739	28	1.6%
LOC420411	chr2	+	269	2	0.6%
MDM2	chr1	+	556	5	0.9%
ACTA1	chr3	-	204	16	7.6%
BCL2L1	chr20	-	440	3	0.7%
CTSB	chr3	-	342	2	0.4%
SPG7	chr11	+	1,013	11	1.0%
TNRC15	chr9	+	1,878	23	1.2%
VEZF1	chr19	+	572	3	0.5%
SLMAP	chr12	+	955	8	0.8%
STAT5B	chr27	-	1,027	8	0.7%
ASXL2	chr3	-	1,991	13	0.7%
SEC24B	chr4	-	1,599	14	0.8%
ANXA11	chr6	-	870	9	1.0%
SLC25A36	chr9	-	1,861	19	1.0%
MIR107	chr6	-	28	0	0.0%
MOSPD2	chr1	-	1,292	14	1.0%
MIR125B	chr1	+	30	0	0.0%
TMEM66	chr4	-	805	7	0.9%
SPINZ	chrZ	+	1,344	27	2.0%
BRAF	chr1	-	923	7	0.8%
STRAP	chr1	+	671	7	1.0%
MAPRE2	chr2	+	992	7	0.7%
GLYR1	chr14	+	671	4	0.6%
EIF4H	chr19	-	1,767	18	1.0%
CDC42	chr21	-	722	6	0.8%
DGCR6	chr15	-	426	7	1.5%
SBDS	chr19	-	1,053	15	1.4%
ACADL	chr7	-	636	6	0.9%
USP15	chr1	+	1,564	23	1.5%
FURIN	chr10	-	1,006	10	1.0%
MED22	chr17	-	150	2	1.0%
SOX4	chr2	-	0	0	#DIV/0!
TIMP3	chr1	-	308	1	0.3%

HNRNPR	chr23	+	886	8	0.9%
VPS29	chr15	-	748	8	1.1%
N4BP2L2	chr1	+	1,374	19	1.3%
GSTA3_dup2	chr3	+	292	3	1.0%
LUC7L2	chr1	+	621	7	1.1%
EIF5B	chr1	+	1,463	16	1.1%
SLU7	chr13	+	851	15	1.8%
C13H5orf15	chr13	+	759	11	1.4%
ATP6V1A	chr1	-	1,378	15	1.1%
NXT2	chr4	-	480	4	0.8%
IK	chr13	-	532	8	1.4%
MMADHC	chr7	-	1,215	13	1.1%
ATP6V0E1	chr13	+	434	6	1.3%
CWC22	chr7	+	1,003	12	1.1%
ARF1	chr2	-	701	9	1.2%
MIER1	chr8	+	750	6	0.8%
SEPT2	chr15	+	40	1	1.3%
CNPPD1	chr7	+	625	10	1.5%
WAPAL	chr6	-	1,747	15	0.8%
EIF2S3	chr1	-	555	4	0.7%
XPO1	chr3	-	1,501	15	1.0%
ZNF326	chr8	-	814	12	1.4%
KLHL7	chr2	+	675	7	1.0%
DFFB	chr21	-	423	5	1.1%
EXD2	chr5	-	1,087	12	1.1%
SNX14	chr3	+	950	14	1.4%
PSMC6	chr5	+	465	4	0.8%
ARIH2	chr12	-	933	10	1.1%
KARS	chr11	+	689	11	1.5%
CASC4	chr10	-	763	8	1.0%
FXYD6	chr24	-	169	2	1.2%
TRIM27_dup2	chr16	+	419	1	0.1%
BRD1	chr1	-	1,653	16	1.0%
COBRA1	chr17	+	662	7	1.0%
BZW1	chr7	+	517	6	1.1%
ENTPD1	chr6	+	1,257	12	0.9%
CHMP4B	chr20	-	538	10	1.8%
HDLBP	chr9	-	1,450	13	0.9%
KDM5B	chr26	+	1,583	12	0.8%
MIR130C	chr19	-	11	0	0.0%
MIR30B	chr2	-	27	0	0.0%

DERL1	chr2	-	1,114	11	0.9%
SERBP1	chr8	-	887	10	1.1%
HMG1	chr1	-	390	6	1.4%
IRF8	chr11	-	540	3	0.5%
CTSL2	chrZ	+	436	4	0.9%
TGM2	chr20	+	825	9	1.0%
TNFSF13B	chr1	-	1,202	12	1.0%
MRPS26	chr4	+	512	4	0.7%
ANGEL1	chr5	-	1,062	7	0.6%
MIR1768	chr2	+	22	1	2.3%
MYST2	chr27	-	1,230	9	0.7%
TPM3	chr25	-	486	9	1.9%
SH3GLB1	chr8	-	549	6	1.0%
MIR18B	chr4	-	13	0	0.0%
ZBTB7A	chr28	+	235	2	0.9%
MIR1692	chr9	+	27	1	1.9%
ATP5A1	chrZ	+	508	6	1.1%
HINT1	chrZ	+	152	2	1.3%
RAD21	chr2	-	1,194	14	1.2%
PDIA3	chr10	-	605	6	1.0%
THOC7	chr12	-	427	6	1.4%
VMA21	chr4	-	646	8	1.2%
COPS3	chr14	-	504	3	0.6%
CCT5	chr2	-	576	5	0.8%
G3BP1	chr13	-	745	7	0.9%
PAFAH1B1	chr19	+	1,532	15	0.9%
BOK	chr9	+	321	1	0.2%
FAM133	chr2	-	897	15	1.7%
VAMP3	chr21	-	211	1	0.2%
PUF60	chr2	-	701	5	0.7%
ANP32E	chr25	+	1,102	20	1.8%
ASB9	chr1	+	547	8	1.5%
NRBF2	chr6	-	559	7	1.3%
GRB2	chr18	-	203	3	1.5%
MIR181B-1	chr8	+	29	0	0.0%
BTBD1	chr10	-	709	7	1.0%
WASH1	chr1	-	626	5	0.8%
MIR17	chr1	-	20	0	0.0%
VPS4B	chr2	+	1,050	16	1.5%
BECN1	chr27	-	563	6	1.1%
LIG3	chr19	-	1,008	12	1.1%

CCND3	chr26	-	680	4	0.6%
MCAM	chr24	+	346	1	0.1%
LOC422249	chr4	+	743	12	1.6%
GLS	chr7	+	615	8	1.2%
EAPP	chr5	-	401	3	0.7%
WDR82	chr12	-	657	7	1.1%
DTD1	chr3	-	397	2	0.5%
SEP15	chr8	+	467	4	0.9%
TMEM57	chr23	-	967	6	0.6%
TGFBR1	chr2	+	579	5	0.9%
TIA1	chr6	-	347	2	0.6%
PPP1R21	chr3	+	1,010	14	1.3%
CIAPIN1	chr11	+	598	4	0.6%
ASNS	chr2	-	908	12	1.3%
PCID2	chr1	+	212	3	1.2%
MYL12A	chr2	-	283	5	1.6%
CEP63	chr9	+	702	4	0.5%
PDHA1	chr1	-	453	7	1.4%
PDPK1	chr14	+	1,765	23	1.3%
JAZF1	chr2	-	853	10	1.1%
UBE2E3	chr7	-	924	14	1.5%
VDAC2	chr6	-	270	3	1.1%
ING5	chr9	-	228	1	0.4%
LOC416354	chr13	+	1,341	16	1.2%
COPA	chr25	-	1,113	6	0.5%
TMED10	chr5	-	635	7	1.1%
BCAP29	chr1	+	537	7	1.2%
PDCD4	chr6	+	381	6	1.4%
HMGCR	chrZ	-	996	14	1.4%
PSMA7	chr20	-	224	5	2.2%
PCYT2	chr18	-	784	7	0.8%
PRKAR1A	chr18	+	955	14	1.4%
MAFK	chr14	+	166	2	1.2%
PTBP1	chr28	+	1,280	16	1.3%
GATAD2A	chr28	-	678	5	0.7%
RAB3IL1	chr5	-	448	3	0.7%
CLASP2	chr2	-	1,429	7	0.5%
SRSF5A	chr5	+	617	10	1.5%
IFNGR2	chr1	+	599	9	1.5%
GPR126	chr3	-	1,148	9	0.7%
MCMBP	chr6	-	929	8	0.9%

SRSF11	chr8	+	660	12	1.7%
ARCN1	chr24	-	899	8	0.8%
ACTR1A	chr6	-	697	5	0.7%
RPS6KB1	chr19	+	762	8	1.1%
CDC73	chr8	-	911	10	1.1%
PDCD6IP	chr2	+	1,382	20	1.4%
THRAP3	chr23	-	1,022	11	1.1%
DNM1L	chr1	-	864	6	0.6%
NADK	chr21	+	1,273	26	2.0%
FGFR1OP2	chr1	+	837	11	1.3%
UBE4A	chr24	-	1,049	10	1.0%
HN1	chr18	-	396	6	1.4%
SNX3	chr3	+	236	2	0.8%
TRIM41	chr16	-	487	7	1.3%
COX7A2	chr3	+	241	1	0.4%
PPP4R2	chr12	+	751	9	1.2%
CBWD1	chrZ	-	445	7	1.6%
UBL7	chr10	+	434	2	0.5%
TST	chr1	+	280	4	1.3%
GABPA	chr1	+	1,106	12	1.0%
ZNF335	chr20	-	1,151	9	0.7%
PTPN2	chr2	+	503	4	0.7%
MBLAC2	chrZ	+	1,005	16	1.6%
HNRNPD	chr4	+	288	3	1.0%
TPRA1	chr12	+	1,022	11	1.1%
IFNAR2	chr1	+	485	6	1.1%
ITGB3	chr27	+	852	6	0.7%
MIR1611	chr10	+	17	0	0.0%
DEGS1	chr3	-	571	6	1.1%
PRELID1	chr13	-	126	2	1.2%
POLR2F	chr1	-	135	0	0.0%
RNASEH1	chr3	-	346	5	1.4%
C22H2orf42	chr22	-	597	5	0.8%
MIR146C-1	chrUn_random	+	34	0	0.0%
PLEK	chr3	+	303	3	0.8%
NRBP1	chr3	-	748	10	1.3%
H2AFZ	chr4	-	240	2	0.6%
PPP2CB	chr4	-	316	3	0.9%
MED20	chr26	-	289	3	0.9%
PRDX6	chr8	-	341	6	1.6%
ZFAND5	chrZ	-	633	9	1.3%

EXOC7	chr18	+	562	5	0.9%
TMX4	chr3	+	1,178	13	1.1%
MAGOH	chr8	-	167	1	0.3%
CAT	chr5	+	205	2	1.0%
XRN2	chr3	-	955	7	0.7%
CARS	chr5	+	788	7	0.9%
SRPR	chr24	+	807	14	1.7%
NUCKS1	chr26	-	325	6	1.7%
IKBKB	chr22	+	633	6	0.9%
ADAM17	chr3	-	1,128	9	0.8%
MIR138-1	chr2	-	26	0	0.0%
FOXO1	chr1	+	1,281	20	1.5%
YIPF4	chr3	-	643	2	0.3%
GFPT1	chr22	+	1,487	11	0.7%
ZRANB2	chr8	-	597	6	0.9%
IL2RG	chr4	+	383	5	1.2%
KDM3A	chr4	+	1,181	16	1.3%
MLF2	chr1	-	390	3	0.8%
NANP	chr3	-	967	6	0.6%
DHX15	chr4	+	691	7	0.9%
CLPX	chr10	+	897	13	1.4%
CLP1	chr5	-	420	1	0.1%
MIR128-2	chr2	+	19	0	0.0%
CELF1	chr5	+	1,098	11	1.0%
EXOC5	chr5	+	1,070	14	1.3%
GOLGA7	chr22	+	469	5	1.0%
GOSR1	chr19	+	568	10	1.7%
TERF2IP	chr11	-	551	5	0.8%
POLDIP3	chr1	+	768	13	1.6%
CCZ1	chr14	-	462	5	1.1%
NCOA7	chr3	-	825	5	0.5%
LLPH	chr1	-	179	2	1.1%
EIF2S1	chr5	-	359	5	1.3%
CYBASC3	chr5	+	299	1	0.3%
ADD3	chr6	+	555	6	1.0%
DIAPH1	chr4	-	1,558	18	1.2%
ANKHD1	chr13	+	1,912	17	0.9%
C20H20orf11	chr20	+	819	12	1.4%
FECH	chrZ	+	344	5	1.3%
PPP1R12A	chr1	-	1,187	21	1.8%
TTC14	chr9	-	712	8	1.1%

C1H2orf49	chr1	+	1,011	10	1.0%
MKKS	chr3	+	740	8	1.0%
RPRD1A	chr2	+	664	11	1.6%
HSP90B1	chr1	-	684	7	1.0%
FEM1B	chr10	+	719	4	0.5%
FLII	chr14	-	856	6	0.7%
DPY30	chr3	+	168	2	0.9%
TOLLIP	chr5	+	689	11	1.5%
SNX2	chrZ	+	472	4	0.8%
SNX12	chr4	+	496	5	1.0%
RIT1	chr25	-	750	9	1.2%
ASH2L	chr22	+	574	7	1.1%
CTCF	chr11	-	998	8	0.8%
MTPN	chr1	+	847	13	1.5%
SLC25A46	chrZ	-	488	2	0.4%
PPP2R5C	chr5	+	980	13	1.3%
PPP3R1	chr3	-	668	13	1.9%
ADAM10	chr10	+	502	8	1.6%
RANGAP1	chr1	+	586	5	0.8%
CTDSPL	chr2	+	253	4	1.4%
SNAP29	chr15	-	1,136	15	1.3%
LBH	chr3	-	660	7	1.1%
PSMD2	chrUn_random	-	492	3	0.6%
BAP1	chr12	-	789	10	1.2%
HARS	chr13	+	451	4	0.9%
NARS	chrZ	+	464	5	1.1%
NDUFV3	chr1	+	321	7	2.0%
MAPK1	chr15	+	225	2	0.9%
HDAC1	chr23	-	776	9	1.1%
COPS4	chr4	-	396	2	0.4%
OPTN	chr1	+	559	4	0.7%
NUMA1	chr1	-	1,333	8	0.6%
AP1G1	chr11	+	824	13	1.5%
CEPT1	chr26	-	515	4	0.8%
IP6K2	chr12	+	382	5	1.2%
B4GALT1	chrZ	-	446	5	1.1%
TMEM30A	chr3	+	696	5	0.6%
ANKRD27	chr11	-	824	11	1.3%
OPA1	chr9	-	1,180	17	1.4%
C25H1orf43	chr25	-	301	2	0.5%
UBXN2A	chr3	+	466	5	1.0%

RAP2C	chr4	-	173	0	0.0%
ABCE1	chr4	+	517	9	1.7%
ABCC1	chr14	+	1,326	19	1.4%
MX1	chr1	+	560	6	1.1%
MIR26A	chr2	+	8	0	0.0%
RIC8A	chr5	-	664	6	0.9%
FAM53A	chr4	+	525	5	0.9%
CUTC	chr6	-	263	4	1.3%
SETD1B	chr15	+	1,327	12	0.9%
TCEB1	chr2	-	675	9	1.3%
TBL1XR1	chr9	+	1,046	25	2.3%
MXD4	chr4	+	416	3	0.7%
ARFGAP2	chr5	+	509	6	1.2%
TIRAP	chr24	+	200	2	0.8%
CRIPT	chr3	+	521	6	1.1%
DYM	chrZ	+	400	5	1.3%
LAMP2	chr4	+	340	4	1.2%
WHSC2	chr4	+	1,321	14	1.1%
ING3	chr1	-	418	4	1.0%
REV1	chr1	-	945	5	0.5%
KLHL15	chr1	+	861	19	2.2%
PIP4K2A	chr2	+	701	9	1.3%
DNAJC18	chr13	+	233	2	0.9%
GTF2A1	chr5	-	1,271	16	1.2%
EIF3J	chr10	-	405	5	1.1%
NAP1L4	chr5	+	484	7	1.4%
RBMX	chr4	-	346	4	1.0%
FBXO9	chr3	-	622	6	0.9%
USP34	chr3	-	2,536	31	1.2%
PAK1IP1	chr2	+	323	7	2.0%
ACTR3	chr7	-	374	3	0.7%
IKZF1	chr2	+	339	4	1.0%
SMU1	chrZ	-	680	6	0.9%
HSPH1	chr1	+	724	7	0.9%
SRSF2	chr18	+	518	7	1.4%
TRAPPC2	chr1	+	382	3	0.8%
PDHB	chr12	-	259	1	0.4%
U2AF1	chr1	-	770	7	0.8%
DNAJB14	chr4	-	523	3	0.5%
HDAC3	chr13	-	367	2	0.4%
RAB9A	chr1	-	508	8	1.5%

VPS18	chr5	+	745	7	0.9%
P2RY1	chr9	-	287	3	0.9%
PHF20L1	chr2	+	1,033	16	1.5%
MIRLET7J	chr26	-	16	0	0.0%
SPCS1	chr12	+	161	4	2.2%
OAT	chr6	-	445	6	1.3%
ARPP19	chrUn_random	+	106	2	1.4%
ZBTB8B	chr23	+	234	2	0.9%
HBZ	chr14	+	87	0	0.0%
AARS	chr11	+	613	7	1.1%
ATXN3	chr5	-	291	5	1.5%
MIR130A	chr15	-	6	0	0.0%
CPNE1	chr20	+	569	4	0.6%
SEC62	chr9	-	507	10	2.0%
CNDP2	chr2	-	460	4	0.8%
DDX19B	chr21	-	695	10	1.4%
SPTLC2	chr5	-	505	6	1.1%
DAZAP1	chr28	+	413	4	0.8%
STRADA	chr27	-	571	1	0.2%
CHMP1A	chr11	-	213	0	0.0%
LOC424740	chr9	+	811	10	1.2%
CHUK	chr6	+	541	3	0.5%
BRAP	chr15	-	587	10	1.7%
C14H17orf103	chr14	+	660	7	1.0%
SNRK	chr2	-	648	10	1.5%
DDB1	chr5	+	804	5	0.6%
MRPL23	chr5	-	142	2	1.1%
NDUFS1	chr7	+	560	4	0.6%
PSMF1	chr20	-	426	4	0.9%
SRRM1	chr23	-	769	12	1.5%
SLC2A3	chr1	+	310	7	2.1%
AKAP9	chr2	+	2,505	28	1.1%
GNS	chr1	-	1,121	9	0.8%
GALNT1	chr2	-	736	7	1.0%
MIR1451	chr3	+	17	0	0.0%
RAB2A	chr2	+	114	2	1.3%
NUP85	chr18	+	425	8	1.8%
RNF166	chr11	-	785	5	0.6%
MAVS	chr4	-	992	5	0.5%
EIF2S2	chr20	+	270	3	1.1%
TFIP11	chr15	-	843	12	1.4%

MIR1764	chr15	+	23	0	0.0%
ATP6AP2	chr1	-	408	5	1.1%
PHB2	chr1	-	268	5	1.9%
MIR16-2	chr9	-	18	1	2.9%
MIRLET7A-1	chr12	-	10	0	0.0%
SNAP23	chr5	+	296	2	0.7%
C5H14orf166	chr5	+	181	2	1.1%
TMEM111	chr12	+	191	0	0.0%
YIPF3	chr3	+	303	3	0.8%
NFYA	chr26	+	715	9	1.3%
NDUFB1	chr5	-	48	1	1.0%
YBX1	chr21	-	288	6	2.1%
FAM125B	chr17	+	1,090	14	1.2%
CRK	chr8	+	242	2	0.6%
MORN4	chr6	+	327	6	1.7%
DNAJC3	chr1	-	1,055	16	1.5%
RNF126	chr28	-	353	4	1.1%
FYCO1	chr2	+	908	8	0.9%
C11H16orf70	chr11	+	623	10	1.6%
ITGB1	chr2	+	705	14	1.9%
OGDH	chr22	+	372	3	0.8%
FKBP4	chr1	-	512	8	1.5%
LYSMD3	chrZ	+	445	11	2.5%
ZNF706	chr2	-	584	4	0.7%
RNF141	chr5	+	696	12	1.7%
PPP3CB	chr6	+	406	6	1.5%
USP12P1	chr4	+	1,063	15	1.4%
NR1H3	chr5	-	634	3	0.4%
EIF4A3	chr3	+	237	4	1.7%
UFD1L	chr15	-	302	4	1.3%
COPS5	chr2	-	295	2	0.7%
STUB1	chr14	+	295	3	1.0%
YAF2	chr1	-	516	9	1.6%
HPSE	chr4	-	324	2	0.6%
CNOT2	chr1	+	500	2	0.3%
SRP14	chr5	+	231	4	1.5%
SUDS3	chr15	-	536	6	1.0%
RNF220	chr8	+	475	6	1.2%
POLK	chrZ	-	624	7	1.0%
SNX13	chr2	-	639	9	1.3%
BAG1	chr2	-	270	5	1.9%

SDC4	chr20	+	112	1	0.9%
AKAP17A	chr1	-	718	10	1.3%
ALDH3A2	chr19	+	511	2	0.4%
DNAJB12	chr6	+	481	7	1.4%
BTF3L4	chr8	+	574	5	0.9%
MTF1	chr23	+	479	4	0.7%
SUMO3	chr9	+	197	2	1.0%
ENSA_dup2	chr25	-	325	6	1.7%
PAM16	chr14	-	96	1	1.0%
LMBRD1	chr3	+	371	6	1.5%
SNX27	chr25	+	308	1	0.2%
SEPP1	chrZ	-	8	0	0.0%
NDUFA5	chr1	+	202	2	0.7%
SMC3	chr6	+	659	9	1.4%
ZCCHC8	chr15	-	560	7	1.2%
CDC27	chr27	+	743	7	0.9%
C26H6orf89	chr26	+	981	10	1.0%
MEF2A	chr10	+	433	7	1.6%
RER1	chr21	-	326	2	0.6%
AHCYL1	chr26	+	587	6	1.0%
ING4	chr1	-	312	2	0.6%
HSPA9	chr13	+	559	4	0.6%
RBM25	chr5	-	775	8	1.0%
GSPT1	chr14	-	706	11	1.5%
CAPZB	chr21	-	283	4	1.2%
POLR2B	chr4	-	733	3	0.4%
SDF4	chr21	+	535	8	1.4%
VAPB	chr20	-	349	6	1.6%
GGA3	chr18	-	827	9	1.1%
SPPL2A	chr10	+	798	12	1.5%
YWHAG	chr19	+	578	8	1.4%
RAP1B	chr1	+	842	8	0.9%
YWHAE	chr19	+	222	3	1.1%
PRKAB2	chrUn_random	-	191	0	0.0%
LPP	chr9	-	561	5	0.8%
TRAPPC11	chr4	-	850	10	1.2%
LOC422426	chr4	+	295	3	0.8%
TMEM11	chr14	+	159	2	1.3%
MVP	chr28	+	464	4	0.8%
CFLAR	chr7	+	544	4	0.6%
CLK2	chr25	+	358	4	1.0%

RLIM	chr4	-	402	3	0.7%
LMBR1	chr2	-	271	4	1.3%
UBN1	chr14	+	942	8	0.8%
FAM86A	chr14	-	288	2	0.7%
MAPT	chr27	-	276	6	2.2%
TTC7B	chr5	-	657	6	0.9%
ELOVL1	chr8	-	417	3	0.6%
INTS2	chr19	+	909	11	1.2%
ST3GAL6	chr1	+	419	4	0.8%
THOC5	chr15	+	392	4	0.9%
RB1	chr1	+	791	8	1.0%
COPS2	chr10	-	357	8	2.2%
CCT2	chr1	+	335	4	1.0%
SLMO2	chr20	+	478	7	1.5%
NUBP2	chr14	-	308	3	1.0%
GAPDH	chr1	+	205	2	1.0%
ATE1	chr6	-	505	5	1.0%
PTP4A1	chr3	-	493	6	1.2%
UBQLN4	chr25	-	402	3	0.7%
RALGAPB	chr20	-	1,012	10	0.9%
FAM116A	chr12	-	608	5	0.8%
SLC23A2	chr22	+	377	2	0.5%
GPR107	chr17	+	515	7	1.4%
LETM1	chr4	+	429	2	0.5%
RBM22	chr13	+	281	5	1.8%
RAP1GAP2	chr19	+	818	6	0.7%
CASP3	chr4	+	252	3	1.2%
ABHD13	chr1	-	496	6	1.2%
CZH5orf44	chrZ	+	251	2	0.8%
SLC26A5	chr1	-	473	6	1.3%
LOC769174	chr1	-	165	0	0.0%
YPEL2	chr19	+	858	15	1.7%
TFEB	chr26	-	587	7	1.1%
E2F6	chr3	-	339	6	1.8%
CTDSPL2	chr10	-	657	10	1.4%
LIN7C	chr5	-	706	7	0.9%
LOC395787	chr22	+	335	5	1.5%
VPS39	chr5	-	858	8	0.9%
TNKS	chr4	-	677	8	1.1%
CORO1C	chr15	-	386	3	0.6%
KLHL24	chr9	+	696	5	0.7%

TPH1	chr5	-	274	2	0.7%
SMARCA2	chr2	+	706	7	0.9%
LAMTOR3	chr4	-	207	1	0.5%
SASS6	chr8	+	526	7	1.3%
SATB1	chr2	-	608	9	1.4%
P2RX5	chr19	+	727	7	0.9%
CDC40	chr3	-	358	6	1.5%
USO1	chr4	-	620	7	1.1%
BCAS2	chr26	-	158	3	1.9%
C3H6orf120	chr3	-	342	5	1.5%
XPOT	chr1	+	586	5	0.8%
ARID4A	chr5	-	847	14	1.6%
UBE2I	chr14	+	242	6	2.5%
SRSF10	chr23	-	491	3	0.6%
COG1	chr18	+	481	5	0.9%
LYRM4	chr2	+	116	2	1.3%
FAM104A	chr18	-	520	8	1.4%
HACE1	chr3	+	650	12	1.8%
POLR3F	chr3	-	265	5	1.7%
TSC22D1	chr1	-	706	9	1.2%
ARID3B	chr10	-	308	6	2.0%
XIAP	chr4	-	307	3	0.8%
MEF2BNB	chr28	+	147	1	0.7%
SF3A2_dup1	chr28	-	52	2	2.9%
TOR1A	chr17	-	379	2	0.5%
TSSC1	chr3	-	616	8	1.3%
RAB35	chr15	+	515	7	1.3%
TSN	chr7	+	164	3	1.5%
HNRNPM	chr28	-	415	5	1.1%
TAP1	chrUn_random	-	140	2	1.1%
YTHDF3	chr2	+	484	7	1.4%
GPS1	chr18	-	336	4	1.0%
NR2C1	chr1	-	401	5	1.2%
LY6E	chr2	-	180	2	1.1%
ZYX	chr1	-	467	4	0.8%
WWP2	chr11	+	603	8	1.2%
PCSK7	chr24	-	586	2	0.3%
KATNA1	chr3	-	249	2	0.6%
DSTYK	chr26	-	499	6	1.1%
SELS	chr10	-	224	1	0.4%
SPCS3	chr4	+	88	0	0.0%

NKAP	chr4	+	292	3	0.9%
ARL6IP4	chr3	+	241	7	2.7%
UBE2F	chr7	+	135	1	0.4%
RAB11B	chr28	-	401	4	1.0%
YARS	chr23	-	388	4	0.9%
NCDN	chr23	-	422	3	0.6%
DDX27	chr20	-	429	3	0.7%
SAR1B	chr13	+	183	3	1.6%
LDHA	chr5	+	246	2	0.8%
MTERFD1	chr2	-	236	3	1.1%
KPNA1	chr1	-	765	5	0.6%
CBR1	chr1	+	142	1	0.4%
MAP2K1	chr10	+	316	3	0.8%
SLC30A7	chr8	-	190	1	0.3%
TCEB3	chr23	+	708	6	0.8%
FBXW5	chr17	+	502	5	0.9%
HIAT1	chr8	-	449	5	1.1%
RNF25	chr7	+	265	5	1.7%
HDAC2	chr3	+	278	3	0.9%
NFU1	chr22	+	145	2	1.4%
FAM76A	chr23	+	436	10	2.2%
SEC23B	chr3	-	441	5	1.1%
PPP6C	chr17	-	217	3	1.2%
ZC3HAV1	chr1	-	625	9	1.4%
MFAP3	chr13	-	759	4	0.5%
ASNSD1	chr7	-	374	3	0.8%
PDS5A	chr4	+	729	10	1.4%
PPP2R2A	chr22	-	348	2	0.4%
SF3A1	chr15	+	494	7	1.3%
MIR128-1	chr7	+	13	1	4.0%
CAPN1	chr3	-	537	7	1.2%
FBXO7	chr1	-	506	6	1.1%
C26H6orf130	chr26	-	276	2	0.5%
SPG21	chr10	-	259	2	0.8%

Appendix 4: Table with information regarding all sequencing tracks shown in this study (total read counts, mapped read counts, MAPQ threshold and median, percentage of reads uniquely mapped).

Track	Experiment description	Type of sequence reads	Total reads	Mapped reads	MAPQ threshold, median	% of reads uniquely mapped
F1-1	F1-1 DNA-seq of cell sample sA	single end	73,667,288	51,421,376	10, 82	45
F1-2	F1-2 DNA-seq of cell sample sB	single end	8,768,621	6,963,103	10, 91	88
SE	SE DNA-seq of cell sample sB	single end	9,981,058	8,669,633	10, 94	91
Transcript (+)	Total RNA-seq of cell sample s1	paired end	55,946,958*	18,293,547	10, >30	>90
Trascript (-)	Total RNA-seq of cell sample s1	paired end	55,946,958*	32,509,582	10, >30	>90
	Total RNA-seq of cell sample s1	paired end	64,858,188	55,946,958*	10, 31	91
Transcript (+)	Nuclear RNA-seq of cell sample s1	paired end	47,049,131	5,635,315	10, >30	>90
Trascript (-)	Nuclear RNA-seq of cell sample s1	paired end	47,049,131	38,331,023	10, >30	>90
	Nuclear RNA-seq of cell sample s1	paired end	53,899,876	47,049,131	10, 18	97
H3K4me3	H3K4me3 CHIP-seq of cell sample sD	single end	24,167,622	15,735,764	10, 72	92

H3K27ac	H3K27ac ChIP-seq of cell sample sD	single end	30,405,304	20,084,812	10, 75	92
<p>MAPQ (MAPping Quality) = $-10 \log_{10} \text{Pr}(\text{mapping position is wrong})$. A MAPQ score of 10 means that the probability of correctly mapping a random read is 90%. Paired end reads contain a pairing quality value which is usually lower than that of single end reads.</p>						
* We used the total number of mapped reads from RNA-seq						